ETUDE DU MANTEAU ARCHEEN. APPORTS ET LIMITES DES TRACEURS GEOCHIMIQUES (REE, Nd, Hf, Sr et 0)

Gérard Gruau

Thèse d' Etat
Université de Rennes I

ETUDE DU MANTEAU ARCHEEN APPORTS ET LIMITES DES TRACEURS GEOCHIMIQUES (REE, Nd, Hf, Sr et O)

par

Gérard GRUAU

Soutenue le 19 Mars 1993 devant la Commission d'Examen

Membres du Jury

B. M. JAHN
S. FOURCADE
F. ALBAREDE
N.T. ARNDT
Ph. GILLET
A.W. HOFMANN
E.G. NISBET

SERIE : C
N° d'Ordre : 526
N° de Série : 176

THESE

Présentée

DEVANT L'UNIVERSITE DE RENNES I

pour obtenir

le grade de Docteur ès Sciences

Par

Gérard GRUAU

Sujet de la Thèse : Etude du manteau Archéen : Apports et Limites des Traceurs Géochimiques (REE, Nd, Hf, Sr et O).

Soutenue le 19 Mars 1992 devant la Commission d'Examen

B. M. JAHN (Président)
S. FOURCADE (Rapporteur)
F. ALBAREDE (Rapporteur)
N.T. ARNDT (Examinateur)
Ph. GILLET (Examinateur)
A.W. HOFMANN (Examinateur)
E.G. NISBET (Examinateur)

Résumé

Dans ce travail nous utilisons les propriétés de traceurs géochimiques des systèmes isotopiques du Sm-Nd, Lu-Hf et Rb-Sr, ainsi que des éléments majeurs et des éléments en trace (Terres Rares) pour apporter une contribution à la connaissance de la composition et de l'évolution du manteau archéen terrestre (T compris entre 2500 et 3800 Ma). Nous étudions aussi le comportement de ces systèmes et/ou éléments lors de l'altération et du métamorphisme, étant entendu que les roches archéennes présentent toutes des signes d'altération et/ou de métamorphisme, deux processus qui peuvent avoir effacer leurs caractéristiques géochimiques originelles. Les objets d'étude sont des roches de composition basique à ultrabasique (komatiites, basaltes et gabbros) et proviennent d'Afrique du sud (ceintures de Barberton et de Schapenburg; T≈3500 Ma), d'Australie (craton de Pilbara; T≈3500 Ma), de Finlande (T≈2700 Ma) et du Groënland (ceinture d'Isua; T≈3800 Ma).

Les résultats géochimiques obtenus sur les komatiites d'Afrique du Sud et du craton de Pilbara, couplés avec ceux publiés sur des komatiites provenant d'autres régions du monde (Canada, Zimbabwe, Inde), montrent qu'il existe, dans ces roches, des variations systématiques des rapports CaO/Al_2O_3, Al_2O_3/TiO_2 et $(Gd/Yb)_N$ telles que trois groupes géochimiques de komatiites archéennes peuvent être reconnus et définis: un Groupe I dans lequel les trois rapports précités présentent des valeurs proches des celles mesurées dans les chondrites; un Groupe II dans lequel les roches montrent des appauvrissements relatifs en Aluminium et en Terres Rares Lourdes; enfin, un Groupe III dans lequel les roches présentent, au contraire, des enrichissements relatifs en Aluminium et en Terres Rares Lourdes. En règle générale, les komatiites archéennes précoces (T≥3400 Ma) appartiennent aux Groupes II et III, celles provenant des terrains archéens tardifs (T≈2700 Ma) étant principalement du Groupe I. Les modélisations géochimiques montrent que les variations observées sont attribuables à des "pertes" (Groupe II) ou à des "gains" (Groupe III) de grenat. Les résultats isotopiques Lu-Hf obtenus sur des échantillons de komatiite du Groupe II de la ceinture de Barberton ($\varepsilon_{Hf}(T)\approx 0$) indiquent que le fractionnement de grenat se produisait lors des épisodes de fusion partielle mantélique (grenat au résidu solide). Couplé avec les données de la pétrologie expérimentale qui montrent que, dans le manteau, la phase au liquidus est le grenat majorite lorsque la pression est ≥15 GPa, ce résultat nous conduit à proposer un modèle reliant les variations géochimiques observées dans les komatiites archéennes à des différences dans la profondeur de fusion des diapirs mantéliques. En tout état de cause, ces variations ne sont pas la trace fossile d'une stratification chimique et minéralogique du manteau archéen, engendrée par un épisode "océan magmatique terrestre" qui se serait développé il y a 4400 Ma.

D'une manière générale, et sans remettre en cause les résultats précédemment énoncés, l'étude du comportement des systèmes isotopiques ainsi que des éléments majeurs et des éléments en trace lors des processus d'altération et/ou de métamorphisme affectant les roches basiques et ultrabasiques archéennes nous conduit à nous interroger sur la capacité réelle de ces systèmes à fournir des traceurs fiables de la composition chimique et isotopique du manteau archéen. En particulier, les résultats obtenus sur les coulées de komatiites de Finlande Orientale (régions de Tipasjärvi et de Siivikkovaara) montrent que la recristallisation métamorphique peut effacer l'ensemble des mémoires magmatiques initialement contenues dans les roches, y compris celles affèrent à des éléments ou des systèmes isotopiques réputés être réfractaires, comme les Terres Rares ou le système isotopique Sm-Nd. A Siivikkovaara, par exemple, nous montrons que la recristallisation métamorphique s'est accompagnée d'une ré-équilibration complète des systématiques Sm-Nd roche-totale: alors que les coulées se sont mises en place il y a 2700 Ma, l'âge isochrone Sm-Nd roche-totale calculé est de 1800 Ma, ce qui correspond à l'épisode métamorphique enregistré dans les minéraux métamorphiques présents dans les échantillons. Les résultats isotopiques de l'oxygène montrent que la recristallisation métamorphique s'opèrait dans des conditions de température de l'ordre de 450°C et que la phase fluide jouait un rôle important dans la mobilité des Terres Rares. Le fait que les ré-équilibrations isotopiques se soient produites 1Ga après la mise en place des coulées conduit à la production d'une gamme aberrante de valeurs $\varepsilon_{Nd}(T)$ (de -8 à +3), sans signification aucune quant à la nature des sources mantéliques impliquées. Le même type de comportement est observé dans les roches de la ceinture d'Isua au Groenland. Alors que certains auteurs ont voulu voir dans la gamme isotopique initiale définie par les roches de cette ceinture ($\varepsilon_{Nd}(3800)$ compris entre -1.0 et +3.5) la trace de composants crustaux d'âge >3800 Ma et/ou de domaines mantéliques très appauvris en Terres Rares Légères, nous montrons que les valeurs $\varepsilon_{Nd}(3800)$ calculées servant de base à ces interprétations ne sont pas des valeurs vraies, mais des valeurs apparentes résultant de fractionnements isotopiques secondaires survenant 1Ga après la mise en place des roches. En fait, des quatres régions étudiées, seules les komatiites de Schapenburg paraissent avoir préservé la quasi-intégralité de leurs mémoires magmatiques originelles.

Abstract

In this study, an attempt is made to constrain further the compositional heterogeneity and evolution of the Archaean mantle (T ranging from 2500 to 3800 Ma) using major, trace element (Rare Earth Elements) and isotopic (Nd, Hf, Sr, and O) compositions of ancient basic-ultrabasic rocks (komatiites, basalts and gabbros). We also investigate the behaviour of chemical elements and isotopic systems during alteration and metamorphism; the aim is to evaluate the effects of non-magmatic processes on the preservation of primary chemical and isotopic memories in old terrestrial rocks. The samples come from (1) West Greenland (Isua supracrustal belt; T≈3750 Ma); (2) South Africa (Barberton and Schapenburg geenstone belts; T≈3500 Ma); (3) Western Australia (Pilbara Craton; T≈3500 Ma); and (4) Eastern Finland (Khumo and Tipasjärvi greenstone belts; T≈2700 Ma).

An intriguing aspect of many komatiites in early Archaean grrenstone belts (T≥3400 Ma; e.g. komatiites from South Africa and Western Australia) is their Al- and HREE-depleted signature. In fact, many early Archaean komatiites have CaO/Al_2O_3 and $(Gd/Yb)_N$ higher, but Al_2O_3/TiO_2 lower than in chondrites, whereas most late Archaean komatiites (T≈2700 Ma; e.g. komatiites from Canada and Zimbabwe) have roughly chondritic ratios of these elements. A third less common type, also largely restricted to early Archaean komatiites, has relative enrichment of Al and HREEs. Geochemical modelling conducted during the course of this study show that these variations are best explained by the removal or addition of garnet. Lu-Hf isotopic results obtained on komatiite samples from the Barberton greenstone belt in South Africa ($\varepsilon_{Hf}(T)\approx 0$) indicates that the garnet fractionation processes took place during the melting events that led to the various groups of komatiites. This result, together with the recent finding that majorite garnet is the high-temperature mantle phase when P≥15GPa, provides a vehicle for discussing the origin of the various groups of komatiites. Most likely, the Archaean mantle had essentially chondritic ratios of CaO/Al_2O_3, Al_2O_3/TiO_2 and $(Gd/Yb)_N$, and the various groups of komatiites arise from differences in the depth of melting which controlled whether or not garnet was residual during the melting process. At any rate, the contrasted geochemical signatures of komatiites are not the consequence of a long-lived mineralogical and chemical stratification in the early Archaean mantle, such as might have formed during the solidification of a 4500-4400 Ma-old terrestrial magma ocean.

As a general rule, the study of the behaviour of chemical elements and isotopic systems during metamorphism of basic-ultrabasic rocks leads us to question the capacity of these rocks to preserve their primary (magmatic) signatures. Results from the komatiite flows from Eastern Finland (Tipasjärvi and Siivikkovaara areas) show that metamorphic recrystallization may erase all the primary chemical and isotopic memories, including the REE patterns and $\varepsilon_{Nd}(T)$ values. The open system type of behaviour is particularly well documented by the komatiite flows from Siivikkovaara; although the age of emplacement of the lava flows is 2700 Ma, whole-rock Sm-Nd data yield an age of 1800 Ma, which corresponds to the age of the metamorphic episodes recorded in the secondary mineral phases present in the samples. The fact that the Nd-isotopic re-equilibration occurred ≈1Ga after the emplacement of the flows cause strong shifts in the calculated $\varepsilon_{Nd}(T)$ values (-8 to +3) relative to the true magmatic values (≈+2.0?). A consideration of petrographic and Oxygen isotopic data indicates that temperature conditions were in the range 400-500°C and that the REE carrier was likely a CO_2-rich fluid. The same type of behaviour is observed in the rocks from the Isua supracrustal belt of West Greenland. Although some authors have interpreted the scatter in calculated $\varepsilon_{Nd}(T)$ values displayed by the rocks from this belt ($\varepsilon_{Nd}(3750)$ ranging from -1.0 to +3.5) as a true initial isotopic variation, new Sm-Nd results obtained during the course of this study provide firm evidence that the Sm-Nd system did not become a closed system in Isua rocks ca. 3750 Ma ago. A Sm-Nd mineral isochron age of 2849±116 Ma indicates that the earliest recognizable amphibolite facies metamorphism of the Isua belt is of mid-Archaean age. Very probably, all the rocks from Isua underwent some Nd isotopic reequilibration and/or fractionation of their $^{147}Sm/^{144}Nd$ ratios during the 2850 Ma-old metamorphic episode. Nevertheless, Nd-rich rocks (> 20 ppm) - such as the Amîtsoq grey gneisses and certain metasediments of the Isua belt - are relatively resistent to secondary fractionation due to the presence of REE-acceptor phases. In view of this behaviour, only $\varepsilon_{Nd}(T)$ values calculated from rocks having Nd contents greater than 20 ppm ($\varepsilon_{Nd}(T) \approx +2.0$) appear to be sufficiently reliable for use in characterizing the ε_{Nd} value of the Earth's mantle at 3800-3700 Ma. In fact, among the four investigated rock sequences, only the komatiites and komatiitic basalts from South Africa (Barberton and Schapenburg greenstone belts) appear to have preserved most of their primary isotopic and chemical memories.

INTRODUCTION

INTRODUCTION

Les études dédiées à la connaissance de la composition chimique et isotopique du manteau archéen (T>2500 Ma) peuvent apporter des contributions importantes dans plusieurs domaines clés des Sciences de la Terre, comme:

-a) les modalités de l'accrétion terrestre et de la formation du noyau

-b) l'histoire thermique précoce de notre Planète

-c) la composition chimique de la Terre Globale

-d) les éventuels effets chimiques et physiques du bombardement météoritique

Par ailleurs, étant entendu que les roches constitutives de la croûte continentale dérivent du manteau par fusion partielle, on peut s'attendre à ce que l'étude du manteau archéen débouche sur une meilleure compréhension des modalités de genèse et de recyclage de la croûte continentale primitive.

L'histoire précoce de la Terre peut avoir été compliquée par plusieurs processus, comme l'accrétion hétérogène, la formation du noyau, l'impact d'astéroïdes géants, ou la fusion partielle intensive de ses envelopes externes (e.g. Newsom and Jones, 1990). Chacun de ces processus peut avoir induit des hétérogénéités minéralogiques et chimiques considérables dans le manteau; certaines de ces hétérogénéités pouvant avoir perduré tout au long de l'histoire de la Terre, et donc influencer la composition du manteau actuel. A l'inverse, il est possible que le brassage convectif vigoureux qui devait exister dans le manteau de la Terre précoce empêchait la préservation des hétérogénéités ainsi créées et que, par conséquent, ces processus n'aient eu, en final, que peu d'influence sur la composition et la structure du manteau terrestre.

Le concept d'océan magmatique terrestre: théorie et modèles

L'un des processus les plus importants susceptibles d'avoir induit de profondes hétérogénéités chimiques et minéralogiques dans le manteau archéen (et peut-être dans le manteau actuel) est le processus d'océan magmatique. Le concept d'océan magmatique doit beaucoup aux études pétrologiques et géochimiques conduites sur les échantillons de roches lunaires (e.g. Hartmann et al., 1984). D'après les résultats de ces études, en effet, il est a peu près établi que les parties externes de la Lune - jusqu'à des profondeurs de l'ordre de, ou excèdant, 500 km - subissaient un épisode précoce de fusion, épisode qui conduisait à la formation d'un océan de magma tout autour de la planète (e.g. Taylor, 1979). La croûte anorthositique serait l'un des produits de cristallisation de cet océan de magma, les

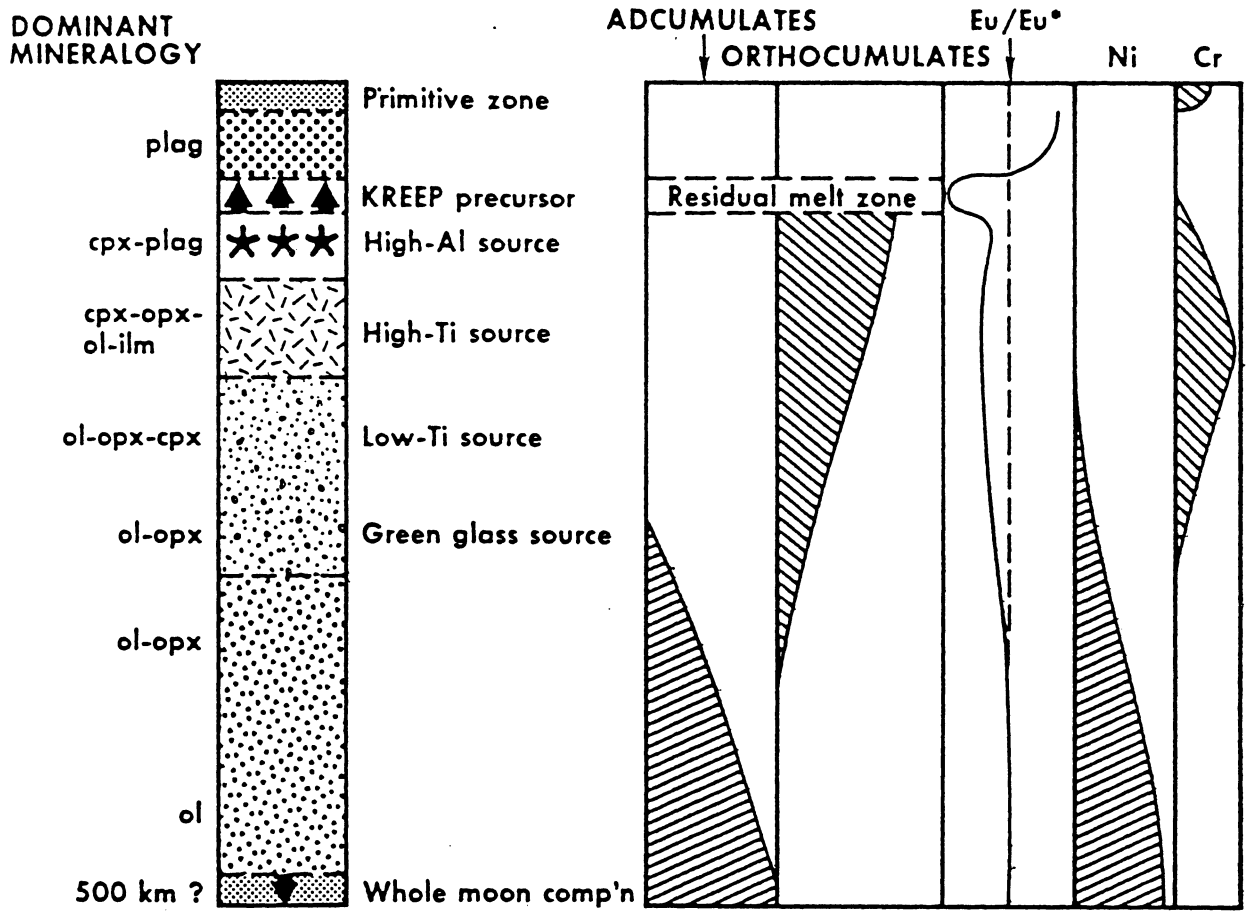

Figure 1: Schéma illustrant le litage minéralogique et chimique des parties externes de la Lune, engendré par la cristallisation d'un océan magmatique profond de 500 km. D'après Taylor (1979).

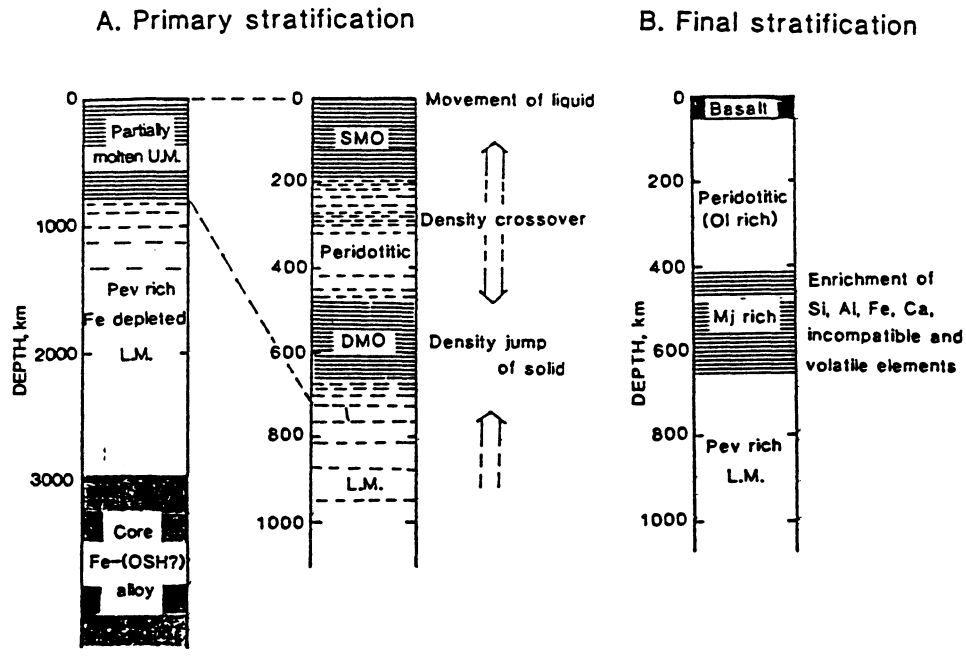

Fig. 4. The stratification of the Earth formed by differentiation during the course of accretion and subsequent solidification of the magma ocean. A. The primary stratification immediately after the accretion of the Earth, which is composed of an Fe-core, perovskite-rich lower mantle, and the partially molten upper mantle. The lower mantle contains some amount of Al_2O_3 and is depleted in FeO. The melt tends to accumulate in two regions (SMO—shallow magma ocean, and DMO—deep magma ocean) in the upper mantle. B. The final stratification of the mantle resulting from solidification of the magma ocean; this stratification is composed of a perovskite-rich lower mantle and a stratified upper mantle with a majorite-rich layer overlain by a peridotitic (olivine-rich) layer. The majorite-rich layer may be relatively enriched in incompatible and volatile elements together with Al_2O_3, FeO, and CaO.

Figure 2: Conséquences possibles d'un océan magmatique terrestre sur la structure et la minéralogie des parties externes de la Planète: modèle proposé par Othani (1988).

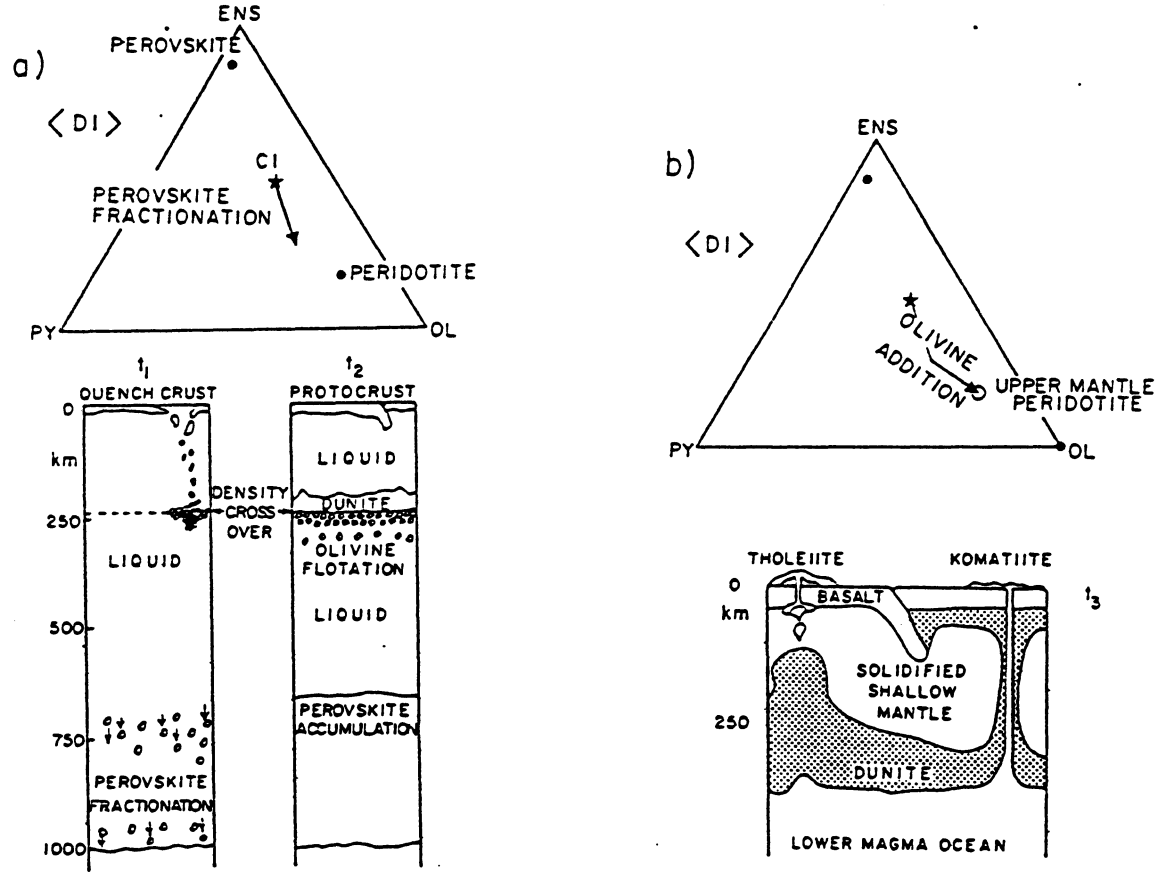

Fig. 4. (a) Cross-sectional sketches of the evolving magma ocean at times t_1 and t_2. The accompanying compositional diagram shows the change in the bulk magma ocean liquid brought about by perovskite fractionation (arrow). Dunite septum is established at the level of the olivine/liquid density crossover. At t_2 the upper and lower magma oceans are isolated by the neutrally buoyant dunite septum. (b) Cross sectional sketch at time t_3, after the Earth has cooled to the extent that the shallow upper mantle is mostly solidified. Lower magma ocean resides stably beneath a buoyant dunite septum, however, Rayleigh-Taylor instabilities develop between the septum and the denser freshly solidified shallow mantle above. Advective olivine addition (shown by the arrow in the compositional diagram) shifts the bulk shallow mantle composition towards peridotite.

Figure 3: Conséquences possibles d'un océan magmatique terrestre sur la structure et la minéralogie des parties externes de la Planète: modèle proposé par Agee and Walker (1988).

autres étant consitués d'une série de cumulats à olivine et/ou pyroxène, cumulats qui allaient devenir par la suite la source des divers types de Mare Basalts (voir Figure 1). D'après les résultats isotopiques, la cristallisation de l'océan magmatique lunaire aurait été éffective vers 4400 Ma (e.g. Hartmann et al., 1984).

Partant de l'idée que l'énergie mise en jeu pour produire l'océan magmatique lunaire devait trouver sa source soit dans l'énergie libérée lors de l'accrétion de la planète, soit dans celle induite par la formation d'un noyau, et étant entendu que les quantités d'énergie libérée par ces deux processus ont du être incomparablement plus élevées sur la Terre que sur la Lune, un certain nombre d'auteurs (e.g. Ringwood, 1975; Anderson, 1982; Nisbet and Walker, 1982; Othani, 1988; Agee and Walker, 1988) ont émis l'hypothèse que si un stade océan magmatique se produisait sur notre satellite, à fortiori, ceci devait être vrai pour la Terre. Par analogie avec le modèle lunaire (Fig. 1), il est possible qu'un épisode océan magmatique terrestre ait conduit à la formation d'une série d'envelopes concentriques, possèdant des compositions minéralogiques et chimiques différentes. Dans les Figures 2 et 3, nous présentons deux modèles parmi les plus récents traitant de la nature des différentes envelopes qui pourraient avoir été ainsi engendrées (Othani, 1988; Agee et Walker, 1988). Les deux modèles sont assez comparables en ce sens que, dans les deux cas, l'océan magmatique est supposé avoir été très profond ($P \geq 1000$ km) et avoir abouti, par cristallisation fractionnée, à la formation d'une envelope interne ($P \geq 700$ Km) constituée de cumulats à perovskite. Par contre, ils diffèrent sensiblement en ce sens que dans un cas (Fig. 2) les zones situées au dessus de la limite des 700 km comprendraient un niveau inférieur constitué de cumulats riches en grenat majorite ($P \geq 400$ Km) et un niveau supérieur constitué de cumulats riches en olivine ($P \leq 400$ Km), alors que dans l'autre cas (Fig. 3) il y aurait formation d'une envelope dunitique isolant une envelope externe (<200 Km) à olivine + pyroxene + grenat d'une envelope plus profonde (300 km <P<700 km), plus pauvre en olivine.

Les effets possibles de l'extraction et du recyclage crustal

Le deuxième grand phénomène pouvant avoir engendré des hétérogénéités chimiques et minéralogiques importantes dans le manteau archéen est le phénomène d'extraction et de recyclage crustal (le terme crustal englobant à la fois croûte océanique et croûte continentale). L'un des systèmes les plus efficace dont nous disposions pour tracer les effets éventuels de ce phénomène est le

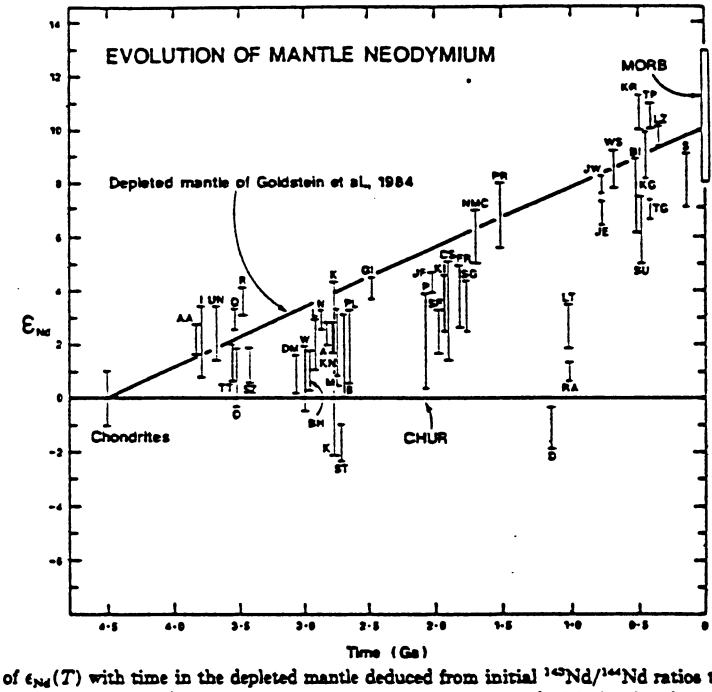

Fig. 2. Evolution of $\epsilon_{Nd}(T)$ with time in the depleted mantle deduced from initial $^{143}Nd/^{144}Nd$ ratios through time. The range shown at 4.55 Ga B.P. for chondrites is the maximum uncertainty associated with the chondritic uniform reservoir (CHUR) of Jacobsen and Wasserburg (1980). Plotted $\epsilon_{Nd}(T)$ are obtained as individual whole-rock samples of known age or from isochron regression initial ratios; uncertainties are quoted errors or ranges of published values. The depleted mantle evolution proposed by Goldstein et al. (1984, table 1 caption) is also shown. *Sources of data*: *A* = Alexo - Ontario, Canada (Dupré et al., 1984); *AA* = Akilia association - Greenland (Gruau et al., 1985b); *B* = Belingwe - Zimbabwe (Chauvel et al., 1986); *BH* = Big Horn Mts. - Wyoming, U.S.A. (Carlson and Diez de Medina, 1982); *BI* = Bay of Islands - Newfoundland, Canada (Jacobsen and Wasserburg, 1979a); *chondrites* (Jacobsen and Wasserburg, 1980); *CS* = Cape Smith - Quebec, Canada (Zindler, 1982); *D* = Duluth gabbro, - Minnesota, U.S.A. (DePaolo and Wasserburg, 1976); Diemals-Marda - Western Australia (Fletcher et al., 1984); *FR* = Front Range - Colorado, U.S.A. (DePaolo, 1981); *GI* = Georgetown Inlier - northern Australia (Black and McCulloch, 1984); *I* = Isua - West Greenland (Hamilton et al., 1978, 1983); *JE* = Jabal Eas - Saudi Arabia (Claesson et al., 1984); *JF* = Jouttiaapa Fm. - Finland (Huhma, 1984); *JW* = Jabal al Wask - Saudi Arabia (Claesson et al., 1984); *K* = Kambalda - Western Australia (McCulloch and Compston, 1981; Chauvel et al., 1985); *KG* = Kempersai gabbro - Urals, U.S.S.R. (Edwards and Wasserburg, 1985); *KI* = Kiruna greenstones - Sweden (Skiold and Cliff, 1984); *KN* = Kanowna - Western Australia (Fletcher et al., 1984); *KR* = Kings River - California, U.S.A. (Shaw et al., 1987); *L* = Lewisian gneisses - Scotland, U.K. (Hamilton et al., 1979a, 1983); *LT* = Llano - Texas, U.S.A. (DePaolo and Wasserburg, 1976); *LZ* = Lizard Complex - Cornwall, U.K. (G.R. Davies, 1984); *ML* = Mulcahy Lake - Ontario, Canada (Morrison et al., 1985); *MORB* = mid-ocean ridge basalts (cf. White, 1985); *N* = Newton lavas - Ontario, Canada (Cattell et al., 1984); *NMC* = New Mexico - Colorado, U.S.A. (Nelson and DePaolo, 1984); *O* = Onverwacht Group - South Africa (Hamilton et al., 1979b, 1983); *P* = Paramaco - French Guiana (Gruau et al., 1985a); *PL* = Preissac-Lacorne - Quebec, Canada (DePaolo and Wasserburg, 1976); *PR* = Pedlar River - Virginia, U.S.A. (Pettingill et al., 1984); *Q* = Qianan - China (Huang et al., 1986), data corrected to conform to CHUR; *R* = Rajasthan - India (Macdougall et al., 1983); *RA* = Roseland anorthosite - Virginia, U.S.A. (Pettingill et al., 1984); *S* = Semail - Gulf of Oman (McCulloch et al., 1981); *SF* = southern Finland (Patchett and Kuovo, 1986); *SG* = southern Greenland (Patchett and Bridgwater, 1984); *ST* = Stillwater Complex - Montana, U.S.A. (DePaolo and Wasserburg, 1979); *SU* = Southern Uplands - England, U.K. (Hooker et al., 1981); *SZ* = Swaziland (Carlson et al., 1983); *TG* = Trinity gabbro - California, U.S.A. (Jacobsen et al., 1984); *TP* = Trinity peridotite - California, U.S.A. (Jacobsen et al., 1984); *TT* = Talga-Talga - Western Australia (Hamilton et al., 1981, 1983); *UN* = Uivak-Nuniak - Labrador, Canada (Collerson and McCulloch, 1982); *W* = Warriedar - Western Australia (Fletcher et al., 1984); *WS* = Wadi Shwas - Saudi Arabia (Bokhari and Kramers, 1981).

Figure 4: Diagramme montrant la variation des valeurs $\varepsilon_{Nd}(T)$ dans les roches basiques et ultrabasiques terrestres. Nota: seules les roches susceptibles de dériver de régions sources mantéliques appauvries ont été reportées. D'après Galer et al. (1989)

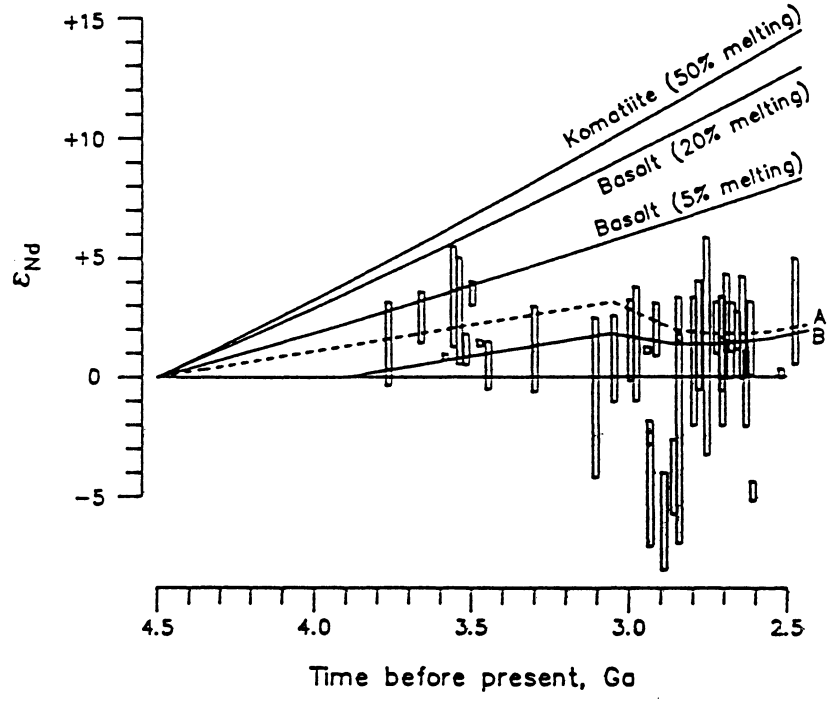

Fig. 3. Modelled ϵ_{Nd} changes in depleted mantle 4.5 to 2.5 Ga. Data ranges from Fig. 1 shown by open bars. Curves for mantle depleted by extraction of continental crust in amounts given by Fig. 2 are *A* (dashed, corresponds to dashed line, Fig. 2b): extraction starts at 4.5 Ga; *B* (lower solid line, corresponds to solid line, Fig. 2b): extraction starts at 3.9 Ga. The sudden decrease in ϵ_{Nd} at 3.0 Ga is caused by the rapid increase then of stable continental mass, which requires involvement of more undepleted mantle and thus dilutes the average isotopic composition of the depleted reservoir. The degree of partial melting of 0.015 chosen to represent the overall process (Table 1) results in a very limited volume of complementary depleted mantle. Depletion caused by 100% storage of tholeiitic oceanic crust formed by 5% or 20% partial melting or by komatiitic crust formed by 50% partial melting is shown by upper, labelled curves, all for oceanic crustal growth curve as given in Fig. 2a. Table 1 lists the distribution coefficients, degree of melting, and residual compositions for the five models shown.

Figure 5: Diagramme illustrant le modèle de Chase et Patchett (1988), modèle d'après lequel les valeurs $\varepsilon_{Nd}(T)$ très élevées (+3 à +4) trouvées dans certaines roches basiques archéeennes précoces ($T \geq 3.5$ Ga) seraient à relier à l'extraction précoce et au stockage d'une croûte océanique basique/ultrabasique enrichie en Nd.

système isotopique Samarium-Néodyme (Sm-Nd). En effet, le Nd étant plus incompatible que le Sm lors de la fusion mantélique, les roches crustales (océaniques et continentales) ont la propriété d'acquérir un rapport Sm/Nd inférieur à celui de leur source, le résidu solide (manteau appauvri) subissant, lui, par effet de bilan, une augmentation de ce même rapport. Comme par ailleurs le ^{147}Sm se désintègre en ^{143}Nd au cours du temps (λ=0.00654 Ga^{-1}), la différence de rapport père/fils ainsi engendrée conduira à l'émergence de différences au niveau du rapport $^{143}Nd/^{144}Nd$ ou des valeurs ε_{Nd} (la valeur ε_{Nd} représentant la déviation en partie pour 10^4 du rapport $^{143}Nd/^{144}Nd$ du système géologique considéré, par rapport à la valeur de ce rapport dans les chondrites - et/ou la Terre Globale - au même âge), différences qui seront d'autant plus marquées que le système aura eu une durée de vie longue.

Dans la Figure 4, nous présentons une compilation des valeurs $\varepsilon_{Nd}(T)$ calculées dans les roches basiques et ultrabasiques terrestres (Galer et al., 1989), T représentant l'âge de cristallisation magmatique présumé des roches. Dans ce diagramme, la droite joignant la composition initiale de la Terre et/ou des chondrites à la valeur ε_{Nd} de +10 mesurée dans les MORBs actuels est censée représenter la croissance isotopique du manteau appauvri (rapport Sm/Nd supérieur aux chondrites), manteau représentant le "résidu" laissé par l'extraction de la croûte continentale (rapport Sm/Nd inférieur aux chondrites). On note immédiatement la présence, à l'archéen précoce ($T \geq 3.5$ Ga), de valeurs $\varepsilon_{Nd}(T)$ très élevées (+3.0 à +4.0), situées significativement au dessus de la droite d'évolution du réservoir mantélique appauvri ainsi défini.

Dans un article publié en 1988, Chase et Patchett ont discuté la signification possible de ces valeurs $\varepsilon_{Nd}(T)$ très élevées (Fig. 5). Ces auteurs ont montrés que de telles valeurs ne pouvaient pas être contrebalancées par la quantité relativement réduite de croûte continentale qui se formait avant 3.5 Ga (courbes A et B dans la Figure). Ce faisant, ils ont proposé que le réservoir enrichi (rapport Sm/Nd inférieur aux chondrites), complémentaire des régions mantéliques sources de ces roches, était une croûte océanique enrichie formée très tôt dans l'histoire de la Terre, et qui aurait été stockée dans le manteau jusque vers 3.5-3.0 Ga.

Buts et Méthodes

Le seul moyen vraiment efficace dont nous disposions pour tenter de percer à jour la composition et la structure du manteau archéen (et en particulier répondre à la question de savoir si oui ou non le manteau terrestre subissait un stade océan magmatique avec les conséquences précitées) consiste à déterminer la composition

chimique des roches basiques et ultrabasiques archéennes. On peut en effet penser que si des hétérogénéités chimiques et minéralogiques existaient dans le manteau archéen, elles devaient engendrer des différences de compositions chimiques et isotopiques dans les magmas qui en dérivaient par fusion partielle. Qui plus est, en étudiant des roches basiques et ultrabasiques d'âge différent, c'est à dire en regardant l'évolution de leur composition au cours du temps, on devrait être capable de préciser la durée de vie des hétérogénéités ainsi crées, et en particulier de voir dans quelle mesure elles peuvent expliquer la structure et la composition du manteau actuel.

Ceci étant, il existe un certain nombre de facteurs limitant qui peuvent compliquer l'interprétation des résultats. Le facteur limitant de premier ordre est que, plus on recule dans le temps, plus les roches que nous allons être capable d'étudier auront des chances d'avoir été altérées ou métamorphisées, parfois plusieurs fois depuis leur mise en place. Tout dépendra alors de la façon dont les systèmes chimiques et isotopiques auront réagi au cours des transformations. Si les éléments et les systèmes isotopiques se sont comportés en système clos, alors les informations que l'on en tirera auront effectivement valeurs d'information quant à la composition des matériaux sources, et seront donc utilisables pour élaborer des modèles de manteau. Si, à l'inverse, les systèmes étaient ouverts lors des évènements d'altération ou de métamorphisme (par exemple des échanges chimiques et isotopiques se produisaient avec les fluides qui percolaient durant le métamorphisme), alors les mémoires initiales pourront avoir été effacées, et si le phénomène n'est pas reconnu, des interprétations erronées pourront s'ensuivre.

Dans ce travail, nous nous sommes principalement intéressés à la chimie des komatiites archéennes. Le choix des komatiites a été dicté par deux considérations. L'une est que ces roches se rencontrent en relativement grande abondance dans les terrains archéens, avec des âges compris entre 3.5 Ga et 2.7 Ga. Donc, en étudiant ces roches ont peut intégrer le facteur temps, facteur fondamental compte tenu des problèmes posés. La deuxième considération vient de ce que ces roches ayant des compositions ultrabasiques (MgO jusqu'à 30%), il n'y a pas d'ambigüité quant au fait qu'elles proviennent du manteau par fusion partielle.

Pour ce qui est du traçage des sources et du problème de l'océan magmatique, la démarche utilisée a été essentiellement une démarche géochimique et isotopique. Les objets d'études ont été principalement les komatiites d'âge ≈3500 Ma de Barberton, en Afrique du Sud, et du crâton de Pilbara, dans l'Ouest de L'Australie. Les systèmes principalement étudiés ont été les éléments majeurs, les REEs, les isotopes du Nd et dans le cas des komatiites de Barberton les isotopes du Hf. Nous avons également fait appel à des données de la littérature.

Pour ce qui des aspects liés à la mobilité des systèmes isotopiques et des éléments majeurs/traces lors de l'altération et/ou du métamorphisme, la démarche a été de coupler les études isotopiques et géochimiques (Sm-Nd, Rb-Sr, REE, éléments majeurs) sur échantillons roche-totales et sur minéraux séparés. En particulier, nous nous sommes éfforcé, chaque fois que cela nous a été possible, de déterminer l'âge des évènements métamorphiques affectant les roches cibles étudiées (Sm-Nd sur minéraux; Ar-Ar), étant entendu que, comme nous le montrons, l'âge de la dernière recristallisation métamorphique est un paramètre fondamental qu'il faut connaître si l'on veut être capable d'interprêter correctement les données isotopiques roche-totale. De même, des études utilisant les isotopes stables ont été entreprises, dans le but de déterminer les températures de recristallisation ainsi que d'estimer les rapports eau/roche et/ou la nature et l'origine des fluides. Pour ce qui concerne ce deuxième axe de notre recherche, les objets d'eétude sont des coulées de komatiite provenant des ceintures de roches vertes de Finlande Orientale (T=2700 Ma) et de Schapenburg (T=3450 Ma), en Afrique du Sud. Nous avons également effectué une étude sur des amphibolites de la ceinture supracrustale d'Isua (T=3800 Ma).

Organisation du mémoire

Dans un soucis de gain de temps et d'éfficacité, j'ai choisi d'organiser ce mémoire autour d'une série d'articles publiés, ou en voie de l'être. Ce procédé a le défaut de produire un mémoire manquant parfois d'homogénéité, et présentant un certain nombre de répétitions. De plus, il n'est pas toujours facile de regrouper des articles traitant d'aspects aussi divers que la mobilité des éléments lors des processus métamorphiques, le problème de l'océan magmatique terrestre et de ces effets éventuels sur la composition du manteau archéen, où encore de la signification des isochrones Sm-Nd roche-totale. Ceci étant, il m'est apparu que je pouvais présenter logiquement mes travaux en insistant tout d'abord sur la contribution "positive" qu'ils apportent à la connaissance de la composition et de l'évolution du manteau archéen terrestre ("les apports"), puis, dans un deuxième temps, sur les limites qu'ils révèlent quant à l'utilisation des traceurs géochimiques et isotopiques dans les roches anciennes à des fins pétrogénétiques.

Dans une première partie, j'ai donc rassemblé quatre articles tournant, à des degrés divers, autour de la question de la signification de la variation des rapports CaO/Al_2O_3, Al_2O_3/TiO_2, $(Gd/Yb)_N$ dans les komatiites archéennes. Le lecteur decouvrira dans ces articles (1) la banque de données établissant la variation de ces rapports; (2) les questions que cela pose en ce qui concerne la genèse des

komatiites et la composition du manteau archéen, et, la présentation détaillée des deux grandes théories qui ont vu le jour pour expliquer pourquoi ces trois rapports varient ("théorie du manteau lité et/ou de l'océan magmatique terrestre" contre "théorie de la différence de profondeur de fusion partielle"); (3) les résultats d'un test que nous avons effectué en utilisant le système isotopique Lu-Hf, test qui, nous le croyons, met un terme au débat.

Dans la deuxième partie, le lecteur trouvera quatre autres articles, traitant cette fois-ci de l'aspect "limite", c'est à dire de la capacité qu'a la recristallisation métamorphique à effacer les mémoires magmatiques primaires des roches, et donc de "brouiller" l'image que l'on peut en déduire de l'hétérogénéité compositionnelle du manteau archéen.

Références

Agee C.R. and D. Walker (1988) Mass balance and phase density constraints on early dfferentiation of chondritic mantle. *Earth Planet Sci Lett.* **90**, 144-156.

Anderson D.L. (1982) Isotopic evolution of the mantle: a model. *Earth Planet. Sci. Lett.* **57**, 13-24.

Chase C.G. and Patchett P.J. (1988) Stored mafic/ultramafic crust and early Archean mantle depletion. *Earth Planet. Sci. Lett.* **91**, 66-72.

Galer S.J.G., Godstein S.L. and R.K. O'Nions (1989) Limits on chemical and convective isolation in the Earth's interior. *Chem. Geol.* **75**, 257-290.

Hartmann W.K., Phillips R.J. and Taylor G.J. *Origin of the Moon.* Lunar and Planetary Institute, Houston, 781p.

Newsom E. and Jones J.H. (1990) *Origin of the Earth* . Oxford University Press, New York, 375 p.

Nisbet E.G. and Walker D. (1982) Komatiites and the structure of the Archaean mantle. *Earth Planett. Sci. Lett.* **60**, 105-113.

Othani E.J. (1988) Chemical stratification of the mantle formed by melting in the early stage of the terrestrial evolution. *Tectonophys.* **154**, 201-210.

Ringwood A.E. (1975) *Composition and Petrology of the Earth's Mantle*. McGraw-Hill, New York 618 p.

Taylor S.R. (1979) Structure and evolution of the Moon. *Nature* **281**, 105-109.

PREMIERE PARTIE

Essai sur la signification de la variation des rapports CaO/Al_2O_3, Al_2O_3/TiO_2 et $(Gd/Yb)_N$ observée dans les komatiites archéennes

Contrib Mineral Petrol (1982) 80:25–40

Contributions to Mineralogy and Petrology

Komatiites of the Onverwacht Group, S. Africa: REE Geochemistry, Sm/Nd Age and Mantle Evolution

Bor-ming Jahn[1], G. Gruau[1], and A.Y. Glikson[2]

[1] C.A.E.S.S., Université de Rennes, Institut de Géologie, 35042 Rennes, France
[2] Bureau of Mineral Resources, Geology and Geophysics, Canberra, A.C.T., Australia

Abstract. Komatiites of the Tjakastad Subgroup of the Onverwacht Group (S. Africa) were dated by the Sm/Nd method. A whole-rock isochron yields an age of 3.56 ± 0.24 (2σ) AE, with initial $^{143}Nd/^{144}Nd$ ratio of 0.50818 ± 23 (2σ), corresponding to $\varepsilon_{Nd}(T) = +1.9 \pm 4.5$. This age is interpreted as the time of initial Onverwacht volcanism. This result agrees with earlier Sm/Nd data of Hamilton et al. (1979) and is consistent with the Rb–Sr result of Jahn and Shih (1974).

Komatiites may be divided into 3 groups based on the typology of heavy REE distributions (Jahn and Gruau 1981). According to this scheme, the Onverwacht komatiites of the present study belong to two groups: the predominant Group II rocks showing $(Gd/Yb)_N \simeq 1.4$, $CaO/Al_2O_3 = 1.33$, $Al_2O_3/TiO_2 \simeq 10.6$; and the subordinate Group III rocks with $(Gd/Yb)_N < 1.0$; $CaO/Al_2O_3 \simeq 0.6$ and $Al_2O_3/TiO_2 \simeq 40$. This contrasting feature is best explained by garnet fractionation within the mantle sources.

Younger komatiites (~2.7 AE) from Finland, Canada, Rhodesia, and Australia have $(Gd/Yb)_N \simeq 1.0$, $CaO/Al_2O_3 < 1.1$ and $Al_2O_3/TiO_2 \simeq 21$ based on 58 analyses. These ratios are nearly chondritic or of the bulk earth value (Anders 1977). It appears that some late Archean komatiites are different in chemistry from many early Archean komatiites. This may imply that the upper mantle chemistry has evolved through Archean times. However, the age connotation of the chemical parameters, such as CaO/Al_2O_3, $(Gd/Yb)_N$ or Al_2O_3/TiO_2 ratio has not been firmly established. The characteristic "high" CaO/Al_2O_3 or $(Gd/Yb)_N$ ratios in many Onverwacht Group rocks can also be explained as a result of local short-term mantle heterogeneity.

Introduction

Komatiites, particularly the peridotitic variety (MgO > 18%), are generally believed to be produced by large degrees of partial melting of upper mantle materials (e.g. Viljoen and Viljoen 1969a, b; Green 1975; Green et al. 1975; Sun and Nesbitt 1978; Nesbitt et al. 1979; Jahn et al. 1980a; among others). Komatiites occur mainly in the Archean and very rarely in post-Archean times. This remarkable skewed time distribution could be related to the different thermal regimes in the Archean and post-Archean times (see Nesbitt et al. 1982, for a brief review).

Reprint requests to: G. Gruau

Since komatiitic rocks, like other volcanic components of greenstone belts, are invariably metamorphosed, their recognition is usually based upon both spinifex textures and chemical composition. In their original definition of komatiites from the Onverwacht Group, Viljoen and Viljoen (1969a) emphasized the high CaO/Al_2O_3 (>1.5) ratio, but subsequent studies of komatiites from Canada, Australia, Rhodesia and Finland have indicated that this is not universally the case and CaO/Al_2O_3 ratios are more commonly about 1.0 (Arndt et al. 1977; Nisbett et al. 1977; Sun and Nesbitt 1978; Nesbitt et al. 1979, 1982; Blais et al. 1978; Jahn et al. 1980a, b). Assuming a "normal" phase assemblage in the Archean mantle, the likely residual phases would be olivine (±orthopyroxene) after large degrees of melting. Because these two phases contain insignificant amounts of Ca and Al, the CaO/Al_2O_3 ratio of the derived liquids (komatiites) should reflect that of their mantle sources, provided post-magmatic alteration, if any, has not modified this ratio.

Why are then the CaO/Al_2O_3 ratios of the Onverwacht komatiites significantly greater than 1.0, the value commonly thought to represent chondritic or pyrolitic mantle sources? Are they indeed abnormal in comparison with other komatiites? Could this difference be related to the effect of alteration-metamorphism, fractional crystallization of komatiitic magmas, or a fundamental difference in mantle chemistry, i.e. chemical evolution or heterogeneity of Archean mantle sources. These questions are addressed in this paper.

Based on a few analyses of Onverwacht Group komatiites, Sun and Nesbitt (1978) and Nesbitt et al. (1979) have suggested a plausible age connotation with the chemical differences between early and late Archean komatiites, and emphasized the role of garnet in the fractionation of CaO/Al_2O_3 and Gd/Yb ratios. However, the small body of REE data available on Archean komatiites may lead to accidental conclusions. In view of the important consequences regarding the chemical evolution of the upper mantle, we have performed geochemical and isotopic analyses on 15 samples from the lower three formations of the Onverwacht Group (Tjakastad Subgroup) of the Barberton Mountain Land and 3 samples from the Sagur Supergroup of India. The principal aims are:

1) to determine the age of the Onverwacht rocks by the Sm/Nd method,

2) to employ the high quality REE data and major and other trace element data to discuss the problem of the CaO/Al_2O_3 variation as outlined above,

0010-7999/82/0080/0025/$03.20

3) to present possible petrogenetic models for the Overwacht komatiites

4) to discuss the possible age connotation of the komatiite chemistry and implications for the mantle evolution or heterogeneity.

Samples and Analytical Procedures

A total of 27 samples collected by A.Y. Glikson from the lower three Formations of the Onverwacht Group (Sandspruit, Theespruit and Komati formations) and additional three samples from the Holenarsipur and the Sagur greenstone belts of India were chosen for major and trace element analyses. Among them, 18 were determined for their REE concentrations by the isotopic dilution method. These samples include komatiites[1] and tholeiitic basalts.

Accounts of the general geology of the Barberton Mountain Land were given by Viljoen and Viljoen (1969c,

1 At a Penrose Conference in 1979 (see Arndt and Brooks, 1980) it was suggested that Komatiite should be defined as the volcanic equivalent of a periodotite (of non-cumulate origin), and should have MgO > 18% (anhydrous). Arndt (1981) has further suggested that if mafic rocks can be demontratably linked with the komatiites, they should be termed the komatiitic association. In fact, this usage has been proposed and used by our group (Blais et al. 1978; Jahn et al. 1980a), but the term "komatiitic series" was used instead. Here, peridotitic komatiite is used for rocks with MgO > 18%, and basaltic komatiites, MgO ≃ 10% to 18%

Table 1. Major element data for Onverwacht Group volcanic rocks (analyses-BMR Laboratories)

Formation	Sandspruit								Theespruit					
Sample No.	5038	5042	5046	5048	5049	5050	5052	5053	5001	5003	5010	5012	5016	5019
Rock type	T	BK	BK	PK	BK	BK	BK	T	BK	BK	T	BK	T	PK
SiO_2 (%)	51.08	50.12	48.48	45.72	47.20	46.48	46.32	50.63	54.31	54.29	52.60	54.32	53.29	42.60
TiO_2	1.66	1.21	1.30	0.91	1.19	1.15	1.43	1.19	0.71	0.78	0.61	0.76	0.79	0.27
Al_2O_3	12.96	9.91	10.03	7.74	9.72	8.66	10.94	11.62	8.88	7.96	13.81	9.08	14.03	2.87
Fe_2O_3 (ΣFe)	15.03	13.46	14.52	15.44	15.28	15.39	14.62	13.33	11.43	12.59	12.15	12.50	13.65	15.12
MnO	0.26	0.18	0.23	0.23	0.29	0.30	0.34	0.26	0.18	0.201	0.17	0.19	0.23	0.36
MgO	4.22	10.95	10.79	19.43	11.70	12.88	10.94	7.52	9.01	10.60	6.32	8.74	5.76	34.18
CaO	9.36	11.80	12.08	8.04	12.59	11.95	12.96	12.38	11.27	9.72	9.17	12.81	8.04	2.29
Na_2O	4.21	1.24	1.54	0.61	1.07	1.08	0.97	2.20	1.82	2.35	2.72	0.39	3.10	0.02
K_2O	0.15	0.26	0.22	–	0.24	0.20	0.32	0.10	0.19	0.08	0.17	0.11	0.20	0.02
P_2O_5	0.20	0.16	0.14	0.12	0.13	0.15	0.13	0.15	0.08	0.10	0.07	0.13	0.15	0.05
H_2O^+	0.29	0.80	0.59	3.46	0.54	1.00	0.82	0.47	1.88	1.34	2.51	1.35	1.22	1.78
Total	99.42	100.09	99.92	100.61	99.95	99.24	99.79	99.85	99.77	100.01	100.30	100.38	100.42	99.43
CaO/Al_2O_3	0.72	1.19	1.20	1.04	1.30	1.38	1.19	1.07	1.27	1.22	0.66	1.41	0.57	0.80
Al_2O_3/TiO_2	7.80	8.19	7.71	8.50	8.17	7.53	7.65	9.76	12.50	10.21	22.64	11.95	17.76	10.63

Formation	Theespruit					Komati								
Sample No.	5025	5026	5031	5067	SA39	5077	5080	5084	5085	5088	5092	5095	AB9	AB9
Rock type	T	BK	PK	BK	PK	BK	BK	BK	BK	T	BK	T	BK	BK
SiO_2 (%)	48.69	52.75	44.28	55.57	38.26	52.72	54.80	52.59	55.03	52.86	50.86	50.92	53.05	52.42
TiO_2	1.51	0.37	0.31	0.32	0.24	0.64	0.82	0.65	0.49	0.40	0.30	0.69	0.66	0.72
Al_2O_3	11.02	13.19	3.31	12.15	2.72	7.37	9.94	6.96	7.14	16.04	2.83	14.38	8.49	8.64
Fe_2O_3 (ΣFe)	18.90	9.68	15.03	7.95	12.40	12.15	10.05	11.10	9.98	8.19	9.35	11.07	12.62	12.00
MnO	0.36	0.16	0.18	0.13	0.21	0.17	0.17	0.17	0.14	0.11	0.16	0.17	0.21	0.23
MgO	5.59	10.62	31.34	9.79	32.86	11.34	9.39	13.12	13.65	6.48	11.19	7.31	11.52	11.42
CaO	10.54	9.54	3.30	7.27	1.74	10.56	9.40	10.83	8.24	9.02	8.38	11.29	10.49	10.63
Na_2O	1.75	1.59	0.09	1.97	0.00	2.97	3.08	1.61	1.55	2.29	1.76	1.67	2.87	2.88
K_2O	0.44	0.49	0.05	1.62	0.00	0.05	0.17	0.11	0.22	1.67	1.71	0.20	0.05	0.06
P_2O_5	0.14	0.11	0.07	0.08	0.05	0.08	0.11	0.08	0.06	0.11	0.04	–	0.06	0.07
H_2O^+	0.92	3.07	2.38	2.16	10.26	1.21	1.66	2.05	2.75	2.64	2.97	2.74	1.09	1.69
Total	99.86	101.57	100.34	99.01	98.74	99.26	99.62	99.27	99.25	99.81	99.55	100.44	101.11	100.76
CaO/Al_2O_3	0.96	0.81	1.00	0.60	0.64	1.43	0.95	1.56	1.15	0.56	0.65	0.79	1.24	1.23
Al_2O_3/TiO_2	7.30	35.64	11.03	37.97	11.33	11.52	12.12	10.71	14.57	40.10	42.77	20.84	12.86[a]	12.00[b]

[a] Sun and Nesbitt (1978)

[b] Viljoen and Viljoen (1969c)

2% other REE. The concentrations of Sm and Nd on samples subject to Nd isotopic analysis were better determined at 1% uncertainty.

The procedures of Nd isotopic analysis were essentially similar to those reported in Jahn et al. (1980c), with a slight modification in chemical separation. All isotopic ratios were normalized using $^{146}Nd/^{144}Nd = 0.7219$. The Nd isotopic compositions ($^{143}Nd/^{144}Nd$) of Johnson-Matthey standard salt (Nd_2O_3) give 0.511136 ± 16 (2 σm) on 18 separate runs and of BCR-1, 0.512650 ± 40 (2 σm) on 6 runs. The decay constant for $\lambda\,^{147}Sm$ used is 6.54×10^{-12} year^{-1}. The Sm–Nd isochron age was calculated using the method of York (1966).

Results

Results of major and trace element analyses are given in Tables 1 and 2. Sm–Nd and Rb–Sr isotopic data for selected samples are presented in Tables 3 and 4. The geochronological results are discussed first, followed by a discussion of the REE distribution patterns.

Sm–Nd Geochronology

Previous studies of stratigraphic relationship between the Barberton greenstone sequence and the associated granitic gneisses using the Rb–Sr method have only achieved partial success, mainly due to the problems of alteration and metamorphic effects on the Rb/Sr isotopic systems (Allsopp et al. 1968; Hurley et al. 1972; Jahn and Shih 1974). An age of about 3.5 AE was determined by the Rb–Sr mineral (density fractions) isochron method on a basaltic komatiite (AB9) from the komati Formation (Jahn and Shih 1974). The age of 3.43 ± 0.20 AE (recalculated using $\lambda\,^{87}Rb = 1.42 \times 10^{-11}$ yr^{-1}) was interpreted as the time of the low grade metamorphism. However, since in many Archean greenstone-granite terrains, volcanism, sedimentary deposition, subsequent metamorphism and granitic intrusions are commonly found to have taken place over relatively short time intervals (Jahn and Murthy 1975; Moorbath 1977; Hart et al. 1969; Vidal et al. 1980), this age was also considered close to the time of the Onverwacht volcanism (Jahn and Shih 1974). This interpretation is supported by the new data reported here and the recently published Sm–Nd results (Hamilton et al. 1979). However, it must be borne in mind that individual greenstone sequences may be separated by long intervals, as, for example, are the Sebakwian (ca. 3.6 AE) and Bulawayan (ca. 2.7 AE) greenstones in Rhodesia (Wilson et al. 1978).

The results of Sm–Nd isotopic analyses are displayed in Fig. 1. The isochron yields an age $T = 3.56 \pm 0.23$ (2σ) AE and $I_{Nd} = 0.50818 \pm 23$ (2σ), which corresponds to $\varepsilon_{Nd}(T) = +1.9 \pm 4.5$. Hamilton et al. (1979) have reported a Sm–Nd isochron age of $T = 3.54 \pm 0.03$ AE with corresponding $I_{Nd} = 0.50809 \pm 4$ for the Onverwacht lavas, mainly from the Komati Formation. Excluding the acid tuff and sodic porphyry data, they obtained $T = 3.51 \pm 0.06$ AE and $I_{Nd} = 0.50813 \pm 7$. Our results are in agreement with theirs, though the uncertainties in both T and I values are greater.

Table 3. Sm–Nd isotopic data for Onverwacht Group volcanic rocks

Sample No.	Rock type	Formation	Sm (ppm.)	Nd (ppm.)	$^{147}Sm/^{144}Nd$[a]	$^{143}Nd/^{144}Nd \pm 2\,\sigma$m
5038	Tholeiitic basalt	Sandspruit	5.645	24.69	0.1392	0.511437 ± 50
5049	Basaltic komatiite	Sandspruit	2.994	9.42	0.1935	0.512805 ± 53
5067	Basaltic komatiite	Theespruit	2.317	12.31	0.1146	0.510891 ± 45
5092	Basaltic komatiite	Komati	1.242	5.79	0.1307	0.511260 ± 35
AB9	Basaltic komatiite	Komati	1.862	6.36	0.1783	0.512315 ± 36

[a] Error in this ratio is $\pm 1/2\%$

[b] Isochron slope $= 0.0253 \pm 0.00156$ (2σ); intercept $= 0.50818 \pm 0.00023$ (2σ); age $= 3{,}557 \pm 235$ (2σ) m.y; $\varepsilon(T) = +1.87 \pm 4.50$

Table 4. Rb–Sr isotopic data for Onverwacht Group volcanic rocks

Sample No.	Rock type	Formation	Rb (ppm)	Sr (ppm)	$^{87}Rb/^{86}Sr$	$^{87}Sr/^{86}Sr$	$\pm 2\,\sigma$m
5067	BK	Theespruit	50.07	122.5	1.186	0.74467	12
5085	BK	Komati	1.43	24.28	0.172	0.70844	15
5088	T	Komati	51.2	240.3	0.619	0.73636	6
5092	BK	Komati	70.53	202.8	1.006	0.73461	10
5095	T	Komati	5.74	206.1	0.080	0.70577	7
A-27[a]	PK	Komati	0.577	49.12	0.034	0.70623	5
BK-2[a]	BK	Komati	0.450	38.37	0.034	0.70214	3
BK-3[a]	BK	Komati	5.41	67.55	0.232	0.70628	4
BK-4[a]	BK	Komati	0.929	32.25	0.083	0.70544	5
DN-3[a]	Gabbro	Komati	0.685	25.16	0.079	0.70663	7

[a] Major and trace element (including REE) data for five samples (A-27 through DN-3) have been published by Herrmann et al. (1976). Isotopic analyses for these samples were made at the NASA-Johnson Space Center in 1975. Analytical procedures have been described in Jahn and Shih (1974)

1970), Anhaeusser (1973, 1978), Anhaeusser et al. (1969) and Hunter (1974). A brief summary of age relationship between the layered successions and surrounding granitic batholiths was given by Jahn and Shih (1974). Sampling localities, assessment of alteration effects on primary chemistry, as well as metamorphic mineralogy are all presented in Appendix 1.

Major and trace elements, except for REE, were determined in the Metalliferous Laboratories of the Australian Bureau of Mineral Resources (BMR) using a Philips PW-1210 automated XRF spectrometer and atomic absorption spectrometer. Procedures, precision and accuracy controls were given by Glikson and Hickman (1981). Rare earth elements (REE) were determined by the isotopic dilution method at Université de Rennes. A brief account was given by Jahn et al. (1980a). The overall uncertainty, including errors derived from sample preparation, chemical procedure, mass analysis, etc., is 3% for La, Gd and Lu and

Table 2. Trace element data for Onverwacht Group volcanic rocks

Formation	Sandspruit								Theespruit					
Sample No.	5038	5042	5046	5048	5049	5050	5052	5053	5001	5003	5010	5012	5016	5019
Rock type	T	BK	BK	PK	BK	BK	BK	T	BK	BK	T	BK	T	PK
La (ppm.)	18.25	–	6.74	–	4.636	–	3.541	9.323	–	–	–	–	–	1.938
Ce	43.409	–	16.904	–	12.632	–	11.07	20.38	–	–	–	–	–	–
Nd	24.75	–	11.312	–	9.416	–	8.966	12.524	–	–	–	–	–	2.498
Sm	5.645	–	3.98	–	2.987	–	2.978	3.442	–	–	–	–	–	0.658
Eu	1.526	–	1.189	–	1.251	–	1.02	1.119	–	–	–	–	–	0.245
Gd	5.661	–	4.168	–	3.810	–	3.90	3.892	–	–	–	–	–	0.832
Dy	5.79	–	4.485	–	4.157	–	5.216	4.020	–	–	–	–	–	0.888
Er	3.32	–	2.499	–	2.11	–	2.40	2.284	–	–	–	–	–	0.548
Yb	3.29	–	2.229	–	2.065	–	2.11	2.065	–	–	–	–	–	0.465
Lu	0.509	–	0.338	–	–	–	0.325	0.305	–	–	–	–	–	0.080
$(Gd/Yb)_N$	1.38	–	1.50	–	1.48	–	1.48	1.51	–	–	–	–	–	1.43
Rb	3	9	–	2	3	3	3	3	3	3	3	–	4	–
Sr	254	166	158	30	78	52	164	138	144	100	100	166	197	–
Zr	144	76	77	57	78	67	80	90	38	36	36	47	45	15
Nb	19	7	4	4	5	4	4	6	2	2	2	3	3	–
Y	29	20	19	16	25	15	17	20	12	14	14	14	12	–
V	134	213	273	241	337	278	266	301	221	224	228	237	203	91
Cr	303	1,005	1,400	2,251	2,477	1,750	1,900	619	639	744	29	595	8	5,200
Co	71	104	113	90	87	136	110	57	88	103	86	89	94	224
Ni	65	439	479	822	784	751	508	156	132	197	93	149	52	1,640

Formation	Theespruit					Komati							
Sample No.	5025	5026	5031	5067	SA39	5077	5080	5084	5085	5088	5092	5095	AB9
Rock type	T	BK	PK	PK	BK	PK	BK	BK	BK	T	BK	T	BK
La (ppm.)	–	–	3.38	16.06	0.731	3.78	5.503	2.872	–	16.497	6.095	–	3.272
Ce	–	–	–	31.18	–	10.470	14.09	7.784	–	35.87	13.78	–	8.893
Nd	–	–	3.569	12.329	1.733	7.465	7.866	5.972	–	13.38	5.791	–	6.399
Sm	–	–	0.949	2.317	0.497	2.122	2.255	1.857	–	2.555	1.241	–	1.862
Eu	–	–	0.358	0.573	0.162	0.712	0.712	0.644	–	0.716	0.413	–	0.647
Gd	–	–	1.21	2.18	0.626	2.732	2.825	2.351	–	2.435	1.461	–	2.274
Dy	–	–	1.078	2.494	0.695	2.843	3.083	2.709	–	2.901	1.987	–	2.654
Er	–	–	0.599	1.678	0.407	1.710	1.767	1.557	–	1.759	1.559	–	1.650
Yb	–	–	0.568	1.742	0.368	1.652	1.614	1.450	–	1.799	1.700	–	1.528
Lu	–	–	0.084	0.287		0.263	0.251	0.207	–	0.296	0.284	–	0.237
$(Gd/Yb)_N$	–	–	1.70	1.00	1.36	1.32	1.40	1.30	–	1.08	0.69	–	1.19
Rb	6	17	–	50.07	0.26	–	–	–	1.43	51.12	70.53	5.74	–
Sr	119	131	9	122.5	1.17	26	22	14	24.3	240.31	202.8	206.14	–
Zr	58	29	17	42	10.9	41	56	37	23	49	53	32	–
Nb	8	3	–	6	0.1	5	2	3	2	5	34	–	–
Y	12	11	4	12	3.3	12	13	11	8	13	12	13	–
V	288	116	102	110	81	179	188	182	212	97	130	227	–
Cr	689	1,070	5,020	1,140	2,647	982	576	1,340	1,220	441	1,350	188	–
Co	110	92	216	80	123	99	84	101	99	70	90	86	–
Ni	274	339	1,450	326	2,285	156	128	273	273	246	411	156	–

30

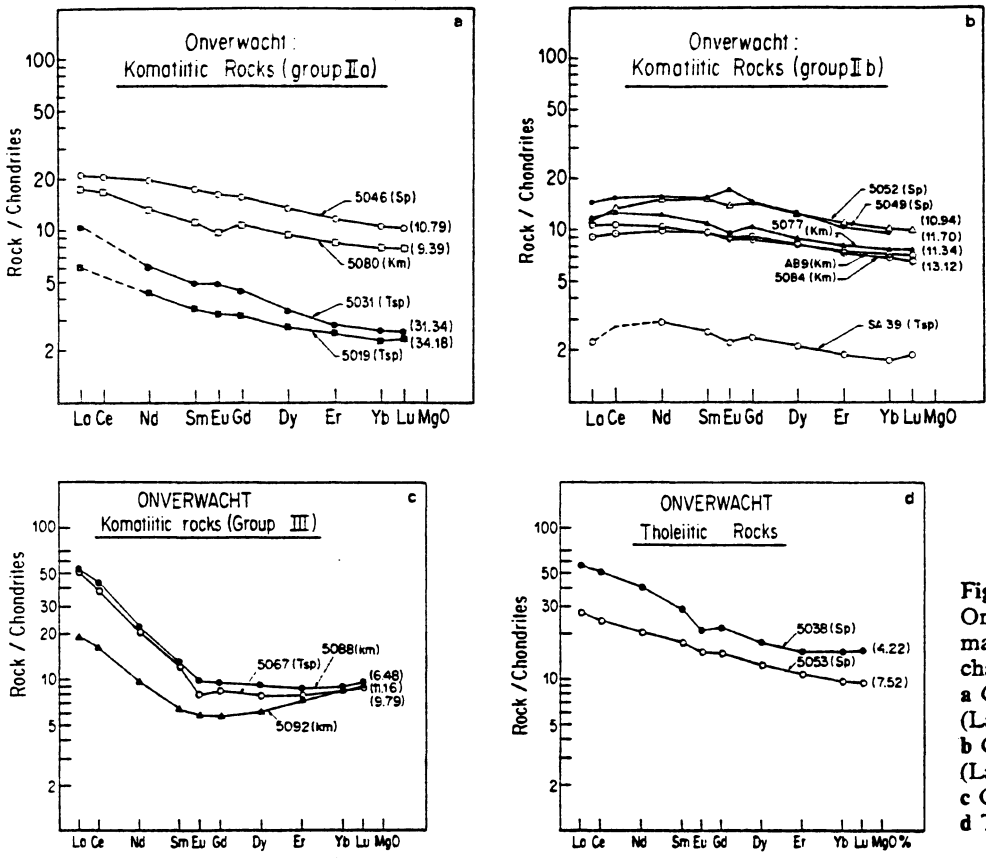

Fig. 4a–d. REE distribution patterns for Onverwacht komatiites. The grouping is made according to their HREE characteristics, i.e., Gd/Yb ratios.
a Group IIa komatiites: $(Gd/Yb)_N > 1.0$; $(La/Sm)_N > 1.0$.
b Group IIb komatiites: $(Gd/Yb)_N > 1.0$; $(La/Sm)_N < 1.0$.
c Group III komatiites: $(Gd/Yb)_N < 1.0$.
d Tholeiitic rocks

two series (Arndt et al. 1977; Blais et al. 1978; Jahn et al. 1980a).

The present results of Onverwacht rocks are plotted in Fig. 3. Most rocks are found well within the defined fields except for sample 5088, which is a tholeiite possessing special geochemical characteristics. It will be further discussed in conjunction with trace element data.

REE Distribution Patterns

In a REE typological study of komatiites, Jahn and Gruau (1981) recently proposed that all komatiites could be subdivided into 3 major groups based on their HREE distributions as follows:

Group I: HREE flat, $(Gd/Yb)_N \simeq 1.0$
Class 1: LREE flat, $(La/Sm)_N \simeq 1.0$
Class 2: LREE depleted, $(La/Sm)_N < 1.0$
Class 3: LREE enriched, $(La/Sm)_N > 1.0$

Group II: HREE depleted, $(Gb/Yb)_N > 1.0$
Class 4: LREE depleted, $(La/Sm)_N < 1.0$
Class 5: LREE enriched, $(La/Sm)_N > 1.0$

Group III: HREE enriched, $(Gd/Yb)_N < 1.0$

The REE distributions in the Onverwacht komatiitic rocks encompass all groups, with Group II dominating.

Group I Komatiites are common in Archean greenstone belts in Canada, Finland, Western Australia and Zimbabwe-Rhodesia (Arth et al. 1977; Whitford and Arndt 1978; Jahn et al. 1980a; Sun and Nesbitt 1978; Hawkesworth and O'Nions 1977; Jahn and Sun 1979), but are of less importance in the Onverwacht Group, being represented by sample 49 J (Sun and Nesbitt 1978). In this study, Group II rocks seem to dominate, possibly due in part to a sampling bias. Rare Group III rocks are also found. More detailed descriptions are given below:

Group II Komatiites (Fig. 4a and 4b). Included in this group are three peridotitic komatiites (SA39, 5019 and 5031) and 7 basaltic komatiites from different formations. All rocks show relatively coherent HREE fractionation patterns with $(Gd/Yb)_N$ ratios invariably greater than 1.0 (Mean: 1.41 ± 0.13 for 10 rocks). The high $(Gd/Yb)_N$ ratios of the Onverwacht Group II rocks are also accompanied by high CaO/Al_2O_3 ratios (Fig. 5) and low Al_2O_3/TiO_2 ratios (Fig. 6). This relationship, together with other trace element data, is considered very significant in later discussion on petrogenesis and mantle evolution. No similar regularity is found with respect to LREE (light rare earth elements) distributions and Eu anomalies. According to the LREE characteristics, Group II rocks can be further subdivided into two subgroups: (a) those with enriched LREE, and (b) those with depleted or nearly flat LREE (i.e. class 4 and 5). This division may be partly attributed to original source heterogeneity in LREE, mantle metasomatism, or post-magmatic alteration.

It should be noted that the peridotitic komatiites so-called here may not necessarily represent true liquid compositions. Petrographic examination reveals that samples 5019 and 5031 have cumulate textures (Table 6), which are confirmed by their high Cr contents (greater than 5,000 ppm

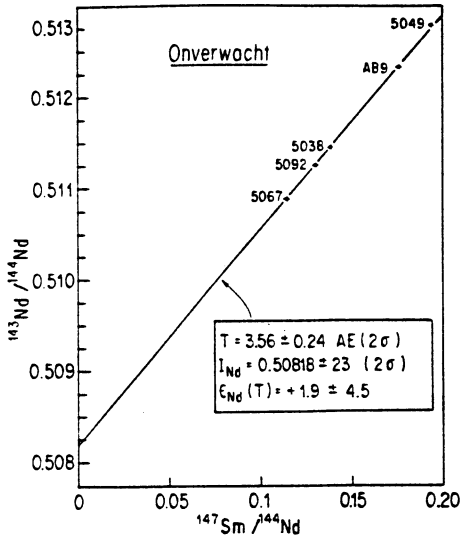

Fig. 1. Sm–Nd isochron diagram for the Onverwacht komatiites. Isochron was calculated using the method of York (1966). $\lambda\,^{147}Sm = 6.54 \times 10^{-12}\ yr^{-1}$.

$$\varepsilon_{Nd}(T) = \frac{I_{Nd}(S) - I_{Nd}\,(\text{chondrite}, T)}{I_{Nd}\,(\text{chondrite}, T)} \times 10^4,$$

where, $I_{Nd}(S)$ = initial $^{143}Nd/^{144}Nd$ ratio of the samples. I_{Nd} (chondrite, T) = 0.50808 in this case (T = 3.56 AE)

It should be noted that included in our isochron calculation are rocks from three different formations (Sandspruit, Theespruit and Komati). Whereas this treatment may not be strictly valid, the choice of samples was made assuming that the lower three formations might have been deposited within a relatively short time interval and their initial isotopic compositions were similar. Moreover, rocks with a maximum Sm/Nd ratio spread were selected to ensure a better isochron statistics. Silicic rocks, pyroclastics or rocks of problematic origin were not included to avoid possible complications in interpretation. The fact that the five data points form a reasonably good linear array favors the hypothesis that the lower Onverwacht lavas were extruded during a time span not resolvable by the present technique, and that the isotopic characteristics of their respective source regions were similar. This is supported by the work of Hamilton et al. (1979) who also included in their isochron calculation a data point of acid tuff from the Theespruit formation. Furthermore, two of their analyses of rocks from the Hooggenoeg Formation (Upper Onverwacht Group) lie on the same isochron. We therefore interpret the age of 3.56 AE as the time of lower Onverwacht Group volcanism.

The stratigraphic relationship between the Onverwacht Group and the Ancient Gneiss Complex (AGC) have been debated for years (Hunter 1974; Viljoen and Viljoen 1969; Anhaeusser 1973; Glikson 1979a) owing to the lack of contact relationships and definitive primary emplacement ages. Recently, leucocratic orthogneisses of the Bimodal Suite of the AGC have been dated (Rb–Sr) by Barton et al. (1980) at $T = 3.56 \pm 0.11$ (2σ) AE, with $I_{Sr} = 0.6999 \pm 16$ (2σ). This age is indistinguishable from that determined by the Sm–Nd method for the Onverwacht rocks. Thus, the relative antiquity of the Onverwacht Group and the Ancient Gneiss Complex is yet to be resolved.

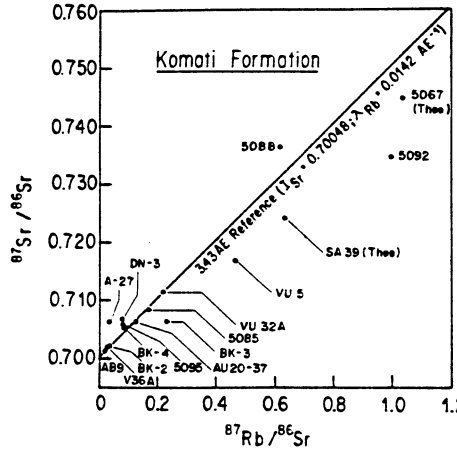

Fig. 2. Rb–Sr isochron diagram for rocks from the Komati Formation (two Theespruit samples are also displayed). $\lambda_{Rb} = 1.42 \times 10^{-11}\ year^{-1}$. Five data (AB9, V36A, VU5, VU32A and AU20–37) are taken from Jahn and Shih (1974)

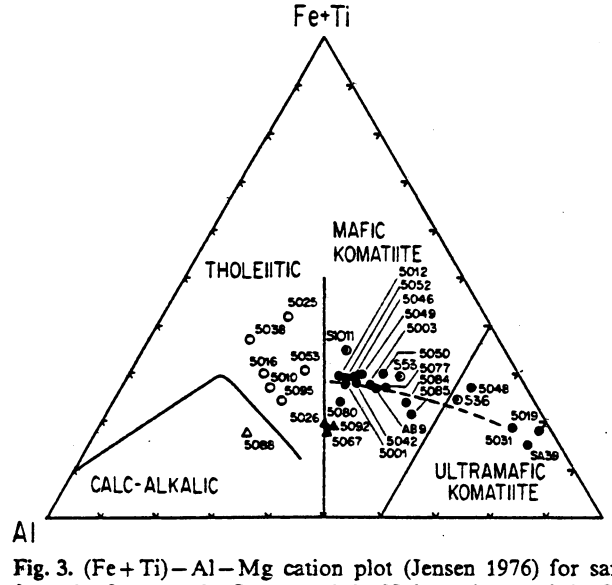

Fig. 3. (Fe + Ti) – Al – Mg cation plot (Jensen 1976) for samples from the Onverwacht Group and the Holenarsipur and the Sargur belts of India

Rb–Sr Isotopic Data

Additional whole-rock Rb–Sr isotopic data on Onverwacht Group rocks have been acquired since the earlier publication of Jahn and Shih (1974). The new data are presented in Table 4 and displayed in Fig. 2. The data points are highly scattered and no isochron relationship could be established. This reiterates the contrasting geochemical behaviors of Sm/Nd and Rb/Sr isotopic systems during alteration and metamorphism.

Classification by Major Element Data

Jensen (1976) has proposed a new classification scheme using the cation proportion of (Fe + Ti) – Al – Mg for volcanic or metavolcanic rocks containing Mg–rich varieties. This cation plot is useful in distinguishing komatiitic from tholeiitic series and it is a complementary to the TiO_2/Al_2O_3 or TiO_2/MgO plots commonly used to separate these

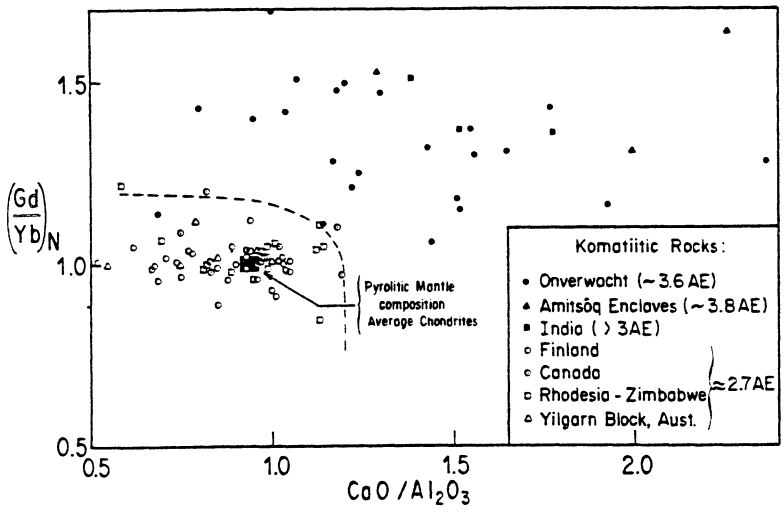

Fig. 5. $(Gd/Yb)_N$ vs CaO/Al_2O_3 diagram. *Solid symbols* are for early Archean rocks ($T > 3.5$ AE; the age of Indian rocks are not determined) and *open symbols* are for late Archean rocks (≈ 2.7 AE). Chondritic CaO/Al_2O_3 ratios are taken from Mason (1979) and pyrolitic mantle values from Ringwood (1979). The early Archean rocks are separated by a dashed boundary from the late Archean rocks by having higher $(Gd/Yb)_N$ and CaO/Al_2O_3 ratios. Data sources: for Onverwacht: present study, Herrmann et al. 1976, Hawkesworth and O'Nions 1977; Sun and Nesbitt 1978; for Amitsoq enclaves: McGregor and Mason 1977; for India: present study; for Yilgarn Block: Sun and Nesbitt 1978; for Rhodesia: Hawkesworth and O'Nions 1977; Bickel et al. 1975; Nisbet et al. 1977; Sun and Nesbitt 1978; for Munro, Canada: Arth et al. 1977; Whitford and Arndt 1978; Sun and Nesbitt 1978; for Noranda, Canada: Jahn, unpublished; for Finland: Jahn et al. 1980a

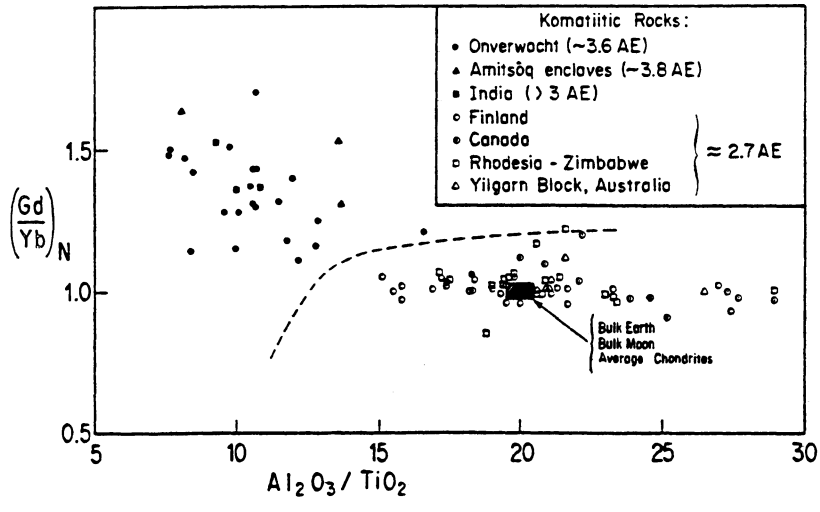

Fig. 6. $(Gd/Yb)_N$ vs Al_2O_3/TiO_2 diagram. The ratios for the bulk earth and the bulk moon are from Anders (1977), and for average chondrites from Mason (1979). The early Archean rocks (*solid symbols*) are distinguised from the late Archean rocks (*open symbols*) by having higher $(Gd/Yb)_N$ but lower Al_2O_3 ratios. Data sources: see Fig. 5 caption

in both cases, Table 2). However, their genetic linkage with true peridotitic komatiites is beyond doubt.

Group III Komatiites (Fig. 4c). This group comprises two basaltic komatiites, one from the Theespruit Formation and one from the Komati Formation. Their LREE are relatively enriched $[(La/Sm)_N > 3.0]$ and their HREE are characterized by $(Gd/Yb)_N < 1.0$, in strong contrast to the Group II rocks. Accompanied with the low $(Gd/Yb)_N$ ratios are the low CaO/Al_2O_3 ratios (< 1.0). Although sample 5067 has a $(Gd/Yb)_N$ ratio of about 1.0, indistinguishable from that of Group I rocks, the concave shape of its HREE pattern and similar TiO_2 and K_2O contents and Al_2O_3/TiO_2 ratio (~ 40) as compared to sample 5092, suggest that 5067 better belongs to Group III komatiites. It is interesting to note that the type of REE pattern as represented by 5092 has not been reported before for komatiites of the Onverwacht Group or elsewhere. However, that of 5067 is quite similar to spinifex-textured basaltic komatiites ($MgO = 12-17\%$) of the Negri volcanics from the Pilbara Block, Western Australia (Sun and Nesbitt 1978).

Tholeiites (Fig. 4d): Three tholeiitic rocks were analyzed for a comparative study. They show LREE enrichment relative to HREE and they have overall REE abundances greater than komatiitic rocks mentioned heretofore.

Samples 5053 and 5038 (Fig. 4d) have REE patterns very similar to some of Group II basaltic komatiites. A comparison of major and trace element data between these rocks suggest that they could be related by fractional crystallisation. Similarly, tholeiite 5088 (Fig. 4c) has a REE pattern almost identical to that of Group III basaltic komatiite 5067. We realize tha the present classification of the three rocks – 5092, 5067, 5088 (Fig. 4c) – is not entirely satisfactory, because they have certain peculiar chemistry that is not well understood: very high K_2O (1.6–1.7%), very low TiO_2 (0.3–0.4%) and hence very high Al_2O_3/TiO_2 ratios (38–43, see Table 1). In addition, the high SiO_2 (55%) in 5067 is puzzling. Nevertheless, their close major element and REE characteristics strongly suggest their derivation (s) from similar sources which have been depleted in Ti but enriched in K_2O. Genetic relationship through fractional crystallisation is considered less likely because many oxides (SiO_2, Al_2O_3, CaO) and HREE patterns cannot be adequately modelled. It is concluded that the source rocks for the Group III komatiites and tholeiite 5088 have been enriched in alkalis and depleted in TiO_2 before the melting event. However, post-magmatic modification of these two oxides cannot be totally discounted either.

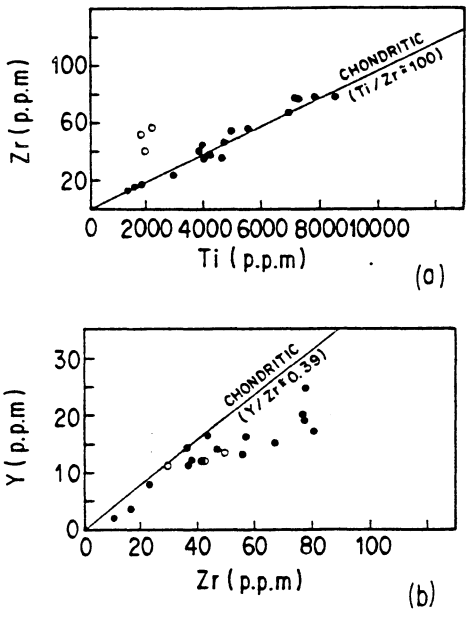

Fig. 7. a Zr vs Ti, and (b) Y vs Zr variation diagrams. Nearly chondritic Zr/Ti ratios are preserved for Onverwacht komatiites (*solid symbols* for Group II and *open symbolds* for Group III rocks). However, in b, Y is shown to be depleted relative to Zr, thus the data points deviate from the chondritic ratio line. Chondritic values are from the compilation of Sun and Nesbitt (1977)

Transition Metals: Zr, Ti, Y, Cr, Ni, Co, V

Recognition of komatiites formed by crystallization of high-Mg liquids may be assisted by transition metal data. From studies of "immobile" transition elements in spinifex-textured rocks, Nesbitt and Sun (1976) and Sun and Nesbitt (1978) established a set of chemical criteria for recognition of komatiites. These include near chondritic ratios of Ti/Zr $\approx$ 110, Y/Zr $\approx$ 0.39 and Ti/Y $\approx$ 290. Figure 7a shows a good correlation between Ti and Zr for all Group II komatiites whose data points fall close to the chondritic line. By contrast, Fig. 7b indicates a significant depletion in Y relative to Zr. It is known that Y behaves like HREE (particularly Dy and Er) therefore it is not unexpected to have Y depletion in rocks which are also depleted in HREE.

It is interesting to note that many komatiites from the Sandspruit Formation have high TiO_2 (>1%) contents, but those from the Komati Formation do not (Table 1). High TiO_2 contents in two basaltic komatiites (VU33, 1.35%; Sandspruit; AB21, 1.43%, Theespruit) have also been reported by Viljoen and Viljoen (1969a). Furthermore, Zr is also correspondingly enriched in these high Ti rocks, thus a near chondritic Ti/Zr ratio is maintained.

Discussion

CaO/Al_2O_3 vs $(Gd/Yb)_N$: Garnet Fractionation

The characteristic high CaO/Al_2O_3 ratios (Mean of 1.33 ± 0.33, on 29 analyses) for Group II komatiites of the Onverwacht Group can be interpreted in terms of two models: (1) the high ratios reflect primary mantle chemical characteristics and (2) the high ratios are a result of secondary alteration or metamorphism. The present results reinforce the first interpretation as proposed by Sun and Nesbitt (1978) and render the proposition of alteration effect untenable (Ludden and Gelinas 1980) for the following reasons.

Figure 5 shows a diagram of $(Gd/Yb)_N$ vs CaO/Al_2O_3 for the known komatiitic rocks from various Archean terrains. It is clear that komatiites of 2.7 AE terrains (shown by open symbols) are characterized by having $(Gd/Yb)_N$ 1.0 ± 0.1 and CaO/Al_2O_3 ratios generally less than 1.0. The variation in CaO/Al_2O_3 ratios of 2.7 AE rocks might be due to pyroxene fractionation, which, however, would introduce only slight HREE fractionation in the komatiites. Thus, most rocks show little deviation from $(Gd/Yb)_N = 1$. As a whole the data points are rather restricted, and the less differentiated (or more magnesian) rocks lie close to the chondritic or pyrolitic mantle values. By contrast, the Onverwacht data show a greater scatter. Almost all Onverwacht rocks have $(Gd/Yb)_N$ and CaO/Al_2O_3 ratios greater than 1.0, whereas their Al_2O_3/TiO_2 ratios ($\simeq 10$) are significantly lower than the chondritic value of about 20. This distinction suggests a fundamental difference in source characteristics and renders accidental alteration phenomena unlikely. It should be understood that Al and Ti are generally considered immobile but Ca occasionally shows its mobility during alteration (Chikhaoui 1981). It is thus possible that the lesser variation in Al_2O_3/TiO_2 ratios (Fig. 6) than in CaO/Al_2O_3 ratios (Fig. 5) might have been a result of some alteration processes. However, Chikhaoui (1981) has also shown that Ca content in volcanic rocks is generally reduced by alteration, hence the CaO/Al_2O_3 ratios are expected to be lowered. This is in contrast to the observed high CaO/Al_2O_3 ratios in the Onverwacht komatiites. Furthermore, the coherent low Al_2O_3/TiO_2 ratios in these komatiites as compared to those of 2.7 AE terrains could hardly be attributed to alteration processes. Nevertheless, if alteration indeed had any effect on CaO/Al_2O_3 ratios, the consistent HREE patterns (Fig. 4) could not be so produded. Further, many komatiites of 2.7 AE terrains have also undergone a similar degree of alteration but do not show a consistent HREE depletion and increased CaO/Al_2O_3 ratios.

Condie et al. (1977) reported that some types of metamorphism (particularly epidotization) release Al, hence increasing the Ca/Al ratio. However, since epidotization is also a common phenomenon in both early and late Archean terrains elsewhere where the majority of rocks show "normal" values for CaO/Al_2O_3 (0.9–1.0) and Al_2O_3/TiO_2 (20–22), it becomes difficult to ascribe a metamorphic cause for the high CaO/Al_2O_3 ratios in the Barberton rocks. It appears, therefore, that the distinct difference in Al_2O_3/TiO_2, CaO/Al_2O_3 and $(Gd/Yb)_N$ ratios between the Onverwacht and younger komatiites are likely related to different mantle chemistry and fractionation processes in early and late Archean times. Arguments on the $CaO-Al_2O_3-TiO_2$ interrelationships by Nesbitt et al. (1979) also dismiss a metamorphic or an alteration hypothesis and favor a magmatic origin of these elemental relationships.

During magmatic processes, the only major phase capable of fractionating both Gd/Yb and Ca/Al ratios is garnet. Al-orthopyroxene is not suitable, because it has very low Kd(HREE) values and is thus not effective enough in HREE fractionation. The fractionation of garnet from either mantle sources or derived liquids at high pressure would be expected to result in depletion of Al relative to Ca, of Yb relative to Gd, and of Y relative to more incompatible elements, such as Zr and Ti. This is clearly demon-

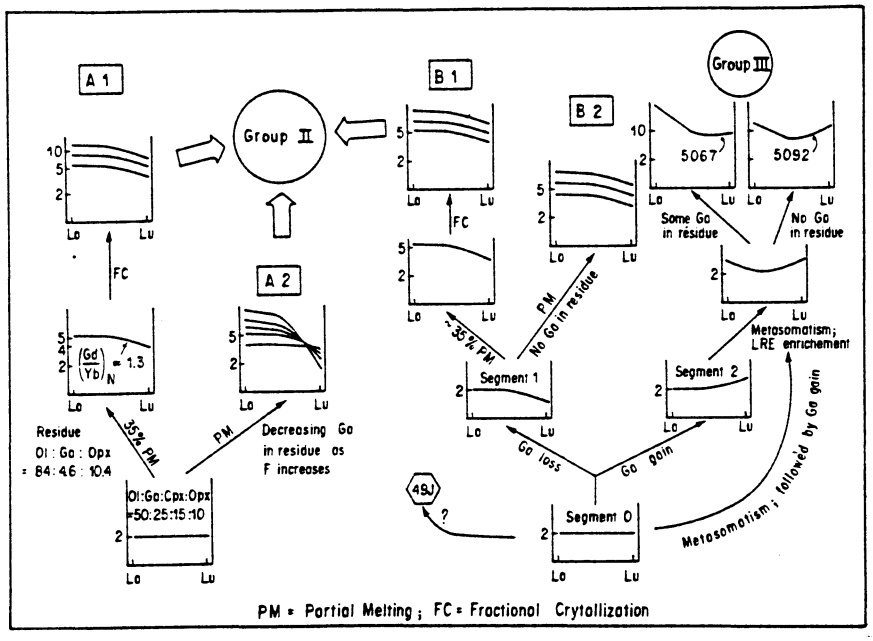

Fig. 8. A summary diagram of petrogenetic models for Onverwacht komatiites

strated in Figs. 5, 6 and 7. The high CaO/Al_2O_3 is more likely caused by Al depletion rather than Ca enrichment.

Petrogenetic Models

If garnet was the only major phase involved in Gd/Yb and Ca/Al fractionation, Group II rocks of Onverwacht Group may find their complementary parts in Group III rocks, which have low $(Gd/Yb)_N = 0.69–1.0$, low $CaO/Al_2O_3 = 0.65–0.60$ and high $Al_2O_3/TiO_2 \simeq 40$. For the genetic relationship between these two groups there may be other interpretations. Possible genetic models are discussed below and portrayed in Fig. 8.

Model 1. Initial mantle source: 2× chondritic, flat REE pattern Olivine:Garnet:Clinopyroxene:Orthopyroxene = 50:25:15:10.

A high-proportion of garnet in the Archean mantle may not be entirely unreasonable, as this mineral could have been common in view of a lesser separation of basaltic component from the mantle at that time. With this assumption, two varieties of Model 1 are examined as follows:

a) In this model, partial melting of the mantle source will be governed by the melting relation proposed by Mysen (1977): 0.63 Ga + 0.41 Cpx + 0.09 Opx = 0.13 Ol (olivine) + Liq. With a 35% of partial melting, the residue will consist of 4.5% Ga + 1% Cpx + 10.5% Opx + 84% Ol. The liquid produced would have relatively flat LREE ($La_N \simeq 6\times$) and fractionated HREE with $(Gd/Yb)_N = 1.3$. Further fractional crystallisation involving mainly olivine and later joined by Cpx could in principle produce REE patterns similar to those known in Fig. 4a and b.

b) In this model, varying degrees of melting of Ga-bearing source leaves varying garnet percentages in the residues. This model will produce (systematic) crossing HREE patterns, and thus is not compatible with the observed data.

Model 2. Initial mantle source: 2× chondritic, flat REE pattern. Garnet separation is assumed during the uprising of mantle diapir as envisaged by Green (1975). In this model, one part of the mantle source (Segment 1) is depleted in garnet and thus in Yb relative Gd and in Al relative to Ca; the other part (Segment 2) is enriched in garnet and thus in Yb and Al (Fig. 6). About 7 to 10% of garnet separation is required to result in a $(Gd/Yb)_N$ ratio between 1.3–1.5 for segment 1. Unfractionated mantle is denoted as Segment 0.

a) Partial melting of Segment 1 producing a parental liquid (no Ga left in the residue) followed by fractional crystallization.

b) Various degrees of melting of Segment 1 without leaving Ga in the residue.

Both models (2a and b) could result in REE patterns mimicking those in Fig. 4a and b.

The complementary mantle (Segment 2) would be enriched in Yb relative to Gd. However, to account for the significant LREE enrichment, Segment 2 might have been metasomatized by invading liquid or fluid enriched in LREE. Partial melting of the metasomatized Segment 2 is considered a possible mechanism to produce the Group III rocks (Fig. 4c).

The above models are based solely on the REE data. Model 1a seems reasonable but has other inherited problems such as: (1) the assumed high proportion of garnet would lower the initial CaO/Al_2O_3 ratio to about 0.7–0.8 and raise the Al_2O_3/TiO_2 to about 30. Liquids produced by melting of such composition are not likely to have high CaO/Al_2O_3 ratios (~1.3) and low Al_2O_3/TiO_2 (~10) as observed in Onverwacht komatiites; (2) Melting of an assemblage with high proportion of garnet and clinopyroxene relative to olivine and orthopyroxene will tend to produce liquids not much enriched in MgO (< 20% even at 35–40% melting). This is not consistent with the MgO contents shown by some peridotitic komatiites in Fig. 4. However, samples 5019 and 5031 have some cumulative nature; (3) so far all the experimental studies on melting of peridotite show that the above-liquidus field of garnet is very restricted and garnet melts before clinopyroxene in most cases and is exhausted before the melting degree is reached to form peridotitic komatiitic liquids (Green 1973; Mysen and

Kushiro 1977; Jaques and Green 1980; Harrison 1981). With regard to point (3), the problem may be circumvented by the fact that none of the experimental studies have been performed on garnet-rich (>20%) peridotite. Nevertheless, the above problems and the failure of Model 1 to account for the Group III rocks may favor the interpretation of Model 2.

Other models of komatiite genesis have been proposed, such as: (1) sequential melting (Arndt 1977), (2) polybaric assimilation: internal variety (Cox 1978), (3) Polybaric assimilation: foreign variety (Bickle et al. 1977), (4) combination of sequential melting and foreign polybaric assimilation (Smith and Erlank 1981). Each of these models has its own problems, and it is not our intention to discuss them here. Interested readers may find some useful comments on the first three models by Nesbitt et al. (1979).

A peridotitic komatiite, 49J, from the Onverwacht has been subject to an experimental study (Green et al. 1975) which demonstrated that the melting temperature of the peridotitic komatiite exceeds 1600° C and the rock represents a product of high degree (≃60%) of melting of mantle material. This specific rock has a high CaO/Al_2O_3 of 1.44 and a flat HREE distribution with $(Gd/Yb)_N = 1.06$ (Sun and Nesbitt 1978). Possibly, in this case a strong Al–Opx fractionation was involved. However, in view of the "normal" Al_2O_3/TiO_2 ratio as shown in Fig. 6, it appears that CaO might be in excess. As far as the REE pattern is concerned, the source region probably corresponds to unfractionated mantle Segment 0.

Possible Age Connotation of CaO/Al_2O_3 and $(Gd/Yb)_N$ ratios?

Figures 5 and 6 show that the Gd/Yb, Ca/Al and Al/Ti ratios of Onverwacht komatiites are different from those of late Archean komatiites (≃2.7 AE). Does this signify an evolutionary feature of the upper mantle chemistry through time? Or does this merely represent a mantle heterogeneity whereby the Onverwacht volcanisms have selectively tapped fractionated yet complementary mantle segments (Segments 1 and 2) in a lopsided proportion (Group II rocks predominate)? The alternative interpretations are given as follows:

Secular Evolution. In this hypothesis it is assumed that the high CaO/Al_2O_3 and Gd/Yb ratios were characteristic of the early Archean mantle (>3.5 AE). However, the data base for such assumption is limited: Rocks of komatiitic affinity occurring as enclaves in the Amitsoq gneisses, West Greenland, have Gd/Yb, CaO/Al_2O_3 and Al_2O_3/TiO_2 ratios similar to those of the Onverwacht rocks (McGregor and Mason, 1977; see Figs. 4 and 5). Komatiitic rocks from India (Holenarsipur and Sargur) also have similar REE distributions (Table 5 and Fig. 9) and CaO/Al_2O_3 ratio. Although the age of these Indian rocks is not determined, in so far as the ratios have any age connotation, these Indian komatiites might be as old as 3.4 to 3.5 AE. The associated Peninsular Gneisses near the Holenarsipur greenstone belt have been dated by the Rb–Sr method at 3.36±0.04 AE (Beckinsale et al. 1980; Beckinsale, pers. communications). Furthermore, three komatiites from the Pilbara Block (3.56 AE of age, Hamilton et al. 1980; Jahn et al. 1981) have been shown by Nesbitt et al. (1979) to possess high CaO/Al_2O_3 (1.4–2.3) and low Al_2O_3/TiO_2 (≃10). However, unpublished data show a wide range of both ratios, many having higher and many lower than 1.0 for CaO/Al_2O_3 and 20 for Al_2O_3/TiO_2 (Glikson 1979). We are currently conducting a systematic REE study of ca 3.6 AE Pilbara komatiites and of Greenland mafic-ultramafic enclaves in order to further examine the possible chemistry-age relationship.

Mantle Heterogeneity. In this hypothesis, it is assumed that the bulk upper mantle (<400 km) chemistry did not change

Table 5. Major elements and REE data for some Indian volcanic rocks

	Holenarsipur	Holenarsipur	Sargur
Rock type	BK	BK	BK
Sample No.	S36	S1011	S53
SiO_2 (%)	46.68	47.51	50.69
TiO_2	0.54	0.85	0.78
Al_2O_3	5.42	9.26	7.22
Fe_2O_3	5.74	2.18	4.30
FeO	8.29	13.29	9.52
MnO	0.17	0.27	0.22
MgO	19.51	9.47	13.14
CaO	9.13	14.14	9.97
Na_2O	0.32	0.71	3.31
K_2O	0.00	0.48	0.25
P_2O_5	0.06	0.10	0.10
H_2O^+	3.94	1.57	0.01
Total	99.75	99.85	99.51
Al_2O_3/TiO_2	10.03	10.89	9.26
CaO/Al_2O_3	1.68	1.53	1.38
La (p.p.m.)	1.696	2.441	6.256
Ce	4.875	7.210	15.131
Nd	3.791	5.657	10.046
Sm	1.231	1.976	2.842
Eu	0.371	0.945	0.894
Gd	1.585	2.688	3.216
Dy	1.753	3.135	3.222
Er	1.020	1.805	1.801
Yb	0.935	1.611	1.650
Lu	0.153	0.247	0.254
$(Gd/Yb)_N$	1.36	1.37	1.53

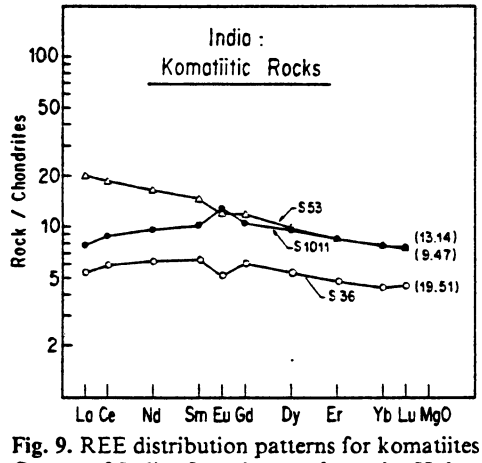

Fig. 9. REE distribution patterns for komatiites from the Dharwar Craton of India. Samples are from the Holenarsipur and Sargur greenstone belts. Their ages are inferred to be ≧3.2 AE (Naqvi et al. 1978)

significantly through Archean times. The mantle sources for the Onverwacht rocks were somehow fractionated by the loss (for Segment 1, see Petrogenetic Model 2) and gain (for Segment 2) of garnet, producing two complementary parts. Only two Group III samples (Fig. 3C) lie on the opposite side of the restricted field defined by the 2.7 AE komatiites (Figs. 5 and 6). This could suggest that the high CaO/Al_2O_3 or Gd/Yb ratios in the Onverwacht rocks (and Amitsoq enclaves, and Indian rocks as well) do not have any age connotation; rather, they only reflect local mantle heterogeneity. In this case, the Nd isotopic data, $\varepsilon_{Nd}(T) \approx 0$, suggest that this heterogeneity was created shortly before the Onverwacht volcanisms. Sample 49J was probably produced by partial melting of unfractionated mantle Segment 0. Chemical and isotopic evidence for Archean mantle heterogeneity has earlier been addressed by several authors (e.g. Sun and Nesbitt 1978; Jahn et al. 1980).

Light Rare Earth Elements (LREE)

It has been shown that komatiites from 2.7 AE terrains are mostly characterized by flat or depleted LREE, some depleted as much as, or even more so than, modern MORB (Sun and Nesbitt 1978; Arth et al. 1977; Whitford and Arndt 1978; Jahn et al. 1980a). Figure 4 shows that the LREE distributions in Group II rocks are not uniform, with $(La/Sm)_N$ ranging from 0.73 (5052) to 2.17 (5031); none of them show as highly depleted LREE as found in komatiites from Finland and Canada (Jahn et al. 1980; Arth et al. 1977; Whitford and Arndt 1978; Sun and Nesbitt 1978). Heterogeneous distribution of LREE is also observed in the Indian komatiites whose HREE, however, show remarkably consistent slope as shown in the Onverwacht rocks (see Fig. 9).

The possible mobility of REE during alteration and metamorphism has been widely debated and is beyond the scope of this paper. However, all workers seem to agree that HREE remain unfractionated, while many suggest LREE mobility. Our preceeding arguments on the HREE, i.e., Gd/Yb ratio, are therefore little affected by this problem. Since alteration might happen at any time, and maybe repeatedly following initial magmatism, the success of dating by the Sm/Nd method and the preservation of primary Sm–Nd isotopic systematics seems to argue against significant change in REE patterns. It follows that the non-uniform LREE distributions may reflect mantle source heterogeneity. It is likely that patterns with $(La/Sm)_N > 1.5$, such as 5019, 5031, 5080 (Fig. 4A), as well as Group III rocks may suggest that their source have been metasomatised by LREE-rich fluids or magmatic liquids shortly before the melting events.

Conclusions

(1) Komatiites of the Tjakastad Subgroup of the Onverwacht Group were dated by the Sm–Nd method yielding a whole-rock isochron age of $T = 3.56 \pm 0.24$ (2σ) AE, and $I_{Nd} = 0.50818 \pm 23$ (2σ), corresponding to $\varepsilon_{Nd}(T) = +1.9 \pm 4.5$. This age is interpreted as the time of initial Onverwacht Group volcanism. The near zero $\varepsilon_{Nd}(T)$ value suggests that the source rocks had a time-integrated near chondritic Sm/Nd ratio. The present result agrees with earlier data of Hamilton et al. (1979) and is consistent with the Rb–Sr results by Jahn and Shih (1974).

(2) Komatiites may be divided into 3 groups based on the typology of REE distributions (particularly HREE; Jahn and Gruau 1981). According to this scheme, the Onverwacht komatiites of the present study belong to two groups: the predominant Group II rocks show $(Gd/Yb)_N = 1.41 \pm 0.13$ (σ), $CaO/Al_2O_3 = 1.33 \pm 0.33$ (σ), and $Al_2O_3/TiO_2 = 10.6 \pm 2.0$ (σ); the subordinate Group III rocks have $(Gd/Yb)_N < 1.0$, $CaO/Al_2O_3 \simeq 0.60$, and $Al_2O_3/TiO_2 \simeq 40$. This contrasting feature is best explained by garnet fractionation within the mantle sources. Mantle Segment 1 was depleted in garnet component and served as the source for the Group II rocks; whereas Segment 2 was enriched in garnet and served as the source for Group III rocks. The exact process of garnet fractionation is not known. However, if a terrestrial magma ocean did exist, as envisaged by Anderson (1980), garnet crystallization and settling due to its greater density than other phases would become possible and maybe important. Consequently, a heterogeneous or even stratified mantle could be so ensued.

Segment 1 may find its modern equivalent in Southern Africa. Morgan et al. (1980) reported that a sheared peridotite nodule PHN 1611 from Lesotho has $Al_2O_3/TiO_2 \sim 10$ and a fractionated REE pattern ($La_N = 3\times$ and $Yb_N = 1.5\times$ chondrites). This composition somewhat resembles that predicted for the source of the Onverwacht Group II rocks. It should be emphasized that the variation in CaO/Al_2O_3 is not likely to have resulted from alteration processes.

(3) Younger komatiites (2.7 AE) from Finland, Canada, Rhodesia and Australia have $(Gd/Yb)_N \simeq 1.0 \pm 0.1$; $CaO/Al_2O_3 < 1.1$ and $Al_2O_3/TiO_2 = 20.5 \pm 3.1$ (σ) (58 analyses). These ratios are nearly chondritic or of the bulk earth value (Anders 1977). It appears that some late Archean komatiites are different in chemistry from many early Archean komatiites. The implication may be that the upper mantle chemistry has evolved through Archean times. However, the age connotation of CaO/Al_2O_3, $(Gd/Yb)_N$ or Al_2O_3/TiO_2 ratio has not been firmly established and further analyses of early Archean komatiites are needed. The aspect of age connotation has been further discussed in a recent paper by Nesbitt et al. (1982). The characteristic Ca/Al or Gd/Yb ratios in Onverwacht Group rocks can be also explained as a result of local short-term mantle heterogeneity.

(4) The non-uniform distribution of LREE in Group II rocks and the highly enriched LREE in Group III rocks may suggest that some part of mantle sources have been metasomatised to various extents by invading LREE-rich fluids or magmatic liquids. The Sm–Nd isotopic data suggest that the heterogeneity developed shortly before the partial melting events.

Acknowledgements. We thank the following komatiitic friends for their useful comments on earlier versions of this paper: B. Auvray (Rennes), A.L. Jaques (Canberra), R.W. Nesbitt (Southampton), and S.S. Sun (North Ryde). Komatiite samples from India were kindly donnated by S.M. Naqvi. Technical assistance of J. Cornichet is much appreciated. This research is supported by ATP-Géochimie (1979–1980) and ATP-Géodynamique (1980–1982) of France. A.Y. Glikson publishes with the permission of the Director, BMR, Australia.

Appendix 1

Petrographic Description

All samples were collected from the type area of the Onverwacht Group (Viljoen and Viljoen 1969c). Localities of all samples ana-

lyzed are shown in Fig. 10. Petrographic description with diagnostic chemical parameters is presented in Table 6. More detailed description can be found in Viljoen and Viljoen (1969b). In general, these rocks have undergone low-grade metamorphism (greenschist facies), which is also true for the entire greenstone belts of the Barberton Mountain Land (Viljoen and Viljoen 1969c). Spinifex textures are not observed in the thin sections examined. Relict primary minerals are occasionally preserved (e.g., 5084, 5085, and AB9). Serpentinization is very restricted except in two cumulate samples (5019 and 5031).

Assessment of Alteration Effects

The single most difficult question inherent in geochemical studies of metavolcanic rocks is the discrimination between primary igneous compositions and superposed secondary element redistribution patterns. Because of the differential nature of open chemical migration of the various elements, references to rock bodies as "fresh" or "altered" must be qualified with respect to the element in question. Thus, it is generally agreed that alkali and alkaline earth elements are prone to redistribution, whereas the high-field strength (HFS) elements (REE, Y, Zr, Nb, Hf, P, Ti) and some ferromagnesian elements (Ni, Co, Cr, Sc) are relatively less mobile (Smith and Smith 1976; Condie et al. 1977; Sun and Nesbitt 1978). The petrogenetic models and interpretations in this article are

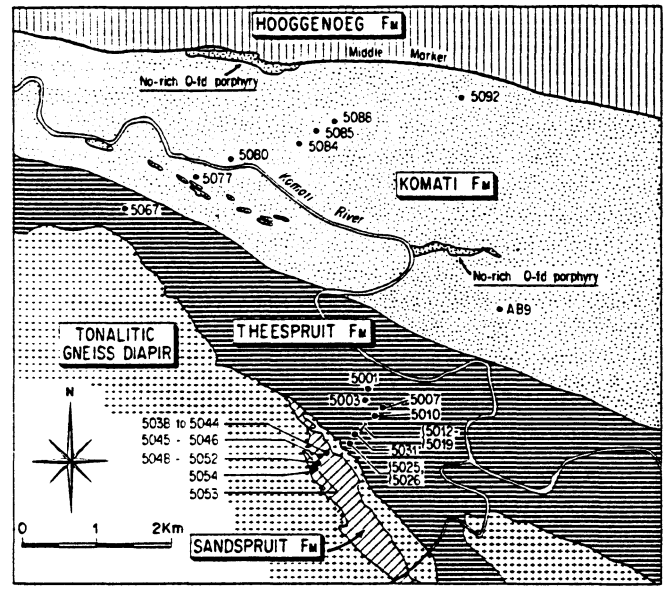

Fig. 10. Sampling localities

Table 6. Petrographic description of analyzed samples from the Onverwacht Group, South Africa (C/A represents CaO/Al_2O_3 ratio; R represents chondrite-normalized $(Gd/Yb)_N$ ratio; Th = tholeiite; BK = basaltic komatiite; PK = peridotitic komatiite)

Sample No.	Texture	Metamorphic mineralogy	Special features	Chemical characteristics		Classification
				Major element	REE	
5038	Microcrystalline, foliated homogeneous	Hb, plag, cpx, Q, sph	No secondary alteration	$SiO_2 = 51\%$, $MgO = 4.2\%$ $TiO_2 = 1.7\%$ $C/A = 0.7$	La = 58 ×, Yb = 16 × R = 1.38	Th
5042	Medium grained porphyroblastic	Trem, alb, ilm, sph	veinlets of alb + clinozo; trace calcite grains	$SiO_2 = 50\%$, $MgO = 11\%$ $TiO_2 = 1.21\%$ $C/A = 1.2$		BK
5046	Microcrystalline, homogeneous	Act, olig, ilm, sph	No secondary alteration	$SiO_2 = 48.5\%$, $MgO = 10.8\%$ $TiO_2 = 1.3\%$ $C/A = 1.2$	La = 21 ×, Yb = 11 × R = 1.5	BK
5048	Microcrystalline, homogeneous	Trem, chl, ilm	trem partly chloritized	$SiO_2 = 45.7\%$, $MgO = 19.5\%$ $TiO_2 = 0.9\%$ $C/A = 1.04$		PK
5049	Microcrystalline, foliated homogeneous	Act, alb, epid, sph	No secondary alteration	$SiO_2 = 47.2\%$, $MgO = 11.7\%$ $TiO_2 = 1.2\%$ $C/A = 1.3$	La = 15 ×, Yb = 10 × R = 1.48	BK
5050	Microcrystalline, foliated homogeneous	Act, olig, ilm, sph	No secondary alteration	$SiO_2 = 46.5\%$, $MgO = 12.9\%$ $TiO_2 = 1.15\%$ $C/A = 1.4$		BK
5052	Microcrystalline homogeneous	Act, alb, sph	No secondary alteration	$SiO_2 = 46.3\%$, $MgO = 10.9\%$ $TiO_2 = 1.43\%$ $C/A = 1.2$	La = 11 ×, Yb = 10 × R = 1.48	BK
5053	Fine grained, homogeneous	Act, alb, clinozo, sph	No secondary alteration	$SiO_2 = 50.6\%$, $MgO = 7.5\%$ $TiO_2 = 1.2\%$ $C/A = 1.1$	La = 30 ×, Yb = 10 × R = 1.51	Th
5001	Microcrystalline, granuloblastic	Act, sauss, alb, cal		$SiO_2 = 54.3\%$, $MgO = 9\%$ $TiO_2 = 0.71\%$ $C/A = 1.27$		BK
5003	Medium grained	Act, alb, Q, ilm, sph		$SiO_2 = 54.3\%$, $MgO = 10.6\%$ $TiO_2 = 0.78\%$ $C/A = 1.22$		BK
5010	Medium grained	Hb, olig, alb, Q, ilm, sph		$SiO_2 = 52.6\%$, $MgO = 6.3\%$ $TiO_2 = 0.61\%$ $C/A = 0.66$		Th

Table 6 (continued)

Sample No.	Texture	Metamorphic mineralogy	Special features	Chemical characteristics		Classification
				Major element	REE	
5012	Microcrystalline, granuloblastic	Act, alb, sauss, Q		$SiO_2 = 54.3\%$, MgO = 8.7% $TiO_2 = 0.76\%$ C/A = 1.41		BK
5016	Medium grained	Hb, olig, alb, sauss, ilm		$SiO_2 = 53.3\%$, MgO = 5.8% $TiO_2 = 0.79\%$ C/A = 0.57		Th
5019	Fine grained homogeneous cumulate text.	Serp, trem, mag	serpentinization completely achieved no prim. relic min.	$SiO_2 = 42.6\%$, MgO = 34.2% $TiO_2 = 0.27\%$ C/A = 0.80	La = 6 ×, Yb = 2 × R = 1.43	PK
5025	Fine to medium grained, banded homogeneous	Hb, alb, sph, ilm	No secondary alteration	$SiO_2 = 48.7\%$, MgO = 5.6% $TiO_2 = 1.51\%$ C/A = 0.96		Th
5026	Fine grained subophitic	Cpx, and, sauss		$SiO_2 = 52.8\%$, MgO = 10.6% $TiO_2 = 0.37\%$ C/A = 0.80		BK
5031	Coarse grained homogeneous cumulate text.	Serp, trem, mag	serpentinization completely achieved no prim. relic min.	$SiO_2 = 44.3\%$, MgO = 31.3% $TiO_2 = 0.31\%$ C/A = 1.00	La = 11 ×, Yb = 3 × R = 1.7	PK
5067	Coarse grained subophitic homogeneous	Cpx, and, serp, sauss, Opx	plag phenocr. saussuritized, trace ol totaly serpentinized	$SiO_2 = 55.6\%$ MgO = 9.8% $TiO_2 = 0.32\%$ C/A = 0.6	La = 51 ×, Yb = 8 × R = 1.0	BK
5077	Fine grained subophitic homogeneous	Cpx, hb, alb, sauss	cpx partly transformed to amph., plag totaly saussuritized	$SiO_2 = 52.7\%$, MgO = 11.3% $TiO_2 = 0.64\%$ C/A = 1.43	La = 12 ×, Yb = 8 × R = 1.32	BK
5080	Occelus textured microcrystalline	Cpx, epid, chl, plag, sauss	trace amount of calcite veinlets	$SiO_2 = 54.8\%$, MgO = 9.4% $TiO_2 = 0.82\%$ C/A = 0.95	La = 18 ×, Yb = 8 × R = 1.40	BX
5084	Medium grained homogeneous	Cpx, trem, chl, plag	relic cpx, chl	$SiO_2 = 52.6\%$, MgO = 13.1% $TiO_2 = 0.65\%$ C/A = 1.56	La = 9 ×, Yb = 7 × R = 1.30	BK
5085	Medium grained porphiritic, skeletal	Trem	relic cpx almost entirely transformed to trem	$SiO_2 = 55.0\%$, MgO = 13.7% $TiO_2 = 0.49\%$ C/A = 1.15		BK
5088	Coarse grained subophitic homogeneous	Cpx, plag, sauss, ilm, serp	trace ol destabilized in serp + chl + cal	$SiO_2 = 52.9\%$, MgO = 6.5% $TiO_2 = 0.4\%$ C/A = 0.56	La = 52 ×, Yb = 9 × R = 1.08	Th
5092	Medium grained subophitic	Cpx, plag, sauss, chl, trem	relic cpx transformed to trem, trace cal crystals	$SiO_2 = 50.9\%$, MgO = 11.2% $TiO_2 = 0.3\%$ C/A = 0.65	La = 19 ×, Yb = 8 × R = 0.69	BK
5095	Microcrystalline	Trem, sauss, sph, clinozo	trace carbonate crystals	$SiO_2 = 50.9\%$, MgO = 7.3% $TiO_2 = 0.69\%$ C/A = 0.79		Th
AB9	Fine grained	Trem, act, olig, chl, sph, opaq	relic cpx	$SiO_2 = 52.4\%$, MgO = 11.4% $TiO_2 = 0.7\%$ C/A = 1.23	La = 10 ×, Yb = 7 × R = 1.19	BK

based primarily on the distribution of the latter group less mobile elements. Although the mineralogy (Table 6) does not in itself allow a precise indication of the degree of alteration, in general departures from primary composition are positively related to the abundance of highly hydrous phases such as chlorite and serpentine. By contrast, the metamorphism of primary pyroxene-plagioclase assemblages to amphibolite can be shown in places to involve limited introduction of water accompanied by little open chemical redistribution (i.e., Hallberg 1972).

While it is not feasible to precisely determine the departure from original igneous composition of any individual sample, overall estimate of the degree of alteration can be obtained from (1) retention or otherwise of magmatic inter-elemental relations and trends; (2) correlation coefficients between magmatically related elements; (3) degree of compositional scatter for individual rock types; and (4) extent of hydration and carbonatization. A measure of departure from igneous compositions is provided by log molecular proportion plots (LMPR) or Beswick and Soucie (1978), wher-

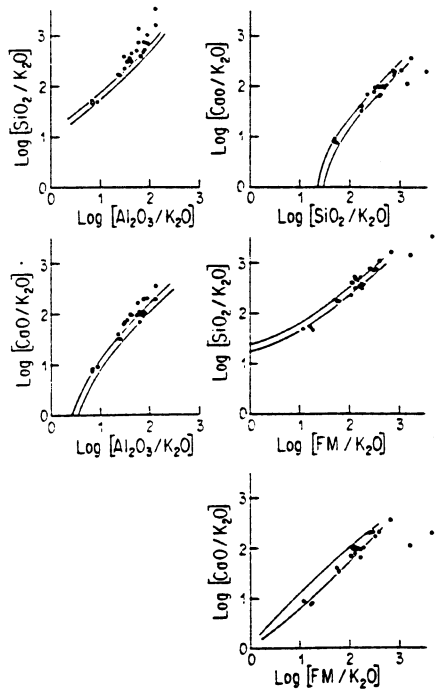

Fig. 11. LMPR (log molecular proportions) plots of the Onverwacht Group volcanic rocks. The delineated central field is of least-altered modern volcanic rocks (after Beswick and Soucie 1978)

eby the log of several major element/alkali ratios are plotted against each other and compared to the field of least altered modern volcanics (Fig. 11). The deviation of any point from the least altered field provides a semi-quatitative parameter of alteration (Glikson 1979).

The samples studied here display high correlation coefficients between the HFS elements, between the ferromagnesian elements, and also between some of the alkalies (Table 7). For example, Ti–Zr ($r=0.83$), Ti–P ($r=0.82$), Ti–Y ($r=0.78$), Y–Zr ($r=0.95$), Cr–Co ($r=0.95$), Ni–Cr ($r=0.98$), Co–Ni ($r=0.96$), K–Rb ($r=0.99$). LMPR plots of the data suggest approximations to the fields of modern volcanics for Ca/Si, Si/FM ($FM=FeO_t+MgO$), and Ca/FM, and some departures in the fields of Si/Al and Ca/Al. The departures may be related to Al depletion in the source regions as developed in the text. The coherent relations suggest that little overall fractionation has taken place with regard to the more stable elements, including the rare earth elements, which may be indicated by erratic REE patterns, including Eu anomalies. However, the regularity of REE patterns and the Sm/Nd isotope systematics reported in this paper lend supporting evidence to their interpretation in terms of near-original compositions. Likewise the relatively limited deviation on the log (CaO/K_2O)–log (Al_2O_3/K_2O) plot suggests that, on the whole, the CaO/Al_2O_3 ratios are not far removed from their primary values. In addition, the process of rodingitization is not identified in the analyzed samples. Notwithstanding these considerations, the possibility of departures of our data from original magmatic chemistry must be constantly borne in mind.

Table 7. Correlation coefficients for komatiitic and tholeiitic rocks of the Onverwacht Group (only values above 0.5 or less than −0.5 are shown)

	Tjakastaad subgroup (major elements)											
	SiO_2	TiO_2	Al_2O_3	Fe_2O_3	FeO	Tot.Fe	MnO	MgO	CaO	Na_2O	K_2O	P_2O_5
SiO_2												
TiO_2												
Al_2O_3												
Fe_2O_3												
FeO	−1.00	1.00	−1.00	1.00								
Tot.Fe	−0.68	0.67		0.53	1.00							
MnO	−0.62	*0.80*			1.00	*0.84*						
MgO	−0.62		−0.80		1.00							
CaO		0.64			−1.00			−0.70				
Na_2O	0.57		0.54		−1.00			−0.66				
K_2O			0.51		1.00	−0.57						
P_2O_5		*0.82*					0.51	−0.50	0.53			
Ba	−1.00	1.00	−1.00	1.00	1.00	1.00	1.00	1.00	−1.00	−1.00	1.00	
Rb		−0.66				−0.73	−0.58		−0.61		*0.99*	−0.54
Sr			*0.72*		1.00			−0.55				
Pb		−0.56		−0.74		−0.74	−0.65				*0.70*	
Th	0.99	−0.89		−0.88		−0.88	−0.80	0.99	−0.93	−0.92	*0.85*	−0.96
U												
Zr		*0.83*			−1.00		0.56		0.54			*0.75*
Nb					−1.00						0.51	
Y		*0.78*			1.00				0.59			*0.72*
La	1.00	−1.00	1.00	−1.00	−1.00	−1.00	−1.00	−1.00	1.00	1.00	−1.00	
Ce												
Li			0.56		1.00						0.51	
V		0.71			1.00		0.64		0.76			
Cr	−0.75		−0.75		1.00			*0.97*	−0.63	−0.69		
Co	−0.81		−0.77					*0.94*	−0.64	−0.67		
Ni	−0.82		−0.66		1.00			*0.93*	−0.61	−0.70		
Cu		0.52			−1.00					0.59		
Zn		*0.89*			−1.00	*0.72*	*0.77*					*0.78*
Ga	1.00	−1.00	1.00	−1.00	−1.00	−1.00	−1.00	−1.00	1.00	1.00	−1.00	

Table 7 (continued)

	Tjakastaad subgroup (trace elements)																	
	Ba	Rb	Sr	Pb	Th	U	Zr	Nb	Y	La	Ce	Li	V	Cr	Co	Ni	Cu	Zn
Ba																		
Rb																		
Sr	1.00																	
Pb		*0.85*																
Th		*0.90*	−1.00	*0.71*														
U																		
Zr	−1.00		0.55		−0.90													
Nb	−1.00				−0.83													
Y	1.00		0.62		−0.89		*0.95*											
La	−1.00		−1.00				1.00	1.00	−1.00									
Ce																		
Li	1.00				0.87					−1.00								
V	1.00	−0.72			−0.64					−1.00								
Cr	1.00				0.93					−1.00								
Co			−0.51		0.82									*0.95*				
Ni	1.00				0.98					−1.00				*0.98*	*0.96*			
Cu	−1.00				−0.87					1.00								
Zn	−1.00	−0.53		−0.56	−0.91		*0.67*		0.56	1.00			0.56				*0.66*	
Ga	−1.00		−1.00				1.00	1.00	−1.00	1.00		−1.00	−1.00	−1.00		−1.00	1.00	1.00

References (Only additional references are listed below; the others are already in the paper reference list)

Beswick AE, Sourcie G (1978) A correction procedure for metasomatism in an Archaean greenstone belt. Precambr Res 6:235–248

Hallberg JA (1972) Geochemistry of Archaean volcanic belts in the eastern Goldfields regions of Western Australia. J Petrol 13:45–56

Smith RE, Smith SE (1976) Comments on the use of Ti, Zr, Y, Sr, K, P, and Nb in classification of basaltic magmas. Earth Planet Sci Lett 32:114–120

References

Allsopp HL, Ulrych TJ, Nicolaysen LO (1968) Dating of some significant events in the history of the Swaziland system by the Rb–Sr isochron method. Can J Earth Sci 5:605–619

Anders (1977) Chemical compositions of the Moon, Earth and Eucrite parent body. Philos Trans R Soc Lond A 285:23–40

Anderson DL (1980) Early evolution of the mantle. Episodes (IUGS) 1980:(3):3–7

Anhaeusser CR (1973) The evolution of the early Precambrian crust of southern Africa. Philos Trans R Soc Lond A 273:359–388

Anhaeusser CR (1978) The geological evolution of the primitive earth-evidence from the Barberton Mountain Land. In: Tarling DH (ed) Evolution of the Earth's crust, Academic Press, London, pp 71–106

Anhaeusser CR, Mason R, Viljoen MJ, Viljoen RP (1969) A reappriasal of some aspects of Precambrian shield geology. Bull Geol Soc Amer 80:2175–2200

Arndt NT (1977) Ultrabasic Magmas and High-Degree Melting of the Mantle. Contrib Mineral Petrol 64:205–221

Arndt NT (1981) What is a Komatiite? Arndt NT and Nisbet EG (ed) Komatiites (in press)

Arndt NT, Brooks C (1980) Komatiites: Penrose conference report. Geology 8:155–156

Arndt NT, Naldrett AJ, Pyke DR (1977) Komatiite and Iron Rich Tholeiitic Lavas of Munro Township, Northeast Ontario. J Petrol 18:319–369

Arth JG, Arndt NT, Naldrett AJ (1977) Genesis of Archean komatiites from Munro township, Ontario: trace element evidence. Geology 5:590–594

Barton JM, Hunter DR, Jackson MP, Wilson AC (1980) Rb–Sr age and source of the bimodale suite of the Ancien Gneiss Complex, Swaziland. Nature 283:756–758

Beckinsale RD, Drury SA, Holt RW (1980) 3,360 Myr old gneisses from the South Indian Craton. Nature 283:469–470

Bickle MJ, Martin A, Nisbet EG (1975) Basaltic and peridotitic komatiites and stromatolites above a basal unconfirmity in the Belingwe Greestone belt, Rhodesia. Earth Planet Sci Lett 27:155–162

Bickle MJ, Ford CR, Nisbet EG (1977) The petrogenesis of peridotitic komatiites: evidence from high pressure melting experiments. Earth Planet Sci Lett 37:97–106

Blais S, Auvray B, Capdevila R, Jahn BM, Hameurt J, Bertrand JM (1978) The Archean greenstone Belt of KARELIA (Eastern Finland) and their Komatiitic and tholeiitic series. In: Windley BF and Naqvi SM (eds) Archean Geochemistry, Elsevier, Amsterdam, pp 87–107

Chikhaoui M (1981) Les roches volcaniques du Protérozoique supérieur de la chaîne Pan-Africaine dans le NW de l'Afrique (Hoggar, Anti-Atlas, Adrar des Iforas): caractérisation géochimique et minéralogique, implications géodynamiques. Thèse d'Etat, Montpellier, 183 pp

Condie KC, Viljoen MJ, Kable EJD (1977) Effects of alteration on element distributions in Archean tholeiites from the Barberton greenstone belt, South Africa. Contrib Mineral Petrol 64:75–89

Cox KG (1978) Komatiites and other high-magnesia lavas: some problems. Philos Trans R Soc Lond A 288:599–609

Glikson AY (1979) Siderophile and Litophile trace element evolution of the Archean mantle. BMR J Aust Geol Geophys 4:253–279

Glikson AY, Hickman AH (1981) Geochemistry of Archaean volcanic successions, eastern Pilbara Block, Western Australia. Aust Bur Miner Resour Record 1981/36

Green DH (1973) Experimental melting studies on a model upper mantle composition at high pressure under water satured and water undersaturated conditions. Earth Planet Sci Lett 19:37–53

Green DH (1975) Genesis of Archean peridotic magmas and constraints on Archean geothermal gradients and tectonics. Geology 3:15–18

Green DH, Nicholls IA, Viljoen M, Viljoen R (1975) Experimental demonstration of the existence of peridotitic liquids in earliest Archean magmatism. Geology 3:11–14

Hamilton PJ, Evensen NM, O'Nions RK, Smith HS, Erlank AJ (1979) Sm–Nd dating of Onverwacht group volcanics, Southern Africa. Nature 279:298–300

Hamilton PJ, Evensen NM, O'Nions RK, Glikson AY, Hicman AH (1980) Sm–Nd dating of the Talga-Talga Subgroup, Warrawoona Group, Pilbara Block, Western Australia. In: Glover JE and Groves DI (eds) Second Int. Archean Symp Perth, pp 11–12

Harrison WJ (1981) Partitioning of REE between minerals and coexisting melts during partial melting of a garnet lherzolite. Am Mineral 66:242–259

Hart SR, Davis GL (1969) Zircon U–Pb and whole rock Rb–Sr ages and early crustal development near Rainy Lake, Ontario. Bull Geol Soc Amer 80:595–616

Hawkesworth CJ, O'Nions RK (1977) The petrogenesis of some Archean volcanic rocks from Southern Africa. J Petrol 18, 487–520

Herrmann AG, Blanchard DP, Haskin LA, Jacobs JW, Knake D, Korotev RL, Brannon JC (1976) Major, Minor and Trace Element Compositions of Peridotitic and Basaltic Komatiites from the Precambrian Crust of Southern Africa. Contrib Mineral Petrol 59:1–12

Hunter DR (1974) Crustal developpment in the Kaapvall craton. I The Archaean. Precambr Res 1:259–294

Hurley PM, Pinson WH, Nagy B, Teska TM (1972) Ancient age of the Middle Marker Horison: Onverwacht Group, Swaziland Sequence, South Africa. Earth Planet Sci Lett 14:360–366

Jahn BM, Chi Yu Shih (1974) On the Age of the Onverwacht Group Swaziland Sequence, South Africa. Geochim Cosmochim Acta 39:1679–1689

Jahn BM, Murthy VR (1975) Rb–Sr ages of the Archean rocks from the Vermilion district, northeastern Minnesota. Geochim Cosmochim Acta 39:1679–1689

Jahn BM, Sun SS (1979) Trace element distribution and Isotopic Composition of Archean Greenstones. In: Ahrens LH (ed) Origin and distribution of the elements. Pergamon Press, Oxford, pp 597–618

Jahn BM, Auvray B, Blais S, Capdevila R, Cornichet J, Vidal F, Hameurt J (1980a) Trace Element Geochemistry and Petrogenesis of Finnish Greenstone Belts. J Petrol 21:201–244

Jahn BM, Vidal P, Tilton GR (1980b) Archaean mantle heterogeneity: evidence from chemical and isotopic abundances in Archaean igneous rocks. Philos Trans R Soc Lond A 297, 353–364

Jahn BM, Bernard-Griffiths J, Charlot R, Cornichet J, Vidal F (1980c) Nd and Sr isotopic compositions and REE abundances of cretaceous MORB (Holes 417D and 418A, Legs 51, 52 and 53). Earth Planet Sci Lett 48:171–184

Jahn BM, Gruau G (1981) Possible significance of REE typology of komatiites to the Archean Mantle Differentiation. (Abstr) Terra Cognita, p 19

Jahn BM, Glikson AY, Peucat JJ, Hickman AH (1981) REE geochemistry and isotopic data of Archean silicic volcanics and granitoids from the Pilbara Block, Western Australia: implications for the early crustal evolution. Geochim Cosmochim Acta 45:1633–1652

Jaques AL, Green DH (1980) Anhydrous Melting of Peridotite at 0–15 Kb Pressure and the Genesis of Tholeiitic Basalts. Contrib Mineral Petrol 73:287–310

Jensen LS (1976) A new cation plot for classifying subalkalic volcanic rocks. Ont dep Mines Misc Pap 66

Ludden JN, Gelinas L (1980) "Fine Tunning" the petrogenesis of komatiite with Ti, Zr and Sc data. (Abstr) EOS 61:386

Mason B (1979) Data of geochemistry, Sixth Edition. Chapter B. Cosmochemistry. Geol Surv Prof Pap 440-B-1:132 pp

McGregor VR, Mason B (1977) Petrogenesis and geochemistry of metabasaltic and metasedimentary enclaves in the Amitsoq gneisses west Greenland. Am Mineral 62:887–904

Moorbath S (1977) Ages, isotopes and evolution of precambrian continental crust. Chem Geol 20:151–187

Morgan JW, Wandless GA, Petrie RK (1980) Earth's upper mantle: volatile element distribution and origin of siderophile element cotent. Lunar and Planetary Science XI, pp 740–742, Abstract of Papers Submitted to the Eleventh Lunar and Planetary Science Conference

Mysen BO (1977) Experimental determination of crystal-vapor partition coefficients for rare earth elements to 30 Kb pressure. Ann Rept Geophys Lab 1977–1978:689–695

Mysen BO, Kushiro I (1977) Compositional variations of coexisting phases with degree of melting of peridotite in the Upper Mantle. Am Mineral 62:843–865

Naqvi SM, Viswanathan S, Viswanatma MN (1978) Geology and geochemistry of the Holenarasipur schist belt and its place in the evolutionary history of the Indian Peninsula. In: Windley BF and Naqvi SM (eds) Archean geochemistry. Elsevier, Amsterdem, pp 109–126

Nesbitt RW, Sun SS (1976) Geochemistry of Archean spinifex-textured peridotites and magnesian and low-magnesian tholeiites. Earth Planet Sci Lett 31:433–453

Nesbitt RW, Sun SS, Purvis AC (1979) Komatiites: Geochemistry and Genesis. Can Mineral 17:165–186

Nesbitt RW, Jahn BW, Purvis AC (1982) Komatiites: an early Precambrian phenomenon. (in press) Sciences de la Terre

Nisbett EG, Bickle MJ, Martin A (1977) The Mafic and Ultramafic Lavas of the Belingwe Greenstone Belt, Rhodesia. J Petrol 18:521–566

Ringwood AE (1979) The origin of the Earth and Moon. Springer Verlag, New York, pp 295

Smith HS, Erlank AJ (1981) Geochemistry and Petrogenesis of Komatiites from the Barberton Greenstone Belt, South Africa. In: Arndt NT and Nisbet EG (eds) Komatiites (in press)

Sun SS, Nesbitt RW (1977) Chemical heterogeneity of the Archaean mantle, composition of the Earth and mantle evolution. Earth Planet Sci Lett 35:429–448

Sun SS, Nesbitt RW (1978) Petrogenesis of Archean Ultrabasic and basic volcanics: evidence from Rare Earth Elements. Contrib Mineral Petrol 65:301–325

Vidal Ph, Blais S, Jahn BM, Capdevila R (1980) U–Pb and Rb–Sr systematics of the Suomussalmi Archean Greenstone belt (Eastern Finland). Geochim Cosmochim Acta 44:2033–2044

Viljoen MJ, Viljoen RP (1969a) The geology and geochemistry of the lower ultramafic unit of the Onverwacht Group and a proposed new class of igneous rocks. In: Upper mantle project. Geol Soc S Africa Spec Publ 2:55–85

Viljoen MJ, Viljoen RP (1969b) Evidence for the existence of a mobile extrusive peridotitic magma from the Komati Formation of the Onverwacht Group. In: Upper mantle project. Geol Soc S Africa Spec Publ 2:86–112

Viljoen MJ, Viljoen RP (1969c) An introduction to the geology of the Barberton Granite-greenstone terrain. In: Upper mantle project. Geol Soc S Africa Spec Publ 2:9–28

Viljoen MJ, Viljoen RP (1970) Archaean vulcanicity and continental evolution in the Barberton (Mountain Land) region, Transvaal. In: Clifford TN and Gass I (eds) African magmatism and tectonics, Oliver and Boyd, Edinburg, pp 27–39

Wilson JF, Bickle MJ, Hawkesworth CJ, Martin A, Nisbet EG, Lorpen J (1978) Granite-greenstone terrains of the Rhodesian Archaean craton. Nature 271:23–27

Whitford DJ, Arndt NT (1978) Rare earth element abundances in a thick layered komatiite lava flow from Ontario, Canada. Earth Planet Sci Lett 41:188–196

York D (1966) Least square fitting of a straight line. Can J Phys 44:1079–1086

Received November 23, 1981; Accepted June 15, 1982

Earth and Planetary Science Letters, 85 (1987) 105–116
Elsevier Science Publishers B.V., Amsterdam – Printed in The Netherlands

[4]

Age of the Archean Talga-Talga Subgroup, Pilbara Block, Western Australia, and early evolution of the mantle: new Sm-Nd isotopic evidence

G. Gruau [1], B.M. Jahn [1], A.Y. Glikson [2], R. Davy [3], A.H. Hickman [3] and C. Chauvel [4]

[1] *C.A.E.S.S., CNRS, Institut de Géologie, Université de Rennes, 35042 Rennes Cedex (France)*
[2] *Bureau of Mineral Resources, Geology and Geophysics, Canberra, A.C.T. (Australia)*
[3] *Geological Survey of Western Australia, Perth, W.A. (Australia)*
[4] *Max-Planck-Institut für Chemie, Postfach 3060, D-6500 Mainz (F.R.G.)*

Received December 5, 1986; revised version accepted May 26, 1987

Archean komatiites, high-Mg basalts and tholeiites from the North Star Basalt and the Mount Ada Basalt formations of the Talga-Talga Subgroup, Warrawoona Group, Pilbara Block, Western Australia, define a linear correlation on the normal $^{143}Nd/^{144}Nd$ vs. $^{147}Sm/^{144}Nd$ isochron plot. The data give an age of 3712 ± 98 Ma and initial $\epsilon_{Nd}(T)$ of $+1.64 \pm 0.40$. The 3712 ± 98 Ma date is consistent with the regional stratigraphic sequence and available age data and the Sm-Nd linear array may be interpreted as an isochron giving the eruption age of the Talga-Talga Subgroup. An alternative interpretation is that the isochron represents a mixing line giving a pre-volcanism age for the Subgroup. Consideration of geochemical and isotopic data indicates that the true eruptive age of the Talga-Talga Subgroup is possibly closer to about 3500 Ma. Regardless of the age interpretation, the new Nd isotopic data support an existence of ancient LREE-depleted reservoirs in the early Archean mantle, and further suggest that source regions for the Pilbara volcanic rocks were isotopically heterogeneous, with $\epsilon_{Nd}(T)$ values ranging from at least 0 to +4.0.

1. Introduction

The systematic study of isotopic composition and REE geochemistry of Archean basic-ultrabasic (komatiitic) series allows new insight into the interpretation of Sm-Nd whole rock "isochron" relationships. A methodological dilemma inherent in geochronological studies is that—in order to obtain a better statistical precision of an isochron age—samples possessing as wide a range in Sm/Nd (or Rb/Sr) ratios as possible are preferentially analysed. However, in view of this variation, especially in the Sm-Nd system, it is possible that the investigated samples are not cogenetic and that different subsets of samples have different initial isotopic ratios. An "isochron" thus obtained may not have an unambiguous chronological meaning.

In this paper we present new Sm-Nd data for fourteen basic-ultrabasic rocks from the North Star Basalt and Mount Ada Basalt formations of the Pilbara Block, Western Australia. On the basis of a Sm-Nd isochron for six samples, ranging in composition from felsic volcanics to ultrabasic komatiite, Hamilton et al. [1,2] have earlier dated the North Star Basalt at 3540 ± 30 Ma. Additional Sm-Nd isotopic data obtained later by Jahn et al. [3] on four samples of felsic volcanics from the same locality yielded a similar but imprecise age of 3560 ± 540 Ma, whose large uncertainty arises from the restricted range of Sm/Nd ratios of the samples. The apparent concordance of these two data sets may suggest that the age of the North Star Basalt is well established at ca. 3550 Ma. However, in the light of the problems discussed in this paper and because of the large error of the second isochron date, this age remains uncertain.

In the present study the approach was to restrict the analyses solely to samples of basic-ultrabasic composition. The main aims of this work are: (a) to independently verify the oldest Sm-Nd isochron age found in the Pilbara Block, and (b) to establish $\epsilon_{Nd}(T)$ values for the mantle in this region, about 3500 Ma ago.

2. Geological setting

The Pilbara Block of northwestern Western Australia, like many other Archean granite-green-

0012-821X/87/$03.50

106

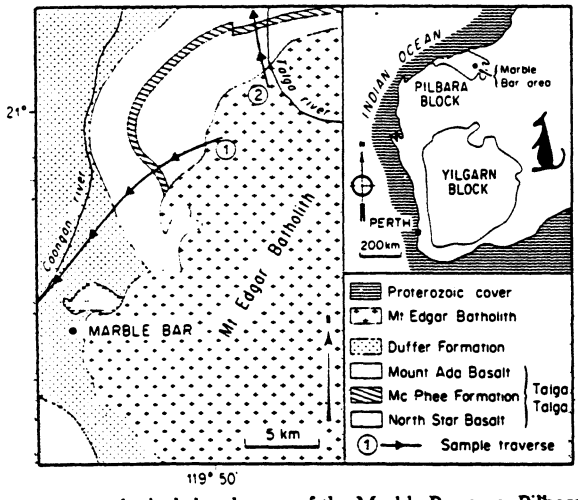

Fig. 1. A geological sketch map of the Marble Bar area, Pilbara Block, Western Australia. Two sample transverses are indicated: (*1*) Talga-Coongan; (*2*) Talga-River. From [5].

stone cratons, consists of low-grade metamorphosed volcanic and sedimentary successions intruded by, or faulted against, granitic batholiths. In the eastern part of the Pilbara Block, near Marble Bar, the stratigraphically lower volcano-sedimentary succession includes the North Star Basalt (NSB), McPhee Formation and Mount Ada Basalt (MAB), which together constitute the Talga-Talga Subgroup [4] (Fig. 1). The Talga-Talga Subgroup consists of pillowed and massive tholeiitic basalts, high-Mg basalts and minor peridotitic komatiites. Subordinate dacitic to andesitic volcanics, minor volcaniclastic sediments and chert occur in the McPhee Formation (Fig. 2). The metamorphic grade ranges from greenschist to lower amphibolite facies [4,5]. The NSB has been dated by the Sm-Nd method as ca. 3550 Ma old [1–3]. Further, Jahn et al. [3] reported a whole rock Rb-Sr isochron yielding a poorly constrained age of 3570 ± 180 Ma. No radiometric age data are available for the Mc Phee Formation nor for the MAB.

Overlying the Talga-Talga Subgroup is the Duffer Formation, composed mainly of dacitic to rhyolitic tuffs and agglomerates, including rare flows. Pidgeon [6] has dated this unit at 3452 ± 16 Ma using the U-Pb method on zircon fractions from dacite flows located 20 km southwest of Marble Bar. This represents the oldest U-Pb zircon age recorded from the layered succession of the Pilbara Block, and is believed to accurately reflect the primary igneous age of the Duffer Formation, providing a minimum age of ca. 3450 Ma for the Talga-Talga Subgroup.

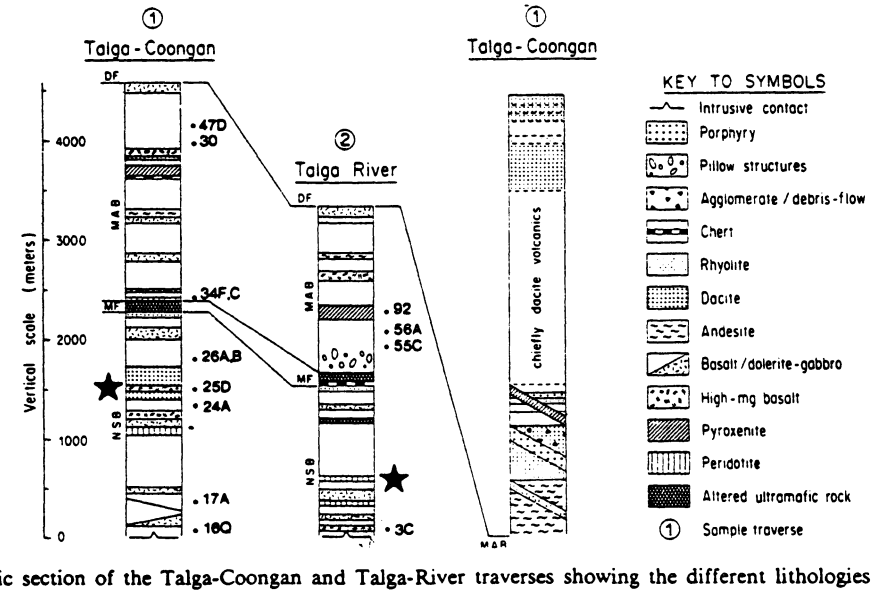

Fig. 2. Stratigraphic section of the Talga-Coongan and Talga-River traverses showing the different lithologies of the Talga-Talga Subgroup and Duffer Formation as well as sampling localities. *NSB* = North Star Basalt Formation; *MF* = McPhee Formation; *MAB* = Mount Ada Basalt Formation; *DF* = Duffer Formation. The star symbols give Hamilton et al.'s [1] and Jahn et al.'s [3] sample localities. From [1,3,5].

3. Sample selection and analytical techniques

In order to determine the ages of the NSB and the MAB the following samples were chosen for Sm-Nd isotopic investigation: (a) five tholeiitic basalts (MgO < 10%) and two high-Mg basalts (10% > MgO < 20%) from the NSB; (b) three tholeiitic basalts, two high-Mg basalts and two peridotitic komatiites (MgO > 20%) from the MAB. Sample localities are indicated in Figs. 1 and 2 and are identical or close to those for rocks analysed by Hamilton et al. [1] and Jahn et al. [3]. Petrographic descriptions can be found in [5].

All Nd isotopic compositions as well as Sm and Nd abundances were determined at the Université de Rennes except for samples 17A, 55C and 92 for which analyses were carried out at the Max-Planck-Institut für Chemie, Mainz. For the latter samples detailed description of chemical procedures and techniques in mass spectrometry analyses was given by Chauvel et al. [7].

Analytical techniques used at the Université de Rennes are as follows: (a) Approximately 500 mg of powder was weighed into closed teflon beakers and treated with HF-HNO_3-$HClO_4$ mixture for several days. (b) After dissolution the sample was dried out and then redissolved on a hot plate in 6*N* HCl. An aliquot of about 1/2 of the sample was used for Nd isotopic composition (IC) and 1/4 was used for Sm-Nd concentration determined by the isotopic dilution (ID) method. The remaining 1/4 was taken for further determination of REE abundances. (c) A mixed $^{149}Sm/^{145}Nd$ spike was added to the Sm-Nd aliquot.

The techniques used for Nd IC and Sm-Nd ID separation are essentially similar to those described in Jahn et al. [8]. Nd IC were run using triple Re filaments. $^{143}Nd/^{144}Nd$ measured ratios were normalized to $^{146}Nd/^{144}Nd = 0.7219$.

A check of our Sm-Nd mixed spike against BCR 1 and the Caltech Standard Solution as well as the mean value of 22 separate runs of La Jolla Nd standard are presented in Table 1. The $^{147}Sm/^{144}Nd$ ratio measured in Rennes for Caltech Standard Solution is in excellent agreement with both the result of Wasserburg et al. [9] and the value given by the Max Planck laboratory [7]. The reproducibility for the $^{147}Sm/^{144}Nd$ ratio is better than 0.2%.

TABLE 1

Sm-Nd results for standards

Samples	Nd (ppm)	Sm (ppm)	$^{147}Sm/^{144}Nd$	$^{143}Nd/^{144}Nd$
BCR-1				
1	28.75	6.574	0.1384	
2	28.84	6.603	0.1384	
3	28.89	6.601	0.1381	
average	28.82	6.592	0.1383	
	±0.2%	±0.2%	±0.1%	
Mainz [a]	28.84	6.590	0.1382	
Caltech Sm-Nd standard solution				
1			0.1963	
2			0.1965	
3			0.1969	
4			0.1965	
average			0.1966	
			±2 (σ)	
Caltech [b]			0.19655	
Mainz [a]			0.19650	
			±4 (σ)	
La Jolla Nd standard solution (22 runs)				0.511875 ±9

[a] Results published by the Max Planck Laboratory, Mainz, [7].
[b] Result given by Wasserburg et al. [9] recalculated against $^{146}Nd/^{144}Nd = 0.7219$.

Regression analyses were carried out using a modified version of the method of York [10]. The error inputs were 0.2% for $^{147}Sm/^{144}Nd$ and 2σ obtained for individual runs for $^{143}Nd/^{144}Nd$. All errors on ages and isotopic ratios are quoted at 2σ or 95% confidence level. Initial $^{143}Nd/^{144}Nd$ (I_{Nd}) ratios are also quoted throughout the text in the ϵ_{Nd} notation of DePaolo and Wasserburg [11] as deviations in part per 10^4 from the chondritic uniform reservoir (CHUR), as determined by Jacobsen and Wasserburg [12]. The errors of the isochron initial $\epsilon_{Nd}(T)$ values were calculated using the method of Fletcher and Rosman [13]. The decay constant of ^{147}Sm used is 0.00654 Ga^{-1}.

4. Results

The Sm-Nd isotopic results obtained for the NSB and MAB basic-ultrabasic suites are presented in Table 2 and displayed on a conventional isochron diagram in Fig. 3. The fourteen data points define an isochron (or errorchron) with an age of 3712 ± 98 Ma (MSWD = 12.8) and I_{Nd} =

108

TABLE 2

Sm-Nd isotopic data for Talga-Talga Subgroup basic-ultrabasic volcanic rocks

Sample	Rock type [a]	Sm (ppm)	Nd (ppm)	$^{147}Sm/^{144}Nd$	$^{143}Nd/^{144}Nd$	ϵ_{Nd} (3500)
North Star Basalt						
3C	HMg-B	1.345	3.233	0.2516	0.514099 ± 20	+3.6 ± 0.4
16Q	TB	2.025	6.754	0.1812	0.512378 ± 32	+1.8 ± 0.6
24A	TB	2.195	7.757	0.1711	0.512126 ± 15	+1.4 ± 0.3
26A	TB	3.398	9.862	0.2083	0.513005 ± 25	+1.8 ± 0.5
26B	TB	2.104	5.513	0.1693	0.512064 ± 17	+1.1 ± 0.3
25D	HMg-B	1.830	6.418	0.1723	0.512112 ± 29	+0.6 ± 0.3
17A	TB	3.120	10.73	0.1758	0.512180 ± 16	+0.6 ± 0.3
Mount Ada Basalt						
30	HMg-B	1.775	4.464	0.1964	0.512742 ± 21	+2.1 ± 0.4
34C	PK	1.199	2.749	0.2638	0.514357 ± 17	+3.2 ± 0.3
34F	PK	1.234	2.698	0.2768	0.514718 ± 29	+4.3 ± 0.6
47D	TB	2.417	8.090	0.1806	0.512360 ± 21	+1.7 ± 0.4
56A	TB	4.766	15.79	0.1824	0.512391 ± 18	+1.5 ± 0.4
92	HMg-B	1.825	5.680	0.1943	0.512574 ± 16	−0.3 ± 0.3
55C	TB	4.884	16.93	0.1744	0.512166 ± 19	+0.7 ± 0.4

[a] HMg-B: high-magnesium basalt; PK: peridotitic komatiite; TB: tholeiitic basalt.

$$\epsilon_{Nd}(3500\ \text{Ma}) = \left[\frac{I_{Nd}(3500)_{sample}}{I_{Nd}(3500)_{CHUR}} - 1\right] \times 10^4$$

For 3500 Ma: $I_{Nd\ CHUR} = 0.50809$.

0.507889 ± 21. The corresponding calculated $\epsilon_{Nd}(T)$ value is +1.6 ± 0.4. If the two sets of data are treated separately the following results are obtained: $T = 3737 \pm 117$ Ma with $\epsilon_{Nd}(T) = +1.8 \pm 0.4$ for the NSB; and $T = 3715 \pm 170$ Ma with $\epsilon_{Nd}(T) = +1.4 \pm 0.8$ for the MAB. The two data sets are indistinguishable within analytical error, and their combined treatment in the isochron calculation is regarded as valid.

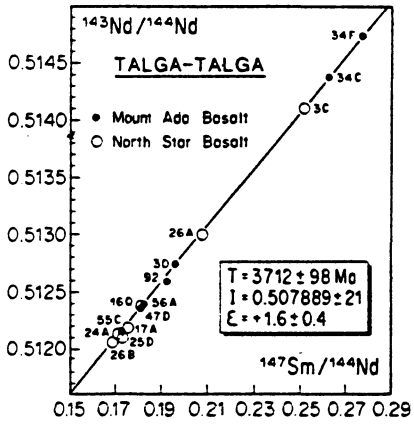

Fig. 3. Sm-Nd isochron diagram for the Talga-Talga Subgroup basic-ultrabasic volcanic rocks.

In Fig. 4, the new Sm-Nd data are plotted along with those published earlier [1–3]. The three samples of basic-ultrabasic composition investigated by Hamilton et al. [1] plot within analytical error on the 3712 Ma array defined by our fourteen rocks. When regressed the seventeen data

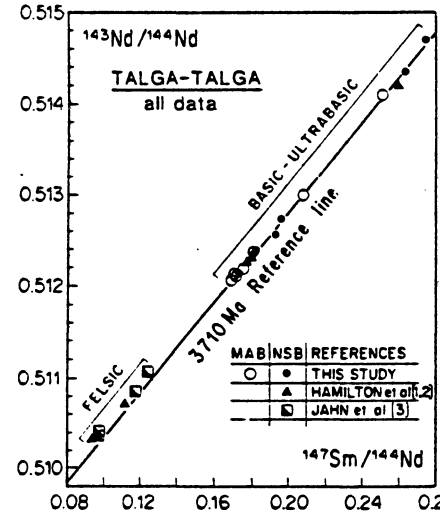

Fig. 4. Sm-Nd isochron diagram showing a comparison of the data from this study with those published earlier [1–3].

TABLE 3

Major and trace element data for Talga-Talga Subgroup basic-ultrabasic volcanic rocks

	North Star Basalt							Mount Ada Basalt						
Sample:	16Q	17A	24A	25D	26A	26B	03C	55C	56A	34F	34C	92	30	47D
Rock type [a]:	TB	TB	TB	HMg-B	TB	TB	HMg-B	TB	TB	PK	PK	HMg-B	HMg-B	TB
SiO_2	53.86	52.23	51.30	51.79	50.57	51.32	49.68	49.91	48.85	44.95	42.07	50.91	52.05	51.34
TiO_2	0.74	1.10	0.58	0.52	1.38	0.58	0.68	1.95	1.89	0.75	0.79	0.70	0.69	0.83
Al_2O_3	14.79	13.46	14.82	13.60	13.52	14.85	5.84	13.70	13.80	5.27	5.58	7.49	6.58	12.12
Fe_2O_3 (Fe)	9.46	12.73	10.47	10.04	15.78	10.81	12.44	14.57	15.56	14.25	15.85	10.83	10.95	11.85
MnO	0.24	0.19	0.25	0.20	0.25	0.32	0.24	0.19	0.23	0.24	0.25	0.22	0.22	0.20
MgO	6.09	7.10	8.61	10.82	6.15	7.69	13.91	6.16	5.71	22.61	23.45	12.19	13.53	7.95
CaO	12.02	8.65	10.15	8.77	9.58	11.83	14.94	8.06	8.95	8.19	6.80	14.79	14.59	10.70
Na_2O	2.41	1.95	1.64	0.82	1.47	0.85	0.42	2.75	2.42	0.06	0.07	1.45	1.00	1.91
K_2O	0.44	0.34	0.30	0.89	0.35	0.27	0.22	0.26	0.25	0.02	0.03	0.08	0.31	0.24
P_2O_5	0.05	0.10	0.04	0.03	0.13	0.03	0.40	0.17	0.15	0.07	0.07	0.04	0.04	0.08
H_2O_4	0.29	1.16	1.33	2.24	1.00	0.17	0.38	1.92	1.96	3.49	4.41	0.45	0.41	1.06
CO_2	0.06	0.02	0.04	0.11	0.12	0.10	0.24	0.46	0.25	0.03	0.03	0.42	0.04	1.93
Total	100.41	99.03	99.53	99.83	100.30	99.82	99.39	100.12	100.02	99.93	99.40	99.57	100.41	100.21
CaO/Al_2O_3	0.81	0.64	0.68	0.64	0.71	0.80	2.55	0.59	0.65	1.55	1.22	1.97	2.22	0.88
Al_2O_3/TiO_2	19.08	12.24	25.60	26.20	9.80	25.60	8.60	7.03	7.30	7.03	7.06	10.70	9.54	14.60
CaO/TiO_2	16.24	7.50	17.50	16.90	6.94	20.40	21.98	4.13	4.74	10.90	8.60	21.13	21.14	12.89
TiO_2/P_2O_5	14.80	11.00	14.50	17.30	10.60	19.30	1.70	11.50	12.60	10.70	11.30	17.50	17.30	10.40
Ba (ppm)	168	49	79	214	89	18	36	117	130	17	9	117	96	120
Rb	15	16	10	40	5	3	2	3	4	–	–	–	16	4
Sr	144	104	71	111	130	95	26	98	163	12	17	61	90	115
Zr	63	94	77	67	105	77	29	141	135	41	42	43	39	75
Nb	2	5	4	3	4	2	–	6	7	–	–	–	2	3
Y	21	27	20	17	29	19	14	39	35	11	11	16	15	23
V	272	364	240	225	420	278	324	425	424	208	203	216	248	218
Cr	985	77	361	752	74	331	1400	220	160	4100	4780	1710	1760	447
Co	44	41	46	44	54	51	66	44	43	90	107	46	47	45
Ni	206	50	115	146	56	108	399	61	74	1450	1480	176	185	94
La	4.25	6.72	5.520	4.53	5.443	5.460	1.183	10.33	7.798	1.027	1.121	2.900	2.620	4.326
Ce	10.21	16.45	12.29	10.24	13.17	12.40	3.506	25.02	20.95	2.385	2.682	7.580	6.924	10.76
Nd	6.754	10.73	7.757	6.418	9.862	7.513	3.233	16.93	15.504	2.698	2.749	5.680	5.464	8.090
Sm	2.025	3.110	2.195	1.830	3.398	2.104	1.345	4.959	4.754	1.234	1.199	1.826	1.775	2.417
Eu	0.688	0.929	0.661	0.560	1.191	0.596	0.539	1.408	1.509	0.324	0.259	0.632	0.604	0.865
Gd	2.642	3.884	2.760	2.249	4.607	2.610	2.289	6.138	5.798	1.904	1.878	2.409	2.295	3.865
Dy	3.197	4.598	3.395	2.830	5.260	3.300	2.589	7.077	6.431	2.083	2.072	2.737	2.709	3.547
Er	2.088	2.891	2.250	1.868	3.050	2.163	0.479	4.459	3.940	1.135	1.156	1.681	1.692	2.240
Yb	2.008	2.729	2.260	1.950	2.728	2.164	1.267	4.256	3.734	0.957	0.991	1.520	1.585	2.194
Lu	0.315	0.416	0.349	0.310	0.400	0.334	0.187	0.647	0.568	0.143	0.149	0.226	0.244	0.336
$(La/Sm)_N$	1.27	1.32	1.55	1.50	0.99	1.57	0.53	1.28	1.01	0.51	0.57	0.97	0.90	1.10
$(Gd/Yb)_N$	1.05	1.14	0.98	0.93	1.36	0.96	1.44	1.19	1.28	1.64	1.56	1.28	1.19	1.14
$(La/Yb)_N$	1.35	1.62	1.55	1.43	1.42	1.55	0.68	1.60	2.09	0.72	0.75	1.26	1.65	1.30
Eu/Eu^*	0.91	0.84	0.82	0.89	0.96	0.78	0.94	0.81	0.88	0.61	0.46	0.94	0.93	1.00
Ti/Y	286	244	243	183	285	183	291	300	324	409	431	262	276	216
Ti/Zr	95	70	63	47	79	45.1	141	83	84	110	113	98	106	66
Zr/Y	3.0	3.49	3.85	3.90	3.6	4.06	2.06	3.6	3.9	3.7	3.8	2.7	2.6	3.3

[a] TB: tholeiitic basalt; HMg-B: high magnesium basalt; PK = peridotitic komatiite.

points yield an age of 3687 ± 83 Ma with $\epsilon_{Nd}(T)$ = 1.6 ± 0.4. By contrast, the felsic volcanics lie well above the 3712 Ma isochron. If all the Talga-Talga Subgroup data are combined, a younger age of 3615 ± 58 Ma with $\epsilon_{Nd}(T) = +1.7 \pm 0.4$ is obtained. If the four komatiite samples with high $^{147}Sm/^{144}Nd$ ratios are excluded, an even younger age of 3517 ± 80 Ma results with corresponding $\epsilon_{Nd}(T) = +1.2 \pm 0.4$. Finally if only the six felsic volcanics data are treated an age as young as 3419 ± 242 Ma is obtained, with $\epsilon_{Nd}(T) = +0.1 \pm 2.7$.

5. Principal geochemical features of Talga-Talga Subgroup basic-ultrabasic volcanics

Table 3 presents major and trace element data including REE concentrations of the fourteen rocks selected for Nd isotope study. The REE data are further displayed in chondrite-normalized diagrams in Fig. 5. While all samples are of basic-ultrabasic composition the elemental abundance data show a large variation, especially when the REE distribution patterns are considered. On the basis of their REE patterns the rocks fall into three categories.

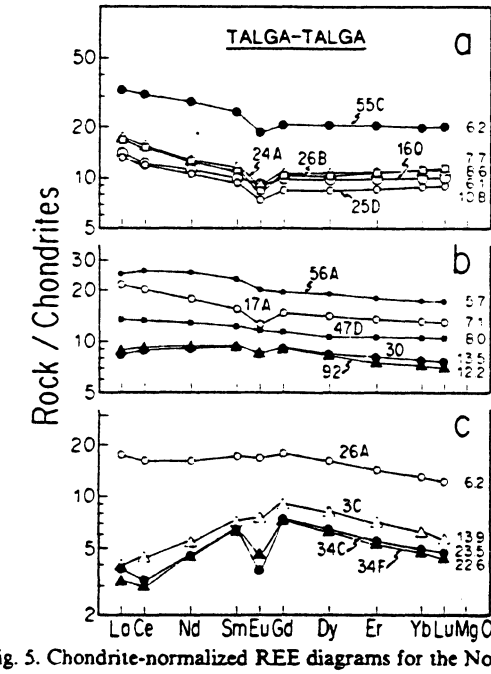

Fig. 5. Chondrite-normalized REE diagrams for the North Star Basalt (open symbols) and the Mount Ada Basalt (closed symbols) basic-ultrabasic volcanics. All analyses were carried out at the Université de Rennes by isotopic dilution mass spectrometry. Analytical techniques and normalizing values are given in [21].

5.1 Markedly depleted HREE patterns

Included in this category are the two MAB peridotitic komatiites, one NSB tholeiitic basalt and one NSB high-Mg basalt (Fig. 5c). All samples show high $(Gd/Yb)_N$ ratios (1.28–1.64) as well as low Al_2O_3/TiO_2 ratios and high CaO/Al_2O_3 ratios, except for the NSB tholeiitic basalt sample which has a CaO/Al_2O_3 ratio less than 1.0. These features resemble those of the Al-depleted Group II komatiites of Jahn et al. [14] common in early Archean terranes [14–18]. It is generally held that such compositions were derived by partial melting of garnet-depleted mantle sources [19].

In contrast, no regular variation is observed for the LREE patterns. The MAB komatiite samples (34F and 34C) and the NSB high-Mg basalt (3C) show strongly depleted LREE patterns, whereas the NSB tholeiitic basalt sample (26A) presents a near-flat LREE pattern. Moreover, the MAB komatiite samples show a strong negative Eu anomaly ($Eu/Eu^* < 0.6$) and a positive La anomaly. The strong depletion in LREE shown by samples 34C and 34F is unusual for early Archean komatiites which commonly have flat or slightly depleted/enriched LREE patterns [14,15,19]. However, because LREE are little fractionated during komatiite genesis the depletion of samples 34F and 34C must be considered very significant for it suggests that depletion events took place in the early Archean mantle. The Eu and La anomalies are both interpreted as resulting from post-magmatic alteration processes. A similar enrichment of La is often observed in altered rocks of ophiolite sequence [20].

Petrogenetic interpretation for tholeiite sample 26A is more difficult. As mentioned above, this rock has a HREE pattern mimicking those of the MAB komatiites and NSB high-Mg basalt, but instead of having a depleted LREE pattern it shows an almost chondritic distribution of LREE (Fig. 5c). This could be due to derivation by a small degree of partial melting of a LREE-HREE-depleted mantle source similar to that of samples 34C, 34F and 3C with some garnet left as residual phase. However, because garnet strongly

fractionates the HREE, sample 26A should display an even higher $(Gd/Yb)_N$ ratio. For this reason we suggest that either sample 26A was derived from a mantle source less depleted in LREE than that of the two MAB komatiites or resulted from mixing between a MAB-komatiite-like component and a component enriched in LREE. In any case a genetic linkage between 26A and the other three HREE-depleted samples is not evident.

5.2. Flat HREE, enriched LREE patterns

Included in this group are one NSB high-Mg basalt, three NSB tholeiitic basalts and one MAB tholeiitic basalt (Fig. 5a). All rocks show consistently fractionated REE patterns with $(Gd/Yb)_N$ ratios close to 1.0, $(La/Sm)_N$ ratios ranging from 1.3 to 1.5 and a negative Eu anomaly. Table 3 shows that the LREE enrichment of these five samples is accompanied by high Zr/Y ratios (up to 4.0), reflecting a coherent enrichment in Zr relative to Y. By contrast, especially in samples 25D and 26B, a relative depletion in Ti results in low Ti/Zr and Ti/Y ratios (45 and 180 respectively) and in high Al_2O_3/TiO_2 ratios (26) relative to chondrites (20). However, the flat HREE patterns and the near-chondritic CaO/Al_2O_3 ratios of these rocks rule out significant garnet fractionation. Thus, these rocks must have originated from mantle sources with chemical characteristics of Al-undepleted Group I komatiites [14,15].

Many Archean basalts are found to have almost flat LREE patterns [15,18,21]. The NSB and MAB tholeiites resemble the Hangingwall Basalts

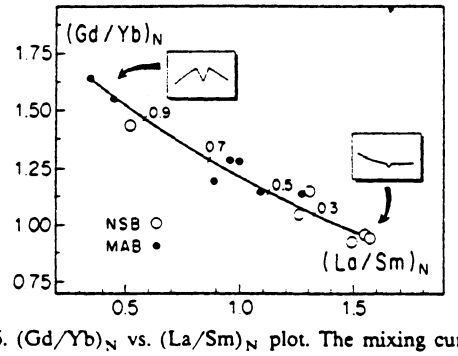

Fig. 6. $(Gd/Yb)_N$ vs. $(La/Sm)_N$ plot. The mixing curve was calculated using samples 34F and 26B as end-members, with $(La/Sm)_N$ corrected for La positive anomaly in sample 34F. Numbers on the curve indicate mixing proportions. *NSB*: North Star Basalt samples; *MAB*: Mount Ada Basalt samples.

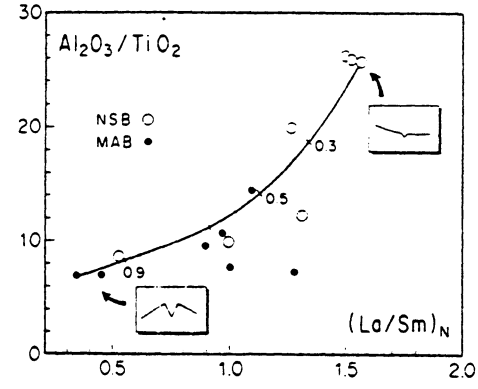

Fig. 7. Al_2O_3/TiO_2 vs. $(La/Sm)_N$ plot. As in Fig. 6, the mixing curve is obtained using samples 34F and 26B as end-members.

of the 2700 Ma old Kambalda greenstone belt of the Yilgarn Block, Western Australia, with respect to their LREE enrichment [7,22]. The Hangingwall Basalts are believed to have formed by contamination of LREE-depleted komatiitic melt by older continental crust and their enrichment in LREE is considered irrelevant to the mantle source characteristics [22]. In view of their identical REE distribution patterns, the NSB and MAB LREE-enriched basalts might be thought to have a similar origin. However, they are found in close association with komatiitic rocks (MgO contents up to 30%) which also have LREE-enriched patterns identical to those of Fig. 5a [23]. Furthermore, the LREE-depleted komatiites of the Talga-Talga Subgroup are also depleted in HREE (Fig. 5c). Crustal rocks (granitoids and sediments) are known to have strongly fractionated HREE patterns and their average $(Gd/Yb)_N$ ratio has been estimated to be about 1.6 [24]. Thus, contamination of LREE-HREE-depleted komatiites should result in basalts with high $(Gd/Yb)_N$ ratios. Since this is not the case with the NSB and MAB basalts it is more likely that their LREE enrichment reflects mantle source characteristics.

5.3. Depleted to flat HREE patterns; depleted to enriched LREE patterns

All the remaining samples are included in this category: two MAB high-Mg basalts; two MAB tholeiitic basalts and one NSB tholeiitic basalt (Fig. 5b). These rocks have chemical characteristics intermediate between the two groups discussed above (cf. Fig. 5a, c; Table 3).

The origin of this intermediate group of rocks may be revealed by the relationships between their MgO and trace element contents. For example, for samples 92, 30 and 47D the decrease in MgO content is accompanied by a flattening of HREE patterns. This cannot be explained by fractional crystallization or by partial melting processes. Since for basic-ultrabasic suites the partition coefficients increase gradually from Gd to Lu, a decrease in MgO should result in an increase in the slope of the HREE. For this reason the main cause of chemical variations may have been mixing of two geochemically distinct components. One component (A) may have been depleted in both LREE and HREE, similar to the MAB komatiites of Fig. 5c, whilst the other (B) may have been enriched in LREE with flat HREE patterns, similar to the MAB and NSB LREE-enriched tholeiites of Fig. 5a. This interpretation is supported by Fig. 6 which presents a plot of $(Gd/Yb)_N$ against $(La/Sm)_N$ for all NSB and MAB basic-ultrabasic volcanics. Also plotted is a mixing curve calculated from end-members (A) LREE-HREE-depleted komatiite 34F and (B) LREE-enriched tholeiite 26B. A reasonably good fit is obtained between the analytical data and the calculated mixing curve.

However, while a mixing model explains the REE distribution patterns of this group of rocks it does not account for all the other chemical variations. This point is illustrated in Fig. 7 in which Al_2O_3/TiO_2 ratios have been plotted against $(La/Sm)_N$ ratios. In this plot the fit between analytical data and calculated mixing curve is far from good. Three samples (55C, 17A and 56A) plot well below the mixing curve. Two of these samples (56A and 17A) belong to the REE-intermediate group of lavas, whereas 55C comes from the LREE-enriched group. The three samples have very high TiO_2 contents (up to 2%; Table 3) resulting in anomalously low Al_2O_3/TiO_2 ratios. The high TiO_2 contents may indicate accumulation of Ti-rich phases through fractional crystallization.

5.4. Summary of geochemical data and petrogenetic considerations

From the preceding description of REE patterns in the NSB and MAB it appears that:

(1) At least two chemically distinct sources were involved in the production of the basic-ultrabasic volcanics of the Talga-Talga Subgroup.

(2) A mixing process is required to explain the chemical variations observed among these volcanics.

One source was clearly LREE and HREE-depleted mantle. The other was either LREE-enriched/HREE-flat mantle (preferred) or HREE-flat mantle mixed with older continental crust. Depending on the nature of the LREE-enriched source, mixing may have operated either (a) directly between mantle sources, (b) between mantle partial melting products within magma chambers or (c) during magma ascent and eruption.

6. Discussion of Sm-Nd isotopic data

6.1. Interpretation of age data

The new and stratigraphically consistent age data of 3712 ± 98 Ma for the Talga-Talga Subgroup is about 150 Ma older than that reported previously by Hamilton et al. [1,2]. Fig. 4 indicates that the date discrepancy probably arises from the combination by Hamilton et al. [1] of felsic samples with rocks of basic and ultrabasic composition. From trace element data, Jahn et al. [3] have argued that the dacitic-andesitic (felsic) volcanics of the Talga-Talga Subgroup could not have been derived by fractional crystallization of LREE-depleted komatiitic or basaltic parental magmas or by partial melting of LREE-depleted basic-ultrabasic sources. The low $^{147}Sm/^{144}Nd$ ratios of the felsic volcanics (Fig. 4) imply highly fractionated LREE patterns. REE modelling shows that these volcanics, whose compositions are similar to the common Archaean TTG (tonalite-trondjhemite-granodiorite) suite, were likely to have been formed by partial melting of LREE-enriched basic sources [3,25–27]. Consequently, their genetic linkage with the LREE-depleted ultrabasic rocks of the NSB and MAB is problematical. The mafic and felsic rock-types could have had significantly different initial $^{143}Nd/^{144}Nd$ ratios and their combined treatment in isochron calculation might lead to an incorrect age. Following this reasoning, the 3712 ± 98 Ma isochron date might represent a more correct age for the eruption of the Talga-Talga Subgroup. We take another view and suggest that

the true (eruptive) age of the Talga-Talga Subgroup is around 3500 Ma, and not as implied above at 3700 Ma. Here are the reasons:

(1) As argued earlier on the basis of major and trace element data the NSB and MAB basic-ultrabasic volcanics were likely derived from chemically distinct mantle sources. Geochemical modelling has suggested that mixing of these heterogeneous sources or their partial melts may explain the chemical compositions of the REE-intermediate lavas. Thus the apparent isochron relationship shown in Fig. 3 may be interpreted in term of a mixing line whose geochronological significance cannot be uniquely determined and depends on the timing of source differentiation. If the differentiation took place shortly before mixing and magmatic eruption (less than 100 Ma), then, despite the non-cogenetic relationship, the rocks could have had identical initial $^{143}Nd/^{144}Nd$ ratios. In this case the linear correlation of Fig. 3 would be an isochron dating the eruption of the Talga-Talga Subgroup. In contrast, if chemical fractionation of sources occurred long (> 100 Ma) before mixing, then the LREE-depleted source should have a higher $^{143}Nd^{144}Nd$ ratio that the LREE-enriched source. In this case the mixing of these two isotopically distinct reservoirs would have created an initial positive slope in the isochron diagram and the linear array as shown in Fig. 3 would yield an age too old for the Talga-Talga Subgroup volcanism.

(2) Two instances have been recently documented in which whole-rock Sm-Nd isochron ages have been shown to exceed the age of the dated rock suites. The first case relates to komatiites and tholeiites from Newton Township, Canada, where the Sm-Nd isochron method gave a date of 2826 ± 64 Ma, whereas the zircon U-Pb data for a dacite sample coming from an underlying stratum yielded an age of 2697 ± 1.1 Ma [28]. The second instance involves a komatiitic-tholeiitic suite from Kambalda, Western Australia, which gave a Sm-Nd whole-rock isochron date of 3230 ± 120 Ma, whereas the U-Pb method on zircon indicated an age not exceeding 2743 Ma [7,29]. In both instances the age discrepancies have been used to suggest that the apparent Sm-Nd isochrons may have resulted from mixing between two components having different initial $^{143}Nd/^{144}Nd$ ratios [7,22,28].

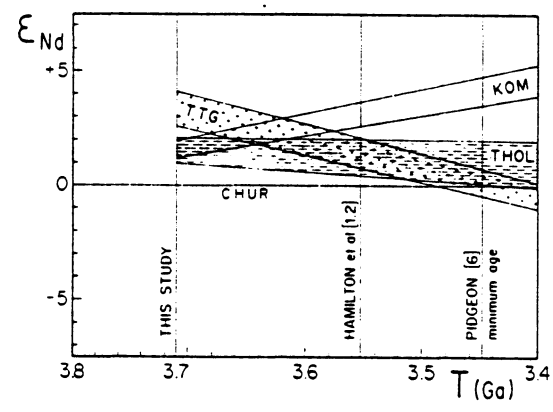

Fig. 8. $\epsilon_{Nd}(T)$ vs. time plot showing isotopic evolution in the three dominant rock types of the Talga-Talga Subgroup: LREE-depleted komatiites (*KOM*); LREE-enriched tholeiites (*THOL*); and LREE-enriched felsic volcanics (*TTG*). Data source: this study and [1–3].

(3) A serious difficulty arises if the 3712 ± 98 Ma date is interpreted as the eruption age of the Talga-Talga Subgroup, for the felsic volcanics would have derived from sources having $\epsilon_{Nd}(T)$ values higher that those of the basic-ultrabasic suites which include strongly LREE-depleted komatiites. This is illustrated by Fig. 8 in which the isotopic evolution lines of the three dominant rock types of the Talga-Talga Subgroup have been plotted, i.e.: (a) the strongly LREE-depleted komatiites; (b) the LREE-enriched tholeiitic basalts; and (c) the strongly LREE-enriched felsic volcanics. Also shown in Fig. 8 are: (a) the 3450 ± 16 Ma minimum age of Pidgeon [6]; (b) the 3540 ± 30 Ma date of Hamilton et al. [1,2]; and (c) the 3712 ± 98 Ma date obtained by us. The felsic and basic-ultrabasic suites constitute intimately intercalated volcanic rocks (Fig. 2) which are believed to have erupted nearly contemporanously [5]. If the date of 3712 Ma is taken as the primary age for the Talga-Talga Subgroup, the $\epsilon_{Nd}(T)$ values for the felsic volcanics would range from +3.4 to +4.2, whereas those for the basic-ultrabasic suite would show a lower range from +1.4 to +2.0. Such a situation conflicts with the geochemical arguments that the felsic volcanics were derived by partial melting of LREE-enriched basic precursors [3]. Furthermore, it is observed that in contemporaneous volcanic association, the variation of $\epsilon_{Nd}(T)$ values seems to correlate with the Sm/Nd ratios of the rocks. This applies to the Archean [7,28] as well as the Proterozoic rocks

[30–33]. The present Pilbara case gives an opposite scenario if 3712 Ma is taken as the eruption age.

(4) The paradoxical situation depicted in Fig. 8 may be resolved if the LREE-enriched basic precursors of the felsic volcanics were originally derived from LREE-depleted mantle and were remelted within a reasonably short time span to produce the felsic volcanics about 3700 Ma ago. But this would encounter a serious geochemical modelling problem. A more satisfactory explanation could be reached if a younger age in the range 3550–3450 Ma was assumed for the eruption of the Talga-Talga Subgroup. In this case the obstacle imposed by the $\epsilon_{Nd}(T)$ argument would be easily removed.

(5) The MAB and NSB LREE-enriched tholeiites may have been the basic precursors of the felsic volcanics. If so the date of 3517 ± 80 Ma obtained from all the available data (including felsic rocks) except the four LREE-depleted basic-ultrabasic rocks could be a meaningful age for the eruption of the Talga-Talga Subgroup. Yet, this age is younger than the 3712 ± 98 Ma date defined by the basic-ultrabasic suite.

In conclusion, we prefer to regard the age of eruption of the Talga-Talga Subgroup as around 3500 Ma ago. At the time of eruption the basic-ultrabasic lavas had a range in $\epsilon_{Nd}(T)$ and the Sm-Nd linear array they define is a mixing line giving an age too old for the emplacement of the Subgroup.

6.2. Isotopic heterogeneity in the early Archean mantle

Accepting a 3500 Ma eruption age we can calculate the $\epsilon_{Nd}(T)$ value of each Talga-Talga Subgroup volcanic rock. They range from +3.2 to +4.3 for the LREE-depleted komatiites; from +0.6 to +1.8 for the LREE-enriched tholeiites; and from 0 to +1.5 for the strongly LREE-enriched felsic volcanics (Fig. 8, Table 2). Such a variation (0 to +4.3) clearly suggests the existence of at least two isotopically distinct sources for the entire Talga-Talga Subgroup volcanic rocks. This conclusion is independent of the age consideration. Should the date of 3712 ± 98 Ma be proved correct for the eruption age of the Subgroup, a similar range (+1.4 to +4.2) would be obtained, the important difference being that, in this case, the highest $\epsilon_{Nd}(T)$ values would not be found in the LREE-depleted komatiites, but in the felsic volcanics (Fig. 8).

The highly positive $\epsilon_{Nd}(T)$ values (+3.2 to +4.3) obtained for the Talga-Talga Subgroup komatiites are comparable with the +2.7 to +3.3 values found in the 3500 Ma old Coazhung amphibolites of China [34,35]. They provide additional evidence for the existence of ancient depleted reservoirs in the mantle ca. 3500 Ma ago. In contrast, they differ from the near zero values found in the coeval komatiites and basalts from the Onverwacht Group of the Barberton greenstone belt of South Africa [2]. Many of the Onverwacht Group komatiites are known to have very low Al_2O_3 content [14,16,17] and cannot be interpreted as contaminated lavas from a depleted source with high $\epsilon_{Nd}(T)$ value. Compared with the Onverwacht Group data, the new Talga-Talga Subgroup results also provide evidence for isotopic heterogeneity in the early Archean mantle.

The lower $\epsilon_{Nd}(T)$ values found in the LREE-enriched tholeiites and in the felsic volcanics (0 to +1.8) reflect the less depleted nature of their source region., From consideration of major and trace element data, the LREE enrichment of the NSB and MAB tholeiitic basalts is not believed to result from crustal assimilation. Thus, the data may indicate that the mantle source of the Talga-Talga Subgroup volcanism was itself isotopically heterogeneous.

Acknowledgements

We thank N.T. Arndt for his review of an earlier version of this paper. The manuscript also benefited by comments and suggestions from S. Moorbath and two other anonymous reviewers. We are also very grateful to J. Cornichet, M. Morin, J. Macé and J. Bernard-Griffiths for their assistance in chemical separations and/or in spike calibration. We thank M.H. Fichet who typed the manuscript. This work was funded in part under contract No. 15-48 of the INSU (France) in connection with ATP "Transferts". A.Y.G. publishes with the permission of the director of the Bureau of Mineral Resources, Australia. R.D. and A.H.H. publish with the permission of the director of the Geological Survey of Western Australia.

References

1 P.J. Hamilton, N.M. Evensen, R.K. O'Nions, A.Y. Glikson and A.H. Hickkman, Sm-Nd dating of the North Star Basalt, Warrawoona Group, Pilbara Block, Western Australia, Geol. Soc. Aust. Spec. Publ. 7, 187–192, 1981.

2 P.J. Hamilton, R.K. O'Nions, D. Bridgwater and A. Nutman, Sm-Nd studies of Archaean metasediments and metavolcanics from West Greenland and their implications for the Earth's early history, Earth Planet. Sci. Lett. 62, 263–272, 1983.

3 B.M. Jahn, A.Y. Glikson, J.J. Peucat and A.H. Hickman, REE geochemistry of Archean silicic volcanics and granitoids from the Pilbara Block, Western Australia: implications for the early crustal evolution, Geochim. Cosmochim. Acta 45, 1633–1652, 1981.

4 A.H. Hickman, Geology of the Pilbara Block and its environs, West. Aust. Geol. Surv. Bull. 127 pp., 1983.

5 A.Y. Glikson and A.H. Hickman, Geochemistry of Archaean volcanic successions, eastern Pilbara Block, Western Australia, Aust. BMR Rec. 36, 1981.

6 R.T. Pidgeon, 3.450 M.y.-old volcanics in the Archaean layered greenstone succession of the Pilbara Block, Western Australia, Earth Planet. Sci. Lett. 37, 421–428, 1978.

7 C. Chauvel, B. Dupré and G.A. Jenner, The Sm-Nd age of Kambalda volcanics is 500 Ma too old!, Earth Planet. Sci. Lett. 74, 315–324, 1985.

8 B.M. Jahn, J. Bernard-Griffiths, R. Charlot, J. Cornichet and F. Vidal, Nd and Sr isotopic compositions and REE abundances of Cretaceous MORB (Holes 417D and 418A, Legs 51, 52 and 53), Earth Planet. Sci. Lett. 48, 171–184, 1980.

9 G.J. Wasserburg, S.B. Jacobsen, D.J. DePaolo, M.T. McCulloch and T. Wen, Precise determination of Sm/Nd ratios, Sm and Nd isotopic abundances in standard solution, Geochim. Cosmochim. Acta 45, 2311–2323, 1981.

10 D. York, Least square fitting of a straight line, Can. J. Phys. 44, 1079–1086, 1966.

11 D.J. DePaolo and G.J. Wasserburg, Inferences about magma sources and mantle structure from variations of $^{143}Nd/^{144}Nd$, Geophys. Res. Lett. 3, 743–746, 1976.

12 S.B. Jacobsen and G.J. Wasserburg, Sm-Nd isotopic evolution of chondrites, Earth Planet. Sci. Lett. 50, 139–155, 1980.

13 I.R. Fletcher and K.J.R. Rosman, Precise determination of initial ϵ_{Nd} from Sm-Nd isotopic data, Geochim. Cosmochim. Acta 46, 1983–1987, 1982.

14 B.M. Jahn, G. Gruau and A.Y. Glikson, Komatiites of the Onverwacht Group, S. Africa: REE geochemistry, Sm-Nd age and mantle evolution, Contrib. Mineral. Petrol. 80, 25–40, 1982.

15 S.S. Sun and R.W. Nesbitt, Petrogenesis of Archean ultrabasic and basic volcanics: evidence from rare earth elements, Contrib. Mineral. Petrol. 65, 301–325.

16 R.W. Nesbitt, S.S. Sun and A.C. Purvis, Komatiites: geochemistry and genesis, Can. Mineral. 17, 165–186, 1979.

17 S.S. Sun, Geochemical characteristics of Archean ultramafic and mafic rocks: implications for mantle composition and evolution, in: Archaean Geochemistry, A. Kröner et al., eds., pp. 25–46, Springer-Verlag, Berlin, 1984.

18 B.M. Jahn and S.S. Sun, Trace Element Distribution and Isotopic Composition of Archean Greenstones, in: Origin and Distribution of the Elements, L.H. Ahrens, ed., pp. 597–618, Pergamon Press, Oxford, 1979.

19 N.T. Arndt, Komatiites: a dirty window to the Archean mantle, Terra Cognita 6, 59–66, 1986.

20 B.M. Jahn, Mid-ocean ridge or marginal basin origin of the East Taiwan Ophiolite: chemical and isotopic evidence, Contrib. Mineral. Petrol. 92, 194–206, 1986.

21 B.M. Jahn, B. Auvray, S. Blais, R. Capdevila, J. Cornichet and J. Hameurt, Trace element geochemistry and petrogenesis of Finnish greenstone belts, J. Petrol. 21, 201–240, 1980.

22 N.T. Arndt and G. Jenner, Crustally contaminated komatiites and basalts from Kambalda, Western Australia, Chem. Geol. 56, 229–255, 1986.

23 A.Y. Glikson, C. Pride, B.M. Jahn, R. Davy and A.H. Hickman, RE and HFS (Ti, Zr, Nb, P, Y) element evolution of Archaean mafic-ultramafic volcanic suites, Pilbara Block, Western Australia, Aust. BMR Rec. 6, 1986.

24 S.R. Taylor and S.M. McLennan, The composition and evolution of continental crust: rare earth evidence from sedimentary rocks, Philos. Trans. R. Soc. London, Ser. A, 301, 381–399, 1981.

25 A.Y. Glikson, Early Precambrian tonalite-trondjhemite sialic nuclei, Earth Sci. Rev. 15, 1–73, 1979.

26 H. Martin, Evolution in composition of granitic rocks controlled by time-dependent changes in petrogenetic processes: examples from the Archaean of Eastern Finland, Precambrian Res., in press, 1987.

27 B.M. Jahn and Z.Q. Zhang, Radiometric ages (Rb-Sr, Sm-Nd, U-Pb) and REE geochemistry of archaean granulite gneisses from Eastern Hebei Province, China, in: Archaean Geochemistry, A. Kröner et al., eds., pp. 204–234, Springer-Verlag, Berlin, 1984.

28 A. Cattell, T.E. Krogh and N.T. Arndt, Conflicting Sm-Nd whole rock and U-Pb zircon ages for archean lavas from Newton Township, Abitibi Belt, Ontario, Earth Planet. Sci. Lett. 70, 280–290, 1984.

29 W. Compston, I.S. Williams, I.H. Campbell and J.J. Gresham, Zircon xenocrysts from the Kambalda volcanics: age constraints and direct evidence for older continental crust below the Kambalda-Norseman greenstones, Earth Planet. Sci. Lett. 76, 299–311, 1986.

30 P.J. Patchett and O. Kouvo, Origin of continental crust of 1.9–1.7 Ga age: Nd isotopes and U-Pb zircon ages in the Svecokarelian terrain of South Finland, Contrib. Mineral. Petrol. 92, 1–12, 1986.

31 P.J. Patchett and N.T. Arndt, Nd isotopes and tectonics of 1.9–1.7 Ga crustal genesis, Earth Planet. Sci. Lett. 78, 329–338, 1986.

32 N.T. Arndt, G.E. Brugmann, K. Lehnert, B.W. Chappel and C. Chauvel, Geochemistry petrogenesis and tectonic environment of Circum-Superior Belt basalts, Canada, in press.

33 H. Huhma, Sm-Nd, U-Pb and Pb-Pb isotopic evidence for the origin of the Early proterozoic Svecokarelian crust of Finland, Bull. Geol. Surv. Finland 337, 1986.

34 X. Huang and D.J. DePaolo, Sm-Nd isotope study of early

116

Archaean rocks, Qianan, Hebei Province, China, Geochim. Cosmochim. Acta 50, 625–631, 1986.

35 B.M. Jahn, B. Auvray, J. Cornichet, Y.L. Bai, Q.H. Shen and D.Y. Liu, 3.5 Ga old amphibolites from eastern Hebei Province, China: field occurrence, petrography, Sm-Nd isochron age and REE geochemistry, Precambrian Res. 34, 311–346, 1987.

Contrib Mineral Petrol (1990) 104:27–34

Contributions to Mineralogy and Petrology

Anomalous Sm–Nd ages for the early Archean Onverwacht Group Volcanics

Significance and petrogenetic implications

G. Gruau [1], C. Chauvel [2], and B.M. Jahn [1]

[1] CAESS, CNRS, Institut de Géologie, Université de Rennes, F-35042 Rennes Cedex, France
[2] Max-Planck-Institut für Chemie, Postfach 3060, D-6500 Mainz, Federal Republic of Germany

Abstract. New Sm–Nd isotopic data for eight samples of basalt and komatiite from the Tjakastad Subgroup (lower Onverwacht Group) of the Barberton Greenstone Belt (BGB) of the Kaapvaal craton in southern Africa are reported. They give new constraints on the interpretation of Sm–Nd ages for the Subgroup and highlight the petrogenesis of Tjakastad volcanics. Although Sm–Nd isotopic data earlier reported for volcanic rocks from the Tjakastad Subgroup yielded an "isochron" age of 3526±48 Ma, the new results give a much younger "isochron" date of 3269±84 Ma. The 3526±48 Ma "isochron" age has been obtained in combining samples ranging in composition from felsic volcanics to ultrabasic komatiites and is thus considered suspect with regard to the pre-requisite of geochronology that all the studied rocks must have had identical initial isotopic compositions. The new "isochron" date of 3269±84 Ma has been obtained in combining samples solely of basic/ultrabasic composition. It might thus represent a more correct age for the eruption of the Tjakastad Subgroup volcanism. In fact, owing to the potential problem of source heterogeneity and also in the light of geochronological and geochemical arguments we show that this date also has little chance to have any strict chronological meaning. Most likely, the Tjakastad volcanics were formed 3450 Ma ago. Also most likely, their source rocks were isotopically heterogeneous and the 3530 Ma and 3270 Ma linear arrays are not true but apparent "isochrons". Based on the calculated ε_{Nd} (3450) values and other geochemical arguments, we show that three possible sources might have been involved: depleted mantle, primitive mantle and older continental crust.

Introduction

One of the most controversial issues in dealing with Archean geochronolgy has always been the interpretation of Sm–Nd "isochron" ages and corresponding $\varepsilon_{Nd}(T)$ values obtained for greenstone successions. The controversy arises owing to the fact that, in order to get statistically more precise ages (and initial $^{143}Nd/^{144}Nd$), samples of maximum compositional variation and hence possibly of diverse origin have been often preferentially included in isochron construction (e.g. Hamilton et al. 1977, 1979, 1981; McCulloch and Compston 1981). This approach neglects the prerequisite of the isochron technique, namely: all analysed samples must have been formed simultaneously from sources with identical initial isotopic compositions. Samples with a wide range of Sm/Nd ratios could have been derived from multiple sources and thus might not satisfy this prerequisite leading in turn to the possibility of incorrect ages and initial ε_{Nd} values. A few such examples have been reported for the Kambalda greenstones of Western Australia (Chauvel et al. 1985; Compston et al. 1986), the komatiite-tholeiite suite of Newton Township, Canada (Cattell et al. 1984), and for the Usushwana gabbroic suite of Swaziland (Hegner et al. 1984). In these cases, the apparent Sm–Nd "isochrons" were thought to result from the mixing of two components with different initial $^{143}Nd/^{144}Nd$ ratios and have no chronological meaning.

The Tjakastad Subgroup of the Onverwacht Group is the lowermost stratigraphic subdivision of the Barberton Greenstone Belt (BGB) of the Kaapvaal craton from southern Africa and consists dominantly of interlayered komatiite and tholeiitic lavas together with subordinate felsic volcanics and intrusives (Viljoen and Viljoen 1969; Viljoen et al. 1983). The Tjakastad Subgroup has already been subject to two whole-rock Sm–Nd isotopic studies. Hamilton et al. (1979, 1983) obtained a whole-rock Sm–Nd "isochron" from the analysis of 10 samples ranging in composition from felsic intrusives/volcanics to ultrabasic komatiites ($^{147}Sm/^{144}Nd$ ratios from 0.1036 to 0.2051). This "isochron" gave a precise date of 3526±48 (2σ) Ma with corresponding $\varepsilon_{Nd}(T)$ of +0.7±0.3 (2σ). Jahn et al. (1982) later reported Sm–Nd isotopic data for 5 samples of basalt and komatiite and obtained a similar but less precise age of 3560±230 (2σ) Ma ($\varepsilon_{Nd}(T) = +3.3 \pm 4.5$ (2σ)). These Sm–Nd dates of 3560–3530 Ma have long been considered as the best estimate for the eruption time of the Tjakastad Subgroup volcanism. However, Kröner and Todt (1988) recently reported $^{207}Pb/^{206}Pb$ isotopic data on zircons based on single grain evaporation and coming from a) a metaquartzite band underlying serpentinized metavolcanics of the Onverwacht Group in north-west Swaziland, and b) a felsic lava flow from the overlying Hooggenoeg Formation (Geluk Subgroup). The data yielded ages of 3451±15 ($2\sigma_m$) Ma and 3438±6 ($2\sigma_m$) Ma, respectively. On this basis, Kröner and Todt (1988) have argued that the Tjakastad Subgroup did not erupt 3460–3530 Ma ago as indicated by the Sm–Nd data but in a short period between 3450 and 3440 Ma ago.

Offprint requests to: G. Gruau

Here we report new Sm–Nd isotopic results for samples of the Tjakastad Subgroup. In order to minimise potential problems that may result from distinct sources we have restricted our analyses to samples of basic-ultrabasic composition. The main aims of this study are: (a) to check the validity of the published Sm–Nd ages; (b) to gain new insight in the interpretation of whole-rock Sm–Nd "isochrons" on Archean greenstones; and (c) to establish $\varepsilon_{Nd}(T)$ values for the early Archean mantle beneath the Barberton region.

Tjakastad Subgroup

Regional geological setting and stratigraphic sub-divisions

The Barberton Greenstone Belt (BGB) is part of the Archean Kaapvaal craton in southern Africa (Fig. 1). It consists of a complex assortment of low-grade metamorphic rocks (greenschist to lower-amphibolite facies) including basic/ultrabasic lava flows (with spinifex textured komatiites), differentiated ultrabasic bodies, metagabbros, basic dykes, intermediate lavas, felsic volcanics/intrusives and various types of sediments (Viljoen and Viljoen 1969; Anhaeusser 1973, 1983). The supracrustal succession is known as the Swaziland Supergroup or Barberton Sequence and has been divided into several groups and subgroups. In ascending stratigraphic order, these are (1) the Tjakastad and Geluk Subgroups – also collectively known as the Onverwacht Group or as the lower ultramafic unit (LUU), and the mafic to felsic unit (MFU), respectively, and (2) the Fig Tree and (3) Moodies Groups (Fig. 1). Both the Tjakastad and Geluk Subgroups are further subdivided into three formations. From base to top and for the Tjakastad Subgroup these are the Sandspruit, Theespruit and Komati Formations. For the Geluk Subgroup these are the Hooggenoeg, Kromberg and Swartkopie Formations.

Type locality and main lithologies

The type section of the Tjakastad Subgroup lies in the southern part of the BGB about 20–30 km east of Baadplaas (Area A in Fig. 1). Virtually all published geochemical and geochronological works (including this study) on the Subgroup are based on samples collected from this area. Because most primary mineral assemblages have been obliterated as a result of alteration and metamorphism, recognition of the Tjakastad Subgroup constituents is mainly based on textural and chemical criteria. At the type locality, the main rock-types are: (a) fine-grained massive and coarse-grained spinifex-textured komatiite flows (MgO > 18% on anhydrous base) and (b) pillowed, fine-grained massive and coarse-grained spinifex textured komatiitic basalt flows (MgO = 18-8%). Subordinate lithologies include pillowed and massive tholeiitic basalts, felsic tuffs, few Na-rich intrusive porphyries and minor sedimentary layers. Komatiites and komatiitic basalts dominate in the Sandspruit and Komati Formations, whereas the Theespruit Formation consists mainly of interlayered komatiite flows and felsic tuffs together with rare thin bands of chert, metapelite and sandstone (Viljoen and Viljoen 1969; Viljoen et al. 1983; De Wit et al. 1983). Note that tectonic slivers of multiply-deformed orthogneiss possibly related to the Ancient Gneiss Complex of Swaziland have been reported in the type section of the Theespruit Formation (De Wit et al. 1983).

Age data

Because the greenstone-granite terrain of the Barberton Mountain Land has been commonly taken as a classic example of Archean crustal development, considerable effort has been unfolded to establish a chronological order of geological events in the region. Available radiometric age data for the Tjakastad Subgroup are summarised in Table 1. It is clear that the oldest dates have been obtained by the whole-rock Sm–Nd method.

Relationships with adjoining granite-gneiss terrains and tectonic implications

Like elsewhere in the Swaziland Supergroup, the Tjakastad Subgroup was deformed into tight, upright synforms during the intrusion of several generations of tonalite-trondhjemite-granodiorite (TTG) domed batholiths (Tegtmeyer and Krõner 1987; Fig. 1). Intrusion ages of these plutons are in the range 3225–3180 Ma (Barton et al. 1983; Barton 1983; Tegtmeyer and Krõner 1987).

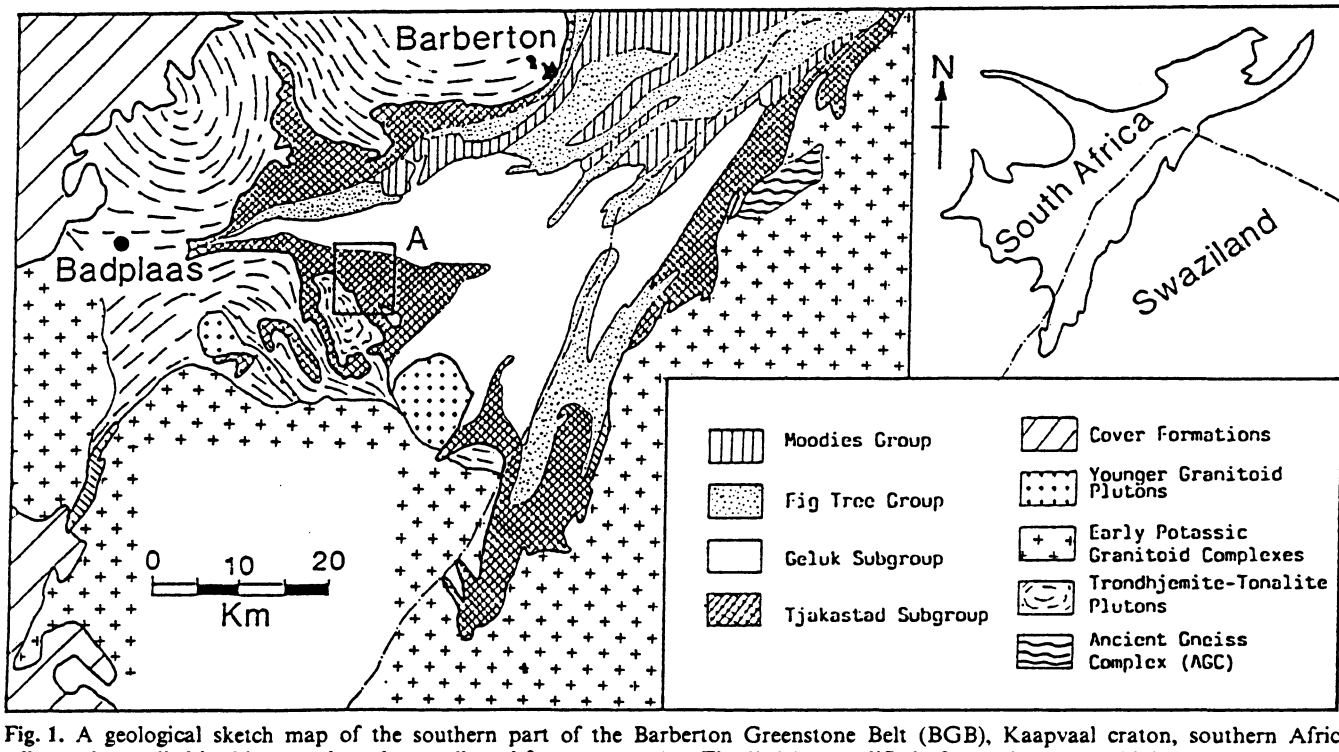

Fig. 1. A geological sketch map of the southern part of the Barberton Greenstone Belt (BGB), Kaapvaal craton, southern Africa. All samples studied in this paper have been collected from Area A (see Fig. 2). Map modified after Anhaeusser (1983)

Table 1. Summary of available age data for the lowermost units of the Barberton Greenstone Belt (BGB), Southern Africa

Method	Age (Ma)	$\varepsilon_{Nd(T)}$, I_{Sr}	Author's interpretation	References
Hooggenoeg Formation				
Flesic lava flows				
$^{207}Pb/^{206}Pb$ age; single zircon evaporation	3438 ± 6	–	Age of eruption; minimum age for the Tjakastad Subgroup	Kröner and Todt (1988)
Tjakastad Subgroup				
Whole-rock Sm – Nd isochron	3526 ± 48	$+0.7 \pm 0.3$	Age of eruption of the Tjakastad Subgroup	Hamilton et al. (1979, 1983)
Whole-rock Sm – Nd isochron	3560 ± 230	$+3.3 \pm 4.5$	Age of eruption of the Tjakastad Subgroup	Jahn et al. (1982)
$^{40}Ar/^{39}Ar$ age	3450 ± 30[b]	–	Age of regional lowgrade metamorphism	Lopez-Martinez et al. (1984)
Pb/Pb whole-rock isochron	3460 ± 70	–	Age of eruption/age of low-grade regional metamorphism (?)	Brévart et al. (1986)
Rb/Sr internal isochron	3430 ± 200[a]	0.70058 ± 5[a]	Age of low-grade regional metamorphism	Jahn and Shih (1974)
Underlying metaquartzite band				
$^{207}Pb/^{206}Pb$ age single zircon-evaporation	3451 ± 15	–	Maximum age for the eruption of the Tjakastad Subgroup volcanism	Kröner and Todt (1988)

[a] Recalculated using $\lambda Rb = 0.0142\ Ga^{-1}$, [b] Average of 4 determinations

Geochemical and petrological modelling studies have concluded that these intrusive batholiths were derived by melting of short-lived LREE-enriched basic precursors (Barton 1983; Glikson and Jahn 1985).

Other rocks of TTG compositions occur in the high-grade and multiple-deformed terrain of the Ancient Gneiss Complex (AGC) of Swaziland (Hunter 1974; Hunter et al. 1984; Fig. 1). Ion-probe U – Pb data for single zircons from the AGC have indicated ages as old as 3644 ± 4 (2σ) Ma (Compston and Kröner 1988). Part of the AGC thus predates (by at least 100 Ma, Table 1) the Tjakastad Subgroup volcanism. This, together with the fact that tectonic slivers of AGC occur in the Theespruit Formation (De Wit et al. 1983), has been used to suggest that the AGC could have been a sialic nucleus on which, or close to which, the BGB volcanics were deposited (Compston and Kröner 1988; Kröner et al. 1988; Kröner and Todt 1988). According to Kröner and Todt (1988),

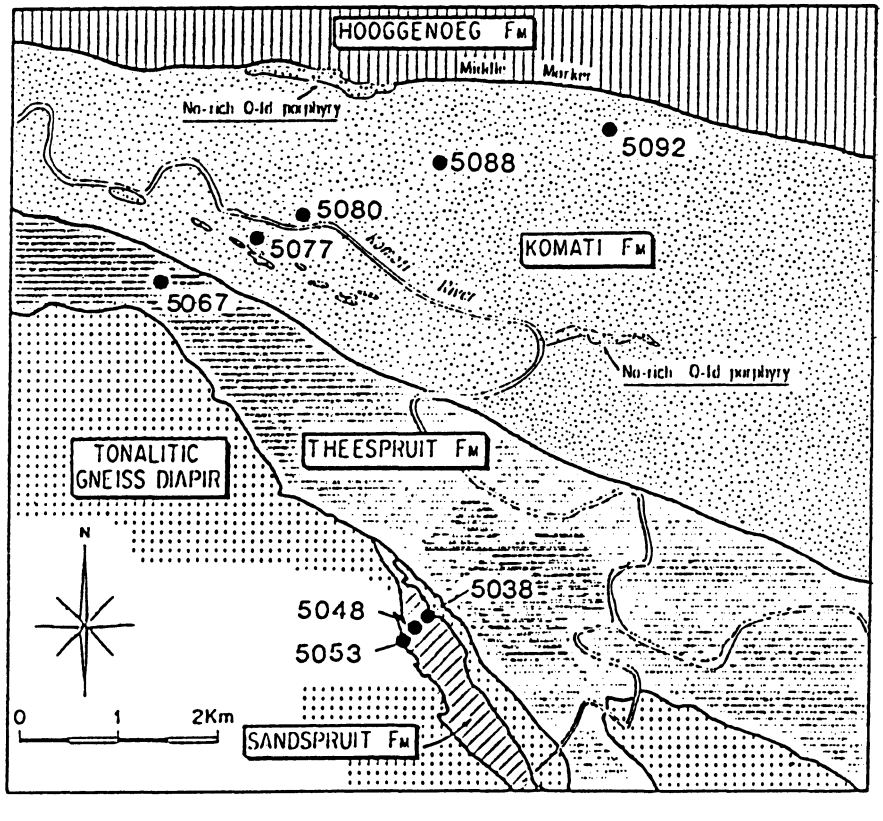

Fig. 2. Simplified geological map showing the sampling localities (= Area *A* of Fig. 1).

the BGB would have evolved either in a marginal basin, intracontinental rift or continental margin setting.

Selection of samples and analytical techniques

The following samples were selected for the renewed Sm–Nd isotopic investigation: (a) one komatiite (MgO > 18%; sample # 5048) and two basalts (MgO < 8%; samples # 5038 and 5053) from the Sandspruit Formation; (b) one high-Mg basalt (18% > MgO > 8%; sample # 5067) from the Theespruit Formation; and (c) three high-Mg basalts (samples # 5077, 5080, and 5092) and one basalt (sample # 5088) from the Komati Formation. Among these samples, three (5038, 5067, and 5092) are part of the earlier Sm–Nd isotopic investigation by Jahn et al. (1982). The sampling localities are given in Figs. 1 and 2. Petrographic description and major and trace element data can be found in Jahn et al. (1982). REE distribution patterns for the eight analysed samples are given in Fig. 3.

Nd and Sm isotopic analyses were carried out at the Max Planck Institut für Chemie, Mainz, following the method described by Chauvel et al. (1985). All samples (≈ 100 mg) were dissolved in Teflon bombs with HF-HNO_3-$HClO_4$ solution and subsequently redissolved after evaporation in 6N HCl. After aliquoting the solutions, a mixed ^{149}Sm–^{145}Nd spike was added to the isotopic dilution (ID) fractions. Nd isotopic compositions (IC) were determined from the unspiked aliquots and the chemical separation of Nd was identical to the method described by White and Patchett (1984). Blanks for Nd and Sm were lower than 100 and 30 pg, respectively.

Isotopic ratios were measured on a Finnigan MAT 261 mass spectrometer. $^{143}Nd/^{144}Nd$ measured ratios were normalized to $^{146}Nd/^{144}Nd = 0.7219$. Isotopic analyses of BCR-1 and La Jolla Nd standard by Chauvel et al. (1985) have indicated $^{143}Nd/^{144}Nd = 0.512661 \pm 24$ ($2\sigma_m$) and $^{143}Nd/^{144}Nd = 0.511847 \pm 21$ ($2\sigma_m$), respectively. Effects of fractionation during Sm and Nd ID runs were eliminated by normalizing to $^{147}Sm/^{152}Sm$ and $^{146}Nd/^{144}Nd$.

Regression analyses were carried out using the method of York (1969). The error inputs were 0.2% for $^{147}Sm/^{144}Nd$ and $2\sigma_m$ obtained for individual runs for $^{143}Nd/^{144}Nd$. All errors on ages and initial isotopic ratios are quoted at 2σ or 95% confidence level. Initial $^{143}Nd/^{144}Nd$ (I_{Nd}) ratios are also quoted throughout the text in the ε_{Nd} notation of DePaolo and Wasserburg (1976). The $^{147}Sm/^{144}Nd$ and $^{143}Nd/^{144}Nd$ ratios for the chondritic uniform reservoir (CHUR) are those determined by Jacobsen and Wasserburg (1980). The errors of the isochron initial ε_{Nd} values were calculated using the method of Fletcher and Rosman (1982). The decay constant of ^{147}Sm is 0.00654 Ga^{-1}.

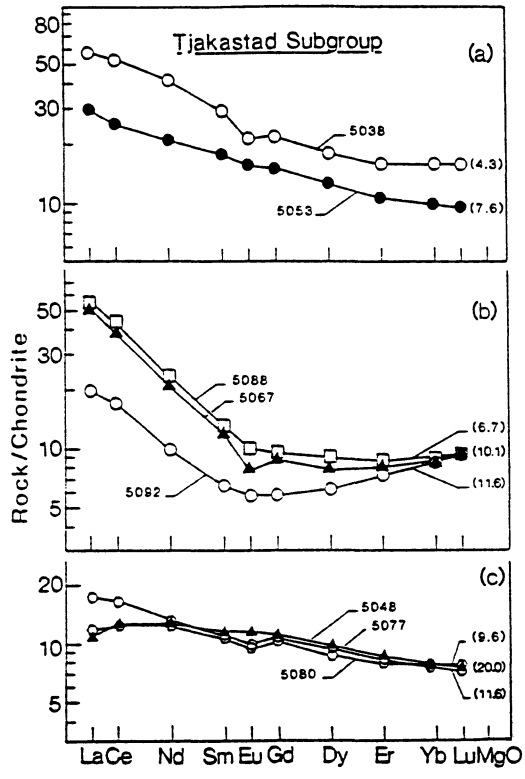

Fig. 3a–c. Chondrite-normalized REE patterns for the Tjakastad Subgroup basic-ultrabasic volcanic suite. The samples have been grouped according to their geochemical affinities: a LREE enriched/HREE depleted basalts; b LREE enriched/HREE enriched to flat basalts and high-Mg basalts; c LREE flat to slightly enriched/HREE depleted komatiite and high-Mg basalts. MgO contents (in wt%) are given on anhydrous basis. Origin of samples – 5038, 5053 and 5048: Sandspruit Formation; 5067: Theespruit Formation; 5077, 5080, 5088 and 5092: Komati Formation (see Fig. 2). Data source: Jahn et al. (1982)

Table 2. Sm–Nd isotopic data for Tjakastad Subgroup basic/ultrabasic volcanic rocks

Sample N°	Rock type	MgO %[1]	Sm(μg/g)	Nd(μg/g)	$^{147}Sm/^{144}Nd$	$^{143}Nd/^{144}Nd$[2]	ε_{Nd} 3.45 Ga[2]
Komati Formation							
5088	bslt	6.7	2.45	12.67	0.1171	0.510889±14	+1.3±0.4
5092	HMg-b	11.6	1.18	5.40	0.1320	0.511180±13	+0.4±0.4
5080	HMg-b	9.6	2.23	7.71	0.1749	0.512143±15	0.0±0.4
5077	HMg-b	11.6	2.10	7.17	0.1775	0.512199±18	0.0±0.5
Theespruit Formation							
5067[a]	HMg-b	10.1	2.28	12.06	0.1142	0.510838±14	+1.6±0.4
5067[b]	–	–	2.36	12.48	0.1143	0.510848±14	+1.8±0.4
Sandspruit Formation							
5038[a]	bslt	4.3	4.96	21.81	0.1375	0.511137±13	−3.0±0.4
5038[b]	–	–	5.41	23.64	0.1383	0.511118±16	−3.7±0.4
5053	bslt	7.6	3.41	12.75	0.1619	0.511827±23	−0.3±0.6
5048	kom	20.0	2.28	7.55	0.1823	0.512296±18	−0.3±0.5

Kom: komatiite; *HMg-b*: high magnesian basalt; *bslt*: basalt
a and *b*: duplicate analyses on different dissolutions of the same rock powder

[1] Recalculated on an anhydrous basis; [2] errors quoted at 2σ level; ε_{Nd} 3.45 Ga $= \left[\frac{I_{Nd(s)}[3.45]}{I_{ND\ CHUR}[3.45]} - 1\right] \times 10^4$

$I_{Nd\ CHUR}[3.45] = 0.512638 - 0.1967\ (e^{\lambda T} - 1) = 0.508150$

$\lambda = 0.00654\ Ga^{-1}$

Results

The new Sm–Nd isotopic results are presented in Table 2 and further displayed on two conventional isochron diagrams in Figs. 4 (present data set alone) and 5 (combined data set including the results of Hamilton et al. (1979, 1983)). Several important points are underlined as follows:

(1) Although all samples are of basic/ultrabasic composition a large variation in $^{147}Sm/^{144}Nd$ ratios is observed. This is also manifested by the distinctly different LREE enrichment patterns shown in Fig. 3.

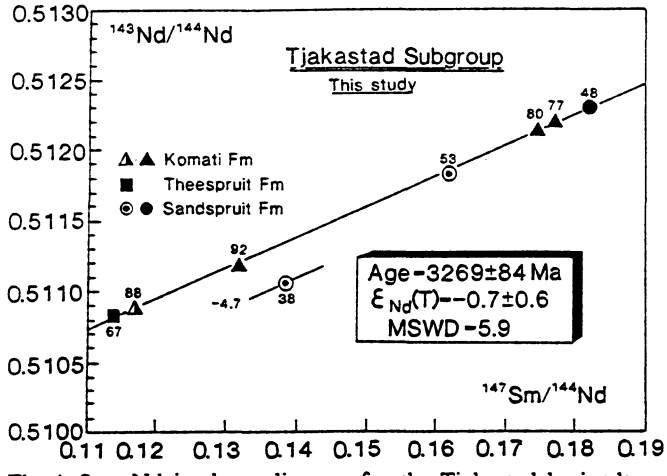

Fig. 4. Sm–Nd isochron diagram for the Tjakastad basic-ultrabasic volcanic suite. *Closed symbols*: high-Mg basalts and komatiites; *other symbols*: basalts. Samples N° 50XX have been simplified into XX. – 4.7 would be the initial ε_{Nd} value of a linear array with a 3269 Ma slope and including sample 5038

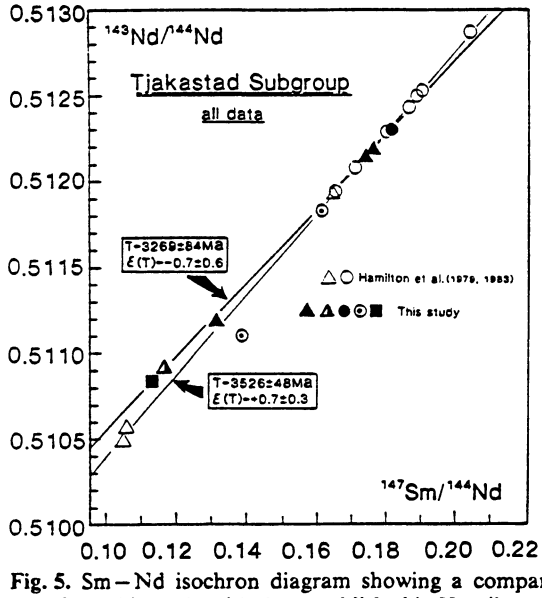

Fig. 5. Sm–Nd isochron diagram showing a comparison of the data from this study with those published in Hamilton et al. (1979). The date of 3526±48 Ma has been recalculated in multiplying the $^{147}Sm/^{144}Nd$ ratios of Hamilton et al. (1979) by 1.0055 as recommended by Hamilton et al. (1983). Likewise, the corresponding ε_{Nd} (3526) value of $+0.7\pm0.3$ has been recalculated following the method of Fletcher and Rosman (1982). Symbols: for this study, see Fig. 4; for Hamilton et al. (1979, 1983) data points: Δ felsic volcanics and intrusives; o basic to ultrabasic volcanics

(2) Duplicate analyses on different dissolutions for two samples (5067 and 5038; Table 2) have indicated that the results obtained during the course and this work were coherent and satisfactory.

(3) The new aliquots of previously analysed samples used in this study (5038, 5067, 5092) yielded the following results. For sample 5067 and 5092, $^{147}Sm/^{144}Nd$ and $^{143}Nd/^{144}Nd$ ratios in agreement with those reported earlier (Jahn et al. 1982) have been obtained. For sample 5038, the same statistical agreement has been found on the $^{147}Sm/^{144}Nd$ ratio. In contrast, some shift has been observed on the $^{143}Nd/^{144}Nd$ ratio. For an unknown reason, while Jahn et al. (1982) reported $^{143}Nd/^{144}Nd=0.511437\pm50$, we repeetedly obtained 0.511137 ± 13 and 0.511118 ± 16 (Table 2).

(4) Regression of the present analytical data except sample 5038 which lies completely off the linear correlation (Fig. 4) yielded a date of 3269 ± 84 Ma (2σ) with a corresponding ε_{Nd} (3269) value of -0.7 ± 0.6 (2σ).

(5) When the data of Hamilton et al. (1979, 1983) are compared (Fig. 5), two separate lines may be recognized: the 3526 ± 48 Ma line as obtained by Hamilton et al. (1979, 1983) and the 3269 ± 84 Ma line as defined by the present data set. It is clear that the age discrepancy between the two data sets mainly arises from the control of the samples with low $^{147}Sm/^{144}Nd$ ratios (<0.14). The samples with $^{147}Sm/^{144}Nd<0.14$ in Hamilton et al. (1979, 1983) study are felsic in composition. If they were excluded, the remaining data points including our data set (except 5038) would give an age of 3346 ± 70 Ma. Such an age is statistically indistinguishable from our date of 3269 ± 84 Ma.

Discussion

Significance of Tjakastad Subgroup whole-rock Sm–Nd data

The two dates shown in Fig. 5 are statistically different from the zircon $^{207}Pb/^{206}Pb$ age of 3451 ± 15 ($2\sigma_m$) Ma given by Krõner and Todt (1988) for the pre-Onverwacht metaquartzite band. The 3526 ± 48 (2σ) Ma date reported by Hamilton et al. (1979, 1983) is clearly too old since the Tjakastad Subgroup lavas necesseraly erupted at $T\leq3460$–3440 Ma (Table 1). The above section has shown that Hamilton et al. (1979, 1983) date is strongly influenced by the two felsic samples with very low $^{147}Sm/^{144}Nd$ (≈0.105, Fig. 5). One of the two samples is a sodic porphyry intrusive into the Komati Formation. Geochemically, sodic porphyry generally resembles Archean TTG granitic gneisses. Archean TTG gneisses are commonly thought to have been produced by remelting of LREE-enriched basaltic or amphibolitic precursors (e.g. Jahn et al. 1981; Martin 1987). The silicic magmas might thus have been formed later than the basic-ultrabasic suite and produced different (lower) initial Nd isotopic ratios. That the date by Hamilton et al. (1978, 1983) does not correspond to the true eruptive age of the Tjakastad Subgroup is therefore not surprising. Our new Sm–Nd date of 3269 ±84 Ma has been obtained in combining solely samples of basic/ultrabasic composition and is younger than the zircon $^{207}Pb/^{206}Pb$ age. It might thus represent a correct age for the eruption of the Tjakastad Subgroup volcanism. In fact, owing to the potential problem of source heterogeneity, even this date is also likely to have no real age connotation. The reasons are as follows:

(1) On the basis of REE distribution patterns and other diagnostic chemical criteria, Jahn et al. (1982) have divided the Tjakastad Subgroup basic-ultrabasic volcanic rocks into three groups: (a) LREE-enriched/HREE-depleted basalts (5038–5053; Fig. 3a); (b) strongly LREE-enriched/HREE flat to enriched basalts and high-Mg basalts (5088-5067-5092; Fig. 3b); and (c) flat to slightly LREE-enriched/HREE-depleted komatiites and high-Mg basalts (5048-5077-5080; Fig. 3c). REE distribution patterns such as those of Fig. 3c are typical of the Al-depleted Group II komatiites commonly found in early Archean terrains (Jahn et al. 1982; Gruau et al. 1987). In addition to high $(Gd/Yb)_N$ ratios, Group II komatiites are known to possess low Al_2O_3/TiO_2 (≈ 10) and high CaO/Al_2O_3 (> 0.8) ratios suggesting an important role of garnet fractionation in their petrogenesis. Current ideas suggest that garnet (marjorite) fractionation could have taken place at depth ≥ 180 Km in ascending mantle diapirs of deep origin (Arndt 1986; Othani 1989). Clearly, Group II rocks (komatiite 5048 and high-Mg basalts 5077 and 5080) may not have been derived from the same mantle domain as tholeiitic basalts 5053 and 5038. In addition, the extreme LREE enrichment of samples 5088, 5067, and 5092 (Fig. 3b) is in marked contrast to the nearly flat LREE patterns of Group II rocks (Fig. 3c). These samples were thought to have been derived from metasomatized garnet-rich mantle sources (Jahn et al. 1982). These garnet-rich sources could have been the solid residue left after extraction of Group II komatiite magmas, while the LREE-enriched metasomatic fluid (melt) could have ultimately originated from the deep upper mantle. If so, provided that the LREE enrichment was short-lived, the mantle precursors of the LREE-enriched basalts and Group II rocks could have maintained nearly identical $^{143}Nd/^{144}Nd$ ratios. If not – i.e. perhaps in the more general case where the metasomatic fluid (melt) would not have originated in a mantle domain chemically equivalent to the source of Group II komatiites – differences in initial $^{143}Nd/^{144}Nd$ ratios would have to be postulated. At any rate, the isotopically analysed basic to ultrabasic samples are unlikely to have had the same initial Nd isotopic ratios.

(2) Serious geochronological difficulties would arise if the date of 3269 ± 84 Ma was interpreted as the eruption age of the Tjakastad Subgroup. First, it would be in conflict with the time of the low-grade metamorphism as established at around 3450-3430 Ma by the $^{40}Ar/^{39}Ar$ and Rb–Sr internal isochron age data (Jahn and Shih 1974; Lopez-Martinez et al. 1984; Table 1). This time represents a minimum age for the eruption of the volcanics and is about 180 Ma older than the new Sm–Nd date. Second, the magmatic zircons of the overlying Hooggenoeg Formation yielded a $^{207}Pb/^{206}Pb$ age of 3438 ± 6 ($2\,\sigma_m$) Ma (Kröner and Todt 1988; Table 2). This date must be regarded as a minimum age for the underlying volcanics. Again the new Sm–Nd date is much too young.

The arguments stated above strongly suggest that the Sm–Nd date of 3269 ± 84 Ma is meaningless with regard to the eruptive age of the Tjakastad Subgroup. This date cannot be interpreted as a "metamorphic age" either, for the Ar–Ar and Rb–Sr systems, both a priori more sensitive to metamorphic perturbation than the Sm–Nd system, yielded ages of about 3440–3450 Ma (Table 1). We suggest that the most likely interpretation is that the Tjakastad Subgroup basic-ultrabasic lavas had a range in initial $^{143}Nd/^{144}Nd$ ratios or $\varepsilon_{Nd}(T)$ values when they erupted 3450 Ma ago. The Sm–Nd whole-rock "isochron" gives an anomalous age because of this initial range.

Meaningless Sm–Nd ages have already been reported for the basalt and komatiite lavas of Newton Township, Canada, the Usushwana gabbroic suite of Swaziland and the Kambalda greenstones of the Yilgarn Block (Cattell et al. 1984; Hegner et al. 1984; Chauvel et al. 1985). The Tjakastad basic-ultrabasic suite thus adds a new case. However a marked difference is found. At Kambalda, Newton Township and for the Usushwana gabbroic suite, the Sm–Nd ages have been proved to be too old compared to the true ages of the dated sample suites. For the Tjakastad basic-ultrabasic suite the Sm–Nd age is not too old but much too young.

At any rate and to conclude, it is clear that the published Sm–Nd isotopic data fail to provide any constraint regarding the age of the Tjakastad Subgroup. When all combined and plotted in the isochron diagram, the Sm–Nd data are scattered (Fig. 5).

Implications for the origin of early Onverwacht Group volcanism and Archean mantle evolution

Accepting an eruption age of ≈ 3450 Ma the calculated initial ε_{Nd} values show a 5.5 ε_{Nd} units range, from -3.4 to $+1.8$ (Table 2). The earlier results of Hamilton et al. (1979, 1983) have also been recalculated. The corresponding data points have been plotted along with ours in Fig. 6 with three important reference reservoirs shown for comparison: (a) Primitive Mantle (CHUR); (b) Depleted Mantle (DM); and (c) the TTG suite of the Ancient Gneiss Complex (AGC) of Swaziland at $T = 3450$ Ma. Since the AGC could have been a basement for the deposition of BGB supracrustals, it might have played a role as contaminant in the basic-ultrabasic magmas. Figure 6 shows that except for the somewhat "aberrant" sample 5038, most rocks have $\varepsilon_{Nd}(T)$

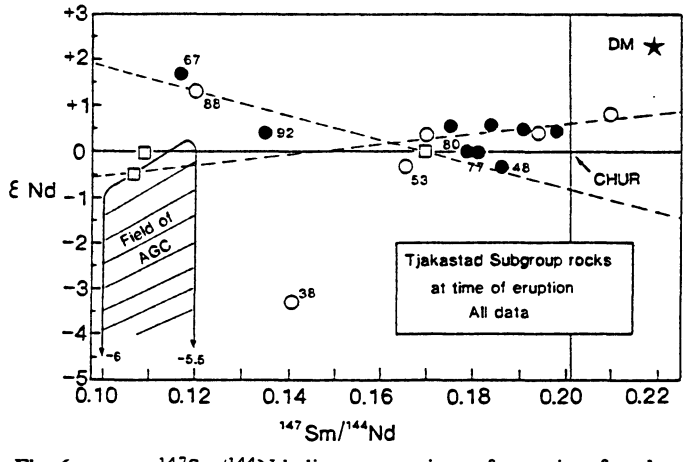

Fig. 6. ε_{Nd} vs $^{147}Sm/^{144}Nd$ diagram at time of eruption for the Tjakastad rocks including the data published in Hamilton et al. (1979; 1983). Also shown are three reference fields: (a) the Ancient Gneiss Complex (AGC) of Swaziland, the field of which at $T = 3450$ Ma was calculated using the Nd isotopic data reported in Kröner et al. (1988) and assuming $^{147}Sm/^{144}Nd$ ratios in the range 0.10–0.12; (b) depleted mantle reservoir (DM) at $T = 3450$ Ma assuming the present $\varepsilon_{Nd} = +10$ and $^{147}Sm/^{144}Nd = 0.2139$; and (c) chondritic mantle reservoir (CHUR). The two dashed lines represent the 3526 ± 48 Ma and 3269 ± 84 Ma linear arrays at $T = 3450$ Ma. Keys to Symbols: □ Felsic vocanics/intrusives; ○ Basalts; ● High-Mg Basalts and Komatiites

values clustering around zero (± 1), irrespective of their Sm/Nd ratios. However two samples (5067 and 5088) distinct themselves from the rest by their positive $\varepsilon_{Nd}(T)$ values of about $+1.5 \pm 0.5$ (Table 2). If the assumed age of 3450 Ma is correct, then these two samples offer the first evidence that a depleted-mantle component has been involved in the Tjakastad Subgroup volcanism.

In summary, the Tjakastad volcanics appear to fall into three isotopically distinct groups, namely: (a) komatiites, high-Mg basalts, basalts and felsic volcanics/intrusives with $\varepsilon_{Nd}(3450) \approx 0$ (± 1); (b) high-Mg basalts and basalts with $\varepsilon_{Nd}(3450) \approx +1.5$; and (c) basalt (5038) with $\varepsilon_{Nd}(3450) = -3.4$. The next question is to understand the petrogenetic implications from such isotopic heterogeneity and their consequences regarding the nature of the Archean mantle beneath the Barberton region.

Interpretation of the near zero $\varepsilon_{Nd}(T)$ for the komatiites and basalts is not unique. These values may suggest derivation from primitive chondritic mantle source(s) or from depleted mantle domains followed by contamination by older crustal material such as the AGC. The AGC certainly is a possible contaminant in the generation of the BGB volcanics but there are several lines of evidence not favourable for such an interpretation:

(1) The Tjakastad Subgroup komatiites and high-Mg basalts with $\varepsilon_{Nd}(3450) \approx 0$ belong to the Al-depleted Group II rocks which typically exhibit low Al_2O_3/TiO_2 ratios of about 10 (Jahn et al. 1982). Archean TTG suites are characterized by a much higher mean value of 40. If Tjakastad Subgroup komatiites have been contaminated by AGC material the uncontaminated komatiites should have had an even lower Al_2O_3/TiO_2 ratio. In the early Archean (3500–3400 Ma) Pilbara Block of Western Australia, strongly LREE-depleted ($(La/Sm)_N = 0.5$–0.6) komatiites with initial ε_{Nd} values of about +4 have been documented (Gruau et al. 1987). As judged from these characteristics, they are unlikely to contain any crustal component. Yet, they belong to the Group II and their Al_2O_3/TiO_2 ratio is about 10.

(2) If crustal contamination has occurred, a positive correlation between $\varepsilon_{Nd}(T)$ and $^{147}Sm/^{144}Nd$ ratios should be expected in normal circumstances, because ancient crustal rocks would have been characterised by a more negative ε_{Nd} value and lower Sm/Nd ratio (Fig. 6). Such a positive correlation has been found in the crustally-contaminated Kambalda valcanics (Chauvel et al. 1985; Arndt and Jenner 1986; Compston et al. 1986). In the Tjakastad volcanics either an opposite trend (Table 2) or no trend was found (Fig. 6). Moreover, the near-zero intial ε_{Nd} values shown in Fig. 6 were obtained for samples ranging in composition from komatiite to tholeiitic basalt.

(3) The Nb/Th ratio is a useful geochemical parameter in assessment of crustal contamination. Jochum et al. (1987) measured Nb/Th ratios in various basic-ultrabasic volcanics including samples from the Tjakastad Subgroup, the Kambalda greenstone belt of Western Australia, and the young komatiite-basalt suite of Gorgona Island. The Kambalda basalts exhibit an extremely low value of Nb/Th (0.9), which is consistent with the interpretation that their parental magmas were affected by crustal contamination. In contrast, basalts from the Tjakastad Subgroup show higher ratios (7–16) that are similar to those of Gorgona samples. Gorgona komatiites and basalts have initial ε_{Nd} values of $\approx +10$ (Aitken and Echeverria 1984).

Although the above lines of the evidence argue against an important role of crustal contamination in the making of the near-zero $\varepsilon_{Nd}(T)$ values, some involvement of ancient crust in the Tjakastad basalt genesis cannot be entirely dismissed. The best example is basalt sample 5038, which has an $\varepsilon_{Nd}(T)$ value of -3.4 (Table 2). This sample might contain an AGC component as visible from Fig. 6.

To sum up, we conclude that the near-zero $\varepsilon_{Nd}(3450)$ values for most Tjakastad volcanics suggest their derivation from chondritic mantle sources. This result is in marked contrast with what we have learned from the published results that most Archean komatiites and basalts are characterised by positive $\varepsilon_{Nd}(T)$ values, suggesting their ultimate derivation from depleted mantle sources (see compilation of Jahn et al. 1987; Cattell et al. 1984; Chauvel et al. 1985; Gruau et al. 1987). In the present study, only basaltic samples 5067 and 5088 are shown to possess positive $\varepsilon_{Nd}(T)$ values (Table 2). The isotopically chondritic nature of Tjakastad komatiites and the LREE enrichment of samples 5067 and 5088 (Table 2, Fig. 3) are the two reasons why the Tjakasted basic-ultrabasic suite gave a scenario so different from the Kambalda and Newton suites, namely: a Sm–Nd age not too old but much too young.

Summary and conclusion

Three important conclusions stem out from this study. The first is that the Tjakastad Subgroup of the Barberton Greenstone Belt (BGB) exemplifies a new case of Archean greenstones succession where the Sm–Nd whole-rock method cannot be used without ambiguity for dating purposes. So far and on the basis of a Sm–Nd "isochron" earlier reported by Hamilton et al. (1979; 1983), the Tjakastad Subgroup was assumed to have been emplaced ca. 3530 Ma ago. Using additional Nd data as well as geochronological and geochemical arguments we believe to have clearly established that this Sm–Nd date has no geological reality. When plot on the conventional Sm–Nd isochron plot, the Tjakastad Sm–Nd data are scattered and no isochron can be confidently drawn.

The second and third conclusions relate to the petrogenesis of the Tjakastad Subgroup volcanics and the nature of their source rocks in the mantle. Two important points are underlined as follows:

(1) the early Archean mantle beneath the Barberton region was isotopically heterogeneous, with primitive mantle domains coexisting with depleted regions.

(2) crustal contamination seems to have played a limited role in the control of the chemistry of the Tjakastad basic-ultrabasic volcanic rocks.

Acknowledgments. We thank J Bernard-Griffiths for his review of an earlier version of this paper. This work also benefited by discussions with N.T. Arndt. We are grateful to A.Y. Glikson who provided the samples. This is a contribution to IGCP project 280 (The oldest rocks).

References

Aitken BG, Echeverria LM (1984) Petrology and geochemistry of komatiites and tholeiites from Gorgona Island, Colombia. Contrib Mineral Petrol 86:94–105

Anhaeusser CR (1973) The evolution of the early Precambrian crust of southern Africa. Phil Trans R Soc Lond 273:359–388

Anhaeusser CR (1983) Contributions to the Geology of the Barberton Mountain Land. Geol Soc S Afr Spec Publ 9

Arndt NT (1986) Komatiites: a dirty window to the Archean mantle. Terra Cognita 6:59–66

Arndt NT, Jenner GA (1986) Crustally contaminated komatiites and basalts from Kambalda, Western Australia. Chem Geol 56:229–255

Barton JM (1983) Isotopic constraints on possible tectonic models for crustal evolution in the Barberton granite-greenstone terrane, southern Africa. In: Anhaeusser CR (ed). Geol Soc S Afr Spec Publ 9:73–79

Barton JM, Robb LJ, Anhaeusser CR, Van Nierop DA (1983) Geochronologic and Sr-isotopic studies of certain units of the Barberton granite-greenstone terrane, South Africa. In: Anhaeusser CR (ed). Geol Soc S Afr Spec Publ 9:63–72

Brévart O, Dupré B, Allègre CJ (1986) Lead-Lead age of komatiitic lavas and limitations on the structure and evolution of precambrian mantle. Earth Planet Sci Lett 77:293–302

Cattell A, Krogh TE, Arndt NT (1984) Conflicting Sm–Nd whole rock and U–Pb zircon ages for Archean lavas from Newton Township, Abitibi Belt, Ontario, Earth Planet Sci Lett 70:280–290

Chauvel C, Dupré B, Jenner GA (1985) The Sm–Nd age of Kambalda volcanics is 500 Ma too old! Earth Planet Sci Lett 74:315–324

Compston W, Kröner A (1988) Multiple zircon growth within early Archean tonalitic gneiss from the Ancient Gneiss Complex, Swaziland. Earth Planet Sci Lett 87:13–28

Compston W, Williams IS, Campbell IH, Gresham JJ (1986) Zircon xenocrists from the Kambalda volcanics: age constraints and direct evidence of older continental crust below the Kambalda-Norseman greenstones. Earth Planet Sci Lett 76:299–311

DePaolo DJ, Wasserburg GJ (1976) Inferences about magma sources and mantle structure from variations of $^{143}Nd/^{144}Nd$. Geophys Res Lett 3:743–746

De Wit MJ, Fripp REP, Stanistreet IG (1983) Tectonic and stratigraphic implications of new field observations along the southern part of the Barberton greenstone belt. In: Anhaeusser CR (ed). Geol Soc S Afr Spec Publ 9:21–29

Fletcher IR, Rosman KJR (1982) Precise determination of initial ε_{Nd} from Sm–Nd isotopic data. Geochim Cosmochim Acta 46:1983–1987

Glikson AY, Jahn BM (1985) REE and LIL elements, eastern Kaapvaal shield, South Africa: evidence of crustal evolution by 3-stage melting. Geol Soc Can Spec Pap 28:303–324

Gruau G, Jahn BM, Glikson AY, Davy R, Hickman AH, Chauvel C (1987) Age of the Talga-Talga Subgroup, Pilbara Block, Western Australia, and early evolution of the mantle: new Sm–Nd isotopic evidence. Earth Planet Sci Lett 85:105–116

Hamilton PJ, O'Nions RK, Evensen NM (1977) Sm–Nd dating of Archean basic and ultrabasic volcanics. Earth Planet Sci Lett 3:263–268

Hamilton PJ, Evensen NM, O'Nions RK, Smith HS, Erlank AJ (1979) Sm–Nd dating of Onverwacht Group volcanics. Nature 279:298–300

Hamilton PJ, Evensen NM, O'Nions RK, Glikson AY, Hickman AH (1981) Sm–Nd dating of the North Star Basalt, Warrawoona Group, Pilbara Block, Western Australia. Geol Soc Aust Spec Publ 7:187–192

Hamilton PJ, O'Nions RK, Bridgwater D, Nutman A (1983) Sm–Nd studies of Archean metasediments and metavolcanics from West Greenland and their implications for the Earth's early history. Earth Planet Sci Lett 62:263–272

Hegner E, Kröner A, Hofmann AW (1984) Age and isotopic geochemistry of the Archaean Pongola and Usushwana suites in Swaziland, southern Africa: a case for crustal contamination of mantle-derived magma. Earth Planet Sci Lett 70:267–279

Hunter DR (1974) Crustal development in the Kaapvaal craton, 1. The Archaean. Precambrian Res 1:259–294

Hunter DR, Barker F, Millard HT Jr (1984) Geochemical investigations of Archaean bimodal and Dwahile metamorphic suites, Ancient Gneiss Complex, Swaziland. Precambrian Res 24:131–155

Jacobsen SB, Wasserburg GJ (1980) Sm–Nd isotopic evolution of chondrites. Earth Planet Sci Lett 50:139–155

Jahn BM, Shih CY (1974) On the age of the Onverwacht Group, Swaziland Sequence, South Africa. Geochim Cosmochim Acta 38:873–875

Jahn BM, Glikson AY, Peucat JJ, Hickman AH (1981) REE geochemistry of Archean silicic volcanics and granitoids from the Pilbara Block, Western Australia: implications for the early crustal evolution. Geochim Cosmochim Acta 45:1633–1652

Jahn BM, Gruau G, Glikson AY (1982) Komatiites of the Onverwacht Group, South Africa: REE geochemistry, Sm–Nd age and mantle evolution. Contrib Mineral Petrol 80:25–40

Jahn BM, Auvray B, Cornichet J, Bay YL, Shen QH, Liu DY (1987) 3.5 Ga old amphibolites from eastern Hebei Province, China: Field occurrence, petrography, Sm–Nd isochron age and REE geochemistry. Precambrian Res 34:311–346

Jochum KP, Hofmann AW, Arndt NT (1987) Nb/Th in precambrian and modern komatiites and basalts. E U G IV Abst Progr, Terra Cognita 7:396

Kröner A, Todt W (1988) Single zircon dating constraining the maximum age of the Barberton greenstone belt, southern Africa. J Geophys Res 93:15329–15337

Kröner A, Milisenda C, Compston W, Tegtmeyer A, Liew TC, Todt W (1988) Combined use of single zircon ages and Sm–Nd isotopes in the analysis of early Archaean crustal growth processes: the Ancient Gneiss Complex of Swaziland, southern Africa. Intern Congr Geochem Cosmochem Abst Progr. Chem Geol 70:146

Lopez-Martinez M, York D, Hall CM, Hanes JA (1984) Oldest reliable $^{40}Ar/^{39}Ar$ ages for terrestrial rocks: Barberton Mountain komatiites. Nature 307:352–355

Martin H (1987) Petrogenesis of Archean Trondjhemites, Tonalites, and Granodiorites from Eastern Finland: Major and Trace Element Geochemistry. J Petrol 28:921–953

McCulloch MT, Compston W (1981) Sm–Nd dating of Kambalda and Kanowna greenstones and heterogeneity in the Archean mantle. Nature 294:322–327

Othani E (1989) Majorite garnet fractionation and genesis of komatiites in the deep mantle. Precambrian Res (in press)

Tegtmeyer AR, Kroner A (1987) U–Pb zircon ages bearing on the nature of early Archean greenstone belt evolution, Barberton Mountainland, southern Africa. Precambrian Res 12:141–160

Viljoen RP, Viljoen MJ (1969) Upper mantle project. Geol Soc S Afr Spec Publ 2

Viljoen MJ, Viljoen RP, Smith HS, Erlank AJ (1983) Geological, textural, and geochemical features of komatiitic flows from the Komati formation. In: Anhaeuuser CR (ed). Geol Soc S Afr Spec Publ 9:1–20

White WM, Patchett PJ (1984) Hf–Nd–Sr isotopes and incompatible elements abundances in island arcs: implications for magma origins and crust-mantle evolution. Earth Planet Sci Lett 67:167–185

York D (1969) Least squares fitting of a straight line with correlated errors. Earth Planet Sci Lett 5:320–324

Received May 8, 1989 / Accepted August 5, 1989
Editorial responsibility: J. Hoefs

ALUMINUM DEPLETION IN KOMATIITES AND GARNET FRACTIONATION IN THE EARLY ARCHEAN MANTLE: HAFNIUM ISOTOPIC CONSTRAINTS

G. Gruau, N.T. Arndt, C. Chauvel and J. Cornichet

Article paru dans *Geochimica et Cosmochimica Acta*, Vol. 54, pp. 3095-3101, 1990.

Abstract-Hafnium isotopic composition were measured in Al-depleted and Al-enriched komatiites from the 3450 Ma old Barberton greenstone belt, South Africa. All samples have initial ε_{Hf} values close to zero. Such values are at variance with the strongly negative or positive values that should be observed if these rocks came from old garnet-depleted or garnet-enriched layers, such as may have formed during the solidification of an ancient terrestrial magma ocean. The garnet fractionation observed in komatiites probably took place during the melting event.

INTRODUCTION

Komatiites are volcanic rocks with extremely high eruption temperature (≈1600°C) and chemical compositions approaching those of mantle peridotites (Arndt and Nisbet, 1982). Even though several occurrences have been documented in Proterozoic and Phanerozoic terrains, komatiites are dominantly an Archean phenomenon and have been reported in Archean greenstone belts with ages ranging from ≈3800 Ma to ≈2700 Ma (e.g. Nesbitt et al., 1982; Jahn et al., 1982). Considerations of chemical composition, geographical distribution and age spectrum indicate that komatiites are an extremely powerful tool for constraining the nature and evolution of the Archean mantle. Most current models dealing with the composition of the primitive mantle, the early evolution of the evolving crust-mantle system, and the chemical and isotopic heterogeneities of the Archean mantle are based on geochemical and isotopic data from komatiites (e.g. Sun and Nesbitt, 1978; Jahn and Sun, 1979; Jahn et al., 1980, 1982; Sun, 1984; Arndt, 1986; Brévart et al., 1986; Albarède and Brouxel, 1987; Chase and Patchett, 1988; Smith and Ludden, 1989).

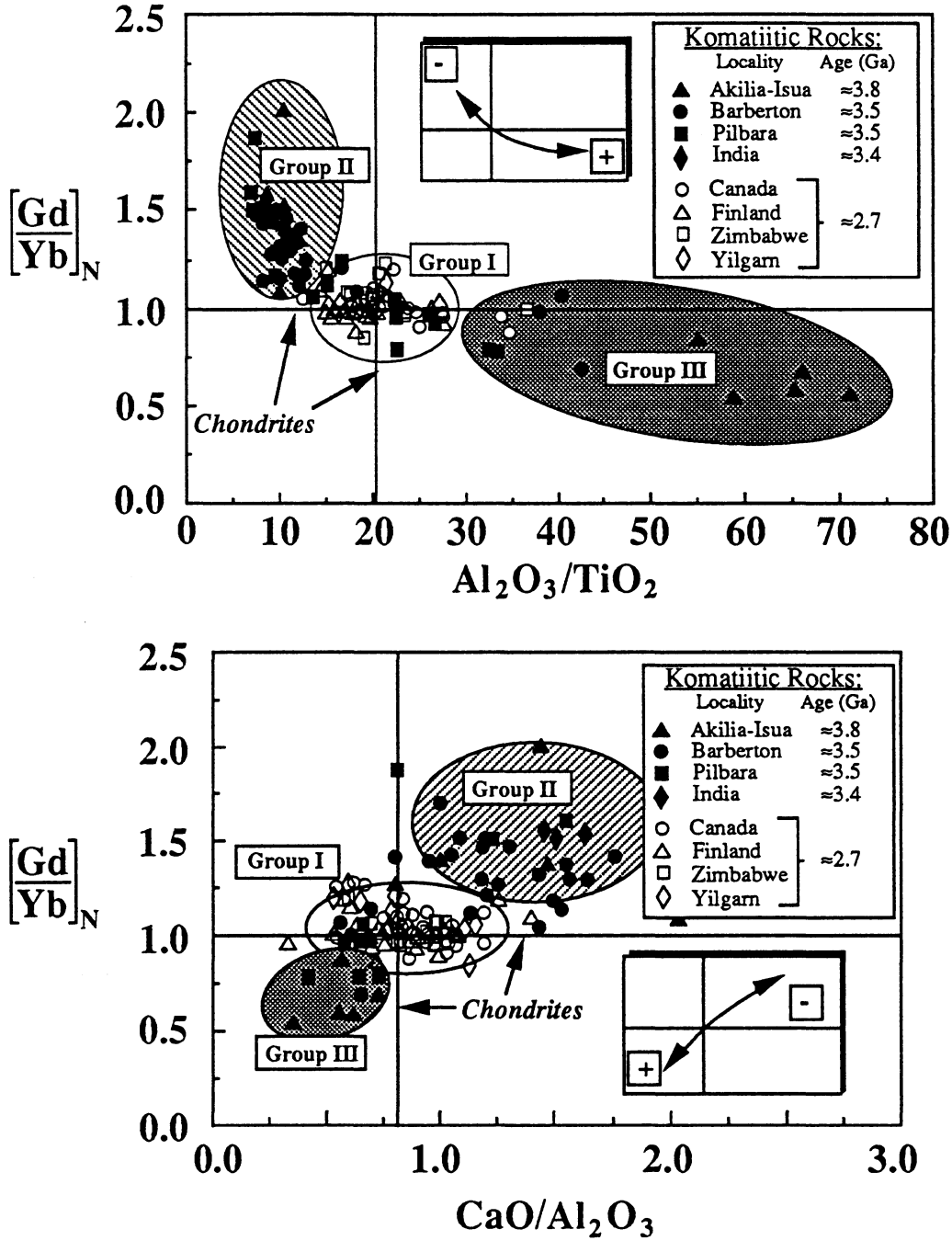

Figure 1: Diagrams illustrating the correlated variations of $(Gd/Yb)_N$, Al_2O_3/TiO_2 and CaO/Al_2O_3 in Archean komatiites and komatiitic basalts. The inset figures show that the correlations fit trends of garnet removal (-) and garnet addition (+) from initially chondritic composition. Solid symbols are for early Archean rocks (T≥3.4 Ga) while open symbols are for late Archean samples (T≈2.7Ga). Chondritic ratios are adopted from Anders (1977). See text for further explanations. Data sources: see caption of Fig. 5 in Jahn et al. (1982); see also Gruau (1983), Cattell et al. (1984), Arndt and Nesbitt (1984), Arndt and Jenner (1986) and Gruau et al. (1987).

An intriguing aspect of many komatiites in early Archean greenstone belts (T ≥ 3400 Ma) is their Al- and HREE-depleted signature. As can be seen in Fig. 1, many early Archean komatiites have CaO/Al_2O_3 and $(Gd/Yb)_N$ higher, but Al_2O_3/TiO_2 lower, than in chondrites, whereas most late Archean komatiites (T≈2700 Ma), have roughly chondritic ratios of these elements. A third less common type, also largely restricted to early Archean komatiites, has relative enrichment of Al and HREEs. Numerous discussions have centered around the cause of such chemical variations. Green (1975) and Sun and Nesbitt (1978) advocated the fractionation of garnet, and proposed that this mineral was a residual phase during the mantle melting that produced Al- and HREE-depleted komatiites. These ideas have recieved support from recent high-P experimental studies (e.g. Takahashi, 1986; Othani et al., 1986; Ito and Takahashi, 1987; Kato et al., 1988) which showed that majorite garnet (the high-pressure garnet-pyroxene solid solution) is a liquidus phase during mantle melting at depths greater than about 450 km. On this basis, Othani (1984) and Arndt (1986) proposed that fractionation of majorite garnet during melting controlled the compositions of Al-depleted and Al-enriched komatiites. An alternative viewpoint was promoted by Jahn et al. (1982) and Gruau and Jahn (1983), who disputed the "garnet fractionation" hypotheses and argued, as had Cawthorn and Strong (1974), Anderson (1982), and most recently Othani et al. (1989), that the depletion or enrichment in garnet was charcteristic of the komatiites source regions. Gruau and Jahn (1983) and Othani et al. (1989) envisaged majorite garnet fractionating during the solidification of a deep terrestrial magma ocean, some 4500-4400 Ma ago. In this study, we report Lu-Hf isotopic analyses of komatiites from the early Archean Barberton greenstone belt in southern Africa which provides a test of the two competing theories.

GARNET FRACTIONATION PROCESSES WITHIN THE EARLY ARCHEAN MANTLE: DATA, CONSTRAINTS AND MODELS*

***Ce chapitre ne figure pas dans l'article paru dans Geochimica et Cosmochimica Acta. Il a été ajouté dans la but de faciliter la compréhension du problème traité par les lecteurs non familiers des résultats de la pétrologie expérimentale haute pression ainsi que de la théorie de l'océan magmatique terrestre.**

Komatiite data bank

Figure 1 comprises a plot of $(Gd/Yb)_N$ vs. Al_2O_3/TiO_2 and $(Gd/Yb)_N$ vs. CaO/Al_2O_3 for 178 analyses of Archean komatiites and komatiitic basalts. The komatiitic affinities of the samples have been determined using textural (spinifex texture) and/or chemical criteria. As recommended in Arndt and Nisbet (1982), the term komatiite refers to a volcanic rock with MgO content ≥18%; komatiitic basalt is used for a volcanic rock of picritic to basaltic composition (MgO<18%) that shares textural or/and chemical characteristics with komatiites and is believed to be genetically related to the ultramafic rocks. Included in Fig. 1 are samples from most of the known occurrences of Archean komatiites, i.e. South Africa (Barberton), Australia (Pilbara and Yilgarn Blocks), Greenland (Akilia and Isua associations), Finland, India (Sargur Supergroup), Zimbabwe (Sebakwaian Group), and Canada.

Figure 1 shows that the ratios of CaO/Al_2O_3, Al_2O_3/TiO_2 and $(Gd/Yb)_N$ are not constant in komatiites but exhibit correlated variations. Three geochemical types or groups can be recognized (Sun and Nesbitt, 1978; Jahn et al., 1982):

(a) an Al-undepleted or Group I type which has chondritic values of Al_2O_3/TiO_2 (≈20); CaO/Al_2O_3 (≈0.8) and $(Gd/Yb)_N$ (≈1.0). This type is mainly (but not exclusively) represented by late Archean (≈ 2700 Ma) samples (open symbols in Fig. 1)

(b) an Al-depleted or Group II type which has Al_2O_3/TiO_2 lower, and CaO/Al_2O_3 and $(Gd/Yb)_N$ higher than chondrites, repectively. Average values for Al-depleted or Group II komatiites and komatiitic basalts are: Al_2O_3/TiO_2 = 10.4±1.9, CaO/Al_2O_3 = 1.60±0.50, and $(Gd/Yb)_N$ = 1.40±0.20. In the diagram it is clearly seen that this type is dominantly observed in early Archean greenstone belts (early Archean samples are represented by closed symbols in Fig. 1).

(c) an Al-enriched or Group III type with $Al_2O_3/TiO_2 > 20$, $CaO/Al_2O_3 < 0.8$ and $(Gd/Yb)_N < 1.0$. This type is by far the least common. Like Group II, Group III samples are confined largely to the early Archean terrains. Group III may be regarded as the chemical counterpart of the Al-depleted or Group II komatiites (Fig.1).

The correlations illustrated in Fig. 1 fit a garnet fractionation trend (Sun and Nesbitt, 1978; Jahn et al., 1982; Gruau 1983; Arndt, 1986). The chemical charcteristics of the Al-depleted or Group II komatiites can be accounted for by

removal of garnet from a chondritic composition, while addition of garnet explains the relative enrichment in Al and HREE of the Group III rocks. Since garnet is unstable in basaltic melts at low pressure, the garnet fractionation must have taken place in the mantle.

Physical and experimental constraints

Accepting that the mechanism responsible for the Al and HREEs depletion of Group II komatiites was the removal of garnet, we now ask how and when the garnet fractionated. It is in this context that the virtual confinement of Al-depleted or Al-enriched komatiites to early Archean terrains is important; apparently, conditions in the early mantle facilitated garnet fractionation. Other constraints come from: (a) the phase relations in mantle systems at very high pressure; (b) the calculated temperatures of komatiite magmas and inferred depth of melting; and (c), the termal history of the young Earth and the concept of a terrestrial magma ocean.

(a) Phase relations at very-high pressure. The phase relations of mantle peridotite at high temperatures and pressures, derived from the experiments of Takahashi and Scarfe (1985), Takahasi (1986), Othani et al. (1986), Ito and Takahashi (1987) and Kato et al. (1988), are summarized in Fig. 2. In the figure, it can be seen that melting at high pressures differs significantly from melting at low pressures. Whereas garnet has a very restricted above-solidus field at pressure lower than 15 GPa (≈450 km), majorite, the high-pressure equivalent of garnet, is the liquidus phase in mantle systems between 15 and 24 GPa (i.e. from ≈450 to ≈700 km). This observation provides the basis for Othani et al's (1989) conclusion that majorite frationation should control the composition of high pressure mantle melts.

(b) The temperature of komatiite magmas and the depth of melting. Experimental studies have shown that, at atmospheric pressure, the liquidus temperature of the most magnesian komatiites (MgO ≈ 30%) is close to 1600°C (Green et al., 1975. Arndt, 1976; Bickle et al., 1977). Since komatiites seem to have been largely volatile-free, this is probably the eruption temperature of their parental magmas, implying still higher temperatures (maybe around 1900°C) for the primary mantle melts (Arndt, 1986; Campbell et al., 1989). Two hypotheses have been proposed to account for the formation of magmas with temperatures so much higher than those of normal, basaltic, partial melts. McKenzie (1984)

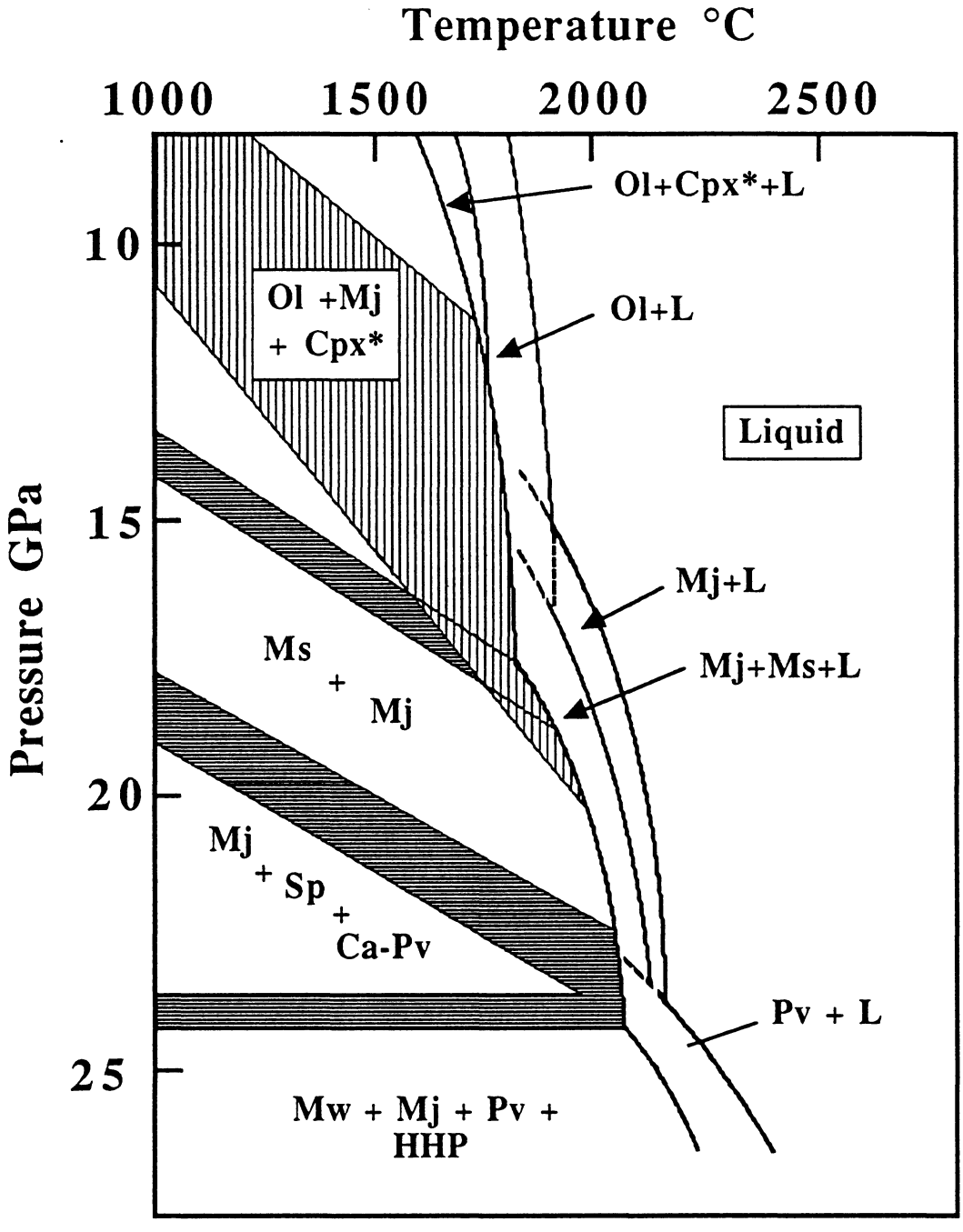

Figure 2: Schematic diagram illustrating the phase relations of mantle peridotites between 10 and 25 GPa. Ol: olivine; Mj: majorite garnet; Cpx*: Ca-poor clinopyroxene; Ms: modified spinel; Sp: spinel; Ca-Pv, Ca-perovskite; Pv: Mg-perovskite; Mw: Mg-wustite; HPP: unknown high pressure phase; L: liquid. Adapted from Othani et al. (1986).

proposed that komatiites form in "hot jets" of mantle material ascending in regions of lithospheric extension while Jarvis and Campbell (1983) and Campbell et al. (1990) developed a model for the formation of komatiites within plumes ascending from a thermal boundary layer deeper in the mantle. In both cases the depth at which melting occurs greatly exceeds 200 km. Under these circumstances, majorite, and not olivine as had earlier been assumed, would have been the high temperature residual phase.

(c) The young Earth and the magma ocean concept. It is generally accepted, on the basis of planetary accretion models and inferred higher abundances of short-lived isotopes, that the outer layers of the Earth were much hotter in pre-Archean times than today (Basaltic volcanism, 1981). In particular, models in which the heat of impact during planetary accretion is evaluated show that much of the upper mantle could have melted leading to the formation of a terrestrial magma ocean (Kaula, 1979; Ransford, 1979). Extensive melting and subsequent crystallization of the young Earth's mantle would have profoundly influenced the structure and the composition of the Achean mantle. Particularly, large effects would be expected if, as suggested by Ransford (1979) and Kaula (1979), the magma ocean was 1000 km deep. In this case, majorite fractionation could have been the dominant process (Othani, 1988) leading to large fractionation of many elemental ratios including CaO/Al_2O_3, Al_2O_3/TiO_2 and the HREEs.

Models

Two main categories of model have been proposed to account for the garnet fractionation processes inferred from komatiite compositions.

(a) Fractionation of garnet during partial melting (Fig.3). In this model, it is assumed that the Archean mantle had essentially chondritic ratios of CaO/Al_2O_3, Al_2O_3/TiO_2 and HREEs ($(Gd/Yb)_N$=1.0) and the various groups of komatiites are supposed to reflect different melting conditions. The "partial melting effect" hypothesis was first proposed by Green (1975) who suggested that garnet would segregate from other residual mantle phases during partial melting in a rising mantle diapir. At the time, available experimental data indicated that olivine and orthopyroxene were the likely liquidus phases during high-degree melting, and that garnet was stable only close to the solidus. To account for the garnet fractionation, Green (1975) called on the significant density difference between garnet and the other mantle phases and he suggested that "suitable values for viscosity and shape

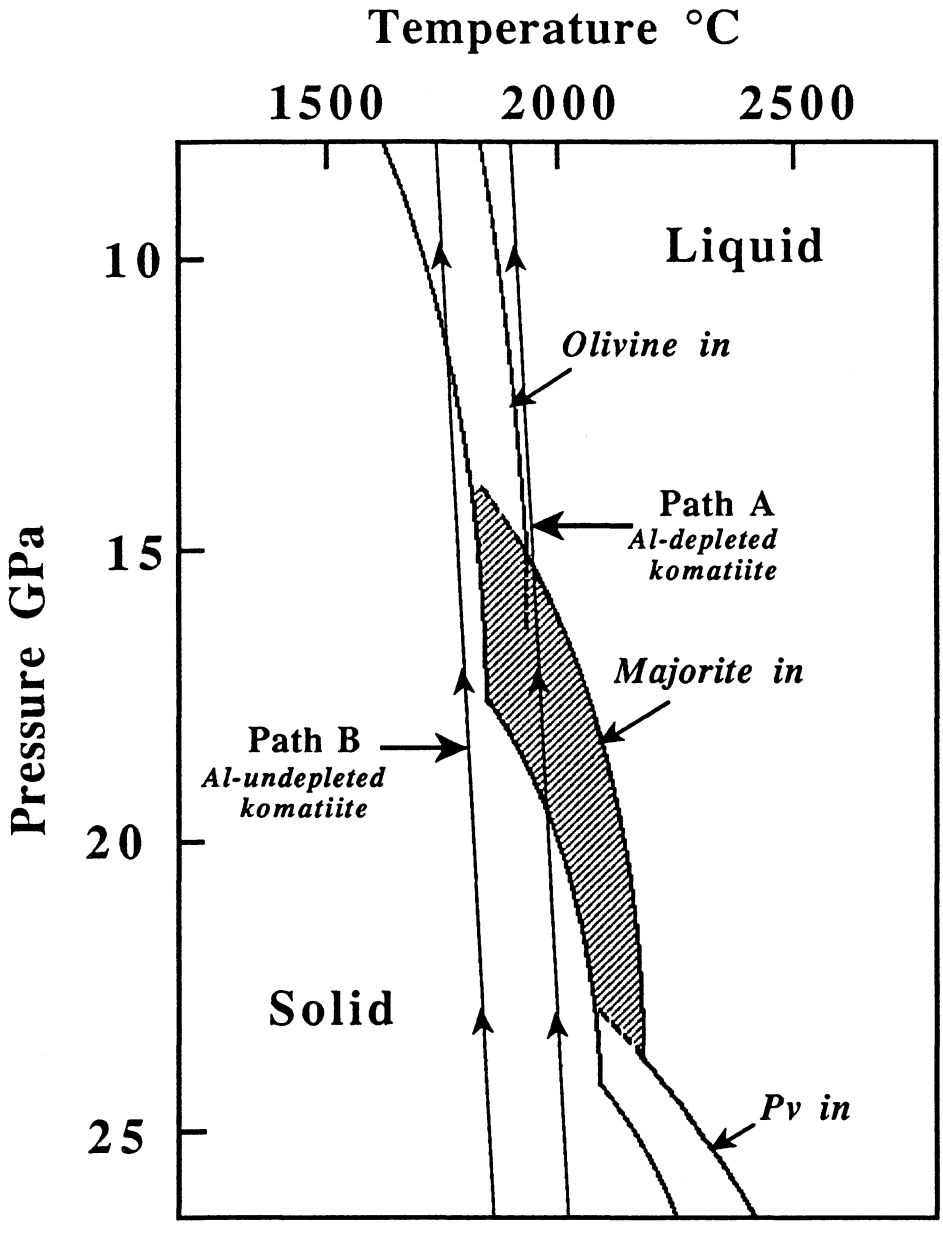

Figure 3: Pressure-Temperature diagram showing Othani's (1984) and Arndt's (1986) scheme whereby the contrasted $(Gd/Yb)_N$, CaO/Al_2O_3 and Al_2O_3/TiO_2 ratios of komatiites would be related to differences in the depth of melting. The starting material is a mantle with chondritic distribution of Ca, Al, Ti and HREE. Path A is the path that Al-depleted (Group II) komatiites would have followed, whereas Group I rocks would be to connect with mantle diapirs having ascented along path B. The predominance of Group II komatiites in the early Archean could be explained because of the higher average temperatures. The phase relations are from Fig. 2.

factors could create conditions for the ascending diapir where olivine and enstatite were entrained but garnet settled through the rising diapir and by its segregation, changed the bulk composition of the diapir". The new high-pressure experimental data provide a more straightforward mechanism for garnet segregation. Othani (1984) and Arndt (1986) proposed that Al-depleted (Group II) komatiite magmas formed by partial melting of the deep upper mantle, between 450 and 650 km, in a domain where majorite is the high-temperature residual phase, whereas Al-undepleted komatiite magmas (Group I) represent mantle melts formed at shallower level, where olivine is the high-temperature residual phase (Fig. 3). In this scheme, Al-enriched (Group III) komatiites are considered to be the remelting products of residual mantle left after separation of the Al-depleted magmas. The temporal distribution of the various groups of komatiites is attributed to secular cooling of the mantle. In the early Archean, average temperature were high and melting at very high pressure was the dominant process. Thus, a majority of early Archean komatiites formed under conditions in which majorite was the residual phase and became depleted in Al and HREE. In the late Archean, average temperatures were lower, melting was shallower, and more komatiites of the Al-undepleted type were generated.

(b) Fractionation of garnet during the cooling of a terrestrial magma ocean (Fig. 4). This alternative model was proposed by Gruau and Jahn (1983) and Othani et al. (1989) who adapted earlier ideas by Cawthorn and Strong (1974) and Anderson (1982). The governing concept of the model is that the young Earth's mantle underwent a magma ocean stage and that the terrestrial magma ocean was deep enough (≈670 km ?) to allow garnet to fractionate during its cooling and subsequent crystallization. The magma ocean is assumed to have solidified soon (≈4400 Ma ago) after it formed, and the mantle to have differentiated into three layers with different mineralogical and chemical composition (Fig. 4b; see also Othani, 1988): an upper layer depleted in garnet and thus with CaO/Al_2O_3, TiO_2/Al_2O_3 and Gd/Yb ratios higher than chondrites; an intermediate layer enriched in garnet and thus with CaO/Al_2O_3, TiO_2/Al_2O_3 and Gd/Yb lower than chondrites; and a deep layer (the lower mantle) unaffected by the magma ocean stage and with chondritic ratios of CaO/Al_2O_3, Al_2O_3/TiO_2 and Gd/Yb. In this scheme, the different types of komatiites observed in early Archean terrains are interpreted as the remelting products of these various layers: Al-depleted (Group II) komatiites from the garnet-depleted upper layer; Al-enriched (Group III) komatiites from the garnet-enriched intermediate layer; Al-undepleted (Group I)

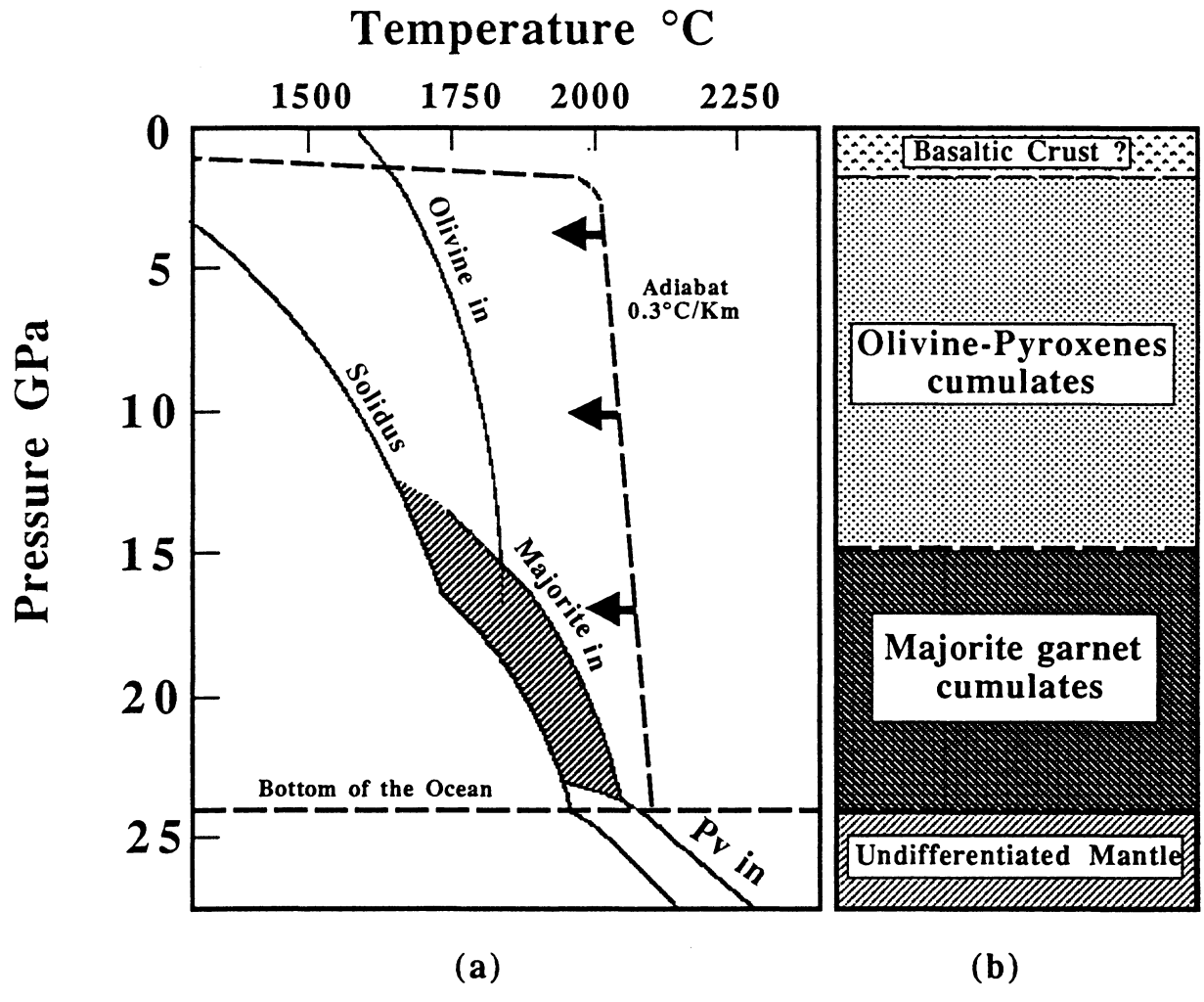

Figure 4: Schematic diagrams illustrating the model of Jahn and Gruau (1983) and Othani et al. (1989) whereby the various types of komatiites would be the remelting products of a three-layers stratified mantle. Fig. 4a gives a sketch of the physical scenario. It is assumed that a 700 km deep magma ocean of ultrabasic composition developed on earth ca 4400-4500 Ma ago. Initially and for most of the history of the ocean, convection will be turbulent, which implies that through the body of magma the temperature follows the adiabat (dashed line in Fig. 4a = thermal profile in the magma ocean). Fractional crystallization takes place where the adiabat intersects the liquidus at the bottom of the magma ocean in regions where majorite garnet is the high temperature mantle phase. Assuming that majorite garnet was allowed to sink and accumulate, the resulting crystallized mantle might have been stratified like shown in Fig. 4b. The phase relations are from Fig. 2.

komatiites from the undifferentiated lower mantle. By the late Archean, mantle convection would have largely homogenized the fossil magma ocean leaving a mantle with essentially chondritic ratios of Al, Ca, Ti and HREEs. Komatiites formed from the homogenized mantle would have roughly chondritic CaO/Al_2O_3, Al_2O_3/TiO_2 and Gd/Yb, as do most of those found in 2700 Ma terrains.

MAJORITE FRACTIONATION AND Lu-Hf ISOTOPIC SYSTEMATICS

Fig. 5 is a summary of measured partition coefficients for REEs and Hf between majorite garnet and liquid, and between pyrope-rich garnet and liquid. Measured majorite-liquid partition coefficient for Hf ($KD_{Hf}^{mj\text{-}liq}$) lie between 0.8 and 0.4 (Kato et al., 1988; Othani et al., 1989; Yurimoto and Othani, 1990). No measurements have been made for Lu, but extrapolation of Yb, Gd and Sm partitioning data yields estimates in the range 1.0-2.0 (Fig.5).

Because Lu and Hf are both refractory elements, the most convenient reference for comparison of initial $^{176}Hf/^{177}Hf$ in terrestrial rocks is an isotopic growth curve based on the evolution of chondritic meteorites (e.g. Patchett et al., 1981). As in the case of Nd isotopes (DePaolo and Wasserburg, 1976), such a comparison is achieved using an ε notation in which:

$$\varepsilon_{Hf}(T) = ((^{176}Hf/^{177}Hf_{(sample,\,T)} / {}^{176}Hf/^{177}Hf_{(chondrites,\,T)}) - 1) \times 10^4$$

where T is the age of interest

During the fractionation of majorite or pyrope-rich garnet, Lu partitions more strongly into the solid phase than Hf, leaving the residue with low Lu/Hf. ^{176}Lu decays to ^{176}Hf with a half live of 35.7 Ga and ^{177}Hf is non-radiogenic. Majorite-depleted material therefore evolves to increasingly lower $^{176}Hf/^{177}Hf$, or lower ε_{Hf} values with time (Fig. 6) This behaviour provides the basis for distinguishing between the two models outline above. Mantle layers that were enriched or depleted in majorite garnet during crystallization of a magma ocean $\approx$ 4400 Ma ago should have acquired distinctly non-chondritic $^{176}Hf/^{177}Hf$ ratios by the time this material remelted to form 3450 Ma old komatiites; Al-depleted komatiites (Group II) should exhibit negative $\varepsilon_{Hf}(T)$ values, and Al-enriched rocks (Group

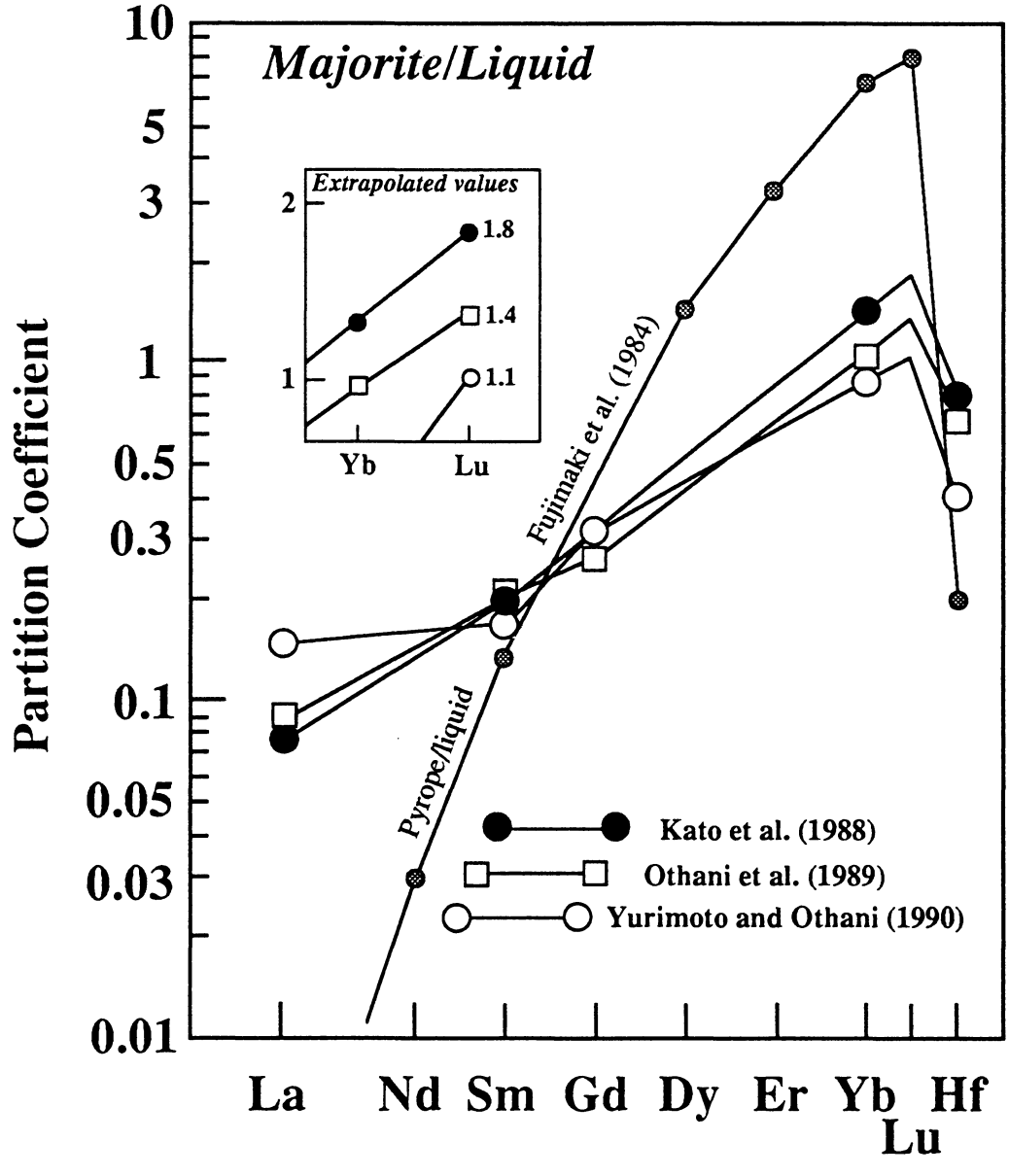

Figure 5: Partition coefficients for REE and Hf between majorite garnet and liquid. The partition cefficient data of Fujimaki et al. (1984) between pyropic garnet and liquid have been plotted for comparison. The partition coefficient of Lu between majorite and liquid has not been experimentaly determined. The values indicated in the inset figure are linearly extrapolated using the data of Sm, Gd and Yb.

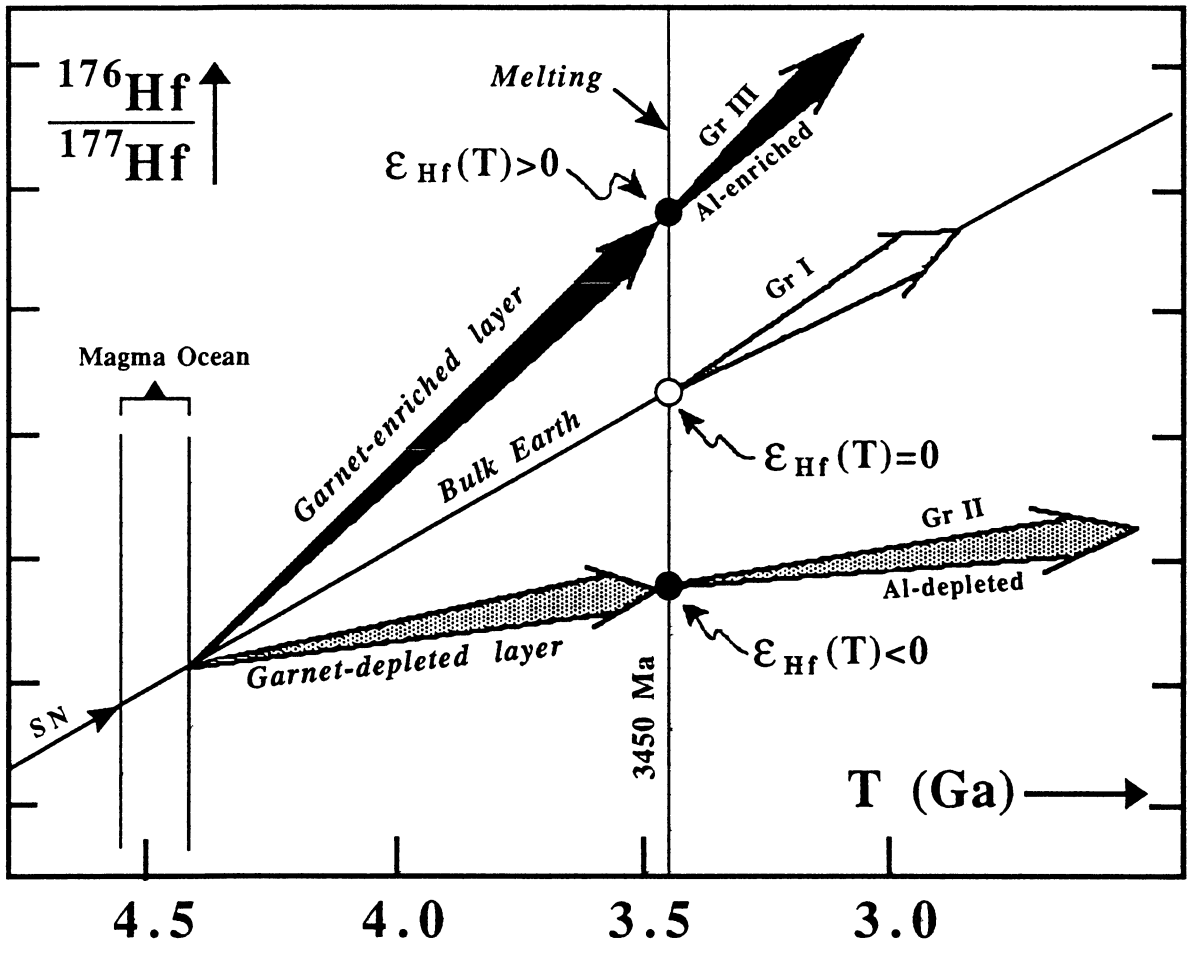

Figure 6: $^{176}Hf/^{177}Hf$ vs. time diagram illustrating the contrasted Hf isotopic trajectories followed by majorite-depleted, majorite-enriched and undifferentiated layers in the stratified mantle model of Jahn and Gruau (1983) and Othani et al. (1989). The trajectories of the majorite-depleted and majorite-enriched layers have been drawn using the partition coefficient data given in Fig. 5, assuming a chondritic or bulk earth Lu/Hf ratio for the ≈700 km deep magma ocean. 3450 Ma corresponds to the time of eruption of Barberton komatiites. SN: Solar Nebular.

III) positive $\varepsilon_{Hf}(T)$ values. As shown in Fig. 6, the degree of departure from chondritic values will depend on the initial composition of the magma ocean, the Lu/Hf ratios of the majorite-depleted and majorite-enriched reservoirs, and the time of later remelting. We show later that ≈3450 Ma old Al-depleted komatiites, if formed from an old majorite-depleted reservoir, should have initial $\varepsilon_{Hf}(T)$ in the range -6 to -5. If majorite fractionates only during the melting event, the Hf isotopic compositions of komatiites will be unaffected (i.e. $\varepsilon_{Hf}(T)\approx 0$).

SAMPLES

The measurement of Hf isotopic compositions of komatiites and komatiitic basalts turned out to be very difficult, for the reasons outlined below, and this limited the number of samples that could be successfully analysed. Three Al-depleted (Group II) samples (one komatiite and two basaltic komatiites) and a single Al-enriched (Group III) basaltic komatiite were finally selected. All are from the classic occurrence of early Archean komatiites in the 3450 Ma old Onverwacht Group of the Barberton greenstone belt, southern Africa. Field locations, age data, petrography, chemical and Nd isotopic analyses have already been presented by Jahn et al. (1982), Gruau (1983), and Gruau et al. (1990). The main geochemical features are summarized in Table 1.

The choice of Al-depleted and Al-enriched samples was dictated by the main goals of this study. Samples from the Onverwacht Group were preferentially selected because of the following:

a) The age of eruption is reasonably well-constrained at 3450 Ma (Kröner and Todt, 1988; Gruau et al., 1990).

b) The grade of metamorphism is greenschist to lower amphibolite facies (Viljoen and Viljoen, 1969). Under these moderate conditions, spinifex and other volcanic textures are preserved, and these, not chemical criteria, provide the basis for recognition of komatiitic rocks. Essentially magmatic trends are retained and refractory elements seem litltle mobilized (Jahn et al., 1982; Vijoen et al., 1983, ***see also the chapter on Schapenburg komatiites, this thesis***).

c) The rocks appear, on the basis of trace element and isotopic compositions, to have escaped contamination with older continental crust (Jochum et al., 1987; Gruau et al., 1990). In this respect, they are unlike komatiites from areas such as Kambalda, Australia, which apparently eroded thermally and assimilated crustal rocks (Huppert et al., 1984; Chauvel et al., 1985; Compston et al., 1986; Arndt and

Table 1: Origin and main geochemical features of selected samples

Sample N°	Classification	MgO %[1,2]	CaO/Al_2O_3[2]	Al_2O_3/TiO_2[2]	$(Gd/Yb)_N$[2]	$(La/Sm)_N$[2]	$\varepsilon_{Nd}(3450)$[3]
	KOMATI Formation						
5077	Gr. II BK	11.6	1.43	11.5	1.32	1.09	0.0±0.5
5080	Gr. II BK	9.6	0.95	12.1	1.40	1.49	0.0±0.4
5088	Gr. III BK	6.7	0.56	40.1	1.08	3.90	+1.3±0.4
	THEESPRUIT Formation						
5031	Gr. II K	32.0	1.00	11.3	1.66	2.15	-

BK: Basaltic komatiites; K: Komatiites

[1] recalculated on a 100% anhydrous basis

[2] data source: Jahn et al., 1982

[3] ε_{Nd} at time of eruption (3450 Ma); errors are ± 2σ; data source: Gruau et al., 1990

Jenner, 1986). Assimilation by komatiites of continental crust would have two disastrous consequences in this study. First, because old continental crust has ε_{Hf} significantly different from mantle rocks, contamination would effectively destroy any record in the komatiite of earlier mantle differentiation. Second, contaminated rocks could contain zircons inherited from the assimilated material. As discussed below, such zircons might escape dissolution during chemical preparation, and because of the high Hf content of zircon (≈1%, cf. <3 ppm in komatiite and komatiitic basalt), their presence would induce large errors in measured Lu/Hf and Hf isotopic ratios. This problem was responsible for strongly negative initial ε_{Hf} values in crustally contaminated komatiitic basalts from the Pilbara Block of Western Australia (Gruau et al., 1986; Gruau, personal observation).

EXPERIMENTAL PROCEDURE

All measurements were performed at the Max Planck Institute für Chemie, Mainz, as were most chemical separations. Aliquots for some Lu/Hf duplicates were separated at the Université de Rennes. Of the four selected samples, only three (5077, 5080, and 5088) were fully analyzed; for the remaining (5031), only the Lu and Hf contents were successfully determined. Lutetium and Hafnium concentrations were determined using isotopic dilution mass spectrometry except for samples 5031 which was analyzed by spark source mass spectrometry (SSMS).

For samples 5077, 5080 and 5088, the chemical procedure was essentially that described in Patchett and Tatsumoto (1980) and Gruau et al. (1988). Because of the problems associated with aliquoting sample solutions (Unruh et al., 1984), Lu and Hf concentrations (ID) and Hf isotopic conmpositions (IC) were determined on separate powders. The low Hf contents of komatiitic rocks meant that large amounts (several grams) of sample had to be dissolved. For Hf-IC, 4 g (sample 5088) to 8 g (samples 5077 and 5080) of powder were used. For Lu- and Hf-ID, a ^{176}Lu-^{179}Hf mixed spike was added and approximately 750 mg were treated. All samples were dissolved in a HF-HNO_3-$HClO_4$ mixture. Because of the large sample size, teflon bomb could not be employed, and the IC fractions were dissolved in open beaker, as was a first set of ID fractions. Problems arising from the potential presence of crustal zircons were assessed by repeating the ID measurements in teflon-bombs. Duplicate measurements of Lu/Hf and of the Hf isotopic composition of sample 5077 were also used to assess sample homogeneity.

The Hf sample/blank ratio was 1000 for samples 5080 and 5077, and 1500 for sample 5088. Lutetium blanks were undetectable (<0.025 ng).

Hf isotopic compositions were measured with Faraday cups of a double-collector Finnigan Mat 261 mass-spectrometer, using analytical techniques similar to those reported in Patchett and Tatsumoto (1980) and Patchett et al. (1981). Total Hf^+ ion currents were of 1.2-2.2 10^{-11} A. Data collection and fractionation correction procedures are described in White and Patchett (1984). All $^{176}Hf/^{177}Hf$ measured ratios were normalized to $^{179}Hf/^{177}Hf = 0.7325$.

Measured and calculated initial $^{176}Hf/^{177}Hf$ ratios are quoted throughout the text and in Table 2 in the ε_{Hf} notation of Patchett et al. (1981) as deviation in part per 10^4 from the chondritic growth curve. The present-day $^{176}Hf/^{177}Hf$ and $^{176}Lu/^{177}Hf$ for the chondritic reference reservoir are those determined by the Denver Laboratory (Patchett et al., 1981). The decay constant of ^{176}Lu is 0.0194 Ga^{-1}.

Fifteen analyses of the Denver JMC 475 Hf standard were made during the course of this study. Previous analyses of this standard in our laboratory were 0.000039 lower than the 0.282200 Denver value (White and Patchett, 1984). In this work, the deviation was slightly reduced: the 15 runs have yielded a mean $^{176}Hf/^{177}Hf$ of 0.282171 ± 15 ($2\sigma_m$). Nevertheless, the discrepancy between Mainz and Denver is still quite large, corresponding to about 1 ε_{Hf} unit, and because the chondritic parameters used in ε_{Hf} are from the Denver laboratory, we increased all the measured $^{176}Hf/^{177}Hf$ ratios by 0.000030 when ε_{Hf} values were calculated.

RESULTS AND DISCUSSION

The Lu-Hf results are listed in Table 2 and illustrated in Figs. 7 and 8. Three important aspects are as follows:

(a) Duplicate analyses (measurements of Lu/Hf using "open beaker" and "teflon bomb" dissolution techniques, respectively, and repeated determination of $^{176}Hf/^{177}Hf$ for sample 5077) gave extremely consistent results (Table 2). The good agreement demonstrates that the samples are homogeneous and free of zircons, which in turn indicates that problems inherent to the preparation of such large samples have been circumvented.

(b) All the samples exhibit Lu/Hf (or $^{176}Lu/^{177}Hf$) ratios lower than chondrites. For the three Al-depleted (Group II) rocks, the deviations are -23.3, -26.9 and -35.8%, respectively. we stress here that the Lu/Hf ratios of these three rocks

Table 2: Lu-Hf isotopic data for Barberton komatiitic rocks

Dissolution	Lu (ppm)	Hf (ppm)	Lu/Hf	$^{176}Lu/^{177}Hf$ [1]	$^{176}Hf/^{177}Hf$ [2]	$f_{Lu/Hf}$ [3]	$\varepsilon_{Hf}(0)$ [4]	$\varepsilon_{Hf}(3450)$ [4]
	5077 - Al-depleted basaltic komatiite							
Open beaker	0.2404	1.337	0.1798	0.02549	0.282294±54	-0.237	-18.9±1.9	+0.4±2.2
Open beaker	-	-	-	-	0.282309±17	-	-14.4±0.6	-
Teflon bomb [4]	0.2434	1.340	0.1816	0.02575	-	-0.229	-	-
Average 5077	**0.2419**	**1.339**	**0.1807**	**0.02562**	**0.282302±30**	**-0.233**	**-18.7±1.1**	**+0.4±1.4**
	5080 - Al-depleted basaltic komatiite							
Open beaker	0.2510	1.451	0.1730	0.02450	0.282248±27	-0.266	-20.6±1.0	+1.2±1.3
Teflon bomb [4]	0.2655	1.549	0.1714	0.02430	-	-0.272	-	-
Average 5080	**0.2583**	**1.500**	**0.1722**	**0.02440**	**0.282248±27**	**-0.269**	**-20.6±1.0**	**+1.5±1.3**
	5031 - Al-depleted komatiite							
(SSMS) [5]	0.0820	0.542	0.1512	-	-	-0.358	-	-
Open beaker [6]	0.0840	-	-	-	-	-	-	-
	5088 - Al-enriched basaltic komatiite							
Open beaker	0.2775	2.118	0.1310	0.01856	0.281852±31	-0.444	-34.6±1.1	+1.7±1.3
Teflon bomb [4]	0.2955	2.255	0.1310	0.01856	-	-0.444	-	-
Average 5088	**0.2865**	**2.187**	**0.1310**	**0.01857**	**0.281852±31**	**-0.444**	**-34.6±1.1**	**+1.7±1.3**

1: error is 0.5%

2: measured values; errors are given at $\pm 2\sigma_m$

3: $f_{Lu/Hf} = (^{176}Lu/^{177}Hf/0.0334) - 1$; 0.0334 = $^{176}Lu/^{177}Hf$ of chondrites

4: $\varepsilon_{Hf}(T) = ((^{176}Hf/^{177}Hf_{sample,\,T} / {}^{176}Hf/^{177}Hf_{chondrites,\,T}) - 1) * 10^4$

T = 0: $^{176}Hf/^{177}Hf_{chondrites} = 0.282860$

T = 3450 Ma : $^{176}Hf/^{177}Hf_{chondrites} = 0.280548$

nota: all measured $^{176}Hf/^{177}Hf$ ratios were increased by 0.000030 in the calculation of $\varepsilon_{Hf}(T)$ values (see text for explanation)

5: concentrations obtained by Spark Source Mass Spectrometry (SSMS)

6: Isotope dilution data from Jahn et al., 1982.

correspond almost exactly to values anticipated from consideration of their Gd/Yb ratios and also appear consistent with the interpretation that Al-depleted komatiites crystallized from magmas depleted in majorite garnet (Fig. 7). For the Al-enriched (Group III) sample 5088, the deviation is -44.4% (Table 2). Such a deviation is contrary to what would be produced by majorite accumulation, a point discussed below.

(c) The three samples fully analyzed for $^{176}Lu/^{177}Hf$ and $^{176}Hf/^{177}Hf$ have calculated initial ε_{Hf} values that are slightly positive but close to zero (Fig.8). The Al-depleted samples 5077 and 5080 yield $\varepsilon_{Hf}(3450)$ values of +0.4±1.4 and +1.5±1.3, repectively, and the Al-enriched sample 5088 an $\varepsilon_{Hf}(3450)$ of +1.7±1.3 (Table 2). These samples also have near zero ε_{Nd} (Fig. 8; Table 1).

A discussion of the significance of these results inevitably involves comparison of the calculated (observed) initial ε_{Hf} values with those predicted by the two alternative garnet fractionation models. It is immediatly clear, on a qualitative basis, that the near zero initial ε_{Hf} displayed by the Barberton rocks do not fit the "magma ocean" scenario of Gruau and Jahn (1983) and Othani et al. (1989). Particularly damning are the initial ε_{Hf} values for the Al-depleted (Group II) samples 5077 and 5080, which are slighlty positive rather than being negative, as would be predicted for samples formed from an old majorite-depleted layer (Fig. 6). Nonetheless, it remains to be shown that the differences between observed and predicted values are *quantitatively* meaningful, particularly in light of the relatively large uncertainties (±1.5 units) on the initial ε_{Hf} values. This can be done most convincingly by considering the compositions of the Al-depleted (Group II) samples.

The problem is as follows: if Al-depleted (Group II) komatiites formed by remelting of a 4400 Ma old majorite-depleted mantle layer, what initial ε_{Hf} should be found in the 3450 Ma old Barberton samples 5077 and 5080? To calculate these values we assume that the Lu/Hf of the komatiites was the same as that of the source; i.e. that the minerals residual during the melting processes did not fractionate these two elements. This assumption is reasonable because olivine and orthopyroxene (the likely residual phases during remelting of the majorite garnet depleted mantle layer) both accomodate insignificant quantities Lu and Hf (Fujimaki et al., 1984). It can be seen from Fig. 9 that majorite-depleted material with Lu/Hf ratios between 0.172 and 0.181 (those of samples 5080 and 5077) diverge from the Bulk Earth or chondritic Hf growth curve at a rate of -6.4 to -5.5 ε_{Hf} units per Ga. Had this material formed 4400 Ma ago, it would have had

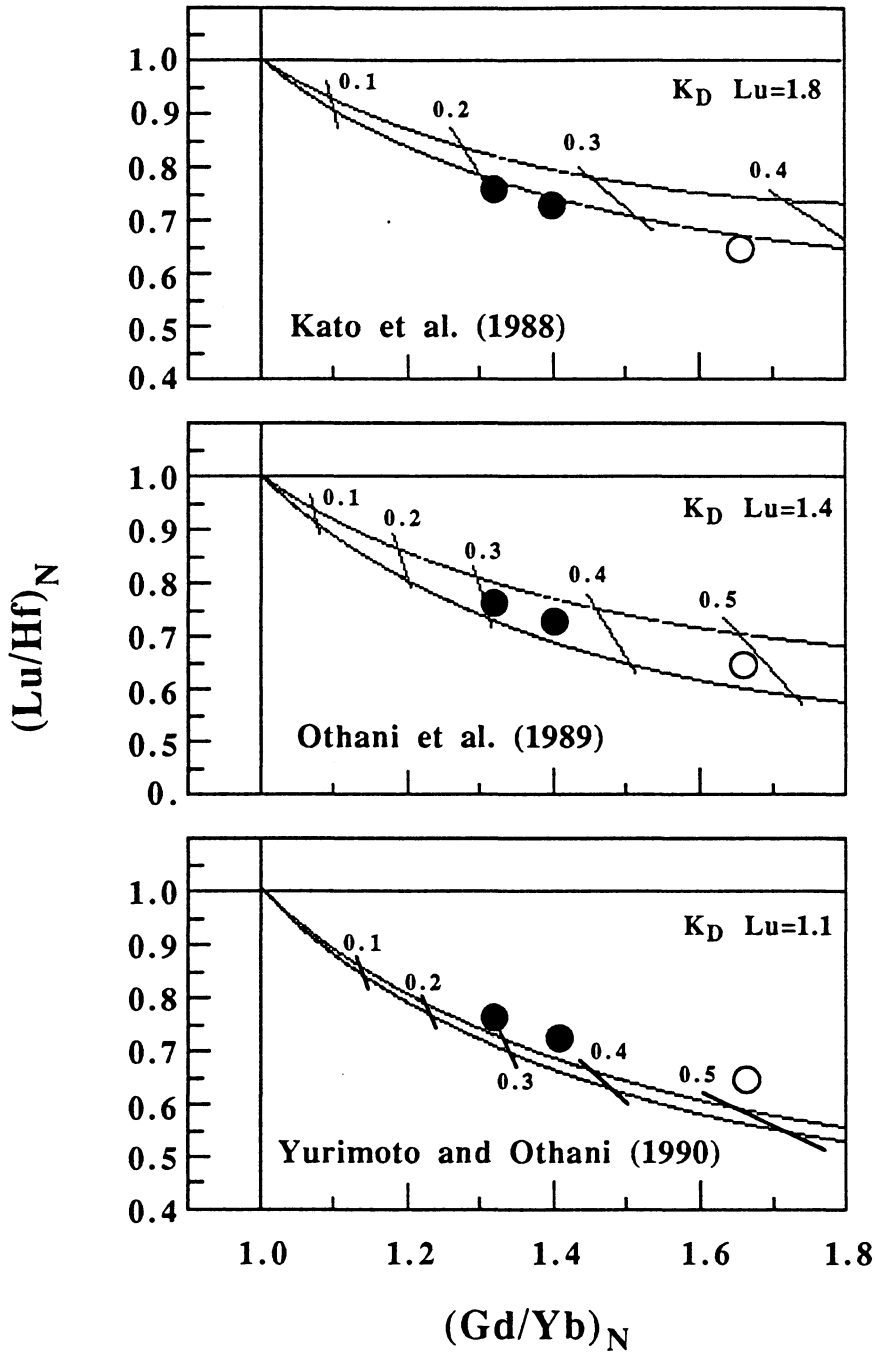

Figure 7: Plots of $(Lu/Hf)_N$ vs. $(Gd/Yb)_N$ showing a comparison between the ratios measured for Al-depleted (Group II) Barberton samples (closed symbols: komatiitic basalts; open symbol: komatiite) and those expected for majorite-depleted magmas (superimposed trends). In each diagram, the lower trend is that of majorite fractional crystallization (the "magma ocean" scenario), and the upper trend is that of partial melting with majorite garnet left as residual phase. The numbers next to the tick marks indicate either the mass fraction of garnet crystallized, or the amount of garnet left as solid residue. All curves have been modelled starting from a chondritic composition. The references refer to the source of the partition coefficients used in the calculations. For KD_{Lu}, the extrapolated values of Fig. 5 were taken.

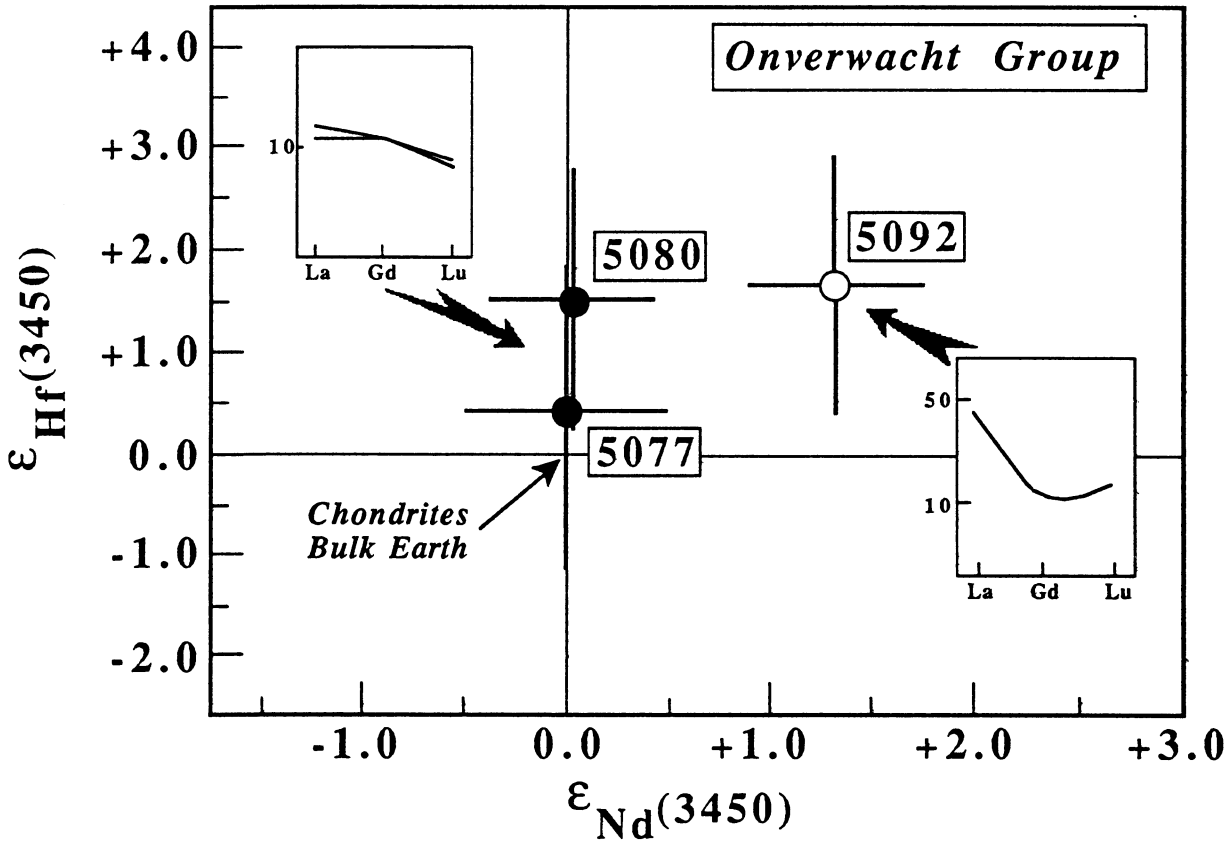

Figure 8: ε_{Hf} vs. ε_{Nd} diagram for Barberton samples at time of their eruption (3450 Ma).

ε_{Hf} = -5.2 to -6.1 at 3450 Ma, values which fall well below those calculated for the Barberton Al-depleted komatiite samples, which have ε_{Hf} values of +0.4±1.4 and +1.5±1.3 (Fig. 9).

But what of the single Al-enriched (Group III) sample? Like all such rocks, 5088 is enriched in Lu relative to Er; i.e. it possesses a Lu/Er ratio higher than chondritic (Jahn et al., 1982). Majorite accomodates Hf in roughly the same proportion as Er (Kato et al., 1988; Othani et al., 1989; Yurimoto and Othani, 1990; Fig. 5). If the composition of 5088 was controlled solely by majorite accumulation, its Lu/Hf ratio should also be higher than chondritic. Yet, as noted above, this sample has a very low Lu/Hf ratio ($f_{Lu/Hf}$ = -0.44; Table 2).

Consideration of the total trace element budget of 5088 leads us to conclude that the low Lu/Hf ratio of this sample is due to an overabundance of Hf. Like all Al-enriched komatiites from Barberton, 5088 is strongly enriched in LREEs (Table 1; Jahn et al., 1982.), whereas a sample enriched in majorite should show a relative depletion in these elements. The LREE enrichment of Barberton Group III komatiites indicates that a process other than majorite accumulation affected these rocks. Jahn et al. (1982) recognized the problem and suggested that the source was metasomatized by a LREE-enriched fluid prior to partial melting. If the metasomatizing fluid was silicate melt, it is not unreasonable to assume that it too was enriched in Hf. Enrichment of the source with such a fluid may then have been responsible for the abnormally low Lu/Hf ratio of sample 5088. The nearly-chondritic initial $^{176}Hf/^{177}Hf$ ratio (Table 2,; Fig. 8) therefore provides little constraint on the nature of its source: although it could indicate an essentially unfractionated chondritic source, the calculated initial isotopic composition could equally well have been imposed by the metasomatic fluid.

IMPLICATIONS FOR THE ORIGIN OF KOMATIITES AND EARLY MANTLE EVOLUTION

It remains to be shown that the model of majorite fractionation during melting, as advocated by Othani (1984), Othani et al. (1988) and Arndt (1986), represents the only alternative to the model of an early magma ocean. One alternative involves a magma ocean that did not crystallized immediatly after it formed but survived until 100-200 Ma before the eruption of Barberton komatiites. Layers enriched or depleted in majorite garnet could have formed during its final cooling. Although this model resembles the LLAMA (large laterally link Archean magma

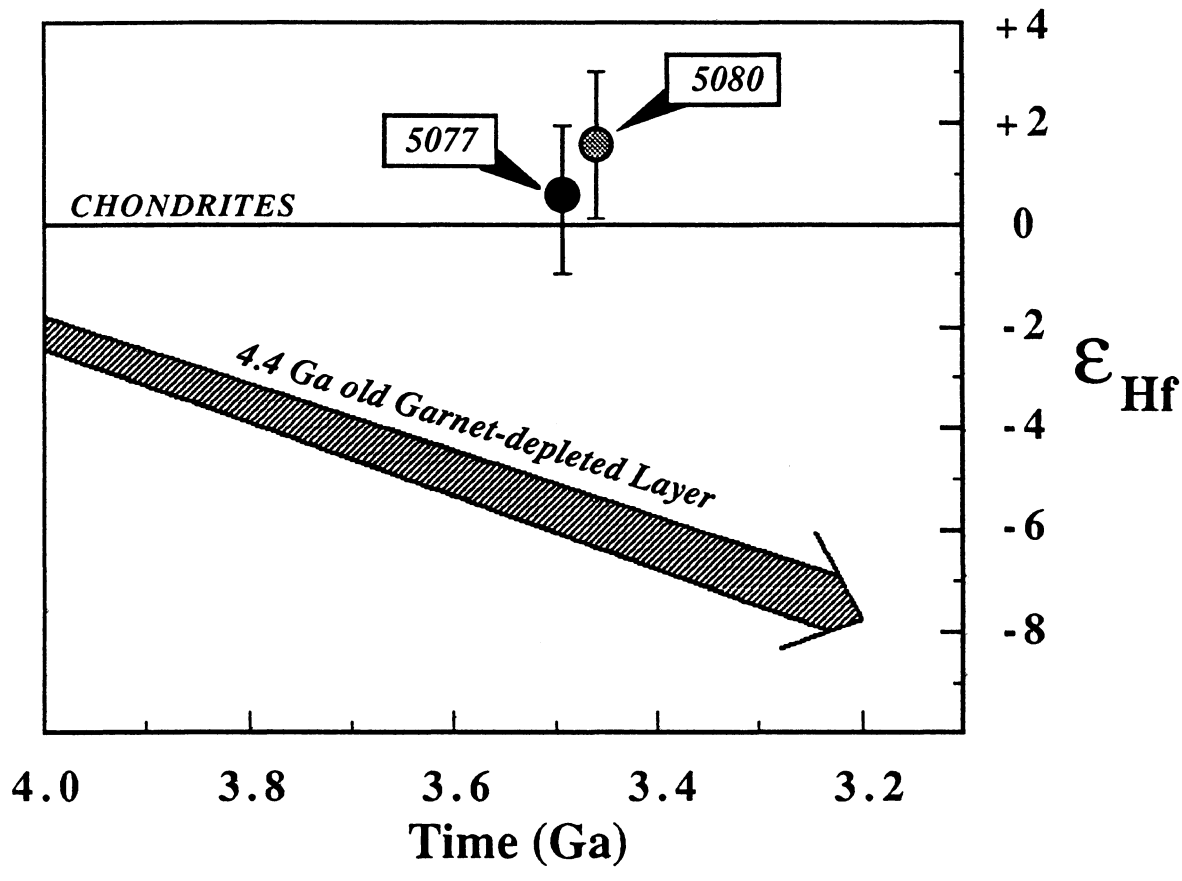

Figure 9: ε_{Hf} vs. time diagram showing a comparison between the observed initial ε_{Hf} of Al-depleted Barberton samples and that of the hypothetical melting products of a 4400 Ma old majorite-depleted mantle layer.

anomalies) concept of Nisbet and Walker (1982), it differs in that we envisage the magma ocean crystallizing and differentiating before the time of komatiite formation. With this model we could explain the near-zero initial ε_{Hf} of Barberton Al-depleted (Group II) komatiitic rocks: a layer depleted in majorite garnet only 200 Ma before the eruption of Barberton komatiites would have had an ε_{Hf} of about -1 by 3450 Ma, i.e., a value not significantly different from the calculated initial ε_{Hf} of samples 5077 and 5080 (Table 2). However, we see a major objection in the range of initial ε_{Nd} values in 3450 Ma old komatiites: coeval Barberton and Pilbara ultramafic lavas exhibit a range in initial ε_{Nd} values from 0 to +4 (Gruau et al., 1987, 1990). A large magma ocean would have convected vigorously and should have been well mixed, and it is difficult to imagine how reservoirs with different Sm/Nd could have remained isolated from one another for the time required (>500 Ma) to produce the observed range in ε_{Nd}. Likewise, we note the positive ε_{Nd} values of Pilbara komatiites (+4) and the indication they give of an origin from a depleted source with Sm/Nd higher than chondrites. A magma ocean produced by partial melting of the mantle should have a Sm/Nd ratio equal to or lower than chondritic ratio (Kato et al., 1988).

Our conclusion that the garnet fractionated during the partial melting that produced komatiites has several implications. The first concerns the development and subsequent evolution of the original terrestrial magma ocean. Many authors (Anderson, 1982; Hofmeister, 1983; Othani, 1988; Agee and Walker, 1988) regard thge formation of a magma ocean as an inevitable stage in the early history of the Earth. Our data indicate that had a magma ocean formed 4400 Ma ago, it either did not differentiate into majorite-enriched and majorite-depleted layers, or, if such layers had formed, they were destroyed soon after by mantle convection or are not samples by magmas reaching the surface of the Earth.

The second implication is that the compositions of komatiites need not correspond to those of their mantle sources. This conflicts with a commonly held concept that komatiites form by high degree mantle melting during which olivine was the sole residual phase. If we accept that majorite was residual during the partial melting that formed Al-depleted komatiites, we must also accept that many elemental ratios of geological interest (e.g. La/Sm, Gd/Yb, Al/Ti, Sm/Nd, Ti/Y) were strongly affected by the melting process.

SUMMARY AND CONCLUSIONS

The results discussed in this paper shows that the chemical variability of Archean komatiites is not inherited from the compositions of garnet-enriched and garnet-depleted layers produced by the crystallisation of an ancient magma ocean. The Archean mantle probably had essentially chondritic ratios of CaO/Al_2O_3, Al_2O_3/TiO_2 and Gd/Yb, and the various groups of komatiites arise from differences in the conditions of melting which controlled whether or not garnet was residual during the melting process.

Acknowledgment- This work was initiated through discussions of G. Gruau with P.J. Patchett. G. Gruau is personaly very grateful to A.W. Hofmann for the access to the Max Planck Institut analytical facilities. We are also grateful to N. Morin and M. LeCoz-Bouhnik for technical assistance for that part of the work done at the Université de Rennes. We also thanks the following for discussions and reviews of various version of the manuscript: A.W. Hofmann, E.J. Othani, S.S. Sun, B.M. Jahn, B. Auvray, P.J. Patchett, V.M.J. Salters and J. Bernard-Griffiths. During his stay in Mainz, G. Gruau benefited by a Max Planck Foundation grant obtained in relation with the french CNRS.

REFERENCES

Agee C.R. and Walker D. (1988) Mass balance and phase density constraints on early differentiation of chondritic mantle. *Earth Planet. Sci. Lett.* **90**, 144-156.

Albarède F. and Brouxel M. (1987) The Sm/Nd secular evolution of the continental crust and the depleted mantle. *Earth Planet. Sci. Lett.* **82**, 25-35.

Anders E. (1977) Chemical composition of the Moon, Earth and Eucrite parent body. *Philos. Trans. R. Soc. Lond. A*, **285**, 23-40.

Anderson D.L. (1982) Isotopic evolution of the mantle: a model. *Earth Planet. Sci. Lett.* **57**, 13-24.

Arndt N.T. (1976) Melting relations of ultramafic lavas (komatiites) at one atmosphere and high pressure. *Carnegie Inst. Wash. Year B.* **75**, 555-561.

Arndt N.T. (1986) Komatiites: a dirty window to the Archean mantle. *Terra Cognita* **6**, 59-66.

Arndt N.T. and Nisbet E.G. (1982) *Komatiites*. George Allen and Unwin. 526p.

Arndt N.T. and Nesbitt R.W. (1984) Magma mixing in Komatiites Lavas from Munro Township, Ontario, in *Archaean Geochemistry* (eds. A. Kröner, G.N. Hanson and A.M. Goodwin), pp. 94-114, Springer-Verlag.

Arndt N.T. and Jenner G.A. (1986) Crustally contaminated komatiites and basalts from Kambalda, Western Australia. *Chem. Geol.* **56**, 229-255.

Basaltic Volcanism Study Project (1981) *Basaltic volcanism on the terrestrial planets*. Pergamon Press. 1286p.

Bickle M.J., Ford C.E. and Nisbet E.G. (1977) The petrogenesis of peridotitic komatiites: evidence from high-pressure melting experiments. *Earth Planet. Sci. Lett.* **37**, 97-106.

Brévart O., Dupré B. and Allègre C.J. (1986) Lead-Lead age of komatiitic lavas and limitations on the structure of the Precambrian mantle. *Earth Planet. Sci. Lett.* **77**, 293-302.

Campbell I.H., Griffiths R.W. and Hill R.I. (1989) Melting in an Archaean mantle plume: Heads its basalts, tails its komatiites. *Nature* **339**, 697-699..

Cattell A., Krogh T.E. and Arndt N.T. (1984) Conflicting Sm-Nd whole-rock and U-Pb zircon ages for archean lavas from Newton Township, Abitibi Belt, Ontario. *Earth Planet. Sci. Lett.* **70**, 280-290.

Cawthorn R.G. and Strong D.F. (1974) The petrogenesis of komatiites and related rocks as evidence for a layered upper mantle. *Earth Planet. Sci. Lett.* **23**, 369-375.

Chauvel C., Dupré B. and Jenner G.A. (1985) The Sm-Nd age of Kambalda volcanics is 500 Ma too old! *Earth Planet. Sci. Lett.* **74**, 315-324.

Chase C.G. and Patchett P.J. (1988) Stored mafic/ultramafic crust and the earlyArchean mantle depletion. *Earth Planet. Sci. Lett.* **91**, 66-72.

Compston W. , Williams I.S., Campbell I.H. and Gresham J.J. (1986) Zircon xenocrists from the Kambalda volcanics: age constraints and direct evidence for older continental crust below the Kambalda-Norseman greenstones. *Earth Planet. Sci. Lett.* **76**, 299-311.

DePaolo D.J. and Wasserburg G.J. (1976) Inferences about magma sources and mantle structure from variations of $^{143}Nd/^{144}Nd$. *Geophys. Res. Lett.* **3**, 743-746.

Fujimaki H., Tatsumoto M. and Aoki K. (1984) Partition coefficients of Hf, Zr and REE between phenocrysts and groundmass. *J. Geophys. Res.* **89**, 662-672.

Green D.H. (1975) Genesis of Archean peridotitic magmas and constraints on Archean geothermal gradients and tectonics. *Geology* **3**, 15-18.

Green D.H., Nicholls I.A., Viljoen M.J. and Viljoen R.P. (1975) Experimental demonstration of the existence of peridotitic liquids in earliest Archean magmatism. *Geology* **3**, 11-14.

Gruau G. (1983) Etude géochimique d'associations volcaniques basiques et ultrabasiques d'age supérieur à 3.5 AE: conséquences sur la structure du manteau archéen précoce. Thèse de 3° cycle. Univ. de Rennes.

Gruau G. and Jahn B.M. (1983) Significance of REE typology of komatiites: argument for early mantle stratification (abstr.). *Terra Cognita* **3**, 130.

Gruau G, Arndt N.T., Chauvel C. and Jahn B.M. (1986) Large scale compositional heterogeneity of the early Archean mantle: Hf isotopic evidence (abstr.). *Terra Cognita* **6**, 245.

Gruau G., Jahn B.M., Glikson A.Y., Davy R., Hickman A.H. and Chauvel C. (1987) Age of the Talga-Talga Subgroup, Pilbara Block, Western Australia, and early evolution of the mantle: new Sm-Nd isotopic evidence. *Earth Planet. Sci. Lett.* **85**, 105-116.

Gruau G., Cornichet J. and Le Coz-Bouhnik M. (1988) Improved dtermination of Lu/Hf ratio by chemical separation of Lu from Yb. *Chem. Geol.(Isot. Geosci. Sec.)* **72**, 353-356.

Gruau G.,Chauvel C.and Jahn B.M. (1990) Anomalous Sm-Nd ages for the early Archean Onverwacht Group volcanics: Significance and petrogenetic implications.*Contrib. Mineral. Petrol.* **104**, 27-34.

Hofmeister A.M. (1983) Effect of a headen terrestrial magma ocean on crust and mantle evolution. *J. Geophys. Res.* **88**, 4963-4983.

Hupper J.E., Sparks R.S.J., Turner J.S. and Arndt N.T. (1984) Emplacement and cooling of komatiite lavas. *Nature* **309**, 19-22..

Ito E. and Takahashi E. (1987) Melting of peridotite at uppermost lower-mantle conditions. *Nature* **328**, 514-517.

Jarvis G.T. and Campbell I.H. (1983) Archean komatiites and geotherms: solution to an apparent contradiction. *Geophys. Res. Lett.* **10**, 1133-1136.

Jahn B.M. and Sun S.S. (1979) Trace element distribution and isotopic composition of Archean greenstones. In *Origin and distribution of the elements* (ed. L.H. Ahrens), pp 597-618, Pergamon Press.

Jahn B.M., Vidal P. and Tilton G.R. (1980) Archean mantle heterogeneity: evidence from chemical and isotopic abundances in Archean igneous rocks. *Philos. Trans. R. Soc. Lond.* **A297**, 353-364.

Jahn B.M., Gruau G. and Glikson A.Y. (1982) Komatiites of the Onverwacht Group, S. Africa: REE geochemistry, Sm-Nd age and mantle evolution. *Contrib. Mineral. Petrol.* **80**, 25-40.

Jochum K.P., Hofmann A.W. and Arndt N.T. (1987) Nb/Th in precambrian and modern komatiites and basalts (abstr.). *Terra Cognita* **7**, 396.

Kato T., Ringwood A.E. and Irifune T. (1988) Experimental determination of element partitioning between silicate perovskite, garnet and liquid: constraints on early differentiation of the mantle. *Earth Planet. Sci. Lett.* **89**, 123-145.

Kaula W.M. (1979) Thermal evolution of the earth and moon growing by planetesimal impacts. *J. Geophys. Res.* **84**, 999-1008.

Kröner A. and Todt W. (1988) Single zircon dating constraining the maximum age of the Barberton greenstone belt, southern Africa. *J. Geophys. Res.* **93**, 15329-15337.

McKenzie D. (1984) The generation of partially molten rock. *J. Petrol.* **25**, 713-765.

Nesbitt R.W., Jahn B.M. and Purvis A.C. (1982) Komatiites: an early precambrian phenomenon. *J. Volc. Geother. Res.* **14**, 31-45.

Nisbet E.G. and Walker D. (1982) Komatiites and the structure of the Archean mantle. *Earth Planet. Sci. Lett.* **60**, 103-113.

Othani E. (1984) Generation of komatiite magma and gravitational differentiation in the deep upper mantle. *Earth Planet. Sci. Lett.* **67**, 261-272.

Othani E. (1988) Chemical stratification of the mantle formed by melting in the early stage of the terrestrial evolution. *Tectonophys.* **154**, 201-210.

Othani E. (1990) Majorite ganet fractionation and genesis of komatiites in the deep mantle. *Precambrian Res.*, in press.

Othani E., Kato T. and Sawamoto H. (1986) Melting of a model chondritic mantle to 20 GPa. *Nature* **322**, 352-353.

Othani E., Moriyama J. and Kawabe I. (1988) Majorite garnet stability and its implication for the genesis of komatiite magmas (abstr.) *Chemic. Geol.* **70**, 147.

Othani E., Kawabe I., Moriyama J. and Nagata Y. (1989) Partitioning of elements between majorite garnet and melt and implications for petrogenesis of komatiite. *Contrib. Mineral. Petrol.* **103**, 263-269.

Patchett P.J. and Tatsumoto M. (1980) A routine high-precision method for Lu-Hf isotope geochemistry and geochronology. *Contrib. Mineral. Petrol.* **75**, 263-267.

Patchett P.J., Kouvo O., Hedge C.E. and Tatsumoto M. (1981) Evolution of continental crust and mantle heterogeneity: evidence from Hf isotopes. *Contib. Mineral. Petrol.* **78**, 279-297.

Ransford G.A. (1979) A comparison of two accretional heating methods. *Proc. Lunar Planet. Sci. Conf.* **10th**, 1867-1879.

Smith A.D. and Ludden J.N. (1989) Nd isotopic evolution of the Precambrian mantle. *Earth. Planet. Sci. Lett.* **93**, 14-22.

Sun S.S. (1984) Geochemical characteristics of Archean ultramafic and mafic rocks: implications for mantle composition and evolution. *In Archaean Geochemistry* (eds. A. Kroner, G.N. Hanson and A.M. Goodwin), pp. 25-46, Springer-Verlag.

Sun S.S. and Nesbitt R.W. (1978) Petrogenesis of Archean ultrabasic and basic volcanics: evidence from rare earth elements. *Contrib. Mineral. Petrol.* **65**, 301-325.

Takahashi E. and Scarfe C.M. (1985) Melting of peridotite to 14 GPa and the genesisi of komatiite. *Nature* **315**, 566-568.

Takahashi E. (1986) Melting of a dry peridotite KLB1 up to 14 GPa: implications on the origin of peridotite upper mantle. *J. Geophys. Res.* **91**, 9367-9382.

Unruh D. M., Stille P., Patchett P.J. and Tatsumoto M. (1984) Lu-Hf and Sm-Nd evolution in lunar mare basalts. *J. Geophys. Res.* **89**, 459-477.

Vijoen R.P. and Viljoen M.J. (1969) Upper mantle Project. *Geol. Soc. S. Afr. Spec. Publ.* **2**.

Viljoen M.J., Viljoen R.P., Smith H.S. and Erlank A.J. (1983) Geological, textural, and geochimical features of komatiitic flows from the Komati formation. *Geol. Soc. S. Afr. Spec. Publ.* **9**, 1-20.

White W.M. and Patchett P.J. (1984) Hf-Nd-Sr isotopes and incompatible elements abundances in island arcs: implications for magam origin and crust-mantle evolution. *Earth Planet. Sci. Lett.* **67**, 167-185.

Yurimoto N. and Othani E. (1989) Trace element partitioning between majorite garnet and the ultrabasic liquid: A secondary ion mass spectroscopic study. Submitted to Nature.

Conseils aux utilisateurs de la méthode Lutetium-Hafnium...

1-Introduction

Dans le chapitre précédent nous avons présenté les résultats isotopiques du Hf obtenus sur trois échantillons de Barberton et montré l'impact que ces résultats ont sur la pétrogénèse des komatiites et la composition du manteau archéen précoce. Dans les faits, nous avons analysé un nombre beaucoup plus important échantillons. En particulier, des résultats complets (rapport Lu/Hf; composition isotopique du Hf) ont été obtenus sur une dizaine d'échantillons de métabasalte provenant du craton de Pilbara dans l'ouest de l'Australie. Les données de Pilbara n'ont toutefois pas pu être exploitées car ne présentant pas le degré de fiabilité requis. De fait, et à l'inverse des roches de Barberton, il ne nous a jamais été possible de reproduire les mêmes résultats d'une analyse à l'autre. Dans un certain nombre de cas nous avons pu mettre à jour les raisons pour lesquelles nous n'arrivions pas à "doubler" les résultats de Pilbara. Deux de ces raisons (présence de quelques grains de zircon dans les échantillons et problème des "aliquots") constituent des sortes de "pièges méthologiques" pour les néophites de la méthode. Compte tenu de la difficulté analytique majeure que représente l'acquisition de données isotopiques Lu-Hf sur échantillon roche-totale (sans parler du coût), il nous est apparu intéressant d'exposer ici ces deux "pièges méthodologiques", et d'essayer de dégager quelques règles simples devant permettre de les contourner. Par ailleurs, le lecteur trouvera en fin de chapitre un article présentant une méthode chimique de séparation quantitative du Lu et de l'Yb, méthode susceptible d'améliorer sensiblement la précision obtenue au niveau de la mesure du rapport Lu/Hf.

2-Les deux "pièges" de la méthode Lu-Hf

Le premier "piège" est à mettre en relation directe avec le haut potentiel d'ionisation de l'élément Hf, haut potentiel responsable de rendements très faibles dans les spectromètres de masse (plus de 100 fois moins que le Nd par exemple). Concrètement, une mesure fiable et précise de la constitution isotopique du Hf par spectrométrie de masse demande la présence de 10 µg de Hf sur le filament. Nous avons personnellement expérimenté trois spectromètres de masse différents (Finnigan MAT 261 avec deux collecteurs, Finnigan MAT 262 avec sept collecteurs et VG Sector) et dans les trois cas ce chiffre limite de 10 µg a été observé. Ceci à deux conséquences pratiques importantes. La première est que les roches de composition ultrabasiques (peridotites et komatiites), du fait de leurs teneurs en Hf très faibles (≤1 p.p.m.; Gruau et al., 1992; cette thèse), sont, pour l'instant, inaccessible à l'analyse. De fait, pour obtenir des résultats exploitables, des

quantités d'échantillon de l'ordre de 10 à 20 g devraient être traitées, ce qui, de notre propre expérience, n'est pas possible en l'état actuel des procédures de dissolution et de purification chimique. La deuxième conséquence est que, même en restreignant les analyses à des roches de composition basique (à priori plus favorables parce que plus riches), les quantités d'échantillon à dissoudre resteront importantes, de l'ordre de 2 à 5g. En effet, mis à part les basaltes alcalins, les teneurs en Hf n'excèderont pas 2 à 5 p.p.m. (e.g. Patchett and Tatsumoto, 1980; White and Patchett, 1984; Gruau et al., 1992; cette thèse). C'est à ce niveau que le premier "piège" survient. De fait, 5 g restant des quantités d'échantillon difficiles à traiter par "voie humide", l'opérateur aura tendance à: (1) sélectionner les échantillons présentant les teneurs en Hf les plus fortes; et (2) effectuer les dissolutions en becher ouvert (et non pas en "bombe" téflon), les quantités de poudre à attaquer demeurant quoi qu'il arrive très supérieures à la centaine de mg (2g au minimum). Là est le problème: qui dit fortes teneurs en Hf (e.g. 5 p.p.m.) dit, en effet, fortes teneurs en Zr (le rapport Zr/Hf est relativement constant dans les roches et les minéraux terrestres, de l'ordre de 40; e.g., Smith et al., 1987), et donc présence possible de zircons dans les échantillons (en particulier lorsque l'on s'adressera à des métabasaltes). Or il faut savoir: (1) que la teneur en Hf d'un zircon oscille entre 4000 et 13000 ppm, avec une valeur moyenne de l'ordre de 10000 ppm (voir Tableau 1); et (2) que la procédure de dissolution en becher ouvert imposée par la grande quantité d'échantillon à traiter aura toute les chances de laisser le zircon non-attaqué - on notera qu'un seul grain de zircon de 100 μm de diamètre contient environ 0.02 μg de Hf. D'où la possibilité d'obtenir des rapports $^{176}Hf/^{177}Hf$ et $^{176}Lu/^{177}Hf$ qui ne seront pas représentatifs des valeurs de l'échantillon roche-totale, et donc de produire des valeurs $\varepsilon_{Hf}(T)$ calculées différentes des vraies valeurs initiales (voir paragraphe suivant).

Le deuxième "piège" a trait à la procédure utilisée pour le dosage du Lu et du Hf. Deux méthodes sont à priori possibles: soit une seule dissolution est effectuée avec ajout du traceur isotopique (un mélange de ^{179}Hf et de ^{176}Lu dans les études que nous avons conduites) dans une fraction de la solution, l'autre fraction servant à mesure du rapport $^{176}Hf/^{177}Hf$ (technique dite des "aliquots" sur solution); soit, deux dissolutions séparées sont éffectuées avec introduction du traceur sur poudre solide dans celle des deux servant à la mesure des concentrations. Lorsque nous avons démaré notre programme de mesure avec les échantillons de Pilbara, notre idée était d'utiliser la méthode des "aliquots" sur solution, cette méthode permettant, normalement, de contrer les effets induits par les éventuelles hétérogénéïtés de poudre. Or il s'avère que la technique des "aliquots" est, appliquée au système Lu-Hf, une technique à "haut risque", dans la mesure où il est très difficile, voir impossible, d'assurer la mise en solution complète et simultanée

Tableau 1: Tableau illustrant les problèmes de mesure du rapport Lu/Hf engendrés par la présence de zircon et/ou l'utilisation de la technique dite des "aliquots" (ajout de traceur Lu-Hf sur solution). Les deux échantillons de référence sont des métabasaltes d'âge 3450 Ma provenant du craton de Pilbara, ouest de l'Australie.

Type d'attaque	"Aliquot" [1]	Lu (p.p.m.)	Hf (p.p.m.)	Lu/Hf	$^{176}Lu/^{177}Hf$
55C PILBARA		*(0.282404±38; -2.9±1.5; 141)*			
Becher ouvert	non	0.606	3.092	0.196	0.0278
Becher ouvert	non	0.598	3.033	0.197	0.0279
Bombe	non	0.657	3.803	0.173	0.0245
Bombe	non	0.651	3.816	0.170	0.0242
Becher ouvert	oui	0.595	3.551	0.168	0.0238
Becher ouvert	oui	0.608	3.222	0.189	0.0268
56A PILBARA		*(0.282256±55; -11.9±2.0; 135)*			
Becher ouvert	non	0.660	3.180	0.208	0.0294
Becher ouvert	oui	0.560	3.037	0.184	0.0261
Bombe	non	0.635	3.569	0.178	0.0252
Zircon [2]		0.5-90	13000-4000	0.000-0.023	0.0000-0.0032

[1] Cette rubrique indique le moment où le traceur ^{176}Lu-^{179}Hf a été ajouté dans la procédure de dissolution. Non veut dire que le traceur ^{176}Lu-^{179}Hf a été ajouté sur la poudre solide avant dissolution de celle-ci; oui signifie que le traceur a été ajouté une fois la dissolution éffectuée, sur une fraction de la solution totale obtenue.

[2] Concentrations en Lu et en Hf, et rapport Lu/Hf (valeurs minimales et maximales) généralement mesurés dans un zircon (e.g., Patchett et al., 1981; Smith et al., 1987; Corfu and Noble, 1992).

Nota: la première valeur entre parenthèses donne le rapport $^{176}Hf/^{177}Hf$ qui a été obtenu suite à la dissolution de l'échantillon en becher ouvert; le deuxième chiffre correspond à la valeur ε_{Hf}(3450 Ma) calculée en combinant ce rapport $^{176}Hf/^{177}Hf$ et le rapport $^{176}Lu/^{177}Hf$ déterminé suivant la même technique de dissolution (becher ouvert) avec ajout de traceur ^{176}Lu-^{179}Hf directement sur la poudre solide (pas "d'aliquot"); le troisième chiffre donne la teneur en zirconium de l'échantillon analysé. On remarquera le caractère fortement négatif des valeurs ε_{Hf}(3450 Ma) ainsi obtenues (voir Fig. 2)..

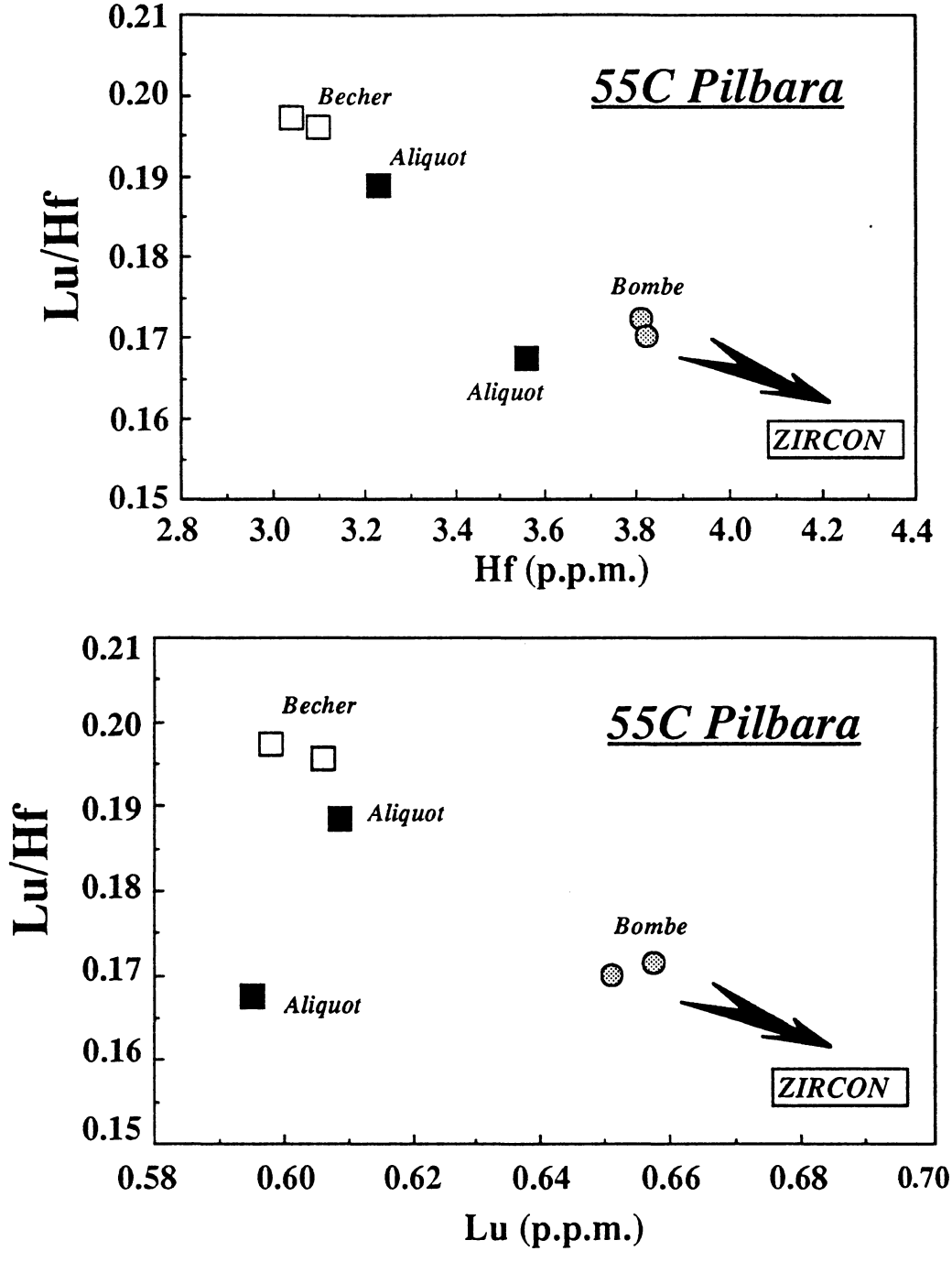

Figure 1: Diagrammes illustrant les différences de concentration en Lu et en Hf, et en rapport Lu/Hf observées lors des analyses répétées de l'échantillon 55C. Au cours des procédures de dissolution conduites en becher ouvert (becher dans le diagramme) et en "bombe", le traceur Lu-Hf était présent dès le début de l'attaque chimique. Le terme "aliquot" réfère à des résultats qui ont été obtenus pour des dissolutions conduites en becher ouvert avec ajout du traceur Lu-Hf une fois la mise en solution éffectuée. Les différences de concentrations et de rapport Lu/Hf entre les dissolutions menées en becher ouvert et celles conduites en "bombe" sont compatibles avec la présence de zircon dans l'échantillon (voir données sur zircon, Tableau 1), présence par ailleurs détectée lors d'opérations de filtration des solutions obtenues par attaque en becher ouvert (5 grains trouvés dans environ 750 mg de poudre traités).

du Lu et du Hf. En effet, si la solution contient un excès d'acide fluorhydrique, il y aura formation de fluorures insolubles qui pourront piéger une partie du Lu naturel contenu dans la solution de départ; à l'inverse, s'il n'y a pas assez de cet acide, il y aura précipitation de phases titanées, phases qui pourront incorporer une partie du Hf naturel (voir aussi Unruh et al., 1984). D'où la possibilité d'un déséquilibre entre le traceur introduit et le Lu et le Hf naturel présent dans la solution, avec comme conséquence des erreurs dans la détermination du rapport $^{176}Lu/^{177}Hf$ de l'échantillon roche-totale analysé.

3-Illustration: le cas des métabasaltes de Pilbara

Dans le Tableau 1 et la Figure 1, nous présentons une série de résultats qui illustrent quantitativement les deux problèmes précédemment énoncés. On notera les différences très importantes de rapport Lu/Hf obtenues lors des dissolutions en "bombe" (0.17) et en becher ouvert (0.20) conduites sur l'échantillon 55C, différences traduisant la présence de quelques grains de zircon dans la roche (5 grains ont été trouvés après filtration d'une solution obtenue après dissolution de 750 mg d'échantillon en becher ouvert). On notera aussi la dispersion très importante des valeurs engendrées par la technique des "aliquots". Par ailleurs, le lecteur trouvera dans la Figure 2 deux diagrammes illustrant les effets induits par la non-dissolution des zircons sur les valeurs $\varepsilon_{Hf}(T)$ calculées, dans l'hypothèse ou les zircons rencontrés seront des zircons d'origine métamorphique (ce qui est probablement le cas des zircons de Pilbara). Pour mémoire, on notera qu'une différence de rapport $^{176}Lu/^{177}Hf$ comme celle observée pour l'échantillon 55C entre les dissolutions en "bombe" et en becher ouvert correspond à une différence d'environ 12 unités d'ε_{Hf} lorsqu'on la propage sur 3450 Ma.

4-Conclusion: quelques conseils pratiques

En conclusion, s'il nous fallait tirer des enseignements des problèmes que nous avons rencontré, nous conseillerions aux nouveaux utilisateurs de la méthode:

-a) s'ils ont dans les roches qu'ils prévoient d'étudier des métabasites avec des teneurs en Zr supérieur à 100 p.p.m., de conduire, en parallèle, des déterminations du rapport Lu/Hf en becher ouvert et en "bombe", afin de s'assurer de l'absence (ou de la présence) de zircon (ne pas se fier aux etudes en lame mince, dans la mesure où quelques grains peuvent suffire à produire des résultats entièrement faux).

-b) d'éffectuer des dissolutions séparées pour le dosage du Lu et du Hf, et la mesure du rapport $^{176}Hf/^{177}Hf$, quite à répéter les mesures afin de s'assurer de l'homogénéïté des poudres analysées

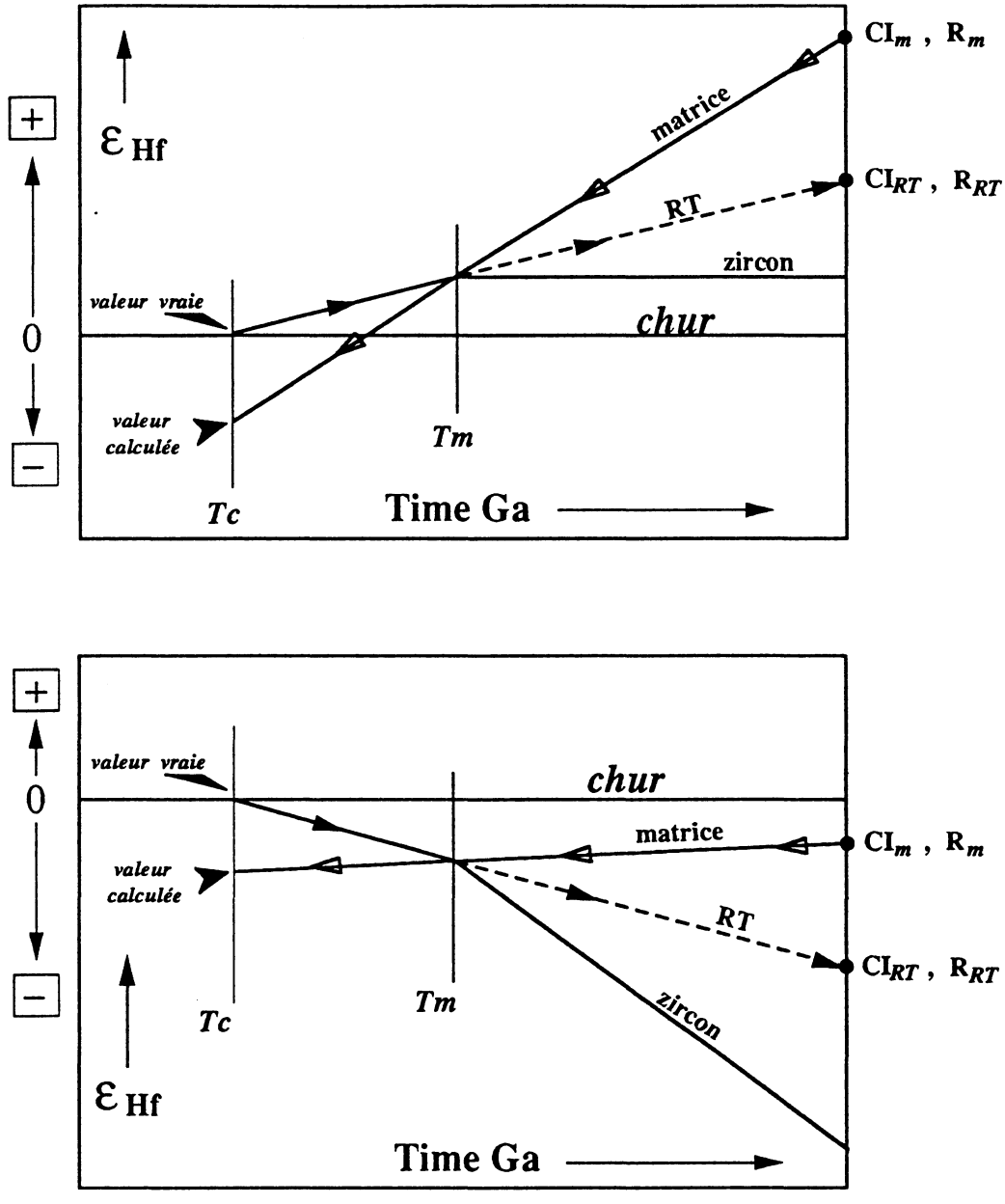

Figure 2: Diagrammes illustrant l'effet engendré par la non-dissolution du zircon sur les valeurs ε_{Hf} (T) calculées de deux roches basiques fictives contenant ce minéral. Dans les deux cas, les zircons sont supposés avoir une origine métamorphique (âge Tm des zircons inférieur à l'âge Tc de cristallisation de la roche hôte). Les trajectoires isotopiques vraies des échantillons sont décrites par les droites porteuses des flêches noires (RT). La non dissolution des zircons conduira à la mesure de rapports isotopiques du Hf (CI_m) et de rapports Lu/Hf (R_m) supérieurs aux valeurs de l'échantillon roche-totale (CI_{RT} ;R_{RT}), l'extrapolation dans le temps (trajectoires marquées par des flêches ouvertes) conduisant, dans les deux cas, à des valeurs ε_{Hf}(Tc) calculées qui seront inférieures aux vraies valeurs ε_{Hf} (Tc) des échantillons roche-totale.

Références

Corfu F. and Noble S.R. (1992) Genesis of the southern Abitibi greenstone belt, Superior Province, Canada: evidence from zircon Hf isotope analysis using a single filament technique. *Geochim. Cosmochim. Acta* **56**, 2081-2097.

Gruau G., Chauvel C., Arndt N.T. and Cornichet J. (1990) Aluminum depletion in komatiites and garnet fractionation in the early Archean mantle: Hafnium isotopic constraints. *Geochim. Cosmochim. Acta* **54**, 3095-3001.

Patchett P.J. and Tatsumoto M. (1980) Hafnium isotope variations in Oceanic Basalts. *Geophys. Res. Lett.* **7**, 1077-1080.

Patchett P.J., Kuovo O., Hedge C.E., and Tatsumoto M. (1981) Evolution of continental crust and mantle heterogeneity: evidence from Hf isotopes. *Contrib. Mineral. Petrol.* **78**, 279-297.

Smith P.E., Tatsumoto M., and Fahrquhar R.M. (1987) Zircon Lu-Hf systematics and the evolution of the Archean crust in the Superior Province, Canada. *Contrib. Mineral. Petrol.* **97**, 93-104.

Unruh D. M., Stille P., Patchett P.J., and Tatsumoto M. (1984). Lu-Hf and Sm-Nd evolution in Mare basalts. Proc. 14th Lunar Planet. Sci. Conf., Part 2, *J. Geophys. Res.* **89** (suppl. B), 459-477.

White W.M. and Patchett P.J. (1984) Hf-Nd-Sr isotopes and incompatible element abundances in island arcs: implications for magma origins and crust-mantle interaction. *Earth Planet. Sci. Lett.* **67**, 167-185.

Chemical Geology (Isotope Geoscience Section), 72 (1988) 353-356
Elsevier Science Publishers B.V., Amsterdam — Printed in The Netherlands

Short Communication

IMPROVED DETERMINATION OF Lu/Hf RATIO BY CHEMICAL SEPARATION OF Lu FROM Yb

G. GRUAU, J. CORNICHET and M. LE COZ-BOUHNIK

Centre Armoricain d'Étude Structurale des Socles, C.N.R.S., Institut de Géologie, Université de Rennes, F-35042 Rennes Cédex (France)

(Received October 21, 1987; revised and accepted February 2, 1988)

Abstract

Gruau, G., Cornichet, J. and Le Coz-Bouhnik, M., 1988. Improved determination of Lu/Hf ratio by chemical separation of Lu from Yb. Chem. Geol. (Isot. Geosci. Sect.), 72: 353-356.

A chemical method for the separation of Lu from silicate rocks and minerals is described. The method permits the separation of Lu from Yb and may be useful for precise determination of Lu/Hf ratios in geological systems.

1. Introduction

Initial $^{176}Hf/^{177}Hf$ ratios, if determined reliably in particular components of the Earth, Moon and meteorites, may provide important clues for the fractionation history of the Lu/Hf ratio during planetary accretion processes, core formation and crust–mantle differentiation. Therefore, the Lu–Hf method may contribute to a better understanding of planetary evolution (Patchett and Tatsumoto, 1980; Patchett et al., 1981; Patchett, 1983; Fujimaki and Tatsumoto, 1984). However, as in the Sm–Nd method, the approach suffers from the fact that the initial $^{176}Hf/^{177}Hf$ ratios are not measured but calculated values. Initial $^{176}Hf/^{177}Hf$ ratios are obtained by subtracting the contribution of radiogenic ^{176}Hf, related to the in situ decay of ^{176}Lu, from the present-day (measured) $^{176}Hf/^{177}Hf$ ratios. Thus, any further development of the ^{176}Lu–^{176}Hf decay scheme as a tracer of planetary evolution relies on precise determination of the $^{176}Lu/^{177}Hf$ ratio. A difference of 1% in the $^{176}Lu/^{177}Hf$ ratio will result in a difference of 1.04 ϵ_{Hf} units in the $^{176}Hf/^{177}Hf$ ratio over the age of the Earth (1 ϵ_{Hf} unit $\equiv$ 1 part in 10^4).

Apart from the problems of spike calibration inherent to any determination of inter-elemental ratios by the isotope dilution method, precise determination of $^{176}Lu/^{177}Hf$ ratios is complicated by two factors: (a) mass interference of ^{176}Yb to ^{176}Lu; and (b) incapacity of classical ion-exchange chromatography to isolate quantitatively Lu from Yb (both elements have very similar ionic radii: 0.85 and 0.86 Å, respectively). In 1980, Patchett and Tatsumoto put forward "a routine high-precision method for Lu–Hf isotope geochemistry and chronology". To avoid the problem of ^{176}Yb interference on ^{176}Lu in mass spectrometry analysis Patchett and Tatsumoto (1980) suggested: (a) to deliberately maintain the chemical recovery of Lu at around 50%, in order to reduce as far

0168-9622/88/$03.50

as possible the level of Yb in the Lu fraction; and (b) to use differences in thermal ionization temperature between Yb (more volatile) and Lu, to burn off Yb in the mass spectrometer before Lu analysis. Notwithstanding, according to Patchett and Tatsumoto (1980) and to our own experience (Gruau et al., 1986), a correction for ^{176}Yb interference is sometimes required. Moreover, when the level of Yb is too high, a significant loss of Lu may be observed during the time necessary to burn off all the Yb.

In this paper, we describe a chemical method of purification of Lu aliquots in rocks and minerals. This method permits a quantitative separation of Lu from Yb and may be useful in increasing the accuracy of the $^{176}Lu/^{177}Hf$ ratio. With respect to the high precision required on the $^{176}Lu/^{177}Hf$ ratio, neither a Lu recovery of ~50%, nor a correction for mass interference are sufficient.

2. Chemical purification of Lu

The method we describe is a two-column ion-exchange chromatographic procedure. Fig. 1 gives the physical properties and the elution profiles of the two columns. After dissolution of a sample with a HF–HNO_3–$HClO_4$ mixture and redissolution in 6 *M* HCl, an aliquot is spiked with a mixed Lu–Hf isotope tracer and loaded onto column *1* in 1 *M* HCl+0.05 *M* HF. Because the procedure was set up to be included in the general scheme of Lu–Hf chemical separation, column *1* is basically identical to column *A* of Patchett and Tatsumoto (1980). On column *1* (Fig. 1a), Hf, Zr, Ti, Cr, P, Al, and some other transition group of trace elements are first eluted with a 1 *M* HCl+0.05 *M* HF mixture and the collected fraction is kept for further isolation of Hf. After this, the remaining components are eluted with 2.5 *M* HCl and 2.5 *M* HNO_3; the Lu, together with a significant amount of Yb, is collected with 50 ml of 4 *M* HNO_3. The fraction containing Lu is then evaporated on a hot plate and the residue is treated with a few drops of 7 *M* HNO_3 and 12

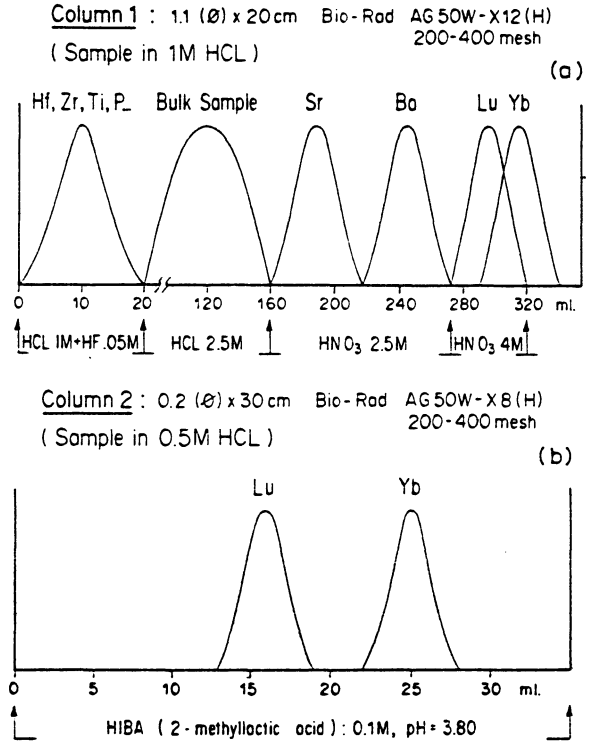

Fig. 1. Physical properties, resin type and elution profile of ion-exchange columns *1* (a) and *2* (b). See text for further explanation.

M $HClO_4$. After heating until dry, 0.05 ml of 0.5 *M* HCl is added and the sample is loaded onto column *2* (Fig. 1b).

The eluant used on column *2* is HIBA (*2*-methyllactic acid). The technique (size of column, type of resin) is basically similar to that earlier used by our group for Sm–Nd separation (Jahn et al., 1980), except that the molarity was adjusted to 0.1 *M* and the pH to 3.80. Under these conditions, Lu is eluted between 13 and 19 ml whereas Yb is collected between 22 and 28 ml (Fig. 1b). The 3-ml gap between Lu and Yb insures an optimal separation of the two elements (see next section). Note that the molarity and pH of HIBA must be precisely adjusted. A survey has shown that a slight increase in the molarity and/or the pH strongly affects the capacity of HIBA to isolate Lu from Yb. For example, an increase of 0.20 in the pH eliminates the 3-ml gap between Lu and Yb.

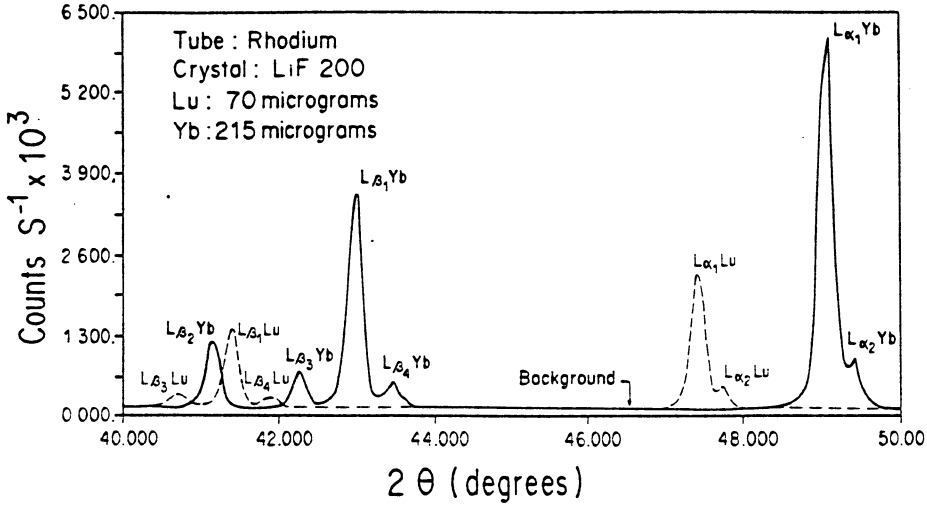

Fig. 2. X-ray fluorescence scan for Lu and Yb between 40° and 50° (2θ, LiF 200) as obtained on a Philips® PW *1014* automatic XRF spectrometer at Rennes University (Institut de Géologie). Estimates of Lu and Yb recovery were calculated from L_{α_1} peak heights measured from ion-exchange paper. The background was taken at 46.6°. Counting time was 40 s.

3. Recovery

In columns *1* and *2*, Lu and Yb contents were monitored and the recovery calculated using an X-ray fluorescence (XRF) spectrometry technique. The method used is similar to that described in Robinson et al. (1986) and is as follows: 70 μg Lu and 215 μg Yb spike were added to the sample aliquot before loading onto column *1* and further separation on column *2*. After evaporation, the eluted fractions containing Lu and/or Yb were taken up with 0.05 ml of 0.5 *M* HCl and loaded on Amberlite® ion-exchange papers (SA-2 Reeve Angel®; diam. = 4.25 cm). The papers were then analyzed using an automatic Philips® PW *1404* XRF spectrometer at Rennes University. During reconnaissance scans it was found that Lu and Yb were ideally separated (Fig. 2) and that there was no need for matrix effect corrections. With this technique, 65% of the Lu loaded onto column *1* was found in the 13–19-ml fraction collected with HIBA on column *2*. In this fraction, Yb was found to be below the detection limit of our XRF spectrometer (< 0.2 μg on each paper sample). This optimal separation of Lu from Yb was later confirmed by mass spectrometry analysis. Indeed, no Yb was found (even at low temperature) in the Lu fraction of a basaltic sample aliquot purified following the above described procedure.

Acknowledgements

The paper was inspired by P.J. Patchett and M. Tatsumoto who, through their pioneering work on the Lu–Hf method, indirectly initiated this study. Dr. M.S.N. Carpenter improved the English version of the manuscript. The manuscript also benefited by comments and suggestions from M. Tatsumoto. This work was funded in part under contract No. 15-48 of the INAG in connection with the ATP project "Transferts".

References

Fujimaki, H. and Tatsumoto, M., 1983. Lu-Hf constraints on the evolution of lunar basalts. Lunar. Sci., 14: 445–458.

Gruau, G., Arndt, N.T., Chauvel, C. and Jahn, B.M., 1986. Large scale compositional heterogeneity of the early Archean mantle: Hf isotopic evidence. Terra Cognita, 6: 245 (abstract).

Jahn, B.M., Bernard-Griffiths, J., Charlot, R., Cornichet,

J. and Vidal, F., 1980. Nd and Sr isotopic compositions and REE abundances of Cretaceous MORB (Holes *417*D and *418*A, Legs *51, 52* and *53*). Earth Planet. Sci. Lett., 48: 171-184.

Patchett, P.J., 1983. Importance of the Lu-Hf isotope system in studies of planetary chronology and chemical evolution. Geochim. Cosmochim. Acta, 47: 81-91.

Patchett, P.J. and Tatsumoto, M., 1980. A routine high-precision method for Lu-Hf isotope geochemistry and chronology. Contrib. Mineral. Petrol., 75: 263-267.

Patchett, P.J., Kouvo, O., Hedge, C.E. and Tatsumoto, M., 1981. Evolution of continental crust and mantle heterogeneity: evidence from Hf isotopes. Contrib. Mineral. Petrol., 78: 279-297.

Robinson, P., Higgins, N. and Jenner, G.A., 1986. Determination of rare earth elements, yttrium and scandium in rocks by an ion exchange-X-ray fluorescence technique. Chem. Geol., 55: 121-137.

DEUXIEME PARTIE

Essai sur le comportement des éléments chimiques (REE) et des systèmes isotopiques (Sm-Nd, Rb-Sr, et O) lors du métamorphisme des roches basiques et ultrabasiques archéennes

Chemical Geology, 90 (1991) 15–29
Elsevier Science Publishers B.V., Amsterdam

[4]

Resetting of REE, and Nd and Sr isotopes during carbonitization of a komatiite flow from Finland

S. Tourpin, G. Gruau, S. Blais and S. Fourcade
CAESS, CNRS, Institut de Géologie, Université de Rennes, F-35042 Rennes Cedex, France

(Received February 20, 1990; revised and accepted October 23, 1990)

ABSTRACT

Tourpin, S., Gruau, G., Blais, S. and Fourcade, S., 1991. Resetting of REE, and Nd and Sr isotopes during carbonitization of a komatiite flow from Finland. Chem. Geol., 90: 15–29.

New isotopic (Nd, Sr, C and O) and trace-element data are reported for a 10-m-thick komatiite flow unit from the 2660-Ma Tipasjärvi greenstone belt of eastern Finland. This unit was selected because of its anomalously variable REE distribution patterns. More specifically, while the lower cumulate zone of the flow exhibits nearly-flat LREE patterns [$(La/Sm)_N = 0.93–1.10$], the spinifex-textured upper zone shows strongly depleted LREE patterns [$(La/Sm)_N \approx 0.40$]. Such a fractionation in REE cannot result from low-pressure differentiation because the flow has MgO contents ranging from 25% to 30%, and only olivine, a phase which does not fractionate the REE, should have crystallized. In previous studies the REE patterns have been interpreted by the assumption that the flow had a composite origin: a LREE-depleted parental magma was inferred for the upper part; the lower part was thought to be derived from a parental magma with a chondritic distribution of LREE. In fact, in the present study, a reassessment of field and petrographic data indicates that the lower part of the flow is rich in secondary carbonate (10–20 wt.%). Determination of the chemical and isotopic composition of the carbonate, and further evaluation of the chemical and isotopic patterns of the flow in the light of the new data clearly show that the addition of carbonate is responsible for the variation in REE patterns.

The Tipasjärvi flow is not a magmatically composite flow, but a single and uniformly depleted flow, whose lower portion has experienced severe alteration of primary chemical and isotopic signatures by invasion of secondary carbonate.

1. Introduction

Komatiites are widespread in the Archean. Examples have been reported in most Archean greenstone belts, ranging from 3.5 to 2.5 Ga in age (Nesbitt et al., 1982). Komatiites are volcanic rocks with compositions approaching those of mantle peridotite (Arndt and Nisbet, 1982). In theory, komatiites represent a window to the nature and evolution of the Archean mantle. Most current models dealing with the composition of the primitive mantle, the early evolution of the crust–mantle system and the chemical and isotopic heterogeneities of the Archean mantle are based on geochemical and isotopic data from komatiites (e.g., Albarède and Brouxel, 1987; Chase and Patchett, 1988; Smith and Ludden, 1989).

However, the use of komatiites as probes for the Archean mantle composition is not so straightforward. One inherent defect is the invariably altered or recrystallized nature of komatiites, which casts some doubt about the preservation of primary chemical and isotopic compositions (e.g., Arndt et al., 1989). One of the more common alteration features of komatiites is carbonate metasomatism (Viljoen and Viljoen, 1969; Bavinton, 1981; Dupré et al., 1984; Arndt and Jenner, 1986; Blais et al., 1987; Arndt et al., 1989). One example of carbonitized komatiite occurs in the 2660-Ma-old Tipasjärvi greenstone belt of eastern Finland. where carbonates have been found in the basal

0009-2541/91/$03.50

part of a single spinifex-textured flow (Blais et al., 1987). Blais et al. (1987) have reported major- and trace-element data (including rare-earth elements, REE) for samples of this flow. Their results set a major problem: while the upper part of the flow exhibits strongly depleted light REE (LREE) patterns, the basal part has nearly-flat LREE patterns. Since the flow is ultrabasic in composition with MgO contents ranging from 25% to 30%, the low-pressure differentiation must have been controlled by olivine fractionation (Arndt, 1986). Olivine does not significantly fractionate the LREE. Consequently, under normal circumstances, the basal and upper parts should have parallel LREE patterns. Blais et al. (1987) recognized this problem and suggested that the basal and upper parts were genetically unrelated. According to Blais et al. (1987), the two parts crystallized from two different parental magmas: one depleted in LREE; the other with a flat LREE pattern.

In this study, we present isotopic data (Nd, Sr) for whole-rock samples from both the upper and basal parts of this flow, as well as C and O isotopic results for interstitial carbonates. We also report isotopic analyses of Nd, Sr, C and O and REE concentrations data for a nearly-pure carbonate vein cross-cutting the flow. The aim of this study was to constrain the effects of carbonitization on the initial isotopic and chemical composition of the flow, and to infer the primary characteristics of the unaltered komatiite.

2. Geological setting

Eastern Finland, like many other Archean granite–greenstone terrains, consists of low-grade metamorphosed volcanic and sedimentary sequences in faulted contact with a gneissic basement of trondjhemitic to granodioritic composition, the whole being intruded by late plutons of essentially granitic composition (Blais et al., 1978; Gaal et al., 1978; Jahn et al., 1980a; Vidal et al., 1980; Martin et al., 1983; Martin, 1985; Taipale, 1983; Martin and Querré, 1984). Tipasjärvi is the southernmost of three greenstone belts (Suomussalmi, Kuhmo, Tipasjärvi), which form an elongate N–S-trending band that extends over 200 km along the Finland–U.S.S.R. border (Fig. 1).

Taipale (1983) and Blais et al. (1987) have described the Tipasjärvi lithologies in detail. Tipasjärvi is a fairly typical Archean greenstone belt consisting of a complex assortment of komatiite lava flows, massive komatiite and basaltic units, felsic volcanics, metasediments and gabbroic intrusives. As is usual in such terrains, these units have been altered and metamorphosed. At Tipasjärvi, the metamorphic grade reached the upper greenschist to lower amphibolite facies. Metamorphic recrystallization and associated deformation has resulted in complete obliteration of the primary mineral assemblages, although some primary

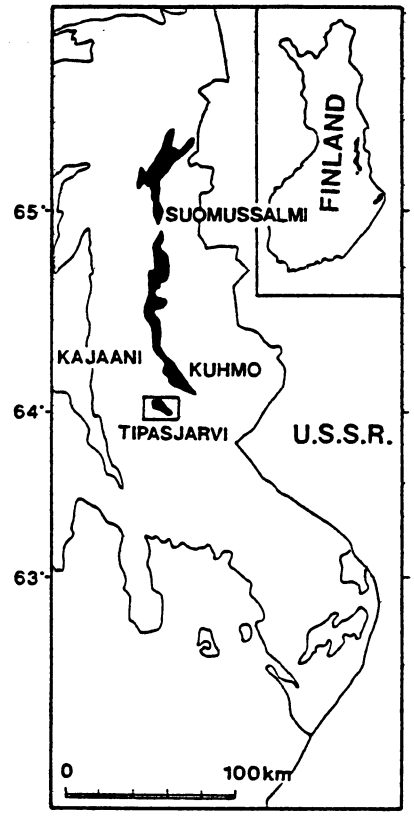

Fig. 1. Sketch map showing location of the Tipasjärvi greenstone belt.

textures (e.g., spinifex in komatiites) have been locally preserved.

Published radiometric data for the various lithologies of eastern Finland yielded the following results: 2860 ± 90 to 2620 ± 70 Ma (Rb–Sr and Pb–Pb) for the gneissic basement (Vidal et al., 1980; Martin et al., 1983; Martin, 1985); 2660 ± 40 Ma (Pb–Pb) for the greenstone successions; 2500 ± 70 to 2400 ± 40 Ma for the late granitic intrusions (Martin and Querré, 1984). Vidal et al. (1980) also reported Rb–Sr ages on micas from both the gneissic basement and the late granitic plutons. For the gneissic basement, the mica age is 2140 Ma, for the late intrusive plutons, it ranges from 1800 to 1700 Ma. Vidal et al. (1980) attributed these reset ages to the Svecokarelian orogeny of northern Scandinavia.

3. Petrography, texture and main geochemical features

The field characteristics and petrology of the Tipasjärvi komatiite flow have been described

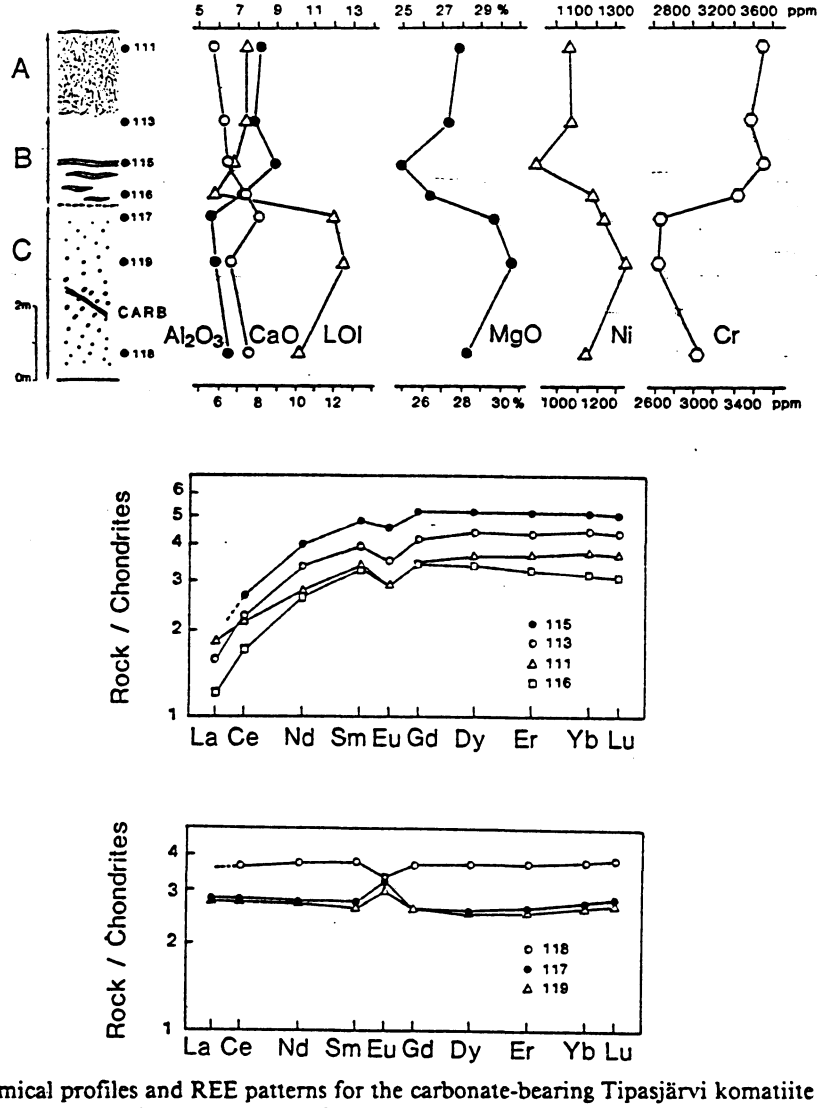

Fig. 2. Textures, chemical profiles and REE patterns for the carbonate-bearing Tipasjärvi komatiite flow (after Blais et al., 1987): (A) upper breccia; (B) intermediate spinifex-textured zone; and (C) lower cumulate zone. *CARB* = localization of carbonate vein sample.

in detail by Blais et al. (1987). The flow is ~10 m thick and consists of three main zones (Fig. 2): an upper breccia (2.3 m thick); an intermediate fine-grained spinifex-textured zone (3.0 m thick); a lower coarse-grained cumulate zone (4.7 m thick). A noticeable feature of this flow is the occurrence of subhorizontal spinifex-textured veinlets in the intermediate zone. In this respect the flow resembles certain komatiite flows from the Abitibi greenstone belt, Canada (Arndt, 1977).

Mineralogically, all parts of the flow exhibit secondary assemblages including tremolite, Mg-chlorite, anthophyllite and opaques. The presence of carbonate in the coarse-grained zone was noted by Blais et al. (1987), but its amount was underestimated. Instead of "rare aggregates of carbonate", careful re-examination of thin sections indicates up to 15–20 vol.% of carbonate. Likewise, Blais et al. (1987) did not mention the presence of carbonate in the breccia zone. In fact, this zone also contains carbonates, even though the amount does not exceed a few percent in volume. Only the intermediate spinifex-textured zone appears virtually free of any carbonate. Moreover, recent field work by two of us (S.T. and S.B.), has revealed that, in addition to interstitial carbonate, the basal part is cross-cut by nearly pure carbonate veins.

Microprobe analyses of both interstitial carbonate and carbonate veins yielded identical molar composition: $Ank_{18.5}Dol_{77.7}Calc_{3.8}$.

Seven samples from the Tipasjärvi flow were earlier analyzed by Blais et al. (1987) for their major- and trace-element (including REE) concentrations. The location of samples in the flow as well as some of the main chemical features are given in Fig. 2.

4. Samples and analytical techniques

Nd and Sr isotopic compositions as well as Sm/Nd and Rb/Sr ratios were determined for the seven samples previously studied by Blais et al. (1987), and for a carbonate vein sample (Fig. 2), for which we also measured the REE concentrations. C and O isotopic compositions were measured in the interstitial and vein carbonates. All analyses were performed at the Université de Rennes.

Nd and Sm/Nd ratios were determined on different aliquots of the same sample dissolution. For Sm and Nd concentrations, a mixed ^{149}Sm–^{145}Nd spike was added. The techniques used for chemical separation were essentially similar to those described in Richard et al. (1976), and the spike calibration results are given in Gruau et al. (1987). Nd blanks were of the order of 0.5 ng. Samples were run on a TSN *206*® single-collector CAMECA® mass spectrometer. Measured $^{143}Nd/^{144}Nd$ ratios were normalized to $^{146}Nd/^{144}Nd = 0.7219$. Results from the La Jolla Nd standard for 39 separate runs yielded $^{143}Nd/^{144}Nd = 0.511878 \pm 0.000012$ ($2\sigma_m$).

REE concentrations in the carbonate vein sample were determined by the isotopic dilution method using the procedure described in Jahn et al. (1980a).

The Sr isotopic compositions and Rb/Sr ratios were determined following the method of Jahn et al. (1980b). Sr blanks were of the order of 1 ng. $^{87}Sr/^{86}Sr$ ratios were all normalized to $^{86}Sr/^{88}Sr = 0.1194$. Results from the NBS *987* Sr standard on 23 separate runs yielded $^{87}Sr/^{86}Sr = 0.71037 \pm 0.00005$ ($2\sigma_m$), so all $^{87}Sr/^{86}Sr$ ratios presented in this paper were corrected by -0.00012 to be consistent with the NBS reference value of 0.71025.

The C and O from interstitial carbonates and the carbonate vein sample were analyzed as CO_2 gas on a triple-collector VG Sira *10*® mass spectrometer. Carbon dioxide was extracted from very finely-ground powders by reacting for 4–7 days with anhydrous orthophosphoric acid at 25°C, following the procedure of McCrea (1950). Fractionation during the liberation of CO_2 from carbonates was approximated to that of dolomite measured by Sharma and Clayton (1965) with $\alpha_{CO_2\text{-Dol}} = 1.01090$. The C and O isotopic compositions for inter-

stitial carbonates and the carbonate vein are given in the conventional δ notation, relative to the PDB and SMOW values, respectively. Duplicate runs of two samples yielded an analytical precision better than $\pm 0.05\delta$ units.

5. Results

5.1. *Nd and* REE *data*

The Sm–Nd results for the seven flow samples and the carbonate vein are given in Table I and reported in the conventional $^{143}Nd/^{144}Nd$ vs. $^{147}Sm/^{144}Nd$ isochron diagram in Fig. 3. The REE results for the carbonate vein sample are illustrated in Fig. 4.

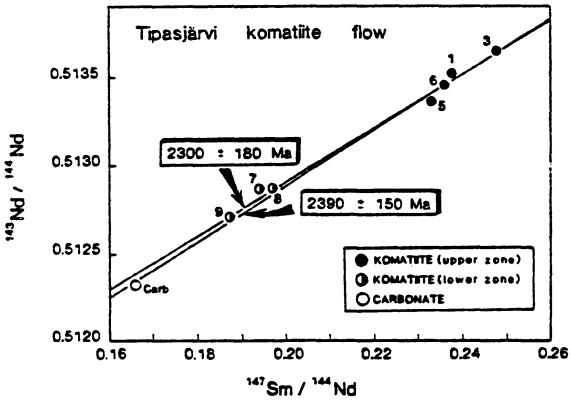

Fig. 3. Sm–Nd isochron diagram for the Tipasjärvi komatiite flow samples and cross-cutting carbonate vein. *2300 ± 180 Ma* refers to the flow samples only and *2390 ± 150 Ma* to the whole sample set (see text). Errors on dates are 2σ.

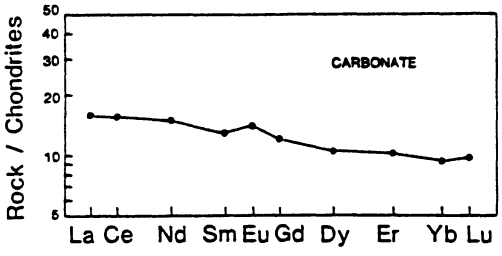

Fig. 4. REE pattern for the carbonate vein sample. Normalized values are those used in Jahn et al. (1980a). REE concentrations are as follows (in ppm): La (5.04); Ce (12.92); Nd (8.98); Sm (2.46); Eu (1.04); Gd (3.17); Dy (3.37); Er (2.15); Yb (1.95); Lu (0.31). Uncertainties are estimated better than ±3%.

The $^{147}Sm/^{144}Nd$ ratios for the seven flow samples are in agreement with the REE data of Blais et al. (1987), ranging from 0.2331 to 0.2478 for the breccia and the intermediate spinifex-textured zone, and from 0.1872 to 0.1969 for the basal zone. For the carbonate vein, the measured $^{147}Sm/^{144}Nd$ ratio is lower (0.1658). Such a ratio indicates a relative enrichment in Nd compared to Sm. Consistently, the carbonate vein sample yielded a LREE-enriched pattern [$(La/Sm)_N = 1.26$; Fig. 4], with an overall REE concentration higher by a factor of 3–4 than the komatiite flow samples (Figs. 2 and 4).

As shown in Fig. 3, there is a positive correlation between the $^{143}Nd/^{144}Nd$ and $^{147}Sm/^{144}Nd$ ratios of the seven flow samples. The corresponding calculated age is 2300 ± 180 Ma. If the carbonate vein sample data are included, this age becomes 2390 ± 150 Ma, which is statistically indistinguishable (Fig. 3).

5.2. *Sr data*

The Rb–Sr results are presented in Table II, and illustrated in a $^{87}Sr/^{86}Sr$ vs. Sr diagram in Fig. 5 and a $^{87}Sr/^{86}Sr$ vs. time diagram in Fig. 6.

All samples exhibit a very low $^{87}Rb/^{86}Sr$ ratio (0.0005–0.0222), such that no Rb–Sr age can be calculated. All the Rb concentrations are very low (0.05–0.22), while Sr is more variable: the lowest Sr concentrations are found in the spinifex-textured zone samples (15.2–20.5 ppm) and in the breccia (23.5 ppm); the carbonate vein sample has the highest Sr concentration (~700 ppm); contents in the carbonate-bearing lower-zone samples are intermediate, between 88 and 126 ppm Sr (Table II).

$^{87}Sr/^{86}Sr$ ratios are also variable. Samples with the highest Sr contents also possess the highest $^{87}Sr/^{86}Sr$ ratios (Fig. 5). $^{87}Sr/^{86}Sr$ ra-

TABLE I

Sm–Nd isotopic results for Tipasjärvi komatiite flow

	Breccia	Intermediate zone		
Sample No.	*111*	*113*	*115*	*116*
Analysis No.	*1*	*3*	*5*	*6*
% Carbonate[*1]	1–2	0.5	0.0	0.0
Sm (ppm)	0.641	0.627	0.857	0.609
Nd (ppm)	1.631	1.530	2.221	1.561
$^{147}Sm/^{144}Nd$[*2]	0.2378	0.2478	0.2331	0.2360
$^{143}Nd/^{144}Nd$[*3]	0.513524 ± 0.000014	0.513648 ± 0.000015	0.513362 ± 0.000015	0.513456 ± 0.000017
$\epsilon_{Nd(0)}$[*4]	+17.3 ± 0.3	+19.7 ± 0.3	+14.1 ± 0.3	+15.9 ± 0.3
$\epsilon_{Nd(2660Ma)}$[*4]	+3.3 ± 0.4	+2.2 ± 0.5	+1.5 ± 0.5	+2.3 ± 0.5

[*1] Amount estimated according to petrographic observations and CO_2 extraction experiments.
[*2] Error on this ratio is ± 0.2%.
[*3] Error on this ratio is $2\sigma_m$.

$$^{*4}\epsilon_{Nd(t)} = \left[\frac{(^{143}Nd/^{144}Nd)_t^{sample}}{(^{143}Nd/^{144}Nd)_t^{chondrites}} - 1\right] \times 10^4$$

with $(^{143}Nd/^{144}Nd)^{chondrites} = 0.512638$, for $t = 0$ Ma; and $(^{143}Nd/^{144}Nd)^{chondrites} = 0.509186$, for $t = 2660$ Ma.

TABLE II

Rb–Sr isotopic results for Tipasjärvi komatiite flow

	Breccia	Intermediate zone		
Sample No.	*111*	*113*	*115*	*116*
Analysis No.	1	3	5	6
% Carbonate[*1]	1–2	0.5	0.0	0.0
Rb (ppm)	0.119	0.092	0.117	0.055
Sr (ppm)	23.5	19.5	15.2	20.5
$^{87}Rb/^{86}Sr$[*2]	0.0146	0.01333	0.0222	0.0078
$^{87}Sr/^{86}Sr$[*3]	0.70506 ± 0.00004	0.70354 ± 0.00004	0.70415 ± 0.00002	0.70295 ± 0.00002
$(^{87}Sr/^{86}Sr)_{(2660Ma)}$[*4]	0.70450 ± 0.00005	0.70303 ± 0.00005	0.70329 ± 0.00004	0.70265 ± 0.00003
$\epsilon_{Sr(2660Ma)}$[*5]	+37.0 ± 0.7	+16.0 ± 0.7	+19.8 ± 0.4	+10.7 ± 0.4

[*1] Amount estimated according to petrographic observations and CO_2 extraction experiments.
[*2] Error on this ratio is ± 2%.
[*3] Error on this ratio is $2\sigma_m$.

$$^{*4}(^{87}Sr/^{86}Sr)_{(2660Ma)} = {}^{87}Sr/^{86}Sr - {}^{87}Rb/^{86}Sr\,[\exp(\lambda t) - 1]$$

with $t = 2.66$ Ga and $\lambda = 1.42 \cdot 10^{-11}$ a^{-1}.

$$^{*5}\epsilon_{Sr(2660Ma)} = \left[\frac{(^{87}Sr/^{86}Sr)_{(2660Ma)}}{(^{87}Sr/^{86}Sr)^{CHUR}_{(2660Ma)}} - 1\right] \times 10^4$$

with $(^{87}Sr/^{86}Sr)^{CHUR}_{(2660Ma)} = 0.70190$ (CHUR stands for chondritic uniform reservoir).

Cumulate zone			Carbonate
117	*118*	*119*	CARB
7	*8*	*9*	CARB
10–20	10–20	10–20	100
0.550	0.714	0.495	2.464
1.727	2.192	1.599	8.984
0.1939	0.1969	0.1872	0.1658
0.512870 ± 0.000023	0.512871 ± 0.000019	0.512710 ± 0.000020	0.512324 ± 0.000013
+4.5 ± 0.5	+4.5 ± 0.4	+1.4 ± 0.4	−6.0 ± 0.3
+5.5 ± 0.6	+4.5 ± 0.5	+4.7 ± 0.5	-

Cumulate zone			Carbonate
117	*118*	*119*	CARB
7	8	9	CARB
10–20	10–20	10–20	100
0.126	0.166	0.226	0.132
113.8	88.1	125.6	693.5
0.0032	0.0055	0.0052	0.0005
0.70604 ± 0.00003	0.70597 ± 0.00004	0.70651 ± 0.00003	0.70599 ± 0.00003
0.70591 ± 0.00003	0.70576 ± 0.00004	0.70631 ± 0.00003	0.70597 ± 0.00003
+57.1 ± 0.6	+55.0 ± 0.7	+62.8 ± 0.4	+58.0 ± 0.6

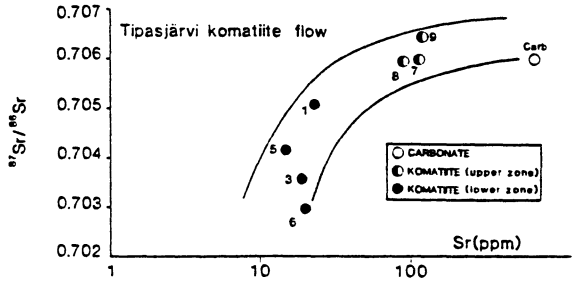

Fig. 5. $^{87}Sr/^{86}Sr$ vs. Sr (ppm) plot for the set of Tipasjärvi flow samples.

tios range from 0.70651 to 0.70597 in the carbonate vein and the lower part of the flow; from 0.70415 to 0.70295 in the intermediate-zone samples; for the breccia sample, the value lies between these two groups at 0.70507. Assuming a maximum age limit of 2660 Ma to correct for present-day $^{87}Sr/^{86}Sr$ from the decay of ^{87}Rb, a similar range is maintained: 0.70631–0.70576 for the carbonate vein and the lower zone of the flow; 0.70329–0.70265 for the intermediate-zone samples, and 0.70450 for the breccia (Fig. 6).

5.3. O and C data

The C and O results are presented in Table III. The carbonate dissolution experiments confirmed the thin-section observations for samples *115* and *116*, since no CO_2 could be extracted. By contrast, although optical studies failed to reveal any carbonate in sample *113*, some CO_2 was released. However, the amount was very small corresponding to <0.5 wt.% of carbonate. Nevertheless, this demonstrates that even the intermediate zone underwent some local carbonate metasomatism. For the other samples the carbonate contents were as follows: between 1 and 2 wt.% for the breccia sample *111*; between 10 and 20 wt.% for the three cumulate zone samples (*117, 118* and *119*).

The most striking feature of the C and O isotopic compositions is the limited range of the isotopic ratios measured in the sample suite: -3.4 to -2.4‰ for $\delta^{13}C$; $+9.3$ to $+12.3$‰ for $\delta^{18}O$ (Table III). Such a result is consistent with the assumption that interstitial and vein carbonates have a common origin.

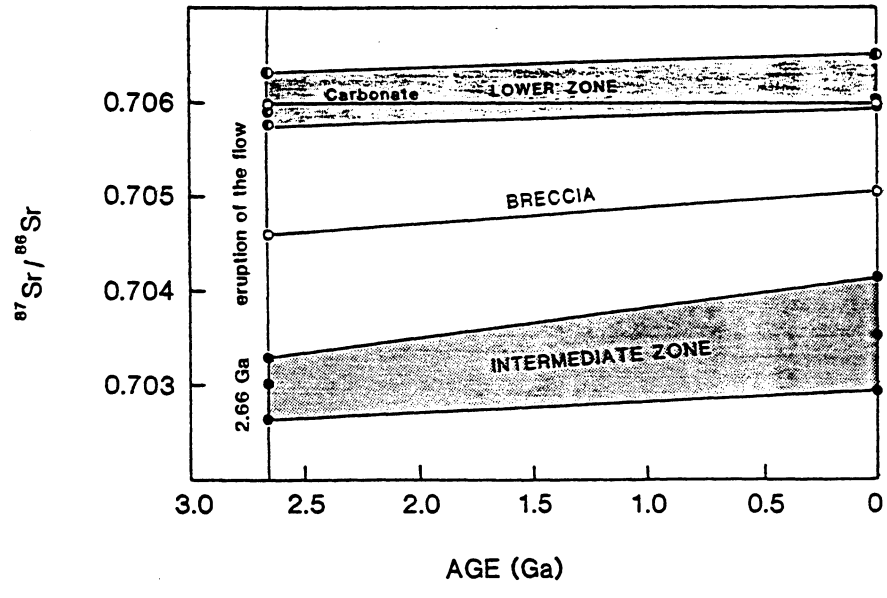

Fig. 6. Diagram illustrating the time evolution of the different $^{87}Sr/^{86}Sr$ ratios for the carbonate and lower-zone samples, and the samples with ≤ 1–2% of interstitial and vein carbonate. *2660 Ma* represents the assumed age of eruption of Tipasjärvi komatiite. See text for further explanation.

TABLE III

C and O isotopic results for Tipasjärvi komatiite flow

	Breccia	Intermediate zone			Cumulate zone			Carbonate
Sample No.	*111*	*113*	*115*	*116*	*117*	*118*	*119*	CARB
Analysis No.	*1*	*3*	*5*	*6*	*7*	*8*	*9*	CARB
% Carbonate*	1–2	0.5	0.0	0.0	10–20	10–20	10–20	100
$\delta^{13}C_{PDB}$ (‰)	−3.43	−2.60	-	-	−2.40	−2.32	−2.39	−3.11
$\delta^{18}O_{SMOW}$ (‰)	+12.27	+11.81	-	-	+9.83	+10.12	+9.89	+9.27

*Amount estimated according to petrographic observations and CO_2 extraction experiments.

6. Discussion

6.1. Sr and LREE *influx during addition of carbonate*

The contrasting REE patterns and Sr concentrations (Figs. 2 and 5; Table II) for the basal and upper zones of the Tipasjärvi flow are features that are clearly at variance with what we expect in a komatiite flow in which low-pressure differentiation was controlled by olivine fractionation (e.g., Arndt, 1986). The Sr and REE partition coefficients between olivine and magmatic liquids are always very low (e.g., Irving, 1978; Fujimaki et al., 1984). Thus, olivine fractionation cannot have produced large variations in $(La/Sm)_N$ or Sr contents such as those observed from the bottom to the top of the Tipasjärvi flow.

The 2300 ± 180-Ma Sm–Nd date calculated here for the seven Tipasjärvi flow samples is also aberrant. The date is much too young to represent the age of eruption of the flow: the Tipasjärvi belt – like the Kuhmo and Suomussalmi belts – is cross-cut by 2500-Ma-old granitic bodies (Taipale, 1983; Martin and Querré, 1984). Moreover, a 2300 ± 180-Ma date for the Tipasjärvi komatiite flow conflicts with the Pb–Pb isochron age at 2660 ± 40 Ma earlier reported by Vidal et al. (1980).

The contrasting REE patterns of the basal and upper parts of the Tipasjärvi flow could possibly represent primary magmatic features. If so, the most likely interpretation would be that of Blais et al. (1987) who proposed that two different parental magmas were erupted, each with distinct initial LREE distribution patterns. These two inferred parental magmas with different LREE patterns could have had distinct $^{143}Nd/^{144}Nd$ ratios, and this difference could explain why the Sm–Nd date is too young. The Tipasjärvi Sm–Nd array could then be interpreted as a magmatic mixing line. Examples of such magmatic mixing lines have been documented in the Kambalda greenstones of Western Australia (Chauvel et al., 1985; Compston et al., 1986), and in the komatiite–tholeiite suite of Newton Township, Canada (Cattell et al., 1984). At Tipasjärvi, however, there are at least two arguments against this interpretation: (1) in the two cited examples, the apparent ages are not too young, but rather older than the true ages (e.g., Chauvel et al., 1985); and (2) the lower-zone samples of the Tipasjärvi flow have nearly chondritic Sm/Nd ratio but $\epsilon_{Nd(2660Ma)}$-values up to +5.5 Table I). This conflicts with the +2 to +3 $\epsilon_{Nd(2660Ma)}$-values calculated for the upper zone samples with very high Sm/Nd ratios (Table I). Normal isotopic evolution would lead to lower ϵ_{Nd}-values in samples with lower Sm/Nd ratios.

A more likely interpretation is that the aberrant chemical and isotopic features of the Tipasjärvi flow are not primary magmatic characteristics. We will argue that the composition of the Tipasjärvi flow can be explained by the addition of metasomatic carbonates enriched

in LREE into uniformly depleted solidified komatiite.

Support for such an explanation is given in Figs. 7 and 3. Fig. 7 illustrates a close correlation between the $(La/Sm)_N$ ratios of Tipasjärvi samples and the amount of interstitial carbonate. The carbonate-bearing rock samples clearly have LREE patterns that are intermediate between the carbonate-free samples and the carbonate vein. For the Sm–Nd isotopic system, evidence is provided through the observation that the carbonate vein analysis lies on the extension of the Tipasjärvi flow Sm–Nd array (Fig. 3).

The role of carbonate is also illustrated by the variations of Ca contents with depth: in Fig. 2, concentration in CaO increases from top to bottom in the flow. Fig. 2 and Table III indicate that this increase correlates with higher proportions of carbonate. Clearly, crystallization of carbonate was accompanied by a strong elemental influx.

Nevertheless, it could be argued that the LREE-enriched character of the Tipasjärvi carbonates does not necessarily imply that LREE were introduced into the solid rock, but results from later redistribution within the flow. If so, the Tipasjärvi Sm–Nd array could be interpreted as a secondary isochron. In fact,

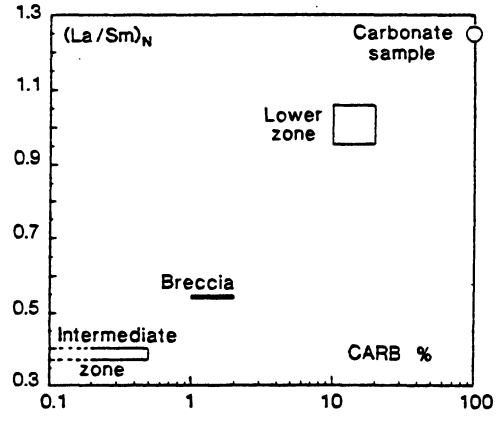

Fig. 7. Diagram illustrating correlation between $(La/Sm)_N$ and amount (in wt.%) of interstitial and vein carbonate for the Tipasjärvi sample suite. Data sources: Blais et al. (1987) and this study.

we do not deny the possibility that Nd and the other LREE were redistributed or re-equilibrated to some extent. Such a process is suggested by the fact that the carbonate-free samples do not have the highest $^{143}Nd/^{144}Nd$ and $^{147}Sm/^{144}Nd$ ratios (Table I; Fig. 3). However, the supposed redistribution must have been limited. It is clear that carbonate metasomatism supplied a significant amount of Sr to the carbonate-bearing samples (Fig. 5). Yet, the $^{87}Sr/^{86}Sr$ ratios of the carbonate-free samples (or of the samples with insignificant amounts of carbonate) are always much lower than those of the carbonate-rich samples (Fig. 6; Section 5.2). Consequently, Sr has not been re-equilibrated in the Tipasjärvi flow. Any re-equilibration hypothesis would thus result in the unexplained paradox that samples that have re-equilibrated for Nd and LREE do not show any $^{87}Sr/^{86}Sr$ effect.

In summary, the anomalously young Sm–Nd date of the Tipasjärvi flow, as well as the flat LREE patterns, high Sr concentrations and high $^{87}Sr/^{86}Sr$ ratios of the cumulate zone samples are all secondary features. Sr and LREE were introduced during the carbonate metasomatism that affected the Tipasjärvi flow. The Tipasjärvi Sm–Nd array gives an anomalously young date because it is not an isochron, but a mixing line between LREE-enriched carbonates and the initially depleted solidified komatiite.

6.2. When did the invasion of carbonate occur? What was the composition and origin of the CO_2-rich fluid?

When was the carbonate introduced to the Tipasjärvi komatiite flow? A temporal upper limit is provided by the Sm–Nd results. We can reasonably speculate that the Nd in the fluid responsible for carbonitization of the flow contained a significant component derived from the older gneisses of eastern Finland. The argument for such a Nd input arises from consideration that in Archean granite–greenstone

terrains, rocks of granitic compositions have by far the highest LREE concentrations. Fluids circulating through such terrains will thus tend to inherit the isotopic composition of the granitic end-member.

All the gneissic basement components in the area have ϵ_{Nd}-values that are much lower than those of Tipasjärvi komatiite samples with high $^{147}Sm/^{144}Nd$ (samples *113, 115* and *116*; Table I; Fig. 8). Thus, a plausible interpretation is that a positive slope already existed in the conventional Sm–Nd diagram by the time the carbonate was added to the solid depleted komatiite. If so, we may infer that 2400 Ma represents an upper limit for the carbonitization event. As already pointed out, biotites from the late Archean granitic plutons of eastern Finland yielded Svecokarelian Rb–Sr ages in the range 1800–1700 Ma (Vidal et al., 1980). The Svecokarelian events are actually the only known thermal events of eastern Finland in the period after 2400 Ma (Vidal et al., 1980). In this respect, 1800–1700 Ma may represent a reasonable age estimate for the introduction of carbonate to the Tipasjärvi flow. It is worth noting here that studies in progress in Rennes on the Kuhmo greenstone belt (20 km north of Tipasjärvi; Fig. 1) reveals that the Svecokarelian thermal events of eastern Finland have had much more influence than previously estimated. This event was able to rehomogenize the whole-rock Sm–Nd systems of Kuhmo komatiites and introduced chemical and isotopic disturbances far greater than those described in the present paper (Tourpin et al., unpublished).

The nature, composition and origin of the fluid which was responsible for the carbonitization remains to be discussed. If we assume that the carbonitization event took place at 1800–1700 Ma, then the fluid was probably metamorphic or hydrothermal. We can estimate the approximate crystallization temperature of the carbonates using the fact that the 1800–1700-Ma event has reset the Rb–Sr ages of the late-Archean granite biotites. A consideration of the blocking temperatures for biotite suggests that the minimum temperature was ~350°C (Jäger et al., 1967). Approximating the Tipasjärvi carbonate–H_2O fractionation coefficient by that of the dolomite–H_2O system (O'Neil et al., 1969; Sheppard and Schwarcz, 1970; Matthews and Kate, 1977), and assuming a temperature of ~350°C, the

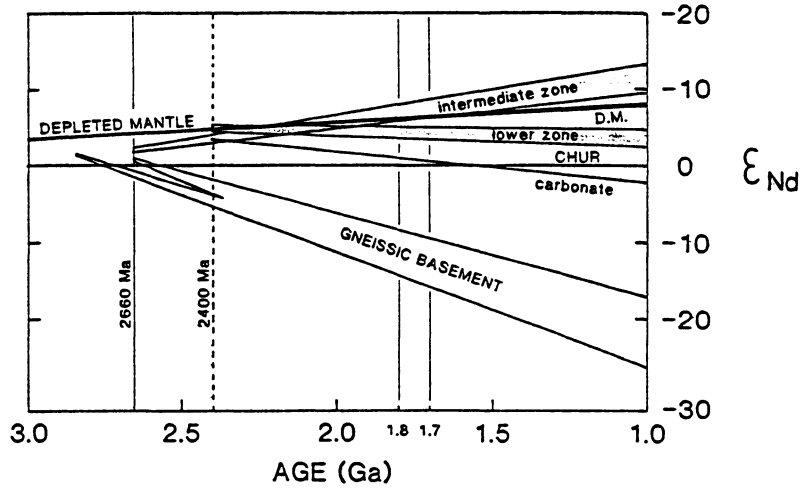

Fig. 8. $\epsilon_{Nd(t)}$ vs. time plot showing isotopic evolution in the various members of the Tipasjärvi flow and in the carbonate vein. The trajectories contrast markedly with the surrounding gneisses which show strongly negative ϵ_{Nd} at the present day. Data sources: Martin (1985) and this study.

calculated $\delta^{18}O$ for the fluid in equilibrium with the Tipasjärvi carbonates falls in the range +5 to +8‰. Such values lie in the field of metamorphic or hydrothermal fluids (rock-dominated fluid systems).

The isotopic compositions of C in carbonates are difficult to interpret since they may result from the control of a number of parameters (see Ohmoto and Rye, 1979), parameters that are not constrained in the present case. However, it is worth noting that the range of $\delta^{13}C$- and $\delta^{18}O$-values in the Tipasjärvi carbonate is quite common in ferroan dolomitic hydrothermal carbonate from Archean greenstone belts, such as the Abitibi province (see a review in Kerrich, 1987).

6.3. The Tipasjärvi flow: a komatiite flow initially homogeneously depleted

Finally, what was the chemical and isotopic composition of the Tipasjärvi komatiite flow before the addition of carbonate?

New results from the Tipasjärvi flow provide definitive arguments against the previous interpretation of Blais et al. (1987). Two different parental magmas, one depleted in LREE, and the other with flat LREE distribution pattern were apparently not emplaced at Tipasjärvi. The less-depleted characters of the cumulate and breccia zones are clearly not primary magmatic features, but features that arise from the input of LREE during introduction of carbonate.

Subtraction of the chemical and isotopic inputs due to carbonitization yields a model flow composition with similar depleted LREE patterns. All the REE patterns probably were identical to the carbonate-free samples *115* and *116* [$(La/Sm)_N = 0.39–0.40$; $(Gd/Yb)_N = 1.0–1.1$], or to that of sample *113* which has <0.5% of interstitial and vein carbonate [$(La/Sm)_N = 0.37$; $(Gd/Yb)_N = 0.93$]. In this respect, the Tipasjärvi flow may initially have resembled some of the komatiite flows from the Abitibi greenstone belt, Canada (Pyke et al., 1973; Arndt and Nesbitt, 1984; Arndt, 1986).

The flow might be also characterized by uniformly positive $\epsilon_{Nd(2660Ma)}$-values as in the carbonate-free samples *115* and *116* which have $\epsilon_{Nd(2660Ma)}$-values of $+1.5 \pm 0.5$ and $+2.3 \pm 0.5$, respectively (Table I; Fig. 8). Subtraction of the <0.5% carbonate of sample *113* gives a similarly positive $\epsilon_{Nd(2660Ma)}$-value of $+2.1 \pm 0.5$. For the cumulate zone samples with an apparent $\epsilon_{Nd(2660Ma)}$ of +4.5 to +5.5, the amount of carbonate is so high (10–20%) that the contamination cannot be accurately subtracted.

An $\epsilon_{Nd(2660Ma)}$ of $\sim +2.0$ indicates derivation of the Tipasjärvi parental magma from depleted mantle sources, a result consistent with the initially strongly depleted LREE patterns. In fact, the true, magmatic $\epsilon_{Nd(2660Ma)}$ value of the Tipasjärvi flow may have been slightly different from +2.0 if the carbonate and the host depleted komatiite experienced some re-equilibration of Nd (Section 6.1). Nevertheless, +2.0 is not an unexpected value for a ~2700-Ma-old komatiite: a similar value of $+2.4 \pm 0.5$ has been obtained for coeval komatiites from Alexo, Canada (e.g., Dupré et al., 1984; Machado et al., 1986; Shirey and Hanson, 1986).

Evaluation of the Sr data is much less straightforward. Although the REE and Nd of samples *115* and *116*, and of the carbonate vein may respectively represent uncontaminated-komatiite and carbonate end-members, this is not necessarily true for their present-day or initial $^{87}Sr/^{86}Sr$ ratios (Figs. 5 and 6). The problem of the initial Sr isotopic composition of the uncontaminated komatiite is well illustrated by sample *115*: the calculated initial $^{87}Sr/^{86}Sr$ ratio of this sample is 0.70329 ($\epsilon_{Sr(2660Ma)} = +19.8 \pm 0.4$), which is far above the value expected for a depleted komatiite. For sample *116*, a similar situation occurs: this sample also shows a high calculated initial $^{87}Sr/^{86}Sr$ ratio corresponding to an $\epsilon_{Sr(2660Ma)}$ of $+10.7 \pm 0.4$.

Another problem concerns the carbonate

end-member since the carbonate vein sample does not exhibit the highest $^{87}Sr/^{86}Sr$ ratio, as would be expected. In fact, the highest value is recorded by sample *119* (Fig. 5; Table II), on which a duplicate run was performed. The second analysis was statistically indistinguishable: 0.70643 ± 0.00005 instead of 0.70651 ± 0.00003.

Thus, Sr isotope data could be explained in two ways: (1) the invading fluid was isotopically heterogeneous with respect to Sr and the vein sample is not accurately representative of all the carbonate contaminant; (2) although the komatiite and the carbonate are not globally in isotopic equilibrium, there has been some limited equilibration effects between the silicate rock and the percolating fluid phase. So, in addition to the introduction of carbonate, the fluid phase could have also altered the initial Sr isotopic composition of "uncontaminated" komatiite by isotope exchange.

7. Summary and conclusions

We offer two main conclusions to this study. The first, and disquieting inference is the statement that the common process of carbonitization observed in many komatiites may result in a profound modification of the initial (magmatic) isotopic and chemical patterns. In such a situation, the ability of metakomatiites to provide straightforward information about the Archean mantle appears questionable. In the Tipasjärvi flow, not only the Sr but also the reputedly less mobile REE were clearly affected.

The second and more positive conclusion is that careful studies can help to eliminate the effects of carbonitization and thus provide, at least partially, a reconstruction of the initial isotopic and chemical composition of the uncontaminated komatiite. At Tipasjärvi, such a reconstruction is possible because the carbonitization is restricted to the basal part of the flow.

Acknowledgments

This paper benefited by critical comments and suggestions from B. Auvray and B.M. Jahn. We thank J. Cornichet and N. Morin for their assistance during chemical preparations, and J. Macé who performed some of the mass analyses. We are also indebted to K. Taipale, I. Tuokko, H. Martin and P. Jegouzo for their support during field work. Dr. M.S.N. Carpenter improved the English version of the manuscript. This work was funded in part under contract DBT No. 89-38-25-05 of the INSU (France). This is a contribution to IGCP project 280 ("The Oldest Rocks").

References

Albarède, F. and Brouxel, M., 1987. The Sm/Nd secular evolution of the continental crust and the depleted mantle. Earth Planet. Sci. Lett., 82: 25–35.

Arndt, N.T., 1977. Thick, layered peridotite–gabbro flows in Munro Township, Ontario. Can. J. Earth Sci., 14: 2620–2637.

Arndt, N.T., 1986. Differentiation of komatiite lava flows. J. Petrol., 27: 279–301.

Arndt, N.T. and Jenner, G.A., 1986. Crustally contaminated komatiites and basalts from Kambalda, Western Australia. Chem. Geol., 56: 229–255.

Arndt, N.T. and Nesbitt, R.W., 1984. Magma mixing in komatiite lavas from Munro Township, Ontario. In: A. Kröner, G.N. Hanson and A.M. Goodwin (Editors), Archaen Geochemistry, Springer, Berlin, pp. 94–114.

Arndt, N.T. and Nisbet, E.G., 1982. Komatiites. Allen and Unwin, London, 526 pp.

Arndt, N.T., Teixeira, N.A. and White, W.M., 1989. Bizarre geochemistry of komatiites from the Crixas greenstone belt, Brazil. Contrib. Mineral. Petrol., 101: 187–197.

Bavington, O.A., 1981. The nature of sulfidic metasediments at Kambalda and their broad relationships to ultramafic rocks and nickel ores. Econ. Geol., 76: 1606–1628.

Blais, S., Auvray, B., Capdevila, R., Jahn, B.M. and Hameurt, J., 1978. The Archean greenstone belts of Karelia (Eastern Finland) and their komatiitic and tholeiitic series. In: B.F. Windley and S.M. Naqvi (Editors), Archaen Geochemistry. Elsevier, Amsterdam, Developments in Precambrian Geology, 1. pp. 87–107.

Blais, S., Auvray, B., Jahn, B.M. and Taipale, K., 1987.

Processus de fractionnement dans les coulées komatiiques archéennes: cas des laves à spinifex de la ceinture de roches vertes de Tipasjärvi (Finlande orientale). Can. J. Earth Sci., 24: 953–966.

Cattell, A., Krogh, T.E. and Arndt, N.T., 1984. Conflicting Sm–Nd whole rock and U–Pb zircon ages for Archean lavas from Newton Township, Abitibi Belt, Ontario. Earth Planet. Sci. Lett., 70: 280–290.

Chase, C.G. and Patchett, P.J., 1988. Stored mafic/ultramafic crust and early Archean mantle depletion. Earth Planet. Sci. Lett., 91: 66–72.

Chauvel, C., Dupré, B. and Jenner, G.A., 1985. The Sm–Nd age of the Kambalda volcanics is 500 Ma too old! Earth Planet. Sci. Lett., 74: 315–324.

Compston, W., Williams, I.S., Campbell, I.H. and Gresham, J.J., 1986. Zircon xenocrysts from the Kambalda volcanics: age constraints and direct evidence for older continental crust below the Kambalda–Norseman greenstones. Earth Planet. Sci. Lett., 76: 299–311.

Dupré, B., Chauvel, C. and Arndt, N.T., 1984. Pb and Nd isotopic study of two Archean komatiitic flows of Alexo, Ontario. Geochim. Cosmochim. Acta, 48: 1965–1972.

Fujimaki, H., Tatsumoto, M. and Aoki, K., 1984. Partition coefficients of Hf, Zr and REE between phenocrysts and groundmass. J. Geophys. Res., 89: 662–672.

Gaal, G., Mikkola, A. and Soderholm, B., 1978. Evolution of the Archean crust in Finland. Precambrian Res., 9: 199–215.

Gruau, G., Jahn, B.M., Glikson, A.Y., Davy, R., Hickman, A.H. and Chauvel, C., 1987. Age of the Archean Talga-Talga Subgroup, Pilbara Block, Western Australia, and early evolution of the mantle: new Sm–Nd isotopic evidence. Earth Planet. Sci. Lett., 85: 105–116.

Irving, A.J., 1978. A review of experimental studies of crystal/liquid trace element partitioning. Geochim. Cosmochim. Acta, 42: 743–770.

Jäger, E., Niggli, E. and Werk, E., 1967. Rb–Sr Altersbestimmungen an Glimmern der Zentral-alpen. Beitr. Geol. Kart. Schweiz, Neue Folge, 134 pp.

Jahn, B.M. and Sun, S.S., 1979. Trace element distribution and isotopic composition of Archean greenstones. In: L.H. Ahrens (Editor), Origin and Distribution of the Elements. Pergamon, Oxford, pp. 597–618.

Jahn, B.M., Auvray, B., Blais, S., Capdevila, R., Cornichet, J., Vidal, F. and Hameurt, J., 1980a. Trace-element geochemistry and petrogenesis of Finnish greenstone belts. J. Petrol., 21: 201–244.

Jahn, B.M., Bernard-Griffiths, J., Charlot, R., Cornichet, J. and Vidal, F., 1980b. Nd and Sr isotopic compositions and REE abundances of Cretaceous MORB (Holes *417*D and *418*A, Legs *51, 52* and *53*). Earth Planet. Sci. Lett., 48: 171–184.

Kerrich, R., 1987. The stable isotope geochemistry of Au–Ag vein deposits in metamorphic rocks. In: T.K. Kyser (Editor), Stable Isotope Geochemistry of Low-temperature Fluids. Mineral. Assoc. Can., Saskatoon, Sask., 13: 287–336.

Machado, N., Brooks, C. and Hart, S.R., 1986. Determination of initial $^{87}Sr/^{86}Sr$ and $^{143}Nd/^{144}Nd$ in primary minerals from mafic and ultramafic rocks: experimental procedure and implications for the isotopic characteristics of the Archean mantle under the Abitibi greenstone belt, Canada. Geochim. Cosmochim. Acta, 50: 2335–2348.

Martin, H., 1985. Nature, origine et évolution d'un segment de croûte continentale archéenne: contraintes chimiques et isotopiques – Exemple de la Finlande orientale. Mém. Doc. Cent. Armoricain Étude Struct. Socles, Rennes, No. 1, 392 pp.

Martin, H. and Querré, G., 1984. A 2.5 Ga reworked sialic crust: Rb–Sr ages and isotopic geochemistry of late Archean volcanic and plutonic rocks from E. Finland. Contrib. Mineral. Petrol., 85: 292–299.

Martin, H., Chauvel, C., Jahn, B.M. and Vidal, P., 1983. Rb–Sr and Sm–Nd ages and geochemistry of Archean granodioritic gneisses from eastern Finland. Precambrian Res., 20: 79–91.

Matthews, A. and Kate, A., 1977. Oxygen isotope fractionation during dolomitisation of calcium carbonate. Geochim. Cosmochim. Acta, 41: 1431–1438.

McCrea, J.M., 1950. On the isotope chemistry of carbonates and a paleotemperature scale. J. Chem. Phys., 18: 849–857.

Nesbitt, R.W., Jahn, B.M. and Purvis, A.C., 1982. Komatiites: an early Precambrian phenomenon. J. Volcanol. Geotherm. Res., 14: 31–45.

Ohmoto, H. and Rye, R.O., 1979. Isotopes of sulphur and carbon. In: H.L. Barnes (Editor), Geochemistry of Hydrothermal Ore Deposits. Wiley, New York, N.Y., 2nd ed., pp. 509–567.

O'Neil, J.R., Clayton, R.N. and Mayeda, T.K., 1969. Oxygen isotope fractionation in divalent metal carbonates. J. Chem. Phys., 51: 5547–5558.

Pyke, D.R., Naldrett, A.J. and Eckstrand, O.R., 1973. Archean ultramafic flows in Munro Township, Ontario. Geol. Soc. Am. Bull., 84: 955–978.

Richard, P., Shimizu, N. and Allègre, C.J., 1976. $^{143}Nd/^{146}Nd$, a natural tracer: an application to oceanic basalts. Earth Planet. Sci. Lett., 31: 269–278.

Sharma, T. and Clayton, R.N., 1965. Measurement of $^{18}O/^{16}O$ ratios of total oxygen of carbonates. Geochim. Cosmochim. Acta, 29: 1347–1353.

Sheppard, S.M.F. and Schwarcz, H.P., 1970. Fractionation of carbon and oxygen isotopes and magnesium between coexisting metamorphic calcite and dolomite. Contrib. Mineral. Petrol., 26: 161–198.

Shirey, S.B. and Hanson, G.N., 1986. Mantle heterogeneity and crustal recycling in Archean granite–greenstone belts: Evidence from Nd isotopes and traces elements in the Rainy Lake area, Superior Province, Ontario, Canada. Geochim. Cosmochim. Acta, 50: 2631–2651.

Smith, A.D. and Ludden, J.N., 1989. Nd isotopic evolution of the Precambrian mantle. Earth Planet. Sci. Lett., 93: 14–22.

Taipale, K., 1983. The geology and geochemistry of the Archean Kuhmo greenstone–granite terrain in the Tipasjärvi area, eastern Finland. Acta Univ. Oulu., Ser. A, No. 151, 98 pp.

Vidal, P., Blais, S., Jahn, B.M., Capdevila, R. and Tilton, G.R., 1980. U–Pb and Rb–Sr systematics of the Suomussalmi Archean greenstone belt (Eastern Finland). Geochim. Cosmochim. Acta, 44: 2033–2044.

Viljoen, M.J. and Viljoen, R.P., 1969. Upper mantle project. Geol. Soc. S. Afr. Spec. Publ. No. 2.

Contrib Mineral Petrol (1992) 112:66–82

Contributions to Mineralogy and Petrology

Loss of isotopic (Nd, O) and chemical (REE) memory during metamorphism of komatiites: new evidence from eastern Finland

G. Gruau, S. Tourpin, S. Fourcade, and S. Blais

CAESS, CNRS, Institut de Géologie, Université de Rennes, F-35042 Rennes Cedex, France

Received October 30, 1991 / Accepted April 1, 1992

Abstract. Komatiites are often considered to depict the chemical and isotopic composition of their source rocks in the Archean mantle. However, a weakness of these rocks in tracking the initial compositional heterogeneity of the Earth's mantle is the ubiquitous presence of metamorphic recrystallization, which casts some doubt about the preservation of primary chemical and isotopic characteristics. Two spinifex-textured komatiite flows from the 2.75 Ga old Kuhmo greenstone belt (Siivikkovaara area) of eastern Finland document this weakness. Both flows have experienced low to medium grade metamorphism ($T = 450 \pm 50$ °C), and now consist entirely of secondary metamorphic assemblages of amphibole ± chlorite ± plagioclase, with minor proportions of magnetite and ilmenite. MgO contents range from 25 to 8%, which suggests that low pressure differentiation was likely controlled by olivine and clinopyroxene fractional crystallization. However, neither major nor trace elements fall on olivine and/or clinopyroxene control lines. This is particularly well illustrated by the REE as there is an overall 60% variation of $(Ce/Sm)_N$ ratios (0.38 to 0.91), which far exceeds that expected from olivine and clinopyroxene fractionation alone. In fact, careful evaluation of petrographic (including mineral composition data) and chemical characteristics shows that most elements of geological interest (including the reputedly immobile REE) were mobile on a whole-rock scale during metamorphic recrystallization of these two flows. This view is fully supported by Sm-Nd isotopic data since both whole-rock and mineral (amphibole and plagioclase) samples lie on a single isochron relationship at $T \approx 1800$ Ma, an age which corresponds to the time of regional metamorphism. Thus, the meta-komatiite flows from Siivikkovaara document a case of komatiite flow units in which metamorphism has induced whole-rock scale resetting of primary REE patterns and Sm-Nd isotope systematics. As regards the nature of the mechanism responsible for this resetting, it is suggested here that the secondary mineralogy played an important role, as there are correlations between whole-rock $^{147}Sm/^{144}Nd$ ratios, major and trace element chemistry, oxygen isotopic ratios and modal proportions of secondary minerals. Consideration of oxygen isotopic data, as well as previous results from a komatiite flow from the nearby Tipasjärvi belt, further enable us to propose that the REE carrier was likely a CO_2-rich fluid. The process of secondary REE redistribution prevents estimation of the true initial Nd isotopic compositions of the two flows. Taken as a whole, the results presented in this paper show that great care should be be exercised in the use of meta-komatiites as probes of Archean mantle composition.

Correspondence to: G. Gruau

Introduction

Initial $^{143}Nd/^{144}Nd$ ratios (or initial ε_{Nd} values) of Archean komatiites are commonly used as key constraints in modelling the earliest stages of the Earth's mantle evolution (e.g. Zindler 1982; Albarède and Brouxel 1987; Chase and Patchett 1988; Smith and Ludden 1989). Though extremely valuable in theory (being ultrabasic volcanic rocks, there is no doubt that komatiites formed by partial melting of the Archean mantle) nevertheless such a use suffers from one severe limitation in practice, namely: the invariably altered and/or metamorphosed nature of komatiites (e.g. Arndt and Nisbet 1982) which may cast some doubt on the capacity of these rocks to preserve primary Nd isotopic compositions.

Recent studies have concluded that significant and at times considerable REE mobility could occur during alteration and metamorphism of komatiites (e.g. Arndt et al. 1989; Tourpin et al. 1991). Assuming that such a secondary mobility of REE is a common process in komatiites, then the possibility emerges that many of the initial ε_{Nd} values calculated for these rocks cannot be true, but apparent values. The difference between true and apparent values will depend on a number of parameters including: (a) the absolute change in Sm/Nd

ratio between the fresh and altered komatiite; (b) the ε_{Nd} value of the reservoir with which the komatiite re-equilibrated; and (c) the time span between the eruption of the komatiite and the event which reset its REE pattern and/or Sm-Nd isotopic systematics (Rosing 1990).

Komatiites with possibly reset Sm-Nd isotope systematics and REE patterns occur in the ca. 2.7 Ga-old Kuhmo, Suomussalmi and Tipasjärvi greenstone belts of eastern Finland. Indeed, an anomalously young Sm-Nd date of 2390±150 Ma, as well as abnormally variable LREE patterns ($(La/Sm)_N$ from 0.40 to 1.10) have been found in a carbonatized komatiite flow from Tipasjärvi, the southermost and the smallest of the three belts (Blais et al. 1987; Tourpin et al. 1991). The possible origin and significance of these anomalies were recently reviewed by Tourpin et al. (1991), who provided unequivocal evidence that they arise from introduction of LREE during invasion of secondary carbonate into the komatiite. As shown by Tourpin et al. (1991), the Sm-Nd date of the Tipasjärvi flow is too young because the Sm-Nd array is not an isochron, but a mixing line between LREE-enriched secondary carbonates ($\varepsilon_{Nd} \leq +1$) and an initially homogeneously LREE-depleted komatiite ($\varepsilon_{Nd} \geq +5$).

However, the process of carbonate metasomatism does not affect all komatiite flows from eastern Finland. Most are amphibolites without any trace of carbonate. In this account, we report the results of a detailed geochemical (major and trace elements, REE) and isotopic (Nd, O) study conducted on whole-rock samples and mineral separates from two meta-komatiite flows which apparently escaped carbonate metasomatism. The two flows come from the Kuhmo greenstone belt, 30 km north of Tipasjärvi. The primary aims of this study are: (a) to determine the age of the upper greenschist or lower amphibolite facies metamorphism affecting Finnish greenstone belts, and (b) to further investigate the effects of alteration and metamorphism on the REE patterns and Nd isotopic compositions of komatiites.

Geological background

Eastern Finland is a typical Archean granite-greenstone terrain consisting of three elongated N-S trending greenstone belts (Suomussalmi, Kuhmo and Tipasjärvi) and of a sialic basement of trondjhemitic to granodioritic gneisses (Gaàl et al. 1978; Blais et al. 1978; Jahn et al. 1980a; Vidal et al. 1980; Taipale 1983; Martin 1985, 1989). Kuhmo, the central and largest belt (100 by 15 km), has been studied in detail by Hanski (1980), Taipale et al. (1980), and Piirainen (1988). The results show this belt to be a most common Archean greenstone succession, consisting of the classical intercalation of spinifex-textured komatiite flows, pillowed and massive basalts, felsic volcanics and sediments.

Late plutons of calc-alkaline granite and swarms of dolerite dykes are intruded into the greenstone-gneissic basement terranes of eastern Finland. Field relationships show that calc-alkaline plutons were intruded in two phases (Martin and Quérré 1984; Quérré 1985): (1) intrusion of augen gneisses of granodioritic composition, and (2) intrusion of pink leucogranites. Augen gneisses, which occur as large plutons (≈10 km in diameter), are concentrated in the belt-basement contact; these gneisses crosscut both the basement gneisses and the greenstones. Pink leucogranites crop out as very small plutons (≈1 km in diameter) which are intruded into the basement gneisses, the greenstone belts and the augen gneisses. Dolerite dykes crosscut all units and mark the end of magmatic activity in the area.

U-Pb data on zircons indicate emplacement ages in the range 3000–2800 Ma for the basement gneisses (Kivijärvi gneisses) of eastern Finland (Hyppönen 1983; Lukkonen 1985; Martin 1989). For the intrusive augen gneisses, the zircon ages are consistently younger, in the range 2770–2703 Ma (Kouvo and Tilton 1966; Kouvo 1978; Hyppönen 1983; Tourpin 1991; Fig. 1). No zircon age data is presently available for the Suomussalmi, Kuhmo or Tipasjärvi greenstone belts. Nevertheless, it is clear from field relationships and available zircon age data on the gneisses that their

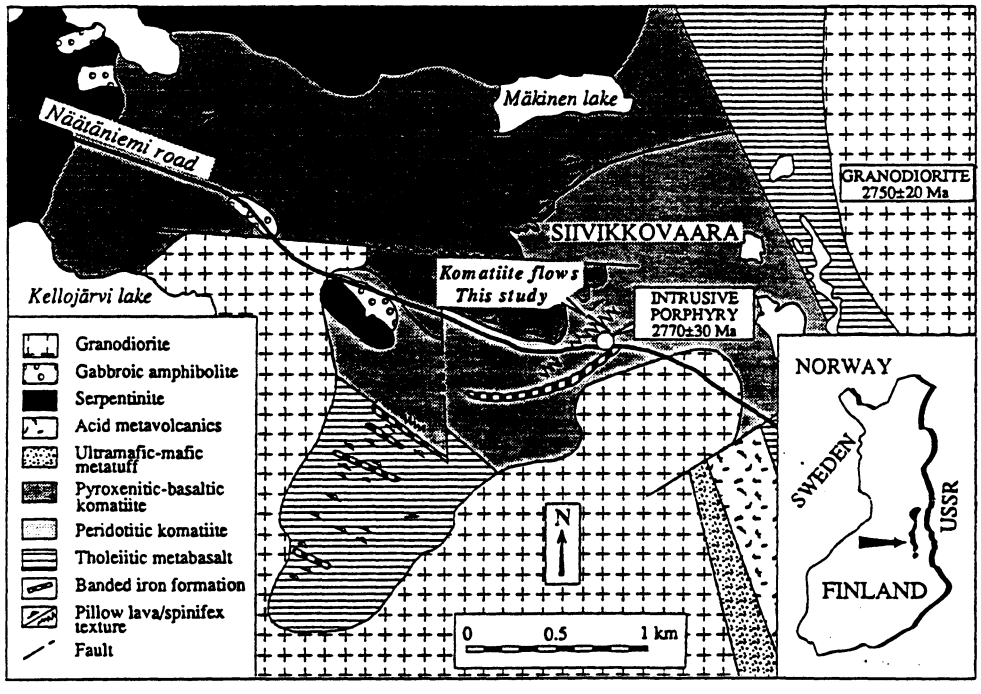

Fig. 1. Geological sketch map of the Siivikkovaara region (after Hanski 1980). The ages quoted on the map (2770±30 Ma and 2750±20 Ma) are $^{207}Pb/^{206}Pb$ zircon ages. Data source: Tourpin (1991)

accumulation is constrained at around 2800–2750 Ma (Vaasjoki 1988).

Radiometric dating of the pink leucogranites and dolerite dyke swarms yields the following results: 2410 Ma (Rb-Sr whole-rock isochron), and 2735 Ma (U-Pb age on zircons) for the pink leucogranites; 2172 to 1990 Ma (U-Pb ages on zircons) for the dolerite dykes (Hyppönen 1983; Martin and Quérré 1984; Tourpin 1991).

According to previous works, the Suomussalmi, Kuhmo and Tipasjärvi belts have experienced at least two distinct tectono-metamorphic episodes. The more recent took place at around 1.7–1.8 Ga, which is defined by the reset Pb-Pb and Rb-Sr ages of K-feldspars and biotites (Vidal et al. 1980), and has been attributed to the Svecokarelian orogeny of northern Scandinavia (Kouvo and Tilton 1966; Vidal et al. 1980; Martin 1989). In the greenstone belts, regional metamorphism corresponds to the upper greenschist or lower amphibolite facies (P = 2–3 Kb; T = 430–480 °C; Hanski 1980; Piquet 1982).

Field occurrence, texture and metamorphic petrography

The two studied flows come from the region of Siivikkovaara, in the southern part of the Kuhmo greenstone belt (Fig. 1; Hanski 1980). The field characteristics and petrography have already been described by Hanski (1980), who also presented detailed descriptions of the geology of the Siivikkovaara region.

As can be seen in Fig. 2, morphology, internal layering and textural variations of Siivikkovaara komatiite flows are typical of ultramafic lava flows from other Archean greenstone belts (e.g. Pyke et al. 1973; Arndt 1977; Viljoen et al. 1983). Each flow comprises a well-developed upper spinifex layer (about 5 m thick) and a lower cumulate zone with no spinifex. In addition, there is a well-preserved breccia zone (about 0.5 m thick) at the top of the lower flow.

Textures in the spinifex zones or in the breccia zone at the top of the lower flow are essentially igneous, and in this respect, the meta-komatiites from Siivikkovaara are also most typical of

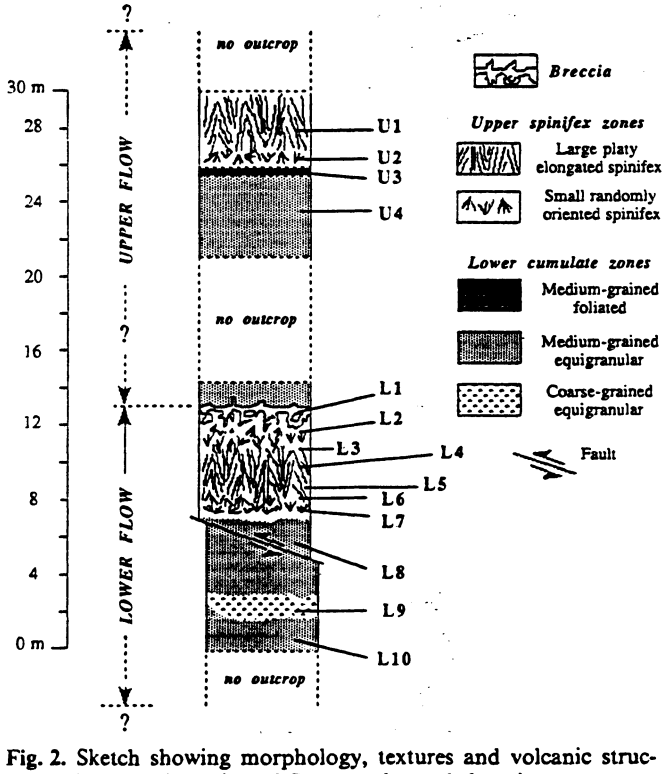

Fig. 2. Sketch showing morphology, textures and volcanic structures of the two investigated flows, and sample locations

Table 1. Modal composition of Siivikkovaara komatiites[a,b]

	Upper flow				Lower flow									
Sample	U1	U2	U3	U4	L1	L2	L3	L4	L5	L6	L7	L8	L9	L10
Vertical location	UPSZ	UPSZ	LCZ	LCZ	Breccia	UPSZ	UPSZ	UPSZ	UPSZ	UPSZ	UPSZ	LCZ	LCZ	LCZ
Amphibole (Wt%)	72.7	65.8	69.8	79.3	79.0	75.7	74.5	69.1	70.8	71.3	66.9	47.7	62.3	41.8
Actinolite	14	29	55	83	66	17	39	45	32	39	26	7	4	98
Mg-Hornblende	86	71	45	17	34	83	61	55	68	61	74	93	96	2
Chlorite	4.2	2.7	32.4	24.9	22.0	5.6	9.0	13.6	11.6	8.8	7.9	49.8	0.0	61.1
Plagioclase	22.7	28.6	0.0	0.0	0.0	19.5	15.4	16.1	16.5	18.0	23.1	0.0	34.8	0.0
Ilmenite	1.8	1.0	0.9	0.7	0.7	0.9	0.9	0.9	0.8	1.0	1.3	1.0	1.1	1.0
Magnetite	0.3	3.6	1.0	0.0	0.0	0.0	2.1	2.0	1.5	2.4	2.2	4.6	3.4	0.4
Biotite	0.0	0.0	0.0	0.0	0.0	0.0	0.0	0.0	0.0	0.0	0.0	0.0	1.9	0.0
Total	101.6	101.7	104.1	104.8	101.7	101.7	101.8	101.7	101.2	101.5	101.3	103.0	103.5	104.2

[a] Calculated from whole-rock and mineral major element compositions using the least-squares method of Bryan et al. (1969)
[b] Errors are typically of the order of ±10 to ±20%
UPSZ: upper spinifex zone; LCZ: lower cumulate zone

Table 2. Major and trace elements in Siivikkovaara whole-rock samples

	Upper flow				Lower flow									
Sample	U1	U2	U3	U4	L1	L2	L3	L4	L5	L6	L7	L8	L9	L10
Vertical location	UPSZ	UPSZ	LCZ	LCZ	Breccia	UPSZ	UPSZ	UPSZ	UPSZ	UPSZ	UPSZ	LCZ	LCZ	LCZ
SiO_2 (%)[a]	51.42	52.41	45.37	49.80	49.29	51.22	50.84	50.38	49.93	50.84	50.74	37.71	52.19	40.54
Al_2O_3	12.42	12.17	10.59	7.05	8.45	12.39	10.51	11.10	11.71	10.97	12.37	16.01	13.85	13.77
Fe_2O_3[b]	11.94	11.50	13.79	10.64	11.27	10.81	12.03	11.82	11.96	11.91	11.77	18.17	11.55	14.15
MnO	0.20	0.19	0.21	0.20	0.21	0.18	0.21	0.22	0.21	0.22	0.22	0.22	0.21	0.19
MgO	11.53	10.74	20.21	21.56	19.82	12.41	13.93	14.69	13.92	13.66	12.14	19.17	8.32	24.51
CaO	8.00	8.30	8.11	9.50	9.34	9.02	9.11	8.43	8.51	8.66	8.22	5.14	7.92	4.94
Na_2O	3.50	3.67	0.36	0.11	0.63	2.94	2.31	2.32	2.50	2.55	3.21	0.58	4.67	0.05
K_2O	0.03	0.10	0.03	0.01	0.03	0.06	0.06	0.06	0.07	0.07	0.08	0.05	0.13	0.01
TiO_2	0.67	0.67	0.69	0.50	0.53	0.69	0.62	0.64	0.61	0.69	0.86	0.82	0.80	0.82
P_2O_5	0.05	0.06	0.05	0.05	0.03	0.05	0.04	0.06	0.06	0.05	0.08	0.05	0.06	0.06
LOI	1.73	1.36	4.76	4.15	3.66	1.71	2.01	2.63	2.28	2.00	1.80	6.25	0.75	7.60
TOT[c]	100.04	99.97	100.1	99.89	100.03	99.98	99.92	100.04	99.77	99.88	99.91	99.15	99.79	100.23
CaO/Al_2O_3	0.64	0.68	0.77	1.35	1.11	0.73	0.87	0.76	0.73	0.79	0.66	0.32	0.57	0.36
Al_2O_3/TiO_2	18.5	18.18	15.29	14.08	15.96	17.91	16.89	17.44	19.07	15.81	14.46	19.48	17.41	16.75
CaO/TiO_2	11.91	12.41	11.70	18.98	17.65	13.04	14.64	13.24	13.87	12.49	9.61	6.26	9.95	6.01
Rb (ppm)	2	2	2	2	1	1	<1	2	1	<1	<1	1	2	1
Sr	67	84	6	6	21	128	57	57	73	56	90	4	116	6
Zr	47	48	44	39	41	50	46	46	42	48	63	43	56	44
Y	16	14	14	9	11	15	14	17	17	17	21	13	18	18
Ni	171	157	476	827	650	243	250	293	287	238	176	1067	105	128
Cr	673	474	2418	1401	1773	1109	713	758	795	657	469	3985	263	281

[a] Major element analyses are presented on a 100% anhydrous basis
[b] Fe_2O_3 = total iron as Fe_2O_3
[c] TOT = sum of oxide and volatile concentrations as obtained during instrumental analysis
UPSZ: upper spinifex zone; LCZ: lower spinifex zone

metamorphosed ultrabasic lava flows elsewhere (e.g. Arndt et al. 1989). In the lower cumulate zones, by contrast, no clear igneous texture could be identified: in these zones, most textures are metamorphic (medium-grained to coarse-grained equigranular), even though some rare relic forms of cumulate olivine have been described by Hanski (1980).

Mineralogically, the two flows now consist entirely of secondary assemblages with no relict igneous phases preserved. In the spinifex zones, amphibole dominates (≥ 65 weight%); other phases include plagioclase, which is unusually abundant (up to 30%), chlorite ($\leq 15\%$), ilmenite ($\leq 2\%$) and magnetite ($\leq 4\%$). In the lower cumulate zones and in the breccia, amphibole and chlorite are by far the most abundant phases (40–80% and 60–10%, respectively); minor phases include ilmenite ($\leq 2\%$), magnetite ($\leq 5\%$), and biotite (few grains); except in the narrow coarse-grained horizon located in the middle of the cumulate zone of the lower flow (Fig. 2), plagioclase is generally absent.

Samples and analytical techniques

Although rocks at Siivikkovaara are generally much better exposed than in the remaining parts of eastern Finland, outcrops are small and discontinuous, in fact neither of the two flows shows a complete section (Fig. 2), and this has limited the number of samples that could be collected and analyzed. Fourteen whole-rock samples weighing 3–5 kg each, 4 from the upper flow (samples No. U1 to U4); ten from the lower flow (samples No. L1 to L10) were finally selected. Separates of amphibole, plagioclase, magnetite and ilmenite obtained from five of these samples (U1, L3, L4, L9, L10) were also analyzed. Sample locations are given in Fig. 2. Modal proportions estimated from whole-rock chemistry and mineral compositions are presented in Table 1.

Mineral purifications were carried out using a Franz magnetic separator combined with heavy liquids, and in some cases, handpicking. All measurements were performed at the Université de Rennes, apart from microprobe analyses which were carried out at the IFREMER laboratory at Brest. Concentrations of major elements, Rb, Sr, Zr, Y, Ni and Cr were determined by the XRF method, while the REE were analyzed by the isotope dilution method (Jahn et al. 1980b). The uncertainties are estimated at 1–5% for major elements, except for MnO whose concentration is precise to only 10%. For Rb, Sr, Zr, Y, Ni and Cr, uncertainties are of the order of 10% for concentrations lower than 30 ppm. For concentrations higher than 30 ppm, uncertainties are reduced to 3%. Analytical errors for the REE, including chemical preparations, blank effects, uncertainties in spike calibration and mass spectrometry runs, are estimated at about 5% for La and Lu, 3% for Gd and 2% for other REE. Blanks were lower than $1*10^{-9}$ g.

$^{143}Nd/^{144}Nd$ ratios and $^{147}Sm/^{144}Nd$ ratios were determined following the procedure described in Gruau et al. (1987). $^{143}Nd/^{144}Nd$ ratios were measured using a five-collector Finnigan MAT 262 mass spectrometer. All ratios were normalized against $^{146}Nd/^{144}Nd = 0.7219$ for isotopic fractionation effect. Results from the La Jolla Nd standard during the course of this study (10 separate runs) were $^{143}Nd/^{144}Nd = 0.511844 \pm 4$ ($2\sigma_m$), so all the $^{143}Nd/^{144}Nd$ ratios presented in this paper are corrected by $+0.000016$ to be consistent with the La Jolla reference value of 0.511860. Blanks for Nd and Sm were lower than $0.2*10^{-9}$ and $0.05*10^{-9}$ g, respectively.

Sm-Nd regression analyses were carried out using the method of York (1969). The errors inputs were 0.2% for $^{147}Sm/^{144}Nd$ and 0.004% for $^{143}Nd/^{144}Nd$. All errors on ages and initial isotopic ratios are reported at a 2σ confidence level. Measured and calculated initial $^{143}Nd/^{144}Nd$ ratios are quoted throughout the text and in Tables 6 and 7 in the ε_{Nd} notation of DePaolo and Wasserburg (1976) as deviations as part per 10^4 from the chondritic growth curve. The presentday $^{143}Nd/^{144}Nd$ and $^{147}Sm/^{144}Nd$ ratio for the chondritic reference reservoir (CHUR) are those determined by Jacobsen and Wasserburg (1980). The errors of the isochrons initial ε_{Nd} values were calculated using the method of Fletcher and Rosman (1982). The decay constant of ^{147}Sm is 0.00654 Ga^{-1}.

Oxygen was extracted using BrF_5 (Clayton and Mayeda 1963), and analyzed as CO_2 gas on a triple-collector VG SIRA 10 mass spectrometer. Isotopic composition are quoted in the standard δ

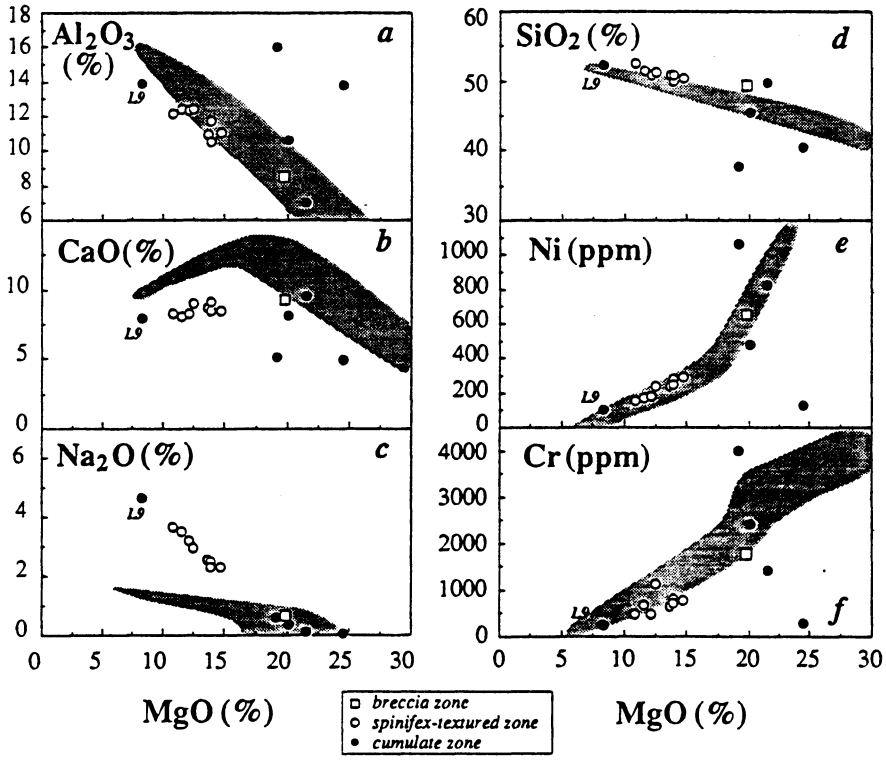

Fig. 3a–f. Variation diagrams. The *shaded field* represents data from the well-preserved Fred's Flow of Canada (Arndt 1977). Note that the significance and origin of the peculiar composition of sample L9 (low MgO, Ni and Cr concentrations) are not fully understood. Should this sample be, in fact, a komatiite cumulate as suggested by its position in the lower flow (Fig. 2), its present-day "basaltic" composition would imply that both the major and trace elements were extraordinarily mobile in the corresponding rock-zone (in any case, much more mobile than in samples L8 and L10, the two adjoining samples with MgO $\geq$ 20%). However, its coarse-grained texture (Fig. 2) suggests that this sample might represent a late gabbroic intrusion, which could also account for the unexpectedly low MgO, Ni and Cr abundances.

notation relative to VSMOW. Duplicate runs yielded an analytical precision better than ± 0.1 δ units. Results from the NBS 28 standard during the course of this study were $\delta^{18}O = +9.47 \pm 0.06$ ($2\sigma_m$). Analytical results are all normalized to NBS 28 = +9.6, applying a systematic correction of +0.13 δ units.

Chemical characteristics and REE profiles of whole-rock samples

Although the komatiite flows from Siivikkovaara have morphological and textural features typical of well-preserved ultrabasic lava flows in other Archean greenstone belts, significant differences appear when one considers their major and trace element compositions. In fact, it is immediately clear that many elements (including the reputedly immobile REE) were mobile during alteration and metamorphism of these flows. Three important points should be underlined:

1. As can be seen from Table 2 and Fig. 3, MgO contents range from ~8 to 25%, which suggests that olivine and clinopyroxene must have been the dominant phases to crystallize in these flows (e.g. Arndt 1977; Kinzler and Grove 1985). However, only a limited number of elements in a limited number of samples exhibit variations consistent with olivine and clinopyroxene fractionation trends (e.g. Al_2O_3, Ni, and Cr in the spinifex-textured samples and in the breccia; Fig. 3a, e, and f). Particularly striking are the compositions of the samples from the cumulate zone of the lower flow (e.g. L8 and L10; Fig. 2). Consider, for example, sample L10 with MgO content ≈25%. If chemically unaltered, a komatiite with such a concentration in MgO should normally contain between 2500 and 3500 ppm Cr, 1000 and 1500 ppm Ni, and 6–8% Al_2O_3 (Fig. 3a, e, f). Yet, L10 has only 128 ppm Ni and 281 ppm Cr, and a concentration in Al_2O_3 as high as 13.8% (Table 2).

2. From Table 2 and Fig. 3, it is evident that there was secondary introduction of considerable amounts of Na into these komatiites. Indeed, the majority of samples have Na_2O concentrations greater than 2% (4.7% in sample L9), a feature that cannot be explained by magmatic processes (see discussion in Hanski 1980). Note for comparison that Na_2O contents in well-preserved komatiites such as Fred's Flow in Canada (MgO between 34.5 and 7.5%), or the komatiites from Gorgona Island (MgO between 20.5 and 14.2%), Colombia, do not exceed 1.5% (Arndt 1977; Dietrich et al. 1981; Echeverria 1982). Interestingly, it appears that, for some reason, the composition of the komatiite controlled the absolute amount of secondary Na that could be introduced into the rocks, which is revealed by the marked negative correlation observed in the Na_2O vs MgO diagram (Fig. 3c). Note that the other alkalis are not affected: concentrations in K_2O and Rb always remain very low, between 0.01 and 0.10%, and between 1 (or less) and 2 ppm, respectively (Table 2).

3. Finally, and most importantly: it is easy to demonstrate that the distribution of REE patterns in these komatiites is not a magmatically inherited distribution. Consider, for example, the variation of $(Ce/Sm)_N$ ratios

Table 3. REE in Siivikkovaara whole-rock samples

	Upper flow				Lower flow									
Sample	U1	U2	U3	U4	L1	L2	L3	L4	L5	L6	L7	L8	L9	L10
Vertical location	UPSZ	UPSZ	LCZ	LCZ	Breccia	UPSZ	UPSZ	UPSZ	UPSZ	UPSZ	UPSZ	LCZ	LCZ	LCZ
La (ppm)	1.78	1.35	1.07	1.19	1.20	2.01	0.55	0.88	1.02	1.13	n.d.	1.73	2.37	1.79
Ce	4.76	4.11	3.51	3.81	3.65	6.09	2.08	2.99	3.32	3.77	5.08	4.74	6.01	5.68
Nd	4.69	4.15	3.29	3.56	3.35	4.96	2.77	3.28	3.39	3.87	4.03	4.47	5.69	4.72
Sm	1.58	1.57	1.35	1.36	1.23	1.65	1.29	1.48	1.32	1.55	1.71	1.59	1.93	1.48
Eu	0.57	0.64	0.49	0.43	0.44	0.61	0.51	0.52	0.51	0.54	0.57	0.58	0.72	0.32
Gd	2.19	2.03	1.96	1.99	1.73	2.19	1.99	2.23	1.96	2.27	2.65	2.26	2.78	2.24
Dy	2.64	2.67	2.56	2.50	2.12	2.64	2.60	2.78	2.43	2.82	3.31	2.80	3.38	2.86
Er	1.66	1.68	1.63	1.63	1.37	1.65	1.63	1.81	1.55	1.81	2.11	1.77	1.77	1.75
Yb	1.52	1.53	1.55	1.57	1.32	1.53	1.54	1.71	1.45	1.68	2.03	1.59	1.59	1.65
Lu	0.23	0.24	0.25	0.25	0.20	0.23	0.24	0.26	0.22	0.26	0.32	0.24	0.24	0.25
$(Ce/Sm)_N$*	0.71	0.62	0.61	0.66	0.70	0.87	0.38	0.48	0.59	0.57	0.70	0.70	0.74	0.91
$(Gd/Yb)_N$*	1.16	1.07	1.02	1.02	1.05	1.15	1.04	1.05	1.09	1.09	1.05	1.14	1.40	1.09
Eu/Eu*[b]	0.95	1.11	0.93	0.81	0.93	0.99	0.99	0.89	0.98	0.89	0.83	0.95	0.96	0.54

* Normalizing values are from Jahn et al. (1980a)
[b] $Eu/Eu^* = Eu_N/(Sm_N * Gd_N)^{0.5}$
n.d.: not determined
UPSZ: upper spinifex zone; LCZ: lower cumulate zone

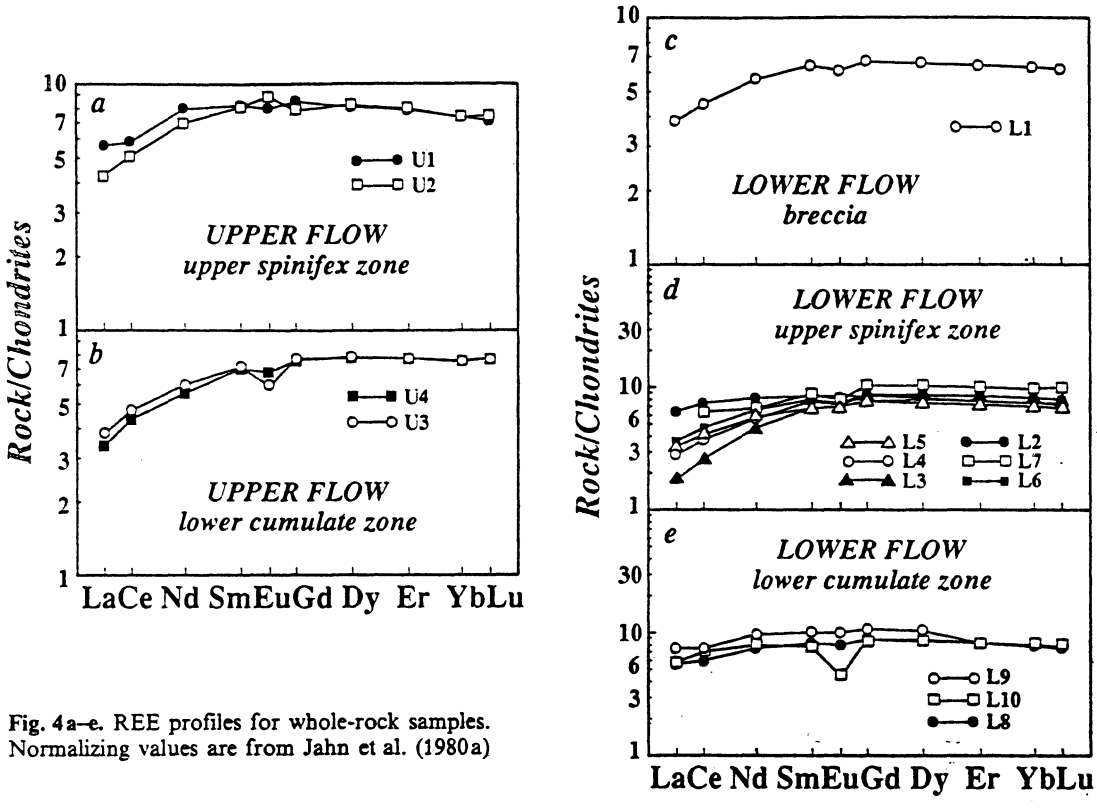

Fig. 4a–e. REE profiles for whole-rock samples. Normalizing values are from Jahn et al. (1980a)

(i.e. the variation in the slope of LREE patterns) in the spinifex-textured samples of the lower flow (L2 to L7). Since a spinifex-textured zone is more or less representative of a liquid composition, it is to be expected that the $(Ce/Sm)_N$ ratios vary over a limited range in these samples. In support of this prediction, note that within the well-preserved Fred's Flow in Canada, the total variation of $(Ce/Sm)_N$ in the spinifex-textured zone is only 5%, from 0.83 to 0.79 (Whitford and Arndt 1978). Yet, $(Ce/Sm)_N$ ratios cover an extraordinarily wide range in the spinifex-textured samples from the lower flow, from 0.87 to 0.38, which represents an overall variation of about 60% (Table 3, Fig. 4c–e). As can be seen in Fig. 2 and Table 3, there is no correlation between the $(Ce/Sm)_N$ ratio and the vertical position of the samples. Instead, the variation is random, with the most extreme values (samples L2 and L3; Table 3) being separated by less than 1 m (Fig. 2). No combination of plausible magmatic processes can introduce such a small scale and erratic variability of LREE patterns into a komatiite lava flow.

Composition of metamorphic minerals

Metamorphic minerals present in the two flows (Table 4) generally yield relatively uniform major element compositions, except for amphiboles which give a continuous compositional spectrum tying Mg-hornblende ($Mg/Mg+Fe^{2+} \approx 0.65$; $Si/Al^{IV} \approx 4.5$) and actinolite ($Mg/Mg+Fe^{2+} \approx 0.85$; $Si/Al^{IV} \approx 80$) as end-members (Leake 1978). The heterogeneity of amphibole composition is observed at all scales (including in a given thin section), even though the amphiboles from the lower cumulate zones and the breccia tend as a general rule to have compositions enriched in actinolite, while those from the upper spinifex-textured zones generally show compositions closer to that of a Mg-hornblende (Table 1).

Compositions of plagioclase are in the field albite-oligoclase (An_7 to An_{21}), which is consistent with the marked positive correlation there is between the proportion of this phase and the Na_2O contents of corresponding whole-rocks (see Tables 1 and 2).

The composition of the chlorite is nearly constant, except for Cr which varies significantly from one crystal grain to another (Table 4). $Fe/Fe+Mg$ ratios are low (0.25 and 0.30); Si/Al^{IV} ratios are also low, ranging from 2.1 to 2.4. When plotted in the Si versus $Fe^{2+}+Fe^{3+}$ diagram of Hey (1954), the chlorite from Siivikkovaara lies in the ripidolite compositional field, very close to the junction between this field and those of sheridanite, clinochlore, and pychnochlorite.

Five amphibole (U1, L3, L4, L9, and L10) and four plagioclase (U1, L4, L3, and L9) separates were analyzed for REE concentrations. The results are presented in Table 5 and illustrated in Fig. 5a–b. Two important points should be mentioned:

1. All amphiboles yield similar REE patterns, with marked depletion of LREE relative to the HREE ($(Ce/Sm)_N = 0.30$ to 0.56; Fig. 5a). The plagioclase patterns also closely resemble each other, all showing a continuous relative enrichment of the REE from Lu to La ($(Ce/Yb)_N = 3.56$ to 13.91; Fig. 5b).

2. There is no correlation between the distribution of REE patterns in amphiboles and the variation in ma-

Table 4. Composition of metamorphic minerals*

	Amphibole						Plagioclase				Chlorite				Ilmenite
Sample	L9	L4	L3	L1	L10		L3	L5	L9		L5	L3	L10		L5
SiO_2	44.37	48.64	53.83	52.77	56.80	SiO_2	62.70	63.03	66.73	SiO_2	26.99	27.55	28.31	SiO_2	0.02
TiO_2	0.51	0.21	0.11	0.19	<0.01	TiO_2	0.05	0.05	0.02	TiO_2	0.10	0.12	0.07	TiO_2	50.89
Al_2O_3	11.61	8.56	3.07	4.17	0.27	Al_2O_3	23.36	23.29	20.36	Al_2O_3	21.63	21.13	20.60	Al_2O_3	0.07
Cr_2O_3	<0.01	<0.01	0.19	0.25	0.08	Cr_2O_3	0.03	0.02	0.11	Cr_2O_3	0.26	<0.01	0.48	Cr_2O_3	0.11
FeO	16.11	12.52	10.25	9.11	6.75	FeO	0.08	0.04	0.13	FeO	17.20	16.75	14.19	FeO	45.96
MnO	0.27	0.31	0.29	0.32	0.14	MnO	0.10	0.15	0.03	MnO	0.29	0.07	0.07	MnO	2.28
MgO	11.38	13.64	16.97	17.77	20.26	MgO	<0.01	<0.01	<0.01	MgO	21.22	21.84	23.28	MgO	0.24
CaO	11.13	11.38	11.86	11.78	12.89	CaO	4.43	4.33	1.57	CaO	0.05	0.10	0.05	CaO	0.04
Na_2O	2.00	1.29	0.41	0.67	0.08	Na_2O	9.14	8.92	11.09	Na_2O	0.02	0.02	<0.01	Na_2O	0.02
K_2O	0.17	0.09	0.08	0.06	0.03	K_2O	0.04	<0.01	0.02	K_2O	0.04	0.01	0.02	K_2O	<0.01
Total	97.55	96.64	97.06	97.09	97.30	Total	99.93	99.83	100.06	Total	87.80	87.59	87.07	Total	99.63
Si	6.53	7.07	7.69	7.49	7.96	Si	2.78	2.79	2.93	Si	5.44	5.54	5.65	Si	–
Al^{IV}	1.47	0.93	0.31	0.51	0.04	Ti	–	–	–	Ti	0.02	0.02	0.01	Ti	0.97
$\sum$	8.00	8.00	8.00	8.00	8.00	Al	1.22	1.22	1.05	Al^{IV}	2.56	2.48	2.35	Al	–
Al^{VI}	0.55	0.54	0.20	0.19	–	Cr	–	–	–	$\sum$	8.00	8.00	8.00	Cr	–
Ti	0.06	0.02	0.01	0.02	–	Fe	–	–	0.01	Al^{VI}	2.57	2.54	2.49	Fe^{3+}	0.06
Cr	–	–	0.02	0.03	0.01	Mn	–	0.01	–	Cr	0.04	–	0.08	Fe^{2+}	0.91
Fe^{3+}	0.47	0.27	0.10	0.26	0.03	Mg	–	–	–	Fe	2.90	2.81	2.37	Mn	0.05
Fe^{2+}	1.40	1.18	1.02	0.71	0.71	Ca	0.21	0.21	0.07	Mn	0.05	0.01	0.01	Mg	0.01
Mn	0.03	0.04	0.04	0.04	0.02	Na	0.79	0.77	0.94	Mg	6.37	6.54	6.92	Ca	–
Mg	2.50	2.96	3.61	3.76	4.23	K	–	–	–	Ca	0.01	0.02	0.01	Na	–
$\sum$	5.00	5.00	5.00	5.00	5.00	$\sum$	5.01	4.99	5.01	Na	0.01	0.06	–	K	–
Fe^{M4}	0.11	0.08	0.11	0.11	0.05	%An	21.1	21.1	7.3	K	0.01	–	–	$\sum$	2.00
Ca	1.76	1.77	1.81	1.79	1.94					$\sum$	11.97	12.02	11.89		
Na^{M4}	0.13	0.15	0.08	0.10	0.01					XFe[b]	0.31	0.30	0.25		
$\sum$	2.00	2.00	2.00	2.00	2.00										
Na^{A}	0.44	0.21	0.30	0.09	0.01										
K	0.03	0.02	0.14	0.01	0.01										
$\sum$	0.47	0.23	0.04	0.10	0.02										
XMg[a]	0.64	0.72	0.78	0.84	0.86										

[a] $XMg = Mg/Mg + Fe^{2+}$; [b] $XFe = Fe^{2+} + Fe^{3+}/Fe^{2+} + Fe^{3+} + Mg$

* The compositions presented in this table are compositions of individual microprobe spots, not average values. Complete data basis (about 150 analyses) can be obtained from the authors on request

Table 5. REE in Siivikkovaara mineral separates

Mineral	Amphibole					Plagioclase			
Sample	U1	L3	L4	L9	L10	U1	L3	L4	L9
La (ppm)	0.74	0.55	0.63	0.68	0.74	1.14	0.64	0.88	3.58
Ce	2.10	2.01	2.45	2.72	2.86	4.18	1.67	3.30	9.24
Nd	2.22	2.88	3.32	4.07	3.94	2.20	1.18	1.43	3.88
Sm	0.88	1.49	1.69	2.01	2.26	0.50	0.27	0.29	0.80
Eu	0.34	0.58	0.60	0.99	0.57	0.18	0.20	0.14	0.31
Gd	1.33	2.43	2.71	3.26	4.27	0.43	0.26	0.33	0.58
Dy	1.69	3.15	3.48	4.08	5.76	0.37	0.22	0.33	0.32
Er	1.07	2.04	2.22	2.54	3.31	0.22	0.13	0.22	0.16
Yb	0.98	1.85	2.12	2.31	2.78	0.21	0.12	0.23	0.17
Lu	0.15	0.27	0.29	0.35	0.39	0.03	0.02	0.04	0.03
$(Ce/Sm)_N$[a]	0.56	0.32	0.34	0.32	0.30	1.97	1.46	2.69	2.73
$(Gd/Yb)_N$[a]	1.09	1.05	1.03	1.13	1.23	1.64	1.74	1.15	2.74
$(Ce/Yb)_N$[a]	0.55	0.28	0.30	0.30	0.26	5.09	3.56	3.67	13.91
Eu/Eu^*[b]	0.97	0.94	0.87	1.19	0.57	1.20	2.33	1.40	1.41

[a] Normalizing values are from Jahn et al. (1980a)
[b] $Eu/Eu^* = Eu_N/(Sm_N * Gd_N)^{0.5}$

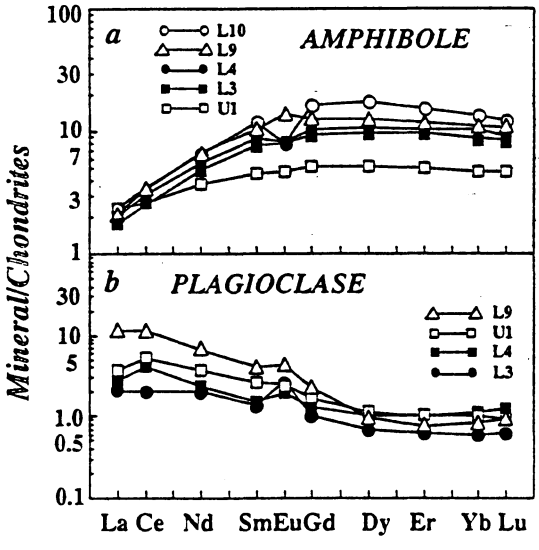

Fig. 5a, b. REE profiles for amphibole and plagioclase separates. Normalizing values are from Jahn et al. (1980a)

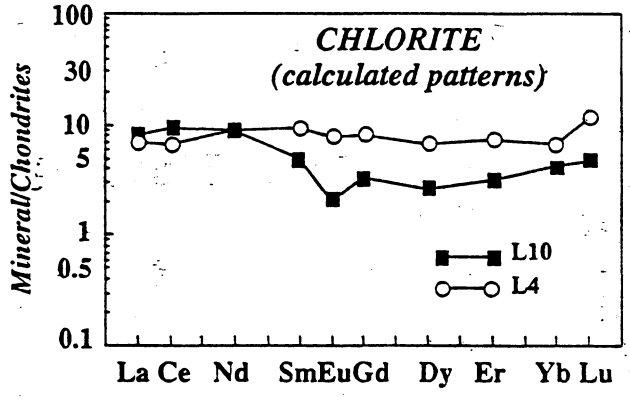

Fig. 6. REE profiles for chlorite as obtained from mass balance calculation. Normalizing values are from Jahn et al. (1980a)

jor element compositions of this mineral. Instead, amphiboles with major element compositions as different as L9 (Mg-hornblende = 86%; actinolite = 14%), L4 (Mg-hornblende = 55%; actinolite = 45%) and L10 (Mg-hornblende = 2%; actinolite = 98%) share nearly identical values of $(Ce/Sm)_N$ (0.30–0.34) and $(Ce/Yb)_N$ (0.26–0.30), as well as similar overall REE concentrations (Table 5; Fig. 5a).

Owing to the intimate small-scale association of amphibole and chlorite, no pure chlorite separate could be obtained, hence preventing direct determination of the REE pattern of this mineral phase. However, a rough evaluation of the REE pattern can be obtained by mass balance calculation using samples L4 and L10, the two samples that contain significant amount of chlorite (≥ 15%; Table 1) and for which we analyzed plagioclase and amphibole. The results are shown in Fig. 6. With respect to plagioclase, chlorite shows approximately the same LREE content, but appears to be somewhat richer in HREE. By contrast with amphibole, both plagioclase and chlorite are seen to be similar phases which preferentially incorporate LREE.

Isotopes

Neodymium and oxygen isotopic data are presented in Tables 6 (whole-rock samples) and 7 (mineral separates); the Nd data are further displayed on two conventional isochron diagrams in Fig. 7a, b.

Neodymium data

Whole-rock Sm-Nd isotopic analyses were carried out on all samples except U4. Five samples were further selected for mineral Sm-Nd isotopic study. These include

Table 6. Isotopic data for Siivikkovaara whole-rock samples

Sample	Vertical location	Sm (ppm)	Nd (ppm)	$^{147}Sm/^{144}Nd$ [a]	$^{143}Nd/^{144}Nd$ [b]	ε_{Nd} (2.75 Ga) [c]	ε_{Nd} (1.81 Ga) [c]	ε_{Nd} (0 Ga) [c]	δO^{18} [d]
	Upper flow								
U1	UPSZ	1.64	4.77	0.2075	0.512846±9	+0.2±0.5	+1.6±0.5	+ 4.1±0.4	+5.12±0.02
U2	UPSZ	1.53	4.03	0.2303	0.513193±4	−1.1±0.6	+3.1±0.5	+10.8±0.4	+5.17±0.01
U3	LCZ	1.34	3.23	0.2498	0.513452±5	−2.9±0.6	+3.6±0.5	+15.9±0.4	+4.74±0.02
	Lower flow								
L1	Breccia	1.10	2.97	0.2237	0.513098±7	−0.6±0.6	+2.7±0.5	+ 9.0±0.4	+4.70±0.01
L2	UPSZ	1.67	5.02	0.2018	0.512761±5	+0.6±0.5	+1.2±0.5	+ 2.4±0.4	+5.12±0.07
L3	UPSZ	1.32	2.83	0.2826	0.513764±7	−8.5±0.6	+2.1±0.5	+22.0±0.4	+4.95±0.06
L4	UPSZ	1.48	3.31	0.2696	0.513598±7	−7.1±0.6	+1.9±0.5	+18.7±0.4	+4.98±0.09
L5	UPSZ	1.34	3.39	0.2395	0.513237±8	−3.5±0.6	+1.8±0.5	+11.7±0.4	+4.98±0.08
L6	UPSZ	1.59	3.94	0.2442	0.513313±3	−3.7±0.6	+2.2±0.5	+13.2±0.4	+4.91±0.03
L7	UPSZ	1.76	4.14	0.2565	0.513384±6	−6.7±0.6	+0.7±0.5	+14.6±0.4	+5.10±0.09
L8	LCZ	1.59	4.47	0.2150	0.512968±8	+0.0±0.5	+2.2±0.5	+ 6.4±0.4	+4.51±0.07
L9	LCZ	1.93	5.77	0.2020	0.512773±5	+0.8±0.5	+1.4±0.5	+ 2.6±0.4	+5.53±0.02
L10	LCZ	1.51	4.79	0.1912	0.512715±5	+3.5±0.5	+2.8±0.5	+ 1.5±0.4	+4.43±0.09

[a] The error on this ratio is 0.2%
[b] The error presented on this ratio is the statistical error obtained during the mass spectrometry run. The true error, including other error sources such as instrumental reproducibility is estimated to be close to ±20
[c] Errors calculated using an error input of ±20 on $^{143}Nd/^{144}Nd$, and ±0.2% on $^{147}Sm/^{144}Nd$ ratios
[d] The error presented on this ratio corresponds to the reproducibility of two separate extractions and mass analyses (duplicate). Total uncertainty with respect to the VSMOW scale is estimated to be lower than 0.1 to 0.15‰.
UPSZ: upper spinifex zone; LCZ: lower cumulate zone

Table 7. Isotopic data for Siivikkovaara mineral separates

Sample	Sm (ppm)	Nd (ppm)	$^{147}Sm/^{144}Nd$ [a]	$^{143}Nd/^{144}Nd$ [b]	ε_{Nd}(1.86 Ga) [c]	ε_{Nd} (0 Ga) [c]	δO^{18} [d]
Amphibole							
U1							+4.73±0.12
L3	1.49	2.88	0.3118	0.514194±6	+2.9±0.5	+30.4±0.4	
L4	1.71	3.34	0.3088	0.514106±7	+1.9±0.5	+28.6±0.4	+4.73±0.08
L9	2.01	4.07	0.2991	0.513965±4	+1.4±0.5	+25.9±0.4	+4.21±0.01
L10	2.26	3.94	0.3464	0.514634±5	+3.2±0.5	+38.9±0.4	
Plagioclase							
U1	0.38	1.84	0.1235	0.511918±5	+3.4±0.5	−14.0±0.4	+7.09±0.13
L3	0.27	1.18	0.1386	0.512084±6	+3.1±0.5	−10.8±0.4	
L4	0.29	1.43	0.1235	0.511833±5	+1.8±0.5	−15.7±0.4	+6.93±0.03
L9	0.92	5.38	0.1039	0.511616±0.5	+2.2±5	−19.9±0.4	
Chlorite							
L10	1.37	3.21	0.2568	0.513544±6	+3.3±0.5	+17.7±0.4	
Ilmenite							
L4							+0.03±0.10
L9							+0.09±0.02

[a] The error on this ratio is 0.2%
[b] The error presented on this ratio is the statistical error obtained during the mass spectrometry run. The true error, including other error sources such as instrumental reproducibility is estimated to be close to ±20
[c] Errors calculated using an error input of ±20 on $^{143}Nd/^{144}Nd$, and ±0.2% on $^{147}Sm/^{144}Nd$ ratios
[d] The error presented on this ratio corresponds to the reproducibility of two separate extractions and mass analyses (duplicate). Total uncertainty with respect to the VSMOW scale is estimated to be lower than 0.1 to 0.15‰.

samples L3, L4, and L9, for which we measured the $^{143}Nd/^{144}Nd$ and $^{147}Sm/^{144}Nd$ ratios of coexisting plagioclase and amphibole. For sample L10, $^{143}Nd/^{144}Nd$ and $^{147}Sm/^{144}Nd$ ratios were determined for a nearly pure amphibole fraction and a mixed fraction of amphibole+chlorite. For the remaining sample (U1), only plagioclase was analyzed. Three important points should be noted:

1. $^{147}Sm/^{144}Nd$ ratios of whole-rock samples turn out to be extremely variable, which is not surprising considering the 60% variation of $(Ce/Sm)_N$ ratios. For the upper flow, the observed variation is of 20%

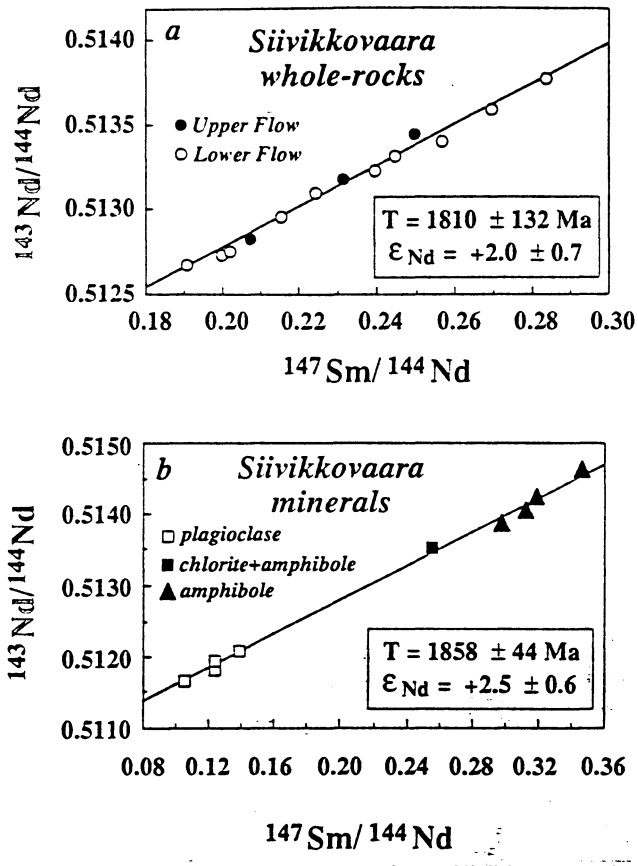

Fig. 7a, b. Sm-Nd isochron diagrams for a, Siivikkovaara whole-rock samples and b, mineral separates. Errors are 2σ. *wr*: whole-rock samples; *amp*: amphiboles; *plg*: plagioclases; *chl*: chlorite

(0.2075–0.2498); for the lower flow, the variation is even larger (48%; 0.1912–0.2826; Table 7). Once again, such variations far exceed the variation normally expected in a komatiite flow (e.g. Whitford and Arndt 1978).

2. As can be seen in Fig. 7a, b, both whole-rocks and mineral separates define isochrons (or "errochrons") when reported on the conventional $^{143}Nd/^{144}Nd$ versus $^{147}Sm/^{144}Nd$ diagram. The 13 whole-rock samples (Fig. 6a) yield an isochron age of 1810 ± 132 Ma (2σ), and an initial ε_{Nd} value of $+2.0 \pm 0.7$ (2σ). The 9 mineral samples (Fig. 7b) give slightly greater, but not statistically different, ages and initial ε_{Nd} values of 1858 ± 44 Ma (2σ), and $+2.5 \pm 0.6$ (2σ), respectively. Thus, it is inferred that the minerals and the whole-rocks shared comparable Nd isotopic composition at around 1800–1850 Ma ago.

3. From geological relationships and previous radiometric data, it is clear that the komatiite flows from Siivikkovaara were erupted around 2800–2750 Ma ago. Thus, the whole-rock Sm-Nd isochron at 1810 ± 132 Ma is a secondary isochron, indicating some stage of later isotopic re-equilibration and fractionation of the $^{147}Sm/^{144}Nd$ ratios at a whole-rock scale. The open-system behaviour of whole-rock Sm-Nd systematics is reflected in the wide range of calculated initial ε_{Nd} values. In Table 6, we took 2750 Ma as the age of magmatic crystallization and calculated what would be the initial ε_{Nd} value of each individual whole-rock sample assuming closed-system evolution since 2750 Ma ago. Upper flow samples give values ranging from -2.9 to $+0.2$; for the lower flow, the range is 12 ε units (-8.5 to $+3.5$). If interpreted as magmatic values, such values would encompass the field of depleted mantle and early Archean crust compositions at 2750 Ma, which is clearly an aberrant situation in the present case.

Oxygen data

Siivikkovaara whole-rock samples show a limited range of $\delta^{18}O$ values, from $+4.43$ to $+5.53$‰ (Table 6). The most striking feature of these values is that, taken as a whole, they are lower than the present-day mantle reference and/or the value found in fresh modern sea floor basalts (Kyser 1986, and references therein). $\delta^{18}O$ values for the Archean mantle and related magmas are not as constrained as their present-day equivalents. However, isotopic studies of fresh Archean komatiites and/or of magmatic minerals from spatially related mafic intrusions showed that these materials generally yielded a $\delta^{18}O$ value of about $+5.5$ to $+6$‰ (e.g. Beaty and Taylor 1982; Smith et al. 1984), which is similar to the average $\delta^{18}O$ of $+5.7 \pm 0.3$‰ observed in modern sea floor basalts (e.g. Muehlenbachs and Clayton 1972; Pineau et al. 1976; Ito et al. 1987). Thus, it is inferred that the oxygen isotopic compositions listed in Table 6 are not primary compositions. They are altered values likely resulting from some stage of later isotopic exchange between the komatiite flows and a secondary fluid phase. Judging from the Sm-Nd data, it is postulated that this episode of isotopic exchange took place around 1800 Ma ago.

Separated mineral phases across the two flows show rather constant oxygen isotopic composition. Measured $\delta^{18}O$ values range from $+4.21$ to $+4.73$‰ for amphibole, from $+6.93$ to $+7.09$‰ for plagioclase, and from $+0.03$ to 0.09‰ for ilmenite (Table 7). It is worth noting that whole-rock samples U3, L1, L8 and L10, which are composed of essentially amphibole and chlorite, display a range of isotopic compositions which overlaps that of amphibole taken on its own (Tables 6 and 7). This means that amphibole and chlorite share identical $\delta^{18}O$ values in these rocks, a fact which was already observed by Smith et al. (1984) for meta-komatiites from the Barberton greenstone belt of southern Africa.

Discussion

Age and temperature of metamorphism

Although the influence of the 1.8–1.7 Ga Svecokarelian orogeny of northern Scandinavia has long been recognized in the greenstone belts of eastern Finland (e.g. Kouvo and Tilton 1966; Bertrand et al. 1978; Vidal et al. 1980; Martin 1989), this orogeny was so far regarded as having played a minor role in their post-depositional tectono-metamorphic history. In particular, the upper greenschist or lower amphibolite facies metamorphism

that affects these belts was claimed to be a much earlier event that took place before or during intrusion of the 2750–2700 Ma-old granodiorite plutons (e.g. Hanski 1980; Blais et al. 1978). We take another view, and suggest, for the following two reasons, that the middle Proterozoic event had a major impact in the region and that the age of metamorphism is not late Archean, but around 1800 Ma:

1. The Sm-Nd mineral age of 1858 ± 44 Ma obtained from the Siivikkovaara komatiite flows (Fig. 7b) is comparable to the reset K-feldspar Pb-Pb and biotite Rb-Sr ages reported earlier by Vidal et al. (1980), and fits the expected age of the Svecokarelian orogeny of northern Scandinavia. In addition, it is evident from Figs. 4 and 7a that the REE patterns and Sm-Nd isotope systematics of the whole-rock samples were reset around 1800–1850 Ma ago.

2. Jegouzo and Blais (1991) recently established that the 2.1–2.0 Ga old dolerite dykes experienced post-injection deformation and metamorphism, and proposed that this deformation and metamorphism developed during the Svecokarelian orogeny. This view is confirmed in a very recent work by Tourpin (1991), who obtained a four-point internal Sm-Nd isochron (whole-rock + plagioclase + amphibole + biotite) at 1719 ± 143 Ma for a deformed and metamorphosed dyke of the Tipasjärvi greenstone belt. Moreover, petrographic studies have revealed that the grade of metamorphism of the dykes also corresponds to the upper greenschist or lower amphibolite facies (Ballèvre personal communication).

It should be understood here that we do not dispute the fact that there was late Archean tectono-metamorphic activity in these belts. In fact, it is not conceivable that granodiorite plutons could have been intruded without producing some metamorphic recrystallization in the adjacent greenstones. We simply stress that the effects of this first event were likely completely erased by the middle Proterozoic metamorphism.

The apparent Sm-Nd age of 2390 ± 150 Ma obtained by Tourpin et al. (1991) for the Tipasjärvi carbonatized komatiite flow provides another, though less direct, argument for the major influence of the Svecokarelian orogeny. As already mentioned, the Sm-Nd age of the Tipasjärvi flow is anomalously young (like the Kuhmo belt, Tipasjärvi is crosscut by granodiorite plutons which were emplaced 2750–2700 Ma ago, and therefore the flow cannot be younger than 2750 Ma) because the Sm-Nd linear array is not an isochron, but a mixing line tying a LREE-depleted komatiite and a LREE-rich carbonate as end-members (see Figs. 3 and 7 in Tourpin et al.'s paper). The occurrence of carbonate in small scale association with the metamorphic minerals indicates that the carbonatization event was synmetamorphic. Yet, as shown by Tourpin et al. (1991), there are geochemical and isotopic arguments to suggest that a positive slope already existed in the Sm-Nd diagram by the time the carbonate was added to the depleted komatiite. The net result of such a positive slope is that the age of the carbonatization process is ≤ 2400 Ma. If this is the case, then metamorphism and carbonatization of the Tipasjärvi flow occurred around 1800 Ma ago since there is no thermal event (other than the Svecokarelian) in the region after 2400 Ma (Tourpin et al. 1991).

Apparent temperatures calculated from the Siivikkovaara mineral oxygen data-base (Table 7) were used to test the presence of internal isotopic equilibrium. Such temperatures are only rough estimates since fractionation coefficients for the amphibole-chlorite, amphibole-ilmenite, plagioclase-ilmenite and plagioclase-amphibole pairs are imperfectly known (especially those involving amphibole) for temperatures lower than 500 °C. Nevertheless, a relatively good agreement is observed between calculated isotopic temperatures and metamorphic conditions (upper greenschist or lower amphibolite facies). Indeed, using the equations of Bottinga and Javoy (1973), Wenner and Taylor (1973), and Javoy (1977) all mineral pairs, except plagioclase-amphibole, give temperatures, in the range 400–500 °C: 500–510 °C for plagioclase-ilmenite, 425–475 °C for ampibole-ilmenite and 410 °C for amphibole-chlorite. For the plagioclase-amphibole pairs, calculated temperatures are much higher: 585–640 °C.

Since oxygen diffusion rates are high in plagioclase (Giletti et al. 1978; Elphick et al. 1986), this mineral has a low closure temperature for oxygen isotopes, and thus considerable capacity to exchange with fluid phases down to relatively low temperatures (e.g. Giletti 1986). Because of this, isotopic disequilibrium is often observed among plagioclase and other metamorphic minerals. Together with the low $\Delta_{\text{plagioclase-amphibole}}$ (less than 3.0 units; Table 7), this may explain why the Siivikkovaara plagioclase-amphibole pairs give such high apparent temperatures. If the $\delta^{18}O$ of plagioclase were altered by late isotopic exchange, the temperature calculated from the plagioclase-ilmenite pair (L4) would be also affected, but the shift would be likely reduced as $\Delta_{\text{plagioclase-ilmenite}}$ becomes very much larger than $\Delta_{\text{plagioclase-amphibole}}$ (Table 7). In every other case, however, the isotopic temperatures calculated from amphibole-chlorite and amphibole-ilmenite pairs (450 ± 50 °C) agree well with the temperature range estimate of 430–480 °C determined previously by Hanski (1980) and Piquet (1983). Thus, the Siivikkovaara mineral oxygen data-base (omitting plagioclase) provides a reliable tool which is suitable for estimating the oxygen isotopic composition of the equilibrium fluid phase (see discussion on *fluid/rock ratios and origin of the fluid phase* later).

Control of secondary mineralogy and possible role of fluids in REE mobility

As already discussed, the extreme variations observed in the $(Ce/Sm)_N$ and $^{147}Sm/^{144}Nd$ ratios, as well as the isochron age relationship at 1810 ± 132 Ma provide firm evidence that the REE were mobile on a whole-rock scale during metamorphism of the Siivikkovaara komatiites. This, in itself, is not so surprising. Previous studies (e.g. Arndt et al. 1989) have shown that the process of metamorphism can redistribute these elements on a whole-rock scale in komatiitic rocks. What is more surprising is the intensity of the process. To our knowledge,

the komatiites from Siivikkovaara are the first example of a komatiite suite in which all whole-rock samples lie on a secondary Sm-Nd isochron giving the age of the metamorphic redistribution. Taken together with the fact that in several other areas, such as Canada or Western Australia, metamorphic recrystallization has had apparently no detectable effect on the REE patterns or Sm-Nd isotope systematics of komatiites (e.g. Dupré et al. 1984; Arndt and Jenner 1986), this consideration gives rise to the following questions: (a) what particular conditions allowed such unusually strong mobility of the REE in these Finnish komatiites; (b) by what exact mechanism did the REE redistribution take place in these rocks?

One of the key issues regarding the interpretation of geochemical and isotopic data in metamorphic rocks is whether (1) the protolith chemistry controlled the nature and proportion of metamorphic phases (closed-system at the sample scale), or whether (2) the actual rock composition depends on the nature and modal abundances of secondary minerals which could themselves be dependent on external parameters (open-system at the sample scale). Neglecting the contribution of accessory phases in the REE mass balance, the whole-rock system can be simplified into a two-component system. Indeed, as previously discussed, the whole-rock REE distribution is controlled, especially at the level of LREE, by the contribution of one LREE-depleted mineral (amphibole), and two LREE-enriched minerals (plagioclase and chlorite). The modal proportions of these three phases are extremely variable among the different samples (Table 1), but we stress the fact that the respective REE distributions of these minerals are not balanced in such a way that whole-rock samples could preserve primary magmatic patterns. This is a general feature throughout the lava flows: Fig. 8 shows that the $^{147}Sm/^{144}Nd$ ratios of all studied samples are controlled by the modal proportions of two types of mineral components possessing a more or less constant REE distribution throughout the flow sections, namely: amphibole (LREE-depleted, high $^{147}Sm/^{144}Nd$ ratio), and plagioclase and/or chlorite (LREE-enriched, low $^{147}Sm/^{144}Nd$ ratio). Thus, it is inferred that the $^{147}Sm/^{144}Nd$ ratio of a given whole-rock sample is controlled by the secondary mineralogy, which in turn confirms the interpretation that the REE were mobile on a whole-rock scale in these flows. It should be pointed out here that this does not necessarily mean that the system was externally buffered. It could just correspond to a REE redistribution among the different units of the flows.

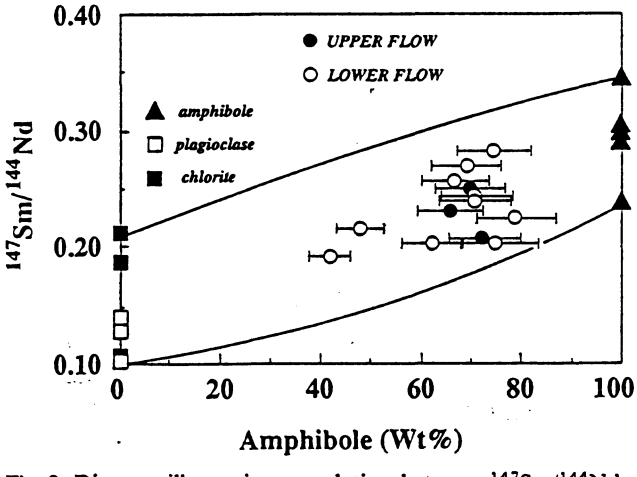

Fig. 8. Diagram illustrating correlation between $^{147}Sm/^{144}Nd$ ratios of whole-rock samples and modal compositions. Mineral data are shown for comparison. The two curves are mixing curves delineating field of $^{147}Sm/^{144}Nd$ ratios obtained in combining chlorite + plagioclase + amphibole in all possible relative proportions

The variation in the proportion of amphibole, chlorite and plagioclase thus appears to have played an important role in the redistribution of REE among the various whole-rock samples. It is possible that this variation ultimately formed from the superimposition of magmatically-induced chemical heterogeneity (e.g. differences in MgO concentrations between the spinifex-textured and lower cumulate zones) and the secondary influx of large amounts of Na. Owing to the high Mg and Fe concentrations, it is indeed to be expected that the more widespread metamorphic phases to crystallize in a komatiite flow will be amphibole and chlorite. However, depending on the Ca/Mg ratio, the relative proportion of these two mineral phases could be highly variable. Within rocks from the lower cumulate zone with high Mg and low Ca contents, chlorite should be an important new mineral. Because chlorite can accomodate Al, most of the Al initially present in this zone should be consumed by the process of chlorite crystallization, so there would be no Al left over to combine with metasomatic Na in order to build plagioclase. The secondary mineralogies in rocks of this zone should thus be composed mainly of chlorite with no plagioclase present, as seen in the samples from the lower cumulate zones of the Siivikkovaara flows (Table 1).

In less Mg-rich rocks from the spinifex-textured zone, on the other hand, the presence of larger amounts of Ca would favour the formation of amphibole. Because amphibole contains much less Al than chlorite, preferential crystallization of amphibole should not use up all the Al present in the rock. Hence, in this case, some Al would be available for trapping metasomatic Na in order to build albitic plagioclase. The secondary mineralogies in rocks of this zone should thus be dominated by amphibole and plagioclase, which is also the assemblage of the present flows. Note that, in such a model, we can predict a negative correlation between Na_2O and MgO contents, a feature which is observed in the Siivikkovaara sample suite (Fig. 3b).

However, the nature of the mechanism that allowed REE mobility remains to be identified. Because diffusion coefficients for REE in crystalline phases are low (e.g. Zindler and Hart 1984; McCulloch and Black 1984), and because metamorphic recrystallization took place under only moderately high temperatures ($\approx$450 °C), it is unlikely that solid state diffusion could account for this mobility. This role was likely played by the fluids which invaded the rocks during their metamorphic recrystallization. Results from the Tipasjärvi belt have already indicated that the fluids which circulated during

the Svecokarelian orogeny could mobilize the REE (Tourpin et al. 1991). The occurrence of secondary metasomatic carbonate at Tipasjärvi suggests that these fluids probably contained a significant CO_2 [or $(CO_3)^{2-}$] component. Judging from the literature, this component might have been the actual complexing agent that allowed these fluids to leach and transport the REE (e.g. McCulloch and Black 1984; Windrim et al. 1984, and references therein).

Fluid/rock ratios and origin of the fluid phase which transported the REE: comparison with the carbonatized komatiite flow from Tipasjärvi

Constraints can be placed on the values of fluid/rock ratios and the origin of the fluid phase which transported the REE using oxygen isotopic data. As already pointed out, the oxygen isotopic composition of each mineral species is more or less constant throughout the two flows (Table 7). If this is true, there should be a correlation between the $\delta^{18}O$ value of the whole-rock sample ($\delta^{18}O_{WR}$) and its corresponding modal composition. Figure 9 illustrates such a correlation, hence demonstrating that the values of $\delta^{18}O_{WR}$ are controlled by the relative proportions of the two types of minerals with different isotopic compositions, namely: chlorite and/or amphibole (similar $\delta^{18}O$), and plagioclase (ilmenite is too scarce to play any significant role in $\delta^{18}O_{WR}$ mass balances). With respect to the fluid-rock interaction, such a correlation may correspond to two extreme situations:

1. The fluid phase is more or less stationary (low fluid/rock ratio). It does not constitute a significant oxygen isotopic reservoir, but acts only as a vector allowing mutual oxygen isotopic equilibration of the minerals within a flow unit. In such a case, measured $\delta^{18}O_{WR}$ is different from initial (magmatic) $\delta^{18}O_{WR}$, but globally, the $\delta^{18}O$ of the whole flow remains unchanged.

2. The oxygen isotopic composition of each mineral species is buffered across the two flows through equilibration with a common external fluid in great excess. In such a case, all rock systems are affected, including

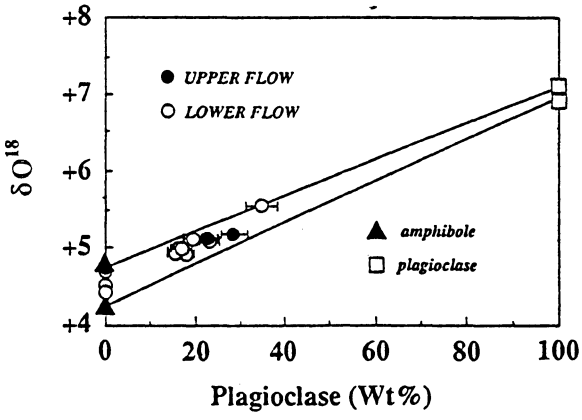

Fig. 9. Diagram illustrating correlation between $\delta^{18}O$ values of whole-rock samples and modal compositions. Mineral data are shown for comparison. Remember that compositions of chlorite (not shown) overlap those of amphibole

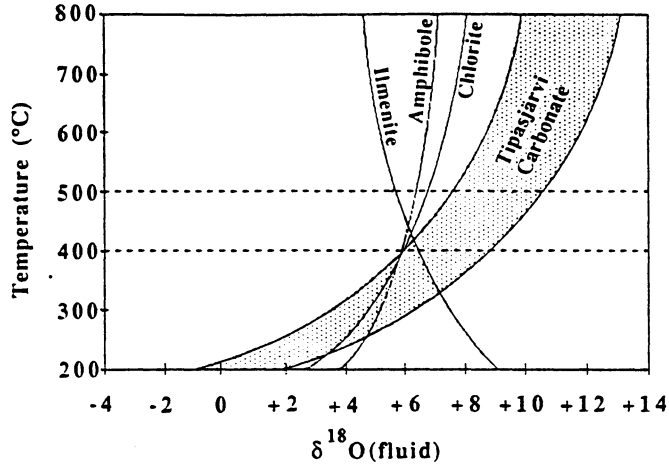

Fig. 10. Diagram showing composition(s) of fluid(s) in equilibrium with Siivikkovaara plagioclase, amphibole and ilmenite as a function of temperature, and comparison with the results obtained for the fluid in equilibrium with the carbonates from the carbonatized komatiite flow from Tipasjärvi. Note that the curve of chlorite was calculated assuming $\delta^{18}O_{chlorite} = \delta^{18}O_{amphibole}$ (see text and Fig. 9). Data sources: this study; Tourpin et al. (1991)

the bulk flow, and all measured $\delta^{18}O$ values are secondary.

Since 12 of the 13 analyzed whole-rock samples have oxygen isotopic ratios lower than the mantle reference (Table 6) we can rule out model 1. A stationary fluid phase model appears also to be somewhat inconsistent with the secondary influx of large amounts of Na, an influx which implies the two flows were connected with the surrounding rocks by means of percolating fluids. So we conclude that: (a) the fluid was external to the komatiite flow units; and (b) fluid/rock ratios were sufficiently large (>1.0?) such that the external fluid could modify all oxygen isotopic compositions.

Using the equations of Bottinga and Javoy (1973, 1975) and Wenner and Taylor (1973) for mineral/water fractionation, we have calculated the $\delta^{18}O$ of the fluid phase in equilibrium with amphibole, ilmenite and chlorite as a function of temperature (Fig. 10). Taking 400 and 500 °C as the minimum and maximum exchange temperatures, it can be inferred that the $\delta^{18}O$ of the fluid phase in equilibrium is located somewhere in between +5.5 and +6.5‰. Such values are typical of rock-dominated fluid systems (magmatic or/and metamorphic fluids), and thus appear consistent with Tourpin et al.'s (1991) conclusion that the fluid responsible for the transport of REE was probably a metamorphic fluid.

Along with Sm-Nd data, Tourpin et al. (1991) presented oygen isotopic results for several carbonate samples from the Tipasjärvi carbonatized komatiite flow. In Fig. 10, we report the field of calculated fluid compositions in equilibrium with these carbonate samples. For a number of samples, calculated $\delta^{18}O_{(fluid)}$ values overlap the compositions found for Siivikkovaara komatiites, but for some, the fluid should have had higher $\delta^{18}O$ values for temperatures in the range 400–500 °C (up to +10.5‰; Fig. 10). It is possible that the carbonates from Tipajärvi were deposited from a fluid phase

with a $\delta^{18}O$ similar to that which circulated in the Siivikkovaara komatiites, but at lower temperatures: assuming carbonate deposition temperatures around 300–350 °C, Figure 10 shows that the two metamorphic fluids would possess similar isotopic signatures.

What were the original REE patterns and ε_{Nd} values?

Let us consider the whole-rock isochron relationship at 1810 ± 130 Ma and its corresponding ε_{Nd} (1810 Ma) value of $+2.0 \pm 0.7$. Such a value may lead to two contrasting interpretations as regards the original compositions depending on whether (a) the bulk flows were closed-system for the REE, or (b) whether they exchanged REE with the surrounding rocks (Fig. 11):

a. *No exchange.* In this case, $+2.0 \pm 0.7$ would be the ε_{Nd} value of the two flows just prior to the middle Proterozoic metamorphic event. If so, provided that the komatiite flows from Siivikkovaara ultimately formed from a mantle source with $\varepsilon_{Nd} \approx +3.0$ – i.e. the value of depleted mantle at 2.7 Ga ago, or the value generally found in crustally uncontaminated and well-preserved 2.7 Ga old komatiites (Dupré et al. 1984; Machado et al. 1986; Chauvel et al. in press), the original REE pattern could have been a flat or slightly LREE-enriched pattern (trajectory A in Fig. 11). If true, the komatiite from Siivikkovaara might have initially resembled some relatively fresh 2.7 Ga-old komatiite flow units from Newton Township in Canada (e.g. Cattell et al. 1984), but would differ from the majority of well-preserved late Archean komatiites as the latter generally yielded LREE-depleted patterns (e.g. Barnes et al. 1983; Arndt and Nesbitt 1984).

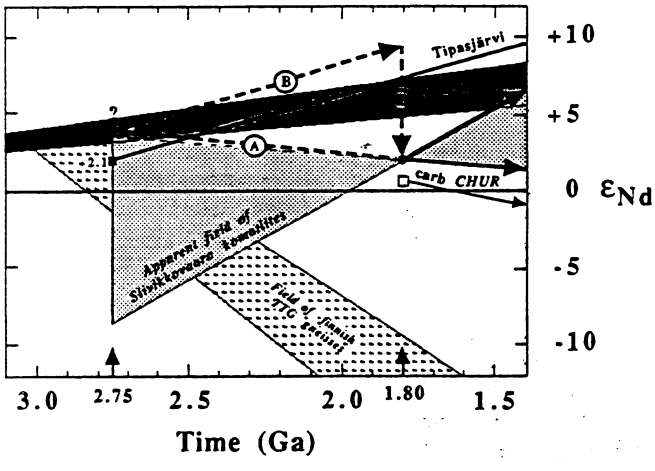

Fig. 11. ε_{Nd} vs. time diagram illustrating possible isotopic trajectories for Siivikkovaara komatiite flows depending on whether these flows were a closed-system at 1800 Ma ago (*trajectory A*) or whether they exchange REE with surrounding rocks (*trajectory B*). The diagram also presents the isotopic evolutions of three important rock-types, namely: (a) the Tipasjärvi uncarbonatized komatiite; (b) the Tipasjärvi metasomatic carbonate; and (c) the TTG gneisses from the surrounding basement. See text for further explanations. Data sources: Martin (1985), Tourpin et al. (1991), and this study

b. *Exchange.* In this case $+2.0 \pm 0.7$ would not be the ε_{Nd} value of the komatiite flows prior to metamorphism, but rather represents some intermediate value between the true pre-metamorphic value and the ε_{Nd} of the external system with which the two flows re-equilibrated. Because the terranes that surround the region of Siivikkovaara are dominated by granitic rocks with strongly negative ε_{Nd} values (-10 to -15; Fig. 11), it is possible that the process of external re-equilibration led to to a reduction of the ε_{Nd} value of the two flows. If so, the ε_{Nd} prior to metamorphism could significantly exceed the value of $+2.0 \pm 0.7$. By making the same assumption as this regarding the ε_{Nd} of the mantle source, the original REE pattern could not have been a flat or slightly LREE-enriched pattern, but a pattern depleted in LREE (trajectory B in Fig. 11).

The fact that the fluid phase which transported the REE on a whole-rock scale was external to the komatiite flows rather favours model (b). Consideration of the results from the Tipasjärvi carbonatized komatiite flow leads to the same conclusion, as these is evidence that the fluid phase which invaded this flow contained Nd (Tourpin et al. 1991).

However, there is still no direct way of determining the exact isotopic composition of the Nd which was present in the invading fluid. Neither do we have the possibility of establishing the exact extent of the isotopic and elemental re-equilibration that took place during the fluid-rock exchange process. In Fig. 11, we present for comparison the ε_{Nd} (1800 Ma) value determined by Tourpin et al. (1991) for the carbonate from the Tipasjärvi carbonatized komatiite flow, as well as the isotopic trajectory of the uncarbonatized Tipasjärvi komatiite. We note that the ε_{Nd} (1800 Ma) value of $+2.0 \pm 0.7$ obtained for the komatiite flows from Siivikkovaara is intermediate between the ε_{Nd} (1800 Ma) value of the Tipasjärvi carbonate ($\approx +1$) and that of the uncarbonatized Tipasjärvi komatiite ($\approx +7$). In the light of this fact and the spatial proximity of the regions of Siivikkovaara and Tipasjärvi, it is possible that the two komatiites initially resembled each other. Thus, the unaltered Siivikkovaara komatiite might have been characterized by an ε_{Nd} (2750 Ma) value of about $+2.0$ and a $^{147}Sm/^{144}Nd$ of about 0.24 (Fig. 11; Tourpin et al. 1991).

Concluding remarks

Two main conclusions stem from this study. The first is that the REE patterns and initial Nd isotopic compositions of komatiites must be treated with caution. The data presented in this paper shows that metamorphism may induce a profound redistribution of REE in these rocks, a phenomenon which may also cause strong shifts of the calculated initial ε_{Nd} values relative to the true magmatic value. As pointed out in the introduction, the absolute shift will depend on a number of factors, one being the time span between the emplacement of the rocks and the subsequent REE redistribution (Rosing 1990). The present case shows importance of this latter factor, as this time span was very large for the komatiite flows from Siivikkovaara (Fig. 11). Taken as a whole, the results presented in this study illustrate the necessity

of dating metamorphic recrystallizations in komatiites, as this may represent crucial data for evaluating the significance of calculated initial ε_{Nd} values. Yet, apart from the case of Barberton (e.g. Jahn and Shih 1974, Lopez-Martinez et al. 1984), the present work is, to our knowledge, the first example of a komatiite study which includes an attempt to establish such a timetable of metamorphic events.

The second conclusion is that fluids played an important role in the resetting of the chemical and isotopic magmatic memories of the two investigated flows. As pointed out, there is reason to believe that the percolating metamorphic fluids were CO_2-rich, and that this component was responsible for the intense secondary mobilization of REE. In this respect, it is worth noting that Lécuyer et al. (in preparation), who recently conducted a similar study on metakomatiite flows from Barberton, did not observe any effect of metamorphism on REE patterns and Sm-Nd isotope systematics. However, the oxygen isotopic results indicate recrystallization temperatures as well as fluid/rock ratios similar to those inferred for the komatiite flows from Siivikkovaara. Lécuyer et al. (in preparation) explain this difference by suggesting that the fluid involved at Barberton was H_2O-rich. Thus, it is possible that the REE mobility in the komatiite flows from eastern Finland does not represent a general case, since the mobility of these elements will likely depend on the composition of the metamorphic fluids. Nevertheless, it is noteworthy that many metakomatiites comprise carbonates (see references in Tourpin et al. 1991), which might suggest that the metamorphic fluids circulating in these rocks often contained a significant amount of CO_2.

Acknowledgements. Field work was sponsored by the Finnish Academy of Sciences, as part of a cooperation project with the French CNRS. We are endebted to MA Fuminier, N Morin, J Cornichet and J Macé for their assistance during sample preparations and/or mass-spectrometry analyses. We also thank the following for discussions and reviews of various versions of the manuscript: J. Hoefs, H.G. Stosch, P.J. Patchett, and N.T. Arndt. Dr. MSN Carpenter improved the English version of the manuscript. The paper is a contribution to IGCP project 275 (Deep Geology of the Baltic Shield).

References

Albarède F, Brouxel M (1987) The Sm/Nd secular evolution of the continental crust and the depleted mantle. Earth Planet Sci Lett 82:25–35

Arndt NT (1977) Thick, layered peridotite-gabbro flows in Munro Township, Ontario. Can J Earth Sci 14:2620–2637

Arndt NT, Nisbet EG (1982) Komatiites. Allen and Unwin, London Boston Sydney, 526 pp

Arndt NT, Nesbitt RW (1984) Magma mixing in komatiitic lavas from Munro Township, Ontario. In: Kröner A, Hanson GN, Goodwin AM (eds) Archaean Geochemistry. Springer Verlag, Berlin Heidelberg New York Tokyo, pp 99–114

Arndt NT, Jenner GA (1986) Crustally contaminated komatiites and basalts from Kambalda, Western Australia. Chem Geol 56:229–255

Arndt NT, Teixeira NA, White WM (1989) Bizarre geochemistry of komatiites from the Crixas greenstone belt, Brazil. Contrib Mineral Petrol 101:187–197

Barnes SJ, Gorton MP, Naldrett AJ (1983) A comparative study of olivine and clinopyroxene spinifex flows from Alexo, Abitibi greenstone belt, Ontario, Canada. Contrib Mineral Petrol 83:293–308

Beaty DW, Taylor HP Jr (1982) The oxygen isotope geochemistry of komatiites: evidence from water-rock interaction. In: Arndt NT, Nisbet EG (eds) Komatiites. Allen and Unwin, London Boston Sydney, pp 267–280

Bertrand JM, Blais S, Capdevila R (1978) Précisions sur l'évolution structurale de l'Archéen de Karélie (Finlande). C R Acad Sci Paris 287:683–686

Blais S, Auvray B, Capdevila R, Jahn BM, Hameurt J (1978) The archean greenstone belts of Karelia (eastern Finland) and their komatiitic and tholeiitic series. In: Wiley BF, Naqvi SM (eds) Developments in Precambrian geology: Archaean geochemistry. Elsevier, Amsterdam Oxford New York Tokyo, pp 87–107

Blais S, Auvray B, Jahn BM, Taipale K (1987) Processus de fractionnement dans les coulées komatiiques archéennes: cas des laves à spinifex de la ceinture de roches vertes de Tipasjärvi (Finlande orientale). Can J Earth Sci 24:953–966

Bottinga Y, Javoy M (1973) Comments on oxygen isotope geothermometry. Earth Planet Sci Lett 20:251–265

Bottinga Y, Javoy M (1975) Oxygen isotope partitioning among the minerals in igneous and metamorphic rocks. Rev Geophys Space Phys 13:401–418

Bryan WB, Finger LW, Chayes F (1969) Estimating proportion in petrographic mixing equations by least-squares approximations. Science 163:926–927

Cattell A, Krogh TE, Arndt NT (1984) Conflicting Sm-Nd whole rock and U-Pb zircon ages for Archean lavas from Newton Township, Abitibi Belt, Ontario. Earth Planet Sci Lett 70:280–290

Chase CG, Patchett PJ (1988) Stored mafic/ultramafic crust and early Archean mantle depletion. Earth Planet Sci Lett 91:66–72

Chauvel C, Dupré B, Arndt NT (1992) Pb and Nd isotopic correlation in Belingwe komatiites and basalts In: Bickle MJ, and Nisbet EG (eds) The development of the Belingwe greenstone belt: a study of the construction of the continental crust. Blackwell (in press)

Clayton RN, Mayeda TK (1963) The use of bromine pentafluoride in the extraction of oxygen from oxides and silicates for isotopic analysis. Geochim Cosmochim Acta 27:43–52

Dietrich VJ, Gansser A, Sommerauer J, Cameron WE (1981) Palaeogene komatiites from Gorgona Island, East Pacific – A primary magma for ocean floor basalts? Geochem J 15:141–161

DePaolo DJ, Wasserburg GJ (1976) Inferences about magma sources and mantle structure from $^{143}Nd/^{144}Nd$. Geophys Res Lett 3:743–746

Dupré B, Chauvel C, Arndt NT (1984) Pb and Nd isotopic study of two Archean komatiitic flows of Alexo, Ontario. Geochim Cosmochim Acta 48:1965–1972

Echeverria LM (1982) Komatiites from Gorgona Island, Colombia. In: Arndt NT, Nisbet EG (eds) Komatiites. Allen and Unwin, London Boston Sydney, pp 199–209

Elphick SC, Dennis PF, Graham CM (1986) An experimental study of the diffusion of oxygen in quartz and albite using an overgrowth technique. Contrib Mineral Petrol 92:322–330

Fletcher IR, Rosman KJR (1982) Precise determination of initial ε_{Nd} from Sm-Nd isotopic data. Geochim Cosmochim Acta 46:1983–1987

Gaàl G, Mikkola A, Soderholm B (1978) Evolution of the Archean crust in Finland. Precamb Res 9:199–215

Giletti BJ (1986) Diffusion effects on oxygen isotope temperatures of slowly cooled igneous and metamorphic rocks. Earth Planet Sci Lett 77:218–228

Giletti BJ, Semet MP, Yund RA (1978) Studies of diffusion – III. Oxygen in feldspars: an ion microprobe determination. Geochim Cosmochim Acta 42:45–57

Gruau G, Jahn BM, Glikson AY, Davy R, Hickman AH, Chauvel C (1987) Age of the Archean Talga-Talga Subgroup, Pilbara Block, Western Australia, and early evolution of the mantle: new Sm-Nd isotopic evidence. Earth Planet. Sci Lett 85:105–116

Hanski EJ (1980) Komatiitic and tholeiitic metavolcanics of the Kellojärvi group in the Siivikkovaara area of the Archaean Kuhmo greenstone belt, eastern Finland. Bull Geol Soc Fin 52:67–100

Hey MH (1954) A new review of the chlorites. Mineral Mag 30:277

Hyppönen V (1983) Geol maps of the Ontojoki, Hiisijärvi and Kuhmo areas. Geol Surv Finland 1:100000. Lehdet 4411, 4412 a 4413 (in Finnish)

Ito E, White WM, Göpel C (1987) The oxygen, Sr, Nd and Pb isotope geochemistry of MORB. Chem Geol 62:157–176

Jacobsen SB, Wasserburg GJ (1980) Sm-Nd isotopic evolution of chondrites. Earth Planet Sci Lett 50:139–155

Jahn BM, Chih CY (1974) On the age of the Onverwacht Group, Swaziland Sequence, South Africa. Geochim Cosmochim Acta 38:873–875

Jahn BM, Auvray B, Blais S, Capdevila R, Cornichet J, Vidal F, Hameurt J (1980a) Trace element geochemistry and petrogenesis of Finnish greenstone belts. J Petrol 21:201–244

Jahn BM, Bernard-Griffiths J, Charlot R, Cornichet J, Vidal F (1980b) Nd and Sr isotopic compositions and REE abundances of Cretaceous MORB (Holes 417D and 418A, Legs 51, 52 and 53). Earth Planet Sci Lett 48:171–184

Javoy M (1977) Stable isotopes and geothermometry. J Geol Soc London 133:609–636

Jegouzo P, Blais S (1991) Structural evidence for a Karelian reworking of the Archean crust in eastern Finland. (Abstr) Res Terrae, Ser A, Vol 5, p 29

Kintzler RJ, Grove TL (1985) Crystallization and differentiation of Archean komatiitic lavas from northeast Ontario: phase equilibrium and kinetic studies. Amer Mineral 70:40–51

Kouvo O, Tilton GR (1966) Mineral ages from the Finnish Precambrian. J Geol 74:421–442

Kouvo O (1978) Annual report on the activities for the year 1982. Abstract Geol Surv Finland, 16–17

Kyser TK (1986) Stable isotope variations in the mantle. In: Valley JW, Taylor HP Jr, O'Neil JR (eds) Stable isotopes in high temperature geological processes. Reviews in Mineralogy 16:141–164

Leake BE (1978) Nomenclature of amphiboles. Am Mineral 63:1023–1059

Lopez-Martinez M, York D, Hall CM, Hanes JA (1984) Oldest reliable $^{40}Ar/^{39}Ar$ ages for terrestrial rocks: Barberton Mountain komatiites. Nature 307:352–355

Luukkonen E (1985) Structural and U-Pb isotopic study of late Archaean migmatitic gneisses of the Presvecokarelides, Lylyvaara, eastern Finland. Trans R Soc Edinburgh, Earth Sci 76:401–410

Machado N, Brooks C, Hart SR (1986) Determination of initial $^{86}Sr/^{87}Sr$ and $^{143}Nd/^{144}Nd$ in primary mineral from mafic ultramafic rocks: experimental procedure and implication for the isotopic characteristics of the Archean mantle under the Abitibi greeenstone belt, Canada. Geochim Cosmochim Acta 50:2335–2348

Martin H (1985) Nature, origine et evolution d'un segment de croûte continentale archéenne: contraintes chimiques et isotopiques. Exemple de la Finlande orientale. Mém Doc Centre Arm Et Struct Socles 1:392 pp

Martin H, Querré G (1984) A 2.5 Ga reworked sialic crust: Rb-Sr ages and isotopic geochemistry of late Archean volcanic and plutonic rocks from E. Finland. Contrib Mineral Petrol 85:292–299

Martin H (1989) Archean chronology in the eastern part of the Baltic Shield: a synthesis. Precamb Res 43:63–77

McCulloch MT, Black LP (1984) Sm-Nd isotopic systematics of Enderby Land granulites and evidence for the redistribution of Sm and Nd during metamorphism. Earth Planet Sci Lett 71:46–58

Muehlenbachs K, Clayton RN (1972) Oxygen isotope studies of fresh and weathered submarine basalts. Can J Earth Sci 9:172–184

Piirainen T (1988) The geology of Archaean greenstone-granitoid terrain in Kuhmo, eastern Finland, Spec Pap 4:39–51

Pineau F, Javoy M, Hawkins JW, Craig H (1976) Oxygen isotope variations in marginal basin and ocean-ridge basalts. Earth Planet Sci Lett 28:299–307

Piquet D (1982) Mécanismes de recrystallisation métamorphique dans les ultrabasites: exemple des roches vertes Archéennes de Finlande Orientale (ceinture de Suomussalmi-Kuhmo). Thèse 3e cycle, Rennes, 246 pp

Pyke DR, Naldrett AJ, Eckstrand OR (1973) Archean ultramafic flows in Munro Township, Ontario. Geol Soc Am Bull 84:955–978

Quérré G (1985) Palingenèse de la croûte continentale à l'Archéen: les granitoïdes tardifs (2.5–2.4 Ga) de Finlande orientale. Pétrologie et géochimie. Mém Doc Centre Arm Et Struct Socles 2:226 pp

Rosing MT (1990) The theoretical effect of metasomatism on Sm-Nd isotopic systems. Geochim Cosmochim Acta 54:1337–1341

Smith AD, Ludden JN (1989) Nd isotopic evolution of the Precambrian mantle. Earth Planet Sci Lett 93:14–22

Smith HS, O'Neil JR, Erlank AJ (1984) Oxygen isotope compositions of minerals and rocks and chemical alteration patterns in pillow lavas from the Barberton greenstone belt, South Africa. In: Kröner A, Hanson GN, Goodwin AM (eds) Archaean geochemistry. Springer, Berlin Heidelberg New York Tokyo, pp 115–137

Taipale K (1983) The geology and geochemistry of the Archean Kuhmo greenstone-granite terrain in the Tipasjärvi area, eastern Finland. Acta Univ Ouluensis 151:98 pp

Taipale K, Tuokko I, Piirainen T (1980) A brief introduction to the geology and the geochemistry of the Kuhmo belt eastern Finland. In: Papunen H (ed) IGCP project 161, field excursion guide for Finland, Helsinki, pp 37–73

Tourpin S (1991) Perte des mémoires isotopiques (Nd, Sr, O) et géochimiques (REE) primaires des komatiites au cours du métamorphisme: exemple de la Finlande orientale. Thèse d'Université, Rennes, 181 pp

Tourpin S, Gruau G, Blais S, Fourcade S (1991) Resetting of REE, and Nd and Sr isotopes during carbonitization of a komatiite flow from Finland. Chem Geol 90:15–29

Vaasjoki M (1988) Zircon U-Pb versus Rb-Sr whole-rock age data from eastern Finland: a critical comment on the papers of Barbey and Martin and Martin, Precambrian Research, Vol 35, 1987. Precamb Res 39:217–219

Vidal P, Blais S, Jahn BM, Capdevila R, Tilton GR (1980) U-Pb and Rb-Sr systematics of the Suomussalmi Archean greenstone belt (eastern Finland). Geochim Cosmochim Acta 44:2033–2044

Viljoen MJ, Viljoen RP, Smith HS, Erlank AJ (1983) Geological, textural, and geochemical features of komatiitic flows from the Komati formation. In: Anhaeusser CR (ed) Geol Soc S Afr Spec Publ 9:1–20

Wenner DB, Taylor HP Jr (1971) Temperature of serpentinization of ultramafic rocks based on $^{18}O/^{16}O$ fractionation between coexisting serpentine and magnetite. Contrib Mineral Petrol 32:165–185

Whitford DJ, Arndt NT (1978) Rare earth element abundances in a thick, layered komatiite lava flow from Ontario, Canada. Earth Planet Sci Lett 41:188–196

Windrim DP, McCulloch MT, Chappell BW, Cameron WE (1984) Nd isotopic systematics and chemistry of Central Australian sapphirine granulites: an example of rare earth element mobility. Earth Planet Sci Lett 70:27–39

York D (1969) Least squares fitting of a straight line with correlated errors. Earth Planet Sci Lett 5:320–324

Zindler A (1982) Nd and Sr isotopic studies of komatiites and related rocks. In: Arndt NT, Nisbet EG (eds) Komatiites. Allen and Unwin, London Boston Sydney, pp 399–420

Zindler A, Hart S (1984) Chemical Geodynamics Ann Rev Earth Planet Sci 14:493–571

Editorial responsibility: J. Hoefs

THE ORIGIN OF FLUIDS AND THE EFFECTS OF METAMORPHISM ON THE PRIMARY CHEMICAL COMPOSITIONS OF BARBERTON KOMATIITES: NEW EVIDENCE FROM GEOCHEMICAL (REE) AND ISOTOPIC (Nd, O, H, $^{39}Ar/^{40}Ar$) DATA

C. Lécuyer, G. Gruau, S. Fourcade and C.R. Anhaeusser

Article soumis à publication dans *Geochimica et Cosmochimica Acta*

Abstract - Numerous greenstone relics, all containing the lowermost formations of the Onverwacht Group, occur in the Archean trondhjemitic/tonalitic gneiss terrains south of the Barberton Greenstone Belt. In this study, we report some detailed petrological, geochemical and isotopic (Nd, O, H, $^{40}Ar/^{39}Ar$) data obtained on komatiites and komatiitic basalts from the Schapenburg Greenstone Remnant (SGR), the largest and best-preserved greenstone relic. The main goals are 1) to date the metamorphism affecting the SGR, using the $^{40}Ar/^{39}Ar$ dating method on amphiboles, 2) to evaluate the effect of metamorphism on the preservation of primary isotopic and chemical signatures and, 3) to estimate the temperature and water/rock ratios that prevailed during metamorphic recrystallization in order to constrain the composition and origin of the reacting fluid phase.

$^{39}Ar/^{40}Ar$ ages of 2.9 Ga obtained on two amphibole separates from the Schapenburg metavolcanics reveal the existence of a metamorphic event younger than the emplacement age (3.5 Ga). This metamorphic event belongs to a series of discrete periods of thermal activity from 3.4 to 2 Ga, each of them coinciding with a major episode of plutonic or volcanic activity. The ultrabasic lava flows acquired their $\delta^{18}O$ values (from +3.2 to +5‰) at high temperature (≈450°C) under high water/rock ratios. The reacting water had initial isotopic values which are typical of metamorphic fluids ($\delta^{18}O$= +5 to +7 ‰; δD= -65 to -50‰), and may contain a major contribution from magmatic fluids derived from the neighbouring TTG plutons.

REE patterns are not disturbed by metamorphic recrystallization. Despite the long time interval between emplacement and metamorphism (≈600 Ma), $\varepsilon_{Nd}(T)$ values are homogeneous throughout the whole magmatic suite, indicating that the Sm-Nd system was a closed system on the sample scale during metamorphism. From the Nd dataset it is deduced that the ultimate mantle source of these greenstones was depleted in LREEs ($\varepsilon_{Nd}(T)$≈+2.5), i.e. the source had a $^{147}Sm/^{144}Nd$ ratio higher than the chondritic reservoir.

Chemical fluxes during metamorphism were calculated for those elements which are unfractionated by olivine removal (e.g. Na, Ca, Ti, Al and Sr), by normalizing to Nd. They suggest a significant mobility of most major elements in the cumulate zones of the lava flows. By contrast, spinifex zones appear to have preserved most of their primary chemical signatures during

metamorphic recrystallization. Their CaO/Al_2O_3 and Al_2O_3/TiO_2 ratios can be used with a high level of confidence in determining the PT conditions of melting in the mantle source.

A general model of water-rock interactions applied to the sedimentary and magmatic rocks of the Onverwacht Group is also presented. The model involves conditions of metamorphism deduced from this study and available data from the literature. In addition to metavolcanic rocks, most of the oxygen isotope compositions of carbonates and cherts (except the highest values) can be explained by reequilibration with metamorphic fluids under greenschist-amphibolite facies conditions

INTRODUCTION

Komatiites are ultrabasic volcanic rocks (MgO contents up to 30%) which occur mainly in Archean greenstone belts. A consideration of chemical compositions, geographical distribution, and age data indicate that komatiites may provide useful evidence of the composition of the Archean mantle (e.g. JAHN et al., 1982; ARNDT, 1986; SMITH and LUDDEN, 1989; GRUAU et al., 1990a-b). However, the invariably altered and/or metamorphosed nature of these rocks casts some doubt on their capacity to preserve primary chemical and isotopic signatures. Authors have recently concluded that many elements, including the reputedly immobile REEs, could be partly or even totally reset during the alteration and metamorphism of komatiites (ARNDT et al., 1989; TOURPIN et al., 1991; GRUAU et al., 1992).

The ca. 3.5 Ga-old Onverwacht Group from the Barberton Greenstone Belt (BGB) of southern Africa (Fig. 1) contains the oldest recognizable komatiites worldwide. Komatiites from the Onverwacht Group are important for two reasons. Firstly, they represent the type locality for Al-depleted or Group II komatiites. Al-depleted or Group II komatiites are a particular category of komatiites, occurring mainly in early Archean terrains, which have lower Al_2O_3/TiO_2 ratios, but higher CaO/Al_2O_3 and $(Gd/Yb)_N$ ratios than chondrites (e.g. JAHN et al., 1982; ARNDT, 1986; GRUAU et al., 1990a). According to recent studies, the peculiar composition of these komatiites would arise because they formed by partial melting of deep mantle diapirs (>400 km) leaving majorite garnet as residual phase (e.g. GRUAU et al., 1990a; HERZBERG, 1992). Secondly, these komatiites have initial $^{143}Nd/^{144}Nd$ ratios close to the chondritic reference ($\varepsilon_{Nd}(T)\approx 0$; HAMILTON et al., 1979; 1983; GRUAU et al., 1990b); this feature is unusual in ancient greenstones worldwide. Other examples, such as the 3.5 Ga-old Pilbara komatiites from Western Australia, give initial $^{143}Nd/^{144}Nd$ ratios that are significantly higher than the chondritic value ($\varepsilon_{Nd}(T)>0$; see compilation in SMITH and LUDDEN, 1989).

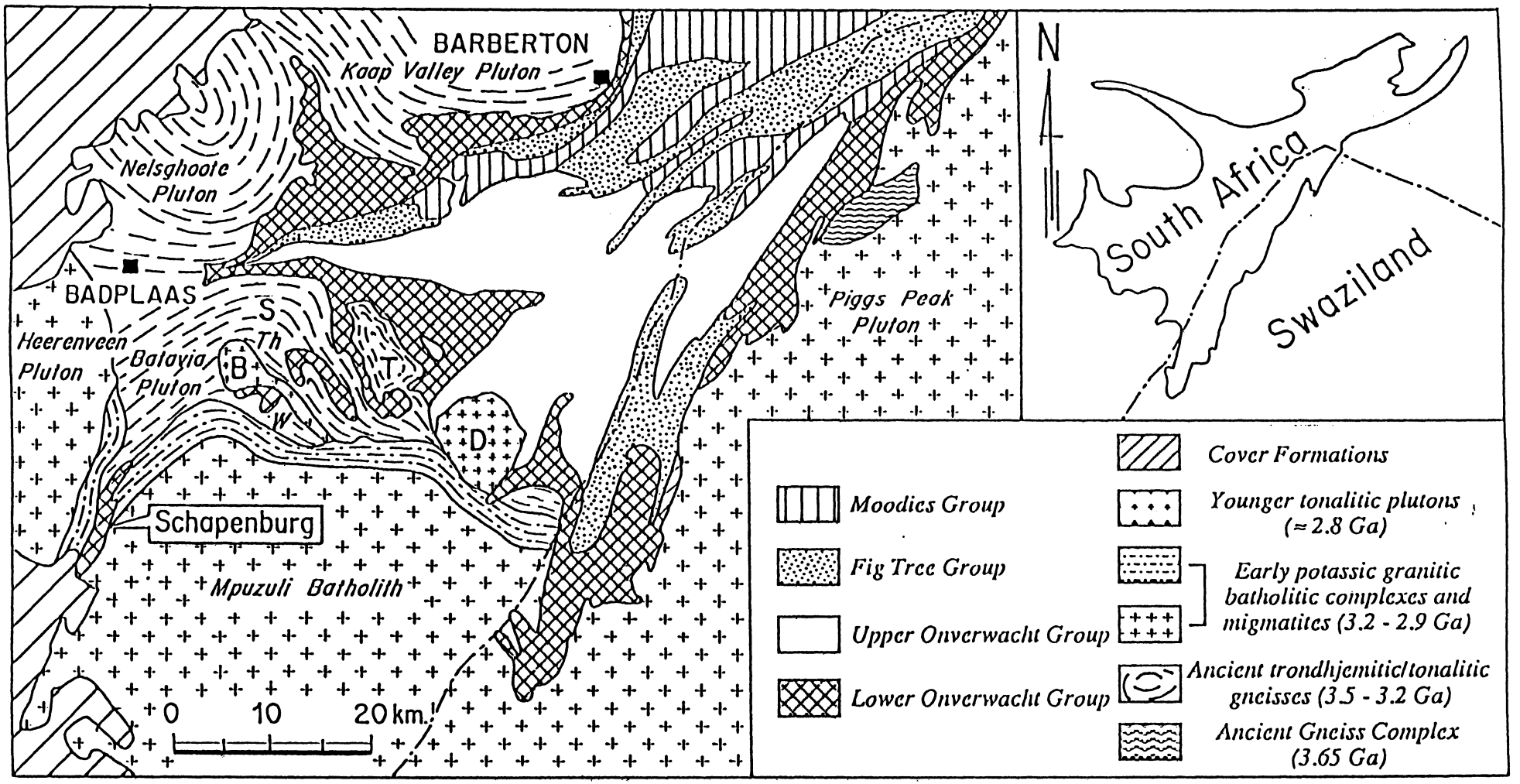

Figure 1: A simplified geological map of the southern part of the Barberton Greenstone Belt, Kaapvaal craton, southern Africa. D: Dalmein Pluton; T: Theespruit Pluton; S: Stolzburg Pluton; B: Boesmanskop Pluton. *W*: Weergevonden farm; *Th*: Theeboom farm.

SAMPLES AND ANALYTICAL METHODS

With the aim of studying elemental mobility and fluid-rock interactions in the Schapenburg greenstones, 23 whole-rock samples - 15 komatiites (MgO = 26 to 32%) and 8 komatiitic basalts (MgO = 15 to 20%) - were selected for geochemical (major and trace elements) and isotopic (Nd, O) analysis. Mineral separates from three of the komatiitic basalt samples (SC16, SC19, and SC20) were also analysed: amphibole (O, H, Ar/Ar) and magnetite (O). The location of samples is given in Fig. 2. Mineral proportions calculated from whole-rock chemistry and mineral compositions are presented in Table 1.

The komatiite samples come from three of four superimposed spinifex-textured komatiite lava flows (Fig.2), the so-called Carl's Flow (samples C1 to C6), Patrick's Flow (samples PD1 to PD4) and Patricia's Flow (samples P1 to P5). Gavin's Flow (68 cm thick), situated between Carl's Flow and Patricia's Flow, was not sampled because of difficulty in obtainning a complete samples set representative of the different textural components of the flow. Magmatic textures in the three flows studied are remarkably well-preserved (Fig. 2): variations in the size and shape of spinifex, for example, are still recognizable and may be mapped in detail. Furthermore, breccia zones are preserved intact at the top of Patricia's and Carl's Flows.

Mineralogically, all samples consist entirely of secondary assemblages with no relic igneous phases. In the komatiite flow samples, serpentine and amphibole are the two dominant phases (up to 70 and 60 weight %, respectively; Table 1). Chlorite and magnetite also occur, but in subordinate amounts (≤10% each) and rare ilmenite grains are locally present. In the basaltic komatiite samples, amphibole is by far the most abundant mineral (up to 99%; Table 1), while serpentine and chlorite are absent. Minor phases are magnetite (≤10%) and ilmenite (a few grains).

All whole-rock analyses were performed at Rennes University, except for the komatiites which were analysed for major elements and Rb, Sr, Zr, Y, V, Ni, and Cr at the University of Witwatersrand, South Africa. Concentrations of major elements and Rb, Sr, Zr, Y, V, Ni, and Cr were determined by XRF, while the REEs were analysed by the isotope dilution method. The precision is estimated at 1-5% for major elements, except for MnO (only 10%). For Rb, Sr, Zr, Y, V, Ni, and Cr, precisions are of the order of 10% for concentrations lower than 30 ppm. For concentrations higher than 30 ppm, the precision is reduced to 3%. Analytical errors for the REE - including chemical processing, blank effects, uncertainty in spike calibration and mass spectrometry runs - are estimated at about 5% for La and Lu, 3% for Gd and 2% for the other REE. Blanks were lower than $1*10^{-9}$g.

However, komatiites from the Onverwacht Group are not fresh rocks; they have all suffered some alteration and metamorphism. The grade of metamorphism is generally in the upper greenschist or lower amphibolite facies (e.g. VILJOEN and VILJOEN, 1969a). The precise context of this metamorphism remains a matter of debate. HOFFMAN et al. (1986) have ascribed recrystallization effects to sea-floor metamorphism on the basis of the apparent similarity between the $\delta^{18}O$ values of Onverwacht Group volcanic rocks and Phanerozoic ophiolites. CLOETE (1991), has recently criticised this interpretation, pointing out that the actual mineral composition of pillow lavas from the Komati Formation in the Onverwacht Group is not consistent with sea-floor metamorphism. VILJOEN and VILJOEN (1969a) and ANHAEUSSER (1983), on the other hand, emphasized the role of dynamothermal contact metamorphism related to the emplacement of numerous granitic batholiths into the BGB (Fig. 1).

Several attempts have been made to date the metamorphic recrystallization event affecting the Onverwacht Group komatiites, mainly by using the $^{40}Ar/^{39}Ar$ method. Very old $^{40}Ar/^{39}Ar$ ages - in the range 3450-3490 Ma - were obtained by LOPEZ-MARTINEZ et al.(1984) for a suite of komatiites and basaltic komatiites from the type section of the Komati Formation in the Onverwacht Group. These ages are indistinguishable from the 3480-3450 Ma zircon ages which are generally thought to represent the eruption age of the Onverwacht Group komatiites (e.g. KRÖNER and TODT, 1988; ARMSTRONG et al., 1990). However, LOPEZ-MARTINEZ et al. (1984) have also obtained $^{40}Ar/^{39}Ar$ ages which are significantly younger: 3300-3225 Ma (see also LOPEZ-MARTINEZ et al., 1992). Furthermore, $^{40}Ar/^{39}Ar$ ages as young as 2700 and 2100 Ma were recently reported for metasediments from the overlying Fig Tree Group (DERONDE et al., 1991). According to this study (op. cit.), the period around 2700 Ma corresponds to final granitic plutonism, or/and craton-scale deformation associated with the Limpopo orogeny.

The estimation of the $\delta^{18}O$ value of ancient seawater is one of the key issues of current research in Earth Sciences (e.g. KARHU and EPSTEIN, 1986; VEIZER et al., 1989a-b). In this respect, the Onverwacht Group komatiites are of particular interest if they contain the oxygen isotopic record of an interaction with Archean seawater, as argued by HOFFMAN et al. (1986). Nevertheless, it should be borne in mind that the similarity of $\delta^{18}O$ values between the Onverwacht Group volcanic rocks and Phanerozoic ophiolites does not necessarily imply that the reacting fluids resembled seawater. The $\delta^{18}O$ values of altered rocks are also a function of water/rock ratios and temperature of interaction, as well as of the nature and relative proportions of the newly-formed mineral phases. These parameters may have been different in Phanerozoic ophiolites as compared with

early Archean komatiites. SMITH et al. (1984), in an investigation of the oxygen isotope compositions of the Onverwacht Group volcanic rocks, concluded that "detailed modelling of $\delta^{18}O$ values in Onverwacht Group komatiite lava flows indicates that magmatic or primitive waters ($\delta^{18}O$=+7 to +5‰) could have been the major fluids responsible for the hydration of the lavas at temperature of 240-450 °C".

Numerous greenstone relics, all containing the lowermost formations of the Onverwacht Group, occur in the Archean trondhjemitic/tonalitic gneiss terrains south of the BGB (e.g. ANHAEUSSER, 1980; Fig. 1). In the present study, we report some detailed petrological, geochemical and isotopic (Nd, O, H, $^{40}Ar/^{39}Ar$) data obtained on komatiites and komatiitic basalts from the Schapenburg Greenstone Remnant (SGR), the largest and best-preserved greenstone relic. The aims of this work are as follows:

1) to determine the age of metamorphism affecting the SGR, using the $^{40}Ar/^{39}Ar$ dating method on amphiboles;

2) to evaluate, in relation to recent studies by ARNDT et al. (1989), TOURPIN et al. (1991), and GRUAU et al. (1992), the effect of metamorphism on the preservation of primary isotopic and chemical signatures in some of the oldest known komatiites; and

3) to estimate the water/rock ratios that obtained during metamorphic recrystallization and to constrain the nature and origin of the associated fluid phase.

GEOLOGICAL SETTING

The geology of the Schapenburg Greenstone Remnant (SGR) and surrounding granite-gneiss terrain is described in detail by ANHAEUSSER (1983; 1991), so only a brief account is given here. The SGR, which is approximately 12 km long with a maximum width of 2.5 km, is a typical greenstone succession consisting largely of alternating volcanic and sedimentary units, and belongs to a trail of km-sized greenstone fragments that crop out within the trondjhemitic/tonalitic gneisses that border the BGB (ANHAEUSSER and ROBB, 1980; Fig. 1). In some cases detailed mapping has revealed a lithological continuity between these fragments and the BGB (VILJOEN and VILJOEN, 1969b). On the basis of this observation, VILJOEN and VILJOEN (1969b) and ANHAEUSSER (1980) proposed that the greenstone lithologies found in the remnants are equivalent to the lowermost formations of the Onverwacht Group of the BGB - namely, the Sandspruit, Theespruit and Komati Formations. Recent high-precision U-Pb zircon results for the Theespruit and overlying Komati Formations of the BGB date the deposition

of the lowermost volcano-sedimentary units of the Onverwacht Group at around 3480-3450 Ma (e.g. ARMSTRONG et al., 1990).

As can be seen in Figure 1, extensive granitic plutonic activity is characteristic of the Barberton Mountain Land. The volumetrically dominant intrusions in the vicinity of Schapenburg are the Mpuzuli and Heerenveen batholiths (Fig. 1). Both batholiths are composite. The Mpuzuli batholith is composed of pinkish medium to coarse-grained adamellite with some minor granodiorite. The Heerenveen batholith is zoned, with a central part made of very coarse-grained trondjhemite, and an outer zone composed of adamellite and granodiorite grading into nebulitic and migmatitic zones near the batholith margins (ANHAEUSSER and ROBB, 1983). The two composite batholiths, together with the Nelspruit batholith located further north, belong to the second magmatic episode of ANHAEUSSER and ROBB (1981), which occurred around 3100-3000 Ma ago (see review of radiometric ages in KAMO and DAVIS, 1991; see also BARTON et al., 1983).

Domes of trondjhemitic/tonalitic gneisses (e.g. the Baadplass and Stolzburg plutons) outcrop to the North and northeast (Fig. 1). They belong to the first magmatic episode defined by ANHAUESSER and ROBB (1981), generally yielding ages older than the Mpuzuli and Heerenveen batholiths: for example, the Stolzburg pluton is dated at 3445±4 Ma by the U-Pb method on zircon (KAMO and DAVIS, 1991).

With rare exception the SGR and the Mpuzuli and Heerenveen batholiths are never in direct contact, the SGR being usually flanked by zones of foliated trondjhemitic gneisses and migmatites. No age data are available on these rock-units in the immediate vicinity of the SGR, although BARTON et al. (1983) has reported whole-rock Rb-Sr isochron ages of 2916±33 Ma and 2939±75 Ma, respectively, for strongly foliated trondjhemitic gneisses occurring in the area north of the Mpuzuli batholith on the farms Weergevonden and Theeboom (Fig. 1). Recent U-Pb zircon dating of the TTG gneiss suite in the southern part of the BGB has indicated, however, that these units are all approximately 3440 Ma old (KAMO and DAVIS, 1991) and are considerably older than the Rb-Sr whole-rock ages previously obtained for this suite.

Minor amounts of syenite were also emplaced in this terrain. The Boesmanskop pluton, which is located approximately 20 km NE of the SGR (Fig. 1) forms part of this suite and yields a Rb-Sr whole-rock isochron age of 2848±31 Ma (BARTON et al., 1983). As with the TTG suite the U-Pb zircon age for this syenite pluton has been shown by KAMO and DAVIS (1991) to be older at 3107±1Ma. It is now evident that the Rb-Sr ages are generally imprecise and, because the BGB has experienced a protacted magmatic history, the Rb-Sr systematics of the older plutons may have been affected by thermal perturbations

and/or hydrothermal alteration associated with the emplacement of younger rocks (KAMO and DAVIS, 1991).

The magmatic episodes involving the emplacement of granitic rocks south of the BGB were followed by other igneous and volcanic events that may have relevance to the thermal history of rocks in the Schapenburg region discussed later in this contribution. Volcanic rocks forming part of the Nsuze Group crop out approximately 20 km SE of the SGR. Similar rocks, which form part of the Pongola Sequence, yielded a U-Pb zircon age of 2490±22 Ma that is consistent with the Sm-Nd whole-rock age of 2934±114 and a younger Rb-Sr whole-rock isochron age of 2883±69 Ma (HEGNER et al., 1984).

Also in this area southeast of the SGR is the Ushuswana Igneous Suite (UIS) comprising mainly olivine pyroxenite and gabbroic rocks. The UIS occurs as a layered dyke-like body extending from NW Swaziland into South Africa in a NW-SE direction parallel to a prominent mafic dyke swarm that extends throughout the region south of the BGB. An internal Sm-Nd isochron age of 2871±30 Ma for the UIS (HEGNER et al., 1984) agrees with an earlier Rb-Sr whole rock age of 2870±38 Ma obtained for the Usushwana Complex by DAVIES et al. (1970). The dykes, which are mainly doleritic, have not been radiometrically dated, but the regional geology and field relationships suggest that dyke intrusion probably culmunated around 1800-2400 Ma (ANHAEUSSER, 1983).

Volcano-sedimentary sequences in the SGR generally comprise peridotitic komatiite flows at the base (MgO contents ranging from 25 to 35%), which are overlain by basaltic komatiites (MgO≈15-20%). Banded silicate-facies iron formations usually form the cap of each sequence. Also present in the SGR is a well-developed succession of metagreywackes and metapelites.

As commonly observed throughout the Barberton Mountain Land, rocks of the SGR have suffered pervasive alteration and metamorphism. Although some primary textures are locally preserved (e.g., spinifex in komatiite lava flows), metamorphic recrystallization has resulted in a complete obliteration of all the primary mineral assemblages.

As shown by ANHAEUSSER (1983), metamorphic grade in the SGR is a function of distance to the granitic-orthogneissic intrusions. Within the predominant mafic/ultramafic rocks, metamorphism grades from upper greenschist to amphibolite facies towards the intrusions, a zonation which suggests a dynamothermal or contact-type metamorphism. The presence of cordierite±staurolite assemblages, as well as the occurrence of local incipient melting in some of the metagreywackes, indicate T-P conditions between 500 and 700°C, and 2.5 and 3.5 Kb for this metamorphism (ANHAEUSSER, 1983).

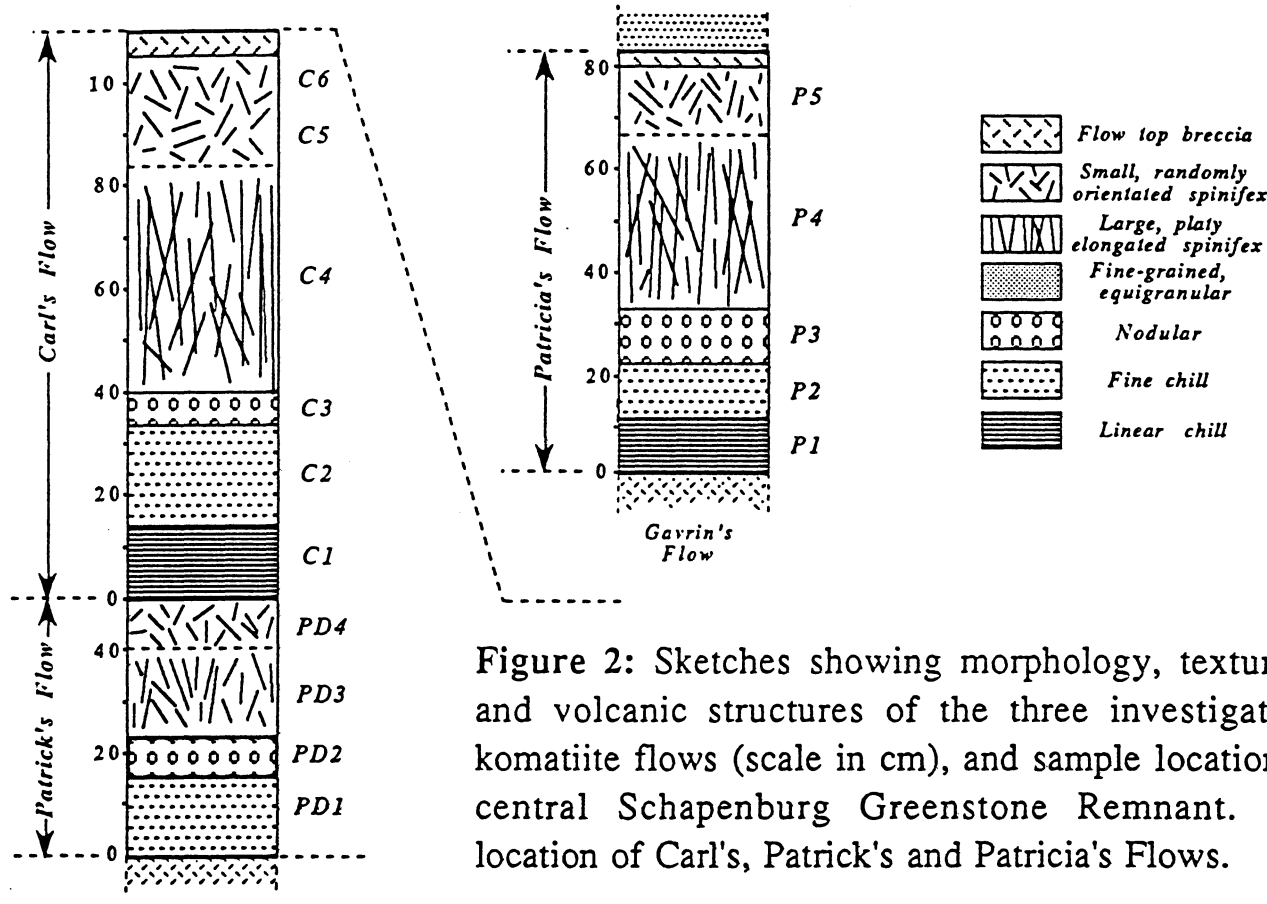

Figure 2: Sketches showing morphology, textures and volcanic structures of the three investigated komatiite flows (scale in cm), and sample locations, central Schapenburg Greenstone Remnant. A: location of Carl's, Patrick's and Patricia's Flows.

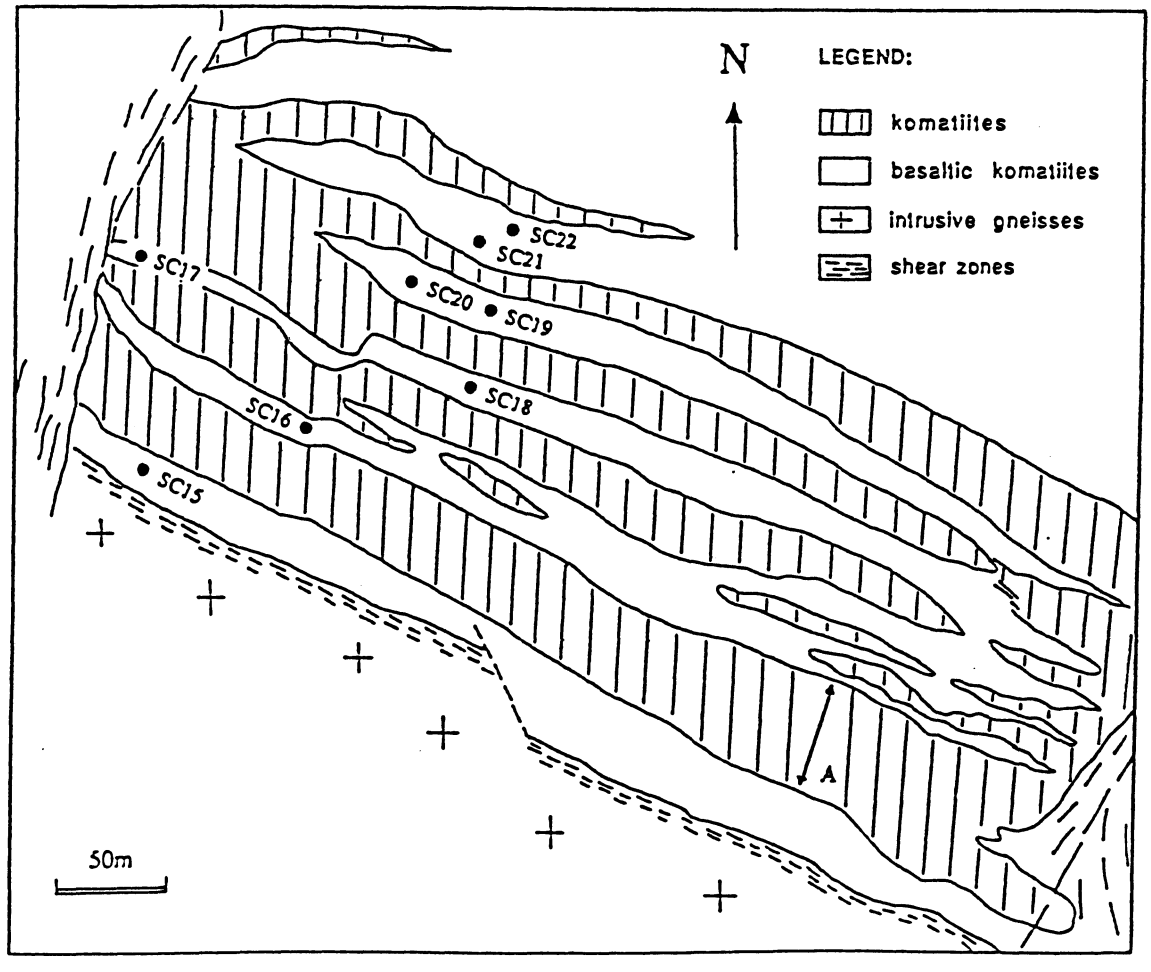

Table 1: Modal composition (in weigh %) of Schapenburg komatiites and komatiitic basalts [a]

Sample N°	Serpentine	Amphibole	Chlorite	Magnetite	MSWD
Carl's Flow					
C1	47.1±6.8	33.4±3.6	12.4±4.6	7.0±1.0	0.41
C2	71.2±9.7	14.3±5.9	6.0±7.5	8.5±1.5	0.66
C3	47.4±9.5	41.6±5.8	5.9±7.3	5.1±1.5	0.64
C4	23.0±6.1	59.9±3.7	7.4±4.7	9.7±1.0	0.41
C5	32.9±6.7	52.7±4.6	5.4±5.0	9.0±1.2	0.51
C6	25.2±1.8	55.8±1.2	10.8±1.3	8.2±0.3	0.13
Patricia's Flow					
P1	70.2±8.4	19.5±5.1	1.4±6.4	8.9±1.3	0.56
P2	39.9±9.2	44.2±5.6	9.3±7.1	6.6±1.5	0.62
P3	23.5±6.0	62.7±3.6	6.2±4.5	7.5±1.0	0.40
P4	27.7±4.3	55.6±2.6	7.5±3.3	9.3±1.0	0.29
P5	28.8±4.6	54.9±2.8	7.0±3.5	9.3±1.0	0.31
Patrick's Flow					
PD1	69.8±8.9	16.3±5.4	4.4±6.8	9.4±1.4	0.60
PD2	26.1±6.8	57.1±4.1	10.0±5.2	6.8±1.0	0.45
PD3	31.7±6.7	50.2±4.1	9.0±5.1	9.1±1.0	0.45
PD4	23.6±6.4	58.4±3.9	9.4±4.9	8.6±1.0	0.43
Komatiitic Basalts					
SC15	0.0	98.8±2.2	0.0	1.1±2.2	0.83
SC16	0.0	94.9±2.0	0.0	5.1±2.0	0.76
SC17	0.0	95.9±2.8	0.0	4.1±2.8	1.05
SC18	0.0	93.9±2.7	0.0	6.0±2.7	1.01
SC19	0.0	91.9±3.0	0.0	8.1±3.0	1.32
SC20	0.0	92.5±1.7	0.0	7.6±1.7	0.73
SC21	0.0	94.0±2.1	0.0	5.9±2.1	0.92
SC22	0.0	91.9±2.2	0.0	8.1±2.2	0.98

[a] Calculated from whole-rock and mineral major element compositions using the least-squares method of Bryan et al. (1969)

$^{143}Nd/^{144}Nd$ and $^{147}Sm/^{144}Nd$ ratios were determined following the procedure described in GRUAU et al. (1987). $^{143}Nd/^{144}Nd$ ratios were measured using a single-collector TSN 206 Cameca mass spectrometer. All ratios were normalized against $^{146}Nd/^{144}Nd = 0.7219$ for isotopic fractionation effects. Results from the La Jolla Nd standard during the course of this study (35 separate runs) were $^{143}Nd/^{144}Nd = 0.511877 \pm 38$ ($2\sigma_{pop}$). All measured $^{143}Nd/^{144}Nd$ ratios were thus corrected (- 0.000017) to be consistent with the La Jolla reference value of 0.511860. Blanks for Nd and Sm were lower than $0.2*10^{-9}$g and $0.05*10^{-9}$g, respectively. Measured and calculated initial $^{143}Nd/^{144}Nd$ ratios are quoted throughout the text and in Table 4 in the ε_{Nd} notation of DEPAOLO and WASSERBURG (1976) as deviations in part per 10^4 from the growth curve. The present-day $^{143}Nd/^{144}Nd$ and $^{147}Sm/^{144}Nd$ ratios for the chondritic reference reservoir are those determined by JACOBSEN and WASSERBURG (1980).

Oxygen was extracted using the BrF_5 method (CLAYTON and MAYEDA, 1963) and analysed as CO_2 gas on a triple-collector VG SIRA 10 mass spectrometer. Isotopic compositions are quoted in the standard δ notation relative to VSMOW. Results from the NBS28 standard during the course of this study gave $\delta^{18}O = +9.5 \pm 0.2‰ (2\sigma_m)$.

Microprobe analyses of minerals were performed at the IFREMER laboratory at Brest. Amphibole and magnetite separates were obtained by using conventional magnetic methods combined with handpicking. Oxygen isotopic compositions of whole-rocks, amphibole and magnetite SC16 were determined at Rennes University, while the D/H compositions of amphiboles SC16, SC19 and SC20 were measured at the University of Michigan at Ann Arbor. The method used for hydrogen isotopic analysis is adapted from KENDALL and COPLEN (1985). After reduction of water extracted with zinc (500°C), hydrogen was analysed on a Finnigan MAT mass-spectrometer with automatic H^{3+} correction. D/H ratios are reported in the conventional δD notation relative to VSMOW. Analyses of the NBS biotite standard at the University of Michigan during the course of this study gave $\delta D = -63 \pm 1‰$.

$^{40}Ar/^{39}Ar$ analyses of amphiboles SC16 and SC19 were carried out at the University of Montpellier, following the procedure described in MONIÉ et al. (1984).

RESULTS

Microprobe analyses of metamorphic minerals

Representative microprobe analyses of the metamorphic minerals, along with their structural formulae, are presented in Table 2. Structural formulae of amphiboles were calculated following the procedure of MÉVEL (1984).

Amphibole compositions in the komatiitic basalt and komatiite samples are not identical. In the former, the amphibole is a Mg-hornblende ($Al^{IV} \approx 0.9$; $Na+K \approx 0.4$; $Mg/Mg+Fe^{2+} \approx 0.8$). In the komatiite samples, the amphibole shows higher $Mg/Mg+Fe^{2+}$ ratios (≈ 0.95) and lower concentrations of Al, Na and Cr (Table 2). In the classification diagrams of LEAKE (1978), amphiboles from the komatiite samples are identified as tremolite.

Chlorite analyses were normalised to 14 anhydrous oxygens, and total Fe was computed as Fe^{2+}. Chlorite, which is present only in the komatiite samples, gives rather uniform compositions, with high $Mg/Mg+Fe^{2+}$ (0.91-0.94). The proportions of Al^{IV} and Al^{VI} are similar (≈ 1.0), suggesting crystallization under low to moderate pressure conditions (LAIRD, 1988). Chlorite is identified as clinochlore in the classification of BAYLISS (1975). Note that the Na_2O, K_2O and CaO contents always remain very low (<0.5%; Table 2), indicating that the common problem of submicroscopic intergrowths of chlorite and other sheet silicates (ERNST, 1983) was not encountered in the present study.

Serpentine in the komatiite samples is dominantly antigorite (X-ray diffractometry). It often contains traces of Cl (0.035-0.072%), while Mg/(Mg+Fe) ratios are in the range 0.91-0.94 (Table 2).

Compositions of Fe-Ti oxides are rather uniform (Table 2). Magnetite and Ti-magnetite are dominant, while ilmenite (systematically found in small-scale association with magnetite grains) is very subordinate (a few grains). TiO_2 and Cr_2O_3 contents in Ti-magnetites and magnetites reach 2% and 6%, respectively. Significant proportions of Al_2O_3 are also measured (up to ≈5%; Table 2)

Major and trace element compositions and REE patterns of whole-rock samples

All studied samples are basic-ultrabasic rocks (Table 3). MgO contents are 14.5-19.6% in the komatiitic basalts and 25.5-31.8% in the komatiites. Major and trace elements contents vary little in the komatiitic basalts (e.g. Al_2O_3=5.3-6.0%; CaO=9.6-12%; TiO_2=0.54-0.65%; Zr=40-45ppm). In the komatiite lava flows, concentrations are also fairly uniform (e.g. Al_2O_3=2.5-5.1%; TiO_2=0.15-0.41%),

Table 2: Composition of metamorphic minerals

Sample N°	C1	C6	C6	SC16
Rock Type	komatiite	komatiite	komatiite	komatiitic basalt
Mineral	amphibole	amphibole	amphibole	amphibole
SiO_2 (%)	55.34	54.11	54.02	49.12
Al_2O_3	2.16	3.11	3.28	6.99
TiO_2	0.14	0.14	0.23	0.35
Cr_2O_3	0.24	0.16	0.05	0.34
FeO	3.29	4.19	3.91	9.37
MnO	0.25	0.11	0.22	0.09
MgO	22.59	21.60	21.77	17.11
CaO	12.35	12.23	12.24	11.66
Na_2O	0.59	0.78	0.75	1.53
K_2O	0.02	0.08	0.07	0.08
Cl	0.00	0.00	0.01	0.01
Total	96.95	96.50	96.55	96.65
Si	7.683	7.592	7.564	7.098
Al_{IV}	0.317	0.408	0.436	0.902
Al_{VI}	0.037	0.106	0.105	0.289
Ti	0.015	0.014	0.024	0.037
Cr	0.026	0.018	0.006	0.038
Fe^{3+}	0.063	0.030	0.062	0.058
Fe^{2+}	0.155	0.302	0.233	0.881
Mn	0.029	0.012	0.026	0.011
Mg	4.674	4.518	4.544	3.685
Fe_{M4}	0.163	0.161	0.164	0.194
Ca	1.837	1.839	1.836	1.806
Na_A	0.158	0.212	0.203	0.428
K	0.003	0.014	0.013	0.014
$Mg/(Mg+Fe^{2+})$	0.968	0.937	0.951	0.807
Fe^{2+}/Mg	0.033	0.067	0.051	0.239

Sample N°	C1	C6	C6	SC16	SC20
Rock Type	komatiite	komatiite	komatiite	komatiitic basalt	komatiitic basalt
Mineral	magnetite	ilmenite	magnetite	magnetite	magnetite
TiO_2 (%)	0.17	49.58	1.76	0.49	1.89
Al_2O_3	2.37	1.44	1.21	1.04	4.67
Cr_2O_3	0.05	0.16	5.91	4.42	3.97
FeO	27.18	38.66	29.52	30.36	32.98
Fe_2O_3	62.07	0.93	52.17	59.38	54.84
MnO	0.07	2.59	0.31	0.00	0.24
MgO	1.50	1.85	0.25	0.03	0.03
Total	93.41	95.22	91.13	95.72	98.63
Ti	0.041	1.934	0.440	0.119	0.450
Al	0.898	0.088	0.477	0.391	1.742
Cr	0.011	0.007	1.558	1.116	0.993
Fe^{3+}	15.008	0.036	13.086	14.257	12.365
Fe^{2+}	7.304	1.677	8.230	8.107	8.372
Mn	0.019	0.114	0.088	0.000	0.065
Mg	0.718	0.143	0.122	0.012	0.013

Table 2: (continue)

Sample N°	C1	C1	C3	C3
Rock Type	komatiite	komatiite	komatiite	komatiite
Mineral	Serpentine	Serpentine	Serpentine	Serpentine
SiO_2 (%)	42.21	42.94	41.39	41.42
Al_2O_3	1.80	1.00	0.55	0.67
FeO	5.43	4.72	5.98	4.03
MnO	0.22	0.05	0.08	0.00
MgO	36.26	37.37	34.90	36.38
CaO	0.04	0.00	0.00	0.01
Na_2O	0.01	0.01	0.01	0.04
K_2O	0.00	0.00	0.00	0.00
Cr_2O_3	0.19	0.04	0.00	0.06
Cl	0.07	0.06	0.04	n.d.
NiO	n.d.	n.d.	n.d.	0.22
Total	86.23	86.18	82.95	82.84
Si	2.015	2.039	2.057	2.046
Al	0.101	0.056	0.032	0.039
Fe	0.217	0.188	0.249	0.167
Mn	0.009	0.002	0.003	0.000
Mg	2.580	2.645	2.586	2.678
Ca	0.002	0.000	0.000	0.001
Na	0.001	0.001	0.001	0.004
K	0.000	0.000	0.000	0.000
Cr	0.007	0.001	0.000	0.002
$Mg/(Mg+Fe^{2+})$	0.922	0.934	0.912	0.941

Sample N°	C3	C3	C3	C6
Rock Type	komatiite	komatiite	komatiite	komatiite
Mineral	Chlorite	Chlorite	Chlorite	Chlorite
SiO_2 (%)	28.99	28.78	29.61	31.22
Al_2O_3	17.52	16.94	17.46	18.80
TiO_2	0.06	0.07	0.04	0.01
FeO	3.92	3.96	3.70	5.03
MnO	0.00	0.00	0.01	0.09
MgO	30.47	29.44	30.42	30.23
CaO	0.03	0.00	0.01	0.05
Na_2O	0.00	0.03	0.04	0.00
K_2O	0.02	0.02	0.00	0.00
Cr_2O_3	0.82	0.94	0.85	0.44
Cl	0.00	0.07	n.d.	0.00
NiO	n.d.	n.d.	0.18	n.d.
Total	81.82	80.24	82.32	85.87
Si	2.925	2.964	2.968	3.002
Al^{IV}	1.075	1.036	1.032	0.997
Al^{VI}	1.009	1.020	1.030	1.132
Ti	0.004	0.006	0.003	0.001
Fe	0.331	0.341	0.310	0.404
Mg	4.583	4.518	4.547	4.333
Mn	0.000	0.000	0.001	0.008
Cr	0.065	0.076	0.067	0.033
Ca	0.003	0.000	0.001	0.005
Na	0.000	0.006	0.008	0.000
K	0.002	0.002	0.000	0.000
$Al^{VI}+2Ti+Cr-1$	0.082	0.108	0.103	0.167
$Mg/(Mg+Fe^{2+})$	0.933	0.930	0.936	0.915
Fe/Mg	0.072	0.075	0.068	0.093

n.d.: not determined

even though samples from the upper spinifex zones generally yield lower MgO, Ni, Cr, and higher SiO_2, CaO, Al_2O_3, TiO_2, Na_2O, Zr, Sr, Y, and V contents than samples from the lower zones with no spinifex. Except for some of the komatiitic basalts (e.g. SC18), the degree of hydration is generally very high (2-9%), being related to variable amounts of serpentine and chlorite (Tables 1, 2 and 3).

As can be seen in Figure 3, the Al_2O_3/TiO_2 and CaO/Al_2O_3 ratios of Schapenburg greenstones are typical of Al-depleted or Group II komatiites (JAHN et al., 1982; GRUAU et al., 1990a). In the komatiitic basalts, both ratios are nearly constant (Al_2O_3/TiO_2=10.0±0.7 (1σ); CaO/Al_2O_3=1.8±0.1 (1σ)). In the komatiites, distributions are more variable, samples from the base of the flows generally yielding higher Al_2O_3/TiO_2 (up to ≈17), but lower CaO/Al_2O_3 ratios (down to 1.1) than samples from the upper zones with spinifex (Table 3; Fig. 3). Average values for the komatiite flow samples are 12.7±2.4(1σ) for Al_2O_3/TiO_2, and 1.6±0.3 (1σ) for CaO/Al_2O_3.

REE concentrations (Table 3; Fig. 4) were determined in 8 komatiites (samples C1 to C6, P3, and PD3) and 4 komatiitic basalts (SC15, SC16, SC20, and SC21). Three important points should be underlined:

-1) Apart from a variable Eu anomaly (Eu/Eu*=0.95-1.62), normalized patterns are remarkably similar (Fig. 4). Besides low Al_2O_3/TiO_2 and high CaO/Al_2O_3 ratios, another typical geochemical feature of Al-depleted or Group II komatiites is the existence of a systematic depletion in HREEs, a feature also observed in the present sample suite. The mean value of the $(Gd/Yb)_N$ ratio - i.e. the slope of the HREE pattern - for Al-depleted or Group II komatiites worldwide (including samples from the type section of the Onverwacht Group in the BGB) is 1.4±0.2 (1σ) (GRUAU, personal compilation; see also JAHN et al., 1982, and ARNDT, 1986). In the komatiites and basaltic komatiites from Schapenburg, the mean values of this ratio are 1.64±0.06 (1σ) and 1.54±0.04 (1σ), respectively.

-2) Although all the LREE patterns display a convex shape (maximum around Nd-Sm; Fig. 4), the depletion in La and Ce always remains moderate ($(La/Sm)_N$=0.92±0.06 (1σ)). A $(La/Sm)_N$ ratio close to 1.0 is common in most komatiites from Barberton (e.g. JAHN et al., 1982; GRUAU et al., 1990b), which is in marked contrast with the heavy depletion of LREEs generally observed elsewhere in this rock-type (see SMITH and LUDDEN, 1989, for data compilation).

-3) good negative correlations are observed between the REEs, and the MgO and Ni concentrations. This is true on the scale of the whole sample suite, the komatiitic basalts having absolute REE concentrations about twice those of komatiites with higher MgO and Ni contents. This also applies at the scale of a

Table 3: Major and trace elements in Schapenburg komatiites and komatiitic basalts

Sample N°	P1	P2	P3	P4	P5	PD1	PD2	PD3	PD4	C1	C2	C3	C4	C5	C6	SC15	SC16	SC17	SC18	SC19	SC20	SC21	SC22
			Patricia's flow				Patrick's flow					Carl's flow											
	LCZ	LCZ	LCZ	USZ	USZ	LCZ	LCZ	USZ	USZ	LCZ	LCZ	LCZ	USZ	USZ	USZ	KB	KB	KB	KB	KB	KB	KB	KB
Major elements																							
SiO_2 (%)	41.25	44.09	47.09	45.60	45.45	40.11	45.91	44.43	45.89	43.14	39.52	45.10	45.69	44.61	45.30	48.84	48.56	49.40	48.33	48.68	48.03	48.75	49.00
Al_2O_3	2.66	3.52	3.85	4.24	4.09	2.90	3.96	4.08	4.45	4.40	2.54	3.47	4.03	3.77	5.07	6.03	5.81	5.89	5.97	6.34	5.48	5.30	5.99
TiO_2	0.18	0.30	0.39	0.37	0.32	0.19	0.39	0.32	0.38	0.26	0.15	0.31	0.41	0.33	0.37	0.54	0.60	0.59	0.65	0.58	0.59	0.56	0.60
Fe_2O_3 (ΣFe)	12.55	9.86	10.68	12.29	12.28	12.83	9.88	12.02	11.69	9.86	11.71	9.38	12.33	12.21	11.86	12.21	15.40	14.82	15.72	15.24	14.85	13.70	15.50
MnO	0.12	0.18	0.18	0.18	0.17	0.11	0.18	0.19	0.18	0.15	0.13	0.18	0.18	0.17	0.18	0.21	0.24	0.23	0.25	0.27	0.23	0.20	0.23
MgO	31.80	28.40	25.95	26.37	26.43	31.77	26.51	26.98	26.19	30.00	31.84	29.89	25.54	26.43	25.86	19.62	17.25	15.83	15.65	14.45	17.95	18.88	15.42
CaO	3.46	6.40	8.15	7.12	7.08	3.14	7.59	6.81	7.73	4.96	2.99	6.16	7.85	7.15	6.77	9.63	10.00	10.65	10.38	12.11	10.26	10.15	10.77
Na_2O	0.10	0.28	0.51	0.48	0.47	0.14	0.42	0.40	0.49	0.13	0.03	0.21	0.47	0.41	0.36	1.18	1.29	1.39	1.55	1.40	1.27	1.30	1.59
K_2O	0.05	0.06	0.07	0.07	0.08	0.05	0.08	0.07	0.07	0.05	0.05	0.06	0.07	0.07	0.09	0.06	0.07	0.08	0.07	0.14	0.11	0.07	0.09
P_2O_5	0.03	0.04	0.05	0.04	0.05	0.03	0.04	0.04	0.05	0.03	0.02	0.03	0.07	0.04	0.05	0.04	0.06	0.04	0.07	0.06	0.05	0.05	0.06
L.O.I.	8.37	4.93	3.39	3.39	3.45	8.53	5.37	5.14	3.33	7.43	9.05	5.36	3.28	4.18	4.32	2.28	0.91	0.80	0.75	0.76	0.84	1.11	0.67
Total	100.57	98.06	100.31	100.15	99.87	99.80	100.33	100.48	100.45	100.41	98.03	100.15	99.92	99.37	100.23	100.64	100.19	99.72	99.39	100.03	99.66	100.07	99.92
Al_2O_3/TiO_2	14.78	11.73	9.87	11.46	12.78	15.26	10.15	12.75	11.71	16.92	16.93	11.19	9.83	11.42	13.70	11.17	9.68	9.98	9.18	10.93	9.29	9.46	9.98
CaO/Al_2O_3	1.30	1.82	2.12	1.68	1.73	1.08	1.92	1.67	1.74	1.13	1.18	1.78	1.95	1.90	1.34	1.60	1.72	1.81	1.74	1.91	1.87	1.92	1.80
Trace elements																							
Rb (p.p.m.)	<2	<2	<2	<2	<2	<2	<2	<2	<2	<2	<2	<2	<2	<2	<2	1	<1	<1	2	<1	5	3	3
Sr	21	61	69	75	76	19	65	60	79	31	2	50	82	71	70	51	104	75	105	87	68	79	75
Y	6	10	12	9	10	5	8	9	12	8	6	10	11	12	7	12	12	11	14	12	10	9	12
Zr	9	16	23	17	17	9	20	22	21	14	32	15	20	19	16	44	42	42	45	41	42	40	43
Nb	3	4	4	3	2	2	2	2	2	3	2	3	2	3	2	5	5	4	5	5	5	4	5
Ni	2016	1523	1313	1325	1335	2049	1293	1475	1253	1846	2165	1644	1070	1436	1485	718	516	443	532	368	624	713	411
Cr	1812	2503	2592	2508	2477	1875	2645	2523	2597	2153	1696	2494	2552	2553	2297	1876	2515	1541	2556	1349	2346	2302	1958
La			1.684					1.510		1.099	0.958	1.217	1.706	1.489	1.459	3.167	2.732				2.910	2.514	
Ce			4.692					4.056		3.080	2.726	3.523	4.685	4.236	3.942	6.618	7.537				7.770	6.904	
Nd			3.681					3.285		2.423	2.143	2.853	3.649	3.304	3.246	5.474	5.618				5.777	5.196	
Sm			1.147					1.029		0.758	0.643	0.887	1.136	1.028	1.002	1.572	1.697				1.714	1.566	
Eu			0.429					0.412		0.279	0.241	0.303	0.422	0.406	0.402	0.670	0.704				0.754	0.903	
Gd			1.412					1.258		0.931	0.784	1.098	1.420	1.257	1.273	1.967	2.069				2.073	1.897	
Dy			1.444					1.315		0.958	0.778	1.138	1.419	1.294	1.273	2.052	2.146				2.154	1.979	
Er			0.781					0.726		0.533	0.441	0.636	0.776	0.729	0.711	1.196	1.208				1.235	1.108	
Yb			0.662					0.624		0.464	0.406	0.552	0.664	0.618	0.611	1.060	1.042				1.068	1.005	
Lu			0.097					0.095		0.072	0.067	0.086	0.096	0.093	0.091	0.155	0.159				0.132	0.151	
$(La/Sm)_N$			0.89					0.89		0.88	0.91	0.84	0.92	0.88	0.89	1.23	0.98				1.03	0.98	
$(Gd/Yb)_N$			1.71					1.62		1.61	1.55	1.60	1.72	1.63	1.67	1.49	1.59				1.56	1.52	
Eu/Eu*			1.04					1.12		1.03	1.05	0.95	1.03	1.10	1.10	1.18	1.16				1.24	1.62	

L.O.I.: loss of ignition; LCZ: lower cumulate zone; USZ: upper spinifex zone; KB: komatiitic basalt

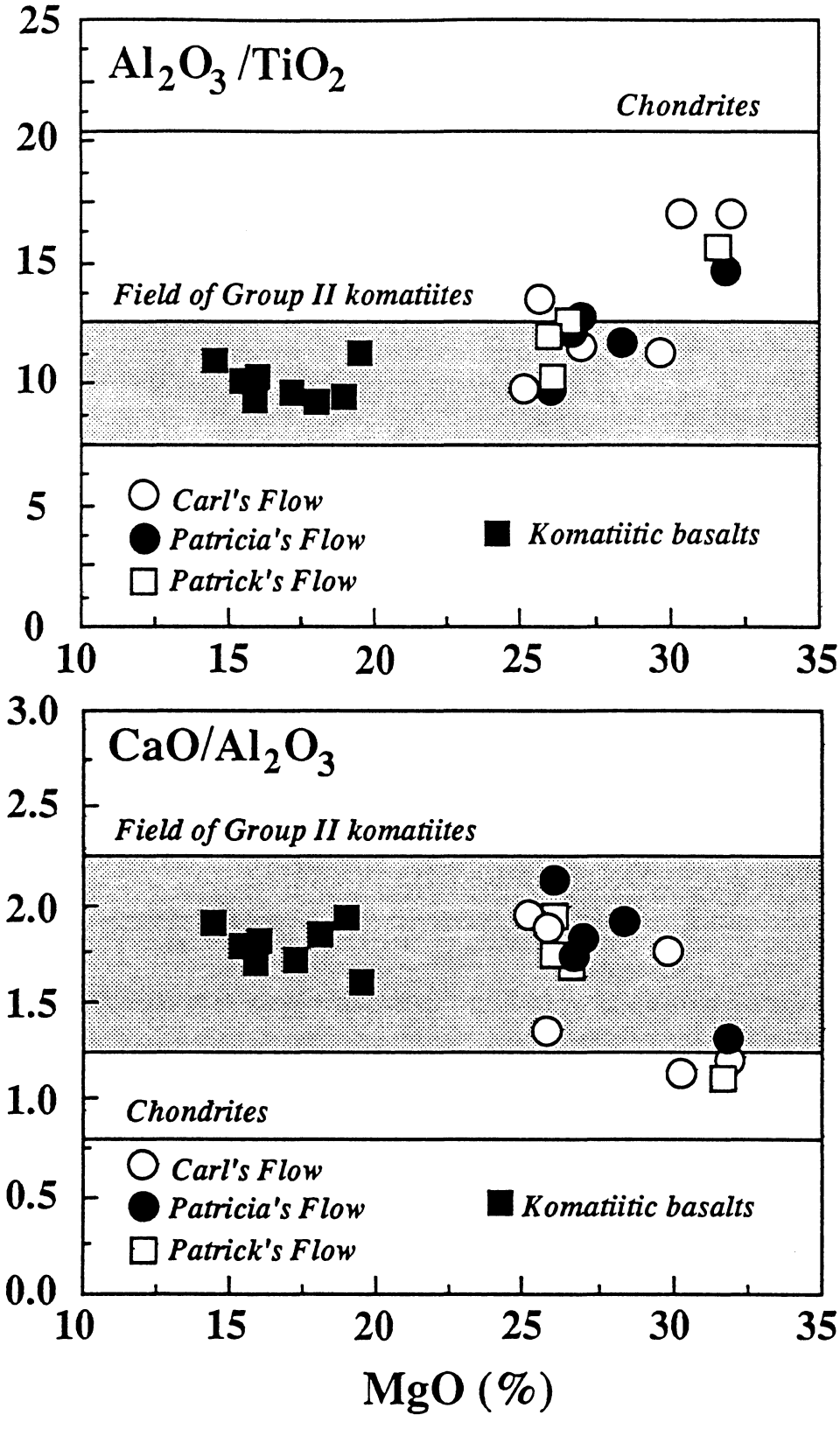

Figure 3: Al_2O_3/TiO_2 vs. MgO and CaO/Al_2O_3 vs. MgO plots. Fields of Group II komatiites are from Jahn et al. (1982) and Gruau et al. (1990a).

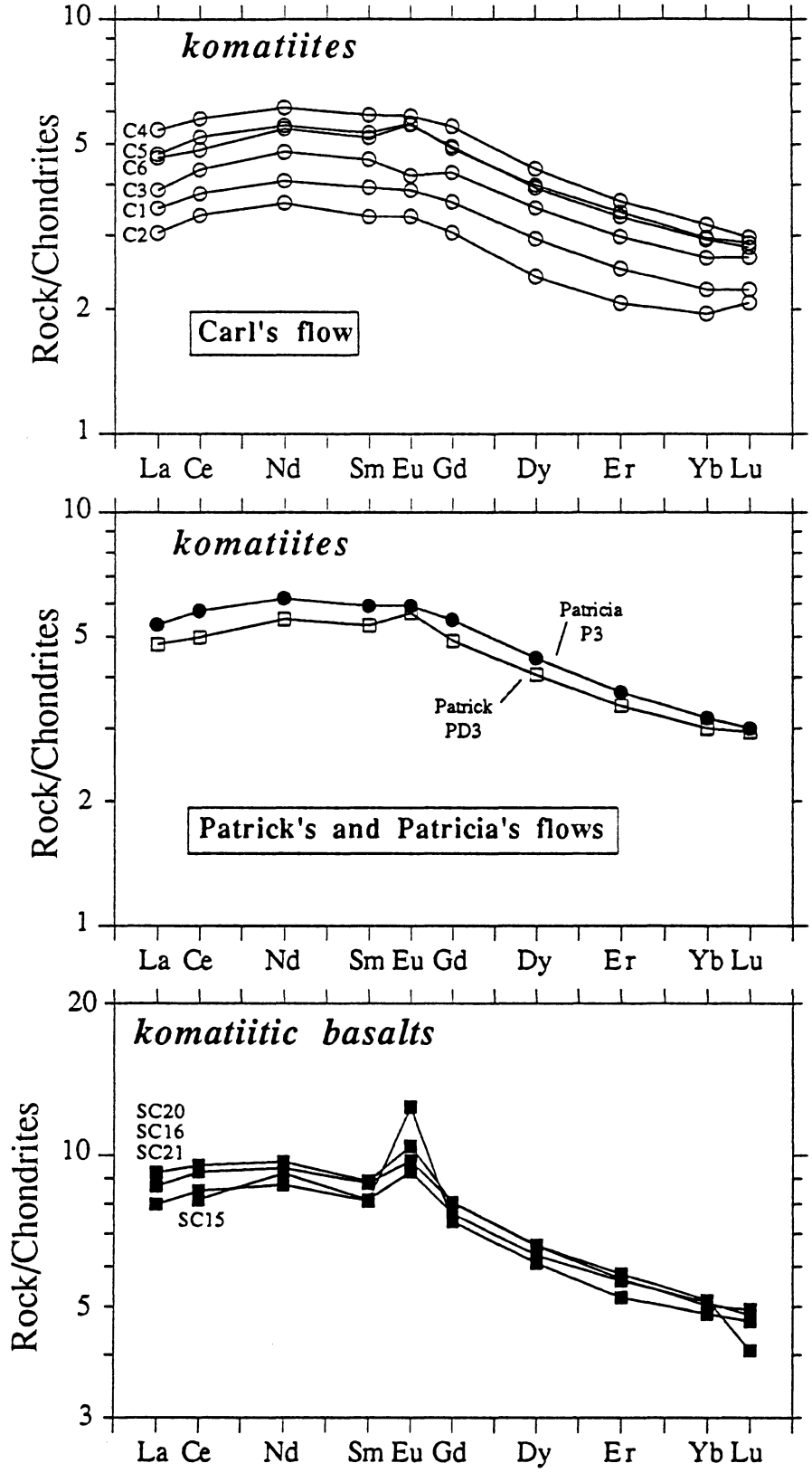

Figure 4: REE profiles. Normalizing values are from GRUAU et al. (1990b).

single komatiite lava flow: samples from Carl's Flow show a regular increase of REE contents for decreasing MgO and Ni contents (Table 3).

Isotopic data

Neodymium

Sm-Nd isotopic ratios were measured on all the komatiite samples and on komatiitic basalts SC20 and SC21 (Table 4). Three important points are to be noted:

-1) All samples share nearly identical $^{147}Sm/^{144}Nd$ ratios (0.1800 to 0.1906; variation≈6%) and $^{143}Nd/^{144}Nd$ ratios (0.512426 to 0.512603; variation≈0.04%), which is not surprising in view of the uniform REE profiles.

-2) T_{CHUR} model ages (Table 4) are extremely variable and unrealistically young (2540-550 Ma). T_{DM} model ages are also somewhat scattered, but the range is much smaller and the values make more geological sense. In fact, by pooling all the available data, a mean T_{DM} model age of 3530±100 (1σ) Ma is obtained, a result which is not significantly different from the zircon ages thought to represent the initial volcanic episode in the Onverwacht Group (3480-3450 Ma; ARMSTRONG et al., 1990).

-3) In Table 4, we list individual initial $\varepsilon_{Nd}(T)$ values calculated using 3450 Ma as the age of magmatic crystallization. All samples (including the two basaltic komatiites) yield positive $\varepsilon_{Nd}(3450)$ values, covering a narrow range around +2.5. Combining all the data, the mean $\varepsilon_{Nd}(3450)$ value is +2.4±0.4 (1σ). Assuming an age of 3480 Ma, the mean value is not significantly different: +2.5±0.4 (1σ).

Oxygen and Hydrogen

Oxygen and hydrogen isotopic data are listed in Table 5. In the komatiitic basalts, $\delta^{18}O$ values are nearly constant (from +4.82 to +5.04‰). In the komatiites, $\delta^{18}O$ values are lower, but are also more variable (from +3.21 to +4.57‰). Comparison of Table 5 and Figure 2 shows that the variation of $\delta^{18}O$ values among komatiites is a feature specific to each flow: ranges as well as absolute values of $\delta^{18}O$ are similar in the three flows, with the lowest values (+3.39‰ for Patricia's Flow; +3.25‰ for Patrick's Flow; +3.21‰ for Carl's Flow) being always observed in samples from the lower cumulate zone.

Amphibole separates (Mg-hornblende) from komatiitic basalts SC16, SC19 and SC20 gave identical $\delta^{18}O$ values, around +5.0‰; δD values are more variable,

Table 4: Sm-Nd isotopic data for Schapenburg whole-rock samples

Sample N°	Sm (ppm)	Nd (ppm)	$^{147}Sm/^{144}Nd$ [a]	$^{143}Nd/^{144}Nd$	2σm	$\varepsilon_{Nd}(0)$ [b]	$\varepsilon_{Nd}(3450)$ [b]	$T_{DM}(Ga)$ [c]	$T_{CHUR}(Ga)$ [b]
Carl's Flow									
C1	0.787	2.524	0.1885	0.512575	18	-1.2±0.4	+2.5±0.5	3.51	1.17
C2	0.672	2.228	0.1823	0.512421	20	-4.2±0.4	+2.2±0.5	3.56	2.29
C3	0.964	3.077	0.1894	0.512562	19	-1.5±0.4	+1.8±0.5	3.72	1.58
C4	1.159	3.712	0.1888	0.512571	24	-1.3±0.5	+2.3±0.6	3.57	1.29
C5	1.021	3.297	0.1872	0.512531	17	-2.1±0.4	+2.2±0.5	3.59	1.72
C6	1.011	3.254	0.1878	0.512574	18	-1.2±0.4	+2.7±0.5	3.42	1.10
Patricia's Flow									
P1	0.643	2.110	0.1842	0.512475	29	-3.2±0.6	+2.4±0.7	3.51	1.99
P2	0.992	3.230	0.1857	0.512482	16	-3.0±0.3	+1.9±0.4	3.65	2.15
P3	1.099	3.570	0.1861	0.512533	14	-2.0±0.3	+2.7±0.4	3.43	1.51
P4	1.085	3.516	0.1866	0.512549	19	-1.7±0.4	+2.8±0.5	3.40	1.34
P5	1.070	3.440	0.1880	0.512549	19	-1.7±0.4	+2.2±0.5	3.56	1.56
Patrick's Flow									
PD1	0.579	1.910	0.1833	0.512443	23	-3.8±0.5	+2.2±0.6	3.56	2.20
PD2	1.148	3.844	0.1806	0.512441	13	-3.8±0.3	+3.4±0.4	3.27	1.85
PD3	1.024	3.272	0.1892	0.512590	21	-0.9±0.4	+2.4±0.5	3.51	0.98
PD4	1.227	3.891	0.1906	0.512616	25	-0.4±0.5	+2.3±0.6	3.56	0.55
Komatiitic basalts									
SC20	1.725	5.794	0.1800	0.512358	20	-5.5±0.4	+2.0±0.5	3.59	2.54
SC21	1.576	5.228	0.1822	0.512426	20	-4.1±0.4	+2.3±0.5	3.52	2.23

[a] The error on this ratio is ±0.2%

[b] Calculated using a $^{147}Sm/^{144}Nd$ ratio of 0.1967 and a $^{143}Nd/^{144}Nd$ ratio of 0.513638 for the present-day chondritic uniform reservoir (CHUR)

[c] Calculated assuming a $^{147}Sm/^{144}Nd$ ratio of 0.2137 and a $^{143}Nd/^{144}Nd$ ratio of 0.513150 for the present-day depleted mantle reservoir (DM)

Table 5: Oxygen and hydrogen isotopic data

Sample N°	$\delta^{18}O$	1σ	δD	1σ
Whole-rocks				
Patricia's flow				
P1	3.39	0.02		
P2	3.95	0.02		
P3	4.50	0.02		
P4	4.46	0.05		
P5	4.50	0.06		
Patrick's flow				
PD1	3.25	0.05		
PD2	4.48	0.02		
PD3	4.03	0.08		
PD4	4.33	0.02		
Carl's flow				
C1	3.64	0.14		
C2	3.21	0.03		
C3	4.16	0.04		
C4	4.57	0.09		
C5	4.30	0.02		
C6	4.39	0.13		
Komatiitic basalts				
SC15	5.02	0.02		
SC16	4.92	0.04		
SC17	4.82	0.06		
SC18	5.04	0.06		
SC19	5.01	0.03		
SC20	4.92	0.02		
SC21	4.91	0.06		
SC22	4.91	0.02		
SC22	4.91	0.02		
Minerals				
Mg-hornblende				
SC16	4.95	0.1	-76.8	0.8
SC19	5.05	0.03	-87.7	1.0
SC20	5.03	0.03	-80.8	0.1
Magnetite				
SC16	0.08	0.05		

Table 6: Argon data

T (°C)	$^{40*}Ar/^{39}Ar$	$^{36}Ar/^{39}Ar*100$	$^{37}Ar/^{39}Ar$	$^{39}Ar/^{40}Ar$	$\%^{39}Ar$ released	Age (Ma)	2σ
	SC19 Amphibole						
500	0.00	63.77	12.94	0.577	0.29	0.0	0.0
600	22.11	27.57	0.00	0.971	0.42	578.1	43.2
700	643.79	45.50	42.45	0.146	0.43	4482.5	17.4
800	133.43	5.97	14.93	0.666	0.74	2142.5	14.5
1050	288.87	0.21	39.32	0.348	1.10	3212.6	14.6
1150	234.68	0.80	36.97	0.424	11.34	2906.6	14.2
1200	237.80	0.04	38.16	0.423	29.92	2925.8	14.1
1250	232.19	0.17	35.83	0.432	61.23	2891.3	14.1
1300	228.03	0.13	35.00	0.440	76.71	2865.3	14.0
1350	233.26	1.30	37.13	0.424	96.56	2897.9	14.3
1400	231.3	0.03	0.00	0.435	99.47	2885.8	14.4
1450	185.22	0.16	0.00	0.542	100.00	2573.4	13.7
	SC16 Amphibole						
500	18.69	14.07	18.74	1.670	2.15	499.7	24.3
600	33.79	5.85	2.11	1.969	6.38	822.1	12.1
700	90.78	1.99	4.97	1.041	7.98	1689.3	11.7
800	118.97	16.91	10.19	0.595	9.56	2001.2	19.9
1000	106.58	8.54	16.36	0.763	11.04	1870.7	15.3
1150	158.35	2.95	53.54	0.602	18.05	2362.7	13.6
1200	227.99	0.80	61.70	0.437	29.06	2865.1	13.9
1250	217.58	1.73	61.97	0.452	42.74	2798.3	14.0
1300	225.29	0.14	63.25	0.446	67.18	2848.0	13.8
1350	236.41	0.00	67.71	0.426	93.19	2917.3	18.8
1400	105.58	0.02	36.27	0.953	95.95	1859.7	11.3
1450	40.1	-0.94	38.45	2.700	100.00	941.2	6.7

ranging from -77 to -88‰. The $\delta^{18}O$ value of SC16 magnetite separate is +0.08‰ (Table 5).

Argon

Argon isotope ratios obtained during the course of step-heating of amphiboles SC16 and SC19 are presented in Table 6; the age spectra are illustrated in Figure 5.

$^{40}Ar/^{39}Ar$ results for amphibole SC19 yield a remarkably flat pattern with a plateau age of 2897±16 Ma corresponding to 98% of the ^{39}Ar released (1050 to 1400°C). The age pattern for amphibole SC16 is not as flat, being saddle - shaped with low ages for low (<1150°C) and high (>1350°C) temperature steps. The plateau for amphibole SC16, corresponding to 75% of the ^{39}Ar released between 1200 and 1350°C, yields an age of 2866±15 Ma.

DISCUSSION

From the results presented above, a number of conclusions can be drawn:

-1) Both amphibole fractions analysed for their $^{40}Ar/^{39}Ar$ age spectrum give consistent results (Fig.5). Because the closure temperature for Ar is high in amphibole (≥600°C for >200μm Mg-hornblende; BERGER and YORK, 1981) and appears to exceed the peak metamorphic conditions recorded by the samples (see below), the calculated plateau ages (2897±16 Ma and 2866±15 Ma) should represent the age of crystallization of the amphibole-bearing metamorphic assemblages, hence fixing the period of metamorphism in the SGR at around 2900 Ma ago. Although the existence of a possible thermal event at around 2900 Ma has long been recognized in the Barberton Mountain Land (e.g. BARTON et al., 1983), this event was so far regarded as having played a minor role on the post-depositional history of the greenstones compared to the 3500-3300 or 3200-3100 Ma history. The revised isotopic data of KAMO and DAVIS (1991) shows that granitic plutonic activity took place south of the BGB at ≈3440 Ma and later at ≈3100 Ma. Because it might be unrealistic to consider that the Mpuzuli batholith (3107+4/-3 Ma) took as long as 200 Ma to cool through the amphibole Ar temperature, it is possible that some other magmatic event may have influenced the thermal evolution of the SGR. The volcanism associated with the Nsuze Group of the Pongola Sequence and the emplacement of the Ushushwana Complex (2940±22 Ma and 2871±30 Ma, respectively; HEGNER et al., 1984) may have played a more significant role in the thermal history of the area south of the BGB than has hitherto been realised.

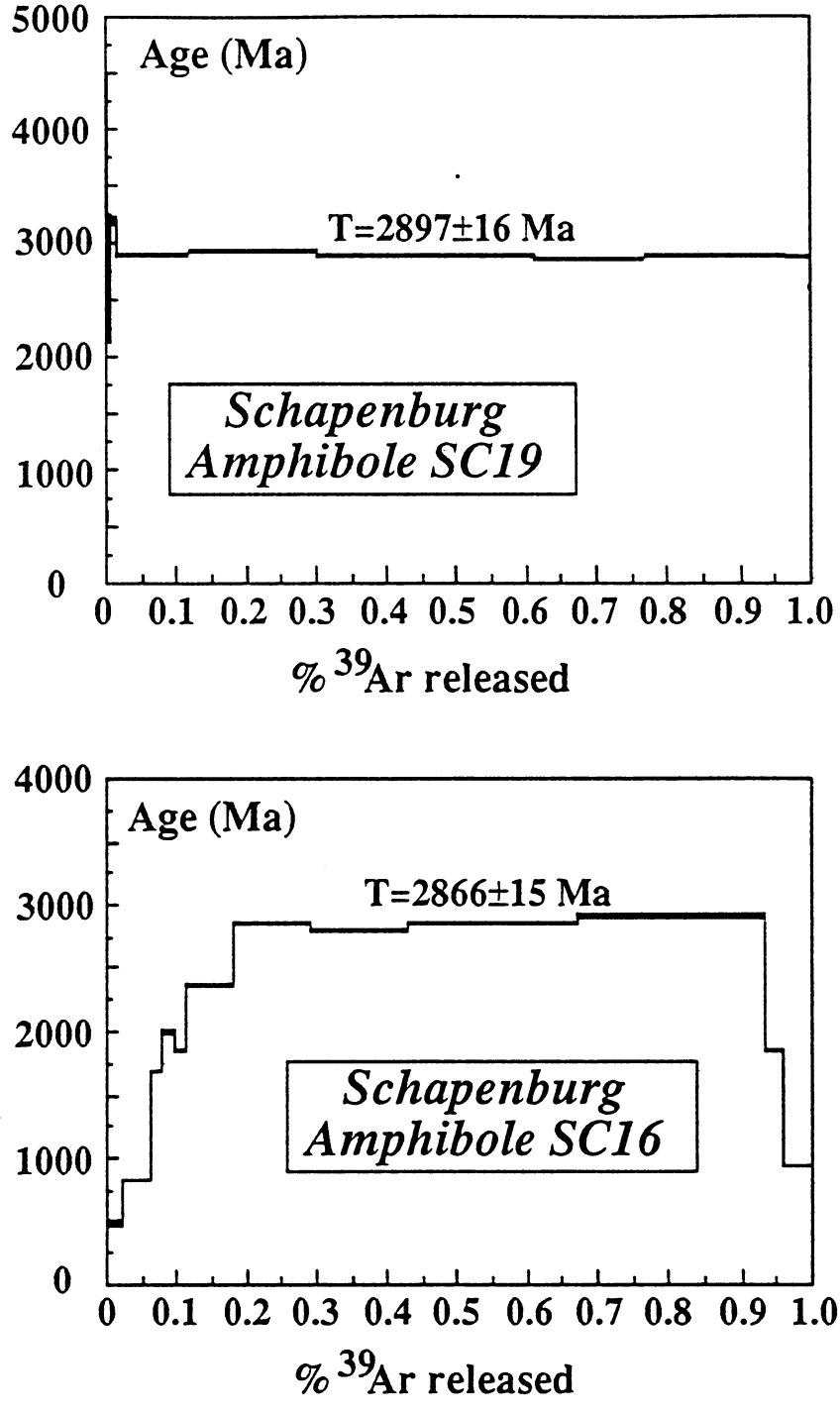

Figure 5: Argon age spectra. Vertical widths of the boxes represent 2σ errors.

-2) Metamorphic parageneses and oxygen isotopic data are consistent with a temperature of metamorphism of 450±50°C. Using the magnetite-water and amphibole-water empirical fractionation coefficients of BOTTINGA and JAVOY (1975), the measured $\Delta_{mag\text{-}amph}$ (4.9 δ units, Table 5) yields an apparent metamorphic temperature of 460±20°C. The presence of antigorite (upper stability temperature of ≈ 500°C for a pressure of the order of 3Kb; HEMLEY et al., 1977), as well as thermometric calculations based on chemical fractionations observed among analysed magnetite-ilmenite pairs (T≈400°C), are also consistent with such a temperature estimate (Table 2). The metamorphic conditions given here (450±50°C) are consistent with the lower limit (500°C) of the temperature range obtained by ANHAEUSSER (1983; 1991) from his study of mineral parageneses.

-3) The $\delta^{18}O$ values of the Schapenburg komatiites and komatiitic basalts are all lower than the present-day mantle reference or/and the values found in modern unaltered sea-floor basalts (+5.7±0.3‰, KYSER, 1986, and references therein). $\delta^{18}O$ values for the Archean mantle and related magmas are not as constrained as their present-day equivalents. However, isotopic study of the least altered komatiites and/or of magmatic minerals from spatially related basic-ultrabasic intrusions yield primary isotopic values not very different from those of modern mantle: $\delta^{18}O$=+5.6 to +6.0‰ (HOEFS and BINNS, 1978; BEATY and TAYLOR, 1982; SMITH et al., 1984). Thus, the oxygen isotopic compositions recorded in the komatiites and komatiitic basalts from Schapenburg are not primary values: they likely result from some degree of isotopic exchange between the rocks and a fluid phase. From the $^{40}Ar/^{39}Ar$ isotopic results, it is postulated that this isotopic exchange corresponds to the metamorphic (re)crystallization event at around 2900 Ma.

-4) From Table 3 and Figure 4, it is clear that the REEs (except Eu) were immobile elements during the evolution of the Schapenburg komatiites and komatiitic basalts. Let us consider Carl's Flow as an example: MgO concentrations range from 25.5 to 31.8% (Table 3), which suggests that low-pressure differentiation was controlled solely by olivine fractionation (ARNDT, 1986). Because the processes of olivine removal and accumulation cannot fractionate the REEs (olivine/liquid partition coefficient are <<1.0 for all the REEs; e.g. FUJIMAKI et al., 1984), both $(La/Sm)_N$ and $(Gd/Yb)_N$ ratios should remain constant from the bottom (olivine cumulate, high MgO and Ni contents) to the top of the flow (quenched liquid with lower MgO and Ni contents), which is basically what we observe in Carl's Flow (Table 3; Fig. 4). Moreover, assuming the REEs to be mobile on the scale of the whole-rock, their should be some relationships between the observed REE patterns and the secondary mineralogy (see GRUAU et

al., 1992). However, such a relationship does not exist in the present greenstone suite: samples with highly contrasted mineral proportions such as komatiite C2 (serpentine>70%) and komatiitic basalt SC16 (amphibole≈95%) yield similar $(La/Sm)_N$ and $(Gd/Yb)_N$ ratios (Table 3; Fig. 4). Recent work carried out on the komatiites from Tipajasjärvi and Kuhmo in eastern Finland (TOURPIN et al., 1991; GRUAU et al., 1992), as well as on the komatiites from Crixàs in Brazil (ARNDT et al., 1989), show that komatiites may experience a partial to total resetting of their REE patterns during low- to medium-grade metamorphic recrystallization. Clearly, the Schapenburg rocks display the opposite type of behaviour: except for Eu, the pervasive low- to medium-grade metamorphic recrystallization did not significantly disturb the REE patterns.

-5) The Sm-Nd results also argue for REE immobility: as already pointed out, the T_{DM} model ages are equal within errors to the zircon ages which are thought to represent the eruption of the Lower Onverwacht Group volcanic rocks. Moreover, the uniformity of initial ε_{Nd} values observed in Carl's, Patrick's and Patricia's Flows is to be expected for the different textural zones of komatiite flows erupted from a common parental magma. Judging from the +2.5 initial $\varepsilon_{Nd}(T)$ values, it is clear that the ultimate source(s) of Schapenburg komatiites and komatiitic basalts was not primitive mantle, but a mantle depleted in LREEs.

Chemical and isotopic effect of serpentinization

The Schapenburg rocks did not behave as closed systems for all elements. Considering the distribution of CaO/Al_2O_3 and Al_2O_3/TiO_2 ratios across the komatiite lava flows, both ratios should remain constant because olivine, the only fractionating phase, does not accomodate any of these three oxides. Yet, CaO/Al_2O_3 and Al_2O_3/TiO_2 are seen to cover a wide range in the komatiite lava flow samples (1.1-2.1, and 9.8-16.9, respectively; Table 3).

As can seen in Figure 3, most of the variation of CaO/Al_2O_3 and Al_2O_3/TiO_2 ratios is located in samples from the lower cumulate zones. By contrast, values in samples from the upper spinifex zones (quenched liquids) are close to those observed in the komatiitic basalts, hence corresponding to the average values of Al-depleted or Group II komatiites worldwide. It appears that the whole-rock chemistry is to some extent controlled by the modal composition of the secondary assemblages. Indeed, a major peculiarity of the cumulate zone samples is their enrichment in secondary serpentine (Table 1), which appears to exert some influence on CaO/Al_2O_3 and Al_2O_3/TiO_2 ratios: in the TiO_2 vs. MgO and CaO vs. MgO diagrams (Fig. 6), the compositions of the cumulate zone samples plot on serpentine control lines. In turn, the abundance of serpentine in the cumulate zone

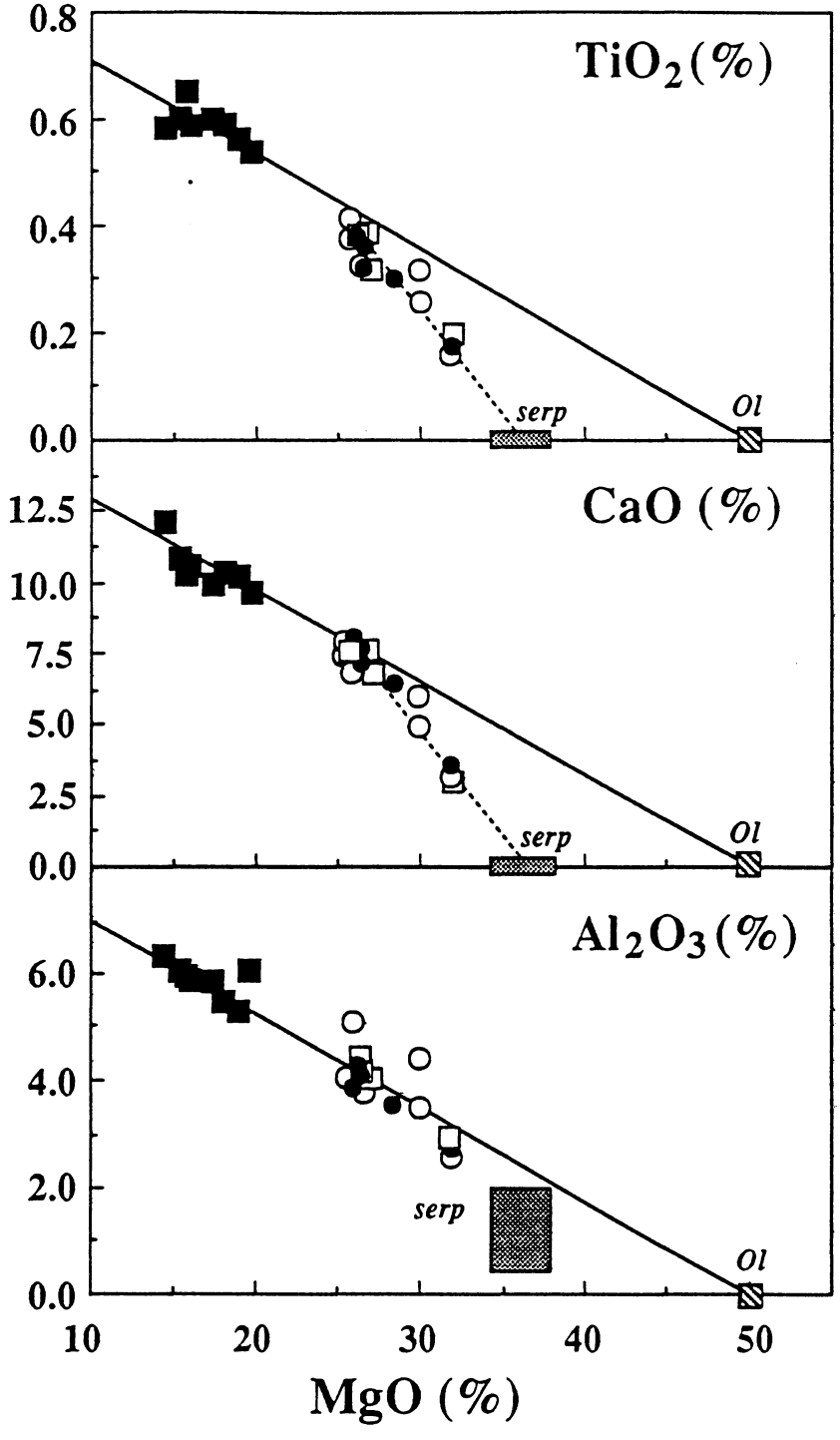

Figure 6: Variation diagrams illustrating control of the serpentine on the composition of the cumulate zone samples. Fields delineating serpentine composition were drawn using the compositions listed in Table 2. Symbols: same as in Figure 3. Ol: olivine; serp: serpentine.

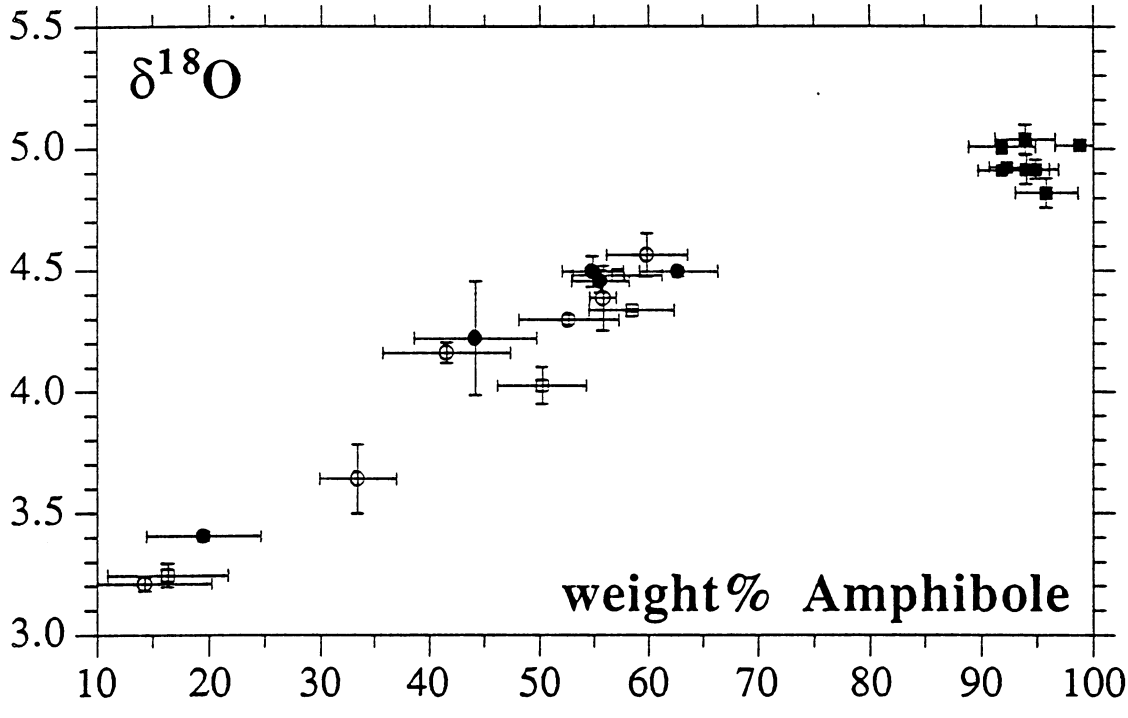

Figure 8: Diagram illustrating positive correlation between $\delta^{18}O$ values of whole-rock samples and the proportion of amphibole. Vertical and horizontal bars represents 1σ errors. Symbols: see Fig. 3.

samples is itself a consequence of the high modal abundance of olivine in the primary paragenesis.

Elemental fluxes in the Schapenburg komatiite flows cannot be properly evaluated because of the lack of primary mineral phases which would allow the calculation of volume and density changes. However, relative variations in elemental abundances can be evaluated. This is made possible by using CaO/Nd, TiO_2/Nd and Al_2O_3/Nd ratios, for two reasons: i) Nd behaved as an immobile element in all samples (see above); ii) CaO/Nd, TiO_2/Nd and Al_2O_3/Nd ratios are not fractionated by olivine addition or removal. Thus, the average CaO/Nd, TiO_2/Nd and Al_2O_3/Nd ratios of the samples that plot on - or very close to - the olivine control lines in Figure 6 (spinifex zone samples) could be taken as the initial (magmatic) bulk flow ratios, and used as reference values to estimate the direction and relative amplitude of elemental fluxes. This procedure is illustrated further on Figure 7, in which we report the vertical distributions of CaO/Nd, TiO_2/Nd and Al_2O_3/Nd ratios in the three flows. Also shown in Figure 7 are the distributions of (i) Sr/Nd and Na/Nd ratios (ii) whole-rock $\delta^{18}O$ values and (iii) H_2O^+ concentrations. Four important points should be stressed:

-1) In each of the cumulate zone flows, significant amounts of Ca and Ti were removed in some of the samples (particularly in sample C2), as inferred from the negative anomalies observed in the CaO/Nd and TiO_2/Nd ratio plots. By contrast, both CaO and TiO_2 appear to have been relatively immobile in samples from the upper spinifex-bearing zones.

-2) Al was also mobile, but this element was added, not lost. The location of Al mobility within the flows is different from that of Ca and Ti, i.e. at the base or the top of the flows.

-3) Profiles of Sr/Nd and Na/Nd contents are also marked by important negative anomalies in the lower parts of the three flows - in fact, the Na/Nd, Sr/Nd and CaO/Nd profiles are closely similar to each other. The sensitivity of the lower cumulate zone samples to chemical alteration is also shown by the anomalously high Zr content of sample C2 (Table 3).

-4) Finally, and most importantly, good correlations exist between the magnitude of elemental variations, the $\delta^{18}O$ values, and the degree of hydration. Moreover, the measured whole-rock oxygen isotopic compositions appear to be controlled by the secondary mineralogy since the $\delta^{18}O$ values of the Schapenburg greenstones are positively correlated with the amount of amphibole in the rock (Fig. 8). In upper greenschist to lower garnet amphibolite-facies rocks, serpentine is commonly less ^{18}O-enriched than amphibole (e.g. GARLICK and EPSTEIN, 1967). Thus, great abundance of serpentine in the lower cumulate zones should result in samples with isotopic compositions lighter than in samples from the

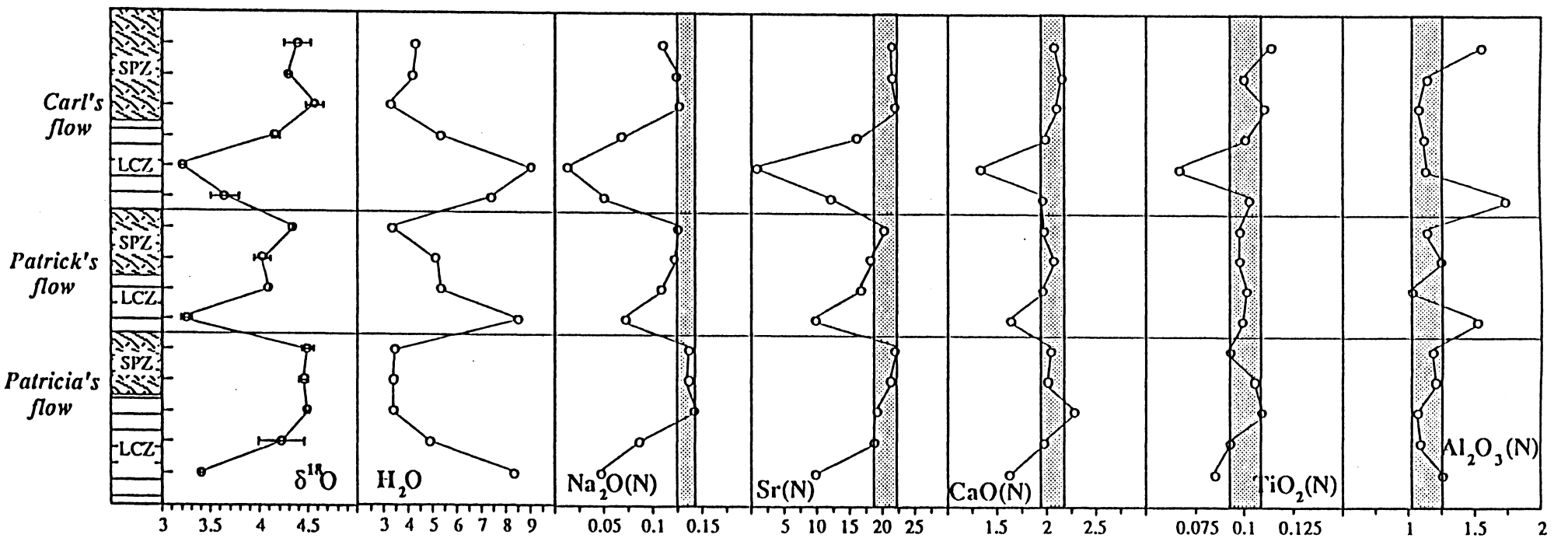

Figure 7: Diagram showing distribution of CaO/Nd, TiO_2/Nd, Al_2O_3/Nd, Na/Nd and Sr/Nd ratios in komatiite samples as a function of their vertical position in the flow units, and comparison with distributions of whole-rock $\delta^{18}O$ values and H_2O^+ concentrations. The two lines in chemical profiles delineate maximum and minimum values of initial (magmatic) bulk flow ratios. See text for further explanations.

upper-spinifex zones with abundant amphibole. Such a relationship is observed in the present sample suite (Fig. 8, Table 5).

The above correlations suggest that fluid/rock interaction was the main process determining the elemental variations as well as the $\delta^{18}O$ values of whole-rock samples. Most of the elemental mobility in samples from the lower cumulate zones of the flows may be related to the initial chemical and mineralogical structure of the flow units. Either the coarse-grained texture of the cumulate zones favoured fluid circulation, or the growth of abundant serpentine in olivine-rich zones enhanced the porosity during recrystallization.

Isotopic composition of the fluid phase

In order to evaluate the oxygen isotopic composition of the fluid present during the metamorphic recrystallization of Schapenburg rocks, it is necessary to estimate the water/rock ratio. Indeed, the $\delta^{18}O$ value of the fluid in equilibrium with a given rock sample may be very different from the initial value if the water/rock ratio is small (due to a mass balance effect during interaction). For the following reasons we argue that the fluid/rock ratio was high enough (>>1) to keep the $\delta^{18}O$ value of the fluid more or less constant during the interaction: i) all the whole-rock samples yield $\delta^{18}O$ values lower than the mantle reference value, which indicates a behaviour distinctly different from that of an infinite isotopic reservoir; ii) the low $\delta^{18}O$ values are buffered on a km-scale (Fig. 2, Table 5); iii) the correlation of whole-rock $\delta^{18}O$ values with the proportions of secondary minerals (Fig. 7) suggests some kind of isotopic buffering by a pervasive fluid flux.

Using the equation for open-system exchange (TAYLOR, 1977), 450°C for the exchange temperature, and $\Delta_{rock\text{-}water}$ values calculated from mineral proportions (Table 1), we obtain a $\delta^{18}O_{fluid}$ value in the range +5.5 to +7‰ (Fig. 9). Using the fractionation equation of SUZUOKI and EPSTEIN (1976), the hydrogen isotopic composition (δD) of water in equilibrium with magnesio-hornblende fractions is -65 to -50‰ (Table 5). These compositions are in the range found for Phanerozoic metamorphic or magmatic fluids (SHEPPARD et al., 1969; BOETTCHER and O'NEIL, 1980; SHEPPARD, 1986); however the possible range of δD values for such fluids during the Archean is not known. Nevertheless, the oxygen isotopic compositions of the SGR rocks are typical of metamorphic fluids. Indeed, since the continental crust has not experienced dramatic changes of $^{18}O/^{16}O$ ratio through time, fluids issued from rock-dominated systems (metamorphic fluids) should possess oxygen isotopic ratios similar to modern values. A magmatic origin for the Schapenburg metamorphic fluids is also

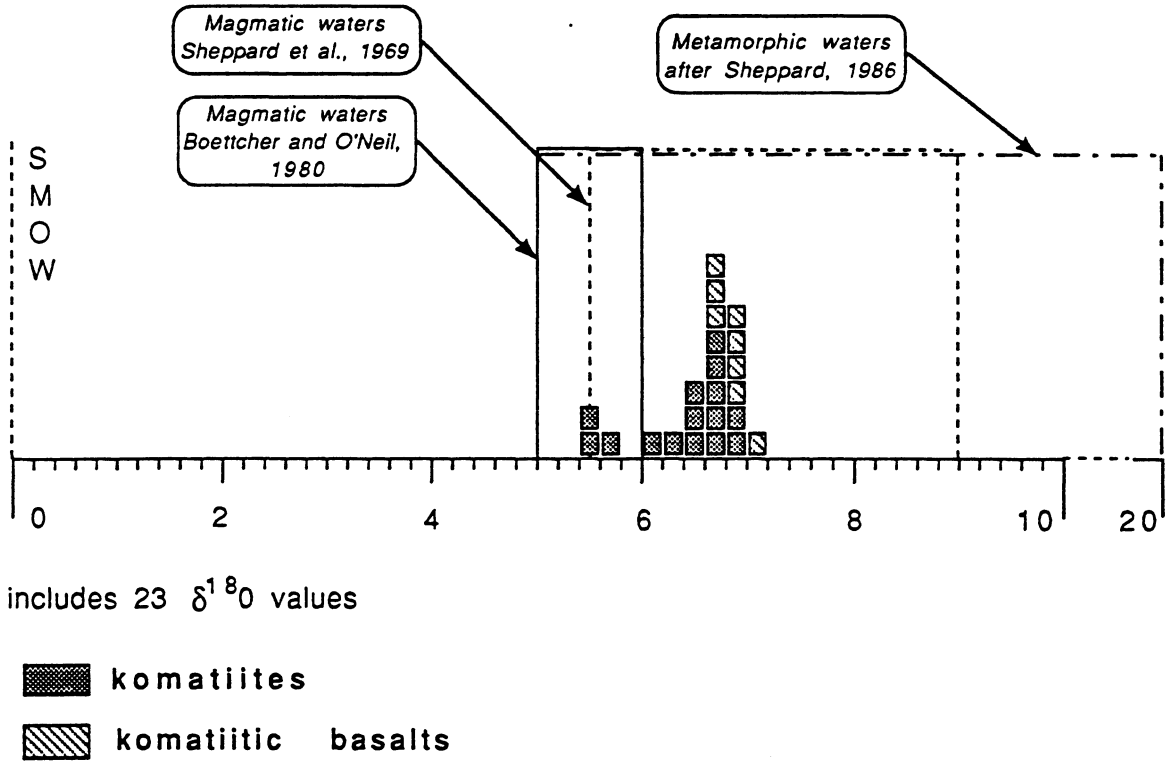

Figure 9: Frequency histogram showing oxygen isotopic composition of fluids in equilibrium with Schapenburg whole-rock samples. Dashed boxes represent fields of metamorphic and magmatic waters as defined by SHEPPARD et al. (1969), BOETTCHER and O'NEIL (1980) and SHEPPARD (1986).

compatible with the $\delta^{18}O$ values in the range +7 to +9‰ measured by TAYLOR (1977) in intrusive tonalitic and granitic plutons of the Barberton Mountain Land. Thus, although the 2900 Ma old magmatic activity that caused the contact metamorphism of the SGR may have been an important fluid source, we have no criteria for distinguishing such magmatic fluids from regional metamorphic fluids. By contrast, the present data rule out the participation of surface-derived water (sea or meteoric water) unless they underwent strong exchanged with the crust at high temperature prior to their interaction with the SGR.

CONCLUDING REMARKS

Preservation of primary chemical and isotopic signatures during metamorphic recrystallization

In contrast with other cases of metamorphosed komatiites (ARNDT et al., 1989; TOURPIN et al., 1991; GRUAU et al., 1992), the metakomatiites and metabasaltic komatiites from Schapenburg appear to have preserved most of their primary chemical and isotopic signatures during metamorphic recrystallization. With the exception of Eu, the REEs were not significantly disturbed. Moreover, the values of CaO/Al_2O_3 and Al_2O_3/TiO_2 ratios which are crucial in determining the PT conditions of melting in the mantle source (see HERZBERG, 1992), remained unchanged in a majority of samples (see above and Fig. 7). Despite the long interval of time between emplacement and metamorphism (≈600 Ma), $\varepsilon_{Nd}(T)$ values are homogeneous throughout the whole magmatic suite, indicating that the Sm-Nd system was closed system on the sample scale during metamorphism. The values we obtain for $(Gd/Yb)_N$, Al_2O_3/TiO_2 and CaO/Al_2O_3 ratios in the less altered samples (1.64±0.06 (1σ), 11±1 (1σ), and 1.8±0.1 (1σ), respectively) corroborate the values of GRUAU et al. (1990a) and HERZBERG (1992) for Barberton komatiites, which are considered as the most representative of Al-depleted komatiites.

Nevertheless, it should be pointed out that such a conclusion is only possible because the present study is focused on individual lava flows. Erratic sampling, biased in favour of particular zones (e.g. sample C2), would have furnished different chemical ratios.

Depleted versus undepleted mantle source

A second implication of this study concerns the composition of the mantle source and the nature of the melting process that formed the komatiites and

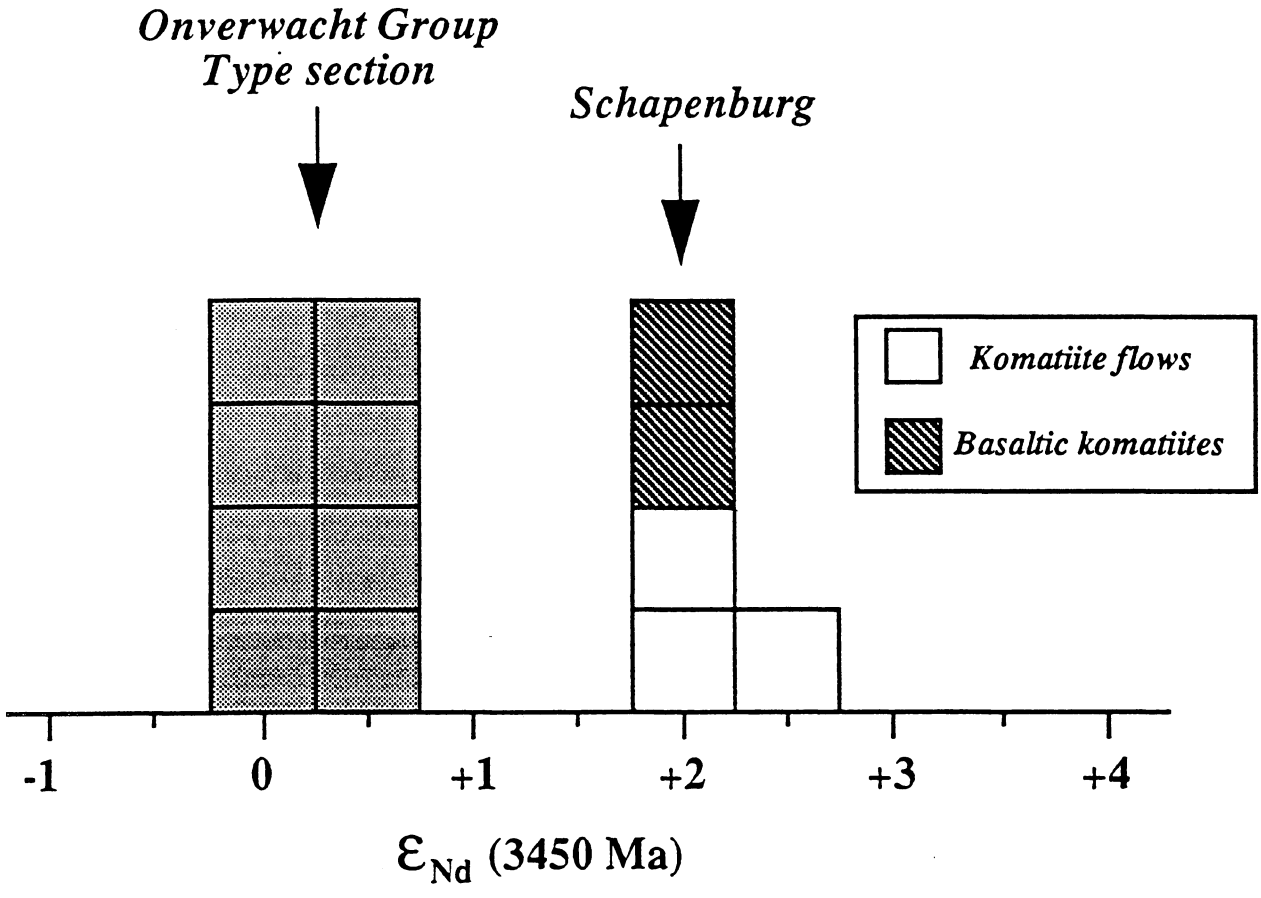

Figure 10: Frequency histogram showing comparison between the $\varepsilon_{Nd}(T)$ values calculated for Schapenburg komatiites and komatiitic basalts and the results obtained for komatiites from the Barberton Greenstone Belt. Note that in the case of BGB komatiites one box represents one sample, whereas in the case of Schapenburg one box represents the mean value of a single lava flow unit. Data sources: HAMILTON et al. (1979; 1983), GRUAU et al. (1990b), and this study.

komatiitic basalts from Schapenburg. From the above Nd dataset it is clear that the ultimate mantle source of these greenstones was depleted in LREEs ($\varepsilon_{Nd}(T)\approx+2.5$), i.e. the source had a $^{147}Sm/^{144}Nd$ ratio higher than the chondritic reservoir. Taken on its own, this result has two important consequences: i) given the fact that measured $^{147}Sm/^{144}Nd$ ratios are all lower than the chondritic value (Table 4), it confirms the hypothesis that garnet (majorite) was residual phase during the partial melting that formed these Al-depleted or Group II komatiites; the sole presence of garnet in the solid residue could lead to simultaneous fractionation of the $(Gd/Yb)_N$, CaO/Al_2O_3, Al_2O_3/TiO_2, and $^{147}Sm/^{144}Nd$ ratios; ii) it significantly modifies the accepted picture of Barberton komatiites tapping undepleted ($\varepsilon_{Nd}(T)\approx0$) mantle source regions (HAMILTON et al., 1979; 1983; GRUAU et al., 1990b, Fig. 10).

The isotopic difference between Schapenburg komatiites ($\varepsilon_{Nd}(T)\approx+2.5$) and the komatiites from the BGB ($\varepsilon_{Nd}(T)\approx0$) could reflect long-term heterogeneity of the early Archean mantle that lay beneath the Barberton Mountain Land. However, it should be noted that none of the Nd isotopic studies so far carried out on BGB komatiites include analyses of samples from a single komatiite flow. In this context, the near-zero $\varepsilon_{Nd}(T)$ values must be treated with caution. Recent studies (e.g. TOURPIN et al., 1991; GRUAU et al., 1992) show that it is only possible to interprete the initial Nd isotopic ratios of metakomatiites as primary (magmatic) isotopic memories *after a detailed study of geochemical and isotopic variations in single flow units.*

The Barberton Mountain Land: a window to the $\delta^{18}O$ value of the early Archean ocean?

The final implication of this study concerns the use of $\delta^{18}O$ values from Barberton Mountain Land rocks to provide information on the isotopic composition of Archean seawater. The $^{39}Ar/^{40}Ar$ ages now available for various metasedimentary and metavolcanic rocks of the BGB and surrounding greenstone remnants indicate the existence of discrete periods of thermal activity at 3480-3450, 3300-3200, 2900-2700 and 2100-2000 Ma (LOPEZ-MARTINEZ et al., 1984, 1992; DERONDE et al., 1991; this study). Each period (except the 2100-2000 Ma event) *coincides with a major episode of granitic plutonism* (KAMO and DAVIES, 1991). At Schapenburg, all record of possible interactions with Archean seawater during emplacement of the volcanic rocks have been lost, and the plutonic activity is likely the cause of this loss due to the recrystallization that occurred during dynamothermal contact metamorphism. On account of the rather general coincidence between $^{39}Ar/^{40}Ar$ metamorphic ages and ages of plutonic

activity, an important question arises: do any of the supracrustal lithologies from the Barberton Mountain Land preserve the isotopic record of their initial interaction with seawater?

As already mentioned, a property of metamorphic and/or magmatic fluids is to display rather constant oxygen isotope composition through time (rocks-buffered fluid systems). Thus, the oxygen isotope compositions of the metamorphic and/or magmatic fluids which circulated at various epochs through the Barberton supracrustral rocks could have fluctuated only within a narrow range (a few δ units). The intervention of magmatic/metamorphic fluids has already been isotopically documented in various sedimentary and volcanic rock units of the BGB. SMITH et al. (1984) identified a significant "magmatic component" ($\delta^{18}O$ values around +5‰) in the fluid reacting with basalts and komatiites from the type section of the Komati Formation. Similar conclusions were drawn for the associated sediments of the Onverwacht Group. More precisely, VEIZER et al. (1989a) concluded that the isotopic signatures of most carbonates coming from the Komati Formation (Lower Onverwacht Gropu), and the Hooggenoeg and Kromberg Formations (Upper Onverwacht Group; Fig. 1) are hydrothermal ($\delta^{18}O$ of fluids around +6‰). They propose that "these hydrothermal waters were derived either from metamorphic dewatering at the base of the piles or from a magmatic source", and that they interacted with the supracrustals at temperatures in the range 200-500°C. Similarly, KNAUTH and LOWE (1978) studied a large number of chert samples from different parts of the Onverwacht Group. Although the highest values recorded by the cherts ($\delta^{18}O$ close to +22‰) were interpreted as evidence for a hot (70°C) Archean ocean ($\delta^{18}O$=0 hypothesis), these authors admitted that some of the lower values (especially those down to +9‰) were problematic and likely resulted from interactions with metamorphic waters. ROBERT (1988) also found evidence for post-formation isotopic disturbances of the C (kerogen fraction) and oxygen isotopic ratios in cherts from the Onverwacht Group. Moreover, WEIS and WASSERBURG (1987) demonstrated from Rb-Sr systematics that the Onverwacht Group cherts "were all produced by a metamorphic or hydrothermal process which replaced and/or at least recrystallized the protolith". This event was dated at approximately 2100-2200 Ma, which is much later than the formation age.

Assuming that the carbonates and cherts from the BGB initially had initial $\delta^{18}O$ values similar to those of Phanerozoic (fresh) marine carbonates and cherts (i.e. ≈0‰ PDB and +32‰ SMOW, respectively), it is possible that their variable measured oxygen isotopic compositions have arisen because these sediments subsequently exchanged with a fluid phase of metamorphic-magmatic origin ($\delta^{18}O \approx +6.0$‰), at various temperatures and under different water/rock ratio

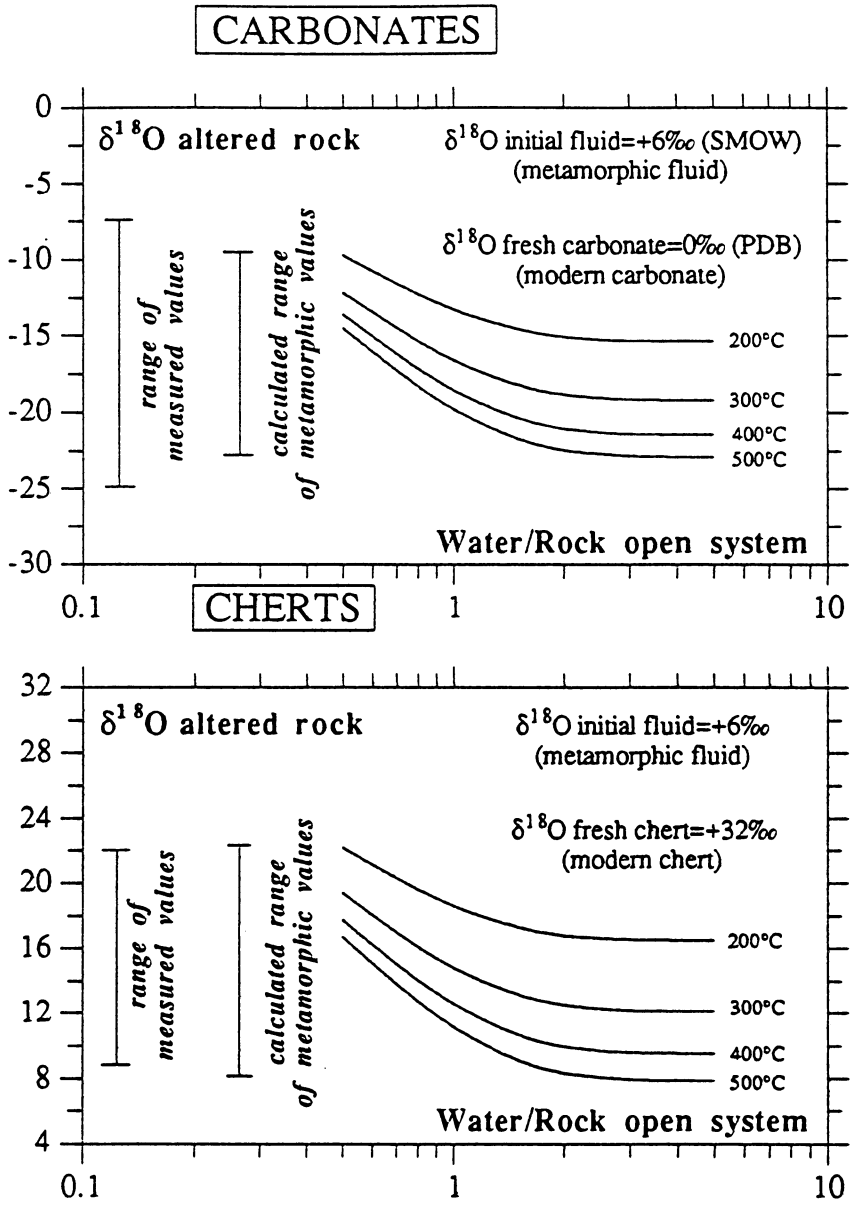

Figure 11: Diagram showing variations of $\delta^{18}O$ values in Barberton carbonates and cherts and comparison with the values calculated assuming isotopic exchange between Phanerozoic (fresh) marine carbonates and cherts and a fluid of metamorphic-magmatic origin ($\delta^{18}O$ around +6‰). Good fit arises between measured and calculated values when exchange temperatures and water/rock ratio conditions are in the range 200-500°C and 0.5-5.0, respectively. The curves were calculated using the isotopic fractionation factors of O'NEIL et al. (1969) - carbonates - and KNAUTH and EPSTEIN (1976) - cherts. The isotopic ratios are reported relative to PDB (carbonates) and SMOW (cherts). Data sources: VEIZER et al. (1989a) and KNAUTH and LOWE (1978).

conditions. We have tested this possibility. The results are presented in Fig. 11. It is a striking fact that, apart from those cherts and carbonates with $\delta^{18}O$ values around +23‰ (SMOW) and -7‰ (PDB), respectively, the oxygen isotopic compositions of all BGB chemical sediments can be explained in such a way. This requires water/rock ratios and exchange temperatures in the range 0.5-5.0 and 200-500°C, respectively. A 200-500°C temperature range corresponds to the widespread greenschist to lower amphibolite facies metamorphic conditions observed in the BGB (e.g. VEIZER et al., 1989a).

Acknowledgments- C. Lécuyer is very grateful to J.R. O.Neil for providing access to the Michigan University analytical facilities. We are also endebted to H. Maluski, who provided the Ar age data, as well as to F. Martineau, N. Morin and J. Macé for their assistance during work carried out at the University of Rennes. Dr. M. S. N. Carpenter improved the English version of the manuscript.

ADDENDUM

J.L. Joron du laboratoire du CEA à Saclay a déterminé les concentrations en Hf des échantillons de Schapenburg, en utlisant la méthode de l'activation neutronique. Des analyses répétées du Sm ont égalément été éffectuées par J. L. Joron, afin de vérifier l'absence de biais entre les concentrations en Hf déterminées par activation neutronique, et celles en Lu obtenues par la méthode de la dilution isotopique (Table 3). Ces données, couplées avec les résultats Lu que nous avons obtenus sont reportées dans le Tableau A et dans la Figure B. Trois faits importants sont à noter:

(a) mis à part un échantillon (P1), on observe une quasi-constance du rapport Hf/Sm dans les coulées de komattiite de Schapenburg. Ceci vaut aussi pour le rapport Lu/Hf (Tableau A).

(b) le rapport Hf/Sm moyen calculé (en excluant l'échantillon P1) est de 0.58±0.04, une valeur qui s'avère être significativement inférieure à la valeur de 0.70 mesurée dans les chondrites (Mc Donnough, 1987). Un tel écart n'est pas surprenant dans la mesure où, pour le grenat majorite (phase au résidu pour les komatiites du Groupe II), les données de coefficients de partage indiquent KdHf>KdSm (voir Fig. 5 dans le chapitre consacré à la présentation des résultats Lu-Hf)

Tableau A: Teneurs en Hf, Sm et Lu , et rapports Hf/Sm et Lu/Hf dans les coulées de komatiite de Schapenburg, région de Barberton

N° Ech.	Hf (ppm)[1]	Sm (ppm)[1]	Hf/Sm	Lu (ppm)[2]	Lu/Hf
	Carl's Flow				
C1	0.44	0.74	0.59	0.072	0.16
C2	0.35	0.65	0.54	0.067	0.19
C3	0.51	0.91	0.56	0.086	0.17
C4	0.67	1.16	0.58	0.096	0.14
C5	0.57	1.01	0.56	0.093	0.16
C6	0.61	0.97	0.63	0.091	0.15
	Patricia's Flow				
P1	0.27	0.63	0.43	-	-
P2	0.54	0.97	0.56	-	-
P3	0.68	1.10	0.62	0.097	0.14
P4	0.54	1.05	0.51	-	-
P5	0.56	1.04	0.54	-	-
	Patrick's Flow				
PD1	0.38	0.57	0.67	-	-
PD2	0.67	1.11	0.60	-	-
PD3	0.54	1.00	0.54	0.095	0.18
PD4	0.71	1.21	0.59	-	-
Moyenne[3]	-	-	0.58±0.04	-	0.16±0.02

[1] Résultats obtenus par la méthode de l'Activation Neutronique (J.L. Joron, Saclay)

[2] Résultats obtenus par la méthode de la Dilution Isotopique

[3] Les incertitudes sont données à 1σ. Nota, pour le rapport Hf/Sm, la moyenne a été calculée en excluant l'échantillon P1.

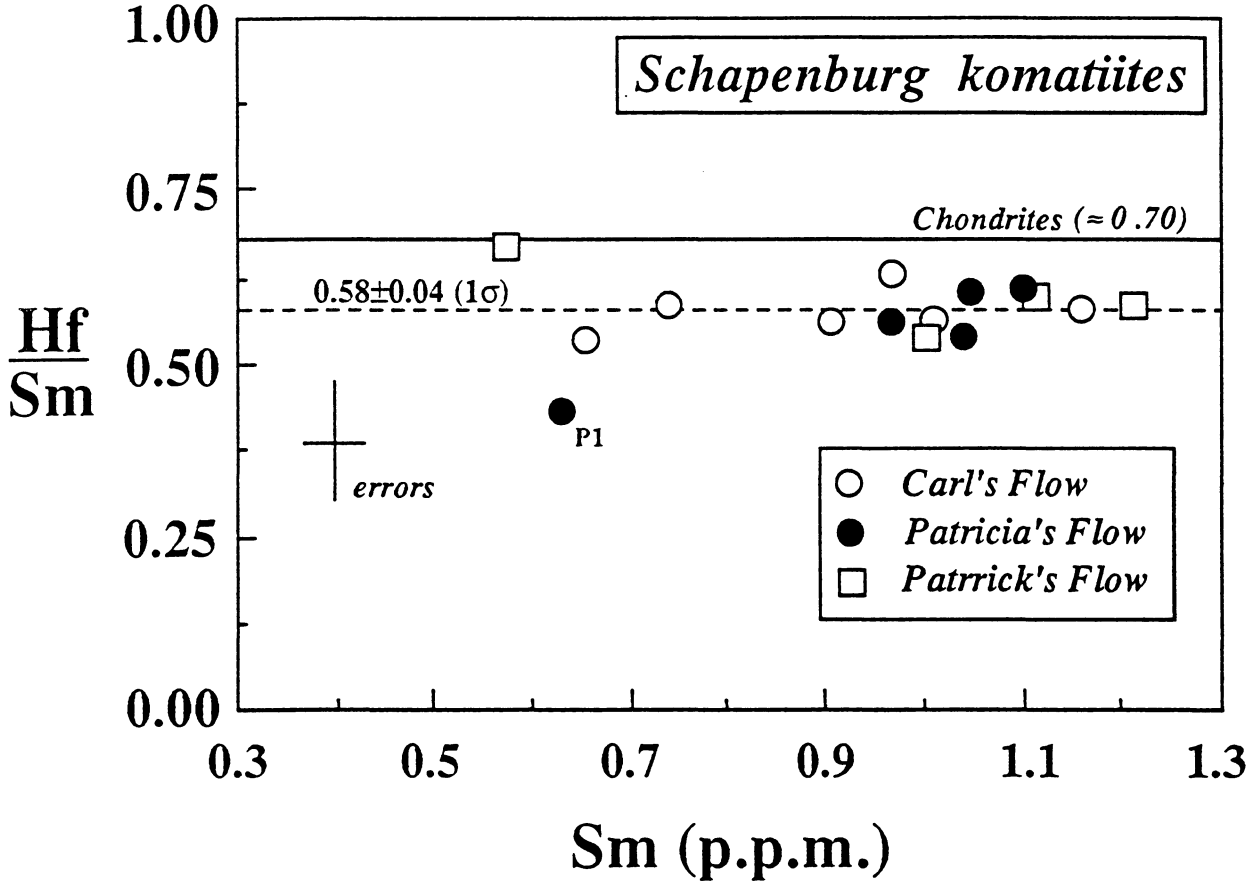

Figure B: Diagramme illustrant la quasi-constance du rapport Hf/Sm dans les coulées de komatiite de Schapenburg. Nota: la valeur moyenne de 0.58±0.04 a été calculée en omettant l'échantillon P1. La valeur des chondrites est tirée de McDonnough, 1987.

(c) le rapport Lu/Hf moyen calculé pour les komatiites de Schapenburg est de 0.16±0.02 ce qui correspond à un rapport $^{176}Lu/^{177}Hf$ de l'ordre de 0.0230 (0.0334 dans les chondrites). Pour mémoire, nous rappellerons que les échantillons de komatiite du Groupe II de Barberton qui nous ont servi de base à la conduite du test isotopique Lu-Hf (5077 et 5080) possèdent, respectivent, un rapport $^{176}Lu/^{177}Hf$ de 0.026 et 0.024 (voir Table 2 dans le chapitre traitant des résultats Lu-Hf).

De ces trois faits, nous concluons que (i) comme les REE, le Hf s'est comporté en système clos lors du métamorphisme des komatiites de Schapenburg; (ii) les rapports Hf/Sm mesurés dans ces komatiites du Groupe II sont compatibles avec l'hypothèse que le grenat majorite était une phase résiduelle lors de la fusion mantélique qui conduisait à ce groupe de komatiite; et enfin (iii) les rapports $^{176}Lu/^{177}Hf$ très voisins observés dans les komatiites de Schapenburg et les échnatillons 5080 et 5077 suggèrent que les signatures isotopiques Lu-Hf de ces deux derniers échantillons sont bien des signatures primaires et qu'il n'y pas de raison de remettre en cause, ici, les interprétations et conclusions précédemment énoncées relativement à la pétrogenèse des komatiites du Groupe II.

REFERENCES

ANHAEUSSER C. R. (1980) A geological investigation of the Archaean granite-greenstone terrane south of the Boesmanskop syenite pluton, Barberton Mountain Land. *Trans. geol. Soc. S. Afr.* **83**, 73-106.

ANHAEUSSER C. R. (1983) The geology of the Schapenburg greenstone remnant and surrounding Archean granitic terrane south of Badplass, Eastern Transvaal. *Spec. Publ. geol. Soc. S. Afr.* **9**, 31-44.

ANHAEUSSER C.R. (1991) Schapenburg greenstone remnant. In *Two Cratons and an Orogen - Excursion Guidebook and Review Articles for a Field Workshop through Selected Archaean Terranes of Swaziland, South Africa and Zimbabwe* (ed. L. D. ASHWAL), pp. 107-115. IGCP 280, Dept. of Geology, Univ. Witwatersrand, Johannesburg.

ANHAEUSSER C. R. and ROBB L. J. (1980) Regional and detailed field and geochemical studies of Archaean trondhjemitic gneisses, migmatites and greenstone xenoliths in the southern part of the Barberton Mountain Land, South Africa. *Precambrian Res.*, **11**, 373-397.

ANHAEUSSER C. R. and ROBB L. J. (1981) Magmatic cycles and the evolution of the Archaean granitic crust in the eastern Transvaal and Swaziland. *Spec. Publ. geol. Soc. Aust.* **7**, 457-467.

ANHAEUSSER C. R. and ROBB L. J. (1983) Geological and geochemical characteristics of the Heerenveen and Mpuzuli batholiths south of the Barberton greenstone belt and preliminary thoughts on their petrogenesis. *Spec. Publ. geol. Soc. S. Afr.* **9**, 131-151.

ARMSTRONG R. A., COMPSTON W., DE WIT M. J. and WILLIAMS I. S. (1990) The stratigraphy of the 3.5-3.2 Ga Barberton Greenstone Belt revisited: a single zircon ion microprobe study. *Earth Planet. Sci. Lett.* **101**, 90-106.

ARNDT N. T. (1986) Komatiites: a dirty window to the Archean mantle. *Terra Cognita* **6**, 59-66.

ARNDT N. T., TEIXEIRA N. A. and WHITE W. M. (1989) Bizarre geochemistry of komatiites from the Crixas greenstone belt, Brazil. *Contrib. Mineral. Petrol.* **101**, 187-197.

BARTON J. M., ROBB L. J., ANHAEUSSER C. R. and VAN NIEROP D. A. (1983) Geochronologic and Sr-isotopic studies of certain units in the Barberton granite-greenstone terrane, South Africa. *Spec. Publ. Geol. Soc. S. Afr.* **9**, 63-72.

BAYLISS P. (1975) Nomenclature of the Trioctahedral chlorites. *Canadian Mineral.* **13**, 178-180.

BEATY D. W. and TAYLOR H. P. J. (1982) The oxygen isotope geochemistry of komatiites: evidence for water-rock interaction. In *Komatiites* (ed. N. T. ARNDT and E. G. NISBET), pp. 267-280. George Allen and Unwin, London.

BERGER G. W. and YORK D. (1981) Geothermometry from $^{40}Ar/^{39}Ar$ dating experiments. *Geochim. Cosmochim. Acta* **43**, 795-811.

BOETTCHER A. L. and O'NEIL J. R. (1980) Stable isotope, chemical and petrographic studies of high pressure amphiboles and micas: evidence for metasomatism in the mantle source regions of alkali basalts and kimberlites. *Am. J. Sci.* **280A**, 594-621.

BOTTINGA Y. and JAVOY M. (1975) Oxygen isotope partitioning among the minerals in igneous and metamorphic rocks. *Rev. Geophys. Space Phys.* **13**, 401-418.

BRYAN W. B., FINGER L. W. and CHAYES F. (1969) Estimating proportions in petrographic mixing equations by least-squares approximation. *Science* **163**, 926-927.

CLAYTON R. N. and MAYEDA T. K. (1963) The use of bromine pentafluoride in the extraction of oxygen from oxides and silicates for isotopic analyses. *Geochim. Cosmochim. Acta* **27**, 43-52.

CLOETE M. (1991) An overview of metamorphism in the Barberton Greenstone Belt. In *Two Cratons and an Orogen - Excursion Guidebook and Review Articles for a Field Workshop through Selected Archaean Terranes of Swaziland, South Africa and Zimbabwe* (ed. L. D. ASHWAL), pp. 84-98. IGCP 280, Dept. of Geology, Univ. Witwatersrand, Johannesburg.

DAVIES R. D., ALLSOPP H. L., ERLANK A. J. and MANTON W. I. (1970) Sr-isotope studies on various layered mafic intrusions in southern Africa. *Spec. Publ. geol. Soc. S. Afr.* **1**, 576-593.

DEPAOLO D. J. and WASSERBURG G. J. (1976) Inferences about magma sources and mantle structure from $^{143}Nd/^{144}Nd$. *Geophys. Res. Lett.* **3**, 743-746.

DeRONDE C. E. J., HALL C. M., YORK D. and SPOONER E. T. C. (1991) Laser step-heating $^{40}Ar/^{39}Ar$ age spectra from early Archean (≈3.5Ga) Barberton greenstone belt sediments: A technique for detecting cryptic tecono-thermal events. *Geochim. Cosmochim. Acta* **55**, 1933-1951.

ERNST W. G. (1983) Mineral parageneses in metamorphic rocks exposed along tailuko Gorge, Central Mountain range, Taiwan. *J. metamorphic Geol.* **1**, 305-329.

FUJIMAKI H., TATSUMOTO M. and AOKI K. (1984) Partition coefficients of Hf, Zr and REE between phenocrysts and groundmass. *J. Geophys. Res.* **89**, 662-672.

GARLICK G. D. and EPSTEIN S. (1967) Oxygen isotope ratios in coexisting minerals of regionally metamorphosed rocks. *Geochim. Cosmochim. Acta* **31**, 181-214.

GRUAU G., JAHN B.M., GLIKSON A.Y., DAVY R., HICKMAN A.H. and CHAUVEL C. (1987) Age of the Talga-Talga Subgroup, Pilbara Block, Western Australia, and early evolution of the mantle: new Sm-Nd isotopic evidence. *Earth Planet. Sci. Lett.* **85**, 105-116.

GRUAU G., CHAUVEL C., ARNDT N. T. and CORNICHET J. (1990a) Aluminum depletion in komatiites and garnet fractionation in the early Archean mantle: Hafnium isotopic constraints. *Geochim. Cosmochim. Acta* **54**, 3095-3101.

GRUAU G., CHAUVEL C. and JAHN B. M. (1990b) Anomalous Sm-Nd ages for the early Onverwacht Group volcanics: significance and petrogenetic implications. *Contrib. Mineral. Petrol.* **104**, 27-34.

GRUAU G., TOURPIN S., FOURCADE S. and BLAIS S. (1992) Loss of isotopic (Nd, O) and chemical (REE) memories during metamorphism of komatiites: new evidence from eastern Finland. *Contrib. Mineral. Petrol.* **112,** *68-82.*

HAMILTON P. J., EVENSEN N. M., O'NIONS R. K., SMITH H. S. and ERLANK A. J. (1979) Sm-Nd dating of Onverwacht Group volcanics, Southern Africa. *Nature* **279**, 298-300.

HAMILTON P. J., O'NIONS R. K., BRIDGWATER D. and NUTMAN A. (1983) Sm-Nd studies of Archaean metasediments and metavolcanics from West Greenland and their implications for the Earth's early history. *Earth Planet. Sci. Lett.* **62**, 263-272.

HEGNER E., KRÖNER A. and HOFMAN A.W. (1984). Age and isotope geochemistry of the Archaean Pongola and Usushwana suites in Swaziland, southern Africa: a case for crustal contamination of mantle-derived magma. *Earth Planet Sci. Lett.* **70**, 267-279.

HEMLEY J. J., MONTOYA J. W., SHAW D. R. and LUCE R. W. (1977) Mineral equilibria in the MgO-SiO_2-H_2O system: II. Talc-antigorite-forsterite-anthophyllite-enstatite stability relations and some geologic implications in the system. *Am. J. Sci.* **277**, 353-383.

HERZBERG C. (1992) Depth and degree of melting of komatiites. *J. Geophys. Res.* **97**, 4521-4540.

HOEFS J. and BINNS R. A. (1978) Oxygen isotope compositions in Archean rocks from Western Australia, with special reference to komatiites. *USGS Open-file Rep.* **78-701**, 180-182.

HOFFMAN S. E., WILSON M. and STAKES D. S. (1986) Inferred oxygen isotope profile of Archaean oceanic crust, Onverwacht Group, South Africa. *Nature* **321**, 55-58.

JACOBSEN S. B. and WASSERBURG G. J. (1980) Sm-Nd isotopic evolution of chondrites. *Earth Planet. Sci. Lett.* **50**, 139-155.

JAHN B. M., GRUAU G. and GLIKSON A. Y. (1982) Komatiites of the Onverwacht Group, S. Africa: REE geochemistry and mantle evolution. *Contrib. Mineral. Petrol.* **80**, 25-40.

KAMO S. and DAVIS D. (1991) A review of geochronology from the Barberton Mountain Land. In *Two Cratons and an Orogen - Excursion Guidebook and Review Articles for a Field Workshop through Selected Archaean Terranes of Swaziland, South Africa and Zimbabwe* (ed.

L. D. ASHWAL), pp. 59-68. IGCP Project 280, Dept. of Geology, Univ. Witwatersrand, Johannesburg.

KARHU J. and EPSTEIN S. (1986) The implication of the oxygen isotope records in coexisting cherts and phosphates. *Geochim. Cosmochim. Acta* **50**, 1745-1756.

KENDALL C. and COPLEN T. B. (1985) Multisample conversion of water to hydrogen by zinc for stable isotope determination. *Anal. Chem.* **57**, 1437-1440.

KNAUTH L. P. and EPSTEIN S. (1976) Hydrogen and oxygen isotope ratios in nodular and bedded cherts. *Geochim. Cosmochim. Acta* **40**, 1095-1108.

KNAUTH L. P. and LOWE D. R. (1978) Oxygen isotope geochemistry of cherts from the Onverwacht Group (3.4 billion years), Transvaal, South Africa, with implications for secular variations in the isotopic composition of cherts. *Earth Planet. Sci. Lett.* **41**, 209-222.

KRÖNER A. and TODT W. (1988) Single zircon dating constraining the maximum age of the Barberton greenstone belt, southern Africa. *J. Geophys. Res.* **93**, 15329-15337.

KYSER T. K. (1986) Stable isotope variations in the mantle. In *Stable Isotopes in High Temperature Geological Processes* (ed. J. W. VALLEY et al.); *Rev. Mineral.*, Vol. 16, pp. 141-164.

LAIRD J. (1988) Chlorites: metamorphic petrology. In *Hydrous Phyllosilicates (Exclusive of Micas)* (ed. S. W. BAILEY); *Rev. Mineral.*, Vol. 19, pp. 405-453.

LEAKE B. E. (1978) Nomenclature of amphiboles. *Am. Mineral.* **63**, 1023-1059.

LOPEZ-MARTINEZ M., YORK D., HALL C. M. and HANES J. A. (1984) Oldest reliable $^{40}Ar/^{39}Ar$ ages for terrestrial rocks: Barberton Mountain komatiites. *Nature* **307**, 352-355.

LOPEZ-MARTINEZ M., YORK D. and HANES J. A. (1992) A $^{40}Ar/^{39}Ar$ geochronological study of komatiites and komatiitic basalts from the Lower Onverwacht Volcanics: Barberton Mountain Land, South Africa. *Precambrian Res.* **57**, 91-119.

McDONNOUGH W.F. (1987) Chemical and isotopic systematics of basalts and peridotite xenoliths: implications for the composition of the Earth's mantle. Ph. D. Thesis, Australian National University, Canberra.

MÉVEL C. (1984) Le métamorphisme dans la croute océanique. Apport de la Pétrologie à la compréhension des phénomènes de circulation hydrothermale (exemples dans l'Atlantique). *Thèse Doctorat ès-Sciences* **Univ. Pierre et Marie Curie**, 434.

MONIÉ P., CABY R. and MALUSKI H. (1984) $^{40}Ar/^{39}Ar$ investigations within the Grande-Kabylie massif (northern Algeria): evidences for its Alpine structuration. *Eclogae Geol. Helv.* **77**, 115-141.

O'NEIL J. R., CLAYTON R. N. and MAYEDA T. K. (1969) Oxygen isotope fractionation in divalent metal carbonates. *J. Chem. Phys.* **51**, 5547-5558.

ROBB L.J., ANHAEUSSER C.R. and VAN NIEROP D.A. (1983) The recognition of the Nelspruit Batholiths north of the Barberton greenstone belt and its significance in terms of Archaean crustal evolution. *Spec. Publ. geol. Soc. S; Afr.* **9**, 117-130.

ROBERT F. (1988) Carbon and oxygen isotope variations in Precambrian cherts. *Geochim. Cosmochim. Acta* **52**, 1473-1478.

SHEPPARD S. M. F. (1986) Characterization and isotopic variations in natural waters. In *Reviews in Mineralogy, Stable Isotopes in High Temperature Geological Processes* (ed. J. W. VALLEY et al.); *Rev. Mineral.*, Vol. 16, pp. 165-183.

SHEPPARD S. M. F., NIELSEN R. L. and TAYLOR H. P. (1969) Oxygen and hydrogen isotope ratios of clay minerals from porphyry deposits. *Econ. Geol.* **64**, 755-777.

SMITH A. D. and LUDDEN J. N. (1989) Nd isotopic evolution of the Precambrian mantle. *Earth Planet. Sci. Lett.* **93**, 14-22.

SMITH H. S., O'NEIL J. R. and ERLANK A. J. (1984) Oxygen isotope compositions of minerals and rocks and chemical alteration patterns in pillow lavas from the Barberton Greenstone Belt, South Africa. In *Archaean Geochemistry* (ed. A. KRÖNER et al.), pp 115-137. Springer-Verlag, Berlin.

SUZUOKI T. and EPSTEIN S. (1976) Hydrogen isotope fractionation between OH-bearing minerals and water. *Geochim. Cosmochim. Acta* **40**, 1229-1240.

TAYLOR H. P. J. (1977) Water/rock interactions and the origin of H_2O in granitic batholiths. *J. Geol. Soc. London* **133**, 509-558.

TOURPIN S., GRUAU G., BLAIS S. and FOURCADE S. (1991) Resetting of REE, and Nd and Sr isotopes during carbonitization of a komatiite flow from Finland. *Chem. Geol.* **90**, 15-29.

VEIZER J., HOEFS J., LOWE D. R. and THURSTON P. C. (1989a) Geochemistry of Precambrian carbonates: II. Archean greenstone belts and Archean sea water. *Geochim. Cosmochim. Acta* **53**, 859-871.

VEIZER J., HOEFS J., RIDLER R. H., JENSEN L. S. and LOWE D. R. (1989b) Geochemistry of Precambrian carbonates: I. Archean hydrothermal systems. *Geochim. Cosmochim. Acta* **53**, 845-857.

VILJOEN M. J. and VILJOEN R. P. (1969a) The effects of metamorphism and serpentinization on the volcanic and associated rocks of the Barberton region. *Spec. Publ. geol. Soc. S. Afr.* **2**, 29-53.

VILJOEN M. J. and VILJOEN R. P. (1969b) The geology and geochemistry of the lower ultramafic unit of the Onverwacht Group and a proposed new class of igneous rocks. *Spec. Publ. geol. Soc. S. Afr.* **2**, 55-85.

WEIS D. and WASSERBURG G. J. (1987) Rb-Sr and Sm-Nd isotope geochemistry and chronology of cherts from the Onverwacht Group (3.5 AE), South Africa. *Geochim. Cosmochim. Acta* **51**, 973-984.

METAMORPHISM AND Sm-Nd REMOBILIZATION IN THE 3800-3700 Ma - OLD ISUA SUPRACRUSTAL BELT OF WEST GREENLAND: IMPLICATIONS FOR EARLY TERRESTRIAL EVOLUTION

G. Gruau, M. Rosing, D. Bridgwater and R.C.O. Gill

Article soumis à publication dans Earth and Planetary Science Letters

Abstract

Initial $^{143}Nd/^{144}Nd$ ratios (or $\varepsilon_{Nd}(T)$ values), if reliably determined for selected components of the 3800-3700 Ma -old Isua Supracrustal Belt of West Greenland may in theory provide important clues regarding the early evolution of the Earth's mantle and crust. However, the Isua Supracrustal Belt, in common with a number of similar early Archaean terrains, shows evidence of multiple periods of metamorphism and deformation, which cast some doubts about the preservation of primary Nd isotopic memories. New Sm-Nd isotopic results obtained on whole-rocks and mineral separates from the so-called Garbenschiefer Amphibolite Unit (GAU) exemply this weakness. Although the GAU likely represents the remains of a basic sill or dyke, that is to say, an intrusive igneous body in which isotopic homogeneity was prevalent during emplacement, whole-rock samples from this unit show large scatter in $\varepsilon_{Nd}(T)$ values (from -1.0 to +5.0), indicaing an open system type behaviour. A Sm-Nd mineral isochron age of 2849 ± 116 Ma shows that the earliest recognizable metamorphism of the Isua belt (amphibolite grade: P≈5Kb-T≈500-600°C) is of mid-Archaean age, which is thought to represent the time of disturbance of the Sm-Nd system in the Garbenschiefer Amphibolite Unit.

Very probably, all the rocks from Isua underwent some Nd isotopic reequilibration and/or fractionation of their $^{147}Sm/^{144}Nd$ ratios during the 2850 Ma-old metamorphic episode. Nevertheless, Nd-rich rocks (> 20 ppm) - such as the Amîtsoq grey gneisses and certain metasediments of the Isua belt - are relatively resistent to secondary fractionation due to the presence of REE-acceptor phases. In view of this behaviour, only $\varepsilon_{Nd}(T)$ values calculated from rocks having Nd contents greater than 20 ppm ($\varepsilon_{Nd}(T) = +2.0 \pm 1.0$) appear to be sufficiently reliable for use in characterizing the ε_{Nd} value of the Earth's mantle at 3800-3700 Ma.

Table 1: Chronological sequence in the Isua area. Modified from Baadsgaard et al. [22] and Nutman [4].

8. ***Proterozoic metamorphism reaching amphibolite facies in local shear-zones (western part of Isua)***	**ca. 1600-1800 Ma**
7. **Proterozoic basic dyke injection**	**ca. 2200 Ma**
6. ***Deformation and amphibolite facies metamorphism***	**ca. 2800-2900 Ma**
5. **Intrusion of Tassartôq (Ameralik) dykes**	**ca. 3200-3100 Ma**
4. ***Deformation and amphibolite facies metamorphism***	**ca. 3600 Ma**
3. **Main intrusion of grey tonalitic (Amîtsoq) gneisses**	**ca. 3750-3800 Ma**
2. **Intrusion (?) of Garbenschiefer Amphibolites parent body**	
1. **Deposition of Isua supracrustal rocks**	

1. Introduction

When reliably determined from selected rock units (e.g. the 3800-3700 Ma Isua supracrustal belt of West Greenland), initial $^{143}Nd/^{144}Nd$ ratios (or $\varepsilon_{Nd}(T)$ values) may in theory provide some useful information on the compositional heterogeneity of the early Earth's mantle and crust [e.g., 1, 2]. However, in practice, the use of Isua rocks as a window on early terrestrial evolution suffers from one severe drawback: the Isua Supracrustal Belt, in common with a number of similar early Archaean terrains, shows evidence of multiple periods of metamorphism and deformation [e.g.,3-5] (Table 1). Moreover, it is now well established that significant and at times considerable Nd mobility and/or fractionation of the Sm/Nd ratio may occur during deformation and metamorphism of terrestrial rocks [e.g. 6-11]. Assuming that secondary Nd mobility and/or fractionation of the Sm/Nd ratio is a common process in deformed and metamorphosed rocks, then the possibility emerges that many of the $\varepsilon_{Nd}(T)$ values calculated for Isua supracrustals are in fact apparent rather than real.

Previous Sm-Nd isotopic studies have documented a large scattering of $\varepsilon_{Nd}(T)$ values in the Isua supracrustal belt: i.e. from -15.0 to +3.0 in the banded iron formations (BIF) [12]; from -0.5 to +3.0 in the so-called Garbenschiefer Amphibolite Unit [1], and from -0.5 to +3.5 in the clastic sediments [2, 13, 14]. As pointed out by Miller and O'Nions [12], a range of ca. 18 ε_{Nd} units such as that claculated for the Isua BIF's at 3800 Ma is "inconsistent with evolution of ^{143}Nd in a reservoir with an initially uniform $^{143}Nd/^{144}Nd$ that became a closed system 3800 Ma ago"; quite clearly, some mobility of the Sm-Nd system has occurred in these rocks, thus resetting their primary isotopic memories. For the Garbenschiefer Amphibolite Unit and the clastic metasediments, the initial isotopic variation is much less pronounced and the computed $\varepsilon_{Nd}(T)$ values make more geological sense, thus leading to more complicated interpretations. In their Sm-Nd study of the Garbenschiefer Amphibolite Unit, Hamilton et al. [1] concluded that "it is not known, a priori, whether the scatter of initial $\varepsilon_{Nd}(T)$ values (i.e. from -0.5 up to +3.0) reflect variable initial $^{143}Nd/^{144}Nd$ ratios because of crustal contamination of the parental magma for example or perturbation of Sm-Nd systematics during metamorphism".

In view of the fundamental importance of Isua as a key point for establishing the Nd growth curve of the early Earth's mantle and crust, an attempt is made here to investigate further the effects of metamorphism on the primary Nd isotopic memories of Isua rocks, combining for the first time the Nd isotopic analyses of whole-rocks as well as secondary mineral phases. All the samples come from the

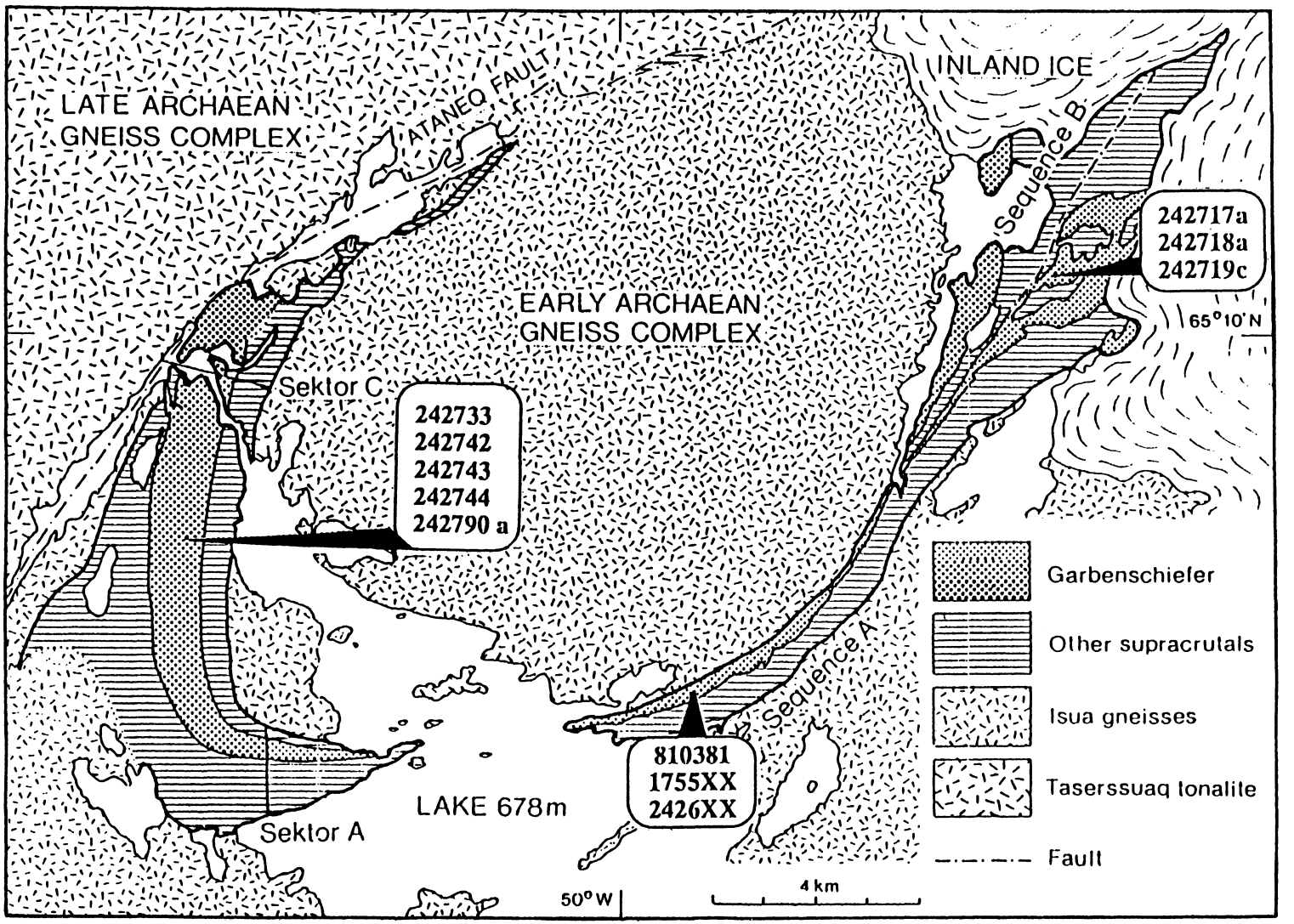

Figure 1: Sketch map of the Isua Supracrustal Belt, West Greenland, showing the location of samples analysed in this study.

Garbenschiefer Amphibolite Unit, which is volumetrically the most important lithological unit of the Isua Supracrustal Belt (ISB).

2. Geological history of the Garbenshiefer Amphibolite Unit

The geology of the ISB and adjacent Amîtsoq gneisses has been described in detail by others [e.g., 3, 4, 15-18], so only information concerning the field occurrence and tectono-metamorphic history of the Garbenschiefer Amphibolite Unit is presented here. A chronological sequence of the magmatic and tectono-metamorphic events in the Isua area is presented further in Table 1.

The Garbenschiefer Amphibolite Unit (GAU) of the ISB is a massive (up to 700 m wide) meta-igneous body of Al- and Mg-rich composition [19] with distinctive sheaf-like amphibole texture. In outcrop, the GAU represents the largest single unit in the Isua succession (Fig.1). Although part of the ISB, the GAU could be younger than the surrounding supracrustals: the GAU cuts obliquely across the Isua metasedimentary and metavolcanic succession, suggesting that it may have originated as a gabbroic sill-like body intruded into the metasediments and metavolcanics [4,19]. However, since the lapse of time between deposition of the supracrustals and emplacement of the GAU cannot be very long - the GAU underwent its earliest phase of folding along with the ISB, which was contemporaneous or even predated the intrusion of the 3750-3700 Ma-old Amîtsoq grey gneisses [e.g., 4] (Table1) - the unit is not chronologically distinguishable from the remaining Isua rocks and is thus regarded also as 3800-3700 Ma old [20-23].

Mineralogically, the GAU now consists entirely of secondary assemblages with no relic igneous phases preserved. The more widespread secondary mineral assemblages include [3]: #1 Fe-Mg amphibole (anthophyllite-gedrite) + plagioclase + quartz + rutile ± kyanite; #2 Fe-Mg amphibole + plagioclase + quartz + hornblende + ilmenite ± kyanite; #3 hornblende + chlorite + quartz + ilmenite + Fe-Mg amphibole ± plagioclase; and #4 hornblende + chlorite + quartz + ilmenite ± plagioclase.

Assemblage #1 is the earliest metamorphic assemblage recognized in the GAU, yielding a minimum pressure-temperature estimate of about 5.5 Kb at 600°C based on the occurrence of kyanite and hypersolvus amphiboles belonging to the anthophyllite-gedrite solid-solution series. Assemblage #1 is not found throughout the GAU; it is mostly observed in the central and eastern parts of the unit (Fig. 1). The pressure-temperature conditions calculated from assemblage #1 are comparable, although slightly higher, to those obtained from the Isua metasediments [24-25].

Assemblages #2 to #4 are more widely developed, being present in all parts of the unit. Assemblage #3 is equivalent to assemblage #4, except that it contains relics of assemblage #1. As a general rule, the appearance of assemblage #4 is accompanied by the development of a new penetrative fabric in the rock. The transition from assemblage #1 to assemblage #2 is interpreted as a local hydration reaction between Fe-Mg amphibole and plagioclase to form hornblende. It is likely that the transition from assemblage #1 to assemblage #2 took place during retrogression from the 600°C/5.5 Kb thermal event, while assemblage #4 formed in response to a different and later tectono-thermal event.

According to previous studies, the ISB and surrounding gneisses experienced at least two episodes of regional metamorphism during the Archaean [e.g., 4] (Table 1). The more recent took place around 2900-2800 Ma ago, corresponding to a well-documented period of intense tectono-thermal activity throughout the Archaean crust of southwest Greenland [e.g., 26-28]. During this event, the mid-Archaean (3200-3100 Ma) Tarssartôq dykes - which are seen crosscutting the ISB - were widely recrystallised to form rodded lineated amphibolites with a plagioclase composition (An>17) indicating metamorphism under amphibolite facies conditions [4]. Later, the ISB and surrounding gneisses both underwent Proterozoic metamorphism (Table 1). This younger thermal event took place at around 1800-1600 Ma [e.g., 29], but recrystallization was not penetrative throughout the ISB, being developed in local faults and shear-zones. In the GAU, the effects of this late event are mainly observed in the western part of the unit, close to the Ataneq fault (Fig. 1). During metamorphism of these rocks, Proterozoic shearing was intense and accompanied by a high flux of CO_2-rich saline fluids. Extensive metasomatism nearly obliterated all the previously described GAU assemblages to form an assemblage (#5) consisting of muscovite + biotite + scapolite + carbonate + sulphides + allanite [3].

3. Samples and analytical methods

In order to investigate the effects of metamorphic recrystallization on the Sm-Nd isotope systematics of the GAU, sixteen whole-rock samples were selected which weighed approximately 3 kg each. Two of these samples (242733 and 242744) have type #4 metamorphic assemblages and have been included in earlier studies of the GAU by Hamilton et al. [1]. All the other samples were collected in the present study; their assemblages comprise type #1 (810381, 175553, and 175558), type #2 (175557, 175563, 242671b, 242790a, and 242719c) and type #3 (242717a, 242718a, and 242743). Nearly pure separates of plagioclase and amphibole were also analysed

from one of the best-preserved type #1 samples (810381). As shown on Fig. 1, samples 24271Xa,b come from the eastern sector of the ISB, while samples 1755XX, 2426XX and 8103881 are located in the central part of the belt; samples 2427XX come from a third locality situated in the western part of the ISB close to the Ataneq fault.

The scale of sampling is twofold: taken separately, sample suites 1755XX, 2426XX, 24271Xa,b and 2427XX each cover an area of ca. 10 m x 10 m (i.e. the distance between sample 175553 and 175557, for example, is < 10 m); the distance between sample suites, however, is of the order of kilometres (Fig. 1).

All chemical separations were carried out at the University of Rennes, following the procedure described in Gruau et al. [30]. $^{143}Nd/^{144}Nd$ and $^{147}Sm/^{144}Nd$ ratios were determined on different aliquots of the same sample dissolution. $^{143}Nd/^{144}Nd$ ratios of whole-rock samples were measured at the University of Rennes using a single-collector CAMECA TSN 206 mass-spectrometer; the Nd isotopic ratios of plagioclase and amphibole separates from sample 810381 were determined at the IFREMER laboratory at Brest, using a five-collector Finnigan MAT 261 mass spectrometer. All $^{143}Nd/^{144}Nd$ ratios were normalized against $^{146}Nd/^{144}Nd$ = 0.7219. Results from the La Jolla Nd standard during the course of this study were $^{143}Nd/^{144}Nd$ = 0.511877 ± 38 ($2\sigma_{pop}$) at Rennes University, and 0.511870 ± 13 ($2\sigma_{pop}$) at the IFREMER laboratory. Accordingly, all the $^{143}Nd/^{144}Nd$ ratios for the whole-rock and mineral samples were corrected by -0.000017 and -0.000010, respectively, to be consistent with the La Jolla reference value of 0.511860. Blanks for Nd and Sm were lower than $0.4*10^{-9}$ and $0.1*10^{-9}$ g, respectively.

Measured and calculated initial $^{143}Nd/^{144}Nd$ ratios are quoted throughout the text and in Table 2, using the ε_{Nd} notation of DePaolo and Wasserburg [31], as deviations in part per 10^4 from the chondritic growth curve. The present-day $^{143}Nd/^{144}Nd$ and $^{147}Sm/^{144}Nd$ ratios for the chondritic reference reservoir (CHUR) are those determined by Jacobsen and Wasserburg [32]. The error of the initial isochron ε_{Nd} value was calculated using the method of Fletcher and Rosman [33]. The decay constant of ^{147}Sm is 0.00654 Ga^{-1}.

4. Results

The Sm-Nd isotopic results (whole-rock samples and mineral separates) obtained in this study are reported in Table 2 and presented in Figs. 2, 3 and 4. Several important points should be noted:

1) The new aliquots of previously analysed samples used in this study (i.e. samples 242733 and 242744) yielded results in agreement with those reported earlier (Table

Table 2: Sm-Nd isotopic data for Garbenschiefer whole-rock samples and minerals

Sample N°	Lithology(1)	Sm (ppm)	Nd (ppm)	$^{147}Sm/^{144}Nd$(2)	$^{143}Nd/^{144}Nd$	εNd(0)	εNd(3750)(3)	εNd(2850)(3)
Central Sector								
Whole-rock data								
810381	1	0.3926	1.143	0.2077	0.513182±23	+10.6±0.5	+5.3±0.7	+6.6±0.6
810381*	1	0.3995	1.158	0.2070	0.513126±15	+9.5±0.3	+4.6±0.5	+5.8±0.4
175553	1	0.7104	2.523	0.1702	0.512108±14	-10.3±0.3	+2.5±0.5	-0.6±0.4
175557	2	0.7797	2.701	0.1745	0.512237±25	-7.8±0.5	+3.0±0.7	+0.3±0.6
175558	1	0.5933	1.697	0.2113	0.513120±19	+9.4±0.4	+2.4±0.6	+4.0±0.5
175563	2	0.3456	0.955	0.2189	0.513230±25	+11.5±0.5	+0.8±0.7	+3.4±0.6
242670	1	0.8110	2.812	0.1744	0.512209±18	-8.4±0.4	+2.5±0.6	-0.2±0.5
242671b	2	0.8430	2.793	0.1825	0.512374±26	-5.1±0.5	+1.7±0.7	+0.1±0.6
242689	2	0.6838	2.139	0.1931	0.512709±13	+1.4±0.3	+3.2±0.5	+2.7±0.4
Mineral data								
810381-amph	1	0.3480	0.707	0.2975	0.514818±20	+42.5±0.4	-	+5.6±0.5
810381-plag	1	0.2841	1.004	0.1710	0.512425±15	-4.2±0.3	-	+5.3±0.4
Eastern Sector								
242717a	3	0.3941	1.076	0.2214	0.513435±22	+15.5±0.4	+3.6±0.6	+6.5±0.5
242718a	3	0.4176	1.189	0.2124	0.513220±23	+11.4±0.5	+3.8±0.7	+5.6±0.6
242719c	2	0.4126	1.068	0.2337	0.513512±23	+17.0±0.5	-0.9±0.4	+3.5±0.6
Western Sector								
242790a	2	0.6443	1.848	0.2108	0.513087±14	+8.8±0.3	+1.9±0.4	+3.6±0.4
242743	3	0.3780	1.633	0.2218	0.513282±27	+12.6±0.5	+0.4±0.6	+3.4±0.6
242742	3	0.5300	1.655	0.1937	0.513512±23	-2.0±0.3	-0.5±0.4	-0.9±0.4
242744	4	0.8020	2.394	0.2026	0.512941±25	+5.9±0.5	+3.1±0.7	+3.8±0.6
242744**	4	0.7997	2.399	0.2015	0.512917±14	+5.4±0.3	+3.1±0.4	+3.7±0.4
242733	4	0.6511	1.608	0.2448	0.513943±25	+25.5±0.5	+2.2±0.7	+7.9±0.6
242733**	4	0.6519	1.601	0.2462	0.513959±16	+25.8±0.3	+1.8±0.4	+7.7±0.4

(1) see text for explanation

(2) the error on this ratio is ±0.2%

(3) values calculated using $^{143}Nd/^{144}Nd=0.512638$ and $^{147}Sm/^{144}Nd=0.1967$ for the present-day chondritic reservoir

* duplicate

** results obtained by Hamilton et al. [1]

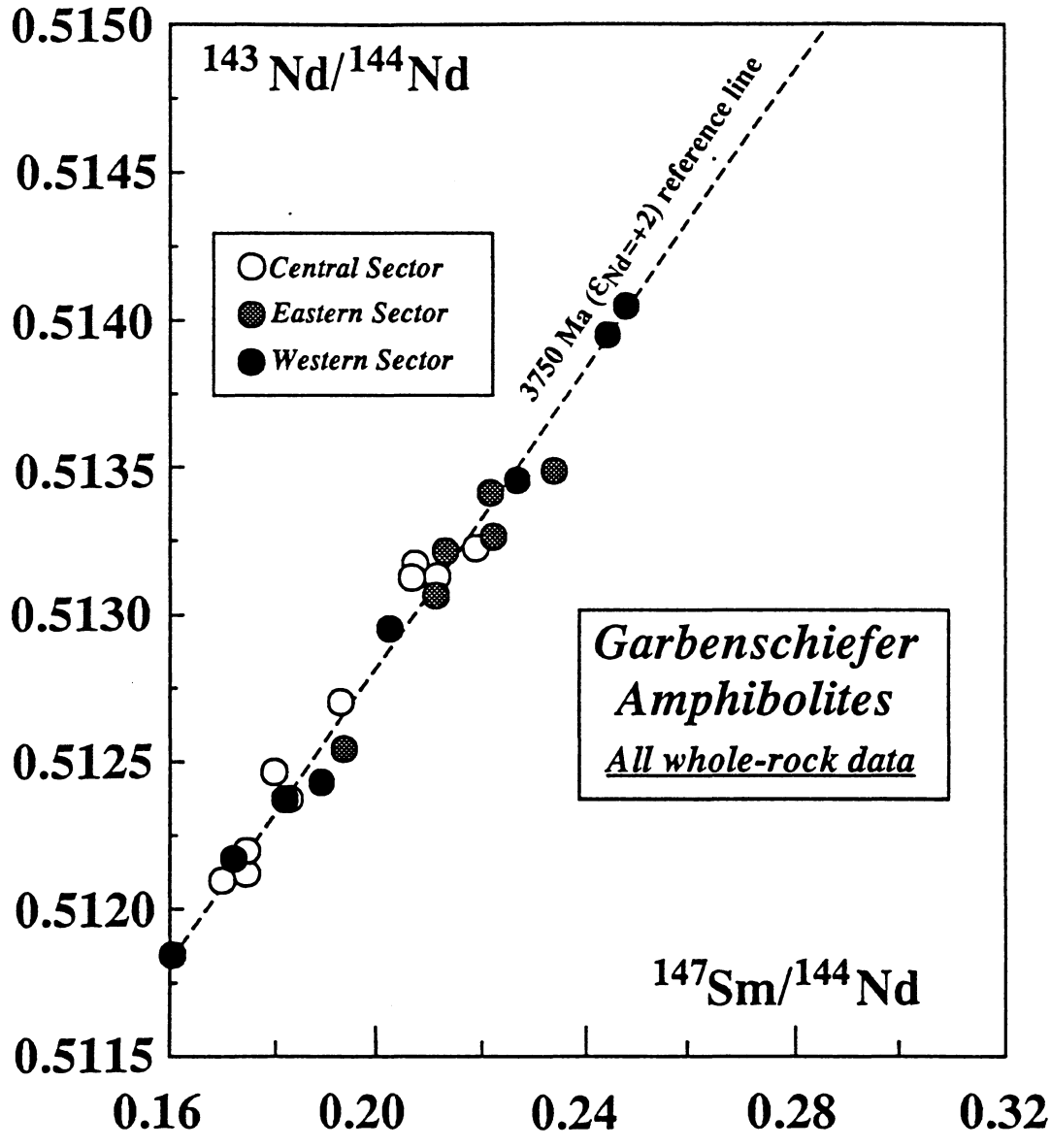

Figure 2: Sm-Nd isochron diagram for Garbenschiefer Amphibolite Unit whole-rock samples. Data sources: this study; Hamilton et al. [1].

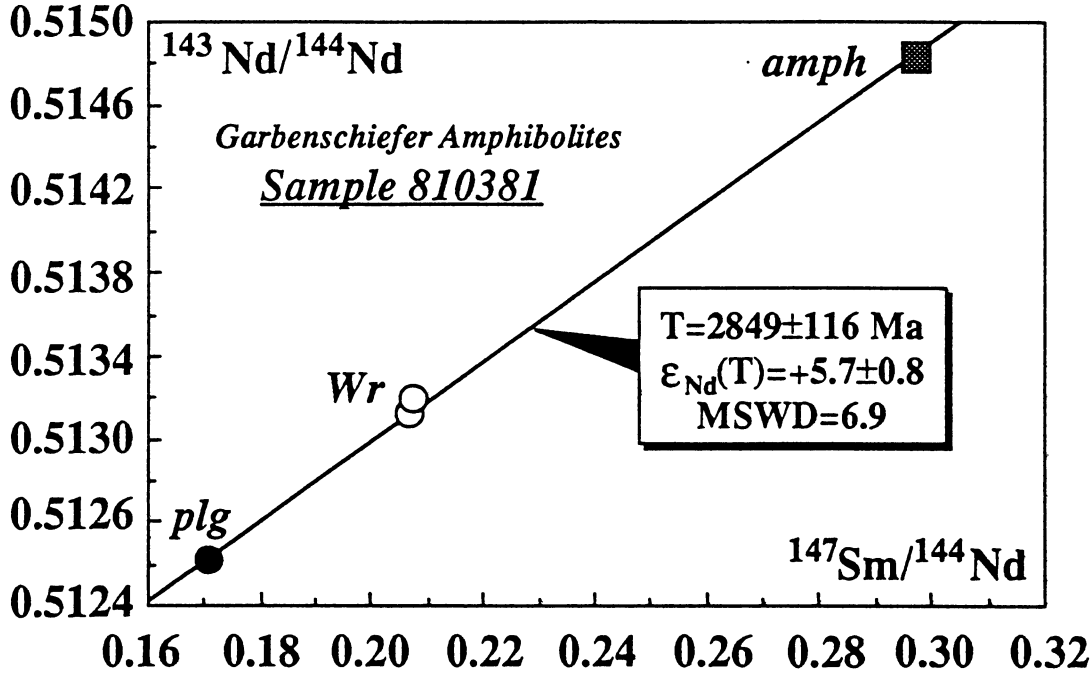

Figure 3: Sm-Nd isochron diagram for plagioclase (plg), amphibole (amph) and whole-rock (Wr) of sample 810381, Garbenschiefer Amphibolite Unit, central sector of the Isua Supracrustal Belt.

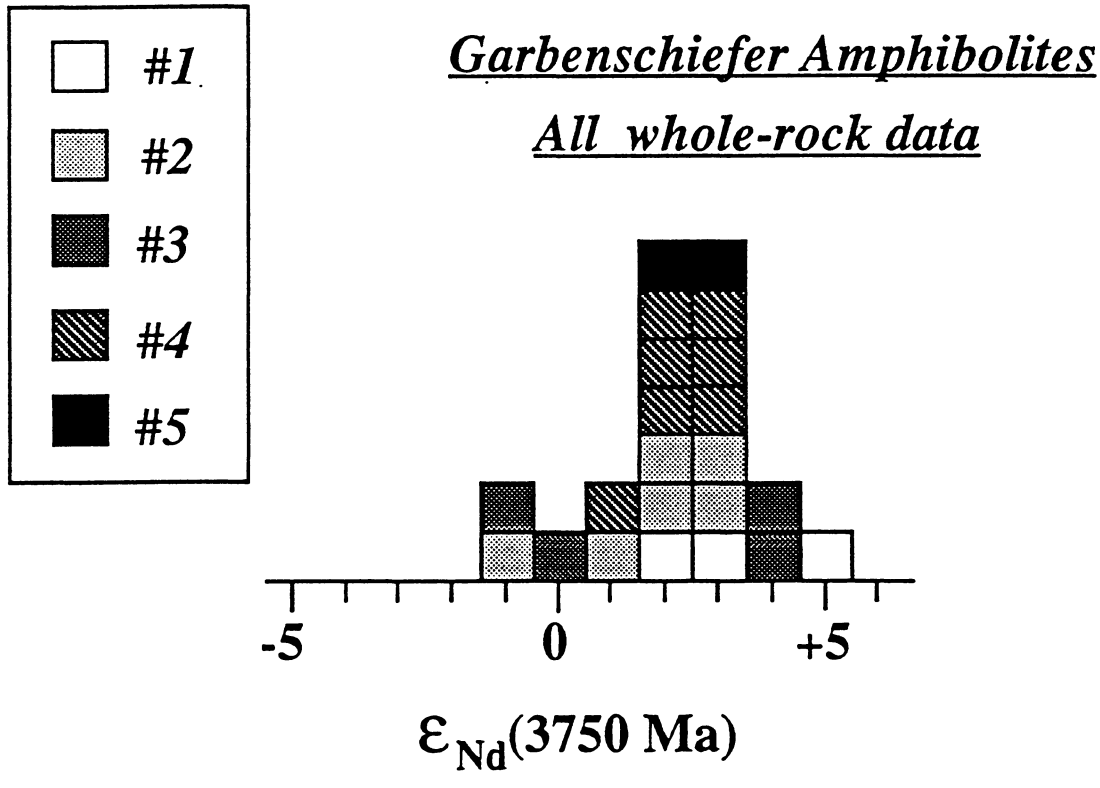

Figure 4: Frequency histogram showing distribution of calculated $\varepsilon_{Nd}(3750)$ values in Garbenschiefer Amphibolite Unit whole-rock samples. #1 to #5: type of metamorphic assemblage present in the analysed samples. Data sources: this study; Hamilton et al. [1].

2). Duplicate analyses of sample 810381 during the course of this study also produced consistent results, even though slight systematic shifts (correlated) were obtained on both the $^{147}Sm/^{144}Nd$ (0.3%) and $^{143}Nd/^{144}Nd$ ratio (0.01%).

2) Previous studies [1,13] have already indicated that measured Sm-Nd isotopic ratios in the GAU exhibit fairly large variations on the whole-rock scale ($^{143}Nd/^{144}Nd$ = 0.511853-0.514038; $^{147}Sm/^{144}Nd$ = 0.160-0.248). This is confirmed by the present results: $^{143}Nd/^{144}Nd$ = 0.512108-0.513438; $^{147}Sm/^{144}Nd$ = 0.170-0.234 (Table 2).

3) As can be seen on Fig. 2, neither samples from one given locality (10 m scale) nor the entire sample suite (km scale) define isochrons when plotted on the conventional $^{143}Nd/^{144}Nd$ vs. $^{147}Sm/^{144}Nd$ diagram (Fig. 2). If all the data are pooled together, the statistical regression gives an age (T) of 3640 ± 275 Ma, with a MSWD value of 32 . By comparison, the results of Hamilton et al. [1] yield an age (T) of 3755 ± 205 Ma with a MSWD value of 19. If samples from one given locality are pooled and regressed separately, the following results are obtained: T = 3531 ± 253 (MSWD = 7) for samples 1755XX; T = 4074 ± 944 Ma (MSWD = 9) for samples 2426XX; T = 2031 ± 1488 Ma (MSWD = 32) for samples 24271Xa,c.

In Table 2, we took 3750 Ma as the age of magmatic crystallization and calculated the model initial ε_{Nd} value of each individual whole-rock sample assuming closed-system growth since 3750 Ma. Calculated $\varepsilon_{Nd}(3750)$ values range from -0.9 to +5.3, with all but two of the samples having a value greater than zero. Similar ranges are found for the upper and lower age limits (-1.1 to +5.3 for T = 3800 Ma; -0.6 to +5.4 for T = 3700 Ma); again, only two samples yield negative values. In fact, the positive and variable $\varepsilon_{Nd}(T)$ values change little with the assumed age of crystallization, since many of the $^{147}Sm/^{144}Nd$ ratios are close to chondritic.

4) Results for samples 810381 (whole-rock + plagioclase + amphibole) define a linear array when plotted on the conventional $^{143}Nd/^{144}Nd$ vs. $^{147}Sm/^{144}Nd$ isochron diagram (Fig. 3). A regression of the data yields an age of 2849 ± 116 Ma (MSWD = 6.9) and an initial ε_{Nd} value of +5.7 ± 0.8.

5) The newly obtained whole-rock $\varepsilon_{Nd}(T)$ values are presented on a histogram (Fig. 4), along with results published earlier for the same unit [1]. Two important points should be stressed. Firstly, high (> +3.5) and low values (< +1.5) are relatively infrequent; many values (13 among 22) are in fact intermediate, in the range +1.5 to +3.5 (see also Table 2). Secondly, there is no relationship between the calculated $\varepsilon_{Nd}(T)$ values and the mineralogy of the samples. Instead, the distribution of $\varepsilon_{Nd}(T)$ values is random, with the extreme values being observed in type #1 (+5.3), type #2 (-0.5) and type #3 (-0.9) samples.

5. Discussion

5.1. Modelling the effect of Sm/Nd fractionation on $\varepsilon_{Nd}(T)$ values

In order to elucidate the interpretation of the isotopic data, it is important to bear in mind the effects of possible REE mobility on model $\varepsilon_{Nd}(T)$ values. If REE mobility comes about, for example, during some secondary event such as metamorphism, then we should expect there to be some modification of the $^{143}Nd/^{144}Nd$ or $^{147}Sm/^{144}Nd$ ratio (or both at the same time) leading to changes in the calculated $\varepsilon_{Nd}(T)$ values of the rocks involved. In the following analysis, we review the effects of secondary fractionation of the $^{147}Sm/^{144}Nd$ ratio on model $\varepsilon_{Nd}(T)$ values. This is illustrated in Fig. 5 in a plot of ε_{Nd} versus time for three model whole-rock systems of ultrabasic-basic composition, where:

$$\varepsilon_{Nd}(T) = \varepsilon_{Nd}(0) - f^{Sm/Nd} * Q * T$$

with

$$\varepsilon_{Nd}(0) = ((^{143}Nd/^{144}Nd_{sample,0} / ^{143}Nd/^{144}Nd_{chondrites,0}) - 1) * 10^4$$

$$f^{Sm/Nd} = (^{147}Sm/^{144}Nd_{sample,0} / ^{147}Sm/^{144}Nd_{chondrites,0}) - 1$$

$$Q = 25.1 \; ; \; T = \text{age in Ga}$$

The reference values for chondrites at T = 0 are 0.512638 for $^{143}Nd/^{144}Nd$ and 0.1967 for $^{147}Sm/^{144}Nd$ [32]. At the age of protolith crystallization (3750 Ma), the $\varepsilon_{Nd}(T)$ value for all three whole-rock systems is taken as +2.0 (i.e. equal to the value of a depleted mantle reservoir at T_c = 3750 Ma, later evolving into the source of present-day MORB's with $\varepsilon_{Nd}(0)$ = +10 and $f^{Sm/Nd}$ = +0.088). Since the three model systems represent ultrabasic/basic rock-types, they are assigned $^{147}Sm/^{144}Nd_{T_C}$ ratios that are identical or very close to the ratios in their mantle sources. The WRI model system is given the same $f^{Sm/Nd}$ (+0.088) as its mantle source, while WR2 and WR3 have ratios of $f^{Sm/Nd}$ that deviate by 10% from this value (+0.197 and -0.021, respectively). From the time of protolith crystallization (T_c) to the metamorphic perturbation (T_m), the three model whole-rocks evolved as closed systems.

The whole-rock systems were metamorphosed at T_m = 2800 Ma, the recrystallization being accompanied by modifications in their $^{147}Sm/^{144}Nd$ ratios. On Fig. 5, these modifications are apparent as changes in slope of the isotopic

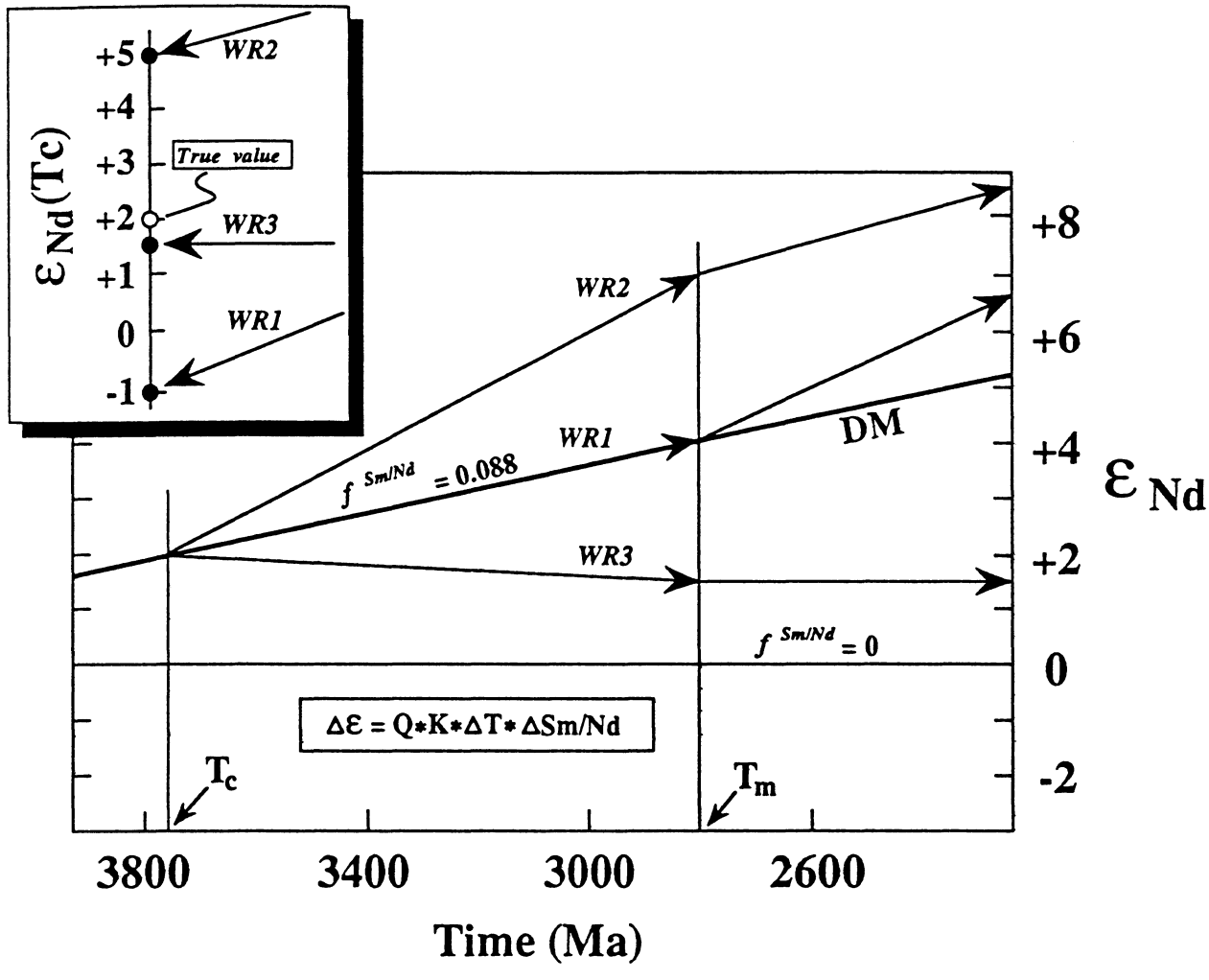

Figure 5: Diagram showing possible effects of secondary fractionation of $^{147}Sm/^{144}Nd$ ratios on the $\varepsilon_{Nd}(T)$ values of three cogenetic whole-rock systems. Samples are derived from depleted-mantle with $\varepsilon_{Nd}(T) \approx +2.0$, and the secondary fractionation of their $^{147}Sm/^{144}Nd$ ratios is assumed to occur ≈ 1 Ga after their initial magmatic crystallization. The box shows that, over this time interval, fractionations of ± 10% of the $^{147}Sm/^{144}Nd$ ratios will result in apparent $\varepsilon_{Nd}(T)$ values ranging from -1.0 to +6.0.

growth curves: system WRI undergoes a relative loss of LREEs (increase of $^{147}Sm/^{144}Nd$ ratio), whereas systems WR2 and WR3 show a gain (decrease of $^{147}Sm/^{144}Nd$ ratio). This syn-metamorphic REE fractionation is of moderate amplitude: +10% for WR1 ($f^{Sm/Nd} = 0.197$), -10% for WR2 ($f^{Sm/Nd} = 0.088$) and - 2% for WR3 ($f^{Sm/Nd} = 0$). Between $T_m = 2800$ Ma and the present-day, the three whole-rocks resumed a closed system type behaviour.

Generally speaking, any scenario of the type illustrated by Fig. 5 will give rise to two main consequences in natural systems:

1) The model $\varepsilon_{Nd}(T_c)$ values calculated for whole-rocks differ from their real $\varepsilon_{Nd}(T_c)$ values.

2) Production of an apparent spread in initial isotopic compositions in a given suite of rocks that, in reality, shared the same ε_{Nd} value at the time of their emplacement.

The deviations which exist between the calculated apparent $\varepsilon_{Nd}(T_c)$ values and the real $\varepsilon_{Nd}(T_c)$ values are given by the following equation (see also [34]):

$$\Delta\varepsilon = \Delta Sm/Nd * Q * K * (T_c - T_m)$$

where $\Delta\varepsilon$ is the difference between the real and apparent values expressed in units of ε_{Nd}, $\Delta Sm/Nd$ is the relative variation of $^{147}Sm/^{144}Nd$ ratio brought about by a perturbation at time T_m and K is the ratio between $^{147}Sm/^{144}Nd$ in the pre-metamorphic protolith and chondritic $^{147}Sm/^{144}Nd$. A value of 25.1 is used for Q, whereas T_m and T_c refer, respectively, to the ages (in Ga) of protolith crystallization and subsequent metamorphism.

The most important point arising from this equation is that, for an identical change in $^{147}Sm/^{144}Nd$ ratio, the difference ($\Delta\varepsilon$) between the apparent calculated and real values of $\varepsilon_{Nd}(T_c)$ becomes larger as the time interval increases between the initial crystallization age of the rocks and their metamorphic perturbation. Moreover, it is clear that a decrease in $^{147}Sm/^{144}Nd$ ratio leads to a $\varepsilon_{Nd}(T_c)_{app}$ value that is higher than $\varepsilon_{Nd}(T_c)_{real}$ ($\Delta\varepsilon > 0$), whereas an increase produces the opposite effect: $\varepsilon_{Nd}(T_c)_{app} < \varepsilon_{Nd}(T_c)_{real}$.

In the context of the model depicted in Fig. 5, where $T_c - T_m = 1$ Ga, the upper left box shows that a 10% decrease of the $^{147}Sm/^{144}Nd$ ratio in WR1 produces - over this time interval - a $\varepsilon_{Nd}(T_c)_{app}$ value which is lower than $\varepsilon_{Nd}(T_c)_{real}$ by three units ($\Delta\varepsilon = -3$). For a 10% increase in $^{147}Sm/^{144}Nd$ (WR2), the difference becomes +3 ε_{Nd} units ($\varepsilon_{Nd}(T_c)_{app} = +5$), while a 2% increase in $^{147}Sm/^{144}Nd$ (WR3) generates a deviation of only -0.5 units ($\varepsilon_{Nd}(T_c)_{app} = +1.5$). The net result of this secondary fractionation is the emergence of a wide spread of model $\varepsilon_{Nd}(T_c)$

values (-1.0 to +5.0) in a set of samples that shared the same initial $\varepsilon_{Nd}(T_c)$ of +2.0. If the T_c - T_m interval is taken as only 0.1 Ga, then the difference in initial ε_{Nd} values is reduced to -0.3 units for WR1, +0.3 units for WR2 and -0.05 units for WR3. The total range of $\varepsilon_{Nd}(T_c)_{app}$ is itself diminished by a factor of ten (-1.7 to +2.3).

5.2. Discussion and interpretation of results

There are two main differences between the whole-rock data presented here and the data previously obtained by Hamilton et al. [1]. Firstly, the range of $\varepsilon_{Nd}(T)$ calculated here is two times greater than in previous studies (6 units compared with 3.5). Secondly, the earlier study (op. cit.) reports a maximum $\varepsilon_{Nd}(T)$ of + 3.1, whereas a maximum of + 5.3 was obtained in the present study; minimum values are practically the same in both studies, being of the order of -1.0 (Table 2).

As already mentioned in the introduction, Hamilton et al. [1] proposed two hypotheses to account for the spread of $\varepsilon_{Nd}(T)$ values obtained from the GAU: either the Sm-Nd pairs behaved as open systems (i.e. the observed spread is an apparent range), or the initial $^{143}Nd/^{144}Nd$ ratios in the parental magmas were variable due to contamination from more ancient crustal materials (i.e. the observed range reflects a true heterogeneity in initial isotopic compositions). In their study, Hamilton et al. [1] recognized metamorphic events at 3600, 2900-2800 and 1800-1600 Ma, admitting that such events could have affected whole-rock Sm-Nd systematics in the GAU. However, they did not clearly advocate an explanation for the spread in $\varepsilon_{Nd}(T)$ values, instead stating: "the preferred interpretation is that the Garbenschiefer unit was derived from a source with positive $\varepsilon_{Nd}(T)$ at the time of its emplacement, and that the low $\varepsilon_{Nd}(T)$ values reflect post-emplacement perturbation of the Sm-Nd system".

It should be borne in mind that, at the time Hamilton et al. [1] carried out their analyses, thermal events at 2900-2800 and 1800-1600 Ma were considered as having only a minor impact in the region. Some authors [e.g., 24-25] even went so far as to claim that the amphibolite-facies parageneses seen at Isua were formed 3600 Ma ago. Subsequent studies have clarified the situation, to the extent that the important role played by younger thermal events is now generally accepted; in fact, the amphibolite-facies metamorphism at Isua is currently thought to be mid-Archaean in age (2900-2800 Ma) rather than early Archaean. Three arguments support this interpretation:

1) The mid-Archaean (3200-3100 Ma) Tassartôq dykes, which cross-cut the Isua region, display assemblages (hornblende + plagioclase + quartz ± garnet) indicating

recrystallization in the amphibolite facies [4]. The linear fabrics in these amphibolites have been correlated with similar fabrics observed in certain metapelitic rocks of the ISB containing biotite + staurotite + muscovite + quartz; the same rock-types have yielded an equilibrium temperature of 541 ± 43°C [24-25].

2) Certain galenas from the ISB define secondary Pb-Pb isochron ages in the range 2.76-2.89 Ga; these ages are interpreted as representing episodes of lead migration in the shear-zones that now contain galena [5]. Furthermore, U-Pb results obtained by ion-probe analysis of zircons from the "conglomeratic metavolcanic" unit of the ISB have revealed that some of the zircons underwent lead loss over an interval of time from 3000 to 2500 Ma [23].

3) Finally, the Sm-Nd mineral isochron presented here (Fig. 3; whole-rock + plagioclase + amphibole from sample 810381) yields a mid-Archaean age (2849 ± 116 Ma) rather than an early Archaean age. It should be noted that the mineral assemblage of sample 810381 is the earliest recognizable metamorphic paragenesis in the GAU (c.f. assemblage #1), yielding pressure-temperature estimates of the order of 5.5 kb at 600°C [3].

Thus, it appears that an interval of 1 Ga elapsed between emplacement of the GAU protolith (ca. 3750 Ma) and its metamorphism in the amphibolite facies (2900-2800 Ma). Moreover, the mineral isochron obtained from sample 810381 (Fig. 3) demonstrates that the REE were mobile in this unit during metamorphism, at least on the scale of the whole-rock. In addition to these considerations, it is very likely that the GAU represents the remains of a basic sill or dyke [3, 19], that is to say, an intrusive igneous body in which isotopic homogeneity was prevalent during emplacement on the scale of the whole-rock. In that case, we may assume that the $\varepsilon_{Nd}(T)$ values in this unit display an apparent heterogeneity due to the perturbation of Sm-Nd whole-rock systems during metamorphism at 2900-2800 Ma.

At this stage, it is useful to recall the model system (Fig. 5) described in the previous section. Ignoring the contribution of accessory mineral phases such as rutile or kyanite on the REE mass balance, the GAU whole-rock systems may be simplified to a two-component system with plagioclase and amphibole. As shown in Table 2 and Fig. 3, these two minerals have strongly contrasting $^{147}Sm/^{144}Nd$ ratios (0.1710 and 0.2975, respectively), which corresponds to a variation of 75%. Let us assume that local compositional variations existed within the GAU, for example, due to the development of differring proportions of amphibole and plagioclase in adjacent whole-rock systems. In such a context, the mobility of the REE could bring about a fractionation of about 10% in the $^{147}Sm/^{144}Nd$, thus leading to the modifications in $\varepsilon_{Nd}(T)$ illustrated on Fig. 5.

In fact, it should be stressed that the GAU is an extremely heterogeneous body in terms of major element composition. This is particularly the case with MgO, CaO and Al_2O_3, in other words, those oxides forming the major components of mineral phases such as amphibole and plagioclase. The contents of these three oxides vary widely from one sample to another, with ranges of 7-22% for MgO, 4-12% for CaO and 10-20% for Al_2O_3 [3,19]. Thus, it is entirely possible that differences in modal abundance of amphibole and plagioclase existed on the small-scale within this unit during recrystallization. Moreover, Gruau et al. [11] have shown recently that mineralogical control on $^{147}Sm/^{144}Nd$ ratios - as invoked in the present model - occurred during the metamorphism of komatiites in the Siivikkovaara area of eastern Finland. This effect arises from variations in modal composition of the rocks, which leads to a secondary fractionation of $^{147}Sm/^{144}Nd$ ratios.

Let us examine the alternative hypothesis of no secondary REE fractionation, i.e. the initial range of ε_{Nd} values (6 units) results from an original isotopic heterogeneity arising from contamination of the parent magma by more ancient crustal materials [1]. Such a hypothesis implies, in the absence of later resetting, the existence of a mantle component with $\varepsilon_{Nd}(3750) \geq +5.0$ ($^{147}Sm/^{144}Nd > CHUR$) and a crustal component with $\varepsilon_{Nd}(3750) \leq -1.0$ ($^{147}Sm/^{144}Nd < CHUR$); these two end-members would have to be mixed together in order to form the protolith magma of the GAU.

Two important objections can be made against the second hypothesis:

1) On the one hand, there is no evidence in the Isua area of a crustal component having a $\varepsilon_{Nd}(3750)$ value equal to or less than -1.0. As can be seen from Fig. 6, all analyses carried out to date - whether on the clastic metasediments or the Amîtsoq grey gneiss - have yielded $\varepsilon_{Nd}(T)$ values which are higher than the pre-3.8 Ga crust, lying in the range -0.5 to +3.5 for the clastics metasediments and +0.8 to +2.3 for the gneisses [1, 2, 13, 14, 18, 13].

2) On the other hand, the analysed samples do not define any geochemical or isotopic correlations consistent with a magmatic contamination hypothesis. In a mixing hypothesis, a broad positive correlation is to be expected between $^{147}Sm/^{144}Nd$ and $\varepsilon_{Nd}(3750)$; on the contrary, the variation of these two parameters in the GAU appears totally random (Table 2). The sample having the lowest $\varepsilon_{Nd}(3750)$ value (-0.9) should, in principle, show the greatest degree of contamination from a crustal component with low $\varepsilon_{Nd}(3750)$ and low $^{147}Sm/^{144}Nd$ ratio. In fact, this sample has one of the highest $^{147}Sm/^{144}Nd$ ratios in the entire set of analyses (0.2337).

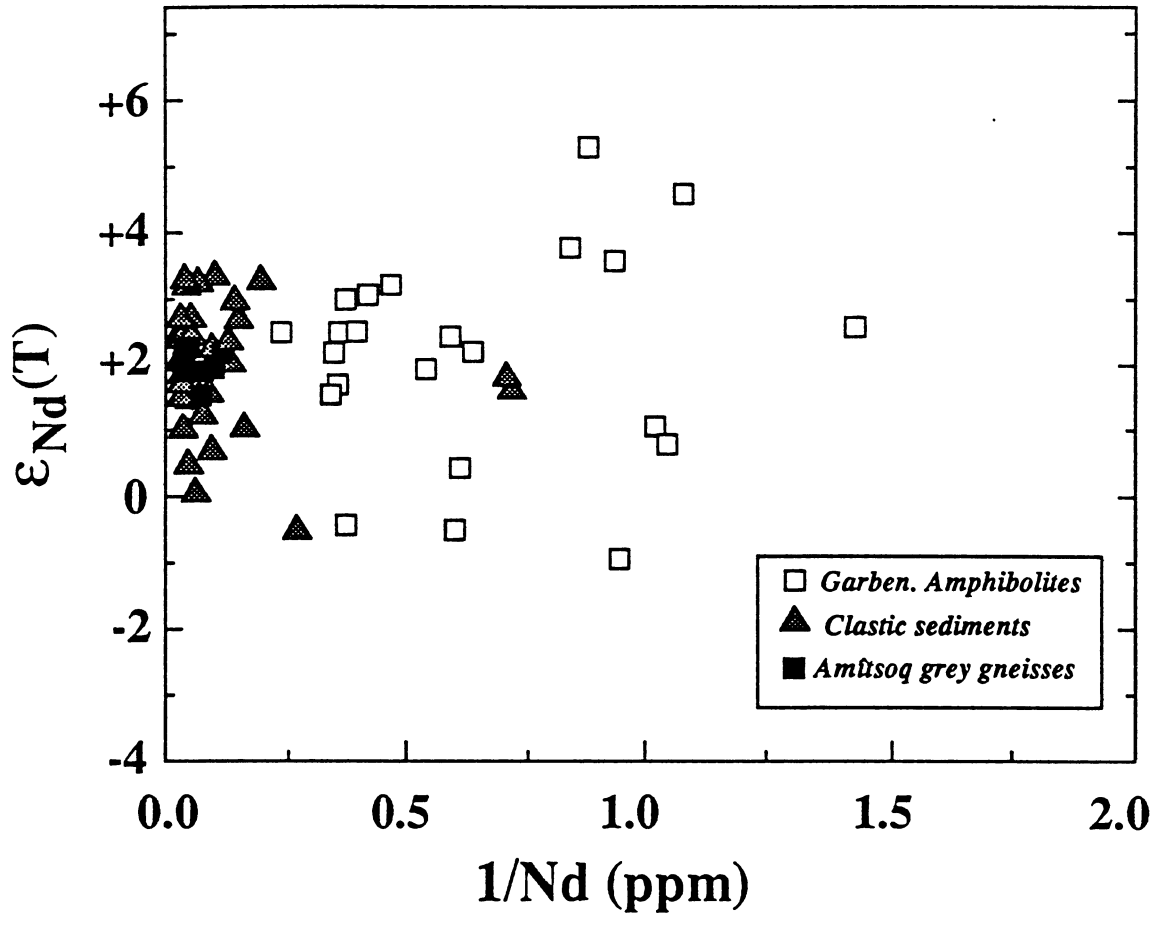

Figure 6: $\varepsilon_{Nd}(T)$ vs. 1/Nd (ppm) diagram comparing results from the Garbenschiefer Amphibolite Unit (T=3750 Ma), Isua clastic metasediments (T=3750 Ma) and Amîtsoq grey gneisses (T=3700 Ma). Data sources; this study; Hamilton et al. [1, 13]; Baadsgaard et al. [18]; Moorbath et al. [14]; Jacobsen and Dymeck [2].

We conclude that local modifications in $^{147}Sm/^{144}Nd$ ratio came about in the GAU during a metamorphic event at 2900-2800 Ma, thus explaining the great variability of calculated $\varepsilon_{Nd}(3750)$ values in this unit

6. Comparison with other Isua rocks: implication for early terrestrial evolution

Two important questions remain unresolved:

- What was the original $\varepsilon_{Nd}(3750)$ value of the GAU protolith?

- Did other rocks of the Isua area undergo perturbations of their Sm-Nd systematics during the metamorphic event at 2900-2800 Ma, and if so, what significance should be attached to their $\varepsilon_{Nd}(T)$ values?

To address the first question, more information needs to be obtained on the precise process by which the $^{147}Sm/^{144}Nd$ ratios are modified. If it takes place through internal fractionation alone, with no exchange outside the system, then the LREEs are partitioned between adjacent recrystallizing phases such as amphibole and plagioclase. Provided that the entire GAU has not suffered any net loss or gain of LREEs, the minimum and maximum calculated values of -1.0 and +5.0 should represent the lower and upper brackets for the original $\varepsilon_{Nd}(3750)$ value in the GAU protolith (Hypothesis A; see Fig. 5). If, by contrast, there has been an overall flux of LREEs on the scale of the GAU (Hypothesis B), then the true value of the original $\varepsilon_{Nd}(3750)$ should be sought either towards the top of the range ($\varepsilon_{Nd}(3750) \geq +5.0$; case of overall LREE loss from the system) or near the minimum ($\varepsilon_{Nd}(3750) \leq -1.0$; case of overall LREE gain).

Two arguments may serve to eliminate Hypothesis B. Firstly, the fact that no isochron relationship is obtained on the scale of the whole-rock suggests that the REEs were not mobile over long distances (i.e. < 10 m). In the second place, isotopic exchanges involving the GAU could only take place with the Amîtsoq grey gneiss and/or the clastic country rocks. These rocks have LREE abundances 10-20 times higher than the GAU, showing ε_{Nd} values at 2840 Ma which are strongly negative (from -5 to -10). If the grey gneisses and clastic sediments had exchanged LREEs with the GAU during the 2900-2800 Ma event, mass balance considerations require that the GAU should take on the isotopic signature of its surrounding formations. However, the results reported in Table 2 show that such exchange has not occurred; most of the GAU samples have positive $\varepsilon_{Nd}(2850)$ values.

Despite the absence of major isotopic exchange, there remains no reliable way of establishing the precise value of $\varepsilon_{Nd}(3750)$ for the GAU. The representivity of the samples studied so far is crucial in assessing the overall composition of the unit. On a histogram (Fig. 3) the frequency of $\varepsilon_{Nd}(3750)$ values in the available dataset shows a peak in the class +2.0 to +3.0. The mean value obtained by pooling all the available whole-rock data is +2.2 ± 1.5 (1σ). Furthermore, there are approximately equal numbers of samples with LREE depletion (i.e. high Sm/Nd) as with LREE enrichment (i.e. low Sm/Nd) relative to chondritic composition (Table 2; [1]). Insofar as this distribution of REE patterns is free of sampling bias, it is possible that the mean value of ca. +2.0 is a relatively good approximation of the initial $\varepsilon_{Nd}(3750)$ in the Garbenschiefer Amphibolites protolith.

As regards the question of whether other Isua belt rocks have suffered perturbations of their Sm-Nd systems during subsequent metamorphism, some indication is provided by studies carried out on the BIFs. As shown by Miller and O'Nions [12], the calculated $\varepsilon_{Nd}(T)$ values for BIFs from Isua (ranging from -15.1 to +2.9) are incompatible with closed system isotopic growth from a reservoir having homogeneous ε_{Nd} at 3800-3700 Ma (c.f. early Archaean seawater). These authors [12] conclude that the opening of Sm-Nd systems in the BIFs is "most probably to be related to the young metamorphic events identified previously in the Isua area". In the light of the results presented here, it is very likely that the 2900-2800 Ma metamorphic episode recorded in the GAU is also responsible for the opening of Sm-Nd whole-rock systems in the Isua BIFs.

In the Godthåb Fjord area, 100 km to the SW of Isua, the Amîtsoq grey gneisses define a whole-rock Sm-Nd isochron with an age of 3720 ± 84 Ma and a $\varepsilon_{Nd}(T)$ value of +2.3 ± 1.2 [14]. Because of a lack of spread in $^{147}Sm/^{144}Nd$ ratios in Isua belt rocks, their correponding isochron age is less precisely determined (3662 ± 198 Ma). Since these results are in agreement with the U-Pb zircon ages of 3700 Ma, they are interpreted as representing the age of emplacement of the igneous precursors [18]. Using this age, the model $\varepsilon_{Nd}(T)$ values calculated for the Amîtsoq grey gneisses of the Isua area are relatively tightly grouped between +0.8 and +2.3. The preservation of the Sm-Nd whole-rock isochron implies that, in contradictinction to the GAU and BIF units, the Amîtsoq grey gneisses generally behaved as closed systems during the 2900-2800 Ma metamorphic event. From this, we may also infer that the $\varepsilon_{Nd}(T)$ value of +2.0 is of primary origin, indicating a LREE-depleted source for the magmas.

By contrast, the situation is quite different for the clastic metasediments of the ISB; their calculated $\varepsilon_{Nd}(T)$ values are far more variable than those obtained for the Amîtsoq grey gneisses: $\varepsilon_{Nd}(3750)$ = -0.4 to +3.4 [2, 14]. In 1988, Jacobsen and

Dymeck [2] proposed that the Sm-Nd whole-rock systems of the Isua metasediments behaved as closed systems during metamorphism at 2900-2800 Ma, thus interpreting the calculated spread in Nd isotopic ratios as a primary sedimentary signature. According to these authors (op. cit.), the wide range of $\varepsilon_{Nd}(3750)$ values calculated for the Isua metasediments can be explained by recycling of 3800 Ma-old continental crust (with $\varepsilon_{Nd}(3750) = -1.0$) combined with contributions of juvenile crust of the same age (with $\varepsilon_{Nd}(3750) = +3.5$).

In view of the present results, it appears more reasonable to assume that the Isua metasediments themselves suffered a post-depositional perturbation of their whole-rock systems, along with the BIFs and the amphibolites. The calculated $\varepsilon_{Nd}(3750)$ values for the metasediments are thus apparent rather than real; three main lines of evidence suport this interpretation:

1) Apart from the Sm-Nd data, no other isotopic evidence points to the existence of pre-3.8 Ga crustal components in the ISB. In particular, numerous U-Pb zircon studies (including ion probe analyses) carried out on the different units of the ISB as well as on the Amîtsoq gneisses have failed to confirm the presence of such a component. All the ages obtained are equal to or younger than 3800 Ma [18, 21-23].

2) Similarly, even though there is little doubt about the existence of a LREE-depleted mantle reservoir with $\varepsilon_{Nd} = +2.0$ at 3800 Ma (c.f. Amîtsoq gneisses), it is difficult to envisage a reservoir having $\varepsilon_{Nd} \geq +3.5$ at that time. In early Archaean terrains, such high values of $\varepsilon_{Nd}(T)$ have only been obtained from three localities, viz: Isua metasediments [18], ultrabasic/basic enclaves of Akilia in the Amîtsoq gneisses of SW Greenland [35] and ultrabasic/basic enclaves in the Sagleck-Hebron gneisses of Labrador [36]. In all three cases, however, there is evidence for a complex multistage tectono-metamorphic history, with thermal events occurring several hundreds of millions of years after the presumed age of magmatic crystallization [35-36].

3) Finally, a particular type of relationship is observed between model $\varepsilon_{Nd}(T)$ values and Nd contents in the Isua metasediments (Fig. 6). The samples with relatively low Nd (<20 ppm) also display the maximum variability of $\varepsilon_{Nd}(T)$ (from -0.5 to ca. +3.5), whereas the samples with high Nd contents yield $\varepsilon_{Nd}(T)$ values that are relatively closely grouped around $+2.5 \pm 0.5$ (c.f. Figs. 12 et 13 in Jacobsen and Dymeck [2]). A similar type of relation is also noted in samples from the GAU (Fig. 6). In fact, this link between spread of $\varepsilon_{Nd}(T)$ and low Nd abundances is a common feature in the ISB (Fig. 7). The maximum spread of $\varepsilon_{Nd}(T)$ in the BIFs (from -15 to +3.0) is observed at Nd < 0.5 ppm [12]. The most tightly clustered group of Nd isotopic compositions is observed in the Amîtsoq gneisses and Isua metasediments with Nd > 20 ppm ($\varepsilon_{Nd}(T) = +2.0 \pm 1.0$).

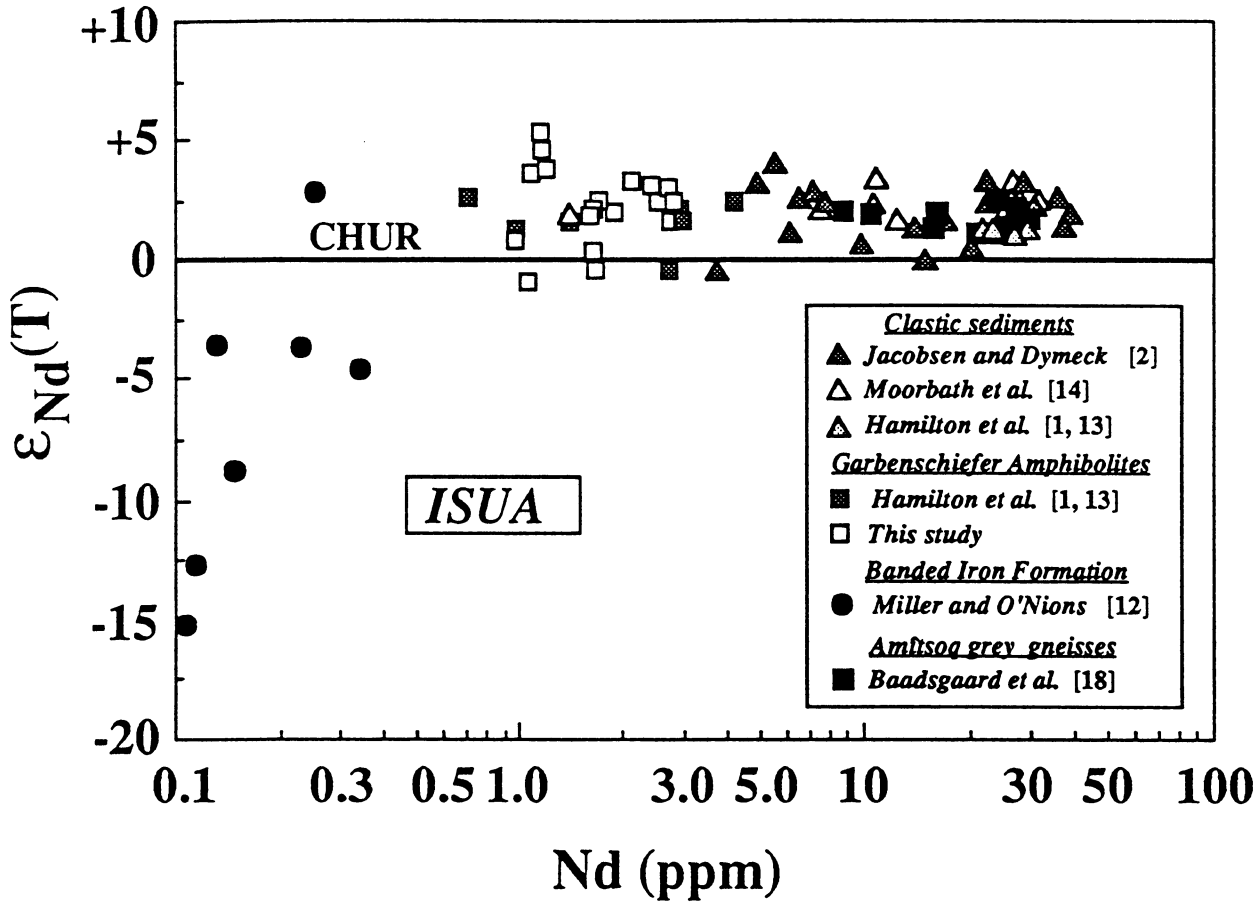

Figure 7: Diagram showing increasing variability of calculated $\varepsilon_{Nd}(T)$ values in Isua rocks with decreasing Nd concentrations. Note that T = 3700 Ma for Amîtsoq grey gneiss samples, whereas for the other samples T = 3750 Ma.

Certain factors which control the opening of Sm-Nd systems in metamorphic terrains may explain the increased scattering of $\varepsilon_{Nd}(T)$ in rocks with low Nd contents. Thus, Nd-rich rocks such as the Amîtsoq gneiss generally form accessory phases which are capable of accepting the REEs into their lattices (e.g. apatite, allanite, zircon, etc.). Furthermore, some of these phases are stable under the conditions that applied during subsequent metamorphism. Due to a mass balance effect, rocks with high Nd contents are less susceptible to possible reequilibration with Nd-poor systems. As a result, the Sm-Nd systematics of Nd-enriched rocks are less likely to be peturbed by metamorphic events. On the contrary, REE-rich accessory phases are rarely developed in Nd-depleted rocks such as the GAU. In this latter case, the REEs are more easily remobilized during metamorphic recrystallization, thus leading to more fragile Sm-Nd systematics.

7. CONCLUSION

In conclusion, it is thought that the type of relation illustrated on Fig. 7 is due to a difference in behaviour of Sm-Nd whole-rock systems in the ISB during a metamorphic event at 2900-2800 Ma. Very probably, all the rocks in this belt underwent some Nd isotopic reequilibration and/or fractionation of their $^{147}Sm/^{144}Nd$ ratios during this metamorphic episode. Nevertheless, Nd-rich rocks (> 20 ppm) - such as the Amîtsoq grey gneisses and certain metasediments of the Isua belt - are relatively resistent to secondary fractionation due to the presence of REE-acceptor phases. In view of this behaviour, only $\varepsilon_{Nd}(T)$ values calculated from rocks having Nd contents greater than 20 ppm ($\varepsilon_{Nd}(T) = +2.0 \pm 1.0$) appear to be sufficiently reliable for use in characterizing the ε_{Nd} value of the Earth's mantle at 3800 Ma.

REFERENCES

1 P.J. Hamilton, R.K. O'Nions, D. Bridgwater and A. Nutman, Sm-Nd studies of Archaean metasediments and metavolcanics from West Greenland and their implications for the Earth's early history, Earth Planet. Sci. Lett. 62, 263-272, 1983.

2 S.B. Jacobsen and R.F. Dymeck, Nd and Sr Isotope Systematics of Clastic Metasediments From Isua, West Greenland: Identification of Pre-3.8 Ga Differentiated Crustal Components, J. Geophys. Res. 93, 338-354, 1988.

3 M.T. Rosing, A metamorphic and isotopic study of the Isua supracrustals, West Greenland, Unpublished Cand. Scient Thesis, Copenhagen University, Copenhagen.

4 A.P. Nutman, The early Archaean to Proterozoic history of the Isukasia area, southern West Greenland, Rapp. Gronlands Geol. Unders. 154, 5-80, 1986.

5 J.R. Richards and P.W.U. Appel, Age of the "least radiogenic" galenas at Isua, West Greenland, Chem. Geol. 66, 181-191, 1987.

6 M.T. McCulloch and L.P. Black, Sm-Nd isotopic systematics of Enderby land granulites and evidence for the redistribution of Sm and Nd during metamorphism, Earth Planet. Sci. Lett. 71, 46-58, 1984.

7 L.P. Black and M.T. McCulloch, Evidence for isotopic equilibration of Sm-Nd whole-rock systems in early Archaean crust of Enderby Land, Antarctica, Earth Planet. Sci. Lett. 82, 15-24, 1987.

8 N.T. Arndt, N.A. Teixeira and W.M. White, Bizarre geochemistry of komatiites from the Crixas greenstone belt, Brazil, Contrib. Mineral. Petrol. 101, 187-197, 1989.

9 S. Li, S.R. Hart and T. Wu, Rb-Sr and Sm-Nd isotopic dating of an Early Precambrian spilite-keratophyre sequence in the Wutaishan area, North China: Preliminary evidence for Nd-isotopic homogeneization in the mafic and felsic lavas during low-grade metamorphism, Precambrian Res. 47, 191-203, 1990.

10 S. Tourpin, G. Gruau, S. Blais and S. Fourcade, Resetting of REE, and Nd and Sr isotopes during carbonitization of a komatiite flow from Finland, Chem. Geol. 90, 15-29, 1991.

11 G. Gruau, S. Tourpin, S. Fourcade and S. Blais, Loss of isotopic (Nd, O) and chemical (REE) memory during metamorphism of komatiites: new evidence from eastern Finland, Contrib. Mineral. Petrol. 117, 66-82, 1992.

12 R.G. Miller and R.K. O'Nions, Source of Precambrian chemical and clastic sediments, Nature 314, 325-329, 1985.

13 P.J. Hamilton, R.K. O'Nions, N.M. Evensen, D. Bridgwater and J.H. Allaart, Sm-Nd isotopic investigations of Isua supracrustals and implications for mantle evolution, Nature 272, 41-43, 1978.

14 S. Moorbath, P.N. Taylor and N.W. Jones, Dating the oldest terrestrial rocks - fact and fiction, Chem. Geol. 57, 63-86, 1986.

15 D. Bridgwater, L. Keto, V.R. McGregor and J.S. Myers, Archaean gneiss complex of Greenland, In A. Escher & W.S. Watt (Editors) Geology of Greenland, Geol. Surv. Greenland, pp. 19-75, 1976.

16 A.P. Nutman, D. Bridgwater, E. dimroth, R.C.O Gill and M. Rosing, Early (3700 Ma) Archaean rocks of the Isua supracrustal belt and adjascent gneisses, Rapp. Gronlands geol. Unders. 112, 5-22, 1983

17 A.P. Nutman, Early Archaean crustal evolution of the Isukasia area, southern West Greenland, In A. Kröner and R. Greiling (Editors), Precambrian Tectonics Illustrated, E. Schweitzerbart (Nägele & Obermiller), Stuggart, pp 79-93, 1984.

18 H. Baadsgaard, A.P. Nutman and D. Bridgwater, Geochronology and isotopic variation of the early Archaean Amitsoq gneisses of the Isukasia area, southern West Greenland, Geochim. Cosmochim. Acta 50, 2173-2183, 1986.

19 R.C.O. Gill, D. Bridgwater and J.H. Allaart, The geochemistry of the earliest known basic metavolcanic rocks, West Greenland: a preliminary investigation, Sec. Publs geol. Soc. Aust. 7, 313-325, 1982.

20 S. Moorbath, R.K. O'Nions and R.J. Pankhurst, The evolution of early precambrian crustal rocks at Isua, West Greenland, Earth Planet. Sci. Lett. 27, 229-239, 1975.

21 A. Michard-Vitrac, J. Lancelot and C.J. Allègre, U-Pb ages on single zircons from the early precambrian rocks of West Greenland and the Minnesota River Valley, Eath Planet. Sci. Lett. 35, 449-453, 1977.

22 H. Baadsgaard, A.P. Nutman, D. Bridgwater, M. Rosing, V.R. McGregor and J.H. Allaart, The zircon geochronology of the Akilia association and Isua supracrustal belt, West Greenland, Earth Planet. Sci. Lett. 68, 221-228, 1984.

23 W. Compston, P.D. Kinny, I.S. Williams and J.J. Foster, The age and Pb loss behaviour of zircons from the Isua supracrustal belt as determined by ion microprobe, Earth Planet. Sci. Lett. 80, 71-81, 1986.

24 J.L. Boak and R.F. Dymeck, Metamorphism of the ca. 3800 Ma supracrustal rocks at Isua, West Greenland: implicatiosn for early Archean crustal evolution, Earth Planet. Sci. Lett. 59, 155-176, 1982.

25 J.L. Boak, R.F. Dymeck and L.P. Gromet, Petrology and rare earth element geochemistry of clastic metasedimentary rocks from the Isua supracrustal belt, west Greenland, Rapp. Gronlands geol. Unders. 112, 23-33, 1983.

26 L.P. Black, S. Moorbath, R.J. Pankhurst and B.F. Windley, $^{207}Pb/^{206}Pb$ whole rock age of Archaean granulite facies metamorphic event in West Greenland. Nature Phys. Sci. 244, 50-53, 1973.

27 P.R.A. Wells, Late Archaean metamorphim in the Buksefjorden region, southwest Greenland. Contrib. Mineral. Petrol. 56, 229-242, 1976.

28 R.T. Pidgeon and F. Kalsbeeck, Dating of igneous and metamorphic events in th Fiskaenesset region of southern West greenland. Can. J. Earth Sci. 15, 2021-2025, 1978.

29 H. Baadsgaard, A.P. Nutman, M. Rosing, D. Bridgwater and F.J. Lonstaffe, Alteration and metamorphism of Amitsoq gneisses from the Isukasia area, West Greenland: Recommendations for isotope studies of the early crust. Geochim. Cosmochim. Acta 50, 2165-2172, 1986.

30 G. Gruau, B.M. Jahn, A.Y. Glikson, R. Davy, A.H. Hickman and C. Chauvel, Age of the Talga-talga Subgroup, Pilbara Block, Western australia, and early evolution of the mantle: new Sm-Nd isotopic evidence. Earth Planet. Sci. Lett. 8, 105-116,1987.

31 D.J. DePaolo and G.J. Wasserburg, Inferences about magma sources and mantle structure from variations of $^{143}Nd/^{144}Nd$, Geophys. Res. Lett. 3, 743-746, 1976.

32 S.B. Jacobsen and G.J. Wasserburg, Sm-Nd isotopic evolution of chondrites, Earth Planet Sci. Lett. 50, 139-155, 1980.

33 I.R. Fletcher and K.J.R. Rosman, Precise determination of initial ε_{Nd} from Sm-Nd isotopic data. Geochim. Cosmochim. Acta 46, 1983-1987, 1984.

34 M.T. Rosing, The theoritical effect of metasomatism on Sm-Nd isotopic systems, Geochim. Cosmochim. Acta 54, 1337-1341, 1990.

35 G. Gruau, A. Nutman and B.M. Jahn, Sm-Nd isotopic systematics of the Akilia association, Greenland, Terra Cognita (abs.) 204-205, 1985.

36 K.D. Collerson, L.M. Campbell, B. L. Weaver and Z.A. Palacz, Evidence for extreme mantle fractionation in early Archaean ultramafic rocks from northern Labrador, Nature 349, 209-214, 1991.

CONCLUSION

CONCLUSION

A propos de l'océan magmatique et de ses conséquences sur la structure et la composition du manteau terrestre

La première et la plus évidente des conclusions que nous dégageons de notre travail est que la variabilité géochimique (différences de rapports CaO/Al_2O_3, Al_2O_3/TiO_2 et $(Gd/Yb)_N$) observée dans les komatiites archéennes n'est pas la trace fossile d'un litage minéralogique du manteau archéen, litage qui aurait été engendré au cours de la cristallisation d'un océan magmatique terrestre profond ($P \geq 700$ km) formé il y a 4500-4400 Ma. En fait, au travers de ce résultat, se trouve une nouvelle fois posé le problème de savoir quelles conséquences exactes a eu le phénomène d'océan magmatique sur la structure du manteau terrestre. Nous avons présenté en introduction et dans l'article traitant des résultats Lu-Hf obtenus sur les komatiites de Barberton les modèles de manteau lité proposé par Othani (1988) et Othani et al. (1989). D'après ces modèles, le phénomène d'océan magmatique aurait conduit à la formation d'un manteau terrestre stratifié, comprenant une envelope externe ($P<400$ Km) dominée par l'olivine et une envelope plus profonde (400 km $< P < 700$ km) riche en grenat majorite. Il est évident que, autant l'obtention de valeurs $\varepsilon_{Hf}(T)$ négatives pour les komatiites de Barberton aurait constitué une sorte de preuve indirecte de la réalité d'une telle stratification, autant le fait que ces valeurs soient voisines de 0 peut être considéré comme un résultat témoignant de l'absence de niveaux appauvris/enrichis en grenat majorite dans le manteau de la Terre.

A ce stade, il nous parait important d'insister sur le fait que les résultats Lu-Hf que nous présentons dans ce mémoire réfutent aussi les modèles de stratification mantélique instituant la présence, dans le manteau profond (≥700 Km), d'un niveau de cumulats riches en Mg-perovskite ($MgSiO_3$). Un certain nombre d'auteurs (par exemple Agee et Walker, 1989) ont suggéré que le rapport Si/Mg (atomique) inférieur aux chondrites observé dans le manteau supérieur actuel (Si/Mg=0.78 contre 0.95 dans les chondrites du type C1) provenait du fait que, lors de la cristallisation de l'océan magmatique terrestre, il y aurait eu fractionnement et accumulation de Mg-perovskite (Si/Mg=1.15) sous la zone des 700 km (voir Fig. 3 de l'introduction). Or, comme l'ont montré Kato et al. (1988), la perovkite est une phase qui fractionne énormément le rapport Lu/Hf ($K_DHf \approx 14$; $K_DLu \approx 3$); les calculs effectués par ces auteurs montrent qu'un fractionnement de 5% de Mg-perovskite (la quantité requise pour passer d'un manteau possédant un rapport

Si/Mg de 0.95 à 0.78 est de 50%) aurait augmenté le rapport Lu/Hf du manteau supérieur de 60% par rapport à la valeur chondritique, soit une croissance isotopique pour le réservoir ainsi créé d'environ +15 unités d'ε_{Hf} par Ga. Autrement dit, un manteau supérieur appauvri en perovskite par fractionnement de ce minéral lors du refroidissement de l'océan magmatique terrestre aurait possédé une valeur ε_{Hf} de l'ordre de +15 vers 3450 Ma. Comme l'a récemment souligné Ringwood (1991), les résultats que nous obtenons sur les komatiites de Barberton ($\varepsilon_{Hf}(3450)\approx 0$) sont incompatibles avec un tel scénario (voir aussi Kato et al., 1988).

A propos de la genèse des magmas komatiitiques et de l'utilisation de ces magmas comme des traceurs de la composition du manteau archéen

La deuxième conclusion importante que nous dégageons de nos résultats est qu'il faut réviser l'idée communément admise jusqu'ici que les magmas komatiitiques se forment par de fort degrés de fusion partielle de la péridotite mantélique laissant uniquement de l'olivine au résidu. Ce point est fondamental dans la mesure où l'hypothèse d'un résidu constitué uniquement d'olivine implique que la plupart des rapports élémentaires mesurés dans ces magmas (sauf ceux incluant Mg, Fe, Si et Ni, c'est à dire les constituants de l'olivine) peuvent être considérés comme représentatifs de ceux de leurs sources, et donc être utilisés pour tracer les éventuelles hétérogénéïtés du manteau archéen. Si l'on accepte les données Lu-Hf, données qui indiquent que le grenat majorite était une phase résiduelle lors de la genèse de certains magmas komatiitiques, force nous est d'admettre que beaucoup de rapports élémentaires (e.g. La/Sm, Gd/Yb, Sm/Nd, Ti/Y ...) mesurés dans les komatiites pourront afficher des valeurs significativement différentes de celles de leurs sources mantéliques.

La démonstration que le grenat majorite était une phase résiduelle lors de la genèse de certains magmas komatiitiques a aussi des incidences sur la profondeur de fusion et l'origine ultime des matériaux qui donnaient naissance aux komatiites. En effet, le grenat majorite n'étant phase de haute température lors de la fusion mantélique qu'à des profondeurs $\geq$ 450 km, ce résultat implique que la fusion et la séparation des liquides de leur résidu solide s'opéraient à des profondeurs au moins équivalentes, voir plus importantes. Ceci veut aussi dire que les matériaux solides sources ultimes des magmas provenaient de régions encore plus profondes du manteau - peut-être de l'interface manteau-noyau (voir Jarvis et Campbell, 1983) - la grandes profondeur de naissance des diapirs mantéliques expliquant pourquoi les komatiites ont des température d'extrusion si élevées (> 1600 °C). En tout état de

cause, et nous rejoignons en cela la conclusion émise par Campbell et al. (1990), nos résultats prouvent que les komatiites sont, avant toutes choses, des traceurs de la composition du manteau profond.

A propos du comportement des éléments chimiques et des systèmes isotopiques lors du métamorphisme

La troisième conclusion qui découle de ce travail a trait à la "fragilité" des signatures géochimiques et isotopiques contenues dans les roches basiques et ultrabasiques archéennes. Les résultats obtenus sur les coulées de komatiite de Finlande montrent que le métamorphisme peut effacer l'ensemble des "signaux" géochimiques et isotopiques initialement contenus dans ces roches, y compris ceux afférent à des éléments (REEs) ou des systèmes isotopiques (Sm-Nd) réputés par ailleurs réfractaires. Nous espérons que le lecteur aura été convaincu de l'ampleur des erreurs que la non reconnaissance de ces "pertes de mémoire" peut entrainer tant au niveau de la caractérisation des sources (caractères apparents des valeurs $\varepsilon_{Nd}(T)$, modification des spectres de Terres Rares), que de la reconnaissance des phases d'altération précoce avec l'eau de mer (perte des mémoires en Oxygène). Il nous semble aussi avoir clairement établi le caractère impératif que revêt la détermination de l'âge du métamorphisme et la nécessité de conduire, en parallèle, des études sur échantillons roche-totale et sur minéraux séparés.

Ceci étant, il est clair que la perte des mémoires géochimiques primaires n'est pas un fait systématique. Très certainement, la différence de comportement observée entre les komatiites de Finlande (perte quasi-totale des mémoires magmatiques) et celles de Barberton (préservation au contraire quasi-totale de ces mêmes mémoires) est à mettre en liaison avec des différences au niveau de paramètres physico-chimiques tels que (i) la composition des fluides (présence ou non de CO_2), (ii) la perméabilité des roches, (iii) ou bien encore l'intensité de la déformation. Dans le cas précis du système Sm-Nd, il est clair aussi que la composition et la minéralogie des protolites (présence ou non de minéraux accepteurs de REEs stables dans les conditions du métamorphisme; faible ou forte concentration en Nd) influeront sur le comportement du système (cf. Isua). Quoi qu'il en soit, et nos études le démontrent, chaque ceinture de roches vertes ou chaque portion de croûte archéenne peut constituer un cas particulier vis-à-vis du problème clé de la mobilité élémentaire et/ou isotopique.

Quelle valeur ε_{Nd} dans le manteau archéen précoce?

Comme nous l'avons souligné en introduction, il y a eu dans les années récentes publication de valeurs $\varepsilon_{Nd}(T)$ très élevées (jusqu'à +4.0) pour un certain nombre de séquences de roches archéennes précoces (cf. la compilation éffectuée par Galer et al., 1989; Fig. 4 de l'introduction). A la lumière des résultats acquis dans le cadre de ce travail, il nous semble important de souligner le caractère non fiable de la plupart de ces données. Nous avons montré dans l'article traitant des résultats de l'Unité Amphibolitique Garbenschiefer que la valeur de +3.5 obtenue par Jacobsen et Dymeck (1988) sur les sédiments clastiques d'Isua entrait dans cette catégorie. Comme nous l'avons indiqué dans cet article, le même doute existe quant à la réalité des valeurs élevées publiées pour les enclaves basiques-ultrabasiques d'Akilia au Groenland (Gruau et al., 1985), et/ou de celles rapportées pour les enclaves basiques-ultrabasiques trouvées dans les gneiss de Saglek-Hebron au Labrador (Collerson et al.,1991). De même, Moorbath et al. (1986) ont montré que la valeur de +3.0, obtenue par Basu et al. (1981) pour les enclaves de TTG prélevées dans le batholite granitique le Singbhum en Inde, était entaché d'erreurs en raison d'une mauvaise prise en compte de l'âge vrai des roches. En fait, si l'on passe les données existantes au crible de critères de fiabilité tels que celui de l'obtention d'âge isochrone Sm-Nd roche-totale identique aux âges sur zircon ou bien encore l'observation dans des coulées de komatiite des valeurs $\varepsilon_{Nd}(T)$ constantes, seules deux données survivent: la valeur de +2.0 obtenue pour les gneiss d'Amîtsoq, d'âge 3700 Ma (Moorbath et al., 1986); celle de +2.5 définie par les coulées de komatiites de Schapenburg, d'âge 3450 Ma (cette thèse).

Ceci nous amène à conclure que des domaines appauvris existaient bel et bien dans le manteau Archéen précoce mais que la valeur ε_{Nd} affichée par ces domaines n'excèdait sans doute pas +2.0.

Références

Agee C.R. and D. Walker (1988) Mass balance and phase density constraints on early dfferentiation of chondritic mantle. *Earth Planet Sci Lett.* **90**, 144-156.

Basu A.R., Ray S.L., Saha A.K. and Sarkar S.N. (1981) Eastern India 3800-Million-Year old crust and early mantle differentiation. *Science* **212**, 1502-1506.

cause, et nous rejoignons en cela la conclusion émise par Campbell et al. (1990), nos résultats prouvent que les komatiites sont, avant toutes choses, des traceurs de la composition du manteau profond.

A propos du comportement des éléments chimiques et des systèmes isotopiques lors du métamorphisme

La troisième conclusion qui découle de ce travail a trait à la "fragilité" des signatures géochimiques et isotopiques contenues dans les roches basiques et ultrabasiques archéennes. Les résultats obtenus sur les coulées de komatiite de Finlande montrent que le métamorphisme peut effacer l'ensemble des "signaux" géochimiques et isotopiques initialement contenus dans ces roches, y compris ceux afférent à des éléments (REEs) ou des systèmes isotopiques (Sm-Nd) réputés par ailleurs réfractaires. Nous espérons que le lecteur aura été convaincu de l'ampleur des erreurs que la non reconnaissance de ces "pertes de mémoire" peut entrainer tant au niveau de la caractérisation des sources (caractères apparents des valeurs $\varepsilon_{Nd}(T)$, modification des spectres de Terres Rares), que de la reconnaissance des phases d'altération précoce avec l'eau de mer (perte des mémoires en Oxygène). Il nous semble aussi avoir clairement établi le caractère impératif que revêt la détermination de l'âge du métamorphisme et la nécessité de conduire, en parallèle, des études sur échantillons roche-totale et sur minéraux séparés.

Ceci étant, il est clair que la perte des mémoires géochimiques primaires n'est pas un fait systématique. Très certainement, la différence de comportement observée entre les komatiites de Finlande (perte quasi-totale des mémoires magmatiques) et celles de Barberton (préservation au contraire quasi-totale de ces mêmes mémoires) est à mettre en liaison avec des différences au niveau de paramètres physico-chimiques tels que (i) la composition des fluides (présence ou non de CO_2), (ii) la perméabilité des roches, (iii) ou bien encore l'intensité de la déformation. Dans le cas précis du système Sm-Nd, il est clair aussi que la composition et la minéralogie des protolites (présence ou non de minéraux accepteurs de REEs stables dans les conditions du métamorphisme; faible ou forte concentration en Nd) influeront sur le comportement du système (cf. Isua). Quoi qu'il en soit, et nos études le démontrent, chaque ceinture de roches vertes ou chaque portion de croûte archéenne peut constituer un cas particulier vis-à-vis du problème clé de la mobilité élémentaire et/ou isotopique.

Quelle valeur ε_{Nd} dans le manteau archéen précoce?

Comme nous l'avons souligné en introduction, il y a eu dans les années récentes publication de valeurs $\varepsilon_{Nd}(T)$ très élevées (jusqu'à +4.0) pour un certain nombre de séquences de roches archéennes précoces (cf. la compilation éffectuée par Galer et al., 1989; Fig. 4 de l'introduction). A la lumière des résultats acquis dans le cadre de ce travail, il nous semble important de souligner le caractère non fiable de la plupart de ces données. Nous avons montré dans l'article traitant des résultats de l'Unité Amphibolitique Garbenschiefer que la valeur de +3.5 obtenue par Jacobsen et Dymeck (1988) sur les sédiments clastiques d'Isua entrait dans cette catégorie. Comme nous l'avons indiqué dans cet article, le même doute existe quant à la réalité des valeurs élevées publiées pour les enclaves basiques-ultrabasiques d'Akilia au Groenland (Gruau et al., 1985), et/ou de celles rapportées pour les enclaves basiques-ultrabasiques trouvées dans les gneiss de Saglek-Hebron au Labrador (Collerson et al.,1991). De même, Moorbath et al. (1986) ont montré que la valeur de +3.0, obtenue par Basu et al. (1981) pour les enclaves de TTG prélevées dans le batholite granitique le Singbhum en Inde, était entaché d'erreurs en raison d'une mauvaise prise en compte de l'âge vrai des roches. En fait, si l'on passe les données existantes au crible de critères de fiabilité tels que celui de l'obtention d'âge isochrone Sm-Nd roche-totale identique aux âges sur zircon ou bien encore l'observation dans des coulées de komatiite des valeurs $\varepsilon_{Nd}(T)$ constantes, seules deux données survivent: la valeur de +2.0 obtenue pour les gneiss d'Amîtsoq, d'âge 3700 Ma (Moorbath et al., 1986); celle de +2.5 définie par les coulées de komatiites de Schapenburg, d'âge 3450 Ma (cette thèse).

Ceci nous amène à conclure que des domaines appauvris existaient bel et bien dans le manteau Archéen précoce mais que la valeur ε_{Nd} affichée par ces domaines n'excèdait sans doute pas +2.0.

Références

Agee C.R. and D. Walker (1988) Mass balance and phase density constraints on early dfferentiation of chondritic mantle. *Earth Planet Sci Lett.* **90**, 144-156.

Basu A.R., Ray S.L., Saha A.K. and Sarkar S.N. (1981) Eastern India 3800-Million-Year old crust and early mantle differentiation. *Science* **212**, 1502-1506.

Campbell I.H., Hill R.I. and Griffiths R.W. (1990) Melting in an Archean mantle plume: Head its basalts, tails its komatiites. Nature **337**, 697-699.

Chase C.G. and Patchett P.J. (1988) Stored mafic/ultramafic crust and early Archean mantle depletion. *Earth Planet. Sci. Lett.* **91**, 66-72.

Collerson K.D., Campbell L.M., Weaver B.L. and Z.A. Palacz (1991) Evidence for extreme mantle fractionation in early Archaean ultramafic rocks from northern Labrador. *Nature* **349**, 209-214.

Gruau G., Nutman A. and Jahn B.M. (1985) Significance of the Sm-Nd isotopic systematics of the Akilia Association. *In Early Crustal Genesis: The World's Oldest Rocks* (Abstract volume) pp. 49-52, Lunar and Planetary Institute, Houston.

Jacobsen S.B. and Dymeck R.F. (1988) Nd and Sr Isotopes Systematics of Clastic Metasediments From Isua, West Greenland: Identification of Pre-3.8 Ga Differentiated Crustal Components. *J. Geophys. Res.* **93**, 338-354.

Jarvis G.T. and Campbell I.H. (1983) Archean komatiites and geotherm: solution to an apparent contradiction. *Geophys. Res. Lett.* **10**, 1133-1136.

Kato T., Ringwood A.E. and Irifune T. (1988) Experimental determination of element partitioning between silicate perovskites, garnets and liquids: constraints on early differentiation of the mantle. *Earth Planet. Sci. Lett.* **91**, 66-72.

Moorbath S., Taylor P.N. and Jones N.W. (1986) Dating the oldest rocks - fact and fiction. *Chem. Geol.* **57**, 63-86.

Othani E.J. (1988) Chemical stratification of the mantle formed by melting in the early stage of the terrestrial evolution. *Tectonophys.* **154**, 201-210.

Ringwood A.E. (1991) Phase transformations and their bearing on the constitution and dynamics of the mantle. *Geochim Cosmochim Acta* **55**, 2083-2110.

ANNEXE

Autres travaux

Precambrian Research, 30 (1985) 63—80
Elsevier Science Publishers B.V., Amsterdam

Rb—Sr AND Sm—Nd GEOCHRONOLOGY OF LOWER PROTEROZOIC GRANITE—GREENSTONE TERRAINS IN FRENCH GUIANA, SOUTH AMERICA

GERARD GRUAU, HERVE MARTIN, BERNARD LEVEQUE and RAYMOND CAPDEVILA

CAESS, Université de Rennes, Institut de Géologie, 35042 Rennes Cedex (France)

ALAIN MAROT

BRGM, BP 552, 97302 Cayenne Cedex, Guyane (France)

(Received March 22, 1984; revision accepted January 22, 1985)

ABSTRACT

Gruau, G., Martin, H., Leveque, B., Capdevila, R. and Marot, A., 1985. Rb—Sr and Sm—Nd geochronology of lower Proterozoic granite—greenstone terrains in French Guiana, South America. Precambrian Res., 30: 63—80.

Nine samples of metavolcanic rock from the lower parts of greenstone belts in central French Guiana (the Paramaca series) and 14 granitic samples from the intrusive gneisses (the Degrad Roche and Arawa gneisses) were selected for Sm—Nd and Rb—Sr analysis.

The Sm—Nd results from the metavolcanic series (including two tholeiites, five peridotitic komatiites and two andesites) yield an isochron age of 2.11±0.09 (2 σ) Ga with an initial $^{143}Nd/^{144}Nd$ ratio (I_{Nd}) of 0.51002±9 (2 σ), corresponding to $\epsilon_{Nd}(T)$ = + 2.1±1.8. This isochron is interpreted as representing the age of initial volcanism of the Paramaca series. Acid intrusives were dated by the Rb—Sr method. A whole rock Rb—Sr isochron, including data points from both the Degrad Roche and Arawa gneisses, yields an age of 2.00±0.07 (2 σ) Ga with initial $^{87}Sr/^{86}Sr$ ratio (I_{Sr} value) of 0.7019±4 (2 σ). This result is considered to be the time of emplacement of the orthogneiss protoliths.

The positive ϵ_{Nd} value (+ 2.1 ± 1.8) obtained from the metavolcanic rocks of French Guiana suggests that their mantle sources have evolved in reservoirs slightly depleted in Light Rare Earth Elements (LREE). This result confirms the possible existence of ancient LREE-depleted reservoirs within the lower Proterozoic mantle. Moreover, the high $\epsilon_{Nd}(T)$ value for these rocks excludes any significant crustal contamination during magma genesis.

The French Guianese orthogneisses yield a low I_{Sr} value (0.7019±4 (2 σ)) which, together with geochemical considerations, suggests that their granitic protoliths could have originated by partial melting of short-lived crustal precursors of basaltic to granodioritic composition.

The present geochronological and isotopic study suggests that the Guiana Shield may represent a major continental accretion event during the lower Proterozoic.

0301-9268/85/$03.30

64

INTRODUCTION

Over the past decade, the detailed geochemical and geochronological investigation of Archaean Cratons has greatly contributed to our knowledge of the petrogenetic and geodynamic processes that were operative during the early stages of the Earth's history. Even if certain analogies can be drawn between present-day and Archaean crustal development, there is also evidence that processes of crustal differentiation during the Archaean were in some respect different from more recent phenomena. However, it is still not clear when and how ancient crustal processes typical of the Archaean began to evolve towards contemporary geodynamic processes. Although this problem of non-uniformitarian crustal evolution is relatively poorly understood, it is very probable that the transition from Archaean to present-day geodynamic regimes occurred sometime during the lower Proterozoic (e.g., De Paolo, 1981a).

In the light of such an evolution of the crust/mantle system, it would appear crucial to obtain precise data from terrains of lower Proterozoic age. From this point of view, the Guiana Shield may well provide a valuable study area — in fact, the available data suggest that this area is made up predominantly of lower Proterozoic greenstone belts and granitic intrusives (e.g., Gibbs and Barron, 1983; Bosma et al., 1983). However, a general lower Proterozoic age for the Guiana Shield cannot be assumed, and certain authors (e.g., Lima et al., 1982) have used structural and petrographic observations to infer Archaean ages for many of the granitic orthogneisses. Owing to the small quantity of reliable geochronological data actually available for the Guiana Shield, controversies over stratigraphic age assignments still continue. In certain parts of the Shield area, geochronological data are totally lacking — and this is particularly the case in French Guiana. The present study was undertaken with two main objectives — firstly to fill in the gaps in our knowledge of the age of the French Guiana basement and, secondly, to provide a basis for further geochemical and petrogenetic research. The aims of this research are:

(1) to determine the age of the volcano-sedimentary belts and associated granitic intrusives of central French Guiana by the use of the Sm—Nd and Rb—Sr methods, respectively;

(2) to elucidate the age relations of the greenstone—granite belts on the scale of the Guiana Shield;

(3) to place constraints on the petrogenesis of the orthogneiss protoliths and to characterize the nature of the lower Proterozoic mantle, source region for the basic and ultrabasic volcanism of French Guiana. The initial isotopic compositions of Nd and Sr (I_{Nd} and I_{Sr} values at time T) can be deduced from whole-rock isochrons, and the data used to constrain petrogenetic models; and

(4) to compare the geochronological and isotopic results obtained from

this basement area with analogous terrains of generally Archaean age to show whether the petrogenetic processes proposed for the Guiana Shield are intermediate in character between Archaean and presentday phenomena.

GEOLOGICAL SETTING

French Guiana is situated in the northeastern part of the Guiana Shield, which itself forms the northern margin of the South American Continent (see Fig. 1). As with the greater part of the Guiana Shield, French Guiana is made up of several orogenic belts which contain a succession of metavolcanics, metasediments and granitic gneisses. In this respect, the French Guianese basement is very similar to the greenstone belt — grey gneiss associations that are so typical of Archaean Cratons (e.g., Superior Province of the Canadian Craton; Goodwin, 1981). The essential difference between the Archaean cratons and the Guiana Shield lies in the fact that most of the dates, whether for metavolcanics or granite gneisses, indicate lower Proterozoic ages of around 2.0—2.1 Ga (Choubert, 1974; Priem et al., 1980; Gibbs and Olzewski, 1982; Gibbs and Barron, 1983; Bosma et al., 1983). The only Archaean ages that have been obtained so far in the general area lie

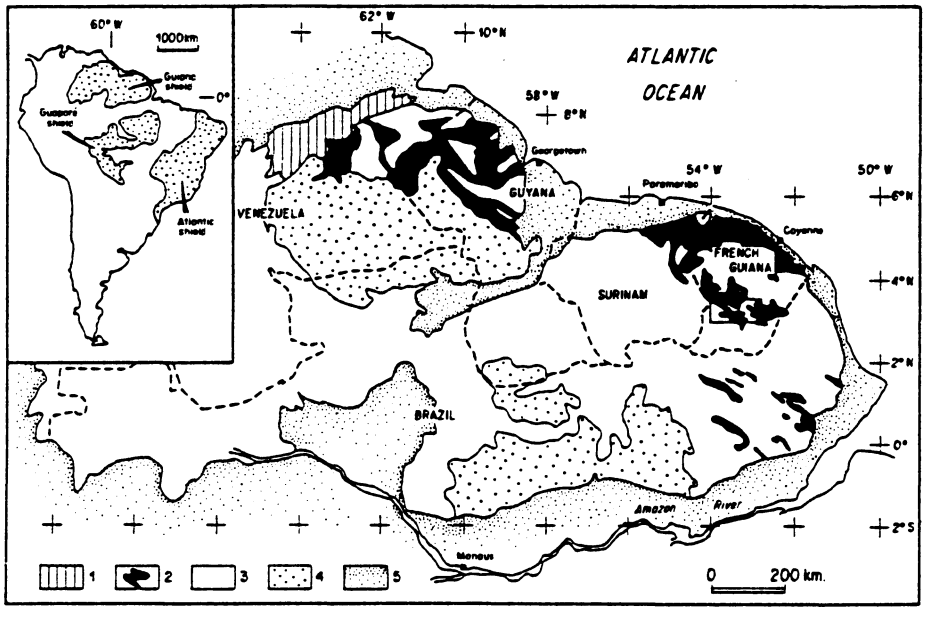

Fig. 1. Geological sketch map of the Guiana Shield (after Gibbs and Barron, 1983) showing location of French Guiana and the study area (rectangle shows limits of area shown in Fig. 2). Legend : 1. Imataca granulitic complex; 2. Greenstone belts; 3. Undivided granites, mostly of ? lower Proterozoic age; 4. Granites and volcano-sedimentary successions of mid-Proterozoic age (Uatuma orogenic cycle, Roraima Group and Urupi Formation); 5. Younger sediments.

TABLE I

Summary of the principal petrographic and geochemical characteristics of the 23 analysed samples from the Inini belt. All values quoted in this table are average values for the three series of formations concerned. Further details are available from manuscripts in preparation by Gruau et al. and Capdevila et al.

Formation of series	Sample No	Compositional Range	Texture	Mineral Paragenesis	Chemical Parameters
Arawa	H 724 — H 715 H 949 — H 718 H 721 — S 539 H 554	— Granitic	Homogeneous Gneissose	Primary : Qz + Plag. + K Felds+Biot.+Zirc. + Apat.+Musc.+Gt+Allan. Secondary : Qz + Plag. +Microcl.±Biot.±Musc.± ± epid.± calc.	SiO_2=74% Al_2O_3=14% Na_2O/K_2O = 1.6 La_N = 30 — 100 X Yb_N = 2 — 20 X $(La/Yb)_N$ = 5 — 15
Degrad Roche	H 921 — S 542 H 924 — H 706 H 104 — S 20 H 922	Tonalitic — Granodioritic	Mylonitic	Primary : Qz + Plag. +K Felds.+Biot.+Hb. +Sph.+Zirc.+Apat. + Ores Secondary : Alb. + Qz + Biot. ±Chlor.± Calc. ± Act.	SiO_2 = 66% Al_2O_3 = 15% Na_2O/K_2O = 2.5 La_N = 130 X Yb_N = 4 — 5 X $(La/Yb)_N$ = 30 — 25
PARAMACA	T 100 — M 111 T 160 — T 188 L 303	Komatiitic	Nemato-Granoblastic oriented fabric	Absence of primary igneous paragenesis Secondary = Act. + Trem.± Ilm.± Magn. ± Talc.	SiO_2 = 45% MgO = 22% TiO_2 = 0.7% CaO/Al_2O_3 = 1.1 La_N =10-30X, Yb_N = 5X $(La/Yb)_N$ = 2-6
	H 919 — R 372	Tholeiitic	Nemato-Granoblastic oriented fabric	Absence of primary igneous paragenesis Secondary : Act. + Hb + Alb+Qz+Epid.± Biot. ± Chlor.± Apat.± Calc.	SiO_2=50%; MgO= 7% TiO_2 = 1% K_2O = 0.15% La_N = 8 X; Sm_N= 10X $(La/Sm)_N$ = 0.8
	L 200 — L 365	Andesitic	Fine-grained more or less porphyroblastic	Primary:relict igneous Cpx (?) Secondary : Hb+Plag. +Biot. +Qz+Epidot. ± Sph. ±Calc.± Chor. ± Apat.	SiO_2 = 60%, MgO = 4% Al_2O_3 = 15% Na_2O=4%, K_2O=1% Sm_N = 20 X Nd_N = 40 X

in the range 2.7 — 3.5 Ga and concern the Imataca Granulite Complex of northeastern Venezuela (Hurley et al., 1976; Montgomery and Hurley, 1978; see Fig. 1).

In French Guiana, volcano-sedimentary rocks are particularly abundant in the central part of the country (see Fig. 1) where they make up, together with later plutonic intrusions, the Inini Orogenic Belt (see inset Fig. 1 and Fig. 2). Field observations and petrographic studies have led to a relative time-scale of tectonic and metamorphic events which can be used to fix the age relations of the various magmatic episodes. The pre-orogenic phase is characterized by the eruption of a suite of ultrabasic, basic, intermediate and acidic lavas, followed by the deposition of a dominantly shale-greywacke type succession. The combined thickness of the volcanic and sedimentary formations attains 4500 m, making up the Paramaca Series (Choubert, 1974). This series is considered to be the stratigraphic equivalent of the Marowijne Group observed in Surinam and the Barama-Mazaruni Super-Group of Guyana (Choudhuri, 1980).

The syn- and post-orogenic period of development is characterized by several phases of deformation and metamorphism, accompanied by the intrusion of various types of pluton. These intrusive rocks occur as sill-like bodies of banded metagabbro (occasionally showing alkaline trends) and more generally as metamorphosed gabbros, tonalites, trondjhemites, granodiorites and granites (sometimes, the late stage granitic plutons are highly potassic). The entire succession of formations within the Inini belt has been affected by several episodes of metamorphism, the highest grade being generally in the amphibolite facies, although some rare granulite facies assemblages are also observed. As a general rule, the intensity of deformation and metamorphism increases from the centre of the orogenic belt outwards towards the rim.

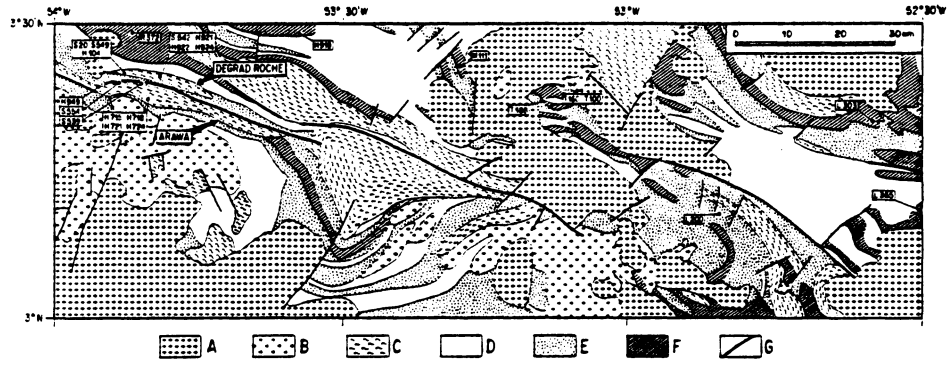

Fig. 2. Generalized geological map of the Inini Belt (inset from Fig. 1) showing samples localities. Legend : A. Post-orogenic granites; B. Post-orogenic granodiorites; C. Undivided gneisses; D—E—F. Paramaca Series; D. Mainly metasediments; E. Predominantly metavolcanics of intermediate composition; F. Ultrabasic and basic meta-volcanics; G. Major fault.

The geochronological results presented in this article have been obtained on samples of metavolcanic rocks from the Paramaca Series and on samples of granitic orthogneiss from two post-orogenic intrusions; the Degrad Roche and Arawa orthogneisses. All 23 studied samples were collected by A. Marot, R. Capdevila, C. Hocquard and B. Levèque — sampling localities are indicated in Fig. 2 and the main geochemical and petrographic characteristics are summarized in Table I.

ANALYTICAL METHODS

All Rb—Sr and Sm—Nd isotopic analyses were performed by mass spectrometric methods at the University of Rennes, according to procedures summarized in Martin et al. (1983a) and Jahn et al. (1980a,b). Elemental concentrations of Rb, Sr, Sm and Nd were determined by isotopic dilution. For the determination of Sr isotopic composition, present-day $^{87}Sr/^{86}Sr$ ratios were calculated assuming an $^{88}Sr/^{86}Sr$ ratio of 0.1194. Eight separate measurements of the $^{87}Sr/^{86}Sr$ ratio of the Standard salt NBS 987 were obtained over the period 1980—1981, yielding an average value of 0.71021+8 (2 σ). The analytical uncertainty in $^{87}Rb/^{86}Sr$ measurements is of the order of ± 2%, whereas measurements of $^{87}Sr/^{86}Sr$ are estimated at 0.05% (2 σ). The decay constant for ^{87}Rb used in age calculation is $1.42 \cdot 10^{-11}$ a^{-1}.

The methods followed for the analysis of Nd isotopes are given in Jahn et al. (1980b), and all Nd isotopic data are normalized to $^{146}Nd/^{144}Nd = 0.7219$. The mean $^{143}Nd/^{144}Nd$ of 24 analysis of the Johnson--Matthey Standard (Nd_2O_3), obtained during the period 1978--1983, is 0.511123 ± 12 (2 σ). The errors for $^{147}Sm/^{144}Nd$ ratios are estimated at ± 1%. A decay constant of $6.54\ 10^{-12}$ a^{-1} for ^{147}Sm is used.

All isochron ages and errors were calculated by the method of York (1966) and errors having an associated MSWD value greater than 1.0 are quoted as 2 σ× MSWD.

RESULTS

Rb—Sr geochronology

The Arawa and Degrad Roche orthogneiss formations have been dated in this study by use of the Rb—Sr whole rock method; the analytical results are given in Table II and displayed in Figs. 3 and 4.

Seven samples of the Arawa orthogneiss were selected to obtain as wide a spread of Rb/Sr ratios as possible and the analytical points define a moderate straight-line fit on a $^{87}Sr/^{86}Sr$ versus $^{87}Rb/^{86}Sr$ isochron diagram (see Fig. 3a). The "isochron age" calculated from these seven analytical points is 2.01± 0.12 (2σ) Ga with an initial $^{87}Sr/^{86}Sr$ ratio (I_{Sr} value of 0.702± 1 (2σ). The observed scatter of points (particularly sample H 718, see Fig. 3a) about the "errorchron" exceeds analytical uncertainty (MSWD value =

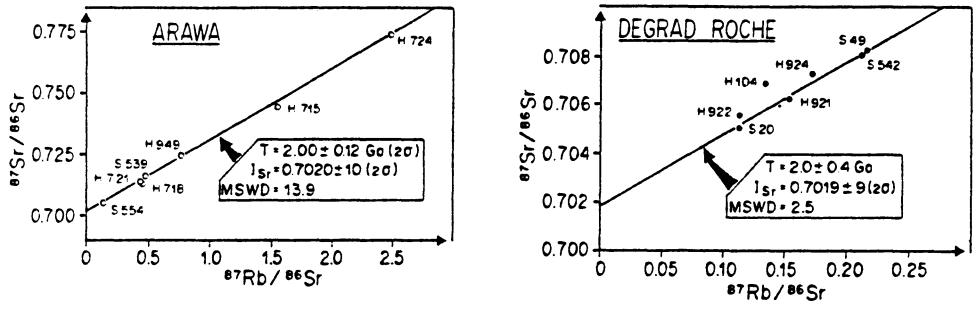

Fig. 3. Rb—Sr whole-rock isochron diagrams for the Arawa (3a) and Degrad Roche (3b) orthogneisses.

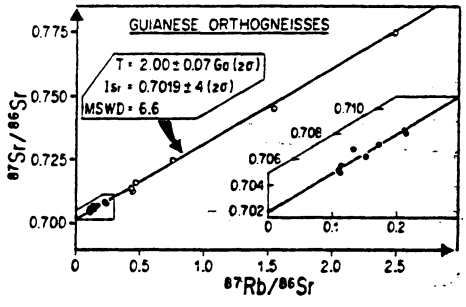

Fig. 4. Composite Rb—Sr whole-rock isochron diagram pooling analytical results from Arawa (open circles) and Degrad Roche (filled circles) orthogneisses)

TABLE II

Rb—Sr data for whole rock samples from the Degrad Roche and Arawa orthogneiss formations

Formation	Sample No	Rb(p.p.m.)	Sr(p.p.m.)	$^{87}Rb/^{86}Sr$[1]	$^{87}Sr/^{86}Sr$[2]
	H 724	138.0	163.5	2.489	0.7744
	H 715	128.4	240.8	1.549	0.7451
	H 949	84.0	320.7	0.758	0.7249
Arawa	H 718	85.3	553.9	0.445	0.7128
	H 721	64.3	579.8	0.429	0.7135
	S 539	40.4	250.5	0.467	0.7163
	S 554	26.0	687.9	0.113	0.7051
	H 921	47.2	282.3	0.155	0.7063
	S 542	43.4	589.6	0.213	0.7080
	H 924	51.2	233.2	0.174	0.7073
Degrad Roche	H 104	44.4	947.0	0.136	0.7068
	H 706	47.3	630.9	0.217	0.7082
	S 20	31.2	789.9	0.114	0.7042
	M 922	38.4	968.9	0.115	0.7055

[1] Analytical error of this ratio is ±2% (2σ).
[2] Analytical error of this ratio is ±0.05% (2σ).

13.9) and could be due to late-stage open system behaviour during metamorphism of the Arawa protoliths.

As far as the Degrad Roche formation is concerned, the seven analyzed samples represent only a very small range in Rb/Sr values (see Table II), and the corresponding points do not yield a statistically valid isochron in Fig. 3b. The calculated "probable errorchron age" is 2.0± 0.4 Ga with an I_{Sr} value of 0.7019± 9 (2σ).

The Arawa and Degrad Roche orthogneisses are very similar in the field, lying within close proximity of each other (see Fig. 2). They have undergone the same series of tectonometamorphic events and, furthermore, share common petrographic characteristics. Such similarities, when taken with the Rb—Sr data presented above, suggest that the protoliths of the two formations were emplaced at the same time, with comparable homogeneous I_{Sr} values. Thus, it is reasonable to pool all the Rb—Sr data obtained from both orthogneisses to obtain a composite isochron diagram as plotted in Fig. 4. The 14 analytical points taken together yield an isochron (MSWD value = 7) which corresponds to an age of 2.00± 0.07 (2σ) Ga with an I_{Sr} value of 0.7019±4 (2 σ). This result is coherent with the results obtained separately on each orthogneiss massif, and leads to an interpretation of the 2.00± 0.07 Ga date as the age of emplacement of the magmatic protoliths for the Arawa and Degrad Roche orthogneisses.

Sm—Nd geochronology

In parallel with Rb—Sr studies on the granitic orthogneisses of the Inini Orogenic Belt, the Sm—Nd method has been applied to nine metavolcanic samples from the pre-orogenic Paramaca Series of central French Guiana. The aim of this approach has been to determine the emplacement age of the Paramaca Series, a series of ultrabasic — intermediate metavolcanics with rather limited range of Rb/Sr ratios that has suffered partial opening of the Rb—Sr isotopic system during regional metamorphism (Gruau et al., in prep.). For these reasons, the Sm—Nd method has been chosen in preference to other whole rock dating methods.

The samples chosen include five rocks of komatiitic composition, two tholeiitic and two andesitic amphibolites. Sm—Nd data obtained on these samples are presented in Table III and plotted in Fig. 5.

The nine analytical points define a fairly good linear correlation (MSWD value =3) when plotted on a $^{143}Nd/^{144}Nd$ versus $^{147}Sm/^{144}Nd$ isochron diagram. The slope of this isochron corresponds to an age of 2.11± 0.09 (2σ) Ga with an initial $^{143}Nd/^{144}Nd$ ratio (I_{Nd} value) of 0.51002 ±9 (2σ). The $\epsilon_{Nd(T)}$ value derived from this result is + 2.1 ±1.8. Even if the two andesitic samples are excluded from the calculation, the seven remaining points still yield a good fit (MSWD value = 1.1) to an isochron of 1.93± 0.11 (2σ) Ga with an I_{Nd} value of 0.5102 ±1 (2σ). The increased errors in this example are due to the more restricted range in Sm/Nd ratios inherent in chosing just the koma-

TABLE III

Sm—Nd data and model age calculations for metavolcanic samples of the Paramaca series

Sample No	Composition type	Sm (p.p.m.)	Nd (p.p.m.)	$\frac{^{147}Sm^{1}}{^{144}Nd}$	$\frac{^{143}Nd}{^{144}Nd}$	2 σm	$\epsilon_{Nd(o)}$[2]	$T_{M(Ga)}$[3]	$T_{DM(Ga)}$[4]
T 100	PK	1.656	6.54	0.1536	0.512182	38	− 9	1.6	2.2
M 111	PK	1.878	7.45	0.1534	0.512162	19	− 9	1.7	2.2
T 160	PK	1.811	6.84	0.1611	0.512302	28	− 7	1.5	2.2
T 188	PK	2.539	10.54	0.1467	0.512070	30	−11	1.7	2.2
L 303	PK	0.831	2.801	0.1805	0.512505	34	− 3	1.3	2.6
H 919	T	2.189	6.512	0.2046	0.512825	38	+ 4	3.5	—
R 372	T	2.475	7.46	0.2021	0.512781	33	+ 3	3.9	—
L 200	And.	4.69	27.65	0.1033	0.511440	16	−23	2.0	2.2
L 365	And.	4.16	20.04	0.1264	0.511722	55	−18	2.0	2.3

Symbols : PK : peridotitic komatiite; T : tholeiite; And. : andesite.

[1] Analytical error on this ratio is ±1%.

[2] $$\epsilon_{Nd(o)} = \frac{^{143}Nd/^{144}Nd\ meas - 0.51264}{0.51264} \times 10^{4}.$$

[3] $$T_{M(Ga)} = \frac{1}{\lambda^{147}Sm} Ln \left[1 + \frac{^{143}Nd/^{144}Nd\ meas - 0.51264}{^{147}Sm/^{144}Nd\ meas - 0.1967} \right]$$

where $^{147}Sm = 6.5410^{-12}\ a^{-1}$ and $T_{M(Ga)}$: Model age assuming chondritic uniform reservoir (CHUR).

[4] $T_{DM(Ga)}$ Model age assuming depleted mantle reservoir (DePaolo, 1981b). Quoted T_{DM} values are calculated by solving eqs. (6) and (7) in DePaolo (1981b). No solution is possible for the tholeiitic samples H 919 and R 372.

72

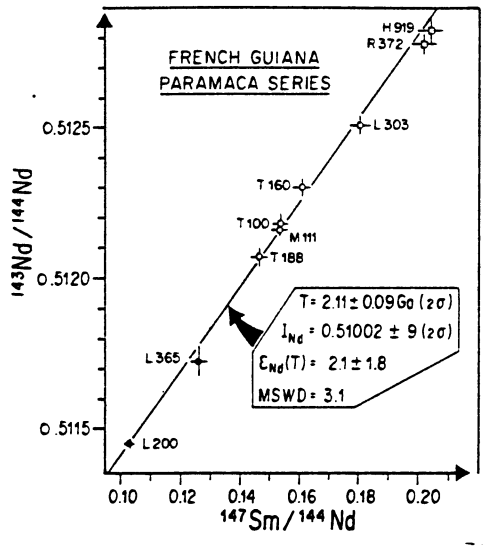

Fig. 5. Sm—Nd whole-rock isochron diagram for metavolcanics from the Paramaca series. Legend : Tholeiites □; Peridotitic komatiites ○; Andesites ●.

$$\varepsilon_{Nd} = \frac{I_{Nd(sample)} - I_{Nd(chondrite,\ T)}}{I_{Nd(chondrite,\ T)}} \times 10^4$$

when $I_{Nd(sample)}$ = initial $^{143}Nd/^{144}Nd$ isotope ratio derived from Sm—Nd isochron. $I_{Nd(chondrite,\ T)}$ = 0.50991 at T = 2.11 Ga.

tiitic and tholeiitic samples. Within the quoted error limits, this seven-point isochron is concordant and thus coherent with the result obtained from the full range of nine samples.

The Sm—Nd whole-rock method, in common with other geochronological methods, suffers from the disadvantage of requiring a wide range of parent/daughter isotope ratios in an initial system of homogeneous daughter isotopic composition. Thus, in order to obtain a wide enough range in Sm/Nd ratio, it is necessary to group together different rock-types that may not be strictly co-genetic, i.e., they may not be derived from the same parent material. As a consequence, the basic assumption in geochronology that initial systems must be co-genetic is quite often violated in practice. The present suite of samples, as well as many other examples in the literature (e.g., Hamilton et al., 1978, 1979; Zindler et al., 1978; DePaolo, 1981a; Jahn et al., 1982), is subject to the same ambiguity as regards compositional range and co-genetic origin. In fact, it is highly unlikely that the three compositional types of rock (komatiites, tholeiites and andesites) in this study could either be derived from partial melting of the same source or result from fractional crystallization of the same parent liquid. Considering the large geographical extent of the sampling area (see Fig. 2) and the wide range of Rare Earth Element (REE) abundance patterns (see Table I), it is not surprising that the metavolcanic rocks of the Paramaca Series should be of various

petrogenetic origins. Simple geochemical models, based on the REE data, show that it is impossible to derive komatiites, tholeiites and andesites cogenetically by any single process of magmatic differentiation (Gruau et al., in prep.). Thus, it is probable that the different samples studied are derived from sources of different composition which possibly also have differing I_{Nd} values.

This being the case, it might appear preferable to interpret the age of 2.11 ±0.09 (2 σ) Ga as the age of differentiation in the source-rocks rather than as the true age of magmatism. However, the good alignment of points on the isochron diagram of Fig. 5 would suggest that the magmatism occurred very close in time to the differentiation of possible sources. Furthermore, these metavolcanics are cut by later granitic orthogneisses whose protoliths were emplaced 2.00 ±0.07 (2 σ) Ga ago (Fig. 4). Hence, the 2.11+ 0.09 (2 σ) Ga Sm—Nd age obtained on metavolcanic rocks from the Paramaca series can be considered as a good estimate of the true emplacement age, despite the possibility of differentiation in the source-rocks shortly before eruption.

Apart from meta-tholeiites and meta-andesites, the Paramaca series contains volcanic rocks of komatiitic composition (viz. five analysed peridotitic komatiites of this study) which are of particular significance when comparisons are made between the Inini Belt of French Guiana and other rare occurrences of post-Archaean ultramafic lavas (e.g., Cape Smith Province, Canada, Schwarz and Fujiwara, 1977; Francis et al., 1981; Gorgona Island, Colombia; Gansser et al., 1979; Echeverria, 1980; Dietrich et al., 1981). The geochemistry and petrogenesis of the komatiites of French Guiana will be discussed elsewhere (Gruau et al., in prep.).

DISCUSSION OF RESULTS

Age of the supracrustal belts of the Guiana Shield

In addition to the determination of the emplacement age of the Paramaca Series, one of the main objectives of the present study is to place more precise constraints on the ages of the other orogenic belts within the Guiana Shield. This extrapolation of results is justified by the great similarity of structural, lithological and metamorphic characteristics between the different belts even though previously obtained geochronological data have suggested a spread in ages from 2.0—2.25 Ga. A Rb—Sr whole-rock isochron of 1.95 ±0.15 Ga has been obtained on metavolcanic rocks of the Marowijne Group in Surinam (Priem et al., 1980), whereas U-Pb dating of zircons from acid volcanics of the Barama—Mazaruni Super-Group in Guyana has yielded an age of 2.25± 0.10 Ga (Gibbs and Olszewski, 1982).

Two main hypotheses have been put forward to explain the disparity of ages obtained from the Guiana Shield basement:

(1) the Rb—Sr isochron age obtained by Priem et al. (1980) corresponds

to a re-opening of the Rb—Sr system during the trans-Amazonian metamorphic event, dated at 2.0 Ga (Hurley et al., 1968; Bosma et al., 1983).

(2) There exists a real spread of ages in the emplacement of supracrustal belts across the Guiana Shield.

Taking into account the rather large analytical errors associated with the Rb—Sr "errorchron" from the Marowijne Group and the somewhat questionable interpretation of Priem et al. (1980), it would seem that controversy over the two hypotheses is inappropriate and premature. If any age significance is to be attached to the Marowijne Group "errorchron", it should, according to Gibbs and Olszewski (1982), be interpreted in terms of a metamorphic event rather than magma emplacement. It follows from such an interpretation that the Surinam belts could have been emplaced at the same time as the Inini Belt and the Guyana belts, around 2.2—2.1 Ga ago. This idea is supported insofar as orogenic belts, usually Archaean in age, generally exhibit volcanism followed by metamorphism after an interval of about 100—200 Ma (e.g., Vidal et al., 1980; Jahn et al., 1982). In the light of this possibility, the available U—Pb, Sm—Nd and even Rb—Sr data from the Guiana Shield would all seem to confirm an age bracket of 2.1—2.2 Ga for the major period of supracrustal belt development in this area. However, by analogy with the Canadian Shield, where Archaean greenstone belts accumulated over a period of 250 Ma (i.e., 2.7—2.95 Ga; Goodwin, 1981), it is not entirely out of the question that certain parts of the Guiana Shield could contain supracrustal successions significantly older than 2.2 Ga.

Age and stratigraphic significance of granitic orthogneiss protolith emplacement

As with the greenstone belts discussed above, there is some disagreement concerning the true age and stratigraphic significance of the intrusive protoliths that have given rise to orthogneisses (such as the Arawa and Degrad Roche formations) in the Guiana Shield. Basing their arguments on the petrographic similarities between certain types of orthogneisses in the Guiana Shield and the Imataca Granulite of Venezuela (protoliths > 2.7 Ga; Montgomery and Hurley, 1978), certain authors consider that such orthogneisses are relicts of an Archaean basement on which the supracrustal belts were later developed (Martin, 1974; Cordani et al., 1979; Lima et al., 1982). By contrast, other authors use the available geochronological data to support the hypothesis that the major part of the orthogneiss protoliths of the Guiana Shield were emplaced during the lower Proterozoic, between 2.3—2.0 Ga ago (Priem et al., 1978; Gibbs and Olszewski, 1982; Gibbs and Barron, 1983).

The limited number of Rb—Sr results obtained on orthogneisses from French Guiana does not permit a general resolution of the age relations throughout the Guiana Shield, but it cannot be ruled out that ancient basement relicts of Archaean age may exist somewhere in the studied area

(Choubert, 1974). However, the present study, added to the previous work of Priem et al. (1978) and Gibbs and Olszewski (1982) and others, would tend to favour the hypothesis that most of the orthogneisses of the Guiana Shield represent intrusive protoliths that were emplaced during the lower Proterozoic.

In the Barama—Mazaruni Super-Group volcanics and neighbouring orthogneisses of the Bartica Complex of Guyana, Gibbs and Olszewski (1982) concluded that the volcanism and intrusive phases of magmatic activity in this part of the Guiana Shield took place almost simultaneously. Similarly, the present Sm—Nd and Rb—Sr results from the Paramaca series, as well as the Arawa and Degrad Roche orthogneisses, appear to show a close grouping of magmatic events, even though the indicated time bracket is 2.0—2.1 Ga rather than clustered around 2.25 Ga. In any case, due to the quite large uncertainties in age estimates — particularly for the emplacement of the Paramaca Series — it is rather unlikely that this apparent age difference has any real significance. On the other hand, there is a clearly significant difference between the age of the Bartica Complex orthogneisses of Guyana (2.23 ±0.04 Ga; Gibbs and Olszewski, 1982) and the orthogneisses of French Guiana (2.07 ±0.07 Ga; this study). This difference probably reflects the existence of several episodes of granitic intrusion in the Guiana Shield.

The contribution of Sr isotope geochemistry to petrogenetic models.

The plutonic protoliths for the French Guianese orthogneisses were emplaced with low I_{Sr} values (0.7019 ±3 (2σ)). This value is comparable with other values obtained on various other granitic plutons of the Guiana Shield (Priem et al., 1966; De Roever and Bosma, 1975; Chaudhuri, 1980). Within analytical uncertainty, the orthogneisses of the Guiana Shield have initial Sr isotope compositions which fall on an undepleted upper mantle growth curve (Main Path of Jahn and Nyquist, 1976).

The mantle-like I_{Sr} values for the Arawa and Degrad Roche orthogneisses restrict the number of possible petrogenetic models for the origin of the magmatic protoliths, and two main explanations can be proposed:

(1) the orthogneiss protoliths are derived directly from the partial melting of mantle-type material; and

(2) the protoliths are indirectly derived from the mantle by a multi-stage process involving the initial formation of a basaltic crust (amphibolites or eclogites) to produce granidioritic liquids. In this latter model, the two main stages need only be separated in time by a matter of c. 100 Ma (Jahn et al., 1981; Martin et al., 1983b).

Strontium isotope geochemistry taken alone cannot decide between direct or indirect derivation from the mantle, but it is possible, using this data, to reject any hypothesis of ancient continental crust involvement in the genesis of the granitic orthogneisses. Geochemical and petrological considerations, however, have lent considerable support to a multistage

petrogenetic model for the derivation of the igneous protoliths (Capdevila et al., in prep.).

To summarize, the mantle-like I_{Sr} values for the Guiana Shield orthogneisses and the lack of evidence for any extensive areas of Archaean basement has led to the conclusion that the major period of continental crust development in the Guiana Shield occurred during the lower Proterozoic with minimal involvement of ancient crustal material.

Contribution of Nd isotope geochemistry to petrogenetic models

The initial $^{143}Nd/^{144}Nd$ isotope ratio (I_{Nd} value) obtained for metavolcanic rocks of the Paramaca series is high (I_{Nd} = 0.51002 ±9 (2σ)) compared with the chondritic uniform reservoir (CHUR) at T = 2.1 Ga. This result corresponds to a positive $\epsilon_{Nd}(T)$ value of + 2.1± 1.8, which places important constraints on possible petrogenetic models.

The positive $\epsilon_{Nd}(T)$ value rules out the possibility of a significant contamination of the protolith magmas by ancient sialic crust and suggests that the mantle source regions for the Paramaca volcanics evolved with Sm/Nd ratios greater than CHUR for some time previous to the eruption of the series. This slight enhancement in mantle Sm/Nd ratios would correspond to a relative depletion in Light Rare Earth Elements (LREE) compared to chondritic mantle sources. From this point of view, the ultrabasic–intermediate volcanism of French Guiana provides new indirect evidence for the existence of LREE-depleted domains in the lower Proterozoic mantle (e.g., DePaolo, 1981a; Allègre, 1982; Chauvel et al., 1983).

When Sm—Nd model ages (T_{DM} in DePaolo, 1981b) are calculated, assuming an I_{Nd} value on DM, the results for komatiites and andesites are

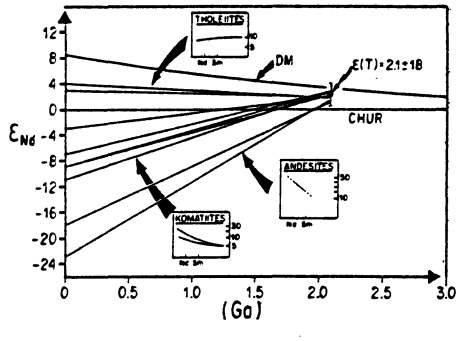

Fig. 6. Nd isotopic evolution diagram showing ϵ_{Nd} variation as a function of time for the studied samples. Schematic REE abundance patterns for each compositional type are shown as insets linked to growth lines by solid arrows. Legend : CHUR — chondritic uniform reservoir. DM — Depleted mantle evolution line (after DePaolo, 1981b). This growth curve has been calculated by use of the equation: $\epsilon_{Nd(T)DM} = 0.25^2 - 3T + 8.5$, where T is the age in Ga, and $\epsilon_{Nd(T)DM}$ is the deviation of the $^{143}Nd/^{144}Nd$ ratio in a DM reservoir compared with CHUR at time T (DePaolo, 1981b).

closely grouped around 2.27± 0.13 (σ) Ga (see Table III and Fig. 6). Taking all samples, the I_{Nd} value determined for the Paramaca series (see Fig. 6) lies between the Depleted Mantle reservoir growth curve proposed by DePaolo (1981b) and CHUR. Within analytical error, the DM reservoir can be considered as a potential source region for at least part of the volcanism in the greenstone belts of French Guiana.

From the $(La/Yb)_N$ values in Table I and the illustrated REE pattern ranges in Fig. 6, it is apparent that the komatiites of the Paramaca series have a very marked LREE enrichment relative to chondrites. Insofar as komatiite REE patterns are generally thought to reflect the REE geochemistry of their mantle source regions (e.g., Sun and Nesbitt, 1978), it is quite likely that the French Guianese komatiites were derived from mantle source regions that had suffered enrichment of the LREE. Furthermore, the constraints provided by the high $\epsilon_{Nd}(T)$ value would suggest that the metasomatic events that enriched the mantle source must have occurred, if they occurred at all, very shortly before the partial melting event that gave rise to the komatiitic magmas. Such problems will be discussed in more detail elsewhere (Gruau et al., in prep.).

CONCLUSIONS

(1) Metavolcanic rocks from the Inini greenstone—granite Belt of central French Guiana have been dated by the whole-rock Sm–Nd method, yielding an age of 2.11 ± 0.09 (2σ) Ga. This age is interpreted as representing the eruption of the Paramaca Series lavas, an age which is concordant with the U/Pb zircon age of 2.25 ±0.10 Ga obtained by Gibbs and Olszewski (1982) on the Barama—Mazaruni Super-Group of Guyana. It is proposed, from this evidence, that most of the supracrustal belts of the Guiana Shield were emplaced between 2.2 and 2.1 Ga ago.

(2) Two granitic orthogneiss formations within the Inini Belt of French Guiana (the Degrad Roche and Arawa plutonic formations) have been dated by the Rb—Sr whole-rock method. The age obtained by pooling the results from both massifs is 2.00 ± 0.07 (2 σ) Ga, an age which is interpreted as the emplacement age of their intrusive protoliths.

(3) The low initial $^{87}Sr/^{86}Sr$ isotope ratio indicated by the Rb–Sr isochron on the French Guianese orthogneisses is close to mantle-type values at 2.0 Ga on the Main Path growth curve of Jahn and Nyquist (1976). This effectively rules out the possibility that the protoliths of the Degrad Roche and Arawa orthogneisses could have been derived from the partial melting of ancient (Archaean) sialic crust. The low I_{Sr} value (0.7019 ±4 (2σ)), taken in conjunction with geochemical arguments, would tend to support an origin by partial melting of juvenile basaltic precursors that had been extracted from the mantle only 100 Ma before. Such a multistage petrogenetic model favours the hypothesis that a major phase of continental crust-building occurred in the Guiana Shield during the lower Proterozoic.

(4) The high initial $^{143}Nd/^{144}Nd$ isotope ratio (I_{Nd} = 0.51002 ± 9 (2σ)) derived from the Sm—Nd isochron on the Paramaca Series has important consequences on the geochemical evolution of the mantle source regions that gave rise to volcanism in the belt. The significant positive deviation of $I_{Nd}(T)$ from the chondritic uniform reservoir value a T = 2.1 Ga excludes any possibility of ancient continental crustal contamination and shows that LREE-depleted mantle reservoirs existed during the lower Proterozoic and contributed to greenstone belt magma genesis in French Guiana.

The present study offers new geochronological and isotopic data that cannot alone provide sufficient information to resolve the more general problem of a transition in geodynamic processes between Archaean times and the present day. Although it remains unclear whether the lower Proterozoic corresponds to a time of crucial change in crustal evolution, there are nevertheless various features in common with Archaean terrains -- i.e., presence of komatiitic lavas, close associations of gneisses with greenstone belts and character of orthogneiss protoliths. Various other characteristics of the French Guianese basement are more typical of present-day phenomena i.e., presence of metabasic rocks with alkaline affinity (Gruau et al., in prep.).

The real significance of such analogies and differences in the behaviour of the crust/mantle system through time is currently being studied at Rennes laboratory and other laboratories by the use of trace element (including REE) and isotope geochemistry.

ACKNOWLEDGEMENTS

Field studies were undertaken with the support of the BRGM; R. Capdevila and B. Levêque would particularly like to thank MM. C. Blanc, P. Dréan, C. Hocquard, A. Noesmoen and J. Testard. Equally, thanks are due to our recently deceased colleague René Charlot who generously supplied a number of Sr isotope analyses. We are also very grateful to N. Morin and J. Cornichet for their assistance in chemical separation work. Drs B. Auvray and B.M. Jahn of the Rennes laboratory have been most helpful in their discussions and critical comments on the manuscript. Finally, we are indebted to Dr. M.S.N. Carpenter, who prepared the English version of our manuscript. Research work for this study has been funded in part under contract no1517 of the INAG in connection with ATP project "Transferts".

REFERENCES

Allègre, C.J., 1982. Chemical geodynamics. Tectonophysics, 81: 109—132.

Bosma, W., Kroonenberg, S.B., Mass, K. and De Roever, E.W.F., 1983. Igneous and metamorphic complexes of the Guiana Shield in Suriname. Geol. Mijnbouw, 62: 241—254.

Chauvel, C., Hofmann, A.W. and Arndt, N.T., 1983. New evidence for early mantle depletion from Nd isotopes in greenstones. Terra Cognita, 3, p. 129 (abstract).

Choubert, B., 1974. Les Précambriens des Guyanes. Mémoires, B.R.G.M., 81, 213 pp.
Choudhuri, A., 1980. The Early Proterozoic greenstone belt of the northern Guiana Shield, South America. Precambrian Res., 13: 363—374.
Cordani, U.G., Tassinari, C.C.G., Teixeira, W., Basei, M.A.S. and Kawashita, K., 1979. Evolucao tectonica da Amazonia com base nos dados geocronologicos. Segundo Congreso Geologico Chileno, Arica, Chile, Aug. 6—11, 1979, pp. 5137- 5148.
DePaolo, D.J., 1981a. Neodymium isotopes in the Colorado Front Range and crust—mantle evolution in the Proterozoic. Nature, 291: 193—196.
DePaolo, D.J., 1981b. A Neodymium and Strontium Isotopic Study of the Mesozoic Calc-Alkaline Granitic Batholiths of the Sierra Nevada and Peninsular Range, California. J. Geophys. Res., 86: 10470—10488.
De Roever, E.W.F. and Bosma, W., 1975. Precambrian magmatism and regional metamorphism in Suriname - Anais 10 ma Conf. Geol. Interguianas, Belem, Brasil, 1: 123—163.
Dietrich, V.J., Gansser, A., Sommerauer, J. and Cameron, W.E., 1981. Paleogene komatiites from Gorgona Island, East Pacific : a primary magma for ocean floor basalts? Geochem. J., 15: 141—161.
Echeverria, L.M., 1980. Tertiary or Mesozoic komatiites from Gorgona Island, Colombia : field relations and geochemistry. Contrib. Mineral. Petrol., 73: 253—266.
Francis, D.M., Hynes, A.J., Ludden, J.N. and Bédard, J., 1981. Crystal fractionation and partial melting in the petrogenesis of a Proterozoic high-MgO volcanic suite, Ungava, Quebec. Contrib. Mineral. Petrol., 78: 27—36.
Gansser, A., Dietrich, V.J. and Cameron, W.E., 1979. Paleogene komatiites from Gorgona Island. Nature, 278: 545—546.
Gibbs, A.K. and Barron, C., 1983. The Guiana Shield Reviewed. Episodes, 2: 7—14.
Gibbs, A.K. and Olszewski, W.J., Jr., 1982. Zircon U—Pb ages of Guyana greenstone—gneiss terrane. Precambrian Res., 17: 199—214.
Goodwin, A.M., 1981. Archaean Plates and Greenstone belts. In: A. Kröner (Editor), Precambrian Plate Tectonics. Elsevier, Amsterdam, pp. 105—130.
Gruau, G., Capdevila, R., Lévêque, B. and Marot, A., 1985. Lower Proterozoic Komatiites in French Guiana: geochemistry and petrogenesis (in preparation).
Hamilton, P.J., O'Nions, R.K., Evensen, N.M., Bridgwater, D. and Allaart, J.H., 1978. Sm—Nd isotopic investigations of Isua supracrustals and implications for mantle evolution. Nature, 272: 41—43.
Hamilton, P.J., Evensen, N.M., O'Nions, R.K., Smith, H.S. and Erlank, A.J., 1979. Sm—Nd dating of Onverwacht group volcanics, Southern Africa. Nature, 279: 298—300.
Hurley, P.M., Melcher, C.C., Pinson, W.H., Jr. and Fairbairn, H.W., 1968. Some orogenic episodes in South America by K—Ar and whole-rock Rb—Sr dating. Can. J. Earth Sci., 5: 633—638.
Hurley, P.M., Fairbairn, H.W. and Gaudette, H.E., 1976. Progress report on early Archean Rocks in Liberia, Sierra Leone, and Guyana, and their general stratigraphic setting. In: B.F. Windley (Editor), The Early History of the Earth. Wiley, London, pp. 511—521.
Jahn, B.M. and Nyquist, L.E., 1976. Crustal evolution in the early Earth—Moon system : constraints from Rb/Sr studies. In: B.F. Windley (Editor), The Early History of the Earth. Wiley, London, pp. 55—76.
Jahn, B.M., Auvray, B., Blais, S., Capdevila, R., Cornichet, J., Vidal, F. and Hameurt, J., 1980a. Trace element geochemistry and petrogenesis of Finnish greenstone belts. J. Petrol., 21: 201—244.
Jahn, B.M., Bernard-Griffiths, J., Charlot, R., Cornichet, J., Vidal, F., 1980b. Nd and Sr isotopic compositions and REE abundances of cretaceous MORB (Holes 417 D and 418 A, legs 51, 52 and 53). Earth Planet. Sci. Lett., 48: 171—184.

Jahn, B.M., Glikson, A.Y., Peucat, J.J. and Hickman, A.H., 1981. REE geochemistry and geochronology of Archaean silicic volcanics and granitoids from the Pilbara block, Western Australia. Geochim. Cosmochim. Acta, 45: 1633—1652.

Jahn, B.M., Gruau, G. and Glikson, A.Y., 1982. Komatiites of the Onverwacht Group, South Africa : REE geochemistry, Sm/Nd age and Mantle Evolution. Contrib. Mineral. Petrol., 80: 25—40.

Lima, M.I.C., De Oliveira, E.P. and Tassinari, C.C.G., 1982. Cinturoes granuliticos da purçao setentrional do craton Amazonico. Anais do I Simposio de Geologia da Amazonia, Belem, Sociedade Brasilera de Geologia, Nucleo Norte, 1: 147- 162.

Martin, H., 1974. Paleotectonica del Escudo de Guyana; Memoria 9th Conferencia Geologica Inter-Guyanas, Puerto Ordaz, 1972, Venezuela. Ministerio de Minas e Hidrocarburos, Boletin de Geologia, Publication Especial no 6, pp. 251—305.

Martin, H., Chauvel, C., Jahn, B.M. and Vidal, Ph., 1983a. Rb—Sr and Sm- Nd ages and isotopic geochemistry of Archaean granodioritic gneisses from eastern Finland. Precambrian Res., 20: 79—91.

Martin, H., Chauvel, C. and Jahn, B.M., 1983b. Major and trace element geochemistry and crustal evolution of Archaean granodioritic rocks from eastern Finland. Precambrian Res., 21: 154—180.

Montgomery, C. and Hurley, P.M., 1978. Total rock U—Pb and Rb—Sr systematics in the Imataca series, Guyana Shield, Venezuela. Earth Planet. Sci. Lett., 39: 281—290.

Priem, H.N.A., Boelrijk, N.A.I.M., Verschure, R.H. and Hebeda, E.H., 1966. Isotopic age determinations on Suriname rocks, 1. Geol. Mijnbouw., 45: 16—19.

Priem, H.N.A., Boelrijk, N.A.I.M., Hebeda, E.H., Kuijper, R.P., De Roever, E.W.F., Verdumen, E.A.Th., Verschure, R.H. and Wielens, J.B., 1978. How old are the supposedly Archean charnockitic granulites in the Guiana Shield basement of western Suriname (South America)? Short Papers, U.S. Geol. Surv., Open File Rep., 78—701, pp. 341—343.

Priem, H.N.A., De Roever, E.W.F. and Bosma, W., 1980. A note on the age of the Paramaka metavolcanics in northeastern Suriname. Geol. Mijnbouw., 59: 171—173.

Vidal, P., Blais, S., Jahn, B.M. and Capdevila, R., 1980. U—Pb and Rb—Sr systematics of the Suomussalmi Archean Greenstone belt (Eastern Finland). Geochim. Cosmochim. Acta, 44: 2033—2044.

Schwarz, E.J. and Fujiwara, Y., 1977. Komatiitic basalts from the Proterozoic Cape Smith Range in northern Quebec, Canada. In: W.R.A. Baragar, L.C. Coleman and J. Hall (Editors), Volcanic Regimes of Canada. Geol. Assoc. Can., Spec. Pap., 16: 429—448.

Sun, S.S. and Nesbitt, R.W., 1978. Petrogenesis of Archaean ultrabasic and basic volcanics : evidence from rare earth elements. Contrib. Mineral. Petrol., 65: 301- 325.

York, D., 1966. Least squares fitting of a straight line. Can. J. Phys., 44: 1079—1086.

Zindler, A., Brooks, C., Arndt, N.T. and Hart, S., 1978. Nd and Sr isotope data from komatiitic and tholeiitic rocks of Munrow Township, Ontario. 4th International Conference of Geochron., Cosmochron., Isotope Geology, Geol. Surv. Open File Rep., 78-701, pp. 469—471.

Origin and Petrogenesis of the Trinity Ophiolite Complex (California): New Constraints from REE and Nd Isotope Data

by G. GRUAU, C. LECUYER, J. BERNARD-GRIFFITHS AND N. MORIN

CAESS–CNRS, Institut de Géologie, Université de Rennes, 35042 Rennes Cedex, France

ABSTRACT

Sm–Nd isotopic results, as well as concentrations of major elements and REE, are reported for nine whole-rock samples of plagioclase lherzolite, lherzolite, harzburgite, clinopyroxene-rich dykes, layered and isotropic gabbros, and a plagiogranite dyke from the central part of the Silurian Trinity Ophiolite Complex (Toad Lake area) of northern California. The data provide new constraints on the origin and petrogenesis of this ophiolite complex and have potentially important implications with regard to the origin of mid-ocean ridge basalts (MORBs) and differentiation of the oceanic lithosphere.

Although Sm–Nd isotopic data published earlier on samples from the northern (China Mountain) and southern (Gray Rock) parts of the complex yielded discordant ages and initial ε_{Nd} values for peridotites [$T = 472 \pm 32$ Myr; $\varepsilon_{Nd}(T) = +10{\cdot}4 \pm 0{\cdot}4$], and crustal rocks from the overlying magma chambers or intrusive dykes [$T \sim 440$ Myr; $\varepsilon_{Nd}(T) \sim +7{\cdot}0$], all the samples investigated in this study define a single array in the Sm–Nd isochron diagram, allowing an age of 423 ± 48 Myr and an $\varepsilon_{Nd}(T)$ value of $+6{\cdot}4 \pm 0{\cdot}7$ to be calculated. Furthermore, although the results published so far on peridotites and gabbroic dykes from Trinity indicated variable LREE depletion, all the basic–ultrabasic samples from Toad Lake are found to exhibit similar, strongly LREE-depleted patterns [$0{\cdot}17 < (Ce/Sm)_N < 0{\cdot}34$].

As elsewhere in the Trinity Ophiolite Complex, peridotites in the Toad Lake area preserved evidence of partial melting (e.g., plagioclase lenses tracking the high-temperature flow plane) and melt extraction (e.g., depleted borders along cross-cutting dykes). Comparison of the new Sm–Nd results with U–Pb zircon ages for plagiogranite samples suggests that 423 ± 48 Myr is a geologically meaningful age, corresponding to the crystallization of plagioclase lenses in plagioclase lherzolites, as well as to the crystallization of dykes and rocks of the Toad Lake magma chamber. Because of the discrepancy in Sm–Nd ages, initial $\varepsilon_{Nd}(T)$ values, and REE patterns, peridotites and crustal rocks of the Trinity Ophiolite Complex have so far been regarded as genetically unrelated. The results from Toad Lake argue for partial reassessment of this view. As far as Sm–Nd isotopic data and REE patterns are concerned, peridotites, dykes, and gabbros from this area have features consistent with a cogenetic rock suite.

Clinopyroxene-rich dykes near Toad Lake have been regarded as the remnants of the conduits which fed the magma chamber, a view which is fully confirmed by the present geochemical and isotopic results. Careful evaluation shows that these dykes have petrographic and geochemical features more representative of crystallized melts, rather than mineral segregates, hence allowing us to propose that their actual picritic composition (MgO ~ 16%) might reflect the composition of the magma which entered the Toad Lake magma chamber.

Comparison of the present results with those published earlier shows the Trinity peridotite to be an isotopically heterogeneous body. Moreover, a difference in age may exist between peridotites from the northern and southern parts of the complex. It is possible that the Trinity Ophiolite Complex represents the remnant of the opening of an ocean, perhaps in an area similar to a modern back-arc or inter-arc basin.

INTRODUCTION

If ophiolites really represent fragments of ancient oceanic crust, as is generally assumed, then the study of these rock units may provide key constraints in important problems such

[*Journal of Petrology*, Special Lherzolites Issue, pp. 229–242, 1991]

as the structure of the oceanic lithosphere or the origin and petrogenesis of mid-ocean ridge basalt (MORB). However, all ophiolites are not genetically identical, and they have been sub-divided into two groups on the basis of the mineralogical variability of their metamorphic peridotites (Nicolas, 1989): (a) the Harzburgite Ophiolite Type (HOT); and (b) the Lherzolite Ophiolite Type (LOT). The LOT comprises lherzolites, harzburgites, and dunites, whereas ultramafic rocks in the HOT are restricted to harzburgites and dunites. Among these three lithologies, only lherzolites contain sufficient amounts of Ca and Al to represent a potential source for MORB. In fact, only LOT offers the opportunity to test directly the possible partial melting relationship between fertile and depleted mantle peridotites during MORB genesis (e.g., Nicolas, 1989; see also Bodinier *et al.*, this volume).

One of the best examples of the LOT is the Trinity ophiolite of northern California (Nicolas, 1989). In contrast to other LOT such as New Caledonia (Sécher, 1981), Canyon Mountain (Himmelberg & Loney, 1980; Misseri & Boudier, 1985), and the Bay of Islands (Girardeau, 1979), where lherzolites might have possibly been formed by magmatic impregnation processes (Nicolas & Dupuy, 1984), the Trinity ophiolite preserves local evidence of partial melting and melt extraction (Boudier & Nicolas, 1985–86). Structural and petrological studies suggest that the crustal sequence (gabbros and dykes) of this ophiolite was derived by partial melting of mantle peridotites in a slow-spreading centre (Le Sueur *et al.*, 1984; Boudier *et al.*, 1989; Nicolas, 1989). However, available Sm–Nd isotopic data (Jacobsen *et al.*, 1984; Brouxel & Lapierre, 1988) are at variance with such a view. Ages of 472 ± 32 Myr and an $\varepsilon_{Nd}(T)$ of $+10{\cdot}4 \pm 0{\cdot}4$ have been obtained from a plagioclase lherzolite sample, whereas a pyroxenite dyke and a suite of gabbros, pillow lavas and plagiogranites have yielded ages of 435 ± 21 and 452 ± 40 Myr, respectively, with corresponding lower $\varepsilon_{Nd}(T)$ ranging from $+6{\cdot}7 \pm 0{\cdot}3$ to $+7{\cdot}1 \pm 0{\cdot}4$. On the basis of these data, Jacobsen *et al.* (1984) concluded that the Trinity peridotites and the Trinity crustal rocks were not genetically related.

The purpose of the present study is two-fold:

(a) to establish, using REE and Nd isotope data, the genetic relationship between peridotites, dykes, and gabbros in a structurally and petrographically well-documented area (the Toad Lake area of the Trinity Complex);

(b) to obtain new insights into the genesis of oceanic lithosphere in a slow-spreading ridge environment.

GEOLOGICAL SETTING AND FIELD RELATIONSHIPS

The Trinity ophiolite includes the 2–4 km thick Trinity Peridotite (Irwin, 1981; Quick, 1981) and a thin (~1 km thick) sequence made up of small gabbroic massifs (Fig. 1a) interpreted as remnants of oceanic magma chambers (Lécuyer, 1990, in press; Cannat & Lécuyer, 1991). Toad Lake is located on the eastern flank of a 6 km wide gabbro body of roughly circular shape. Structural (Le Sueur *et al.*, 1984; Boudier *et al.*, 1989; Nicolas, 1989) and petrological studies (Cannat & Lécuyer, 1991) in this area have established that the Toad Lake magma chamber was rooted in adjacent mantle peridotites.

The exposed Toad Lake gabbroic sequence is ~200 m thick (Fig. 1b). The gabbro–peridotite contact is planar and undeformed, and parallel to the cumulate layering. It is continuously underlain by several metres of ultrabasic–basic breccias (Fig. 1b). Mantle peridotites beneath the magma chamber comprise harzburgites, plagioclase harzburgites, lherzolites, and plagioclase lherzolites. In the plagioclase lherzolites, plagioclase occurs in small elongated lenses. These feldspar lenses define a lineation parallel to the high-

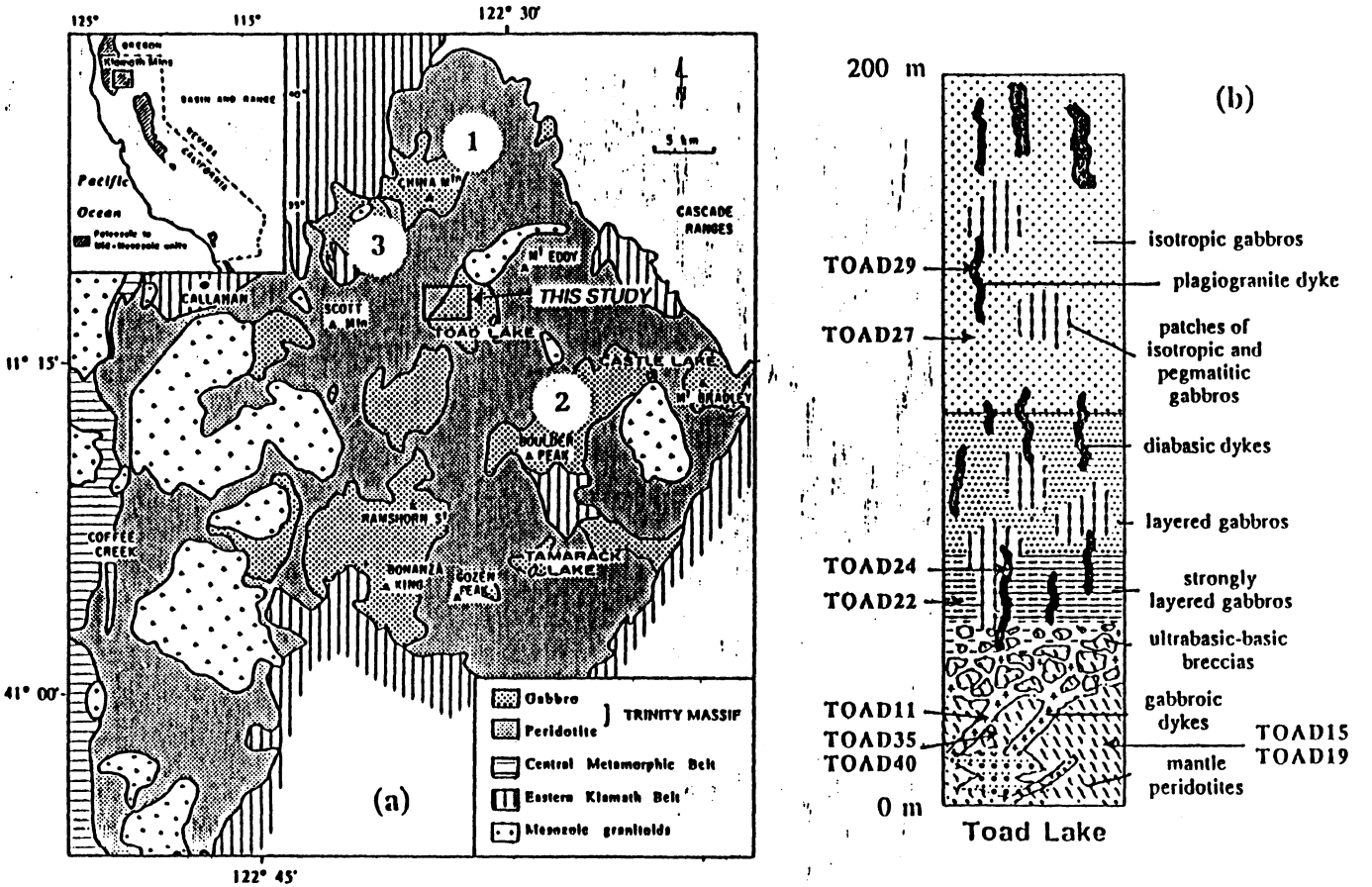

FIG. 1. (a) Geological map [after Wagner & Saucedo (1986)] of the Trinity Ophiolite Complex [1 and 3 refer to areas studied by Quick (1981) and Jacobsen *et al.* (1984), and Wallin *et al.* (1988), respectively; 2 indicates location of the study by Brouxel & Lapierre (1988)]. (b) Sketch showing a simplified stratigraphic column of the NW flank of the Toad Lake magma chamber, with the location of the samples.

temperature flow plane and often surround elongated spinels. Such features suggest that these feldspar lenses probably result from incomplete extraction of melt during high-temperature mantle flow, thus providing evidence that the Trinity peridotite was partially molten when it was incorporated into the oceanic lithosphere (Quick, 1981; Nicolas, 1989).

Undeformed dykes of clinopyroxene-rich gabbro cross-cut both the mantle peridotites and the magma chamber. In the magma chamber, they are fine grained and have no chilled margins, suggesting that they were emplaced before complete consolidation of the country rock (Cannat & Lécuyer, 1991; Lécuyer, in press). In the peridotites, they exhibit parallel borders with depleted lherzolite or harzburgite, and are nearly perpendicular to the spinel foliation (Le Sueur *et al.*, 1984; Boudier *et al.*, 1989). Taken as a whole, these undeformed clinopyroxene-rich dykes are believed to be part of the dyke swarm which fed the original magma chamber (Cannat & Lécuyer, 1991).

SAMPLES

The location of the samples is shown in Fig. 1b. Five samples from the mantle section—one harzburgite (sample TOAD15), one plagioclase harzburgite (sample TOAD19), one lherzolite (sample TOAD35), one plagioclase lherzolite (sample TOAD40), and one clinopyroxene-rich dyke (sample TOAD11)—and four samples from the magma chamber—two gabbros (samples TOAD22 and TOAD27), one clinopyroxene-rich dyke (sample TOAD 24), and one plagiogranite dyke (sample TOAD29)—were selected for the geochemical and isotopic study.

The textures of the peridotites are porphyroclastic (Mercier & Nicolas, 1975). The sizes and shapes of olivine grains (Fo_{90-92}; NiO from 0·2 to 0·45%) are highly variable. The larger grains (0·6–1 mm) are commonly elongated and exhibit regular kink bands. Orthopyroxene porphyroclasts ($Wo_{1-2}En_{89-90}Fs_{8-9}$; 1·5–2·5 mm) often contain clinopyroxene exsolution lamellae. Clinopyroxene ($Wo_{47}En_{50}Fs_3$) is undeformed and generally small (< 1 mm). Spinel grains (magnetite 2–6%, hercynite 52–60%, chromite 35–44%) are reddish brown, commonly elongated (0·4–0·6 mm), and define a lineation which tracks the high-temperature mantle flow direction.

Sample TOAD22 is an ilmenite-rich gabbronorite with mesocumulate to orthocumulate texture. Magmatic layering in the Toad Lake gabbronorites is well developed, and layers of different mineralogy and granulometry are observed. Generally, plagioclase (altered to epidote or albite) dominates in the coarser-grained layers. The pyroxenes are usually fresh, although orthopyroxene is sometimes altered to chlorite, and clinopyroxene to actinolite. The gabbronorites are characterized by early cumulus plagioclase, followed by clinopyroxene, orthopyroxene, and, finally, interstitial ilmenite.

Sample TOAD27 is an isotropic gabbro. Isotropic gabbros lie above the layered cumulates and are ~90 m thick (Fig. 1b). These gabbros *sensu stricto* are characterized by early cumulus clinopyroxene and postcumulus plagioclase.

Clinopyroxene-rich dyke samples TOAD11 and TOAD24 have medium-grained (1–2 mm) and fine-grained (< 1 mm) doleritic textures, respectively. The dominant mineral phases are clinopyroxene (~50–55% in modal proportion) and plagioclase (~30–35% in modal proportion), with olivine (<20% in modal proportion). The clinopyroxene is diopsidic in composition and the plagioclase is highly calcic (An_{90}).

Plagiogranite dyke sample TOAD29 has predominantly hypidiomorphic albite and quartz and corresponds to a medium-grained trondhjemite according to the terminology of Coleman & Peterman (1975). Other minerals include hornblende (< 5% in modal proportion), magnetite, sphene, apatite, and zircon.

ANALYTICAL METHODS

All measurements were performed at the Université de Rennes. Concentrations of major elements, Ni, and Cr were determined by X-ray fluorescence (XRF) spectrometry. Total iron is reported as Fe_2O_3. Analytical uncertainties are lower than 3%, except MnO whose concentration is precise to only 10%.

REE concentrations were determined by the isotopic dilution method following a procedure essentially similar to that described by Jahn *et al.* (1980). Blanks were as follows (10^{-9} g): La (2·07), Ce (1·50), Nd (0·27), Sm (0·65), Eu (0·11), Gd (0·87), Dy (2·95), Er (2·03), Yb (4·36), and Lu (0·77). Analytical errors, including chemical preparations, blank effects, and uncertainties in spike calibration and mass spectrometry runs, were estimated at ~5% for La and Lu, 3% for Gd, and 2% for other REEs in most samples. However, uncertainty on the La concentration of sample TOAD35 (a strongly depleted peridotite) might be much higher because of the high La-blank/La-sample ratio. For sample TOAD15, the REE pattern is so depleted in LREEs (Table 1, Fig. 2a) that concentrations in La and Ce could not be accurately measured.

Nd isotopic analyses were performed on separate powder samples. The method has been described by Gruau *et al.* (1987, 1990). All samples were first dissolved in $HF–HNO_3–HClO_4$ and subsequently redissolved, after evaporation, in 6 N HCl. Approximately 80% of the sample solutions were used for Nd isotopic composition; determinations; the remaining 20% were used for redetermination of Sm/Nd ratios. Nd isotopic compositions were run using Faraday cups on a five-collector Finnigan MAT 262 mass spectrometer. $^{143}Nd/^{144}Nd$ measured ratios were normalized to $^{146}Nd/^{144}Nd = 0{\cdot}7219$. Fourteen individual isotopic analyses of the Nd La Jolla standard during the course of this study indicate a mean $^{143}Nd/^{144}Nd$ ratio of $0{\cdot}511843 \pm 5$ ($2\sigma_m$). Nd blanks were lower than 0·5 $\times 10^{-9}$ g.

Regression analyses were carried out following the method of York (1969). The error inputs for $^{147}Sm/^{144}Nd$ and $^{143}Nd/^{144}Nd$ ratios were 0·2% and 0·005%, respectively. All errors on ages and initial isotopic ratios are reported at a 2σ confidence level. Measured and

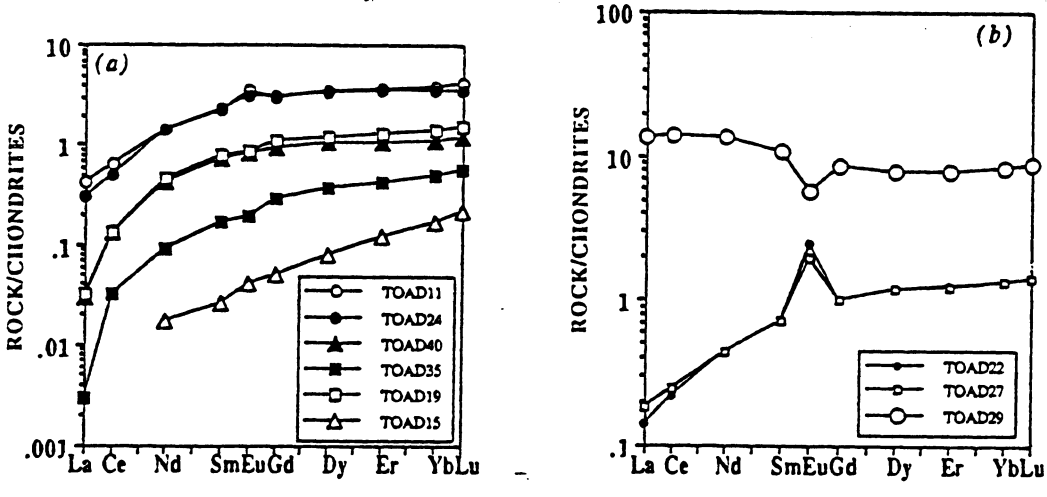

FIG. 2. Chondrite-normalized REE patterns for Toad Lake samples: (a) peridotites and clinopyroxene-rich dykes; (b) cumulate gabbros and plagiogranite dyke. Normalizing values have been reported by Jahn *et al.* (1980). TOAD15: harzburgite; TOAD19: plagioclase harzburgite; TOAD35: lherzolite; TOAD40: plagioclase lherzolite; TOAD11 and TOAD24: clinopyroxene-rich dykes; TOAD22 and TOAD27: cumulate gabbros; TOAD29: plagiogranite dyke.

TABLE 1

Major and trace elements in Toad Lake samples

Samples	*TOAD15 harzburgite*	*TOAD19 plagioclase harzburgite*	*TOAD35 lherzolite*	*TOAD40 plagioclase lherzolite*	*TOAD11 picrite dyke*	*TOAD24 picrite dyke*	*TOAD22 gabbronorite cumulate*	*TOAD27 gabbro cumulate*	*TOAD29 plagiogranite dyke*
SiO_2 (%)	39·03	40·98	42·59	41·03	46·01	48·47	42·35	46·13	77·31
Al_2O_3	0·72	2·62	1·16	2·54	11·75	12·89	19·77	19·46	12·56
Fe_2O_{3t}	7·97	8·21	8·60	8·49	8·27	7·09	11·84	5·89	0·21
MnO	0·11	0·11	0·13	0·12	0·18	0·13	0·16	0·11	0·00
MgO	38·91	36·89	37·32	37·70	15·47	15·16	7·39	9·61	0·09
CaO	0·89	2·27	2·21	2·40	13·96	11·57	13·34	14·41	4·19
Na_2O	0·00	0·05	0·02	0·05	0·81	0·15	0·64	0·30	3·59
K_2O	0·01	0·00	0·00	0·01	0·03	0·00	0·15	0·01	0·24
TiO_2	0·02	0·10	0·04	0·10	0·24	0·23	1·02	0·09	0·18
P_2O_5	0·01	0·01	0·00	0·01	0·00	0·00	0·01	0·01	0·03
L.O.I.	11·43	7·90	7·09	6·76	2·95	3·81	2·78	3·54	0·60
Sum	99·10	99·14	99·16	99·21	99·67	99·5	99·45	99·56	99·00
Ol (%)[1]	76	58	55	53	15	12	—	—	n.d.
Opx	19	27	25	20	—	—	22	—	n.d.
Cpx	3	—	13	21	50	56	14	48	n.d.
Pl	—	8	—	4	35	32	55	52	n.d.
Sp	2	7	7	2	—	—	—	—	n.d.
Ilm	—	—	—	—	—	—	9	—	n.d.
Ni (ppm)	2287	2049	2165	2090	380	411	62	67	0
Cr	2360	2318	2847	2452	825	980	50	36	15
La	b.d.l.	0·010	0·001	0·009	0·124	0·168	0·051	0·069	4·307
Ce	b.d.l.	0·105	0·026	0·105	0·514	0·391	0·172	0·195	11·350
Nd	0·010	0·275	0·054	0·252	0·850	0·851	0·255	0·256	8·000
Sm	0·005	0·150	0·033	0·138	0·433	0·442	0·137	0·135	2·093
Eu	0·003	0·062	0·014	0·059	0·250	0·228	0·179	0·139	0·410
Gd	0·013	0·277	0·073	0·240	0·768	0·789	0·262	0·259	2·248
Dy	0·026	0·395	0·119	0·342	1·130	1·088	0·382	0·386	2·563
Er	0·026	0·271	0·090	0·228	0·771	0·733	0·263	0·261	1·672
Yb	0·035	0·297	0·104	0·227	0·780	0·705	0·269	0·275	1·722
Lu	0·007	0·049	0·018	0·038	0·128	0·110	0·044	0·045	0·282
$(Ce/Sm)_N$	—	0·17	0·19	0·18	0·28	0·21	0·30	0·34	1·28
$(Gd/Yb)_N$	0·30	0·75	0·56	0·85	0·79	0·90	0·78	0·76	1·05
Eu/Eu*	1·11	0·94	0·88	1·00	1·34	1·19	2·92	2·30	0·58

[1] Calculated from bulk-rock chemistry and average mineral composition using the least-squares method of Bryan *et al.* (1969).
b.d.l. = below detection limit.
n.d. = not determined.
Rare earth element data are corrected for blank contributions.

calculated initial $^{143}Nd/^{144}Nd$ ratios are quoted throughout the text and in Table 2 in the ε_{Nd} notation of DePaolo & Wasserburg (1976) as deviations in parts per 10^4 from the chondritic growth curve. The present-day $^{143}Nd/^{144}Nd$ and $^{147}Sm/^{144}Nd$ ratios for the chondritic reference reservoir (CHUR) are those determined by Jacobsen & Wasserburg (1980). The errors of the isochron initial ε_{Nd} values were calculated using the method of Fletcher & Rosman (1982). The decay constant of ^{147}Sm is 0·00654 Gyr^{-1}.

RESULTS

Major and trace element data

Major and trace element data are presented in Table 1. Chondrite-normalized REE patterns are illustrated in Fig. 2a and b.

Fertile plagioclase lherzolite sample TOAD40 and plagioclase harzburgite sample TOAD19 are characterized by relatively high CaO (2·40 and 2·27%, respectively), Al_2O_3 (2·54 and 2·62%, respectively), and TiO_2 (0·1%) contents. Depleted lherzolite sample

TABLE 2

Sm–Nd isotopic results for Toad Lake samples

Sample	*Rock type*	*Sm (ppm)*	*Nd (ppm)*	$^{147}Sm/^{144}Nd$*	$^{143}Nd/^{144}Nd$	2σ	$\varepsilon_{Nd}(0)$†	$\varepsilon_{Nd}(T)$‡
TOAD19	Pl-harzburgite	0·181	0·295	0·3708	0·513450	8	+15·8 ± 0·2	+6·4 ± 0·2
TOAD40	Pl-lherzolite	0·143	0·259	0·3323	0·513388	16	+14·6 ± 0·4	+7·3 ± 0·4
TOAD11	Cpx-rich dyke	0·440	0·850	0·3126	0·513281	7	+12·5 ± 0·1	+6·3 ± 0·1
TOAD24	Cpx-rich dyke	0·460	0·871	0·3189	0·513286	8	+12·6 ± 0·1	+6·0 ± 0·1
TOAD27	Gabbro	0·142	0·273	0·3149	0·513286	6	+12·6 ± 0·1	+6·3 ± 0·1
TOAD29	Plagiogranite	2·088	7·963	0·1585	0·512868	7	+4·5 ± 0·1	+6·6 ± 0·1

* Error on the ratio is 0·2%.

† $\varepsilon_{Nd}(0) = \left[\frac{(^{143}Nd/^{144}Nd)_0^{sample}}{0.512638} - 1\right] \times 10^4$.

‡ $\varepsilon_{Nd}(T) = \left[\frac{(^{143}Nd/^{144}Nd)_T^{sample}}{(^{143}Nd/^{144}Nd)_T^{CHUR}} - 1\right] \times 10^4$

with $T = 423$ Myr.

TOAD35 exhibits lower concentrations of these elements (CaO = 2·21%, Al_2O_3 = 1·16%, and TiO_2 = 0·04%). Values for depleted harzburgite sample TOAD15 are even lower (CaO = 0·89%, Al_2O_3 = 0·72%, and TiO_2 = 0·02%). The REE patterns of these four peridotites are nearly parallel, with a strong depletion in LREEs [$(Ce/Sm)_N$ = 0·17–0·19]. The absolute REE contents of the depleted peridotites are lower by a factor of 5–25 than those of the fertile peridotites (Table 1, Fig. 2a).

The chemical characteristics of the two clinopyroxene-rich gabbroic dykes (TOAD11 and TOAD24) (MgO ~ 15–16%, Ni ~ 400 ppm, and Cr ~ 900 ppm) are similar and resemble those of picritic magmas. As with the peridotites, the REE patterns are strongly depleted in LREEs [$(Ce/Sm)_N$ = 0·28 and 0·21, respectively]. Both samples exhibit a slight positive Eu anomaly (Table 1, Fig. 2a). The absolute content of REE is higher than those of the fertile peridotites by a factor of 3 (Table 1).

The two gabbros (TOAD22 and TOAD27) present petrographic evidence of plagioclase accumulation. Consistently, both samples exhibit high Al_2O_3 contents (19·77 and 19·46%, respectively), as well as marked positive Eu anomalies (Eu/Eu* = 2·92 and 2·30). These two gabbros also have strongly LREE-depleted patterns [$(Ce/Sm)_N$ = 0·30 and 0·34, respectively; Table 1, Fig. 2b].

The plagiogranite dyke (TOAD29) has a major element composition similar to that of other plagiogranites in the Trinity Ophiolite Complex. REE concentrations are consistently higher than in the mafic–ultramafic samples. However, marked differences arise when the REE distribution patterns are considered (Fig. 2a and b). Sample TOAD29 is not LREE depleted; instead, its REE pattern reflects slight enrichment of the LREEs relative to the HREEs. Another noticeable difference is the existence of a pronounced negative Eu anomaly (Fig. 2b).

Nd isotopic data

The Sm–Nd isotopic results are presented in Table 2 and further displayed on two conventional isochron diagrams (Fig. 3). Three important points should be noted:

(1) Consistent with their REE distribution patterns, all samples except the plagiogranite dyke exhibit very high $^{147}Sm/^{144}Nd$ ratios. The $^{147}Sm/^{144}Nd$ ratios of the peridotites, clinopyroxene-rich dykes, and cumulate gabbros cluster between 0·3126 and 0·3708 (Table 2). $^{147}Sm/^{144}Nd$ for the plagiogranite dyke is much lower (0·1585).

(2) The Toad Lake dataset defines a linear correlation on an Sm–Nd isochron diagram. Because of the relatively small range in $^{147}Sm/^{144}Nd$ of the basic–ultrabasic suite, the resulting isochron is basically a two-point isochron. The Toad Lake dataset yields an age of 423 ± 48 Myr with an $\varepsilon_{Nd}(T)$ of $+6{\cdot}4 \pm 0{\cdot}7$.

(3) When the data of Jacobsen *et al.* (1984) and Brouxel & Lapierre (1988) are combined, the dataset defines two separate isochrons (Fig. 3b): one corresponds to the plagioclase lherzolite sample (whole-rock, with clinopyroxene and plagioclase separates) investigated by Jacobsen *et al.* (1984), which yields an age of 472 ± 32 Myr and an initial ε_{Nd} of $+10{\cdot}4 \pm 0{\cdot}4$; the second isochron includes the Toad Lake dataset (peridotites, gabbros, and plagiogranite) and the data from crustal rock-types (including clinopyroxene and plagioclase separates) obtained by Jacobsen *et al.* (1984) and Brouxel & Lapierre (1988). This second isochron gives an age of 421 ± 28 Myr with an initial ε_{Nd} of $+6{\cdot}9 \pm 0{\cdot}4$. Both the age and initial ε_{Nd} defined by this second isochron are identical within error to those obtained for the Toad Lake dataset taken on its own (Fig. 3a and b).

DISCUSSION

The Toad Lake Massif: a cogenetic rock suite

The Sm–Nd isotopic results reported by Jacobsen *et al.* (1984) and Brouxel & Lapierre (1988) implied a non-cogenetic relationship between the Trinity peridotites and associated crustal rock-types. The present results from Toad Lake give an opposite view: all the data from this area are consistent with a close genetic link between peridotites and the crustal rocks. The main evidence is as follows:

(1) Clinopyroxene-rich dykes cross-cutting the peridotites (TOAD11) and overlying gabbros (TOAD24) have nearly identical major and trace element compositions (Table 1, Fig. 2a). Thus, the dykes may well represent magma conduits that fed the magma chamber. Their depleted border zones may represent the residues left after extraction of melts which are now crystallized in the dykes.

(2) Quick (1981) has shown that fertile, depleted peridotites and plagioclase-rich dykes from the China Mountain area (locality 1 in Fig. 1a) define a straight line when plotted in Harker diagrams. Quick (1981) concluded that the lherzolite and harzburgite are refractory residues produced by partial melting of a protolith with a composition similar to that of a plagioclase lherzolite. The Toad Lake samples belong to the same linear trends (Fig. 4a and b). In particular, the clinopyroxene-rich dyke (TOAD24) plots very close to the primary liquid composition (PLV in Fig. 4a and b) of Quick (1981), whereas sample TOAD11 appears to have undergone some clinopyroxene accumulation.

(3) REE patterns for peridotites, cumulate gabbros, and clinopyroxene-rich dykes from Toad Lake are consistent with a cogenetic rock suite. They all show a similar depletion of the LREEs relative to the HREEs and REE concentrations increase with decreasing MgO (Table 1).

(4) All samples (peridotites and crustal rocks) from the Toad Lake area define a linear array in an Sm–Nd isochron diagram (Fig. 3a). This array is even better defined if the crustal rocks and related mineral separates from other areas of the Trinity ophiolite (Jacobsen *et al.*, 1984; Brouxel & Lapierre, 1988) are added, resulting in a 16-point regression line (Fig. 3b).

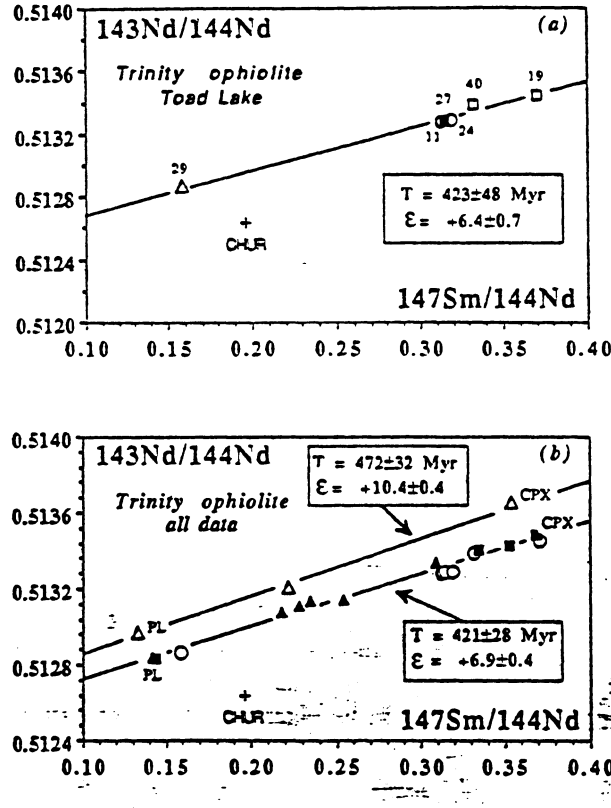

FIG. 3. Sm–Nd isochron diagrams for Trinity rocks: (a) Toad Lake sample suite only; (b) whole dataset including results from Jacobsen *et al.* (1984) and Brouxel & Lapierre (1988). Symbols: (a) □, peridotites; ○, clinopyroxene-rich dykes; ■, cumulate gabbro; △, plagiogranite dyke; (b) ○, this study; △, ▲, Jacobsen *et al.* (1984); ■, Brouxel & Lapierre (1988). Pl = plagioclase; cpx = clinopyroxene.

The corresponding ages (423 ± 48 and 421 ± 28 Myr, respectively) are identical to the U–Pb zircon ages (419 ± 15 to 412 ± 10 Myr) obtained for the Trinity plagiogranites (Wallin *et al.*, 1988), suggesting that they probably represent true ages. Most likely, these ages record crystallization of plagioclase lenses in plagioclase lherzolites, as well as the age of clinopyroxene-rich dykes and crustal gabbros and plagiogranites. The fact that the peridotites from the Toad Lake plot on, or close to, an isochron with an $\varepsilon_{Nd}(T)$ of $\sim +7$ supports a cogenetic relationship between these peridotites and the associated crustal rocks.

Advocates of a non-cogenetic relationship between the Trinity peridotites and their associated crustal gabbros might nevertheless attempt to confront the isotopic argument by suggesting that the Toad Lake Sm–Nd array represents the result of re-equilibration between a ~470-Myr-old peridotite, which has $\varepsilon_{Nd}(T) \sim +10$, and some younger melts (~420 Myr old) with lower $\varepsilon_{Nd}(T)$. However, two important objections against such a model are:

(1) The feldspar lenses of the Toad Lake peridotites define a lineation parallel to the high-temperature mantle flow direction (Quick, 1981; Nicolas, 1989). This is in agreement with the lenses being crystallized trapped melts rather than from impregnation of the peridotites by younger melts. In fact, the invasion of 420-Myr-old melts into 470-Myr-old peridotites would probably result in feldspar lenses with a lineation discordant to the mantle flow direction.

(2) Plagioclase-bearing peridotites (TOAD19 and TOAD40) have $^{147}Sm/^{144}Nd$ ratios (0·3708 and 0·3323, respectively) which are much higher than that of the peridotite investigated by Jacobsen and coworkers (0·2219). If we assume that peridotite samples TOAD19 and TOAD40 initially possessed $\varepsilon_{Nd}(T) = +10{\cdot}4 \pm 0{\cdot}4$ and $^{147}Sm/^{144}Nd = 0{\cdot}2219$, and gained their lower $\varepsilon_{Nd}(T)$ and higher $^{147}Sm/^{144}Nd$ through melt impregnation processes, then simple mass balance considerations indicate that the postulated impregnated melt should have had a $^{147}Sm/^{144}Nd > 0{\cdot}3708$. Figure 3a and b shows that none of the Trinity samples investigated so far exhibit such an extraordinary depletion in LREE. In particular, samples TOAD24 and TOAD11, which could have acted as impregnated melts, have $^{147}Sm/^{144}Nd$ ratios no higher than 0·3189 (Table 2).

In summary, the Toad Lake samples have geochemical and isotopic characteristics consistent with a cogenetic igneous suite. The age of 423 ± 48 Myr records the crystallization of plagioclase lenses in plagioclase lherzolites, as well as the age of clinopyroxene-rich dykes and crustal gabbros. At that time, both the peridotites (plagioclase lherzolites and lherzolites) and the magmatic precursors of dykes and rocks in the magma chamber had an identical ε_{Nd} value of $+6{\cdot}4 \pm 0{\cdot}7$ (see also Bodinier *et al.*, this volume).

Composition of the magma which fed the Toad Lake magma chamber

In addition to establishing a close cogenetic relationship between the peridotites, the clinopyroxene-rich dykes, the gabbros, and the plagiogranite dyke, the above results confirm the view that clinopyroxene-rich dykes represent probable remnants of magma conduits. Accepting this analogy, constraints can be placed on the composition of the partial melt which fed the Toad Lake magma chamber.

Are clinopyroxene-rich dykes representative of the composition of a melt and, if so, can this melt have been a parental magma for rocks of the Toad Lake magma chamber? Two main processes may result in dykes with compositions different from that of circulating melts: (a) crystal segregation during flow crystallization; and (b) mechanical incorporation of crystals and/or xenoliths from the wall rocks. The two processes have been recognized in dykes from orogenic lherzolites and/or in dykes from ultramafic xenoliths in alkalic basalts, and it is clear that the compositions of the affected dykes are by no means representative of a melt (e.g., Irving, 1980; Bodinier *et al.*, 1987). However, such processes do not seem to have been involved in the case of the dykes discussed here. Let us consider those clinopyroxene-rich dykes which cross-cut the cumulate gabbros (TOAD24). As already pointed out, clinopyroxene-rich dykes in the gabbros have fine-grained doleritic textures; they are devoid of phenocrysts and no mineralogical layering is observed. These are not the diagnostic textural and petrological criteria of dykes which result from mineral segregation and/or mineral incorporation processes (e.g., Irving, 1980). Chemical characteristics of sample TOAD24 also support a hypothesis based on a crystallized melt: (a) this sample contains moderately high Cr (~980 ppm) and Ni (~411 ppm) contents; (b) there is no significant Eu anomaly (Fig. 2a); and (c) sample TOAD24 lies on a modelled line of liquid descent when plotted on the CaO vs. MgO and Al_2O_3 vs. MgO diagrams (Fig. 4a and b).

At this stage, the possibility arises that the magnesian composition (MgO ~16%; Table 1) preserved in the clinopyroxene-rich dykes might represent the composition of the magma which fed the Toad Lake magma chamber. Comparison of the REE pattern of clinopyroxene-rich dyke sample TOAD24 with cumulate gabbro samples TOAD22 and TOAD27 may confirm whether this is a reasonable working hypothesis. Assuming that cumulate gabbro samples TOAD22 and TOAD27 crystallized from a melt initially similar in composition to sample TOAD24, we are able to predict the resulting REE patterns. Because partition

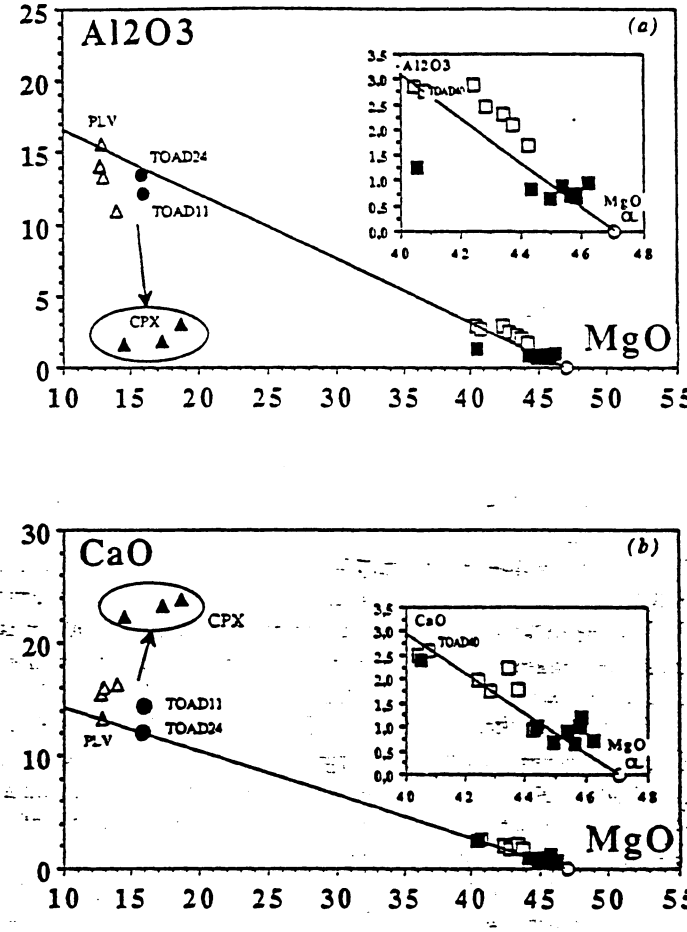

FIG. 4. Al_2O_3 vs. MgO (a) and CaO vs. MgO (b) plots for Trinity peridotites, and clinopyroxene-rich and plagioclase-rich dykes. Symbols: □, fertile peridotites; ■, depleted peridotites; ●, clinopyroxene-rich dykes; △, plagioclase-rich dykes; ▲, composition of clinopyroxene in cumulate gabbros; ○, average composition of olivine in peridotites; PLV: recalculated composition of plagioclase-rich dyke parental magma (from Quick, 1981). Data sources: this study, Quick (1981), and Lécuyer (1990).

coefficients for REE between clinopyroxene, orthopyroxene, plagioclase (the minerals likely to have crystallized and accumulated), and basaltic melt are $<1{\cdot}0$ (e.g., Arth, 1976), concentrations of these elements should be lower in samples TOAD22 and TOAD27 than in sample TOAD24. Partition coefficient data indicate that cumulate gabbros crystallizing from a melt with the REE pattern of sample TOAD24 should display LREE-depleted patterns. Table 1 and Fig. 2 show that these two basic requirements are met: REE concentrations in samples TOAD22 and TOAD27 are lower than in sample TOAD24 by a factor of 3, and both samples are depleted in LREEs (Fig. 2a and b).

Further inspection of the REE patterns provides additional evidence to support the emerging view that clinopyroxene-rich dykes represent a reasonable candidate for a parental magma composition. Here, we wish to stress that the relative depletion in LREEs in cumulate gabbro samples TOAD22 and TOAD27 is, in both cases, accompanied by a depletion of Gd relatively to Dy (Fig. 2b). Because Gd and Dy are nearly equally partitioned between basaltic melts and coexisting minerals, we may deduce that the resulting $(Gd/Dy)_N$ ratios

(< 1·0) are features which were inherited from the composition of the parental magma. In other words, this magma should be similarly depleted in Gd relatively to Dy. Significantly, samples TOAD24, TOAD22, and TOAD27 have nearly identical values of $(Gd/Dy)_N$: 0·90, 0·85, and 0·83, respectively.

However, it is still not clear whether all the magma chambers at Trinity were fed by picritic magmas. Judging from the results of Quick (1981), it is not out of the question that more basic magmas in fact prevailed in other magma chambers (e.g., China Mountain). Nevertheless, Trinity may document a case for an oceanic ridge environment where part of the newly formed oceanic crust differentiated from parental magmas that were picritic in composition.

IMPLICATIONS FOR THE ORIGIN AND SETTING OF THE TRINITY OPHIOLITE COMPLEX

It remains to explore the possible significance of the differences in age and initial ε_{Nd} value between the peridotites from Toad Lake [$T = 423 \pm 48$ Myr; $\varepsilon_{Nd}(T) = +6{\cdot}4 \pm 0{\cdot}7$] and the plagioclase lherzolite from China Mountain [$T = 472 \pm 32$ Myr; $\varepsilon_{Nd}(T) = +10{\cdot}4 \pm 0{\cdot}4$]. As can be seen in Fig. 5, initial ε_{Nd} values often vary in coeval but spatially remote ophiolites (e.g., Kings River and Bay of Islands). By contrast, variations in age and initial ε_{Nd} in closely spatially related ophiolites, or in a given ophiolitic massif, are rarely observed. Apart from Trinity, the only documented example so far is the Saudi Arabian ophiolites where ages of 740–780 Ma have been found with initial ε_{Nd} in the range +6·6 to +7·6 (Claesson *et al.*, 1984).

An attractive working hypothesis is that the Trinity Ophiolite Complex represents the remnant of the opening of an ocean which operated on a previously developed oceanic lithosphere, perhaps in an area similar to a modern back-arc or inter-arc basin. This hypothesis is attractive because it could account for the juxtaposition of oceanic mantle units of different ages and different isotopic signatures. A similar interpretation was proposed by Gõpel *et al.* (1984) for the isotopically heterogeneous Xigaze Ophiolite of Tibet. In fact, several workers have already promoted a hypothesis based on a back-arc or inter-arc

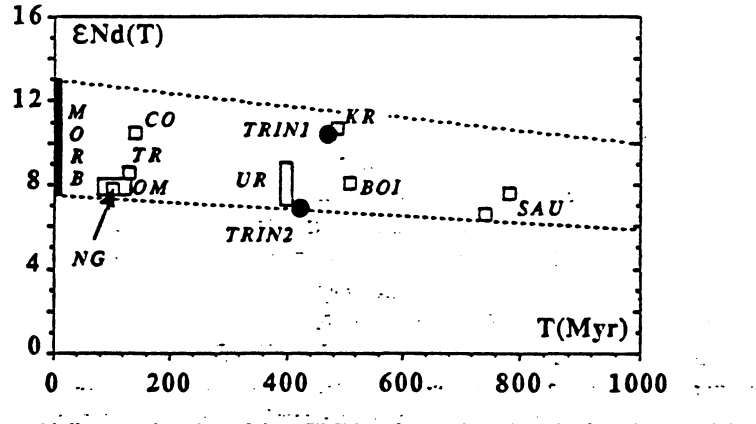

FIG. 5. ε_{Nd} values in ophiolites as a function of time. TRIN1 refers to the value obtained by combining all samples from Trinity, except the plagioclase lherzolite sample investigated by Jacobsen *et al.* (1984), which is indicated as TRIN2. Other symbols: SAU (Saudi Arabia; Claesson *et al.*, 1984); BOI (Bay of Islands; Jacobsen & Wasserburg, 1979); KR (Kings River; Shaw *et al.*, 1987); UR (Urals; Edwards & Wasserburg, 1985); CO (Corsica; Richard & Allègre, 1980); TR (Troodos; Richard & Allègre, 1980); NG (New Guinea; Richard & Allègre, 1980); OM (Oman; McCulloch *et al.*, 1981). The two dashed lines delineate depleted mantle composition at corresponding ages.

basin environment for the emplacement of the Trinity peridotite (e.g., Quick, 1981; Brouxel & Lapierre, 1988). Thus, the Trinity Ophiolite Complex could be a composite body, with old oceanic lithosphere (the China Mountain area) in tectonic contact with a newly risen diapir of asthenospheric mantle (the Toad Lake area). However, it should be noted that, although the difference in initial ε_{Nd} between the peridotites from Toad Lake and China Mountain appears well established (the actual difference is of 4 ε units, which far exceeds analytical uncertainties), the ages (423 ± 48 and 472 ± 32 Myr, respectively) statistically overlap. Should the age difference be proved geologically meaningless, the whole Trinity Ophiolite Complex could be related to an ancient diapir of isotopically heterogeneous asthenospheric mantle (see also Bodinier *et al.*, this volume).

ACKNOWLEDGEMENTS

C. Lécuyer benefited from the experience of M. Cannat during fieldwork. H. Lapierre and the U.S. Geological Survey of Menlo Park are thanked for assistance and financial support during carriage of the samples. We are also grateful to J. Macé for his assistance during mass spectrometry runs. We thank A. Nicolas, F. Boudier, and J.-L. Bodinier for stimulating discussions on various aspects of this work. M. A. Menzies is thanked for his helpful review of an earlier version of the manuscript. This is contribution CNRS-INSU-DBT No. 344.

REFERENCES

Arth, J. G., 1976. Behaviour of trace elements during magmatic processes. A summary of theoretical models and their applications. *J. Res. U.S. Geol. Surv.* **4**, 41–7.

Bodinier, J.-L., Guiraud, M., Fabriès, J., Dostal, J., & Dupuy, C., 1987. Petrogenesis of layered pyroxenites from the Lherz, Freychinède and Prades ultramafic bodies (Ariège, French Pyrenees). *Geochim. Cosmochim. Acta* **51**, 279–90.

Boudier, F., & Nicolas, A., 1985–86. Harzburgite and lherzolite subtypes in ophiolite and oceanic environments. *Earth Planet. Sci. Lett.* **76**, 84–92.

—— Le Sueur, E., & Nicolas, A., 1989. Structure of an atypical ophiolite: the Trinity complex, eastern Klamath Mountains, California. *Geol. Soc. Am. Bull.* **101**, 820–33.

Brouxel, M., & Lapierre, H., 1988. Geochemical study of an early Paleozoic island arc–back arc basin system. Part I: The Trinity ophiolite (Northern California). *Ibid.* **100**, 1111–19.

Bryan, W. B., Finger, L. W., & Chayes, F., 1969. Estimating proportions in petrographic mixing equations by least-squares approximation. *Science* **163**, 926–7.

Cannat, M., & Lécuyer, C., 1991. Ephemeral magma chambers in the Trinity peridotite, Northern California. *Tectonophysics* **186**, 313–28.

Claesson, S., Pallister, J., & Tatsumoto, M., 1984. Samarium–neodymium data on two late Proterozoic ophiolites of Saudi Arabia and implications for crustal and mantle evolution. *Contr. Miner. Petrol.* **85**, 244–52.

Coleman, R. G., & Peterman, Z. E., 1975. Oceanic plagiogranite. *J. Geophys. Res.* **80**, 1099–108.

DePaolo, D. J., & Wasserburg, G. J., 1976. Inferences about magma sources and mantle structure from variations of $^{143}Nd/^{144}Nd$. *Geophys. Res. Lett.* **3**, 743–6.

Edwards, R. L., & Wasserburg, G. J., 1985. The age and emplacement of obducted oceanic crust in the Urals from Sm–Nd and Rb–Sr systematics. *Earth Planet. Sci. Lett.* **72**, 389–404.

Fletcher, I. R., & Rosman, K. J. R., 1982. Precise determination of initial ε_{Nd} from Sm–Nd isotopic data. *Geochim. Cosmochim. Acta* **46**, 1983–7.

Girardeau, J., 1979. Structure des ophiolites de Terre Neuve et modèle de croûte océanique. Thèse Doctorat 3ème cycle, Université de Nantes, 154 pp.

Göpel, C., Allègre, C. J., & Xu, R. H., 1984. Lead isotopic study of the Xigaze ophiolite (Tibet): the problem of the relationship between magmatites (gabbros, dolerites, lavas) and tectonites (harzburgites). *Earth Planet. Sci. Lett.* **69**, 301–10.

Gruau, G., Chauvel, C., & Jahn, B. M., 1990. Anomalous Sm–Nd ages for the early Archean Onverwacht Group volcanics: significance and petrogenetic implications. *Contr. Miner. Petrol.* **104**, 27–34.

—— Jahn, B. M., Glikson, A. Y., Davy, R., Hickman, A. H., & Chauvel, C., 1987. Age of the Archean Talga-Talga Subgroup, Pilbara block, western Australia, and early evolution of the mantle: new Sm–Nd isotopic evidence. *Earth Planet. Sci. Lett.* **85**, 105–16.

Himmelberg, G. R., & Loney, R. A., 1980. Petrology of ultramafic and gabbroic rocks of the Canyon Mountain ophiolite, Oregon. *Am. J. Sci.* **280A**, 232–68.

Irving, A. J., 1980. Petrology and geochemistry of composite ultramafic xenoliths in alkalic basalts and implications for magmatic processes within the mantle. *Ibid.* **280A**, 389–426.
Irwin, W. P., 1981. Tectonic accretion of the Klamath Mountains. In: Ernst, W. G. (ed.) *The Geotectonic Development of California.* Englewood Cliffs, NJ: Prentice-Hall, 29–49.
Jacobsen, S. B., Quick, J. E., & Wasserburg, G. J., 1984. A Nd and Sr isotopic study of the Trinity peridotite; implications for mantle evolution. *Earth Planet. Sci. Lett.* **68**, 361–78.
—— Wasserburg, G. J., 1979. Nd and Sr isotopic study of the Bay of Islands ophiolite complex and the evolution of the source of Mid-Ocean Ridge Basalts. *J. Geophys. Res.* **84**, 7429–45.
—— —— 1980. Sm–Nd isotopic evolution of chondrites. *Earth Planet. Sci. Lett.* **50**, 139–55.
Jahn, B. M., Auvray, B., Blais, S., Capdevila, R., Cornichet, J., Vidal, F., & Hameurt, J., 1980. Trace element geochemistry and petrogenesis of Finnish greenstone belts. *J. Petrology* **21**, 201–44.
Le Sueur, E., Boudier, F., Cannat, M., Ceuleneer, G., & Nicolas, A., 1984. The Trinity mafic–ultramafic complex: first results of the structural study of an untypical ophiolite. *Ofioliti* **9**, 487–98.
Lécuyer, C., 1990. Hydrothermalisme fossile dans une paléocroûte océanique associée à un centre d'expansion lent: le complexe ophiolitique de Trinity (N. Californie, U.S.A.). Thèse Doctorat d'Universite. Université de Rennes. I. *Mémoires et Documents du Centre Armoricain d'Etude Structurale des Socles* **33**, 279 pp.
—— in press. Chemical transfer between ultrabasic xenoliths and basic magmas: evidence from oceanic magma chambers (the Trinity ophiolite, N. California). *Lithos* **24**.
McCulloch, M. T., Gregory, R. T., Wasserburg, G. J., & Taylor, H. P. J., 1981. Sm–Nd, Rb–Sr, and $^{18}O/^{16}O$ isotopic systematics in an oceanic crustal section: evidence from the Samail ophiolite. *J. Geophys. Res.* **86**, 2721–35.
Mercier, J. C., & Nicolas, A., 1975. Textures and fabrics of upper mantle peridotites as illustrated by basalt xenoliths. *J. Petrology* **16**, 454–87.
Misseri, M., & Boudier, F., 1985. Structures in the Canyon Mountain ophiolite indicate an island arc intrusion. *Tectonophysics* **120**, 191–209.
Nicolas, A., 1989. *Structures of Ophiolites and Dynamics of Oceanic Lithosphere.* Dordrecht: Kluwer Academic, 367 pp.
—— Dupuy, C., 1984. Origin of ophiolitic and oceanic lherzolites. *Tectonophysics* **110**, 177–87.
Quick, J. E., 1981. Petrology and petrogenesis of the Trinity peridotite, an upper mantle diapir in the eastern Klamath Mountains, northern California. *J. Geophys. Res.* **86**, 11 837–63.
Richard, P., & Allègre, C. J., 1980. Neodymium and strontium isotope study of ophiolite and orogenic lherzolite petrogenesis. *Earth Planet. Sci. Lett.* **47**, 65–74.
Sécher, D., 1981. Les lherzolites ophiolitiques de Nouvelle-Calédonie et leurs gisements de chromite. Thèse Doctorat 3ème cycle, Université de Nantes, 228 pp.
Shaw, H. F., Chen, J. H., Saleeby, J. B., & Wasserburg, G. J., 1987. Nd–Sr–Pb systematics and age of the Kings River ophiolite, California: implications for depleted mantle evolution. *Contr. Miner. Petrol.* **96**, 281–90.
Wagner, D., & Saucedo, G. J., 1986. Geological map of the Weed quadrangle, 1/250 000, California. *Calif. Div. Min. Geol., Reg. Geol. Map Ser.* **4A**.
Wallin, E. T., Mattinson, J. M., & Potter, A. W., 1988. Early Paleozoic magmatic events in the eastern Klamath Mountains, northern California. *Geology* **16**, 144–8.
York, D., 1969. Least squares fitting of a straight line with correlated errors. *Earth Planet. Sci. Lett.* **5**, 320–4.

RESUME

Dans ce travail nous utilisons les propriétés de traceurs géochimiques des systèmes isotopiques du Sm-Nd, Lu-Hf et Rb-Sr, ainsi que des éléments majeurs et des éléments en trace (Terres Rares) pour apporter une contribution à la connaissance de la composition et de l'évolution du manteau archéen terrestre (T compris entre 2500 et 3800 Ma). Nous étudions aussi le comportement de ces systèmes et/ou éléments lors de l'altération et du métamorphisme, étant entendu que les roches archéennes présentent toutes des signes d'altération et/ou de métamorphisme, deux processus qui peuvent avoir effacer leurs caractéristiques géochimiques originelles. Les objets d'étude sont des roches de composition basique à ultrabasique (komatiites, basaltes et gabbros) et proviennent d'Afrique du sud (ceintures de Barberton et de Schapenburg; T≈3500 Ma), d'Australie (craton de Pilbara; T≈3500 Ma), de Finlande (T≈2700 Ma) et du Groënland (ceinture d'Isua; T≈3800 Ma).

Les résultats géochimiques obtenus sur les komatiites d'Afrique du Sud et du craton de Pilbara, couplés avec ceux publiés sur des komatiites provenant d'autres régions du monde (Canada, Zimbabwe, Inde), montrent qu'il existe, dans ces roches, des variations systématiques des rapports CaO/Al_2O_3, Al_2O_3/TiO_2 et $(Gd/Yb)_N$ telles que trois groupes géochimiques de komatiites archéennes peuvent être reconnus et définis: un Groupe I dans lequel les trois rapports précités présentent des valeurs proches des celles mesurées dans les chondrites; un Groupe II dans lequel les roches montrent des appauvrissements relatifs en Aluminium et en Terres Rares Lourdes; enfin, un Groupe III dans lequel les roches présentent, au contraire, des enrichissements relatifs en Aluminium et en Terres Rares Lourdes. En règle générale, les komatiites archéennes précoces (T≥3400 Ma) appartiennent aux Groupes II et III, celles provenant des terrains archéens tardifs (T≈2700 Ma) étant principalement du Groupe I. Les modélisations géochimiques montrent que les variations observées sont attribuables à des "pertes" (Groupe II) ou à des "gains" (Groupe III) de grenat. Les résultats isotopiques Lu-Hf obtenus sur des échantillons de komatiite du Groupe II de la ceinture de Barberton ($\varepsilon_{Hf}(T)\approx 0$) indiquent que le fractionnement de grenat se produisait lors des épisodes de fusion partielle mantélique (grenat au résidu solide). Couplé avec les données de la pétrologie expérimentale qui montrent que, dans le manteau, la phase au liquidus est le grenat majorite lorsque la pression est ≥15 GPa, ce résultat nous conduit à proposer un modèle reliant les variations géochimiques observées dans les komatiites archéennes à des différences dans la profondeur de fusion des diapirs mantéliques. En tout état de cause, ces variations ne sont pas la trace fossile d'une stratification chimique et minéralogique du manteau archéen, engendrée par un épisode "océan magmatique terrestre" qui se serait développé il y a 4400 Ma.

D'une manière générale, et sans remettre en cause les résultats précédemment énoncés, l'étude du comportement des systèmes isotopiques ainsi que des éléments majeurs et des éléments en trace lors des processus d'altération et/ou de métamorphisme affectant les roches basiques et ultrabasiques archéennes nous conduit à nous interroger sur la capacité réelle de ces systèmes à fournir des traceurs fiables de la composition chimique et isotopique du manteau archéen. En particulier, les résultats obtenus sur les coulées de komatiites de Finlande Orientale (régions de Tipasjärvi et de Siivikkovaara) montrent que la recristallisation métamorphique peut effacer l'ensemble des mémoires magmatiques initialement contenues dans les roches, y compris celles affèrent à des éléments ou des systèmes isotopiques réputés être réfractaires, comme les Terres Rares ou le système isotopique Sm-Nd. A Siivikkovaara, par exemple, nous montrons que la recristallisation métamorphique s'est accompagnée d'une ré-équilibration complète des systématiques Sm-Nd roche-totale: alors que les coulées se sont mises en place il y a 2700 Ma, l'âge isochrone Sm-Nd roche-totale calculé est de 1800 Ma, ce qui correspond à l'épisode métamorphique enregistré dans les minéraux métamorphiques présents dans les échantillons. Les résultats isotopiques de l'oxygène montrent que la recristallisation métamorphique s'opèrait dans des conditions de température de l'ordre de 450°C et que la phase fluide jouait un rôle important dans la mobilité des Terres Rares. Le fait que les ré-équilibrations isotopiques se soient produites 1Ga après la mise en place des coulées conduit à la production d'une gamme aberrante de valeurs $\varepsilon_{Nd}(T)$ (de -8 à +3), sans signification aucune quant à la nature des sources mantéliques impliquées. Le même type de comportement est observé dans les roches de la ceinture d'Isua au Groenland. Alors que certains auteurs ont voulu voir dans la gamme isotopique initiale définie par les roches de cette ceinture ($\varepsilon_{Nd}(3800)$ compris entre -1.0 et +3.5) la trace de composants crustaux d'âge >3800 Ma et/ou de domaines mantéliques très appauvris en Terres Rares Légères, nous montrons que les valeurs $\varepsilon_{Nd}(3800)$ calculées servant de base à ces interprétations ne sont pas des valeurs vraies, mais des valeurs apparentes résultant de fractionnements isotopiques secondaires survenant 1Ga après la mise en place des roches. En fait, des quatres régions étudiées, seules les komatiites de Schapenburg paraissent avoir préservé la quasi-intégralité de leurs mémoires magmatiques originelles.